Photocaged compounds as versatile tools for light-controlled gene expression in bacteria

Inaugural-Dissertation

zur Erlangung des Doktorgrades
der Mathematisch-Naturwissenschaftlichen Fakultät
der Heinrich-Heine-Universität Düsseldorf

vorgelegt von

Dennis Binder

aus Oberhausen

Jülich, September 2016

Aus dem Institut für Molekulare Enzymtechnologie

der Heinrich-Heine-Universität Düsseldorf

Gedruckt mit der Genehmigung

der Mathematisch-Naturwissenschaftlichen Fakultät der

Heinrich-Heine-Universität Düsseldorf

Referent: Prof. Dr. Karl-Erich Jaeger

Korreferent: Prof. Dr. Jörg Pietruszka

Tag der mündlichen Prüfung: 07.11.2016

TABLE OF CONTENTS

A. Conference contributions

A.I. Poster presentations

Binder D, Grünberger A, Loeschcke A, Probst C, Pietruszka J, Wiechert W, Kohlheyer D, Jaeger KE, Drepper T (2013) Characterization of light-triggered gene expression in *E. coli* with respect to population and single cell response. *Symposium on Advanced Imaging in Cell- and Microbiology: Technology and Applications.* Jülich, Germany. 2013-10-10.

Binder D, Grünberger A, Loeschcke A, Probst C, Pietruszka J, Wiechert W, Kohlheyer D, Jaeger KE, Drepper T (2013) Characterization of light-triggered gene expression in *E. coli* with respect to population and single cell response. *Jülicher Biotechday 2013*. Jülich, Germany. 2013-10-11.

Binder D, Grünberger A, Loeschcke A, Probst C, Pietruszka J, Wiechert W, Kohlheyer D, Jaeger KE, Drepper T (2013) Characterization of light-triggered gene expression in *E. coli* with respect to population and single cell response. *EMBL Conference: New approaches and concepts in microbiology.* Heidelberg, Germany. 2013-10-14.

Wandrey G, Hoffmann K, Bier C, **Binder D**, Pietruszka J, Drepper T, Jaeger KE, Büchs J (2014) Online fluorescence spectroscopy combined with light-induced gene expression. *World Talent Campus in Biotechnology Manufacturing*. Kopenhagen, Denmark. 2014-08-15.

Wandrey G, Hoffmann K, Bier C, **Binder D**, Pietruszka J, Drepper T, Jaeger KE, Büchs J (2014) Online fluorescence spectroscopy combined with light-induced gene expression. *Bioprocess Engineering Course 2014*. Island of Brac, Croatia. 2014-09-21.

Loeschcke A, Thies S, Hage-Hülsmann J, Grünberger A, **Binder D**, Domröse A, Klein A, Kohlheyer D, Pietruszka J, Jaeger KE, Drepper T (2015) Heterologous production of antibacterial secondary metabolites from *Serratia marcescens* in *Pseudomonas putida. FEMS 6th Congress of European Microbiologists.* Maastricht, Netherlands. 2015-06-10.

Probst C, Grünberger A, **Binder D**, Steffens I, Drepper T, Wiechert W, Kohlheyer D. (2015) Optical control of gene expression in bacteria on the single-cell level by caged compounds. *Synthetic Biology. Opportunities for Interdisciplinary Research from Biology to Engineering.* Aachen, Germany. 2015-06-24.

Bier C, **Binder D**, Grünberger A, Drobietz D, Hage-Huelsmann J, Kohlheyer D, Loeschcke A, Jaeger KE, Drepper T, Pietruszka J (2015). *Caged Compounds* for Biotechnological and Synthetic Biological Application. *European Society for Photobiology Congress*. Aveiro, Portugal. 2015-09-02.

Bier C, **Binder D**, Grünberger A, Drobietz D, Hage-Huelsmann J, Kohlheyer D, Loeschcke A, Jaeger KE, Drepper T, Pietruszka J (2016). Caged compounds for biotechnological applications. *26th IUPAC International Symposium on Photochemistry*. Osaka, Japan, 2016-04-05.

Steffens I, Grünberger A, **Binder D**, Drepper T, Wiechert W, Kohlheyer D (2016) Bacterial phase diagrams: Analyzing and predicting cell-to-cell heterogeneity of microbial gene expression. *4th BioProScale Symposium.* Berlin, Germany. 2016-04-06.

Grünberger A, Steffens I, **Binder D**, Drepper T, Wiechert W, Kohlheyer D (2016) Bacterial phase diagrams: A novel concept to predict and control bacterial gene expression. *DECHEMA-Himmelfahrtstagung: New Frontiers for Biotech Processes*. Koblenz, Germany. 2016-05-02.

Binder D, Bier C, Hilgers F, Grünberger A, Loeschcke A, Kohlheyer D, Pietruszka J, Jaeger KE, Drepper T (2016). Photocaged Carbohydrates As Versatile Tools For Synthetic Bio(techno)logy And Single Cell Applications. *Conference of the American Society for Photobiology*. Tampa, USA. 2016-05-22.

Thies S, Loeschcke A, Domroese A, Klein A, Pietruszka J, Hilgers F, Weihmann R, **Binder D**, Troost K, Jaeger KE, Drepper T (2016). Novel microbial production strategies for natural products with antimicrobial properties. *IV. International Conference on Antimicrobial Research.* Malaga, Spain. 2016-06-29.

Hage-Hülsmann J, Grünberger A, Thies S, Domroese A, Klein A, **Binder D**, Hilgers F, Kohlheyer D, Pietruszka J, Jaeger KE, Drepper T, Loeschcke A, (2016). Combinatorial antibiotic effects of natural biocide cocktails. *IV. International Conference on Antimicrobial Research.* Malaga, Spain. 2016-06-29.

Grünberger A, Steffens I, **Binder D**, Drepper T, Wiechert W, Kohlheyer D (2016) Microbial metabolic state diagrams: Using microfluidic single-cell cultivation to predict bacterial gene expresssion. *EMBL Conference Microfluidics*. Heidelberg, Germany. 2016-07-24.

Burmeister A, Bitzenhofer NL, Grünberger A, **Binder D**, Drepper T, Wiechert W, Kohlheyer D (2016) Microfluidic heterogeneity analysis of fluorescence-based gene expression of industrially relevant production strains on single-cell level. *18. Heiligenstädter Kolloquium „Technische Systeme für die Lebenswissenschaften“.* Heilbad Heiligenstadt, Germany. 2016-09-19.

Frohwitter J, **Binder D**, Drepper T, Wendisch VF (2016) Metabolic engineering of *Corynebacterium glutamicum* for the production of the sesquiterpenoid (+)-valencene. *6th Int. Bielefeld-CeBiTec Research Conference. Advances in Industrial Biotechnology: New Techniques, Substrates and Products for Bioprocesses.* 2016-09-26.

A.II. Oral presentations

Binder D, Grünberger A, Loeschcke A, Probst C, Bier C, Pietruszka J, Wiechert W, Kohlheyer D, Jaeger KE, Drepper T (2014) Cage me if you can! Optogenetic bacterial gene regulation using photocaged inducers. *Mechanisms of gene regulation 2014, VAAM symposium.* Düsseldorf, Germany, 2014-10-03.

Binder D, Grünberger A, Loeschcke A, Probst C, Bier C, Pietruszka J, Wiechert W, Kohlheyer D, Jaeger KE, Drepper T (2014) Cage me if you can! Optogenetic bacterial gene regulation using photocaged inducers. *Microbiology and infection 2014 – DGHM and VAAM congress*. Dresden, Germany, 2014-10-06.

Binder D (2014) Cage me if you can! Optogenetic bacterial gene regulation using photocaged inducers. *International Autumn School on Synthetic Biology. Biology feat. engineering. Workshop on single cell analysis in microfluidic chips*. Jülich, Germany. 2014-11-18.

Wandrey G, Hoffmann K, Bier C, **Binder D**, Pietruszka J, Drepper T, Jaeger KE, Büchs J (2015) Online fluorescence spectroscopy combined with light-induced gene expression in a high-throughput screening system. *Scale-up and scale-down of bioprocesses; Dechema.* Hamburg, Germany. 2015-05-13

Loeschcke A, Thies S, Hage-Hülsmann J, Grünberger A, **Binder D**, Domröse A, Klein A, Kohlheyer D, Pietruszka J, Jaeger KE, Drepper T (2015) Heterologous production of antibacterial secondary metabolites from *Serratia marcescens* in *Pseudomonas putida. FEMS 6th Congress of European Microbiologists.* Maastricht, Netherlands. 2015-06-09.

Binder D, Bier C, Grünberger A, Loeschcke A, Kohlheyer D, Pietruszka J, Jaeger KE, Drepper T (2015) Light-controlled cell factories - Employing optogenetic plug-and-play expression modules based on photocaged carbohydrates for synthetic bio(techno)logy and single cell applications. *ESP Photobiology conference*. Aveiro, Portugal, 2015-08-31.

Grünberger A, Steffens I, **Binder D**, Drepper T, Wiechert W and Kohlheyer D (2016). Bacterial phase diagrams: Using engineering concepts to predict cell-to-cell heterogeneity of microbial gene expression. *VAAM Conference*. Jena, Germany. 2016-03-15.

Binder D, Bier C, Grünberger A, Hilgers F, Loeschcke A, Kohlheyer D, Pietruszka J, Jaeger KE, Drepper T (2016) Employing photocaged carbohydrates in light-controlled cell factories for synthetic bio(techno)logy and single cell applications. *VAAM Conference*. Jena, Germany. 2016-03-15.

Bier C, **Binder D**, Grünberger A, Drobietz D, Kohlheyer D, Loeschcke A, Jaeger KE, Drepper T, Pietruszka J (2016). Photocaged Carbohydrates: Versatile Tools for Biotechnological Applications. *ICP 2016: 18th International Conference on Photochemistry.* Paris, France. 2016-09-26.

B. List of publications

Binder D,* Grünberger A,* Loeschcke A, Probst C, Bier C, Pietruszka J, Wiechert W, Kohlheyer D, Jaeger K-E, Drepper T (2014) Light-responsive control of bacterial gene expression: precise triggering of the *lac* promoter activity using photocaged IPTG. Integr Biol (Camb) 6:755–65.

Binder D, Probst C, Bier C, Loeschcke A, Grünberger A (2015) Lichtgesteuerte Genexpression auf Einzelzellebene. BIOspektrum 21:612–615.

Binder D, Bier C, Grünberger A, Drobietz D, Hage-Hülsmann J, Wandrey G, Büchs J, Kohlheyer D, Loeschcke A, Wiechert W, Jaeger K-E, Pietruszka J, Drepper T (2016) Photocaged Arabinose - A Novel Optogenetic Switch for Rapid and Gradual Control of Microbial Gene Expression. Chembiochem 17:296–299.

Wandrey G, Bier C, **Binder D**, Hoffmann K, Jaeger K-E, Pietruszka J, Drepper T, Büchs J (2016) Light-induced gene expression with photocaged IPTG for induction profiling in a high-throughput screening system. Microb Cell Fact 15:63.

Binder D,* Probst C,* Grünberger A,* Hilgers F, Loeschcke A, Jaeger K-E, Kohlheyer D, Drepper T (2016) Comparative Single-Cell Analysis of Different *E. coli* Expression Systems during Microfluidic Cultivation. PLoS One 11:e0160711.

Binder D,* Frohwitter J,* Mahr R, Bier C, Grünberger A, Loeschcke A, Peters-Wendisch P, Kohlheyer D, Pietruszka J, Frunzke J, Jaeger K-E, Wendisch VF, Drepper T (2016) Light-controlled cell factories - Employing photocaged IPTG for light-mediated optimization of *lac*-based gene expression and (+)-valencene biosynthesis in *Corynebacterium glutamicum*. Appl Environ Microbiol 82:6141–6149..

Bier C, **Binder D**, Drobietz D, Loeschcke A, Drepper T, Jaeger K-E, Pietruszka J (2016) Photocaged carbohydrates – versatile tools for controlling gene expression by light. Synthesis (Stuttg); doi:10.1055/s-0035-1562617

Binder D, Drepper T, Jaeger KE, Delvigne F, Wiechert W, Kohlheyer D, Grünberger A (2017) Homogenizing bacterial cell factories: Analysis and engineering of phenotypic heterogeneity. Metab Eng 42:145–156.

Binder D, Bier C, Klaus O, Pietruszka J, Jaeger K-E, Drepper T (2016) Using 1,2-dimethoxy-4-nitrobenzene actinometry to monitor UV-A light exposure in photobiotechnological setups. *Manuscript in preparation.*

Binder D, Pietruszka J, Jaeger K-E, Drepper T (2016) Cage me if you can! – From assembly to application of photocaged compounds in microbial biotechnology. *Manuscript in preparation.*

*These authors contributed equally to this work.

C. Abbreviations

°C	degree Celsius	**h**	hour(s)
µM	micromolar	**HC**	hydroxycoumarin
µm	micrometer	**HCY**	heptamethine cyanine
a.u.	arbitrary units	**h*v***	light (energy)
aTc	anhydrotetracycline	**IPTG**	isopropyl-*β*-D-thiogalactopyranoside
ATP	adenosine-5'-triphosphate	**kg**	kilogram(s)
BHC	6-bromo-7-hydroxycoumarin	**l**	liter
BLUF	sensor of blue light using FAD	**LB**	Lysogeny Broth
bp	base pair(s)	**LED**	light-emitting diode
cAMP	cyclic adenosine monophosphate	**LOV**	light oxygen voltage (protein / domain)
CCR	carbon catabolite repression	**LPS**	lipopolysaccharides
c-di-GMP	cyclic diguanylate	**m**	meter
CM	coumarin	**M9CA**	M9 medium with casamino acids
cm	centimeter	**max**	maximal / maximum
CRP	catabolite repression protein	**mg**	milligram(s)
CRY	cryptochrome	**min**	minute(s)
DMNB	1,2-dimethoxy-4-nitrobenzyl/ nitrobenzene	**ml**	milliliter
DMSO	dimethyl sulfoxide	**mM**	millimolar
DNA	deoxyribonucleic acid	**mm**	millimeter
doi	digital object identifier	**mol**	mole (amount of substance)
FACS	fluorescence-activated cell sorting	**mRNA**	messenger RNA
FAD	flavin adenine dinucleotide	**MTP**	microtiter plate
FbFP	flavin-binding fluorescent protein	**mW**	milliwatt
Fig.	figure	**n.d.**	not determined
FMN	flavin mononucleotide	**NB**	*o*-nitrobenzyl
FPP	farnesyl pyrophosphate	**NBE**	1-(6-nitrobenzo[d][1,3] dioxol-5-yl)ethanol
FRET	Förster resonance energy transfer	**NC**	aminocoumarin
GFP	green fluorescent protein	**nl**	nanoliter
GM	Göppert-Mayer unit	**nM**	nanomolar

nm	nanometer
NMR	nuclear magnetic resonance (spectroscopy)
norm.	normalized
NP	6-nitropiperonyl
NPOM	6-nitropiperonyloxymethyl
NV	6-nitroveratryl
NVOC	6-nitroveratryloxycarbonyl
OC	alkoxycoumarin
OD_{580}	optical density at 580 nm
PDMS	polydimethylsiloxane
***p*HP**	*p*-hydroxyphenacyl
pl	picoliter
PTS	phospho-transferase system
RBS	ribosome binding site
RNA	ribonucleic acid
RT	room temperature
SEM	scanning electron microscopy
t	time(point)
T7RP	T7 RNA polymerase
Tab.	table
TC	thiocoumarin
TMG	thiomethyl-*β*-D-galactopyranoside
TPU	two-photo uncaging
tRNA	transfer RNA
UV	ultraviolet (light)
UVR8	UV-B receptor protein
YFP	yellow fluorescent protein
ε	extinction coefficient
λ	wavelength
Φ	quantum yield

D. Summary

Optogenetic tools are light-responsive components that allow for a simple triggering of cellular functions with unprecedented spatiotemporal resolution and in a non-invasive fashion. In this context, photocaged compounds, which release bioactive molecules upon short light exposure, are highly valuable tools for setting up light control and thus regulating and studying crucial bio(techno)logical processes such as gene expression. Due to the unique potential of light to achieve a stringent control of cellular processes, this thesis was concerned with the overall aim to establish light-controlled bacterial expression systems based on photocaged compounds.

Initially, different inducible expression systems were characterized in-depth using microfluidic single-cell analysis and subsequently reengineered towards beneficial expression features such as system tightness or population homogeneity. Consequently, different light-controlled expression tools were established based on P_{lac}/LacI, P_{BAD}/AraC and P_{rhaBAD}/RhaRS promoter/regulator systems in *Escherichia coli* using photocaged derivatives of IPTG, arabinose, galactose, rhamnose and glucose. Here, gene expression was monitored by means of fluorescent reporter based online monitoring and further tuned towards a rapid and highly dynamic control. Essentially, single-cell analyses indicated that by applying photocaged carbohydrates, conventional chemical induction mostly gets superseded at the level of population heterogeneity, expression strengths and temporal resolution. Finally, established optogenetic tools were transferred to alternative expression hosts such as *Corynebacterium glutamicum* and first biotechnological productions such as flavoring terpenoid and secondary metabolite antibiotic biosyntheses.

Conclusively, photouncaging is a sophisticated approach to achieve a gradually adjustable, non-invasive, spatiotemporal and thus high-throughput feasible fine control of simple to complex biological processes within bacterial cultures in picoliter- to liter-scale. In the future, several special applications such as high-throughput screenings as well as closed or multimodal processes are predestined for optogenetic control. Inevitably, plenty of prospective synthetic bio(techno)logical tasks in different key microbes arise for the newly developed and versatile plug-and-play expression toolbox mediating light-controlled gene expression *via* photocaged compounds.

E. Zusammenfassung

In der Optogenetik ermöglichen molekulare Lichtschalter eine unkomplizierte und nicht-invasive Ansteuerung von zellulären Funktionen mit einer enormen räumlichen und zeitlichen Auflösung. Durch die Kopplung mit Licht-sensitiven chemischen Schutzgruppen können sogenannte *photocaged compounds* bioaktive Moleküle nach kurzer Belichtung freisetzen. Folglich sind diese Verbindungen geeignete molekulare Werkzeuge, um eine solche Lichtsteuerung zu realisieren und somit wichtige bio(techno)logische Prozesse, wie etwa die Genexpression, zu regulieren und zu erforschen. Aufgrund dieses einzigartigen Potenzials von Licht eine höhere Form der Kontrolle über zelluläre Prozesse zu erzielen, wurde in dieser Arbeit das übergeordnete Ziel verfolgt, Licht-gesteuerte bakterielle Expressionssysteme basierend auf *photocaged compounds* zu etablieren.

Zunächst wurden unterschiedliche induzierbare Expressionssysteme mithilfe mikrofluidischer Einzelzellanalysen eingehend charakterisiert und anschließend hinsichtlich gewünschter Expressionseigenschaften, wie etwa der strikten Kontrolle des Promotors oder einer erhöhten Homogenität der Zielgenexpression innerhalb einer bakteriellen Population, optimiert. Infolgedessen wurden unterschiedliche lichtgesteuerten Expressionssysteme basierend auf P_{lac}/LacI, P_{BAD}/AraC und P_{rhaBAD}/RhaRS Promotor/Regulator-Kombinationen in *Escherichia coli* unter Verwendung von photo-aktivierbaren IPTG-, Arabinose-, Galactose-, Rhamnose- und Glucose-Derivaten etabliert. Hierbei wurde die Genexpression während der Kultivierung mithilfe Fluoreszenzreporter-basierter Online-Überwachung verfolgt und anschließend ausgewählte Systeme in Hinblick auf ein schnelles und hochdynamisches Ansprechverhalten verbessert. Grundlegend konnte dabei mittels Einzelzellanalysen aufgezeigt werden, dass die *photocaged compounds* herkömmliche chemische Induktoren hinsichtlich der Populationshomogenität, der Expressionsstärke sowie der zeitlichen Auflösung des jeweiligen Expressionssystems zumeist deutlich übertreffen. Abschließend wurden etablierte optogenetische Werkzeuge auf alternative Expressionswirte wie etwa *Corynebacterium glutamicum* sowie auf erste Produktionen biotechnologisch relevanter Terpenoide und Antibiotika übertragen.

Zusammengefasst haben sich *photocaged compounds* als ausgeklügelte Werkzeuge etabliert, um eine graduell steuerbare, nicht-invasive, zeitlich und räumlich hoch aufgelöste und somit Hochdurchsatz-fähige Feinsteuerung von einfachen und komplexen biologischen Prozessen im Pikoliter- bis Liter-Maßstab zu erzielen. In Zukunft sind einige spezielle Anwendungen wie etwa Hochdurchsatz-Screenings sowie

geschlossene oder multimodale Prozesse in besonderem Maße für eine optogenetische Steuerung qualifiziert. Zwangsläufig ergeben sich viele potenzielle Anwendungen im Bereich der synthetischen Bio(techno)logie sowie in verschiedenen relevanten Mikroorganismen für die hier neu entwickelten und vielseitigen optogenetischen Werkzeuge zur Vermittlung einer lichtgesteuerten Genexpression mithilfe von *photocaged compounds*.

I. Introduction

I.1 Natural bacterial gene regulation

Although invisible to the naked eye, bacteria populate every imaginable habitat on earth (Whitman et al. 1998), ranging from the deepest seas over the driest soils and the highest atmospheres (Imshenetsky et al. 1978) to the most miscellaneous bioreactors in biotechnology (Sánchez 2005). Even in the human body, our cells (3×10^{13}) are numerically inferior to those of bacteria (4×10^{13}) (Sender et al. 2016). Furthermore, most bacterial habitats are subjected to drastic and rapid environmental fluctuations with respect to e.g. temperature, pH, humidity or carbon source availability. Beyond that, individual bacterial species such as *Escherichia coli* are not only found in one particular habitat, but are known to colonize numerous quite different environments successfully (Chuang et al. 1993). Closely connected to such habitat diversity and thus vast adaptability of bacteria turns out to be the ability to rapidly respond to fluctuating environmental conditions with a manifold metabolic diversity (Acar et al. 2008; Kussell and Leibler 2005). To realize this flexible responsiveness, bacteria have evolved complex regulatory networks that precisely concert the expression of genes (Smits et al. 2006; Thattai and van Oudenaarden 2004). This seems challenging and crucial at the same time, considering that, for instance, the *E. coli* genome encompasses more than 4000 genes (Blattner et al. 1997; Studier et al. 2009) and protein biosynthesis demands tremendous amounts of energy (Byrgazov et al. 2013; Saier 2013). This renders constitutive expression of all genes unfeasible. Consequently, only the subset of genes is expressed that is required for the adaption to the present extracellular environment e.g. for uptake and metabolism of available nutrients.

To exert straightforward control over such specific sets of genes, they are commonly clustered in transcriptional units that share a single promoter, which is subjected to diverse regulatory stimuli such as carbon source availability, pH or temperature shifting as well as the presence of microbial competitors (Beales 2004; Deutscher et al. 2006; Ponomarova and Patil 2015).

Most prominent operons are those of the carbon metabolism, in particular those for lactose and arabinose consumption, which are subsequently described in further detail.

I.1.1 The lactose utilization network

In 1961, Jacob and Monod first described a set of genes in *E. coli* that was tightly suppressed in the presence of glucose, and efficiently transcribed in the sole presence of lactose (Jacob and Monod 1961). The functional unit was later denoted as the *lac* operon and found to be controlled by two regulatory proteins, a global activator called catabolite repressor protein (CRP) and a specific *lac* repressor (LacI) (Busby and Ebright 1999; Lewis et al. 1996). By means of CRP and LacI, which both bind specifically close to the promoter of the tricistronic *lac* operon, the transcription of *lacZ, lacY* and *lacA* and their contribution to lactose metabolism is controlled (**Fig. I.1 A**). The gene *lacY* codes for a membrane embedded galactoside/H^+-symporter, which is also denoted as the *lac* permease LacY and catalyzes the import of lactose molecules from the environment (Guan and Kaback 2006).

Upon LacY-mediated intracellular accumulation, lactose molecules are further processed by the *lacZ* encoded *β*-galactosidase (LacZ) that converts lactose into either glucose and galactose or 1,6-allolactose (Jobe and Bourgeois 1972). In addition, the *lacA* encoded galactoside transacetylase (LacA) acetylates and thus inactivates wrongly imported inducing, but non-metabolizable thiogalactosides (Andrews and Lin 1976; Marbach and Bettenbrock 2012; Roderick 2005).

Since the actual *lac* inducer allolactose is formed in a *β*-galactosidase side-reaction and lactose import is strictly dependent on the presence of the *lac* permease, an inherent basal expression of the *lac* genes is essential.

Substantial *lac* gene expression, however, is virtually repressed by the *lac* repressor protein, that is encoded by the constitutively expressed *lacI* gene, located upstream of the other three *lac* genes (Wilson et al. 2007). In the absence of inducer molecules, a tetrameric LacI complex binds to two of the three *lac* operator sites within the *lac* operon, and forms a stable DNA loop that impedes the transcription of the three *lac* genes downstream of the P_{lac} promoter (Daber et al. 2007; Wilson et al. 2007). The presence of an inducer, preferentially allolactose, indicates lactose availability in the environment. Inducer binding to LacI entails a conformational change in the tetrameric LacI complex leading to a tremendously decreased affinity for the operator DNA and thus the dissociation from the operator (Daber et al. 2007; Dunaway et al. 1980). Hence, inducer-mediated derepression of the *lac* promoter is the first requirement for an efficient transcription of the *lacZYA* operon.

Furthermore, glucose availability substantially represses the *lac* gene transcription. Here, CRP, whose activity is regulated by cyclic adenosine monophosphate (cAMP),

plays an essential role in *lac* operon repression (Wanner et al. 1978; Wilson et al. 2007).

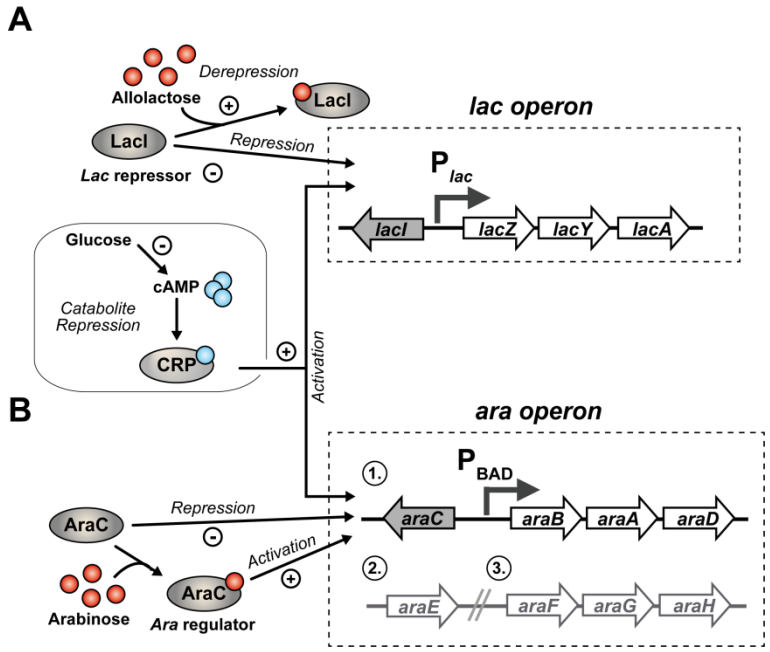

FIGURE I.1 | Natural gene regulation of selected carbon source metabolization operons.
(**A**) Natural *lac*-based gene expression *via* allolactose. Upon LacY (*lac* permease)-mediated import of lactose into the cell, lactose is transformed into allolactose *via* LacZ (*β*-galactosidase) activity, whereas wrongly imported thiogalactosides get acetylated *via* LacA (transacetylase). Inducer binding leads to the dissociation of the LacI repressor from the P_{lac} promoter and thus induces *lac* gene expression. (**B**) Arabinose inducible gene expression. Upon active uptake *via* AraE and AraFGH transport proteins, which are encoded in two separate transcriptional units (2. and 3.), arabinose positively regulates P_{BAD} promoter activity (1.). The three *araBAD* genes code for the proteins involved in arabinose metabolization to D-xylulose-5-phosphate. In the absence of arabinose, AraC tightly represses target gene expression. Furthermore, both operons are subjected to carbon catabolite repression that is basically pursued *via* cAMP level-sensing of the CRP protein.

cAMP, which is generated upon glucose starvation, acts as an allosteric effector for the CRP protein and recruits the RNA polymerase to bind with a higher affinity to the *lac* promoter region (Busby and Ebright 1999). Glucose or rather cAMP-based **carbon catabolite repression** (CCR) (**Box I.1**) is a simplified principle that uses the complex phospho-transferase system (PTS) to coordinate carbon source hierarchy throughout the microbial world (Deutscher et al. 2006).

Besides the pre- and absence of glucose or lactose, *lac* gene expression further depends on stochastic fluctuations of expression and predisposition of induction. Those factors entail a distinct **bistability** (**Box I.1**) and thus heterogeneous population that mainly leads back

Box I.1 | Glossary of terms

Carbon Catabolite repression (CCR) Global microbial control system that mediates the prevalent metabolization of primary carbon sources such as glucose (carbon source hierarchy) *via* the CRP regulator protein.
Bistability Feature of a dynamic biological system in which two discrete states coexist among isogenic cells within a population that was exposed to a defined stimulus.

to unequally distributed LacY proteins among isogenic cells (Eldar and Elowitz 2010; Ozbudak et al. 2004; Robert et al. 2010).

I.1.2 The arabinose utilization network

Another well-known transcriptional unit that is prone to CRP-mediated CCR is the arabinose utilization network of *E. coli*. Here, the three genes coding for L-arabinose metabolization, *araB, araA and araD* are under control of the P_{BAD} promoter, which is positively regulated by the AraC protein (**Fig. I.1 B**) (Brautaset et al. 2009; Guzman et al. 1995). In contrast to the LacI regulator, which exclusively represses transcription in the absence of an appropriate inducer, the dimeric AraC protein effectively activates and represses transcription, in the presence or absence of arabinose, respectively (Schleif 2010). The uptake of the sole inducer arabinose is strictly dependent on a complexly regulated transport system that mainly consists of the AraE and AraFHG transport proteins, whose genes are spread among the genome (Fritz et al. 2014; Schleif 2010; Scripture et al. 1987). Upon successful import of L-arabinose, the carbohydrate is further processed by means of AraA, AraB, and AraD, which catalyze the isomerization, phosphorylation and epimerization of L-arabinose *via* L-ribulose and L-ribulose-5-phosphate to D-xylulose-5-phosphate. Since the incorporation of D-xylulose-5-phosphate into the pentose phosphate pathway is energetically less favorable than glucose consumption, *ara* gene expression is likewise prone to CCR *via* the CRP protein (Miyada et al. 1984). Finally, arabinose inducible gene expression was again found to be subjected to distinct cell-to-cell variations during gene expression (Fritz et al. 2014; Khlebnikov et al. 2000; Siegele and Hu 1997).
The briefly presented regulatory networks illustrate how bacteria have evolved ingeniously controlled circuits to adaptively respond to their environment.

I.2 Artificial gene regulation in biotechnology

In biotechnology, bacteria massively contribute to the industrial production of therapeutic proteins (Schmidt 2004, Huang 2012, Baeshen 2015), bioactive secondary metabolites (Clardy et al. 2006, Berdy 2005, Vaishnav 2010) or chemical building blocks (Lee et al. 2011, Choi et al. 2015). To accomplish such microbial production processes, homologous and especially heterologous genes have to be expressed in a straightforward, precise and frequently temporal fashion (Medema et al. 2011, Keasling

1999, Smanski 2016). Thus, for the successful production of proteins or biosynthetic enzymes suited expression tools have to be developed that allow a feasible control of target gene expression. Therefore, **inducible expression tools** are valuable devices to gain control over gene expression procedures (Keasling 1999, Terpe 2006).

Barely astonishing, the variety of sophisticated natural regulatory circuits massively inspired the development of artificial control strategies in **synthetic biology** (**Box I.2**) and biotechnology. As a consequence, numerous inducible expression systems were developed by combining regulatory gene circuits with suitable expression hosts to exert control over recombinant gene expression (Terpe 2006). Here, exact control over gene expression attains utmost importance to direct cellular resources into the right direction, which most often means to tackle the challenge of balancing biomass and product formation. Typically, bacterial expression cultures are induced in the exponential growth phase to enable sufficient biomass accumulation prior to extensive product formation (Balzer et al. 2013; Rosano and Ceccarelli 2014; Saïda et al. 2006). This becomes further essential regarding toxic gene products, where precise regulation and timing of gene expression acquires increasing relevance (Dumon-Seignovert et al. 2004; Saïda et al. 2006; Wagner et al. 2008).

Prior to setting up sophisticated inducible expression tools, suitable expression hosts should be recruited for the respective application. Four bacterial workhorses, which are most commonly used in biotechnology, will thus be shortly presented in the following.

I.2.1 Expression hosts

Most bacterial expression systems are based on common platform organisms that feature straightforward genetic manageability, non-pathogenicity, rapid growth up to high cell densities and particularly the availability of adequate expression tools. Noteworthy, mainly *Escherichia coli*, *Bacillus subtilis*, *Corynebacterium glutamicum* and *Pseudomonas putida* are prominent key microbes with biotechnological relevance.

One of the most frequently used and best characterized organisms in biotechnology is the Gram-negative enterobacterium ***E. coli*** (Baeshen et al. 2015; Baneyx 1999; Terpe 2006), which is, for instance, consulted for the production of about 30% of currently approved therapeutic proteins (Huang et al. 2012; Sanchez-Garcia et al. 2016; Walsh 2010). Valuable industrial productions with crucial medical relevance include the blood sugar control hormone insulin, the blood clot retractor hirudin as well as interferons or interleukins for antiviral or antitumor immunotherapy (Baeshen et al. 2015; Huang et al. 2012; Schmidt 2004). Generally, for biotechnological productions in *E. coli*, apparent

disadvantages like pyrogenic lipopolysaccharides (LPS) or laborious down-stream processing face a tremendous wealth of ingeniously constructed strains to tackle manifold problems occurring during recombinant gene expression (Rosano and Ceccarelli 2014; Samuelson 2011; Terpe 2006) (see Chapter I.3).

In contrast to *E. coli*, Gram-positive ***Bacillus*** strains lack LPS endotoxins and bear a significant secretion capacity that often facilitates down-stream processing to a large extent. Especially the firmicute *B. subtilis* is a well-characterized and manageable expression host and has been frequently applied for heterologous protein production (Li et al. 2004; Westers et al. 2004). Furthermore, *B. megaterium* appears to be a valuable alternative due to a more stable maintenance and replication of plasmids even in the absence of antibiotics (Korneli et al. 2013; Münch et al. 2015). On this account, numerous *Bacillus* strains have been engineered in the last decades for the large-scale production of, for example, amylases or vitamin B12, that are vital for brewing or as food supplements (Mohammed et al. 2014; Moore et al. 2014; Terpe 2006)

Furthermore, the actinobacterium ***C. glutamicum*** represents another important Gram-positive biotechnological platform organism. It has been massively exploited for the industrial production of lower alcohols (Blombach et al. 2011; Inui et al. 2004; Niimi et al. 2011), organic acids (Litsanov et al. 2012; Wieschalka et al. 2013) and especially amino acids (Wendisch et al. 2016; Wendisch 2014). Notable processes imply the high-titer productions of amino acids such as L-arginine and L-lysine (Eggeling and Bott 2015; Park et al. 2014), that are essential for cattle feed (Patton et al. 2014), or building block chemicals such as succinate or itaconate (Ahn et al. 2016; Otten et al. 2015) that aim to replace petrochemically produced compounds.

Particularly with respect to natural product biosynthesis, ***P. putida*** is one of the key workhorses, since it provides a highly versatile intrinsic metabolism including diverse enzymatic capacities together with a notable xenobiotic tolerance (Loeschcke and Thies 2015; Troeschel et al. 2012). Therefore, the Gram-negative pseudomonad seems highly qualified for several special biotechnological purposes such as the production of rhamnolipids, terpenoids, polyketides, polyhydroxyalkanoates or non-ribosomal peptides (Loeschcke and Thies 2015; Poblete-Castro et al. 2012).

Moreover, numerous **specialized expression hosts** including *Rhodobacter*, *Streptomyces* or *Gluconobacter* have been shown to be highly suited for challenging applications such as membrane protein and antibiotic productions or where specific pH and oxidative capabilities are required (Heck & Drepper 2016; Hiltner et al. 2015; Liebl et al. 2014; Özgür 2015; Terpe 2006).

Irrespective of the finally selected expression host, the success of recombinant gene expression is invariably interconnected with the applied expression tool.

I.2.2 Expression tools

Typical expression tools make use of native or mutagenized promoters and a corresponding transcriptional regulator that represses, derepresses or activates target gene expression in the presence of a specific inducer. In the following, three biotechnologically relevant expression systems that emerged from natural gene circuits over the last decades will be reviewed.

I.2.2.1 Lac-derived promoter systems

Based on the lactose utilization network of *E. coli* (see Chapter I.1.1), different promoters were constructed as tools for recombinant protein production in *E. coli* and various other biotechnological workhorses (Terpe 2006). As initial plasmid-systems using the **native *lac* promoter** (Polisky et al. 1976) showed only moderate expression levels, different promoter mutagenesis and hybridization studies were performed to elevate promoter activity distinctly. The mutagenized ***lacUV5* promoter** (Wanner et al. 1977), for instance, was found to exert stronger expression together with a reduced catabolite repression, yet revealed noticeable basal expression levels (Dubendorff and Studier 1991; Grossman et al. 1998). By combining the -20 bp upstream region of the *trp* promoter and the respective downstream region of the *lacUV5* promoter, a synthetic promoter hybrid construct, denoted as the ***tac* promoter** (de Boer et al. 1983), was designed to further increase gene expression levels up to 10-fold (Amann et al. 1983).

In 1986, however, Studier and Moffatt developed an elaborate expression setup that was since then the expression tool of choice for high-level recombinant protein production in *E. coli* (Gräslund et al. 2008; Studier and Moffatt 1986; Terpe 2006). Here, the **T7 RNA polymerase** (T7RP) (**Box I.2**) gene from the bacteriophage T7 was chromosomally integrated into the *E. coli* BL21 genome. Upon expression of the T7RP gene that is under P_{lacUV5} control, the recombinant phage polymerase features tremendous processivity (Holmes et al. 1983; Iost et al. 1992), exclusive and high specificity for its unique promoter (Chamberlin et al. 1970; Tabor and Richardson 1985) and autonomy of bacterial regulators such as sigma factors and terminators (Arvani et al. 2012; Loeschcke et al. 2013; Tahirov et al. 2002).

Box I.2 | Glossary of terms

Synthetic Biology An emerging interdisciplinary field that applies engineering principles to the fundamental components of biology in order to redesign artificial biological components and systems for various useful functions.

T7 RNA Polymerase Highly processive RNA polymerase from the T7 bacteriophage that specifically drives high-level transcription from its cognate T7 promoter, irrespective of common bacterial regulators and terminators.

Together with suited expression vectors harboring the target genes under control of a synthetic ***T7lac* promoter**, the presented expression strain *E. coli* BL21(DE3) and its derivatives are frequently employed for high-level gene expression (Samuelson 2011) with up to 50% target protein of total protein cell titers (Baneyx 1999).

Appropriate inducer molecules that activate *lac*-based gene expression in the presented promoter systems include natural inducers such as galactose (Xu et al. 2012) or mainly lactose (Menzella et al. 2003; Studier 2005). Moreover, non-metabolizable **synthetic inducers** such as thiomethyl-*β*-D-galactopyranoside (TMG) and isopropyl-*β*-D-thiogalactopyranoside (IPTG) were developed to mediate constant instead of transient induction of *lac* promoter-based gene expression (Boezi and Cowie 1961; Cohn 1957). Among all inducers galactose, exhibits lowest binding affinity to the LacI regulator (Gilbert and Müller-Hill 1966). Compared to galactose, the actual *lac* inducer allolactose, which emerges from lactose upon LacZ activity, shows a more than 80-fold higher LacI binding. Highest binding affinities to LacI, however, are observed for the synthetically modified inducers TMG and IPTG, which feature 3- and 12-fold increased binding properties, respectively (Gilbert and Müller-Hill 1966). Natural inducer uptake basically depends on GalP (mainly galactose) and LacY transport proteins, whereas synthetic inducers are imported *via* both active transport and passive diffusion (**Fig. I.2 A**).

In summary, *lac*-based expression tools were comprehensively reengineered to cope with the demands for straightforward, broad-host range and high-level gene expression. Notably, for common key microbes such as *E. coli*, *C. glutamicum*, *P. putida* or *B. subtilis* *lac*-based gene expression tools were successfully developed over the last decades (Eikmanns et al. 1991; de Lorenzo et al. 1993a; Terpe 2006; Troeschel et al. 2012)

I.2.2.2 Ara-derived promoter systems

Besides *lac*-promoter-mediated gene expression, **P_{BAD} promoter** (see Chapter I.2) based expression tools established as valuable alternatives for recombinant protein production especially in *E. coli,* where it depends on the complex AraEFGH transport system (Brautaset et al. 2009; Terpe 2006). Favorable features of the *ara* system include a rapid and strong expression response, a low basal background activity especially in the presence of glucose, the inexpensiveness of arabinose as well as high inducer-sensitivity in *araBAD*-deletion strains (Balzer et al. 2013; Fritz et al. 2014; Guzman et al. 1995; Rosano and Ceccarelli 2014). Furthermore, the fact that the AraC regulator protein effectively activates and represses transcription (**Fig. I.2 B**) in the presence or absence

of arabinose (Schleif 2010) entails a relatively tight and fine-adjustable regulation of gene expression levels in dependence on arabinose concentrations (Brautaset et al. 2009).

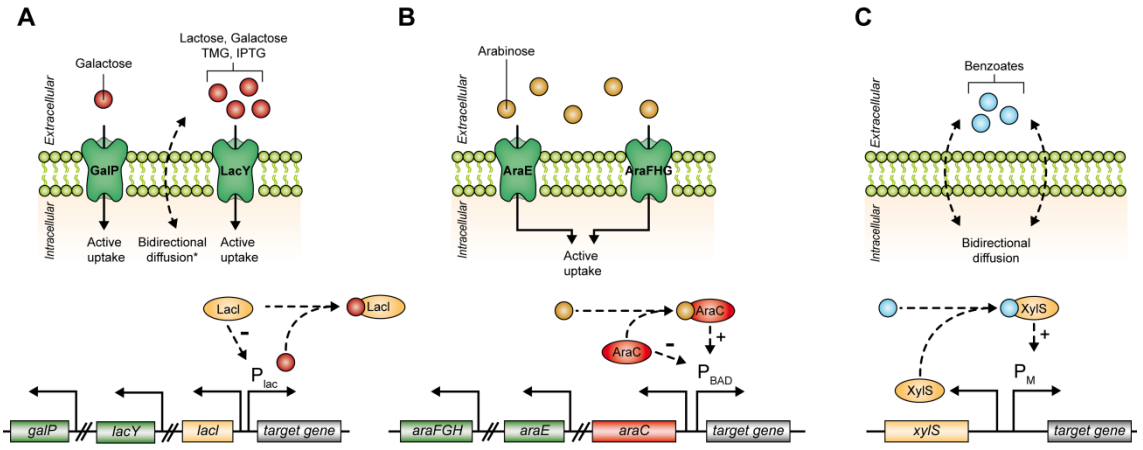

FIGURE I.2 | Synthetic gene regulatory circuits and their inducer uptake.

(**A**) *Lac*-based gene expression *via* natural (lactose, galactose) or synthetic (TMG, IPTG) inducers. Uptake basically occurs through GalP (mainly galactose) or LacY (all inducers) transport proteins and by passive diffusion (* only synthetic inducers TMG and IPTG). Inducer binding leads to the release of the LacI repressor from the P_{lac} promoter and thus induces gene expression. (**B**) Arabinose inducible gene expression upon active uptake *via* AraE and AraFGH transport proteins. In the presence of arabinose AraC positively regulates P_{BAD} promoter activity, whereas in the absence of arabinose AraC tightly represses target gene expression. (**C**) Pm/XylS regulated gene expression driven by benzoates that are imported *via* passive diffusion and initiate the XylS regulator-dependent activation of Pm promoter-based expression. Abbreviations: *galP*: galactose permease gene; *lacY*: lactose permease gene; *lacI*: *lac* repressor gene; *araFGH*: arabinose transporter genes; *araE*: arabinose transporter gene; *araC*: *ara* regulator gene; *araBAD*: arabinose metabolization genes; *xylS*: *xyl* regulator gene. The figure was modified from Binder *et al*. (2016) PLoS ONE 11: e0160711; doi: 10.1371/journal.pone.0160711, under the terms of the Creative Commons Attribution 4.0 International License.

Interestingly, a deletion of the last 12 amino acids of the AraC regulator's C-terminus enlarged arabinose sensitivity and significantly reduced IPTG-crosstalk of P_{BAD} promoter based gene expression at the same time (Lee et al. 2007).

Whereas arabinose inducible expression tools have been broadly applied in *E. coli* for a long time, alternative expression hosts such as *C. glutamicum* and *P. putida* were only quite recently exploited for efficient P_{BAD}-based gene expression (Calero et al. 2016; Zhang et al. 2012). Here, mainly the heterologous expression of additional arabinose uptake genes proved crucial for the adequate application of arabinose induction.

I.2.2.3 Xyl-derived promoter systems

In contrast to afore presented expression tools that strongly depend on the functional expression of complex transport systems, the **Pm/XylS system** features complete autonomy with respect to inducer uptake (**Fig. I.2 C**). The Pm/XylS system imports respective benzoate inducer molecules *via* passive diffusion and has been proven as a promising tool for recombinant protein production (Blatny et al. 1997; Brautaset et al. 2009; Ramos et al. 1988). Imported benzoates bind to the XylS regulator protein, which in turn positively regulates Pm-controlled gene expression. Primarily, *m*-toluic acid serves as main inducer of recombinant Pm/XylS systems, although it has been reported that a variety of different benzoates are able to drive Pm-derived gene expression as well (Ramos et al. 1986). Moreover, single point mutations in the XylS regulator (e.g. R45T) were shown to significantly enhance inducer promiscuity (Ramos et al. 1990; Ramos et al. 1986).

Towards high-level protein production, the native Pm promoter was subjected to random mutagenesis yielding several high-level variants, which exhibited up to 14-fold increased expression responses (Bakke et al. 2009). Among those, especially the ML1-17 variant (P_{M1-17}) was shown to be highly convenient for high-level gene expression (Bakke et al. 2009; Balzer et al. 2013).

Finally, Pm/XylS derived expression tools were shown to be well applicable in different Gram-negatives (Blatny et al. 1997) such as *E. coli* (Balzer et al. 2013) or *P. putida* (Calero et al. 2016; de Lorenzo et al. 1993b). However, their biotechnological potential has probably not yet been fully exploited.

I.2.2.4 Further expression systems

Additional expression systems that are worth mentioning are based on propionate-inducible P_{prpB}/PrpR (Lee and Keasling 2006; Lee and Keasling 2005), rhamnose-inducible P_{rhaBAD}/RhaRS (Brautaset et al. 2009; Haldimann et al. 1998) or anhydrotetracycline (aTc)-inducible P_{tetA}/TetR (Skerra 1994) regulatory systems. However, due to expensive or partly toxic inducers, a restricted expression host spectrum or the need for coexpression of recombinant transport systems, those systems are less often applied for biotechnological purposes.

I.3 Challenges in recombinant gene expression

Despite the opulent wealth of diverse expression systems, recombinant gene expression commonly faces several drawbacks that will be shortly described in the following, together with so far established solution strategies.

I.3.1 Common drawbacks in recombinant gene expression

In principle, challenges during recombinant gene expression can be distinguished into system-specific, gene-specific and cultivation-specific impediments. System-specific drawbacks lead back to the respective expression system, which includes the selected expression host together with the promoter/regulator and transport systems employed for recombinant gene expression. Furthermore, the target gene(s) can cause problems during recombinant gene expression that arise from respective gene and especially protein features and are closely connected to the given expression environment and thus the expression host. Finally, the cultivation approach is capable of decisively interfering with recombinant gene expression. Subsequently, common drawbacks will be described and the complex interplay of system-, gene- and cultivation-specific impediments will be insinuated (**Fig. I.3**).

An obvious **system-specific drawback** illustrates the inherent **phenotypic heterogeneity** (**Box I.3**) of an expression system. Whereas in natural microbial habitats, phenotypic heterogeneity has evolved as the ultimate strategy to survive in fluctuating and competitive environments, such cell-to-cell variations are vastly unfeasible for recombinant gene expression (Lidstrom and Konopka 2010). Likewise unsuited appear **all-or-nothing responses** or **feedback loops** (**Box I.3**), which are, for instance, observed in different *lac*-based expression setups (Novick and Weiner 1957; Robert et al. 2010). Here, defined on- and off-

Box I.3 | Glossary of terms

Phenotypic heterogeneity Cell-to-cell variations within an isogenic population that show variable phenotypes, e.g. with respect to growth or expression, and are independent of genetic or environmental variations.
All-or-nothing response Regulation principle where a biological response is independent of the strength of an applied stimulus. Above certain threshold values the response is always enforced in the same deterministic fashion, quite contrary to gradual regulation (*vide infra*).
Feedback loops Negative or positive feedback loops are implemented into regulatory circuits to attenuate or amplify the biological responses (e.g. metabolization) in dependence on certain metabolite threshold levels.
Gradual regulation Expression of a gene directly correlates to the concentration of a supplied inducer molecule and thus allows for a fine adjustment of gene expression levels.
Basal expression Level of gene expression that occurs in the absence of an inducer. Also denoted as 'leakiness'.
Inclusion bodies Intracellular accumulations of recombinantly produced proteins in in-soluble aggregates that are usually incorrectly folded and thus functionally inactive.

states impede a finely adjustable, **gradual regulation** (**Box I.3**) of gene expression and thus complicate the optimization of overall expression levels (Keasling 1999). Further system-specific challenges are tightness and timing of gene expression as just-in-time induction upon sufficient biomass accumulation is a general prerequisite for numerous applications (Keasling 1999). Tight, temporal, homogeneous and gradual control attains increasing relevance if additional gene-specific impediments come into play. This becomes most evident for toxic gene products, where excessive, **leaky** (**Box I.3**) and thus early expression leads to tremendously reduced biomass formation, negative selection pressure and thus significantly lowered overall yields (Saïda et al. 2006). Notably, not only specific gene products may appear toxic for the host cell, also the overexpression of arbitrary genes may lead to tremendous growth impairments in individual expression systems e.g. due to the depletion of cellular resources. Likewise, for **inclusion bodies** (**Box I.3**), which are known to occur e.g. for hydrophobic proteins or massive protein overproduction in general, the precise adjustment of gene expression levels plays a major role (Terpe 2006).

General gene-specific drawbacks include a mal-adjusted codon usage that frequently occurs in heterologous gene expression especially for eukaryotic genes.

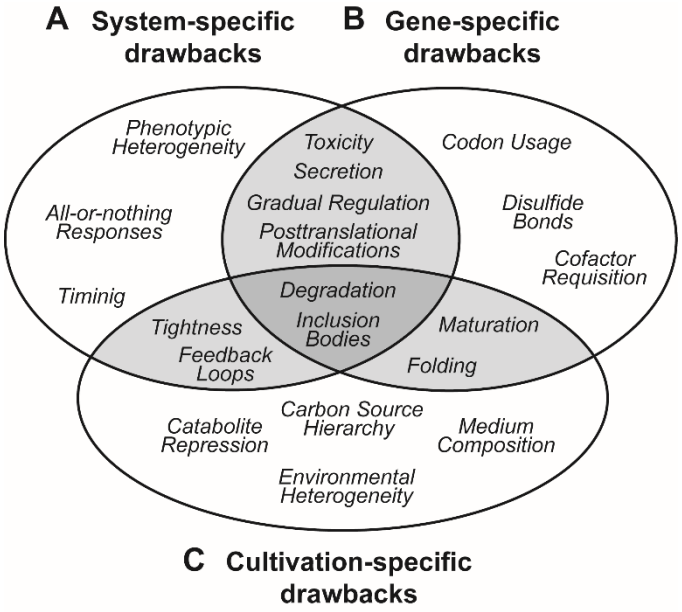

FIGURE I.3 | Simplified Venn diagram highlighting and classifying common system-, gene- and cultivation-specific challenges in recombinant gene expression and their functional interactions.

(**A**) Numerous gene expression drawbacks can be attributed to the respective expression system, yet commonly depend on the respective target gene(s) as well as the applied cultivation conditions. (**B**) Several impediments during gene expression are gene-specific and may lead back to the gene sequence or the protein maturation or activity in general. (**C**) Further drawbacks may originate from the cultivation approach, for instance, due to unfavorable nutrient selection, fluctuations or the cultivation temperature. Additional overlaps, challenges and functional interactions are expected to arise for individual setups.

Rather ubiquitous issues pose mRNA and protein degradation and may lead back to system-, gene- as well as cultivation-specific impediments. Especially, protein degradation is interconnected to frequent gene-specific obstacles such as folding, disulfide bonding, cofactor requisition or maturation (e.g. oxidation) that are likewise strictly dependent on applied expression strains or cultivation conditions. Upon successful translation of target proteins, finally posttranslational modifications or the secretion into the extracellular medium are gene-specific challenges that may depend on the applied expression strategy, though. Besides the respective expression strategy, the applied **cultivation conditions** play a non-negligible role in recombinant gene expression (Jana and Deb 2005). For instance, culture oxygenation or cultivation temperatures were shown to decisively influence folding or maturation issues (Drepper et al. 2010; Terpe 2006). Further cultivation conditions that impair or rather influence recombinant gene expression include e.g. catabolite repression, carbon source hierarchy, choice of medium, **environmental heterogeneity** (**Box I.4**) or nutrient depletion and complete the intricate image of challenges during recombinant gene expression (**Fig. I.3**).

I.3.2 Current strategies to encounter expression drawbacks

Based on such versatile and entangled challenges during recombinant gene expression, extensive work has been ventured over the past decades to tackle at least some of the most recurring issues (Rosano and Ceccarelli 2014; Saïda et al. 2006; Terpe 2006). In the following, selected strategies to approach most common drawbacks will be discussed in brief (**Tab. I.1**).

Toxicity is the most apparent issue in recombinant gene expression. Hence, countless approaches have been conducted to provide expression tools that are suited for toxic gene products (Saïda et al. 2006) such as toxic proteins or enzymes forming toxic metabolites. Basically, such strategies involve tightly titratable expression systems (Guzman et al. 1995), the delay of expression responses (Miroux and Walker 1996) and particularly the reduction of leaky gene expression.

Thus, tightness is of pivotal importance for recombinant expression of toxic or difficult-to-express genes. In this context, next to the application of inherently tighter expression tools (Guzman et al. 1995), the supplementation of glucose seems an appropriate approach to

Box I.4 | Glossary of terms

Environmental heterogeneity Cell-to-cell variations in an isogenic population caused by fluctuating environmental (extrinsic) factors such as insufficient aeration or stirring.
T7 Lysozyme Natural T7 RNA polymerase inhibitor from the bacteriophage T7.

minimize basal expression of systems that are prone to carbon catabolite repression such as P_{lac}, P_{xyl}, P_{BAD} or P_{rhaBAD} systems (Balzer et al. 2013; Brautaset et al. 2009; Terpe 2006). In this context, also the specific ratio of regulator binding sites and available regulator proteins dictates the extent of basal expression. Thus, the coexpression of additional negative regulator (Dubendorff and Studier 1991) or accessory inhibitory genes (Studier 1991) are able to significantly enhance the tightness of an expression system. In particular, for P_{T7lac}-based expression setups the supply of additional copies of the *lac* repressor gene *lacI* or *lysY*, a gene encoding the **T7 lysozyme** (**Box I.4**) and thus a natural inhibitor of the T7RP, proved valuable for the reduction of basal expression (Dubendorff and Studier 1991; Studier 1991). This approach was further elaborated with the *E. coli* Lemo21(DE3) expression host presented by Wagner *et al*. in 2008 (Wagner et al. 2008). Here, an optimized *lysY* gene was tightly controlled *via* an L-rhamnose inducible *rha*BAD promoter on the so-called pLemo plasmid to enable finely adjusted downregulation of P_{T7lac}-controlled membrane protein production in the conventional *E. coli* BL21(DE3) host.

Furthermore, it seems favorable that a uniform induction response is provided upon induction. Phenotypic heterogeneity is under reasonable suspicion for lowered yields and lacking control of target gene expression in biotechnology and synthetic biology. In this context, a detailed single-cell analysis is a pivotal prerequisite (Grünberger et al. 2014) to tackle potential phenotypic heterogeneity, for instance by means of transport system modifications (Khlebnikov et al. 2001; Khlebnikov et al. 2000). Due to the crucial relevance of single-cell analysis as a means of unravelling phenotypic heterogeneity, cutting-edge single-cell methodologies will be presented in the subsequent chapter in further detail (**Chapter I.4**).

Moreover, several gene-specific factors such as codon-usage, folding, disulfide bonding and secretion commonly restrain the success of functional gene expression. On this account, multiple expression strains have been engineered (Rosano and Ceccarelli 2014; Samuelson 2011; Terpe 2006), to provide for instance additional tRNAs to address codon usage bias (e.g. *E. coli* Rosetta), improved disulfide bond formation (e.g. *E. coli* Origami) or proper folding at low temperatures (e.g. *E. coli* ArcticExpress).

Notably, also the optimization of target genes to the codon-usage of the respective host and thus the re-synthesis of genes provides a valuable, yet pricey alternative. Regarding issues in secretion, cofactor supply and posttranslational modifications, however, the application of completely different, alternative expression hosts seems to be most promising. While *Bacillus* strains offer high secretion capacities (Harwood and Cranenburgh 2008) and *Rhodobacter* strains might be suited to improve cofactor supply (Katzke et al. 2012; Heck & Drepper 2016), for proteins requiring posttranslational

modifications, eukaryotic expression platforms such as *Saccharomyces cerevisiae*, *Pichia pastoris* or *Kluyveromyces lactis* are the method of choice (Porro et al. 2011; Schmidt 2004).

TABLE I.1 | Selected strategies to tackle drawbacks in recombinant gene expression.

Drawback	Solution approaches	Reference
Toxicity	▪ Increasing system tightness ▪ Delaying / Reducing expression responses ▪ Applying titratable expression tools	(Saïda et al. 2006), (Miroux and Walker 1996) (Guzman et al. 1995; Wagner et al. 2008)
Tightness	▪ Glucose supplementation (for CCR-sensitivity) ▪ Repressor overexpression	(Balzer et al. 2013; Guzman et al. 1995) (Studier 1991; Wagner et al. 2008)
Phenotypic heterogeneity	▪ In-depth single-cell analysis to unravel the cause of heterogeneity ▪ Transport System Modification	(Grünberger et al. 2014) (Khlebnikov et al. 2001; Khlebnikov et al. 2000)
Codon usage	▪ Adaption to host codon usage ▪ Specialized hosts (e.g. *E. coli* Rosetta)	(Samuelson 2011; Terpe 2006)
Folding	▪ Lowering temperature ▪ Chaperone coexpression ▪ Specialized hosts (e.g. *E. coli* ArcticExpress)	(Ferrer et al. 2003; Hartinger et al. 2010; Samuelson 2011; Terpe 2006)
Disulfide bonds	▪ Direction to the periplasm ▪ Specialized hosts (e.g. *E. coli* Origami)	(Rosano and Ceccarelli 2014; Samuelson 2011)
Secretion	▪ Alternative hosts / strains with high secretion capacity	(Harwood and Cranenburgh 2008; Terpe 2006)
Cofactor supply	▪ Alternative expression hosts (e.g. *R. capsulatus*)	(Katzke et al. 2012; Katzke et al. 2010; Heck & Drepper 2016)
Posttranslational modifications	▪ Alternative (eukaryotic) expression hosts	(Porro et al. 2011; Schmidt 2004)
Inclusion bodies	▪ Lowering temperature ▪ Applying titratable expression tools ▪ Direct protein to the periplasm	(Rosano and Ceccarelli 2014; Terpe 2006)
Degradation	▪ Lowering temperature ▪ Protease-deficient hosts	(Samuelson 2011; Terpe 2006)
Yields	▪ Promoter mutagenesis ▪ Plasmid copy number ▪T7RP implementation	(Bakke et al. 2009) (Balzer et al. 2013) (Katzke et al. 2010; Kortmann et al. 2015; Studier and Moffatt 1986)

More general problems that probably occur in most expression hosts portray undesired mRNA and protein degradations as well as inclusion body formations. Here, challenges may generally be tackled applying lowered cultivation temperatures, protease-deficient expression strains or the downregulation of expression (Terpe 2006).

Finally, it is further conceivable that overall expression yields do not cope with originally intended amounts despite the fact that none of the aforementioned individual challenges appears to be obviously responsible. In this context, the superior goal is simply to increase expression levels. Promising approaches on this behalf include the implementation of the highly processive T7RP (Katzke et al. 2010; Kortmann et al. 2015;

Studier and Moffatt 1986; Troeschel et al. 2012), the increment of plasmid copy numbers (Balzer et al. 2013) or extensive promoter mutagenesis (Bakke et al. 2009).
Noteworthy, a selected approach often solves the problem at hand, yet raises another. Such an example poses the extensive random mutagenesis of the wildtype Pm promoter reported by Bakke and coworkers (Bakke et al. 2009). Whereas mutagenized promoter variants depicted up to 8-fold improved overall expression levels, all high-level variants involved enlarged basal expression, which increased leakiness up to 400-fold. This example illustrates that challenges in recombinant gene expression are complexly entangled.
Although plenty of individual cases prove that most challenges can be approached, some consistently recur so that rather systematic and global approaches should be considered (Balzer et al. 2013; Calero et al. 2016). Evidently, recombinant gene expression would benefit from novel broad-host-range expression tools that provide higher-order control of microbial gene expression. In this context, tightly controlled high-level gene expression that can be triggered in a rapid, homogeneous and gradual fashion is the superior goal for reengineering recombinant expression tools. One approach to tackle these ambitious objectives will be discussed in-depth in chapter I.5.
Prior to setting up well-defined expression tools that provide a higher-order control of gene expression, it is important to uncover existing regulatory impairments down to single-cell level. Inevitably, the existence of subpopulations can have a large impact on productivity and overall yields, as solely adequate producer cells with moderate growth are desired in biotechnological and synthetic biology applications. An important prerequisite to approach those limitations is thus an in-depth single-cell analysis of respective expression setups (Delvigne and Goffin 2014; Grünberger et al. 2014).

I.4 Single-cell analysis tools – Principles and distinctions

Quantitative and dynamic single-cell analyses of microbial populations provide a powerful tool to gain valuable insights into the complexity of cell-to-cell-variations with respect to cell morphology, growth and expression (Delvigne and Goffin 2014; Grünberger et al. 2014; Young et al. 2012). Those insights are an important prerequisite to reengineer recombinant gene expression and microbial productions towards higher degrees of control, robustness and precision.
To monitor population dynamics, **flow cytometric analyses** (**Box I.5**) (**Fig. I.4 A**) are frequently engaged to investigate millions of single cells in an appropriate amount of time (Delvigne and Goffin 2014; Müller and Nebe-von-Caron 2010; Neumeyer et al. 2013).

Here, the obtained data reveal a highly representative picture of the microbial population at a given time-point. Analysis of population dynamics can be accomplished as a snapshot-like accumulation of broad data sets. This way, just the pre- or absence of heterogeneity is visualized for specific time points rather than a real dynamic decoding of phenotypic heterogeneity including mother-daughter cell correlations and the knowledge how single cells behave over time (**Fig. I.4 B**). In addition, using flow cytometric analysis it appears difficult to investigate cell-to-cell variations in growth. Conclusively, flow cytometry illustrates a highly quantitative approach to uncover population heterogeneity. However, an analysis of population dynamics at high spatiotemporal resolution seems impeded, as single-cell lineages as well as a distinction between environmental (extrinsic) and actual phenotypic (intrinsic) heterogeneity cannot be displayed.

These bottlenecks were tackled in recent years by means of **microfluidic single-cell analysis** (**Box I.5**) (Dusny and Schmid 2015; Grünberger et al. 2015; Grünberger et al. 2014).

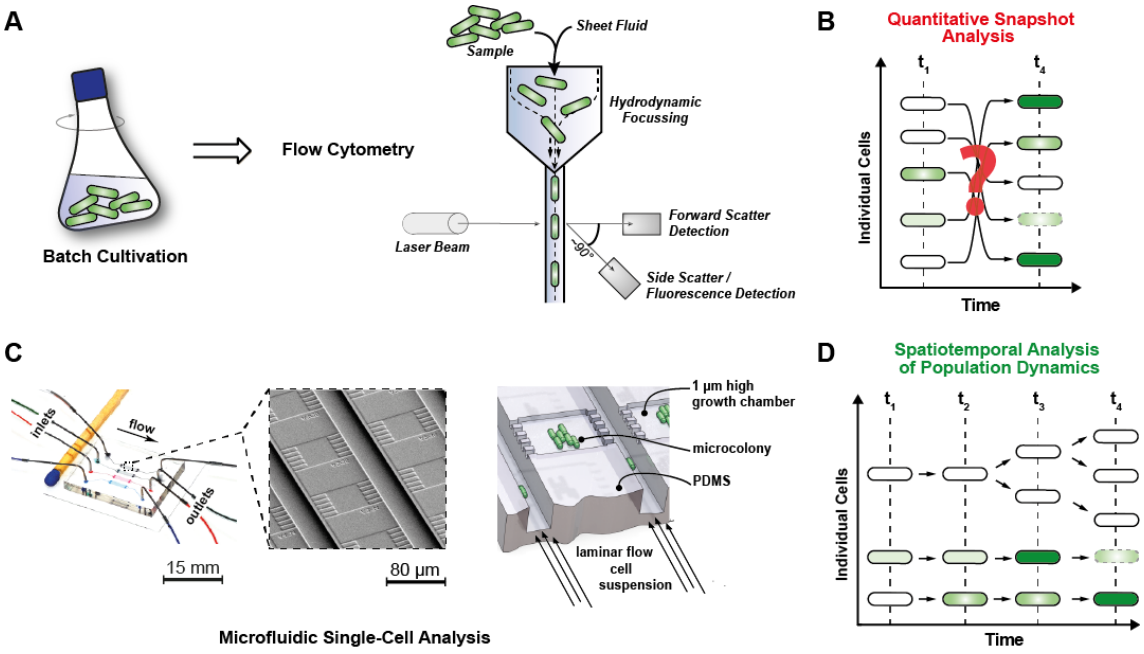

FIGURE I.4 | Common single-cell analysis tools – Principles and distinctions.

(**A**) Flow cytometric single-cell analysis upon conventional batch cultivation allows the analysis of thousands of cells with respect to size (forward scatter), granularity / density (side scatter) and specific fluorescence signals. (**B**) Flow cytometric analysis enables to quickly measure large amounts of cells without visualization of population dynamics or lineages, respectively. (**C**) Left - Photograph of a microfluidic PDMS single-cell cultivation chip next to a match. The inset shows a SEM micrograph of a monolayer cultivation section among several hundreds of single cultivation chambers. Right - Schematic illustration of microscale growth chamber that is perfused with cell suspensions and media for cultivation of trapped cells. Modified from Binder *et al.* (2014) *Integr Biol (Camb)* 6: 755–65; doi: 10.1039/c4ib00027g, under the terms of the Creative Commons Attribution-NonCommercial 3.0 Unported Licence. (**D**) Microfluidic single-cell analysis provides spatiotemporally resolved, detailed insights into population dynamics and lineages, yet in a less quantitative fashion.

Single-cell microfluidics allows a detailed investigation of thousands of cells in terms of morphology, expression and growth to provide in-depth knowledge on the single-cell dynamics of population heterogeneity. Here, several hundred polydimethylsiloxane (PDMS)-based monolayer growth chambers can be monitored in a high-throughput and spatiotemporal fashion using time lapse microscopy (**Fig. I.4 C, D**). Furthermore, well-defined environmental conditions can be established by a constant perfusion of cultivation medium e.g. through 10 µm high nutrient supply channels to the growth chambers (typical dimensions for the cultivation of *E. coli*: 1 x 40 x 40 µm). In contrast to classical agar pad based single-cell analysis technologies (Dusny et al. 2015; Young et al. 2012), long-term cultivations and environmental homogeneity are key benefits that allow for an in-depth analysis of phenotypic heterogeneity independent of perturbing extrinsic factors. Moreover, in contrast to flow cytometric analysis, single-cell lineages can be traced in a spatiotemporal fashion (Grünberger et al. 2015; Helfrich et al. 2015).
Irrespective of the selected single-cell analysis technology, readout systems to quantitatively report and monitor the respective bioprocess at single-cell level have to be implemented. This seems crucial, especially if the experimental setup is complex regarding the number of analyzed parameters, modifications and conditions and reaches the limitations of currently developing single-cell omics technologies (Saliba et al. 2014; Zenobi 2013). Whereas single-cell transcripts may be amplified *via* appropriate technologies prior to quantification (Saliba et al. 2014), metabolite sensitivity cannot be easily enhanced and remains a big challenge for small cells like bacteria (Zenobi 2013). Consequently, for direct bioprocess monitoring, optical **biosensors** (**Box I.5**) provide a valuable and widely established method for bio-product detection with broad applicability and adequate sensitivity (Delvigne et al. 2015; Delvigne and Goffin 2014). In addition, special staining technologies to report e.g. metabolic activity, membrane potential or cell viability were developed for application in microfluidics and flow cytometry (Brehm-Stecher and Johnson 2004; Krämer et al. 2015; Neumeyer et al. 2013). Most commonly, however, fluorescing reporters are employed to monitor cellular processes such as gene expression (Drepper et al. 2013; Shaner et al. 2005). In this context, also transcription factor-based biosensors play a pivotal role in single-cell analysis of biotechnological production processes

Box I.5 | Glossary of terms

Flow cytometry. A laser-based technology that counts thousands of single cells separately and conducts optical measurements to provide information on individual cell length, granularity and fluorescence. Often those measurements are coupled to fluorescence-activated cell sorting (FACS) to allow automated parameter dependent high-throughput single-cell sorting.
Single-cell microfluidics Analytical tool to cultivate and analyze thousands of single cells with high spatial and temporal resolution in a dynamic fashion. Commonly cells are trapped in a defined microenvironment (e.g. in a microchip) where defined environmental conditions can be created by means of continuous liquid perfusion.
Biosensor A biomolecule, e.g. protein that dynamically alters its properties e.g. fluorescence in response to environmental changes such as pH or metabolite concentrations.

(Mahr et al. 2015; Mahr and Frunzke 2016; Mustafi et al. 2014; Xiao et al. 2016). Moreover, FRET- or riboswitch-based biosensors pose sophisticated alternatives to unravel phenotypic heterogeneities appropriately (Fowler and Li 2014; Moussa et al. 2014).

Concisely, an in-depth single-cell analysis and particularly unraveling and minimizing phenotypic heterogeneity is a key aspect in understanding and optimizing recombinant gene expression. In this context, optical monitoring, for instance by means of fluorescent gene expression markers or fluorescent metabolite biosensors, is an established method to quantitatively report cellular processes such as gene expression in a spatiotemporal fashion. Logically consistent, the question emerges, to what extent it might be beneficial not only to report but also to trigger cellular events by optical means. Therefore, the final chapter will focus on recent approaches to control cellular functions by light.

I.5 Optogenetic tools – Light as a key player to increase the degree of control over cellular functions?

In nature, biological key processes in bacteria such as growth, gene expression or protein activity underlie highly complex regulation and control patterns that originate from millions of years of evolutionary selection. For instance, natural effectors often require uptake or conversion processes, which in turn are interconnected to cellular growth states or carbon source availability (see Chapter I.1.1). Thus, phenotypic diversity, differential expression, feedback loops, and carbon source hierarchy significantly dictate biological processes with respect to responsiveness and functionality. For synthetic biology or biotechnological applications, however, contrary features such as strict, robust, homogeneous and rapid control are desired.

To gain elevated precision and high spatiotemporal resolution, the external stimulus light is currently evolving as a key player in providing a higher-order control over cellular functions (Brieke et al. 2012; Drepper et al. 2011). The advantages of light control comprise an unprecedented spatiotemporal resolution together with high variability and selectivity, which jointly empower the triggering of biological functions in a precise and non-invasive fashion. In this context, especially biological photoreceptors and photocaged compounds arise as valuable so-called **optogenetic tools** (**Box I.6**) to achieve spatiotemporally resolved light-control for studying and regulating biological functions in a more robust and predictable fashion (Deiters 2009; Gardner and Deiters 2012; Krauss et al. 2011; Young and Deiters 2007a).

I.5.1 Biological photoreceptors

A highly valuable attempt to control cellular functions by light is conveyed using **genetically encoded photoreceptors** (**Box I.6**) (Christie et al. 2012b; Fenno et al. 2011). This optogenetic approach, which originally arose from neurosciences, employs both naturally occurring and artificially designed photo-switchable proteins to conduct *in vivo* signal transduction in biological applications (Drepper et al. 2011). Here, the light-response is usually implemented in a reversible fashion and enables to apply a broad spectrum of different light colors ranging from UV-B to near infrared light (Pathak et al. 2013; Ziegler et al. 2016; Ziegler and Möglich 2015).

To sense such a wide range of electromagnetic radiation and conduct proper *in vivo* signal transduction emanating from the photoreceptor protein, different chromophores are incorporated within the respective photoreceptors. Applied chromophores include, for instance, intramolecular tryptophan residues for UV-B perception in UVR8 photoreceptor (Christie et al. 2012a), different blue-light-sensing flavins in LOV, BLUF and CRY photoreceptors (Christie et al. 2012b; Gomelsky and Hoff 2011; Losi and Gärtner 2012), retinals in rhodopsins (Fenno et al. 2011; Kandori 2015) or red-light-sensing bilin chromophores in phytochrome photoreceptors (Ikeuchi and Ishizuka 2008; Rockwell et al. 2006; Rockwell and Lagarias 2010).

In addition to this variety of sensing domains, a comparable functional versatility is currently arising due to the modular organization and thus enabled continuous redesign of existing photoreceptors with novel functional output modules (Ziegler et al. 2016; Ziegler and Möglich 2015). Most common effector modules are kinases or c-di-GMP turnover domains that drive plenty of cellular processes (Ikeuchi and Ishizuka 2008; Losi and Gärtner 2012). Biological photoreceptors generally require continuous light exposure due to usually quick dark recovery from the light-activated signaling state.

A prominent example of a photoreceptor ingeniously engineered to drive bacterial gene expression poses the blue-light sensing LOV histidine kinase YF1 (Möglich et al. 2009). Here, the YtvA LOV sensing-domain from *B. subtilis*

Box I.6 | Glossary of terms

Optogenetics Methodology using genetically encoded light-responsive elements to achieve light-control of cellular functions, which originally arose from neuroscience. In a broader sense, both genetically encoded photoreceptors and photocaged compounds together with the actuated genetic element can be conceived as optogenetic tools.

Photoreceptor Light-sensitive protein-chromophore complex that conducts light-initiated signal transduction to modulate cellular behavior.

Two-component system Predominant bacterial signal transduction system which typically consists of a histidine kinase that senses a specific environmental stimulus and a corresponding response regulator that mediates the cellular response (e.g. transcription factor activity) in dependence on its phosphorylation state.

was fused to the FixL kinase effector-domain of *Bradyrhizobium japonicum* to yield a blue-light repressed **two-component system** (**Box I.6**). Together with the response regulator FixJ, the recombinant photoreceptor was in an initial setup able to repress gene expression approximately 70-fold upon continuous blue-light exposure in *E. coli*. Moreover, a redesign using an inversion cassette based on the lambda cI repressor resulted in an additional blue-light activated expression setup that was capable to induce gene expression up to 460-fold in a highly dynamic fashion (Ohlendorf et al. 2012).
In summary, both natural and recombinant photoreceptors represent valuable tools to control cellular functions such as bacterial gene expression by light (Ziegler and Möglich 2015).

I.5.2 Photocaged compounds

Another sophisticated approach of controlling cellular functions by light, uses **photocaged compounds** (**Box I.7**) to implement optogenetic control into biological applications. This concept was pursued in this work and will thus be introduced subsequently in more detail. In photocaged compounds, biomolecule activity is masked by photolabile protection groups and can be fully restored upon short light exposure (Brieke et al. 2012; Goeldner and Givens 2005). Already in 1977, Engels and Schlaeger successfully introduced the first photocaged biomolecule, namely *o*-nitrobenzyl-caged cAMP (Engels and Schlaeger 1977), which was shortly after followed by photocaged ATP (Kaplan et al. 1978). Since then, tremendous work has been ventured to photocage vital biomolecules properly in order to gain spatiotemporal light-control over chemical and biological processes (Brieke et al. 2012; Deiters 2009; Gardner and Deiters 2012). Several requirements have to be met to empower favorable photocaging and photouncaging efficiencies.

I.5.2.1 General prerequisites for photouncaging

To realize smooth functionality and straightforward *in vivo* applicability of photocaged compounds, several criteria, concerning development, physicochemical properties and photo-release have to be fulfilled.
Generally, a feasible and cost-efficient synthesis based on readily available precursors is clearly favored for the employment of photocaged compounds. Moreover, the photocaging group should be readily installable to the chosen effector molecule. At best, a photoprotection group should be highly stable both *in vitro* and *in vivo* and provide easy

coupling to different common effector molecule functionalities such as hydroxyl-, carboxy-, amino-, or amide moieties (Brieke et al. 2012; Goeldner and Givens 2005). To this end, alcohol or aldehyde precursors seem to qualify as versatile photocaging group functionalities (Goeldner and Givens 2005; Szymański et al. 2014).

Upon successful caging of the respective biomolecule, a diverse set of beneficial physicochemical properties facilitates the employment of the photocaged compound at hand. Appropriate absorptivity, solubility, non-toxicity as well as stability *in vivo* and *in vitro* are crucial for the success of the respective application. Furthermore, an adequate **uncaging quantum yield** (**Box I.7**), i.e. the efficiency of photo-induced bond scission, seems beneficial for most applications. Highly interesting in this context are also compounds that bear an appropriate **two-photon cross section** (**Box I.7**) and are thus suited for **two-photon uncaging** (**Box I.7**), so that light of approximately twice the wavelength can be applied (Bort et al. 2013; Brieke et al. 2012). This prospective, yet elaborate method of two-photon-uncaging will be discussed in a later chapter (**III.4.2**) in further detail.

In addition to mentioned physicochemical properties, the photocaged compound should exhibit no residual biological activity at all to fully suppress the respective function in the absence of light. In the presence of light, the actual photo-release is a key feature for the success of the *in vivo* application. It should be realized in a reasonable amount of time, so that no excessive light exposure is required and may thus bring the otherwise harmless irradiation into cytotoxic dimensions that entail phototoxic reactions or the heating-up of microbial cultivations. Furthermore, it is beneficial if a complete photo-release takes place and accordingly biological activity can be fully restored upon light exposure.

Upon successful and, ideally, complete photo-release of the biological effector molecule, any interference of resulting photo-products with cellular activity is undesired. A welcome feature, however, poses the ability to monitor the photoreaction online, for instance, in form of decreasing photocaged compound fluorescence or increasing photo-product fluorescence. Here, strongly fluorescing photocages are often favored to enable distinct visualization of the uncaging process by means of a significant shift

Box I.7 | Glossary of terms

Photocaged Compounds Light-responsive molecules that are rendered biologically inactive by means of photo-labile protection groups and regain their primal function upon short light exposure.

Uncaging quantum yield Percentage of photocaged compounds that undergo the intended photocleavage reaction in the excited state.

Two-photon uncaging (TPU) An optical technique that applies two photons of approximately twice the usual wavelength simultaneously to the same molecule to evoke the photoreaction in very small excitation volumes of several femtoliters. Special high-frequency lasers in the NIR-IR range have to be used.

Two-photon cross section Photo-chemical efficiency of two-photon uncaging that relates to the two photon-areas and the time, in which the two photons have to be applied to drive the photoreaction. To drive TPU applications properly cross sections above 0.1 GM (Göppert-Mayer unit; 10^{-50} cm^4 s $photon^{-1}$) are favored.

of fluorescence (Goeldner and Givens 2005; Luo et al. 2014).
This challenging and diversified requirement profile led to the establishment of various photocages, whereof most prevalent ones will be subsequently highlighted.

I.5.2.2 Commonly applied photocaging groups

Nowadays, a plethora of different photocaging groups with auspicious features is available and absorptivity spans from UV to red light (Hansen et al. 2015). Most frequently consulted photocages, however, are based on nitrobenzyl- and coumarin-derived photocaging groups (Brieke et al. 2012; Goeldner and Givens 2005).
For nearly 40 years, **nitrobenzyl-derived photocages** have been readily applied for photouncaging applications (Engels and Schlaeger 1977; Kaplan et al. 1978). Straightforward syntheses together with well-known photocleavage reactions are key benefits that still warrant their continuous employment (Deiters 2010; Goeldner and Givens 2005; Young and Deiters 2007a). Despite various examples highlighting applicability (Barth and Corrie 2002; Chou et al. 2010; Zhao et al. 2013), *o*-nitrobenzyl (NB) compounds mainly absorb in the UV-B/-C range (**Fig. I.5 A**), wherein radiation is rather cell-toxic and thus less appropriate for *in vivo* applications. On this account, NB uncaging is usually conducted using excessive UV-A light exposure, where the respective compounds provide moderate to low absorptivity. Hence, advanced nitrobenzyl-derivatives were developed that featured a bathochromic shift towards a longer-wavelength absorption and thus improved biocompatibility (Görner 2005; Schaper et al. 2010). Especially 6-nitroveratryl (NV), also denoted as 1,2-dimethoxy-4-nitrobenzyl (DMNB) or 6-nitroveratryloxycarbonyl (NVOC), and 6-nitropiperonyl-type photocages (NP), which include the frequently used 6-nitropiperonyloxymethyl (NPOM) derivative, were shown to exhibit adequate UV-A absorptivity and efficient photolysis (Görner 2005; Lusic and Deiters 2006; Schaper et al. 2010). In addition to NV and NP-photocages for longer-wavelength absorption, different carboxy-nitrobenzyls (CNB) were designed to improve compound solubility (Ni et al. 2007; Schaper et al. 2010).
Further prevalent photocages are coumarins or rather **coumarin-4-ylmethyl derivatives** (Brieke et al. 2012; Goeldner and Givens 2005), that are significantly red-shifted compared to nitrobenzyl-cages (**Fig. I.5 A**). Here, different moieties such as alkoxy-, amine, bromo- or hydroxyl-groups in the C6, C7 and C8-position are able to decisively shift the absorptivity into the visible range and improve water-solubility or membrane-permeability, respectively (Eckardt et al. 2002; Furuta et al. 1999; Goeldner and Givens 2005; Hagen et al. 2003; Klán et al. 2013). Novel promising coumarin-

derivatives are, for instance, 7-diethylamino-4-thiocoumarinmethyl- or 6-bromo-7-hydroxycoumarinmethyl that were shown to be well-suited for green light or two-photon uncaging, respectively (Fournier et al. 2013a; Fournier et al. 2013b; Luo et al. 2014).

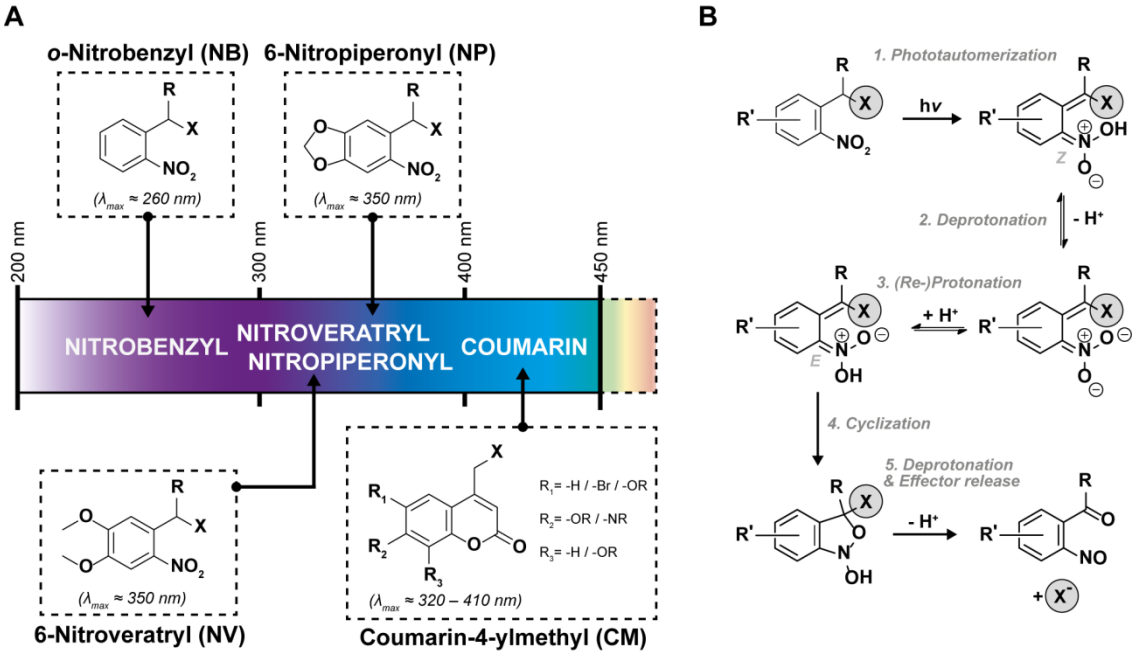

FIGURE I.5 | Absorption maxima of common photocaging groups along the UV-Vis spectrum and simplified photorelease mechanism of most prevalent *o*-nitrobenzyl derived caged compounds.

(**A**) Common photocaging groups that are applied to temporarily mask biological activities of respective effector molecules (X) include *o*-nitrobenzyl (NB) (λ_{max}~260 nm), nitroveratryl (NV) (λ_{max}~350 nm), nitropiperonyl (NP) (λ_{max}~350 nm) and diverse coumarin-4-ylmethyl (CM) (λ_{max}~380-450 nm) photocages (Brieke et al. 2012; Klán et al. 2013; Pelliccioli and Wirz 2002). Approximate long-wavelength absorption maxima, which slightly differ in dependence on chosen residues and effector molecules, are presented alongside the excerpt of the UV-Vis spectrum, with absorption at wavelengths between 200 and 450 nm. (**B**) Simplified photorelease mechanism of common *o*-nitrobenzyl based caged compounds (Goeldner and Givens 2005; Il'ichev et al. 2004; Schaper et al. 2009). R: -H, $-CH_3$, $-CO_2H$. R': -H (NB), -OMe (NV) or 4,5-methylenedioxy-bridge (NP) residues as presented in Fig. I.5 A.

In contrast to NB phototriggers, CM-based derivatives bear a highly promising chromatic diversity and are partly well-suited for two-photon-uncaging applications (Amatrudo et al. 2014; Furuta et al. 1999; Klán et al. 2013). However, synthesis of CM photocaged compounds proved to be less straightforward, more challenging or dependend on rather expensive precursors (Goeldner and Givens 2005).

Next to NB- and CM-derived photocages a huge variety of different photocaging groups, such as nitroindolines (Papageorgiou et al. 2005), *p*-hydroxyphenacyls (Givens et al. 2012), BODIPYS (Umeda et al. 2014) or heptamethine cyanines (Gorka et al. 2014) exists, whose facile and versatile applicability has to be evaluated in the near future. In a later chapter the applicability of novel photocages will be discussed in further detail (see Chapter II.6). Most prevalent photocages, however, are still *o*-nitrobenzyl derived compounds, whereof mainly NV- and NP-type caging groups are well applicable for

numerous *in vivo* applications. One key feature is the well-characterized and efficient photolysis.

To efficiently release the effector molecule, the *o*-nitrobenzyl compound undergoes five essential steps (**Fig. I.5 B**) that all occur in a millisecond time scale (Bley et al. 2008). Upon initial UV light absorption, the *o*-nitrobenzyl compound forms an *aci*-nitro intermediate in a phototautomerization reaction (Il'ichev et al. 2004). Here, a benzylic proton is abstracted by the nitro group to yield the Z-isomer of the corresponding nitronic acid. In a next step, the *aci*-nitro intermediate gets deprotonated to form the *aci*-nitro anion. Thereupon, the *aci*-nitro anion has to be (re-)protonated to the E-isomeric nitronic acid, to undergo cyclization in the following. Here, the *aci*-nitro E-isomer can cyclize to form the N-hydroxybenzisoxazoline intermediate. In a final step the unstable bicyclic benzisoxazoline degrades irreversibly *via* deprotonation to yield the respective effector molecule and the final nitrosocarbonyl photoproduct (Goeldner and Givens 2005).

In summary, the effector release from *o*-nitrobenzyl derived caged compounds occurs in a well-known, rapid and quantitative fashion in both aqueous and organic solutions, thus providing the groundwork for countless photochemical applications. Logically consistent, NB-derived photocaged compounds were together with other sophisticated derivatives employed to control biochemical processes *in vitro* and *in vivo* with utmost precision and in a spatiotemporal and non-invasive fashion. Despite far-reaching fields of application from neurobiology (Ellis-Davies 2007) over biomedicine (Bao et al. 2015; Nani et al. 2015) and material sciences (San Miguel et al. 2011) to photopharmacology (Fan et al. 2012; Lerch et al. 2016; Velema et al. 2014b), the subsequent chapter will solely focus on light-controlled gene expression by means of photocaged compounds (Deiters 2009).

I.5.2.3 Photocaged compounds for light-controlled gene expression

Optogenetic tools bear the tremendous potential for achieving a higher-order control of gene expression. As natural gene regulation mechanisms underlie immense complexity, elaborate control mechanisms and phenotypic variability (**see Chapter I.1**), optogenetic approaches such as photouncaging offer to remedy lacking precision, spatiotemporal resolution and invasiveness of conventional chemical induction. Here, a brief overview of existing attempts to control microbial gene expression by light using photocaged compounds will be provided.

In general, three main photouncaging principles are employed to realize light-controlled microbial gene expression, namely the optogenetic control of promoter, protein or riboswitch activity (**Fig. I.6**). The most common approach poses the utilization of

photocaged inducer molecules to drive microbial promoter activity. Whereas the biological activity of the inducer molecule is efficiently prohibited by means of photocaging, light exposure fully restores inducer functionality and thus enables the inducer to bind to the respective regulator protein, which in turn activates or represses gene expression (**Fig. I.6 A**).

Essentially, the most prominent photocaged inducer is **photocaged IPTG** that was shown to drive *lac*-based bacterial gene expression (Young and Deiters 2007b). NP-photocaged IPTG efficiently releases IPTG in a **two-step photocleavage** (**Box I.8**) process upon short UV-A light exposure and subsequent enzymatic hydrolysis of the photoproduct esters. Using photocaged IPTG, a ten-fold photoactivation of P_{lac}/LacI-regulated gene expression could be achieved in *E. coli*, which roughly corresponded to 85% of expression levels obtained with conventional equimolar induction. Although functionality was distinctly proven in principle, full applicability of the caged inducer, e.g. with respect to temporal resolution, gradual regulation or single-cell responsiveness, was since then not further elucidated.

By contrast to the presented bacterial photocaged inducers, additional photocaged biomolecules were shown to enable light-controlled gene expression in mammalian cells. Those include caged estradiol (Cruz et al. 2000), *β*-ecdysone (Lin et al. 2002), hydroxytamoxifen (Link et al. 2005), and toyocamycin (Young et al. 2009). Noteworthy, photocaged doxycycline (Cambridge et al. 2009; Cambridge et al. 2006; Sauers et al. 2010) was shown to drive P_{tet}/TetR-based gene expression upon UV-A light exposure. Despite likewise elaborated microbial P_{tet}/TetR-based expression tools that respond to either doxycycline itself or the structural analog anhydrotetracycline (Berens and Hillen 2003), photocaged doxycycline derivatives have not yet been recruited for light control of microbial gene expression, for instance in yeasts.

Besides the approach of exerting light-control of promoter activity using caged inducers, it is further feasible to obtain photocontrol of **riboswitches** (**Box I.8**) (**Fig. I.6 B**). In this context, a synthetic theophylline-sensing riboswitch (Lynch and Gallivan 2009) was recently employed in combination with **NP-photocaged theophylline** (Young and Deiters 2006) to photoactivate gene expression in *E. coli* (Walsh et al. 2014). Here, LacZ reported gene expression was strikingly upregulated up to 276-fold in response to UV-A light-mediated release of the NP-photocaged theophylline ligands.

Box I.8 | Glossary of terms

Two-step photocleavage In contrast to one-step photocleavages, upon initial photolysis the photoproduct of two-step photocleavage reactions requires further processing such as oxidation or enzymatic cleavage prior to release the bioactive effector molecule.

Riboswitch A regulatory mRNA segment that specifically binds small target molecules and regulates the transcription or translation of the respective mRNA e.g. *via* differential folding in response to the effector molecule concentration.

In addition to small-molecule photocaged effectors to control promoter or riboswitch activity, also biological macromolecules such as proteins may be caged effectively (Baker and Deiters 2014). Chou *et al*. successfully introduced an **NB-photocaged tyrosine** into the catalytic sites of recombinantly expressed T7 RNA polymerases (T7RP) to control gene expression (Chou et al. 2010). Therefore, NB-photocaged tyrosine was implemented into the proteins using genetic code expansion *via* orthogonal tRNA synthase-tRNA pairs from *Methanococcus jannaschii*. Finally, photo-functionality of recombinant T7RP proteins could be achieved to drive P_{T7}-based gene expression in both *E. coli* and mammalian cells (**Fig. I.6 C**).

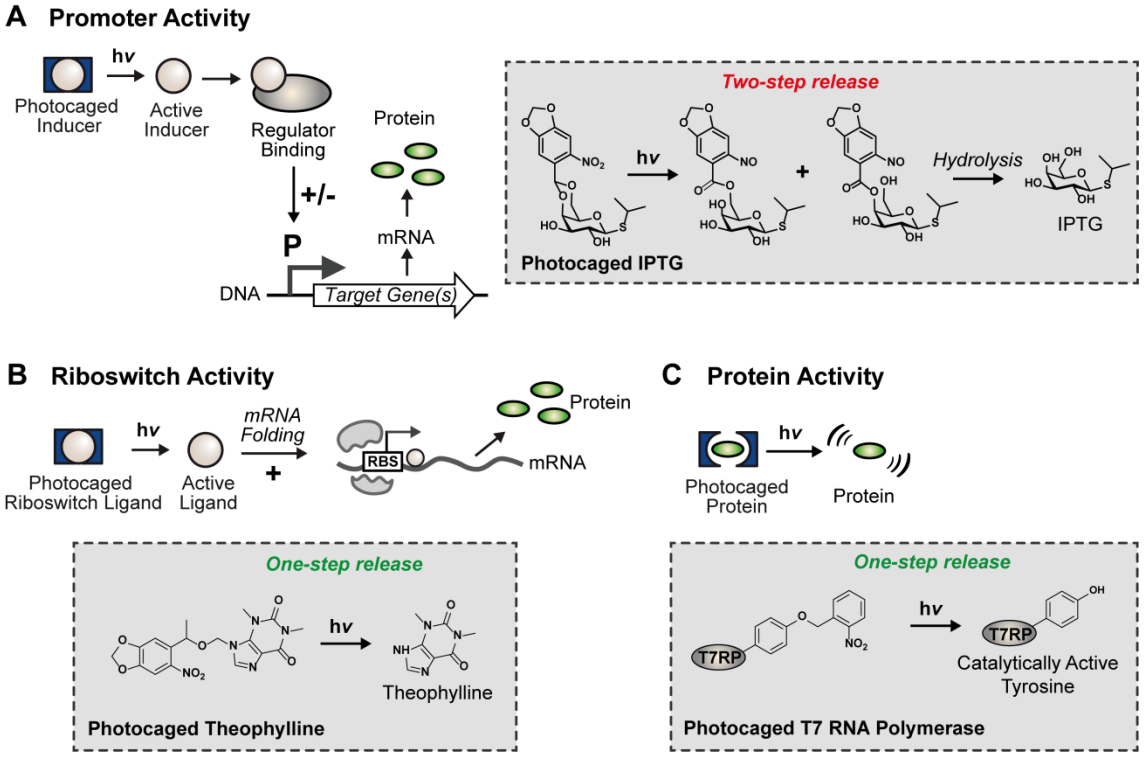

FIGURE I.6 | Light-controlled bacterial gene expression using photocaged compounds.
Light-dependent control over gene expression using photocaged compounds, which effectively release bioactive effector molecules upon short light exposure. Uncaged compounds can promote cellular behavior such as promoter (**A**), riboswitch (**B**) or specific protein (**C**) activity. Sophisticated photocaged compounds (grey boxes) that have been successfully applied to control bacterial gene expression include photocaged IPTG (Young and Deiters 2007b), photocaged theophylline (Walsh et al. 2014) and photocaged T7RP (Chou et al. 2010).

Moreover, photocaged oligonucleotides pose a sophisticated approach of controlling RNA and DNA molecules (Liu and Deiters 2014; Yamazoe et al. 2014). Whereas benefits could be proven mainly *in vitro* and for some mammalian applications including splicing (Hemphill et al. 2015) and even plasmid control (Hemphill et al. 2014), *in vivo* applicability in microbes has to be elucidated in the near future.

The presented examples illustrate how diverse approaches may be employed to establish optogenetic tools for bacterial gene expression in principle. However, current

tools inevitably require in-depth characterization, optimization and redesign to compete with currently available conventional expression tools, and finally to supersede them in suited lab-scale applications. In this context, it will be an appealing challenge to entirely exploit the versatile features of electromagnetic radiation, in favor of miscellaneous microbial application in biotechnology and synthetic biology.

I. 6 Outline of the thesis

Light is currently evolving as a key player in providing a higher-order control over cellular functions. Here, unique features such as high variability and selectivity meet with unprecedented spatiotemporal resolution to trigger cellular events in a precise, straightforward and non-invasive fashion. In this context, it was the overall aim of this thesis to establish **light-controlled expression systems based on photocaged compounds in bacteria**.

Initially a set of different *E. coli* expression systems was (**I**) characterized down to the single-cell level in order to recruit suited systems for the subsequent application in a light-controlled setup (Chapter II.1). Here, a focus was laid onto the cell-to-cell heterogeneity of expression, which should be (**II**) tuned towards homogeneity (Chapter II.2). Upon identification of suited expression systems, (**III**) light-controlled expression tools were established applying photocaged inducer molecules (Chapter II.3). Thereby, the attention was turned on elevating the temporal resolution of obtained light-responsiveness.

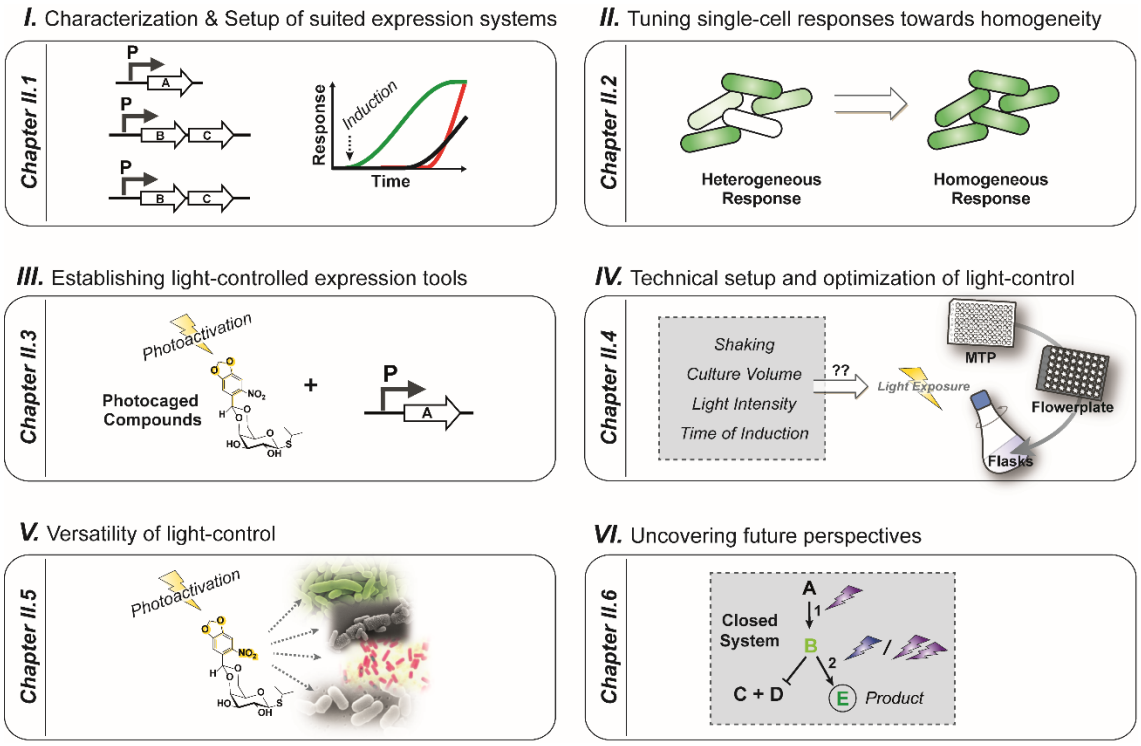

FIGURE I.5 | Graphical outline of this thesis.

Within the scope of this thesis different *E. coli* expression systems were (***I.***) characterized down to the single-cell level and recruited for the overall aim to achieve light-control of gene expression. A special focus was laid onto cell-to-cell heterogeneity of expression that was (***II.***) tuned towards homogeneity. Subsequently, (***III.***) light-controlled expression tools were established and (***IV.***) optimized with respect to technical setup and general light-control. Based on established optogenetic tools, (***V.***) the transfer of light-controlled tools to alternative platform organisms was tackled prior to (***VI.***) uncovering future perspectives in-depth.

Next, (**IV**) parameters affecting light exposure were systematically characterized from a technical point of view in different cultivation setups and optimized applying a newly developed photomicrobioreactor (**Chapter II.4**).

Further, (**V**) established light-controlled setups were transferred to **a**) alternative expression hosts, and **b**) biotechnological applications (**Chapter II.5**).

Finally, (**VI**) future perspectives for light-controlled expression tools using photocaged compounds were uncovered and evaluated (**Chapter II.6**).

II. Results

The following results section of this thesis includes nine manuscripts that were compiled in close and essential collaborations with the Institute of Bioorganic Chemistry (Heinrich-Heine University Düsseldorf), the Institute of Bio- and Geosciences (IBG-1, FZ Jülich), the Group of Biochemical Engineering (RWTH Aachen) as well as the Group of Genetics of Prokaryotes (University of Bielefeld). On this account, the own contributions were estimated for all manuscripts taking into account the following aspects: Design of experiments / performance of experiments / data analysis / writing the manuscript. Specific contributions to the articles at hand are a listed below. Furthermore, the current status of the presented manuscript was specified.

Chapter II.1

Binder D,* Probst C,* Grünberger A,* Hilgers F, Loeschcke A, Jaeger K-E, Kohlheyer D, Drepper T (2016) Comparative Single-Cell Analysis of Different *E. coli* Expression Systems during Microfluidic Cultivation. PLoS One 11:e0160711.

Status: Published

Own contribution: 35%

- Designing and performing experiments, plasmid constructions, analyzing data, writing the manuscript

Chapter II.2

Binder D, Drepper T, Jaeger KE, Delvigne F, Wiechert W, Kohlheyer D, Grünberger A (2016) Analysis and engineering of microbial phenotypic heterogeneity – From tools to applications and beyond.

Status: Published

Own contribution: 65%

- Writing the manuscript

Chapter II.3.1

Binder D,* Grünberger A,* Loeschcke A, Probst C, Bier C, Pietruszka J, Wiechert W, Kohlheyer D, Jaeger K-E, Drepper T (2014) Light-responsive control of bacterial gene expression: precise triggering of the *lac* promoter activity using photocaged IPTG. Integr Biol (Camb) 6:755–65.

Status: Published

Own contribution: 45%

- Designing and performing experiments, cIPTG synthesis, analyzing data, writing the manuscript

Chapter II.3.2

Binder D, Bier C, Grünberger A, Drobietz D, Hage-Hülsmann J, Wandrey G, Büchs J, Kohlheyer D, Loeschcke A, Wiechert W, Jaeger K-E, Pietruszka J, Drepper T (2016) Photocaged Arabinose - A Novel Optogenetic Switch for Rapid and Gradual Control of Microbial Gene Expression. Chembiochem 17:296–299.

Status: Published

Own contribution: 65%

- Designing experiments, performing *in vivo* experiments, analyzing data, writing the manuscript

Chapter II.3.3

Bier C, Binder D, Drobietz D, Loeschcke A, Drepper T, Jaeger K-E, Pietruszka J (2016) Photocaged carbohydrates – versatile tools for controlling gene expression by light. Synthesis; doi: 10.1055/s-0035-1562617.

Status: Published

Own contribution: 25%

- Performing *in vivo* experiments, writing parts of the manuscript

Chapter II.4.1

Binder D, Bier C, Klaus O, Pietruszka J, Jaeger K-E, Drepper T (2016) Using 1,2-dimethoxy-4-nitrobenzene actinometry to monitor UV-A light exposure in phozobiotechnological setups.

Status: To be submitted

Own contribution: 80%

- Designing and performing experiments, analyzing data, writing the manuscript

Chapter II.4.2

Wandrey G, Bier C, Binder D, Hoffmann K, Jaeger K-E, Pietruszka J, Drepper T, Büchs J (2016) Light-induced gene expression with photocaged IPTG for induction profiling in a high-throughput screening system. Microb Cell Fact 15:63.

Status: Published

Own contribution: 20%

- Plasmid construction, initial cIPTG synthesis, spectral Analysis, analyzing data, writing parts the manuscript

Chapter II.5.1

Binder D,* Frohwitter J,* Mahr R, Bier C, Grünberger A, Loeschcke A, Peters-Wendisch P, Kohlheyer D, Pietruszka J, Frunzke J, Jaeger K-E, Wendisch VF, Drepper T (2016) Light-controlled cell factories - Employing photocaged IPTG for light-mediated optimization of *lac*-based gene expression and (+)-valencene biosynthesis in *Corynebacterium glutamicum*. Appl Environ Microbiol. doi: 10.1128/AEM.01457-16

Status: Published

Own contribution: 45%

- Designing and performing experiments, initial cIPTG synthesis, analyzing data, writing the manuscript

Chapter II.6

Binder D, Pietruszka J, Jaeger K-E, Drepper T (2016) Cage me if you can! – From assembly to application of photocaged compounds in microbial biotechnology.

Status: To be submitted

Own contribution: 80%

- Writing the manuscript

* These authors equally contributed to this work

II.1 Characterization and setup of suited expression systems

II.1.1 Microfluidic analysis of E. coli expression systems

Comparative single-cell analysis of different *E. coli* expression systems during microfluidic cultivation

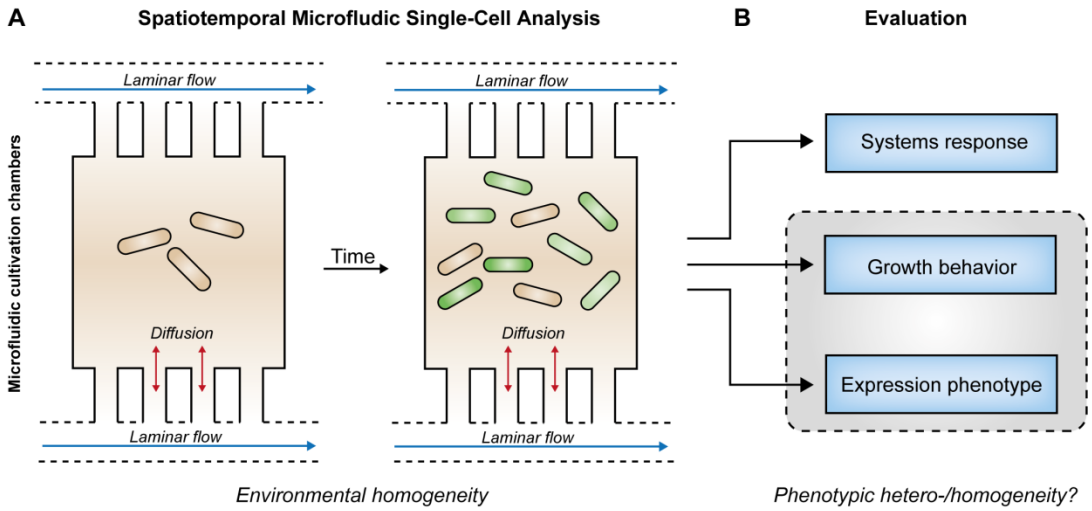

Dennis Binder, Christopher Probst, Alexander Grünberger, Fabienne Hilgers, Anita Loeschcke, Karl-Erich Jaeger, Dietrich Kohlheyer and Thomas Drepper

PLoS One 2016; 11:e0160711.

The full online version may be found at:
http://dx.doi.org/10.1371/journal.pone.0160711

For the complete supporting information see Appendix (**Chapter V.1**) turn to page **189.**

PLOS | ONE

RESEARCH ARTICLE

Comparative Single-Cell Analysis of Different *E. coli* Expression Systems during Microfluidic Cultivation

Dennis Binder[1☯], Christopher Probst[2☯], Alexander Grünberger[2☯], Fabienne Hilgers[1], Anita Loeschcke[1], Karl-Erich Jaeger[1,2], Dietrich Kohlheyer[2], Thomas Drepper[1]*

1 Institute of Molecular Enzyme Technology, Heinrich-Heine-University Düsseldorf, Forschungszentrum Jülich, Jülich, Germany, **2** Institute of Bio- and Geosciences (IBG-1), Forschungszentrum Jülich, Jülich, Germany

☯ These authors contributed equally to this work.
* t.drepper@fz-juelich.de

OPEN ACCESS

Citation: Binder D, Probst C, Grünberger A, Hilgers F, Loeschcke A, Jaeger K-E, et al. (2016) Comparative Single-Cell Analysis of Different *E. coli* Expression Systems during Microfluidic Cultivation. PLoS ONE 11(8): e0160711. doi:10.1371/journal.pone.0160711

Editor: Paul D. Riggs, New England Biolabs Inc, UNITED STATES

Received: March 1, 2016

Accepted: July 22, 2016

Published: August 15, 2016

Data Availability Statement: All relevant data are within the paper and its Supporting Information files.

Funding: Supported by grants from the Federal Ministry of Education and Research (OptoSys, FKZ 031A16), Ministry of Innovation, Science and Research of North-Rhine Westphalia and German Research Foundation (INST 208/654-1 FUGG). Moreover, the Helmholtz Association (VH-NG-1029 and PD-311) is gratefully acknowledged for funding. This work was partly performed at the Helmholtz Nanoelectronic Facility (HNF) of Forschungszentrum Jülich. The funders had no role in study design, data

Abstract

Recombinant protein production is mostly realized with large-scale cultivations and monitored at the level of the entire population. Detailed knowledge of cell-to-cell variations with respect to cellular growth and product formation is limited, even though phenotypic heterogeneity may distinctly hamper overall production yields, especially for toxic or difficult-to-express proteins. Unraveling phenotypic heterogeneity is thus a key aspect in understanding and optimizing recombinant protein production in biotechnology and synthetic biology. Here, microfluidic single-cell analysis serves as the method of choice to investigate and unmask population heterogeneities in a dynamic and spatiotemporal fashion. In this study, we report on comparative microfluidic single-cell analyses of commonly used *E. coli* expression systems to uncover system-inherent specifications in the synthetic M9CA growth medium. To this end, the P_{T7lac}/LacI, the P_{BAD}/AraC and the Pm/XylS system were systematically analyzed in order to gain detailed insights into variations of growth behavior and expression phenotypes and thus to uncover individual strengths and deficiencies at the single-cell level. Specifically, we evaluated the impact of different system-specific inducers, inducer concentrations as well as genetic modifications that affect inducer-uptake and regulation of target gene expression on responsiveness and phenotypic heterogeneity. Interestingly, the most frequently applied expression system based on *E. coli* strain BL21(DE3) clearly fell behind with respect to expression homogeneity and robustness of growth. Moreover, both the choice of inducer and the presence of inducer uptake systems proved crucial for phenotypic heterogeneity. Conclusively, microfluidic evaluation of different inducible *E. coli* expression systems and setups identified the modified *lacY*-deficient P_{T7lac}/LacI as well as the Pm/XylS system with conventional *m*-toluic acid induction as key players for precise and robust triggering of bacterial gene expression in *E. coli* in a homogeneous fashion.

collection and analysis, decision to publish, or preparation of the manuscript.

Competing Interests: The authors have declared that no competing interests exist.

Introduction

While in natural environments, cell-to-cell variations in gene expression and growth may prove beneficial and are considered as bet-hedging or division of labor strategies to enhance environmental adaptability within an isogenic bacterial population [1,2], such phenotypic heterogeneity is unfavorable in biotechnology and synthetic biology. Here, phenotypic homogeneity is needed to reliably predict and control target gene expression [3,4]. In this context, strength, velocity and tightness of gene expression responses seem essential for processes where, for instance, a general interconnection between biomass formation and product accumulation exists. Hence, expression systems should be critically evaluated down to single-cell level with respect to responsiveness, growth behavior and expression phenotype, to gain detailed insights into these processes and, subsequently, to yield a higher degree of control over target gene expression.

The last decades gave rise to several sophisticated inducible bacterial expression systems that were predominantly inspired by natural regulatory circuits. Mainly catabolic regulatory networks such as those for lactose, arabinose or benzoate utilization were employed as useful tools for heterologous gene expression [5–7]. These expression systems commonly consist of native or mutagenized promoters and a corresponding transcriptional regulator that represses, derepresses or activates target gene expression in the presence of a specific inducer that can enter the cell *via* an appropriate transport system or by passive diffusion.

For *E. coli*, which is the most commonly applied microbial expression host [5,8], the *lac*-based regulation of expression is typically the first-to-try system for recombinant protein production [9,10]. *E. coli* BL21(DE3) [11] and its derivatives [12–14] are the most frequently used strains for high-level protein production that make use of the highly processive T7-RNA polymerase (T7RP) [15]. Usually, the expression of the chromosomally integrated T7RP gene is controlled by the *lac* promoter and the phage polymerase in turn exclusively drives expression of a synthetic T7*lac* promoter, usually present on an additional expression plasmid. Both, *lac* and T7*lac* promoters, are negatively regulated by the LacI repressor, which dissociates from the operator region upon binding of an appropriate inducer [16,17]. Several natural inducers, such as lactose and galactose [18,19], or synthetic inducers such as methyl-1-thio-β-D-galactopyranoside (TMG) [20] and isopropyl β-D-1-thiogalactopyranoside (IPTG) [21] are able to promote gene expression in this system. Uptake of the natural inducers lactose and galactose in *E. coli* mainly depends on the lactose (LacY) and galactose (GalP) permeases [22,23]. The synthetic *lac* inducers IPTG and TMG, however, pass the bacterial cell membrane both by diffusion and by LacY-mediated active transport [24] (Fig 1A).

Another widely used expression system in *E. coli* is based on the arabinose utilization network, which positively regulates the P_{BAD} promoter controlled gene expression using the AraC regulator protein [7,25]. In contrast to the LacI regulator, which solely represses transcription in the absence of an appropriate inducer, AraC effectively activates and represses transcription, in the presence or absence of arabinose, respectively, thus allowing for extremely fine-adjustable expression levels [7]. The uptake of arabinose mainly occurs by a complex regulated transport system including the AraE and AraFHG transport proteins [26] (Fig 1B). Furthermore, the Pm/XylS system, which originates from the *Pseudomonas putida* TOL meta operon for the degradation of toluenes and benzoates, finds increasing application for controlling gene expression in *E. coli* [7,27]. Here, benzoate inducers such as *m*-toluic or salicylic acid [28] bind to the XylS regulator protein that in turn activates Pm-mediated target gene expression. Opposite to previously mentioned *lac* and *ara*-based expression systems, benzoate inducers for the activation of Pm/XylS systems do not depend on active transport systems but enter the cells solely *via* passive diffusion (Fig 1C) [29].

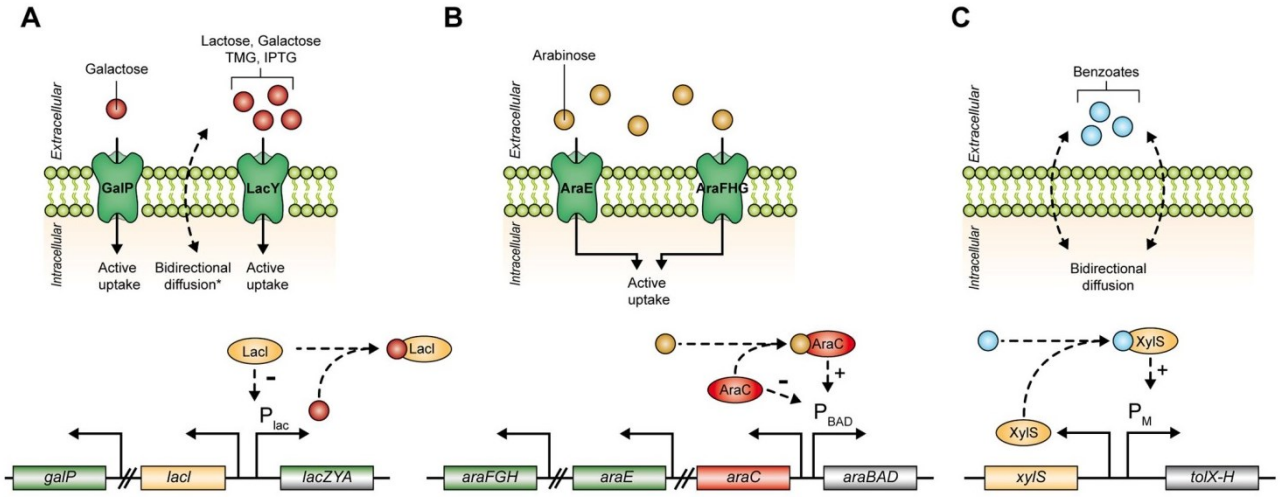

Fig 1. Simplified mechanisms of inducer uptake and regulation of target gene expression in common *E. coli* expression systems. (A) *Lac* based gene expression *via* natural (lactose, galactose) or synthetic (TMG, IPTG) inducers. Uptake basically occurs through GalP (mainly galactose) or LacY (all inducers) transport proteins and by passive diffusion (* only synthetic inducers TMG and IPTG). Inducer binding leads to the release of the LacI repressor from the P_{lac} promoter and thus induces gene expression. (B) Arabinose inducible gene expression upon active uptake *via* AraE and AraFGH transport proteins. In the presence of arabinose AraC positively regulates P_{BAD} promoter activity, whereas in the absence of arabinose AraC tightly represses target gene expression. (C) Pm/XylS regulated gene expression driven by benzoates that are imported *via* passive diffusion and initiate the XylS regulator-dependent activation of Pm promoter based expression. Abbreviations: *galP*: galactose permease gene; *lacI*: *lac* repressor gene; *lacZYA*: lactose metabolization and uptake genes; *araFGH*: arabinose transporter genes; *araE*: arabinose transporter genes; *araC*: *ara* regulator gene; *araBAD*: arabinose metabolization genes; *xylS*: *xyl* regulator gene; *tolX-H*: toluene degradation operon.

doi:10.1371/journal.pone.0160711.g001

Additional *E. coli* expression systems are based on propionate-inducible P_{prpB}/PrpR [30,31], rhamnose-inducible P_{rhaBAD}/RhaRS [7,32] or tetracycline-inducible P_{tetA}/TetR [33] regulatory systems. Due to costly or toxic inducers, a restricted spectrum of expression hosts or the need for coexpression of recombinant transport systems, those systems are less often applied for biotechnological purposes and are thus not subject of this study.

Here, we comparatively analyzed commonly used *E. coli* expression systems, namely the P_{T7lac}/LacI, P_{BAD}/AraC and Pm/XylS systems, in order to gain more detailed knowledge at the single-cell level. We used the synthetic M9CA medium of defined composition to characterize the inducibility of the three expression systems in response to different inducer molecules and investigated the influence of inducer-uptake affecting genetic modifications on phenotypic heterogeneity. Our results provide new insights into individual strengths and weaknesses of each expression system in terms of system responsiveness, growth behavior and phenotypic heterogeneity.

Materials and Methods

Microfluidic chip fabrication and experimental setup

Microfluidic polydimethylsiloxane (PDMS) chips incorporating media supply channels of 10 μm height and cultivation chambers of 1 μm height were fabricated by common silicone elastomer molding. Therefore, a 100 mm silicon wafer carrying inverted SU-8 microstructures processed by cleanroom photolithography served as the replication mold. A PDMS base and crosslinker mixture (1:10) was then poured onto the mold and thermally polymerized. After releasing the PDMS slab containing the structure imprint, individual chips were cut and inlet and outlets were punched manually. Before each experiment, PDMS chips were cleaned,

oxygen plasma activated and finally permanently bonded to a microscopy cover slide. Detailed information regarding the device layout and fabrication can be found in previous studies [34–36].

Fluidic connections were established by silicone tubing (Tygon S-54-HL, ID = 0.25 mm, OD = 0.76 mm, VWR International) and dispensing needles (dispensing tips, ID = 0.2 mm, OD = 0.42 mm, Nordson EFD). A medium flow rate of approximately 200 nl min^{-1} was generated by a syringe pump (neMESYS, centoni GmbH, Germany). Prior to cultivation, cells at the exponential growth phase (OD_{580} of 0.3–0.5) were inoculated into the chip. Then specific growth chambers which were most suitable for imaging were manually selected, leading to a short delay between the initial induction and start of the experiment. The maximum cultivation duration was determined by the growth rate and the fixed chamber volume.

Microscopy setup

Microscopy images were taken using an inverted microscope (Nikon TI-Eclipse, Nikon Instruments, Germany) equipped with a 100x oil immersion objective (CFI Plan Apo Lambda DM 100X, NA 1.45, Nikon Instruments, Germany) and a temperature incubator (PeCon GmbH, Germany). Phase contrast and fluorescence time-lapse images were recorded every 10–15 minutes using an ANDOR LUCA R DL604 CCD camera. Fluorescence images were recorded with an exposure time of 200 ms using the Nikon Intensilight as light source with an ND filter of 1/8 (Nikon, Japan) and an appropriate YFP filter (EX 490–550 nm, DM 510 nm, BA 520–560 nm).

Image and data analysis

Time-lapse movies of monolayer growth chambers were analyzed using a custom, specialized workflow implemented as an ImageJ/Fiji plugin [37]. Cell identification was performed using a segmentation procedure tailored to detect individual rod-shaped cells in crowded populations. Maximum growth rates were derived for each colony by fitting an exponential function to the cell number increase applying the method of least squares [38,39]. Basal expression factors were calculated as ratios of averaged fluorescence values for non-induced expression cultures and non-induced control cultures (lacking the respective expression vector) at the end of the respective experiment. System responsiveness was measured as the positive slope of linear fitting functions for the averaged fluorescence of single-cell fluorescence values increase during the first 60 min of the experiment. The dynamic range of induction was calculated as the highest ratio of averaged fluorescence values for induced and non-induced cultures over the whole course of the experiment.

Growth Media

Solid Lysogeny Broth (LB) plates were prepared using 25 g l^{-1} ready-to-use mix Luria/Miller (Carl Roth, Karlsruhe, Germany) and 15 g l^{-1} agar-agar (Carl Roth, Karlsruhe, Germany).

Liquid cultivations were performed using M9CA medium: 4 g l^{-1} Bacto™ casamino acids (BD Biosciences, Franklin Lakes, NJ, USA), 6.8 g l^{-1} Na_2HPO_4, 3 g l^{-1} KH_2PO_4, 0.5 g l^{-1} NaCl, 1 g l^{-1} NH_4Cl, adjusted to pH 6.8 at 25°C. Supplementation of 2 mM $MgSO_4$ (from separately autoclaved 1 M stock solution) and 8 g l^{-1} glycerol (from sterile-filtrated stock solutions) was performed after autoclaving.

Plasmid-containing strains were maintained by applying 25 μg ml^{-1} of kanamycin in both solid and liquid cultivation media.

Table 1. *E. coli* expression systems characterized in this study.

System	UptakeMechanism	Inducer	Inducer concentrations*	*E. coli* strain (plasmid)	Cultivation temperature	References
P_{T7lac}/LacI	active(*lacY*$^+$)	IPTG	0, 0.05, 0.1 mM	BL21(DE3) (pRhotHi-2-EYFP)	37°C	[47]
P_{T7lac}/LacI	passive (*lacY*)	IPTG	0, 0.05, 0.1 mM	Tuner(DE3) (pRhotHi-2-LacI-EYFP)	37°C	[14]
P_{T7lac}/LacI	*active (galP*$^+$ *lacY*$^+$*)*	galactose	0, 0.4, 1 mM	BL21(DE3)** (pRhotHi-2-LacI-EYFP)	37°C	[14]
P_{BAD}/AraC	*active (araEFGH*$^+$*)*	arabinose	0, 1, 2.5 mM	Tuner(DE3)*** (pAra-GFPmut3)	37°C	[48]
$P_{M1\text{-}17}$/XylS	passive	*m*-toluic acid	0, 0.05, 0.1 mM	Tuner(DE3) (pM-117-R45T-GFPmut3)	30°C	[6,28] & this study
$P_{M1\text{-}17}$/XylS	passive	salicylic acid	0, 0.5, 1.5 mM	Tuner(DE3) (pM-117-R45T-GFPmut3)	30°C	[6,28] & this study

* w/o inducer, intermediate inducer concentrations, high inducer concentrations

** *galK*$^-$ strain: inability to metabolize galactose, enables sufficient galactose accumulation for induction

*** *araBAD*$^+$ strain: metabolizes arabinose, increased inducer concentrations are essential

doi:10.1371/journal.pone.0160711.t001

Bacterial strains and plasmids

All bacterial strains, plasmids and oligonucleotides used in this study are listed in S1 Table. The construction of expression vectors and recombinant DNA techniques were carried out in *E. coli* DH5α as described by Sambrook *et al.* [40]. To yield a benzoate induction with a broader inducer spectrum and a stronger induction response, an afore-described R45T mutation [28,41] was introduced into the XylS regulator protein *via* overlap extension PCR [42] using Primers 1–4 (S1 Table). The resulting PCR product as well as the target vector pSB-M117-2-g [6] were digested *via* *Sal*I and *Sac*I restriction. The mutagenized *xylS* PCR product was then inserted into the vector backbone *via* ligation, yielding the vector pM117-R45T-GFP. The resulting construct was verified *via* sequencing. Prior to application of the expression systems listed in Table 1, the corresponding expression vectors were freshly heat-shock transformed into the respective expression hosts.

Precultivation

To obtain comparable microfluidic expression cultures, precultivation was performed exactly as described using fresh LB-Agar transformation plates. First, an overnight preculture was inoculated from a fresh transformation plate in 0.8 ml of the final cultivation medium. After 16 h of cultivation a fresh culture was inoculated in again 0.8 ml of the final cultivation medium to a cell density corresponding to an optical density of 0.01 at a wavelength of 580 nm (OD_{580}). This culture was cultivated until an OD_{580} of 0.3–0.5 was reached. Exponentially growing cells were then immediately seeded into the microfluidic cultivation chips. All precultivations (30 or 37°C, 1500 rpm) were performed in sterile 48-well flowerplates (m2p-labs GmbH, Aachen, Germany) using a deep-well plate incubator (Thermomixer C; Eppendorf, Hamburg, Germany).

Results

In synthetic biology and biotechnology, expression processes are mainly observed on average-based population scale, thus ignoring phenotypic heterogeneity especially in case of adequate overall yields and functionality. However, cell-to-cell heterogeneity may distinctly hamper overall product yields [43]. This becomes most evident for toxic gene products [44] and if non-

producing cells overgrow the culture due to a faster growth [45]. Unraveling phenotypic heterogeneity is therefore a key aspect in understanding and optimizing recombinant protein production.

In order to precisely analyze expression systems at single-cell level, cells have to be characterized under well-defined environmental conditions, enabling one to distinguish between phenotypic (intrinsic) and environmental (extrinsic) heterogeneity [36,43].

This challenge was strikingly tackled in recent years by means of microfluidic single-cell cultivation approaches. These allow for cultivations under precisely controlled cultivation conditions implemented by continuously perfused cultivation medium (Fig 2A). Here, laminar flow conditions and diffusion-dominated mass transport lead to well predictable environmental homogeneity. Furthermore, microfluidics in combination with time-lapse imaging facilitates the analysis of cellular behavior and physiology with high spatiotemporal resolution [34–36]. We thus employed novel microfluidic bioreactor systems [36] for cultivation and *in vivo* fluorescence reporter-based monitoring of gene expression in common *E. coli* expression systems to uncover system-inherent specifications including responsiveness, growth behavior and expression phenotype (Fig 2B).

Complex growth media such as LB medium are widely used for the cultivation of *E. coli* in both bulk and single-cell analysis. In contrast to synthetic media, they contain yeast extracts, which are chemically not accurately defined, thus limiting exact knowledge about the nutrient composition. Moreover, distinct variations between different yeast extract suppliers or lots might occur [46]. Our preliminary analyses of the carbohydrate composition of different LB cultivation media (S2 Table, S1 Appendix) and its impact on expression strength and homogeneity (S1 Fig) revealed striking differences.

These results clearly demonstrate that complex LB cultivation media should not be applied for microfluidic cultivations where precise control over gene expression is of primary interest;

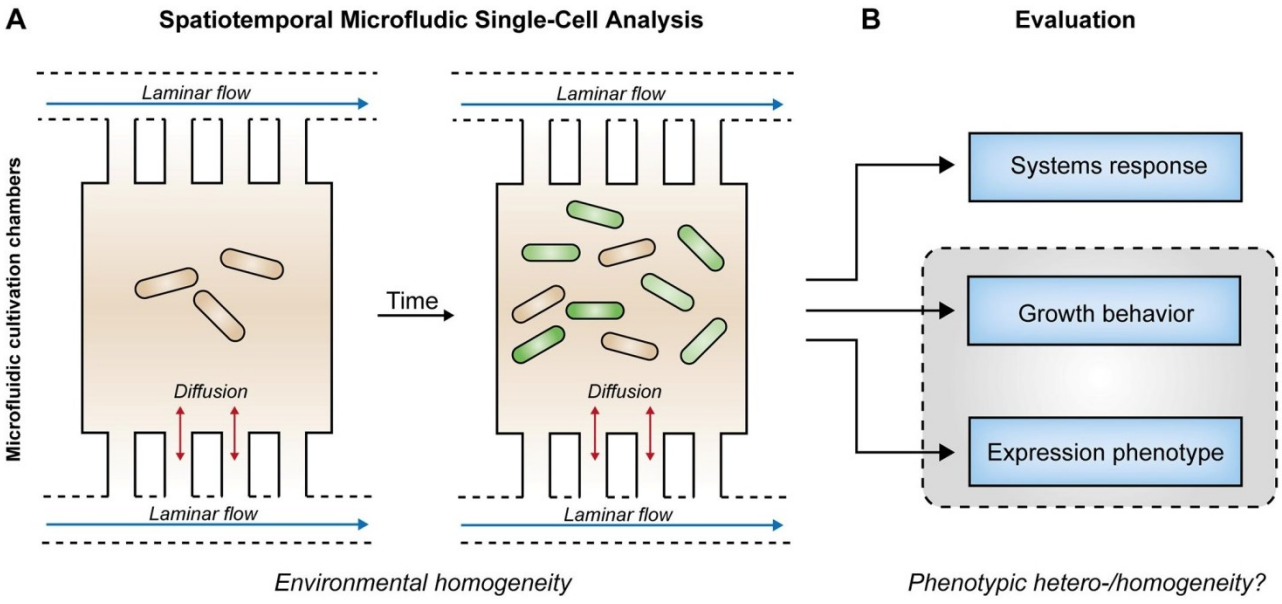

Fig 2. Microfluidic single-cell cultivation experiments. A) Spatiotemporal microfluidic single-cell analysis of isogenic populations enables well-defined environmental conditions (environmental homogeneity) within growth chambers due to constant laminar media flow through nutrient supply channels. **B)** Exact evaluation of expression systems response, growth behavior and expression phenotype to expose phenotypic heterogeneity (grey box) of analyzed expression systems.

doi:10.1371/journal.pone.0160711.g002

we therefore selected for growth of *E. coli* the synthetic M9CA as an alternative medium, which lacks in residual carbohydrates (S2 Table). M9CA is a rich cultivation medium that contains well-defined components that can be individually adjusted if necessary and enables fast growth of *E. coli* cells.

Comparative system specification analysis of selected *E. coli* expression systems

With microfluidic single-cell analysis and the synthetic M9CA medium we choose a well-defined experimental setup, providing high environmental homogeneity, to enable detailed insights into relevant microbial expression systems on the single-cell level.

Hence, we comparatively analyzed system-inherent specifications of a defined set of commonly applied *E. coli* expression systems using different inducer molecules, concentrations and uptake mechanisms (Table 1). In contrast to other studies focusing on high-transformation efficiency, low background of target gene expression [6] or natural P_{lac} constructs with *E. coli* K12 wildtype strain derivatives [21], we solely analyzed expression systems that were based on the most commonly used high-level production host in biotechnology, namely *E. coli* BL21 (DE3) and its *lacZY*⁻ derivative Tuner(DE3). These two strains, in contrast to commonly used K12 strains, are deficient in the proteases encoded by *ompT* and *lon*, which has proven beneficial for high-level protein production [9]. Moreover, due to the implementation of the highly processive T7RP, the strains are well suited for applying the frequently used expression vectors harboring hybrid T7*lac* promoters for target gene expression (P_{T7lac}/LacI system).

P_{T7lac}/LacI-based IPTG induction of target gene expression was analyzed in both BL21 (DE3) (*lacY*⁺) and Tuner(DE3) (*lacY*⁻) expression strains since previous studies indicated crucial differences in responsiveness and phenotypic heterogeneity [14]. Whereas the *lacY*⁺ system represents the 'what to try first' *E. coli* expression system, the here applied *lacY*⁻ system was expected to bear improved expression features due to the absence of permease LacY and elevated amounts of repressor LacI. We further analyzed galactose induction in the *lacY*⁺ system as well as an arabinose inducible P_{BAD}/AraC system [48]. Moreover, we tested benzoate induction using a Pm/XylS system with the high-level expression promoter P_{M117} [6,27]. To enable a promiscuous benzoate induction with diverse benzoate derivatives [28], in particular to empower salicylic acid induction in addition to conventional *m*-toluic acid induction, we introduced an R45T mutation into the XylS regulator protein. For the non *lac*-based expression systems, we consistently used the *lacY*⁻ *E. coli* strain Tuner(DE3) as it exhibits strict inhibition of (in this case) undesired T7RP gene expression under the here applied conditions.

To uncover system-inherent specifications for all analyzed *E. coli* expression systems, microfluidic cultivations were compared using no inducer as well as intermediate and high inducer concentrations (for exact concentrations and setups see Table 1). All cultivations were conducted at 37°C, except for benzoate induction systems which worked best at 30°C.

First, we aimed to analyze the system responsiveness of the respective expression systems since temporally precise control is of utmost importance for several synthetic biology and biotechnological applications. For instance, in rapidly growing cultures, exclusively prompt induction responses might enable sufficient product formation prior to nutrient depletion or the transition into the less productive stationary phase.

Thus, the system responsiveness (Fig 3A) was evaluated using the initial increase of single-cell fluorescence (linear slope of fluorescence for the first 60 min) for all six expression strains (Table 2). IPTG induction of the P_{T7lac}/LacI system using the *lacY*⁺ strain *E. coli* BL21(DE3) showed the strongest initial target gene expression response. Notably, a likewise rapid and strong response was observed for salicylic acid induction of the Pm promoter, albeit the here

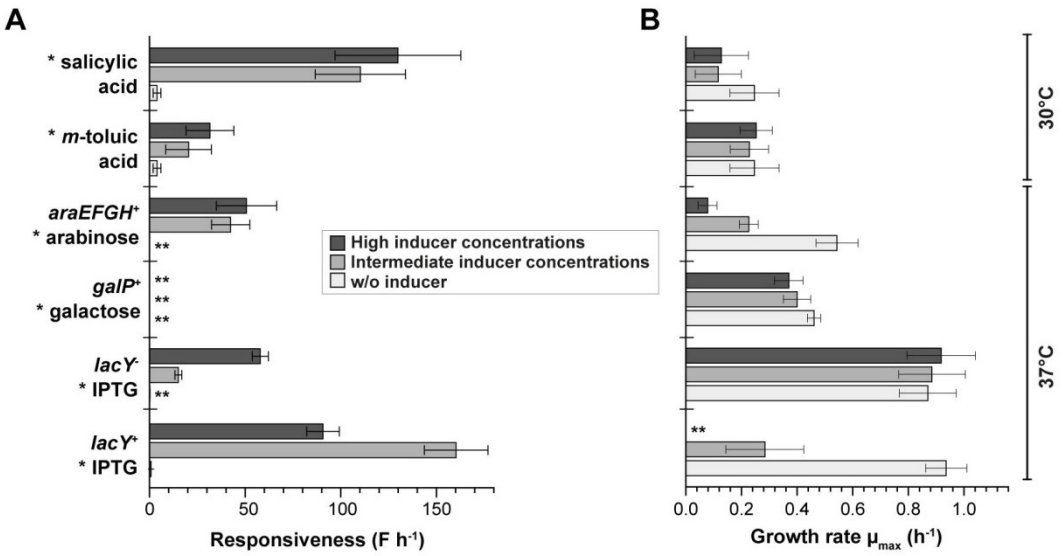

Fig 3. System responsiveness and growth analysis of characterized *E. coli* expression systems. A) Responsiveness was calculated using the initial linear slope of the averaged single-cell fluorescence increase in the first 60 min of cultivation. **B)** For the correlation between cellular growth and the level of induction, growth rates were calculated for at least 10 populations of microfluidic expression cultures without inducer (light grey), as well as with intermediate (grey) and high inducer concentrations (dark grey). Mean and standard deviations derive from 10 individual colonies. Inductors are labeled by asterisks (*). Double asterisks (**) indicate that no calculation was possible.

doi:10.1371/journal.pone.0160711.g003

applied lower cultivation temperature. An intermediate responsiveness of gene expression was observed for IPTG induction with the *lacY*$^-$ system, as well as for arabinose induction and *m*-toluic acid induction. For galactose induction no detectable increase of fluorescence was initially monitored, and only a slight increase occurred over the course of cultivation (S2 Fig).

In addition to the velocity of induction response, the interplay between growth and target gene expression is a key aspect that decisively affects the productivity of a given bioprocess. Here, slowly growing overproducers might fall behind with respect to overall yields due to poor biomass formation. It is thus essential, that production of target proteins does not result in substantial inhibition of cellular growth.

Table 2. System responsiveness, growth interference, basal expression and dynamic range of different *E. coli* expression systems. Values were calculated using fluorescence values obtained during microfluidic cultivation of at least 10 microcolonies. All shown data were obtained from highest values (see Fig 3 and S2 Fig for details and respective maxima).

System	Systems responsiveness [F h^{-1}]	Growth interference** [x-fold reduction]	Basal expression factor	Dynamic range
LacY$^+$ & IPTG	160.3	>> 3.3 *	2.1	63.4
LacY$^-$ & IPTG	57.9	n.d.	1.4	67.0***
galactose	2.3	1.2	1.3	2.3
arabinose	50.7	7.0	1.0	106.6
m-toluic acid	31.6	1.1	8.9	5.4****
salicylic acid	129.9	2.1	8.9	27.2****

* difficult to determine due to complete growth arrest

** calculated from Fig 3B by comparing cultivations without inducer and with high inducer concentrations

*** due to fast growth and thus short cultivation times, expected to significantly increase in long-term setups [14]

**** might be improved by the application of the low background wildtype Pm promoter [6]

doi:10.1371/journal.pone.0160711.t002

Hence, we subsequently evaluated growth of respective expression cultures (Fig 3B) and compared it without inducer as well as using intermediate and high inducer concentrations (see Table 1). Strikingly, tremendous growth interferences were revealed for BL21(DE3) (*lacY*$^+$) when cultures were supplemented with IPTG, which seemed to correlate with the strength of induction since intermediate inducer concentrations already resulted in a 3.3-fold reduction of growth whereas high inducer concentrations almost completely abrogated growth (Table 2). A similarly strong growth impairment was observed for arabinose induction of target gene expression as intermediate and high inducer concentrations decreased growth 2.4- and 7.0-fold, respectively. In contrast, minor effects on cellular growth were observed for galactose (up to 1.2-fold reduction) and salicylic acid induction (up to 2.1-fold reduction), respectively. Remarkably, induction with *m*-toluic acid (up to 1.1 fold reduction) and especially IPTG induction using the *lacY*$^-$ system revealed hardly any interference with growth compared to respective non-inducing conditions (Table 2). Further, growth rates were generally about 3.8-fold decreased for reduced working temperatures of 30°C (μ_{max} = 0.25 ± 0.09 h^{-1}) as compared to cultivations at 37°C (μ_{max} = 0.94 ± 0.07 h^{-1}) (Fig 3B).

Conclusively, analysis of systems responsiveness and cellular growth during microfluidic cultivation revealed that the most rapidly responding expression systems, namely the P_{7lac}/LacI system using the *lacY*$^+$ strain BL21(DE3) as well as the salicylic acid induction system, suffer from a significant growth impairment upon induction. In some production processes this could lead to low overall yields due to poor development of biomass. In this context, moderately responding expression systems, such as the *m*-toluic acid induction system or especially IPTG induction using the *lacY*$^-$ system, may prove beneficial with respect to overall productivity.

In general, the interplay between growth and protein production might even be enlarged for toxic proteins, so that a low background expression activity is highly favorable. In this context, a full inhibition of basal target gene expression in the absence of specific inducers, allowing sufficient biomass formation prior to induction of the protein production process, is an important prerequisite for a robust bacterial expression system.

We thus further calculated basal expression factors as fluorescence ratios of strains harboring respective expression plasmids under non-inducing conditions and corresponding strains without expression plasmid. IPTG induction using the *lacY*$^+$ system was moderately leaky (2.1-fold), whereas IPTG induction with the *lacY*$^-$ system (1.4-fold) as well as galactose induction (1.3-fold) showed a low basal expression. Noteworthy, for those two later systems, a modified expression vector providing elevated amounts of the LacI regulator [14] was applied. In contrast, the here selected promiscuous (XylS R45T) benzoate induction system using the high-level P_{M117} promoter [27] revealed a significantly leaky expression with basal expression factors of up to 8.9 (Table 2). Notably, the wildtype Pm promoter instead of the here applied mutagenized high-level expression variant should offer a reduced leakiness [6]. The tightest promoter observed during microfluidic cultivations was the arabinose inducible P_{BAD} as no basal expression could be detected.

To further evaluate the controllability of expression response, the dynamic range of the expression response was quantified as the ratio of the maximum fluorescence (upon induction) and the basal fluorescence of non-induced cultures. The dynamic range of induction was highest for arabinose induction (up to 107), and remarkable for both IPTG induction in the *lacY*$^+$ system (up to 63) and the *lacY*$^-$ system (up to 67). A moderate dynamic range of gene expression response, was observed for salicylic acid induction (up to 27), whereas *m*-toluic acid (up to five) and especially galactose induction (up to two) showed poor inducibility. The moderate dynamic ranges for the generally (in absolute fluorescence values) well inducible benzoate induction systems, in terms of both expression strength and responsiveness (S2 Fig), mainly emerge from the high basal expression levels. In contrast, galactose induction is slow and extremely weak under

applied conditions. For IPTG induction using the *lacY*$^-$ system it should be further noted that the rapidly responding system exhibits fast growth so that the respective values were calculated after cultivation times of only 3 h. In general, the dynamic range is expected to rise with the course of cultivation in microfluidic setups for long-term cultivations [49,50].

Uncovering expression heterogeneity in selected *E. coli* expression systems

Upon characterization of valuable expression system specification parameters such as responsiveness, effect of protein production on growth, promoter tightness and dynamic range of induction in a bulk single-cell analysis, the focus was subsequently laid on cell-to-cell variations during the expression response within a specific *E. coli* microcolony. To this end, the single-cell fluorescence distributions were comparatively analyzed in ten individual microcolonies for all six expression systems, respectively. Due to a slight fluorescence reduction for high inducer concentrations (S2 Fig), which was likewise observed in literature [26,51], the P_{BAD}/AraC system was analyzed for intermediate inducer concentrations, whereas all other expression systems were analyzed for high inducer concentrations. The results of the fluorescence distribution analyses are shown as a boxplot for a descriptive depiction of the recorded data sets (Fig 4). IPTG induction in the *lacY*$^+$ system led to a high number of cells that significantly deviated from the mean fluorescence (red dotted line) and the coefficient of variation (CV) interval of 25% (grey box), where only 63% of all data fitted in.

For IPTG induction in the *lacY*$^-$ system 83% of all single-cell fluorescence values fell into the 25% CV interval, beyond which merely individual outliers were detected. The fit into the 25% CV interval was even more distinct for galactose induction (98%), yet an overall poor inducibility was detected and a rather separate evaluation might be appropriate. Arabinose induction revealed a moderate fluorescence distribution as the majority of cells exhibited average fluorescence levels (77%). Some colonies, however, significantly deviated from the mean and showed a strikingly increased deviation.

The same is true for *m*-toluic acid induction *via* the Pm/XylS system as medians generally varied inside of the 25% CV interval (79%). For the same Pm/XylS system, salicylic acid induction revealed a much more wide-spread single-cell fluorescence distribution (just 42% lay within the interval). Half of all medians did not fit into the CV interval and antenna indicated distinct variations.

Boxplot diagrams therefore proved as a suitable depiction to describe cell-to-cell differences in the expression response of single-cell cultivations from different *E. coli* expression systems upon induction. Evidently, heterogeneous expression systems showed a significant quantity of cells outside the selected 25% CV interval (grey box).

In a next step, we intended to further classify and rank the expression systems with respect to expression heterogeneity. We thus aimed to identify further quantitative parameters suitable for a conclusive determination of expression homogeneity or heterogeneity, respectively. To this end, we determined the normed coefficient of variation (CV) as well as the number of outliers as significant parameters to visualize and appropriately identify system-inherent cell-to-cell variations. First, the CV was used to roughly assign homogeneity or heterogeneity to the respective expression system. For intermediate inducer concentrations (Fig 5), the *lacY*$^-$ system with IPTG induction revealed the smallest CV observed (9 ± 2%), indicating homogeneity. Similarly low CVs were found for *m*-toluic acid (14 ± 3%) as well as galactose (11 ± 16%) and arabinose induction (18 ± 7%). Significantly higher CVs, and thus a rather heterogeneous expression behavior, were observed for salicylic acid (36 ± 8%) and IPTG induction with the *lacY*$^+$ system (41 ± 11%).

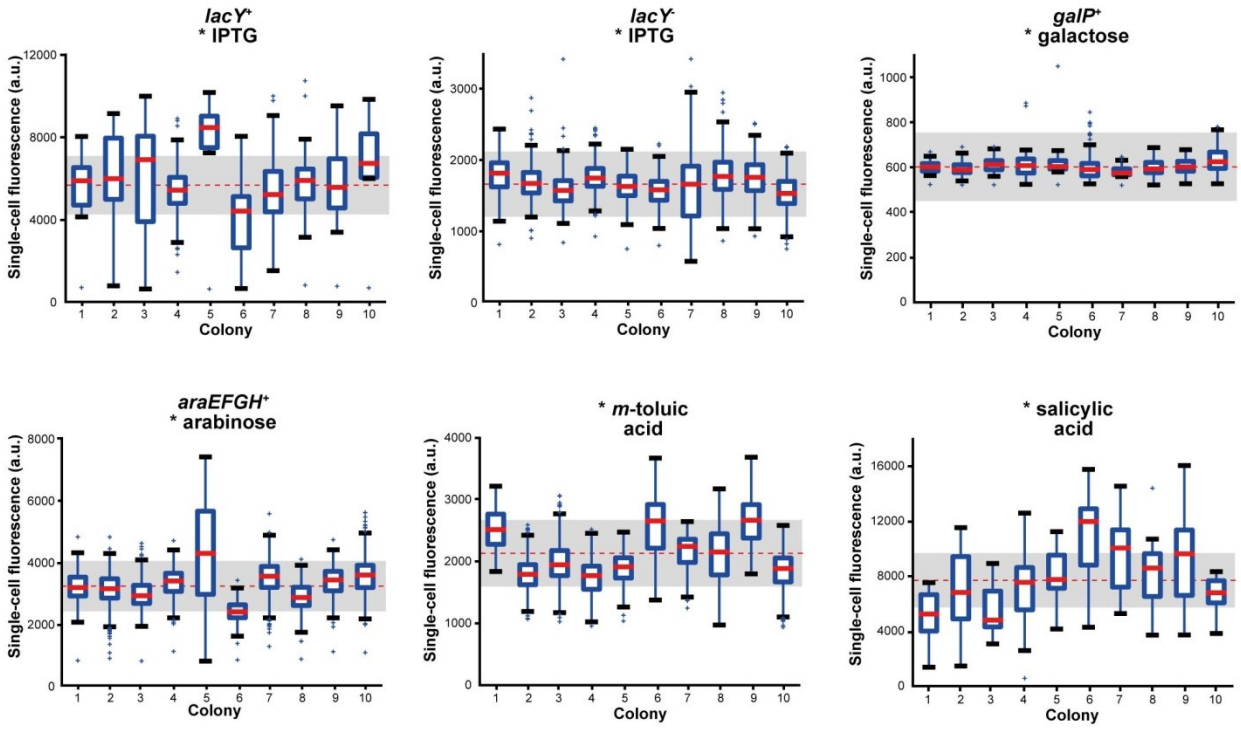

Fig 4. Box plot analysis depicting cell-to-cell variations in gene expression for different optimally induced *E. coli* expression systems. Cell-to-cell fluorescence distributions of optimally induced expression systems are depicted with the total mean (dotted red line) and the spread interval (25% of mean, grey box) for ten individual microcolonies evaluated at the end of each experiment (end point criteria: cultivation chambers fully filled with cells or $\mu_{max} \sim 0$). Exact inducer concentrations for optimal induction were 0.1 mM IPTG (for each system), 1 mM galactose, 1 mM arabinose, 0.1 mM m-toluic acid and 1.5 mM salicylic acid. For each individual colony, medians (bold red line) indicate values above which 50% of cells are located, blue boxes indicate interval into which 50% of fluorescence values fall. Top or bottom of the box show areas, where 25% of cells are located above or below, respectively. Antenna indicate the 1.5-fold interquartile distance (IQR, 1 IQR = box height) or the last data point detected inside the 1.5-fold IQR. Outliers outside of the 1.5-fold IQR were marked as crosses.

doi:10.1371/journal.pone.0160711.g004

For high inducer concentrations (Fig 5), galactose induction showed the lowest CV (7 ± 3%). Due to poor inducibility, however, it is difficult to evaluate the expression heterogeneity appropriately. In contrast, *m*-toluic acid (16 ± 3%) and IPTG induction with the *lacY*$^-$ system (17 ± 5%) showed low CVs together with appropriate inducibility so that their expression responses can be characterized as clearly homogeneous. A rather heterogeneous expression response was observed for arabinose (26 ± 5%) and salicylic acid induction (30 ± 7%), whereas a distinct expression heterogeneity was depicted for IPTG induction using the *lacY*$^+$ system (43 ± 12%).

Outliers exhibited a rather chaotic distribution in the plots and did not follow the expectation that homogeneity would go along with a low number of outliers and heterogeneity in reverse, with a high number of outliers (S5 Fig). Most evident examples were galactose induction, which depicts an increased number of outliers despite a very low CV, or salicylic acid induction, which just sporadically showed outliers despite obvious expression heterogeneity. As no direct correlation between outliers and the CV could be obtained and outliers seemed further specific for some expression systems, the fraction of outliers proved rather unsuited as a criterion for the evaluation of expression heterogeneity. It rather seems that the number of outliers correlated with system-specific rare heterogeneity events such as low inducibility

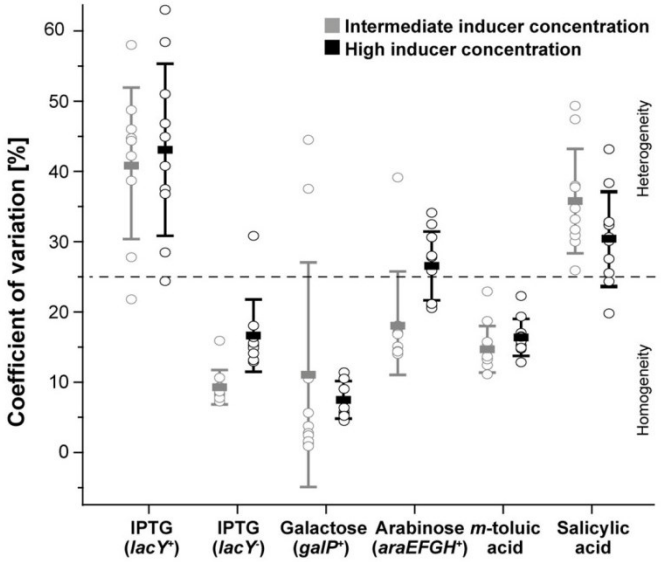

Fig 5. Expression heterogeneity analysis of different *E. coli* expression systems during microfluidic cultivation for intermediate (grey) and high inducer concentrations (black). CVs for ten individual colonies (open circles) are plotted together with the respective overall mean (bold dash) and the corresponding standard deviation. The grey dotted line indicates the threshold for expression heterogeneity (CV > 25%) above which colonies are considered as heterogeneous.

doi:10.1371/journal.pone.0160711.g005

(e.g. for galactose induction) or cellular stress due to high expression levels (e.g. for high inducer concentrations with arabinose and IPTG in the *lacY*$^+$ system).

In this context, however, IPTG induction using the *lacY*$^-$ system as well as *m*-toluic acid induction showed most robust expression performances as they constantly exhibited low CVs and negligible fractions of outliers (bottom left quadrants in S5 Fig) irrespective of the applied inducer concentration. Moreover, for IPTG induction using the *lacY*$^+$ system and for arabinose induction it became evident that the degree of induction influenced the fraction of outliers, as higher inducer concentrations led to increased numbers of outliers (S5 Fig).

Taking into account both visual and statistical analyses of expression heterogeneity, the selected CV (22 ± 5% for all systems on average) threshold of 25% (roughly average plus deviation) seemed appropriate for the characterization of expression homogeneity. For the fraction of outliers (3.4 ± 2.9% on average) more than 6% (roughly average plus deviation) appeared unusual for both homogeneous and heterogeneous expression systems and may be seen as an indicator of lacking systems robustness and of rare cellular events such as spontaneous mutations or rare phenotypes. Therefore, rare phenotypes observed during here conducted microfluidic cultivations were subsequently compiled to provide insights into unusual phenomena during employment of an inducible expression system (Fig 6). Rare heterogeneities of cell phenotypes that were observed during microfluidic cultivations include cell filamentation (Fig 6A), protein aggregation (dark non-fluorescing spots), which is potentially attributed to inclusion body formation (Fig 6B), dormant cells that rest in growth and expression (Fig 6C), single cells that show a high productivity within sparely producing cells (Fig 6D), or sudden cell lysis (Fig 6F).

The phenomenon of overgrowth (Fig 6E) clearly illustrates why phenotypically homogeneous expression systems are crucial for the optimization of synthetic and systems biology as well as biotechnological applications. For growth-interfering overexpression, it becomes

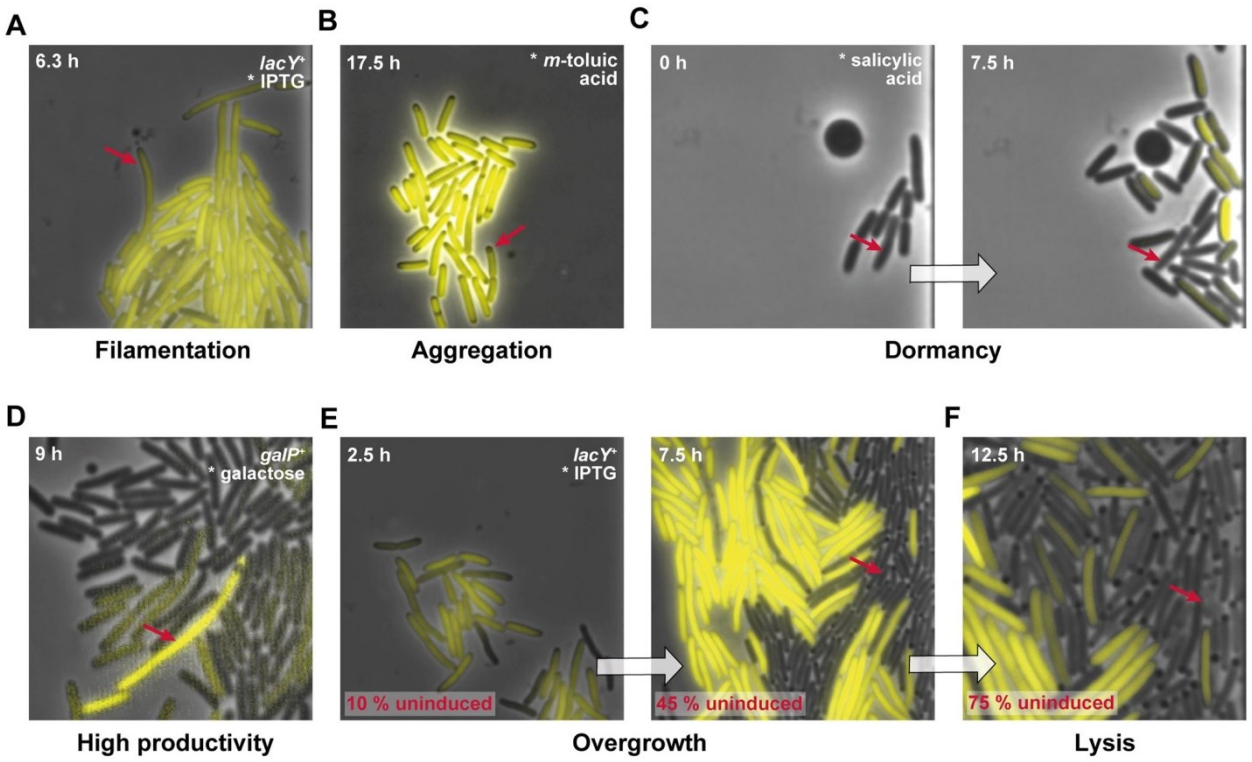

Fig 6. Rare cell-to-cell variation phenomena selected from conducted microfluidic analyses. (A) Filamentous cells that grow but do not divide. (B) Formation of dark spots indicating aggregates in highly producing cells. (C) Dormant cells, which are significantly delayed or irresponsive in growth and expression. (D) Highly producing cells in an otherwise sparely producing population. (E) Overgrowth of slowly—dividing producer cells by rapidly growing non-producers. (F) Cell lysis of stressed overproducer cells or even rapidly growing non-producer cells. Red arrows indicate cells exhibiting the respective phenomena.

doi:10.1371/journal.pone.0160711.g006

apparent that rapidly dividing non-producers can outperform the number of slowly growing producers during the course of cultivation, distinctly reducing overall product yields. This important observation became evident only by applying microfluidic single-cell analysis with its high spatiotemporal resolution. Specifications of all tested *E. coli* expressions systems during microfluidic cultivation are summarized in Table 3.

Table 3. Summary of system specifications of *E. coli* expression systems during microfluidic cultivation.

Inducer (System)	Responsiveness	Strength	Tightness	Working concentration	Growth impairment	Population
IPTG (*lacY*$^+$)	+++	+++	++*	low	very high	heterogeneous
IPTG (*lacY*$^-$)	++	++	+++*	low	very low	homogeneous
Galactose (*galP*$^+$)	-	-	++	high	moderate	n.d.***
Arabinose (*araEFGH*$^+$)	++	++	++*	high	high	partly homogeneous
m-toluic acid	+	++	-**	moderate	very low	homogeneous
Salicylic acid	+++	+++	-**	high	high	heterogeneous

* If leakiness has to be reduced further, glucose supplementation can be applied [25].

** The wildtype P_M Promoter (instead of the P_{M117}) can be applied for reduced basal expression [6].

*** Due to poor inducibility during microfluidic cultivation exact evaluation is impeded.

doi:10.1371/journal.pone.0160711.t003

Discussion

Unraveling phenotypic heterogeneity is a key aspect for the optimization of biotechnological and synthetic biology applications; however, well-defined conditions have to be applied to avoid the influence of environmental heterogeneity on microbial expression setups.

In this study, we demonstrated that cultivation in the synthetic M9CA medium and spatio-temporal microfluidic single-cell analysis provide a constant and homogeneous environment allowing for an extensive comparative analysis of *E. coli* expression systems at the single-cell level. We could identify distinct differences in performance relevant parameters of diverse systems and have uncovered distinct differences in responsiveness, controllability and homogeneity of target gene expression (Table 3). Interestingly, the most commonly applied P_{T7lac}/LacI expression system based on *E. coli* BL21(DE3) clearly exhibited significant deficits with respect to expression homogeneity and growth. Throughout the whole cultivation, significant cell-to-cell variations of target gene expression were observed for both intermediate and high inducer concentrations. A similar system based on the lactose permease LacY-deficient *E. coli* strain Tuner(DE3), however, showed a remarkable homogeneity with regard to both expression and growth. Here, the beneficial features of this strain could be clearly attributed to the absence of LacY as the *lacY*$^+$ system using likewise elevated amounts of LacI depicted similar expression heterogeneity as the original *lacY*$^+$ system (S6 Fig).

In addition, promoter tightness under non-inducing conditions as well as robustness of cellular growth during protein production of this system distinctly outperformed all other monitored expression systems. A favorable performance was also observed for the tested benzoate inducible Pm/XylS system, as *m*-toluic acid induction produced a clearly homogeneous, rapid and strong expression response. The choice of benzoate inducer, however, was crucial for the systems performance as the alternative benzoate inducer salicylic acid evoked an even stronger but also highly heterogeneous target gene expression, which resulted in distinctly impaired cellular growth. Arabinose induction *via* the P_{BAD}/AraC system, in turn, yielded a strong and only partly homogeneous expression response. Growth impairment for high inducer concentrations was relatively high, though. The galactose-inducible *E. coli* expression system was found not to be suited for microfluidic perfusion but well-functioning in batch cultivations (S3 Fig). Thus, inducer uptake might be impeded by the continuous perfusion of inducer supplemented cultivation medium or inducibility might be reduced, in general, by the cells being basically trapped in the exponential growth state, which might for instance interfere with galactose uptake. Here, microfluidic batch cultivations might be an opportunity to unravel system inherent differences with regard to the respective cultivation mode in further detail [52]. To the best of our knowledge, this is the first description of galactose and salicylic acid based induction systems analyzed by microfluidic single-cell cultivation. It has to be noted that systems performances may differ for induction in other media and, in particular, in discontinuous cultivation approaches. This becomes most evident for galactose induction as microfluidically grown cells in the synthetic M9CA medium revealed only poor induction, whereas conventional batch cultivation produced a significant expression response (S3 Fig).

Compared to existing studies using other cultivation media, such as LB [6,14] or minimal medium [21,53], and different single-cell analysis tools, we detected comparable features for our *lac*-based expression setups. Flow cytometric analysis of *lac* expression systems with *lacY*$^+$ [6] and *lacY*$^-$ [21] strains as well as microfluidic cultivations [14] ascribe similar expression characteristics to both variants, with and without the LacY transporter, for IPTG or TMG induction. Interestingly, the overexpression of *lacY* also appears to be a valuable alternative to gene deletion for implementation of homogeneous expression with *lac*-based gene expression circuits [54]. In contrast to the here depicted results, arabinose induction is mostly described in literature as

being heterogeneous [6,48,55]. Here, we found partly homogeneous arabinose induction for the tested arabinose-metabolizing strain *E. coli* Tuner(DE3). Presumably, this homogeneous response is due to the presence of the *araBAD* genes encoding the arabinose metabolizing operon, and the choice of the specific expression host strain resulting in increased arabinose concentrations. For lower arabinose concentrations in *araBAD*-deficient strains, expression is known to be heterogeneous and thus extensive work has been invested to achieve a homogeneous arabinose-induced gene expression response by means of AraE transporter overproduction [55,56], mutagenized LacY transporter variants [57] or novel photocaged arabinose inducers [48]. As complex inducer uptake systems have repeatedly been shown to cause expression heterogeneity [14,55,56], easily membrane-permeable photocaged inducers, that bypass specific uptake systems, enable a more homogeneous expression response [14,48]. As another advantage of photocaged inducers, induction processes might be simplified in handling due to the non-invasive and straightforward applicability of light exposure. Especially, where experimental evaluation of diverse, e.g. temporally variable, induction setups is required, rapid triggering of hundreds of different cultures grown in parallel typically causes labour-intensive effort with conventional inducers. In the future, novel optogenetic methods offer to remedy these efforts, and moreover enable attractive control over single cells with high spatiotemporal resolution [14,48].

Microfluidic single-cell analysis proved to be a powerful tool to unravel limitations of biotechnological production processes on single cell level before [43,45]. This study further corroborates that microfluidics methodology is of utmost importance to fully optimize control over bacterial response circuits for biotechnological production processes or synthetic biology applications. Besides the determination of valuable system-inherent specifications for different *E. coli* expression systems based on single-cell data, the technique enabled us to zoom in to cell-to-cell variations and their development over time, and finally allowed uncovering rare cellular phenotypes.

Gained in-depth insights will inevitably encompass the optimization of recombinant protein production approaches in the future. Here, phenotypically homogeneous expression systems such as the modified *lacY*-deficient P_{T7lac}/LacI as well as the Pm/XylS system with conventional *m*-toluic acid induction might emerge as key players for precise and robust triggering of bacterial gene expression in *E. coli* in a homogeneous fashion.

Supporting Information

S1 Appendix. Supporting methods. Exact LB growth media recipes and quantification of galactose, lactose and glucose.
(PDF)

S1 Fig. Expression responses and growth of *E. coli* BL21(DE3) with (A-C) and without (D) the pRhotHi-2-EYFP expression vector in different complex LB cultivation. (A) Representative micro-colonies, weakly induced (2.5 μM) with IPTG after approximately 4 h of cultivation in four different LB media. (B) Mean fluorescence distribution for the representative microcolonies shown above. Mean values and coefficient of variations are plotted above the bar, indicating the complete spread. (C) Mean fluorescence for ten EYFP-expressing colonies cultivated in the four different media. (D) Comparison of maximum growth rates for non-induced cultivations in the different LB media (grey bars) with growth rates obtained for uninduced cultivation in the novel defined rich medium M9CA (dark grey bars).
(TIF)

S2 Fig. Fluorescence profiles for conducted microfluidic expression setups. Averaged single-cell fluorescence development for at least ten populations cultivated without (blue), as well

as using intermediate (green) and high inducer concentrations. Shaded areas indicate respective standard deviations. The end of the experiment corresponds to the time were cultivation chambers are almost fully loaded or where cells completely stopped growing.
(TIF)

S3 Fig. Bulk fluorescence profiles for batch cultivations of different *E. coli* expression systems. Expression response of the selected expression systems 1–6 (**A-F**) in a BioLector microbioreactor system (m2plabs, Germany) under constant monitoring of biomass accumulation and reporter fluorescence. Indicated fluorescence was biomass-normalized. Expression cultures were inoculated to cell densities corresponding to an optical density of 0.05 at 580 nm. Gene expression was induced when cell cultures reached the logarithmic growth phase (cell density of OD580 ~0.5). Cultures induced with 1 mM arabinose start to consume arabinose, while the are still growing, whereas induction with 2.5 mM arabinose leads to tremendous growth impairment and thus no arabinose consumption was observed during the observation period of 10 h. Expression cultures were performed at least in triplicates. Shaded areas indicate respective standard deviations. a.u.: arbitrary units.
(TIF)

S4 Fig. Time-resolved fluorescence reporter expression patterns of microfluidic cultivations using intermediate and high inducer concentrations. Histograms were plotted using single-cell fluorescence values obtained from representative populations at the initial (blue, $N>8$), intermediary (green, halftime of experiment) and end state (red, $\mu_{max} \sim 0$) of conducted microfluidic cultivation experiments.
(TIF)

S5 Fig. Expression heterogeneity analysis of different *E. coli* expression systems during microfluidic cultivation using (A) intermediate and (B) high inducer concentrations for induction of target gene expression. Percentaged coefficient of variation and fraction of outliers (outside the 1.5-fold IQR) are plotted as potential indicators of expression heterogeneity for ten individual microcolonies. Cross lines reveal respective means and standard deviations. Grey dotted lines show thresholds for expression heterogeneity ($CV > 25\%$) or increased number of rare events (outliers $> 6\%$) selected for the expressions systems at hand. The bottom left quadrant indicates the region of expression robustness and homogeneity.
(TIF)

S6 Fig. Comparison of representative microcolonies from conducted microfluidic analyses, which differ in their *lacY* and *lacI* constitution. $lacY^+$: *E. coli* BL21(DE3), $lacY^-$: *E. coli* Tuner (DE3),—additional LacI: pRhotHi-2 expression vector, + additional LacI: pRhotHi-2-LacI expression vector. The white scale bar corresponds to 10 μm.
(TIF)

S1 Table. Bacterial strains, plasmids and oligonucleotides used in this study.
(PDF)

S2 Table. Quantification of known inducing or repressing carbohydrates in different *E. coli* cultivation media.
(PDF)

Author Contributions

Conceived and designed the experiments: DB CP AG TD.

Performed the experiments: DB CP AG FH.

Analyzed the data: DB CP AG.

Contributed reagents/materials/analysis tools: FH AL KEJ DK.

Wrote the paper: DB CP AG AL KEJ DK TD.

References

1. Veening J-W, Smits WK, Kuipers OP. Bistability, epigenetics, and bet-hedging in bacteria. Annu Rev Microbiol. 2008; 62: 193–210. doi: 10.1146/annurev.micro.62.081307.163002 PMID: 18537474
2. Eldar A, Elowitz MB. Functional roles for noise in genetic circuits. Nature. Nature Publishing Group; 2010; 467: 167–73.
3. Wang Y-H, Wei KY, Smolke CD. Synthetic Biology: Advancing the Design of Diverse Genetic Systems. Annu Rev Chem Biomol Eng. 2013; 69–102. doi: 10.1146/annurev-chembioeng-061312-103351 PMID: 23413816
4. Sleight SC, Bartley BA, Lieviant JA, Sauro HM. Designing and engineering evolutionary robust genetic circuits. J Biol Eng. 2010; 4: 12. doi: 10.1186/1754-1611-4-12 PMID: 21040586
5. Terpe K. Overview of bacterial expression systems for heterologous protein production: from molecular and biochemical fundamentals to commercial systems. Appl Microbiol Biotechnol. 2006; 72: 211–22. PMID: 16791589
6. Balzer S, Kucharova V, Megerle J, Lale R, Brautaset T, Valla S. A comparative analysis of the properties of regulated promoter systems commonly used for recombinant gene expression in *Escherichia coli*. Microb Cell Fact. 2013; 12: 26. doi: 10.1186/1475-2859-12-26 PMID: 23506076
7. Brautaset T, Lale R, Valla S. Positively regulated bacterial expression systems. Microb Biotechnol. 2009; 2: 15–30. doi: 10.1111/j.1751-7915.2008.00048.x PMID: 21261879
8. Rosano GL, Ceccarelli EA. Recombinant protein expression in *Escherichia coli*: advances and challenges. Front Microbiol. 2014; 5: 172. doi: 10.3389/fmicb.2014.00172 PMID: 24860555
9. Samuelson JC. Recent developments in difficult protein expression: a guide to *E. coli* strains, promoters, and relevant host mutations. In: Evans TC, Xu M-Q, editors. Methods in molecular biology. 1st ed. Totowa, NJ: Humana Press; 2011. pp. 195–209.
10. Gräslund S, Nordlund P, Weigelt J, Hallberg BM, Bray J, Gileadi O, et al. Protein production and purification. Nat Methods. 2008; 5: 135–46. doi: 10.1038/nmeth.f.202 PMID: 18235434
11. Studier FW, Moffatt BA. Use of bacteriophage T7 RNA polymerase to direct selective high-level expression of cloned genes. J Mol Biol. 1986; 189: 113–30. PMID: 3537305
12. Wagner S, Klepsch MM, Schlegel S, Appel A, Draheim R, Tarry M, et al. Tuning *Escherichia coli* for membrane protein overexpression. Proc Natl Acad Sci U S A. 2008; 105: 14371–6. doi: 10.1073/pnas.0804090105 PMID: 18796603
13. Dumon-Seignovert L, Cariot G, Vuillard L. The toxicity of recombinant proteins in *Escherichia coli*: a comparison of overexpression in BL21(DE3), C41(DE3), and C43(DE3). Protein Expr Purif. 2004; 37: 203–6. PMID: 15294299
14. Binder D, Grünberger A, Loeschcke A, Probst C, Bier C, Pietruszka J, et al. Light-responsive control of bacterial gene expression: precise triggering of the *lac* promoter activity using photocaged IPTG. Integr Biol (Camb). 2014; 6: 755–65.
15. Iost I, Guillerez J, Dreyfus M. Bacteriophage T7 RNA polymerase travels far ahead of ribosomes in vivo. J Bacteriol. 1992; 174: 619–22. PMID: 1729251
16. Lewis M, Chang G, Horton NC, Kercher MA, Pace HC, Schumacher MA, et al. Crystal structure of the lactose operon repressor and its complexes with DNA and inducer. Science. 1996; 271: 1247–54. PMID: 8638105
17. Daber R, Stayrook S, Rosenberg A, Lewis M. Structural analysis of *lac* repressor bound to allosteric effectors. J Mol Biol. 2007; 370: 609–19. PMID: 17543986
18. Jacob F, Monod J. Genetic regulatory mechanisms in the synthesis of proteins. J Mol Biol. 1961; 3: 318–56. PMID: 13718526
19. Xu J, Banerjee A, Pan S-H, Li ZJ. Galactose can be an inducer for production of therapeutic proteins by auto-induction using *E. coli* BL21 strains. Protein Expr Purif. 2012; 83: 30–6. doi: 10.1016/j.pep.2012.02.014 PMID: 22425658

20. Ozbudak EM, Thattai M, Lim HN, Shraiman BI, Van Oudenaarden A. Multistability in the lactose utilization network of *Escherichia coli*. Nature. 2004; 427: 737–40. PMID: 14973486

21. Marbach A, Bettenbrock K. *lac* operon induction in *Escherichia coli*: Systematic comparison of IPTG and TMG induction and influence of the transacetylase LacA. J Biotechnol.; 2012; 157: 82–8. doi: 10.1016/j.jbiotec.2011.10.009 PMID: 22079752

22. Guan L, Kaback HR. Lessons from lactose permease. Annu Rev Biophys Biomol Struct. 2006; 35: 67–91. PMID: 16689628

23. Henderson PJ, Giddens RA, Jones-Mortimer MC. Transport of galactose, glucose and their molecular analogues by *Escherichia coli* K12. Biochem J. 1977; 162: 309–20. PMID: 15558

24. Fernández-Castané A, Vine CE, Caminal G, López-Santín J. Evidencing the role of lactose permease in IPTG uptake by *Escherichia coli* in fed-batch high cell density cultures. J Biotechnol.; 2012; 157: 391–8. doi: 10.1016/j.jbiotec.2011.12.007 PMID: 22202176

25. Guzman LM, Belin D, Carson MJ, Beckwith J. Tight regulation, modulation, and high-level expression by vectors containing the arabinose PBAD promoter. J Bacteriol. 1995; 177: 4121–30. PMID: 7608087

26. Fritz G, Megerle JA, Westermayer SA, Brick D, Heermann R, Jung K, et al. Single cell kinetics of phenotypic switching in the arabinose utilization system of *E. coli*. PLoS One. 2014; 9: e89532. doi: 10.1371/journal.pone.0089532 PMID: 24586851

27. Bakke I, Berg L, Aune TEV, Brautaset T, Sletta H, Tøndervik A, et al. Random mutagenesis of the PM promoter as a powerful strategy for improvement of recombinant-gene expression. Appl Environ Microbiol. 2009; 75: 2002–11. doi: 10.1128/AEM.02315-08 PMID: 19201973

28. Ramos JL, Stolz A, Reineke W, Timmis KN. Altered effector specificities in regulators of gene expression: TOL plasmid xylS mutants and their use to engineer expansion of the range of aromatics degraded by bacteria. Proc Natl Acad Sci USA. 1986; 83: 8467–71. PMID: 3022293

29. Ramos JL, Marqués S, Timmis KN. Transcriptional control of the Pseudomonas TOL plasmid catabolic operons is achieved through an interplay of host factors and plasmid-encoded regulators. Annu Rev Microbiol. 1997; 51: 341–73. PMID: 9343354

30. Lee SK, Keasling JD. A propionate-inducible expression system for enteric bacteria. Appl Environ Microbiol. 2005; 71: 6856–62. PMID: 16269719

31. Lee SK, Keasling JD. Effect of glucose or glycerol as the sole carbon source on gene expression from the Salmonella prpBCDE promoter in *Escherichia coli*. Biotechnol Prog. 2006; 22: 1547–51. PMID: 17137300

32. Haldimann A, Daniels LL, Wanner BL. Use of new methods for construction of tightly regulated arabinose and rhamnose promoter fusions in studies of the *Escherichia coli* phosphate regulon. J Bacteriol. 1998; 180: 1277–86. PMID: 9495769

33. Skerra A. Use of the tetracycline promoter for the tightly regulated production of a murine antibody fragment in *Escherichia coli*. Gene. 1994; 151: 131–5. PMID: 7828861

34. Grünberger A, Paczia N, Probst C, Schendzielorz G, Eggeling L, Noack S, et al. A disposable picolitre bioreactor for cultivation and investigation of industrially relevant bacteria on the single cell level. Lab Chip. 2012; 12: 2060–8. doi: 10.1039/c2lc40156h PMID: 22511122

35. Gruenberger A, Probst C, Heyer A, Wiechert W, Frunzke J, Kohlheyer D. Microfluidic picoliter bioreactor for microbial single-cell analysis: fabrication, system setup, and operation. J Vis Exp. 2013; (82:): e50560.

36. Grünberger A, Probst C, Helfrich S, Nanda A, Stute B, Wiechert W, et al. Spatiotemporal microbial single-cell analysis using a high-throughput microfluidics cultivation platform. Cytometry A. 2015; 87: 1101–15. doi: 10.1002/cyto.a.22779 PMID: 26348020

37. Schneider CA, Rasband WS, Eliceiri KW. NIH Image to ImageJ: 25 years of image analysis. Nat Methods. 2012; 9: 671–5. PMID: 22930834

38. Grünberger A, van Ooyen J, Paczia N, Rohe P, Schiendzielorz G, Eggeling L, et al. Beyond growth rate 0.6: *Corynebacterium glutamicum* cultivated in highly diluted environments. Biotechnol Bioeng. 2013; 110: 220–8. doi: 10.1002/bit.24616 PMID: 22890752

39. Dusny C, Grünberger A, Probst C, Wiechert W, Kohlheyer D, Schmid A. Technical bias of microcultivation environments on single-cell physiology. Lab Chip. 2015; 15: 1822–34. doi: 10.1039/c4lc01270d PMID: 25710324

40. Sambrook J, Fritsch EF, Maniatis T. Molecular cloning: a laboratory manual. 2 nd. New York City, USA: Cold Spring Harbor Laboratory Press; 1989.

41. Ramos JL, Michan C, Rojo F, Dwyer D, Timmis K. Signal-regulator interactions. Genetic analysis of the effector binding site of xylS, the benzoate-activated positive regulator of *Pseudomonas* TOL plasmid meta-cleavage pathway operon. J Mol Biol. 1990; 211: 373–82. PMID: 2407853

42. Urban A, Neukirchen S, Jaeger KE. A rapid and efficient method for site-directed mutagenesis using one-step overlap extension PCR. Nucleic Acids Res. 1997; 25: 2227–8. PMID: 9153325

43. Grünberger A, Wiechert W, Kohlheyer D. Single-cell microfluidics: opportunity for bioprocess development. Curr Opin Biotechnol. 2014; 29: 15–23. doi: 10.1016/j.copbio.2014.02.008 PMID: 24642389

44. Saïda F, Uzan M, Odaert B, Bontems F. Expression of highly toxic genes in *E. coli*: special strategies and genetic tools. Curr Protein Pept Sci. 2006; 7: 47–56. PMID: 16472168

45. Mustafi N, Grünberger A, Mahr R, Helfrich S, Nöh K, Blombach B, et al. Application of a Genetically Encoded Biosensor for Live Cell Imaging of L-Valine Production in Pyruvate Dehydrogenase Complex-Deficient *Corynebacterium glutamicum* Strains. PLoS One. 2014; 9: e85731. doi: 10.1371/journal.pone.0085731 PMID: 24465669

46. Diederichs S, Korona A, Staaden A, Kroutil W, Honda K, Ohtake H, et al. Phenotyping the quality of complex medium components by simple online-monitored shake flask experiments. Microb Cell Fact. 2014; 13: 149. doi: 10.1186/s12934-014-0149-5 PMID: 25376163

47. Katzke N, Arvani S, Bergmann R, Circolone F, Markert A, Svensson V, et al. A novel T7 RNA polymerase dependent expression system for high-level protein production in the phototrophic bacterium *Rhodobacter capsulatus*. Protein Expr Purif. 2010; 69: 137–46. doi: 10.1016/j.pep.2009.08.008 PMID: 19706327

48. Binder D, Bier C, Grünberger A, Drobietz D, Hage-Hülsmann J, Wandrey G, et al. Photocaged Arabinose—A Novel Optogenetic Switch for Rapid and Gradual Control of Microbial Gene Expression. Chembiochem. 2016; 17: 296–299. doi: 10.1002/cbic.201500609 PMID: 26677142

49. Ullman G, Wallden M, Marklund EG, Mahmutovic A, Razinkov I, Elf J. High-throughput gene expression analysis at the level of single proteins using a microfluidic turbidostat and automated cell tracking. Philos Trans R Soc Lond B Biol Sci. 2013; 368: 20120025. doi: 10.1098/rstb.2012.0025 PMID: 23267179

50. Mather W, Mondragón-Palomino O, Danino T, Hasty J, Tsimring LS. Streaming instability in growing cell populations. Phys Rev Lett. 2010; 104: 208101. PMID: 20867071

51. Lee SK, Chou HH, Pfleger BF, Newman JD, Yoshikuni Y, Keasling JD. Directed evolution of AraC for improved compatibility of arabinose- and lactose-inducible promoters. Appl Environ Microbiol. 2007; 73: 5711–5. PMID: 17644634

52. Dai J, Yoon SH, Sim HY, Yang YS, Oh TK, Kim JF, et al. Charting microbial phenotypes in multiplex nanoliter batch bioreactors. Anal Chem. 2013; 85: 5892–9. doi: 10.1021/ac400648z PMID: 23581968

53. Robert L, Paul G, Chen Y, Taddei F, Baigl D, Lindner AB. Pre-dispositions and epigenetic inheritance in the *Escherichia coli* lactose operon bistable switch. Mol Syst Biol. 2010; 6: 1–12.

54. Khlebnikov A, Keasling JD. Effect of *lacY* expression on homogeneity of induction from the P(tac) and P(trc) promoters by natural and synthetic inducers. Biotechnol Prog. 2002; 18: 672–4. doi: 10.1021/bp010141k PMID: 12052093

55. Khlebnikov A, Risa O, Skaug T, Carrier TA, Keasling JD. Regulatable arabinose-inducible gene expression system with consistent control in all cells of a culture. J Bacteriol. 2000; 182: 7029–34. PMID: 11092865

56. Khlebnikov A, Datsenko KA, Skaug T, Wanner BL, Keasling JD. Homogeneous expression of the P(BAD) promoter in *Escherichia coli* by constitutive expression of the low-affinity high-capacity AraE transporter. Microbiology. 2001; 147: 3241–7. PMID: 11739756

57. Morgan-Kiss RM, Wadler C, Cronan JE. Long-term and homogeneous regulation of the *Escherichia coli* araBAD promoter by use of a lactose transporter of relaxed specificity. Proc Natl Acad Sci USA. 2002; 99: 7373–7. PMID: 12032290

II.2 Tuning single-cell expression responses towards homogeneity

II.2.1 Analysis and engineering of phenotypic heterogeneity

Homogenizing bacterial cell factories: Analysis and engineering of phenotypic heterogeneity

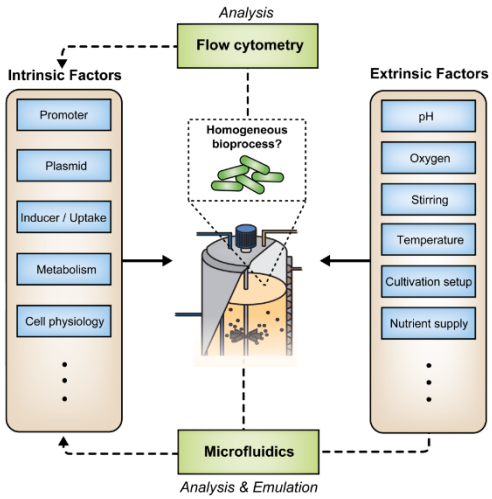

Dennis Binder, Thomas Drepper Karl-Erich Jaeger, Frank Delvigne, Wolfgang Wiechert, Dietrich Kohlheyer and Alexander Grünberger

Metab Eng. 2017*;* 42:145–156.

The full online version may be found at:
https://doi.org/10.1016/j.ymben.2017.06.009.

Metabolic Engineering 42 (2017) 145–156

Contents lists available at ScienceDirect

Metabolic Engineering

journal homepage: www.elsevier.com/locate/meteng

Homogenizing bacterial cell factories: Analysis and engineering of phenotypic heterogeneity

Dennis Binder[a,*], Thomas Drepper[a], Karl-Erich Jaeger[a,b], Frank Delvigne[c], Wolfgang Wiechert[b,d], Dietrich Kohlheyer[b,e], Alexander Grünberger[b,f,**]

[a] Institute of Molecular Enzyme Technology, Heinrich-Heine-University Düsseldorf, Forschungszentrum Jülich, 52425 Jülich, Germany
[b] Institute of Bio- and Geosciences, IBG-1: Biotechnology, Forschungszentrum Jülich, 52425 Jülich, Germany
[c] University of Liege, Gembloux Agro-Biotech, 5030 Gembloux, Belgium
[d] RWTH Aachen University – Computational Systems Biotechnology (AVT.CSB) – 52074 Aachen, Germany
[e] RWTH Aachen University – Microscale Bioengineering (AVT.MSB) – 52074 Aachen, Germany
[f] Multiscale Bioengineering, Bielefeld University, Universitätsstr. 25, Bielefeld 33615, Germany

A B S T R A C T

In natural habitats, microbes form multispecies communities that commonly face rapidly changing and highly competitive environments. Thus, phenotypic heterogeneity has evolved as an innate and important survival strategy to gain an overall fitness advantage over cohabiting competitors. However, in defined artificial environments such as monocultures in small- to large-scale bioreactors, cell-to-cell variations are presumed to cause reduced production yields as well as process instability. Hence, engineering microbial production toward phenotypic homogeneity is a highly promising approach for synthetic biology and bioprocess optimization.

In this review, we discuss recent studies that have unraveled the cell-to-cell heterogeneity observed during bacterial gene expression and metabolite production as well as the molecular mechanisms involved. In addition, current single-cell technologies are briefly reviewed with respect to their applicability in exploring cell-to-cell variations. We highlight emerging strategies and tools to reduce phenotypic heterogeneity in biotechnological expression setups. Here, strain or inducer modifications are combined with cell physiology manipulations to achieve the ultimate goal of equalizing bacterial populations. In this way, the majority of cells can be forced into high productivity, thus reducing less productive subpopulations that tend to consume valuable resources during production. Modifications in uptake systems, inducer molecules or nutrients represent valuable tools for diminishing heterogeneity.

Finally, we address the challenge of transferring homogeneously responding cells into large-scale bioprocesses. Environmental heterogeneity originating from extrinsic factors such as stirring speed and pH, oxygen, temperature or nutrient distribution can significantly influence cellular physiology. We conclude that engineering microbial populations toward phenotypic homogeneity is an increasingly important task to take biotechnological productions to the next level of control.

1. Introduction

Isogenic populations display tremendous phenotypic heterogeneity to cope with rapidly changing environments (Acar et al., 2008; Kussell and Leibler, 2005; Smits et al., 2006; Veening et al., 2008a). Hence, stochastic fluctuations (i.e., regulatory noise) in regulatory circuits have evolved to control key cellular functions such as gene expression (Eldar and Elowitz, 2010; Ozbudak et al., 2002), growth (Kiviet et al., 2014; Martins and Locke, 2015), lysogeny (Frunzke et al., 2008; Nanda et al., 2015) and sporulation (De Jong et al., 2010; Veening et al., 2009). In this way, a certain species can produce populations with multiple phenotypes with respect to metabolism, expression and growth to achieve the ultimate goal of survival in a naturally multispecies and competitive environment (Eldar and Elowitz, 2010; Lidstrom and Konopka, 2010). Vitally, population heterogeneity simply provides a basis to adaptively respond to unpredictable changes in natural habitats. This form of risk spreading, which is commonly termed bet-hedging, characterizes the phenomenon whereby diversified phenotypes bear no apparent instantaneous benefit, yet provide a significant long-term fitness advantage for the respective species during temporally

* Corresponding author.
** Corresponding author at: Multiscale Bioengineering, Bielefeld University, Universitätsstr. 25, Bielefeld 33615, Germany.
E-mail addresses: dennis.binder@uni-duesseldorf.de (D. Binder), alexander.gruenberger@uni-bielefeld.de (A. Grünberger).

http://dx.doi.org/10.1016/j.ymben.2017.06.009
Received 2 March 2017; Received in revised form 2 June 2017; Accepted 18 June 2017
Available online 20 June 2017

variable conditions (Grimbergen et al., 2015; Stewart and Cookson, 2012; Veening et al., 2008a, 2008b). Moreover, differential gene expression patterns may favor a division of labor strategy to cope with complex tasks in specific environments (Healey et al., 2016; Martins and Locke, 2015; Stewart and Cookson, 2012). Furthermore, phenotypic heterogeneity, in terms of metabolically inactive subpopulations, has been shown to be beneficial in promoting survival in conditions of cellular stress. Metabolically inactive persister cells successfully enduring antibiotic treatments represent prominent examples of this persistence strategy (Allison et al., 2011; Amato and Brynildsen, 2015; Balaban et al., 2004).

In summary, phenotypic cell-to-cell variation is an innate and ultimate bacterial survival strategy in natural microbial populations to tackle suddenly changing environmental conditions in a flexible and robust fashion, thus strongly increasing their overall fitness. However, in artificial habitats such as simplified monoculture bioprocesses, interspecies competition and rapidly changing environments are minimized compared to those in natural habitats. For most artificial bioprocesses, the ultimate goal is to achieve precise control over the respective process of interest in a predictable and robust fashion. Consequently, in synthetic biology and biotechnology, homogeneous populations are favored to promote an increased degree of process stability, predictability and precise control over the balance between growth and production (Grünberger et al., 2014). As multiple phenotypes are under suspicion for lowered yields and a cause of the low robustness of bioprocesses, the aims of uncovering and diminishing phenotypic heterogeneity have gained increasing interest (Delvigne and Goffin, 2014). In the investigation of phenotypic heterogeneity in isogenic populations, different types of populations may be observed that are presumed to show a diversified impact on productivity (Huang, 2009). Most obvious phenotypic heterogeneity that is subsequently described as macro-heterogeneity depicts a multi-modal distribution behavior. Furthermore, uni-modal distributions that feature a rather broad-spread production behavior with one common maximum can be denoted as micro-heterogeneity (Fig. 1**A, left**). Thus, uni-modality does not suffice as a suited criterion to describe homogeneous productions. To distinguish between micro-heterogeneity and homogeneity and also between homo- and heterogeneity in general, heterogeneity indices based on statistical analysis are required. One such parameter that is frequently calculated for quantifying heterogeneity is the coefficient of variation (CV). For a set of inducible *E. coli* expression systems a (CV) threshold level of 25% was recently used to distinguish between phenotypic homo- and heterogeneity (Binder et al., 2016c). Similarly, Vasdekis *et al.* used a robust coefficient of variation to determine phenotypic diversity fairly neglecting outlier cells that are commonly included during single-cell analysis (Vasdekis et al., 2015). Furthermore, totally different statistic approaches such as Kolmogorov-Smirnov-based non-normality and quadratic entropy were suggested in another context to be highly appropriate for the description of phenotypic heterogeneity (Gough et al., 2014). A sharp separation of those three phenotypic states, however, might further depend on the conducted single-cell analysis approach since e.g. extra-large cells are not captured and some measurements are too insensitive to detect weak fluorescences in small bacterial cells. Moreover, it appears difficult to compare cell-to-cell variations with significantly different expression levels since expression noise is usually decreasing with elevated expression levels according to the scaling law (Baert et al., 2015).

In contrast to macro- and micro-heterogeneous populations, a homogeneous population exhibits a single bell-shaped distribution of cells with equal production levels and a narrow spread, thus exhibiting minor deviations from the population average (Fig. 1**A, right**). Although all three types of single-cell distribution profiles may lead to exactly the same production average within a population, single-cell productivities and their impact on overall productivity can be highly dissimilar (Fig. 1**B**).

Whereas both macro- and micro-heterogeneous distribution profiles consist of low- and high-producing cells, the production behavior in homogeneous populations is uniform, with significantly smaller deviations (Fig. 1**B, right**). Besides homogeneous populations that solely consist of high-producing cells, it may be further crucial to create intermediate or rather well-adjustable homogeneous expression responses if toxic or difficult-to-express proteins come into play (Medema et al., 2011; Rosano and Ceccarelli, 2014; Saïda et al., 2006). Here, a precise and homogeneous adjustment is supposed to be key for toxic gene products or complex metabolic pathways; and “cheater cells”, whose production is too low, too high or simply not in-time, would significantly hamper overall productivity. Furthermore, production heterogeneity is a significant impediment for bioprocesses, whereby a tight interconnection between growth and production exists and rapidly dividing non-producers tend to overgrow slower-growing producer cells. Currently, it is hypothesized that the overall productivity of bioprocesses can be optimized if cells are forced into a homogeneous production state with high or rather optimally adjusted productivity, in contrast to populations consisting of cells in producing and non-producing states.

Thus, unraveling and diminishing phenotypic heterogeneity have emerged as key aspects in bioprocess optimization and are of the utmost relevance for critical and complex productions, wherein fine adjustments of gene expression levels in time and magnitude are essential.

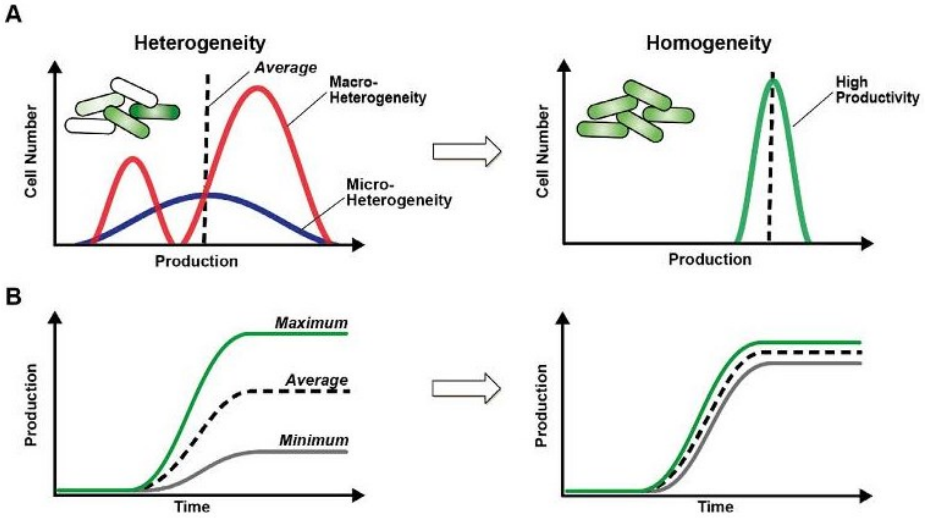

Fig. 1. Types of phenotypic heterogeneity and their impact on productivity. A) Obvious and multi-modal macro-heterogeneity manifests in clearly different phenotypes. Less obvious micro-heterogeneity exhibits no clear phenotypes and is characterized by large deviations from the mean value. Homogeneity, by contrast, features a unimodal response with significantly lower deviations from the mean value. **B**) In heterogeneous populations, diverse cellular production levels are obtained, whereby average values might not reflect single-cell productivities, especially in the case of macro-heterogeneity. In homogeneous populations, single-cell productivities show only small deviations from the average. Here, a higher level of control over single-cell productivity is assumed, which might be essential for toxic gene products or complex metabolic pathways in particular.

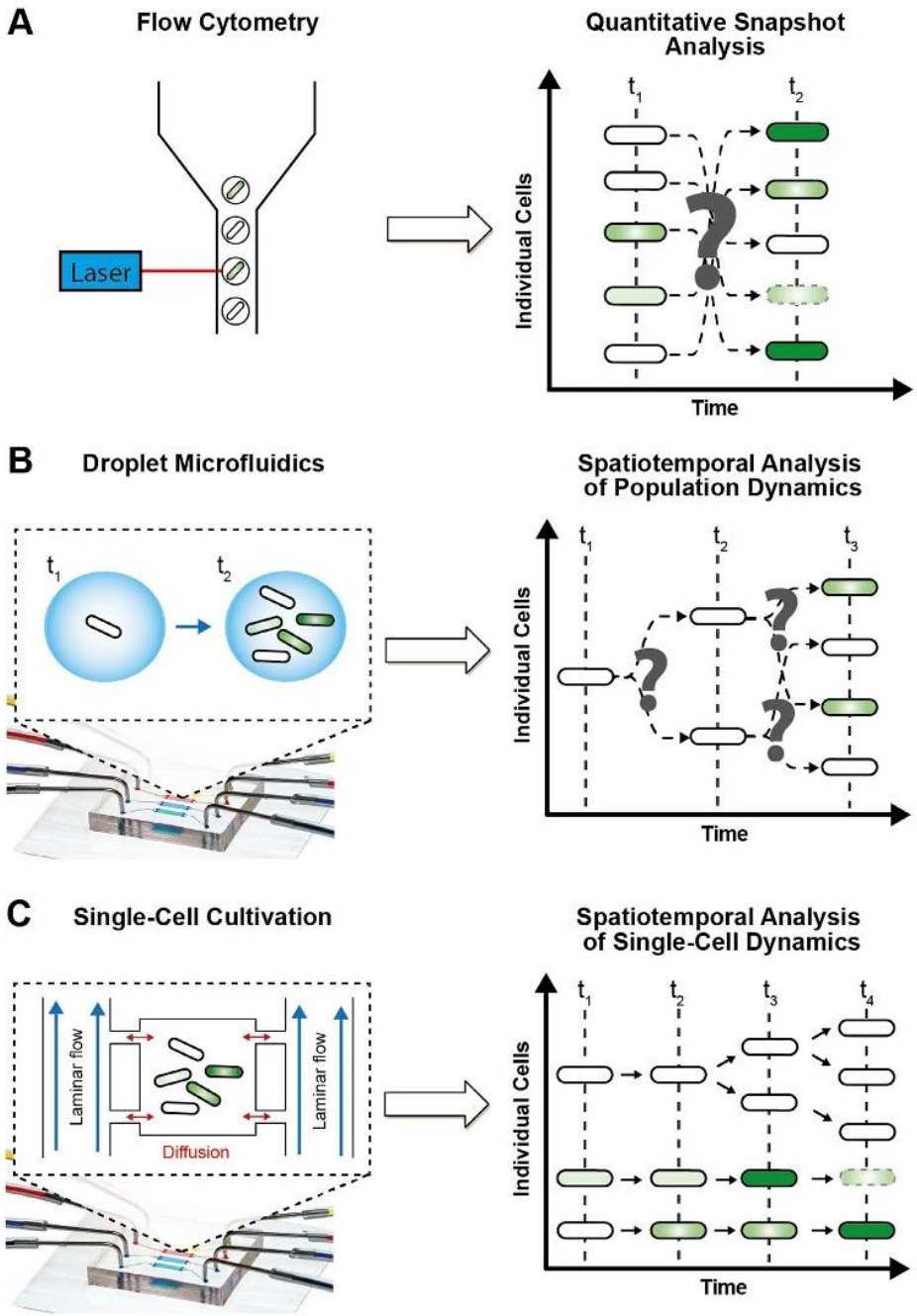

Fig. 2. Application of quantitative flow cytometric and spatiotemporal microfluidic single-cell analysis for the investigation of phenotypic heterogeneity. A) Snapshot-like flow cytometric analysis enables reliable and high-throughput analyses of millions of cells in a highly representative manner. B) Sub-population analysis of isogenic bacterial colonies in microfluidic droplet systems. C) Spatiotemporal microfluidic analysis enables a more detailed and time-resolved investigation of both growth and expression using only a few thousand cells under well-defined environmental conditions.

1.1. Investigation of phenotypic heterogeneity

Flow cytometric (FC) analyses (Fig. 2**A, left**) are frequently employed to investigate millions of cells in an appropriate amount of time (Delvigne and Goffin, 2014; Müller and Nebe-von-Caron, 2010; Neumeyer et al., 2013) with respect to phenotypic heterogeneity. The obtained data reveal a highly representative picture of the process at a given time point. Temporal analysis can be accomplished as a snapshot-like accumulation of broad data sets. In this manner, however, solely the presence or absence of heterogeneity is indicated rather than the real dynamic behavior of phenotypic heterogeneity, including mother-daughter cell correlations and information regarding how single cells behave over time (Fig. 2**A, right**). Despite emerging staining technologies to unravel population dynamics (Müller and Nebe-von-Caron, 2010; Neumeyer et al., 2013), FC analysis appears less straightforward than microfluidics especially when it comes to growth analysis. For instance, it is difficult to perform detailed lineage analysis, to cross-link cellular functions detected with invasive staining methods or to detect filamentous growth. One alternative method to FC are droplet microfluidic methods (Fig. 2**B**). These allow cultivating small populations based on single cells and provide insights into the behavior of different subpopulations over time. Detailed insights into single-cell dynamics are limited. Although these systems are ideal for screening studies (Jang et al., 2016; Lino et al., 2013), due to their "batch-like" behavior, environmental conditions are difficult to control and thus the inherent phenotypical heterogeneity at an defined extracellular environment is unmasked. These challenges were strikingly tackled in recent years using spatiotemporal microfluidic single-cell analysis (Grünberger

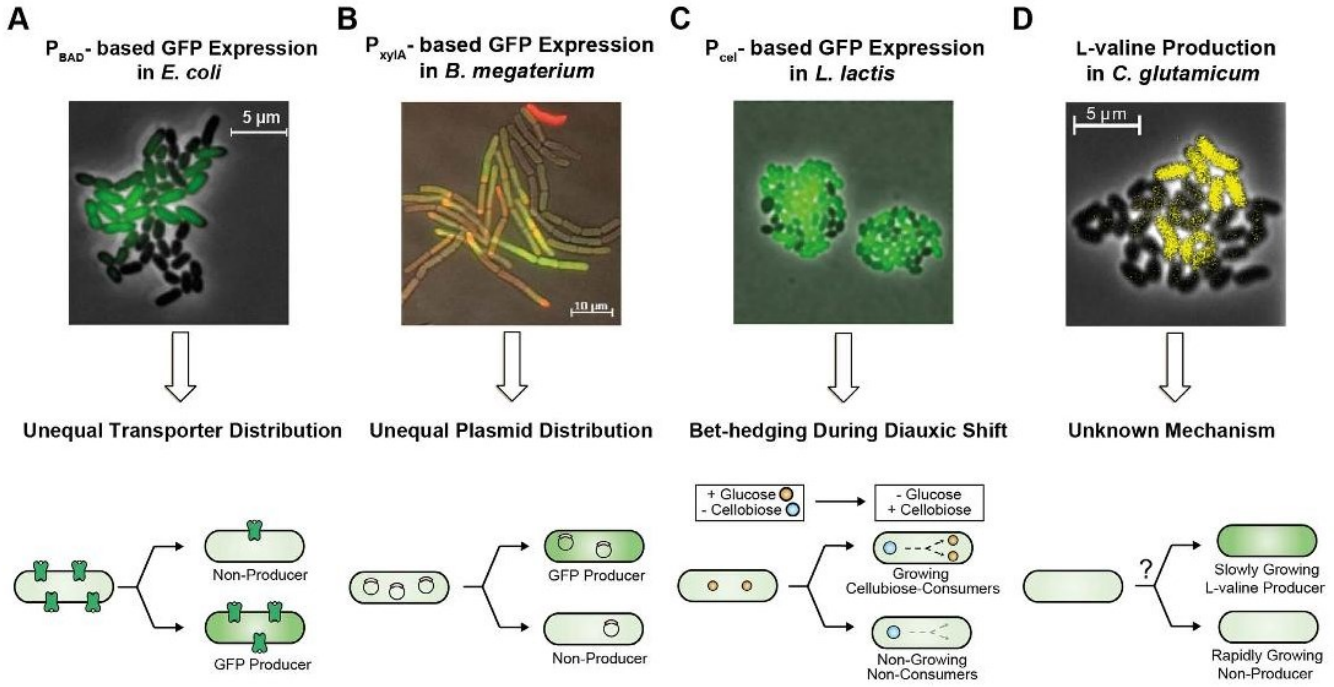

Fig. 3. Phenotypic heterogeneity in different bacterial production hosts. A) Phenotypic GFP expression heterogeneity upon L-arabinose induction in *E. coli* using the P_{BAD}/AraC system. Adapted and reproduced with permission from Ref. (Binder et al., 2016a). Cell-to-cell variations are evoked by the unequal distribution of the complex AraEFGH transport system. **B**) GFP-producing *B. megaterium* cells. Adapted and reproduced with permission from Ref. (Münch et al., 2015). Due to the asymmetric distribution of plasmids and thus polar localization of XylR-mCherry (red)/plasmid complexes, cell division yields daughter cells with varying plasmid accumulation and thus varying GFP levels. **C**) A diauxic shift from glucose to cellobiose produces a heterogeneous population of cellobiose-consuming and non-consuming cells. Adapted and reproduced with permission from Ref. (Solopova et al., 2014). Here, stochastic fluctuations of cellobiose-metabolizing enzymes appear to result in a bet-hedging strategy. **D**) Biosensor-based monitoring of L-valine production in *C. glutamicum* reveals phenotypic heterogeneity with slowly growing producers and rapidly growing non-producers. Adapted and reproduced with permission from Ref. (Mustafi et al., 2014). Here, the mechanisms involved in biological heterogeneity are not yet understood.

et al., 2015, 2014) (Fig. 2**C**). Using this technique, a detailed time-resolved investigation of thousands of cells concerning both growth and expression can provide in-depth knowledge of the dynamics of phenotypic heterogeneity, e.g., in the form of lineage trees (Helfrich et al., 2015). In contrast to FC analysis, conventional microfluidic perfusion cultivation has the advantage of analyzing cells under well-defined environmental conditions (Fig. 2**C**), thus excluding environmental (extrinsic) fluctuations as the primary source of phenotypic heterogeneity (Gruenberger et al., 2013; Grünberger et al., 2012). Classical agar pads are also used to study single-cell dynamics, but they lag behind regarding environmental control and long-term studies compared to the aforementioned single-cell analysis methodologies (Dusny et al., 2015; Young et al., 2012). However, in order to circumvent those bottlenecks combinatorial approaches of agar pads and PDMS-based microfluidics were developed (Moffitt et al., 2012; Wakamoto et al., 2013).

To adequately analyze and describe phenotypic heterogeneity, irrespective of the selected single-cell analysis technology, it seems indispensable to report and monitor a bioprocess in terms of gene expression or metabolite production at the single-cell level (Vasdekis and Stephanopoulos, 2015). A common and valuable approach is to directly characterize bacterial gene expression using fluorescent reporter proteins (Drepper et al., 2013; Shaner et al., 2005). This approach is highly feasible, especially if the number of analyzed parameters, modifications or conditions increases, and currently outperforms single-cell omics technologies (Saliba et al., 2014; Zenobi, 2013). Although single-cell transcripts can be amplified prior to quantification (Saliba et al., 2014), microbial single-cell RNAseq is not yet available (Lasken and McLean, 2014; Santana et al., 2016). At the same time, the sensitivity of metabolite analytics for small cells such as bacteria remains a substantial challenge (Zenobi, 2013). Notably, commonly applied green and red fluorescent proteins are crucially dependent on cellular growth and oxygen availability (Hebisch et al., 2013). Thus, in heterogeneous populations with e.g. differently growing cells the fluorescent output might not be regarded as fully quantitative. In this regard, for instance Flavin-based fluorescent proteins can be a valuable alternative since their maturation was shown to be completely independent of oxygen availability and thus cellular growth (Drepper et al., 2010, 2007). For monitoring metabolite production, optical biosensors are the method of choice with broad applicability and adequate sensitivity (Delvigne and Goffin, 2014; Delvigne et al., 2015). In this context, transcription factor-based biosensors play a pivotal role in the single-cell analysis of biotechnological production processes (Mahr and Frunzke, 2016; Mahr et al., 2015; Mustafi et al., 2014; Xiao et al., 2016). Moreover, FRET- (Frommer et al., 2009; Moussa et al., 2014; Potzkei et al., 2012), RNA- (Michener et al., 2012; Paige et al., 2012; Strack and Jaffrey, 2013) or riboswitch-based (Fowler and Li, 2014) biosensors represent sophisticated alternatives to monitor cellular production processes, and can further help to unravel phenotypic heterogeneities.

One emerging alternative is subpopulation “omics”, in which cells are sorted based on their fluorescence characteristics and are then analyzed independently (Jahn et al., 2014).

In summary, optical monitoring, for instance, by expressing in vivo reporters or fluorescent metabolite biosensors, is a prerequisite for a comparative investigation of phenotypic heterogeneity.

In the following sections, we will highlight several examples of phenotypic heterogeneity in biotechnologically exploited expression systems, production processes and cultivation events that have been uncovered in recent years by optical means.

1.2. Microbial phenotypic heterogeneity

Cell-to-cell variations are often based on fluctuations in transport protein distributions, which are further amplified during cell division

(Choi et al., 2008; Eldar and Elowitz, 2010). Because the amount of membrane- and especially non-membrane-permeable molecules inside a cell is tightly connected to the number of existing uptake systems, distinct transport protein distribution diversity entails phenotypic heterogeneity. Well-studied examples include both the *lac* and *ara* genetic circuits (Eldar and Elowitz, 2010; Lidstrom and Konopka, 2010; Maloney and Rotman, 1973; Siegele and Hu, 1997).

In the lactose utilization network, fluctuating expression levels of the lactose transporter gene *lacY* were shown to produce distinct *lac* gene expression heterogeneity. Due to a positive feedback loop, in which LacY-imported inducers induce an even higher expression of *lacY*, bistable populations arise, exhibiting both high producing and non- or low producing cells (Binder et al., 2014; Marbach and Bettenbrock, 2012; Ozbudak et al., 2004).

A similar effect has been observed for the arabinose utilization system, in which the arabinose inducer is imported via the complex AraE and AraFGH transport systems (Fritz et al., 2014). Here, an unequal distribution of transport proteins leads to a heterogeneous induction response, as shown for arabinose-induced GFP production using P_{BAD}/AraC systems in *E. coli* (Binder et al., 2016a; Khlebnikov et al., 2001, 2000; Siegele and Hu, 1997) (Fig. 3**A**).

In addition to an unequal distribution of transport proteins, heterogeneous plasmid distributions have recently been shown to induce distinct cell-to-cell variations in both the growth and expression of *Bacillus megaterium* (Münch et al., 2015). In that study, a previously described phenotypic heterogeneity in xylose-induced high-level GFP production (Biedendieck et al., 2007) was intensively characterized at the single-cell level, indicating an asymmetric localization of plasmids. Due to predominant plasmid accumulation at old cell poles, cell division produced both high-level (old pole-based) and low-level (new pole-based) GFP producers (Fig. 3**B**).

In *Lactococcus lactis,* phenotypic heterogeneity was observed during the diauxic shift from glucose to cellobiose (Solopova et al., 2014). Here, a GFP reporter gene, whose expression was under control of the P_{cel} promoter, was used to report the expression of the *celB* gene, which encodes a cellobiose uptake system component. This construct monitored the ability to take up and metabolize cellobiose. Upon glucose consumption, a mixture of cellobiose-consuming (growing) and non-cellobiose-consuming (non-growing) cells arose (Fig. 3**C**). GFP-monitored P_{cel} promoter activity indicated that the lag phase during the diauxic shift was primarily based on cell-to-cell variations of cellobiose-metabolizing operon expression. These observations were further shown to act in agreement with the general bet-hedging strategy because cells growing on cellobiose exhibited significantly less growth on galactose, whereas cells that did not grow on cellobiose performed well on galactose. Although bet-hedging cells may only offer a partial impairment of biotechnological productions, the case is different if production negatively interferes with growth in a heterogeneous population.

Slowly growing producers might be overgrown by rapidly dividing non-producers, thus drastically impeding overall yields. This phenomenon was recently shown for L-valine production in *Corynebacterium glutamicum* (Mustafi et al., 2014) monitored at the single-cell level via a specific genetically encoded L-valine fluorescence biosensor, based on the transcriptional regulator Lrp (Mustafi et al., 2012). High-level L-valine production revealed distinct phenotypic heterogeneity (Fig. 3**D**). Specifically, highly producing cells exhibited poor growth, whereas rapidly growing cells showed low L-valine production levels. In contrast to the aforementioned examples of bioprocess heterogeneity, the exact mechanism of phenotypic heterogeneity during L-valine production has not yet been elucidated. A similar phenomenon is often observed for the production of recombinant proteins, in which the metabolic burden associated with protein production tends to impair growth (Dong et al., 1995).

Similarly, micro-heterogeneous populations can significantly impede overall productivity. For instance, Xiao *et al.* recently uncovered tremendous cell-to-cell variations in both L-tyrosine and free fatty acid (FFA) biosynthesis. Applying both tyrosine-responsive fluorescent biosensors and lipophilic dye-based cell staining, broad but single-bell-shaped single-cell productivity profiles were identified that depicted a wide range of FFA and L-tyrosine titers within isogenic *E. coli* producer strains (Xiao et al., 2016). Similarly, a salicylic acid-inducible expression system in *E. coli* was found to exhibit a micro-heterogeneous expression response (Binder et al., 2016c).

Overall, both micro- and macro-heterogeneity are commonly found in diverse microbial production hosts, ranging from simple expression systems to elaborate biosynthetic production setups, yet are under suspicion to be decisive for lowered yields and reduced bioprocess stability.

1.3. Tools and strategies for engineering phenotypic heterogeneity

Upon pinpointing the cause of cell-to-cell variations, under, at best, constant environmental conditions, numerous approaches for minimizing these cell-to-cell variations have been conducted over the last decades. In this regard, favored strategies can be classified into general system modifications, including strain and inducer modifications, or general physiology manipulations.

Strain modifications, namely, promoter, plasmid or transport system modifications, as well as metabolic engineering, are most prominent in shifting heterogeneous populations toward homogeneity. For example, promoters can be engineered to mediate a more uniform induction behavior. A novel benzoate-inducible system using the M1-17 promoter (Bakke et al., 2009), for instance, was shown to provide a sharper expression response with a reduced spread regarding gene expression as compared to the wild-type Pm promoter (Balzer et al., 2013). Moreover, the choice of plasmid may be crucial in yielding a uniform expression response. Expression heterogeneity can be significantly influenced by the plasmid construct or by changing the plasmid copy number, stability and distribution (Kortmann et al., 2015). Modifications in transport systems can significantly contribute to achieving population homogeneity. Given that uptake systems are unequally distributed during cell division, transporter gene overexpression (Khlebnikov et al., 2001, 2000), deletion (Binder et al., 2014; Marbach and Bettenbrock, 2012) or mutation (Morgan-Kiss et al., 2002) can lower phenotypic heterogeneity. Furthermore, the effect of inducer metabolization should not be underestimated in diminishing phenotypic heterogeneity. For instance, in inducible expression setups, the metabolization of the applied inducer molecules can reduce phenotypic heterogeneity due to an increased inducer working concentration and, thus, an accompanied decrease in the fluctuations of intracellular inducer molecules (Binder et al., 2016c).

If the manipulation of transport systems appears difficult — e.g., due to the different loci of genes that encode for different transporter proteins (Binder et al., 2014; Scripture et al., 1987) — the chemical manipulation of inducer molecules is a valuable alternative. In particular, the introduction of hydrophobic moieties can result in transporter-independent inducer uptake of otherwise non-membrane permeable inducers. This behavior can be observed for the modified galactose derivative isopropyl-β-D-thiogalactopyranoside (IPTG), which, in contrast to the natural inducers galactose or lactose, can readily diffuse into most cells due to its hydrophobic isopropyl-thio-group (Boezi and Cowie, 1961; Cohn, 1957). Given that no unequally distributed transport systems are present, the transition from galactose to IPTG can suffice to homogenize bacterial gene expression (Binder et al., 2014).

Furthermore, photocaged inducers, which release the actual biological inducer upon brief light exposure, represent a sophisticated alternative for diminishing phenotypic heterogeneity because light-responsive photocages commonly include a hydrophobic moiety that facilitates passive diffusion into the cell (Bier et al., 2017; Binder et al., 2016a; Young and Deiters, 2007). Furthermore, the introduction of

groups such as thio-based or halogenated moieties that impede consumption of the respective inducer molecule can prove crucial to minimize phenotypic heterogeneity. Besides inducible promoters to control gene expression, also non-inducible promoters can be applied. Here, for common cell factories such as *E. coli* or *B. subtilis* a large set of promoters has already been analyzed down to single-cell level and rather homogeneous non-inducible promoters could be identified (Guiziou et al., 2016; Silander et al., 2012). Interestingly, Silander *et al.* found that primarily promoters of highly essential and conserved genes exhibited a reduced degree of phenotypic heterogeneity in *E. coli*, suggesting a strong correlation of gene function and noise (Silander et al., 2012).

Cell physiology in terms of metabolic or growth states has been proven valuable for cellular fitness and productivity (Müller and Nebe-von-Caron, 2010). Thus, preculture management —for instance, in terms of inoculum size or age (Jõers et al., 2010; Luidalepp et al., 2011) — may be another key aspect to achieving population homogeneity because the age of the inoculum turned out to be essential for the appearance of persisters and resisters. The choice of cultivation medium is also crucial (Jõers et al., 2010; Mustafi et al., 2014). Furthermore, the continuity of nutrient supply may be a key aspect for tuning bacterial populations toward homogeneity; for example, diauxic shifts were recently revealed as a major source of cell-to-cell variations (Boulineau et al., 2013; Solopova et al., 2014).

Although several events in biotechnology have been shown to depict distinct phenotypic heterogeneity, the actual homogenization of these bioprocesses is significantly lagging. However, there are some examples of bacterial populations that were tuned toward homogeneity, as described below.

1.4. Paradigms of minimizing phenotypic heterogeneity

The most obvious and commonly used approaches of diminishing phenotypic heterogeneity are those based on strain modifications, including regulator or transporter deletions.

For instance, chromosomal deletion of the carbon catabolite repression transcriptional regulator gene *ccpA* in *Lactococcus lactis* can abolish the heterogeneous diauxic response upon shifting from glucose to cellobiose. Instead of shifting from glucose to cellobiose consumption in a non-uniform fashion, *L. lactis* strains lacking *ccpA* directly start to metabolize cellobiose together with glucose (Solopova et al., 2014).

For inducible expression setups, extensive transport system modifications are believed to contribute to a more uniform intracellular inducer accumulation. One valuable approach includes the transport protein overproduction that was conducted for abolishing the phenotypic heterogeneity of arabinose-inducible P_{BAD} promoter-based gene expression in *E. coli* (Fig. 4**A**). Here, the AraE transport protein was overexpressed on a plasmid, yielding significantly homogenized expression profiles (Khlebnikov et al., 2000). The same effect was observed for P_{BAD}-promoter-controlled gene expression in *C. glutamicum,* wherein the plasmid-based overexpression of *araE* shifted heterogeneous expression toward homogeneity (Zhang et al., 2012).

A similar example of minimizing phenotypic heterogeneity is based on the well-known *lac* operon. Here, the lactose permease LacY translocates both synthetic and natural *lac* inducer molecules into the cell, thereby abrogating the repression of *lac* operon gene expression. Because *lacY* expression, however, underlies stochastic fluctuations (Choi et al., 2008; Ozbudak et al., 2004), the LacY distribution and thus intracellular inducer concentrations as well as *lac* gene expression levels vary distinctly from cell to cell. For the frequently applied biotechnological workhorse *E. coli* BL21 (DE3), which enables T7 RNA-polymerase-based, high-level gene expression, the deletion of *lacY* was recently shown to clearly induce homogeneous expression responses (Binder et al., 2014). Furthermore, for native expression setups, similar behavior was reported for *lacY* deletion mutants (Marbach and Bettenbrock, 2012). Due to the resulting uniform diffusion of the synthetic inducer IPTG into the cells, remarkable phenotypic homogeneity was revealed for both growth and expression. Here, the inducer modification by an additional thio-isopropyl group, initially intended for non-metabolization of galactose and thus a reduced demand of inducer, proved essential because it enabled diffusion into the cell, which is impeded for the natural inducers galactose or lactose.

For some production hosts, however, IPTG seems to be unable to freely enter cells in a homogeneous fashion. For instance, poor permeability for IPTG has been described for *C. glutamicum* (Pátek et al., 2003). Here, elevated amounts of IPTG compared to *E. coli* and a heterogeneous expression response were observed (Kortmann et al., 2015). Further inducer modification, namely, the photocaging of IPTG with a hydrophobic nitropiperonal photocaging group (Young and Deiters, 2007), was recently shown to produce a clearly homogeneous expression response (Binder et al., 2016b), in contrast to conventional IPTG induction (Fig. 4**B**). In addition to expression homogeneity, photocaged inducers generally enable a spatiotemporal, non-invasive, high-throughput-feasible and thus straightforward induction of gene expression by light (Bier et al., 2017; Binder et al., 2016a; Wandrey et al., 2016).

Bioprocess homogenization for L-valine production by *C. glutamicum* was also realized via physiology manipulation (Mustafi et al., 2014) (Fig. 4**C**). During microfluidic single-cell analysis, the omission of complex compounds within the minimal medium was shown to alter L-valine production in *C. glutamicum* from distinct heterogeneity to a homogeneous production profile. Unfortunately, exact compounds responsible for heterogeneity are not yet identified.

Similarly, for α-amylase production in *B. subtilis*, the application of EnPressoB medium instead of LB medium shifted AmyM production, as monitored using both transcriptional and translational GFP-promoter fusions, toward population homogeneity with higher overall production levels (Ploss et al., 2016).

Moreover, it will be interesting to see in how far cell-free protein synthesis (Hodgman and Jewett, 2012; Rollin et al., 2013; Zemella et al., 2015), or fully synthetic genome-minimized microbes (Gibson et al., 2010; Glass et al., 2006; Hutchison et al., 2016) will contribute to homogenizing protein production. Here, the absence of complex transport systems, unequal plasmid distributions, complex regulatory systems or simply the reduction of unknown parameters might be key to setting up homogeneous bioprocesses in the future.

Finally, recently reported examples of FC-assisted approaches to sort top-performing cells could provide a powerful tool to homogenize bacterial populations. Firstly, adaptive evolution approaches could be used to augment phenotypic heterogeneity and subsequently to sort for highly producing clones with stable and homogeneous phenotypes (Mahr et al., 2015). Secondly, already non-genetic variations can suffice to distinctly alter population performances. In this context, Xiao et al. recently reported an in vivo population quality control (PopQC) system to continuously select for high-producer cells based on non-genetic phenotypic variations. This study suggests a highly versatile potential to directly employ phenotypic heterogeneity for the improvement of biosynthetic productions (Xiao et al., 2016). Here, it will be interesting to see how biosensor-driven adaptive evolution might assist in tuning microbial populations toward homogeneity in the future.

In conclusion, this broad range of examples highlights the finding that bacterial gene expression can be efficiently tuned toward homogeneity (Fig. 5). In most cases, diminishing phenotypic heterogeneity enabled improved and more predictable process control that is frequently accompanied by improved overall productivity.

2. Outlook and future perspective

2.1. From intrinsic to extrinsic factors influencing phenotypic heterogeneity

Although bacteria employ phenotypic heterogeneity in natural habitats to survive in suddenly changing, multispecies and competitive

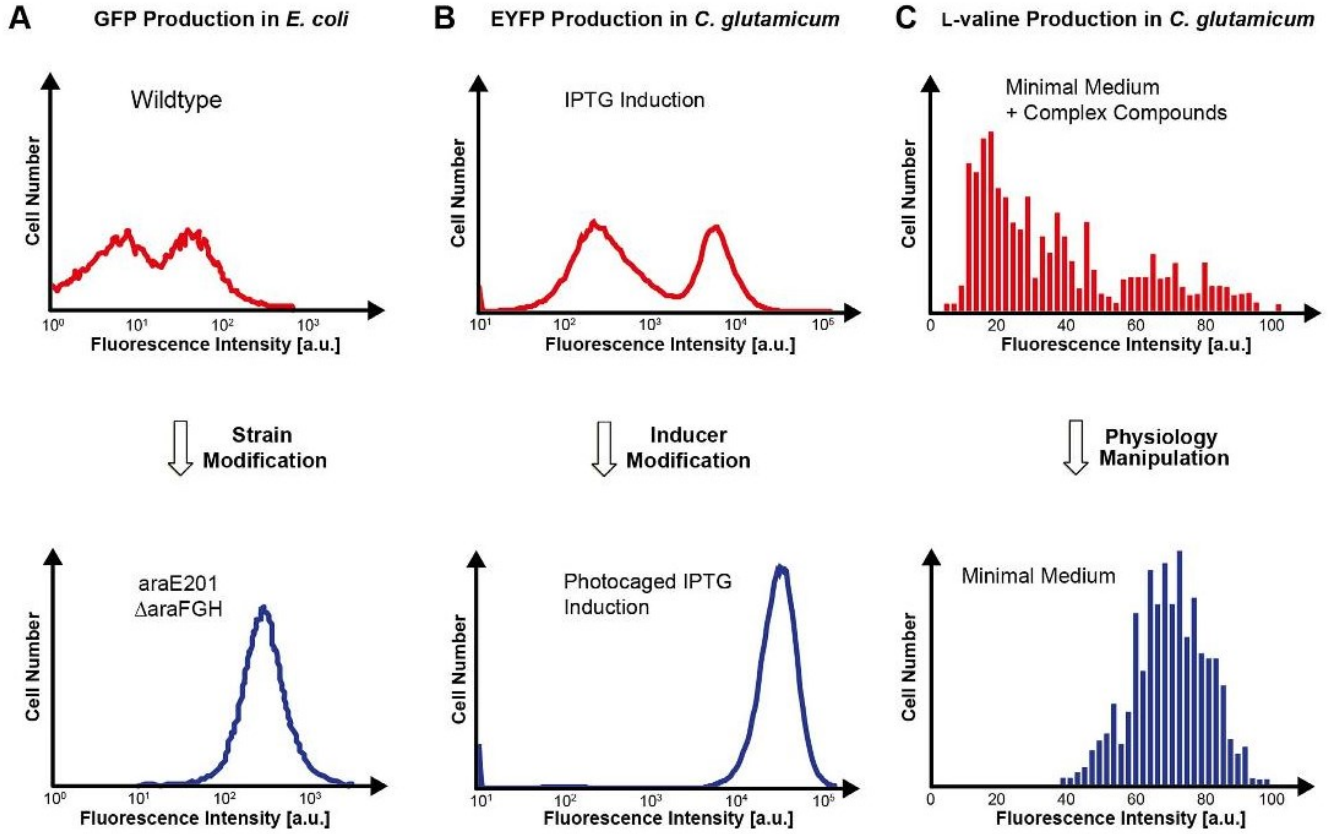

Fig. 4. Paradigms of engineering phenotypic heterogeneity. **A**) The approach of AraE transporter overproduction proved crucial in abolishing GFP-monitored phenotypic heterogeneity of arabinose-inducible P_{BAD} promoter-based gene expression. Modified from Ref. (Khlebnikov et al., 2000). **B**) Modification of EYFP production through inducer engineering. *C. glutamicum* shows bistable gene expression upon induction with IPTG. Using photocaged IPTG, a homogeneous profile was obtained. Modified from Ref. (Binder et al., 2016b). **C**) Using the concept of medium modification, L-valine production in *C. glutamicum* was altered. During perfusion with minimal medium supplemented with complex compounds (0.5% BHI), cells showed strong heterogeneity during growth and production. A homogeneous production profile was obtained when complex compounds were omitted in the production medium. Modified from Ref. (Mustafi et al., 2014). a.u.: arbitrary units.

environments, the impact of cell-to-cell variations on robustness and productivity in artificial bioprocesses remains under discussion. On the one hand, cellular heterogeneity is seen as unfeasible or even impedimental for bioprocesses. On the other hand, heterogeneity may play an important role in adaptation to environmental gradients, particularly within large-scale setups (Delvigne and Goffin, 2014), and if top-performing cells are selectively enriched from phenotypically heterogeneous populations (Xiao et al., 2016). Thus, unraveling, understanding and engineering phenotypic heterogeneity are emerging as key aspects in the optimization of bioprocesses and are of utmost relevance for critical and complex production processes. To efficiently tackle cell-to-cell variations, an in-depth analysis of the phenomenon at different cultivation scales seems crucial prior to applying convenient strategies for reengineering bacterial populations toward homogeneity.

2.2. Design of robust bioprocesses—an interdisciplinary challenge

One major challenge to expanding bioprocesses to the industrial scale is the transfer of homogeneous engineered strains into large volumes in which gradients within environmental conditions are common. This task is complex and will require an interdisciplinary research team of biologists and engineers. Fig. 6 provides an overview of how knowledge regarding the complex interplay between intrinsic and extrinsic factors influencing cell-to-cell heterogeneity can be gained and used to develop cells with uniform production behavior. Gradients of environmental factors can occur within the nutrient, oxygen or pH distributions that inevitably emerge during the typical scaling up process (Lara et al., 2006). These fluctuations might lead to specific responses at different levels of microbial physiology (Käß et al., 2014a, 2014b). To investigate environmental heterogeneity at laboratory and industrial scales, typically so-called scale-down reactors are used (Neubauer and Junne, 2010; Takors, 2012) (Fig. 6, **bottom**). These reactors consist of at least two compartments that allow the primary characteristics of large-scale bioprocesses, occurring on the m^3 scale, to be mimicked at the L scale (Lemoine et al., 2015; Noorman, 2011). Gradients occur due to the insufficient mixing within large volumes and can lead to variations within the solubility of gases, substrates, pH and pressure (Neubauer et al., 2013; Takors, 2012). Most studies typically investigate the impact of environmental factors on the complete population performance and largely neglect population dynamics. The investigation of *C. glutamicum*, for example, showed robustness in metabolism regarding a lack of oxygen and substrate when exposed to temporary gradients. The cells exhibited only minor metabolic and regulatory changes at the transcriptome and proteome levels (Käß et al., 2014a, 2014b). The behavior can be significantly different for alternative strains and varying gradients. For *E. coli* significant differences in gene expression were observed upon exposure to local glucose gradients for more than 100 s (Löffler et al., 2016).

To evaluate cell-to-cell heterogeneity in large-scale bioprocesses, FC methods are commonly applied (Brehm-Stecher and Johnson, 2004; Tracy et al., 2010) to validate production processes and to determine whether and to what extent environmental factors influence phenotypic heterogeneity in terms of cell physiology and production (Fig. 6, **bottom**). FC enables insights to be gained into population behavior but fails to resolve single-cell responses in a dynamic and spatiotemporal fashion.

A

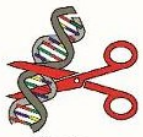

Strain Modification

System	Strategy	Features	Reference
E. coli P_{BAD}/AraC	Plasmid- & chromosome-based *araE* overexpression	Homogeneous inducer uptake and thus induction due to equal AraE distribution	Khlebnikov et al., 2001 Khlebnikov et al., 2000
E. coli P_{BAD}/AraC	*araBAD* and *araEFGH* deletion and expression of LacY transporter mutants with relaxed specificity	Homogeneous and continuous uptake of arabinose by means of equally distributed LacY mutants	Morgan-Kiss et al., 2002
C. glutamicum P_{BAD}/AraC	Plasmid-based *araE* overexpression	Homogeneous inducer uptake and thus induction due to equal AraE distribution	Zhang et al., 2012
E. coli P_{T7lac}/LacI	LacY transporter deletion	Solely diffusion- based and thus homogeneous induction of high-level P_{T7lac}-based gene expression (works as well using photocaged IPTG-based light induction)	Binder et al., 2014
L. lactis P_{cel}/CcpA	CCR transcriptional regulator CcpA deletion	Regulator deletion abolishes the heterogeneous diauxic growth and enables the continuous metabolization of cellobiose	Solopova et al., 2014

B

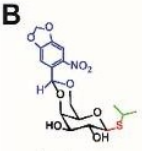

Inducer Modification

E. coli P_{BAD}/AraC	Applying photocaged (membrane-permeable) arabinose that is solely taken up by diffusion	Rapid, strong and homogeneous light-induction of P_{BAD} - controlled gene expression	Binder et al., 2016a
C. glutamicum P_{tac}/LacI	Applying photocaged (membrane-permeable) IPTG that is solely taken up by diffusion	Homogeneous light-induction of P_{tac} - based gene expression in contrast to conventional IPTG induction	Binder et al., 2016b

C

Physiology Manipulation

C. glutamicum L-Valine production	Applying alternative cultivation media	Homogeneous L-valine production together with uniform growth	Mustafi et al., 2014
E. coli P_{BAD}/AraC	Adjusting cultivation mode, medium and inducer concentrations in an *ara*$^+$ strain	Partly homogeneous expression response for selected parameters	Binder et al., 2016c
B. subtilis P_{amy}/AmyM	Optimized growth conditions i.e. application of slow / limited glucose feeding from complex polysaccharides	More homogeneous and improved production	Ploss et al., 2016

Fig. 5. Bacterial expression/production systems engineered toward phenotypic homogeneity. A) Examples of systems engineered through strain modifications such as promoter engineering, plasmid modification, transport system modification or metabolic engineering. **B)** Chemical inducer modifications, such as non-metabolizable groups, as well as hydrophobic and photocaging moieties. **C)** Cell physiology manipulations during pre- and main cultivation. Here, key aspects include medium development and optimization of the cultivation mode.

Future efforts should aim for a more detailed analysis of phenotypic heterogeneity through FC in combination with scale-down reactors. A proof-of-principle study was performed by Hewitt et al. (2000). This study showed that for *E. coli*, changing microenvironments with respect to glucose and dissolved oxygen concentrations had a significant effect on cell physiology and cellular heterogeneity and hence on viable biomass yields. Furthermore, the results obtained with a scale-down reactor were comparable to large-scale bioprocesses at the m^3 scale (Hewitt et al., 2000). The inclusion body formation by a recombinant *E. coli* strain, producing the mammalian protein AP50, was investigated under different scale-down conditions associated with large-scale bioprocesses. Upon exposure to different environmental conditions, inclusion body formation was shown to be strongly dependent on individual cell physiology (Hewitt et al., 2007).

These examples indicate the potential of scale-down reactor studies combined with FC to fully understand a cell's metabolic response to environmental conditions in large-scale bioreactors. The obtained information can then be used to optimize process conditions (Fig. 6, **right**) or cellular parameters through genetic engineering (Fig. 6, **left**).

Microfluidic single-cell cultivation can be used to determine the cellular physiology in response to certain environmental factors (e.g., glucose concentrations, pH) to screen for optimal cultivation parameters—e.g., via droplet microfluidics (Kaminski et al., 2016; Mazutis et al., 2013)—as well as for a detailed understanding of cell-to-cell variations caused by specific environmental factors (Grünberger et al., 2013; Unthan et al., 2013). At the same time, novel microfluidic systems allow one to emulate environmental gradients within bioprocesses. Similar to FC studies combined with scale-down reactors, the obtained information may allow one to better control and fine-tune phenotypic heterogeneity (Fig. 6, **bottom**).

A first proof-of-concept study was reported by Uhlendorf et al. (2012). These researchers established a microfluidic platform for the real-time control of gene expression in yeast; this platform integrated microscopy, microfluidics and tailor-made software for automated imaging, cell behavior quantification and dynamic environmental control. This setup could be adjusted to emulate bioprocesses, especially for the investigation of dynamic changes within nutrients, temperature or pH (Lapin et al., 2006, 2004). These studies can be combined with computational fluidic dynamics (Westerwalbesloh et al., 2015) or flux variability analysis (Unthan et al., 2013) to obtain a deeper understanding of the intrinsic and extrinsic factors that are responsible for cell-to-cell variations. In this context, the automatization of single-cell analysis (Helfrich et al., 2015), as well as robust mathematical models and software tools to precisely define and distinguish

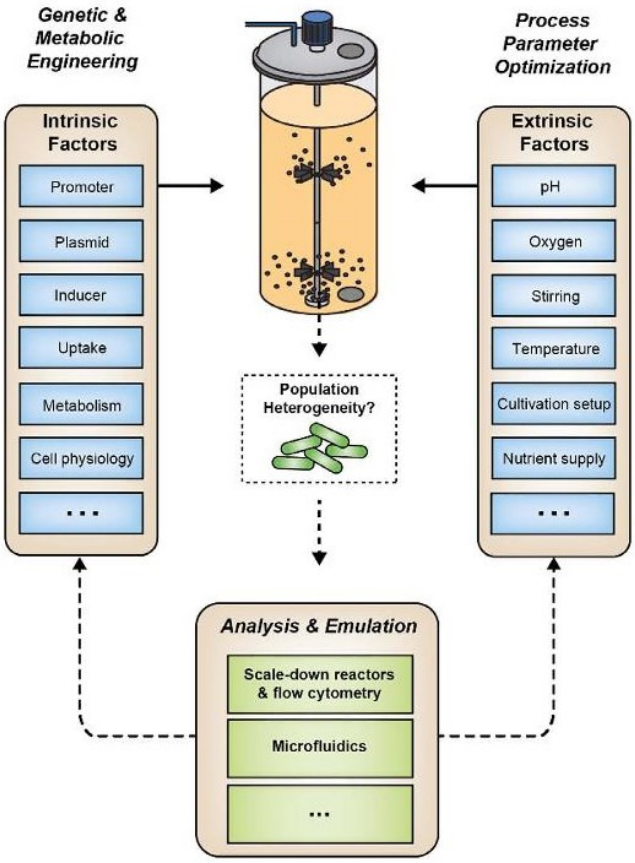

Fig. 6. Analyzing and tuning bioprocess homogeneity. Typically, intrinsic factors (left) are to be tuned by strain, inducer and metabolic engineering to obtain improved bioprocesses. Thereafter, process parameters — i.e., extrinsic factors — are optimized to increase the productivity and robustness of bioprocesses. To investigate and determine the influence of phenotypic heterogeneity on bioprocesses, scale-down reactors combined with flow cytometry can be used. Alternatively, novel microfluidic setups allow for detailed single-cell studies and, moreover, the emulation of large-scale reactor conditions. The findings of these studies can be used to optimize both intrinsic and extrinsic factors to obtain productive, robust and stable bioprocesses.

micro-heterogeneity and macro-heterogeneity from homogeneity in microbial populations, is required (Gough et al., 2014; Huang, 2009).

For significant heterogeneities, additional sorting and offline analysis of selected subpopulations can be performed to obtain a detailed molecular understanding of the observed cell-to-cell heterogeneity (Jahn et al., 2014). These methods can be supplemented and combined with different traditional omics technologies, enzyme assays or microscopic methods.

Certainly the exploitation of microfluidic single-cell cultivation to understand and improve bioprocess applications has just started. First studies, analyzing and comparing cellular behavior and heterogeneity at different scales have been reported e.g. for growth (Grünberger et al., 2013; Unthan et al., 2013), gene expression (Dusny and Schmid, 2016) and the production of lipids (Vasdekis et al., 2015). Yet, a direct comparison and transfer of microfluidic results into large-scale is difficult to date. Especially differences in the cultivation modes (e.g. batch vs. perfusion), mass and heat transfer as well the artificial environmental conditions make a direct transfer challenging or even a complete new research field within the scientific community. Nevertheless, first concepts to control heterogeneity in large-scale bioreactors were developed and have been reviewed recently (Delvigne et al., 2017).

These approaches lay the foundation for further metabolic engineering of homogeneous microbial production strains. Finally, biologically engineered homogeneous systems seem ideally suited to investigate environmental heterogeneity and thus represent a prerequisite to tackle extrinsic factor optimization. Specifically, phenotypically homogeneous setups could be employed to detect extrinsic heterogeneities; however, for intrinsically heterogeneous systems, it appears difficult to distinguish between intrinsic and extrinsic heterogeneity.

3. Concluding remarks

Phenotypic heterogeneity can have a significant impact on microbial production, as shown here for several bacterial gene expression setups. Thus, unraveling and diminishing cell-to-cell heterogeneity can be a valuable approach. Nevertheless, we have only begun to understand the full role of heterogeneity within applied biotechnology. Novel single-cell analysis tools, together with emerging strategies to combat phenotypic heterogeneity, will enable the shift of microbial production toward homogeneous and robust productivity. Here, synthetic biology and metabolic engineering tools merge with cultivation and inducer modification technologies to take biotechnological production to the next level. The final transfer to the industrial scale remains a key challenge, which requires future interdisciplinary research efforts.

Acknowledgments

We gratefully acknowledge the support of grants from the Federal Ministry of Education and Research (OptoSys, FKZ 031A16). Moreover, the Helmholtz Association (PD-311 and VH-NG-1029) is gratefully acknowledged for funding. We also thank Christopher Probst for discussion and graphical support.

References

Acar, M., Mettetal, J.T., van Oudenaarden, A., 2008. Stochastic switching as a survival strategy in fluctuating environments. Nat. Genet. 40, 471–475. http://dx.doi.org/10.1038/ng.110.

Allison, K.R., Brynildsen, M.P., Collins, J.J., 2011. Heterogeneous bacterial persisters and engineering approaches to eliminate them. Curr. Opin. Microbiol. 14, 593–598. http://dx.doi.org/10.1016/j.mib.2011.09.002.

Amato, S.M., Brynildsen, M.P., 2015. Persister heterogeneity arising from a single metabolic stress. Curr. Biol. 25, 2090–2098. http://dx.doi.org/10.1016/j.cub.2015.06.034.

Baert, J., Kinet, R., Brognaux, A., Delepierre, A., Telek, S., Sorensen, S.J., Riber, L., Fickers, P., Delvigne, F., 2015. Phenotypic variability in bioprocessing conditions can be tracked on the basis of on-line flow cytometry and fits to a scaling law. Biotechnol. J. 10, 1316–1325. http://dx.doi.org/10.1002/biot.201400537.

Bakke, I., Berg, L., Aune, T.E.V., Brautaset, T., Sletta, H., Tøndervik, A., Valla, S., 2009. Random mutagenesis of the PM promoter as a powerful strategy for improvement of recombinant-gene expression. Appl. Environ. Microbiol. 75, 2002–2011. http://dx.doi.org/10.1128/AEM.02315-08.

Balaban, N.Q., Merrin, J., Chait, R., Kowalik, L., Leibler, S., 2004. Bacterial persistence as a phenotypic switch. Science 305, 1622–1625. http://dx.doi.org/10.1126/science.1099390.

Balzer, S., Kucharova, V., Megerle, J., Lale, R., Brautaset, T., Valla, S., 2013. A comparative analysis of the properties of regulated promoter systems commonly used for recombinant gene expression in Escherichia coli. Microb. Cell Fact. 12, 26. http://dx.doi.org/10.1186/1475-2859-12-26.

Biedendieck, R., Yang, Y., Deckwer, W.-D., Malten, M., Jahn, D., 2007. Plasmid system for the intracellular production and purification of affinity-tagged proteins in Bacillus megaterium. Biotechnol. Bioeng. 96, 525–537. http://dx.doi.org/10.1002/bit.21145.

Bier, C., Binder, D., Drobietz, D., Loeschcke, A., Drepper, T., Jaeger, K.-E., Pietruszka, J., 2017. Photocaged carbohydrates: versatile tools for controlling gene expression by light. Synthesis (Stuttg) 49, 42–52. http://dx.doi.org/10.1055/s-0035-1562617.

Binder, D., Bier, C., Grünberger, A., Drobietz, D., Hage-Hülsmann, J., Wandrey, G., Büchs, J., Kohlheyer, D., Loeschcke, A., Wiechert, W., Jaeger, K.-E., Pietruszka, J., Drepper, T., 2016a. Photocaged arabinose – a novel optogenetic switch for rapid and gradual control of microbial gene expression. Chembiochem 17, 296–299. http://dx.doi.org/10.1002/cbic.201500609.

Binder, D., Frohwitter, J., Mahr, R., Bier, C., Grünberger, A., Loeschcke, A., Peters-Wendisch, P., Kohlheyer, D., Pietruszka, J., Frunzke, J., Jaeger, K.-E., Wendisch, V.F., Drepper, T., 2016b. Light-controlled cell factories - Employing photocaged IPTG for light-mediated optimization of lac-based gene expression and (+)-valencene biosynthesis in Corynebacterium glutamicum. Appl. Environ. Microbiol. 82, 6141–6149. http://dx.doi.org/10.1128/AEM.01457-16.

Binder, D., Grünberger, A., Loeschcke, A., Probst, C., Bier, C., Pietruszka, J., Wiechert, W., Kohlheyer, D., Jaeger, K.-E., Drepper, T., 2014. Light-responsive control of bacterial gene expression: precise triggering of the lac promoter activity using photocaged

IPTG. Integr. Biol. (Camb.) 6, 755–765. http://dx.doi.org/10.1039/c4ib00027g.
Binder, D., Probst, C., Grünberger, A., Hilgers, F., Loeschcke, A., Jaeger, K.-E., Kohlheyer, D., Drepper, T., 2016c. Comparative single-cell analysis of different E. coli expression systems during microfluidic cultivation. PLoS One 11, e0160711. http://dx.doi.org/10.1371/journal.pone.0160711.
Boezi, J.A., Cowie, D.B., 1961. Kinetic studies of β-galactosidase induction. Biophys. J. 1, 639–647. http://dx.doi.org/10.1016/S0006-3495(61)86913-0.
Boulineau, S., Tostevin, F., Kiviet, D.J., ten Wolde, P.R., Nghe, P., Tans, S.J., 2013. Single-cell dynamics reveals sustained growth during diauxic shifts. PLoS One 8, e61686. http://dx.doi.org/10.1371/journal.pone.0061686.
Brehm-Stecher, B.F., Johnson, E.A., 2004. Single-cell microbiology: tools, technologies, and applications. Microbiol. Mol. Biol. Rev. 68, 538–559. http://dx.doi.org/10.1128/MMBR.68.3.538-559.2004.
Choi, P.J., Cai, L., Frieda, K., Xie, X.S., 2008. A stochastic single-molecule event triggers phenotype switching of a bacterial cell. Science 322, 442–446. http://dx.doi.org/10.1126/science.1161427.
Cohn, M., 1957. Contributions of studies on the beta-galactosidase of Escherichia coli to our understanding of enzyme synthesis. Bacteriol. Rev. 21, 140–168.
De Jong, I.G., Veening, J.-W., Kuipers, O.P., 2010. Heterochronic phosphorelay gene expression as a source of heterogeneity in Bacillus subtilis spore formation. J. Bacteriol. 192, 2053–2067. http://dx.doi.org/10.1128/JB.01484-09.
Delvigne, F., Baert, J., Sassi, H., Fickers, P., Grünberger, A., Dusny, C., 2017. Taking control over microbial populations: current approaches for exploiting biological noise in bioprocesses. Biotechnol. J. 12, 1600549. http://dx.doi.org/10.1002/biot.201600549.
Delvigne, F., Goffin, P., 2014. Microbial heterogeneity affects bioprocess robustness: dynamic single-cell analysis contributes to understanding of microbial populations. Biotechnol. J. 9, 61–72. http://dx.doi.org/10.1002/biot.201300119.
Delvigne, F., Pêcheux, H., Tarayre, C., 2015. Fluorescent reporter libraries as useful tools for optimizing microbial cell factories: a review of the current methods and applications. Front. Bioeng. Biotechnol. 3, 147. http://dx.doi.org/10.3389/fbioe.2015.00147.
Dong, H., Nilsson, L., Kurland, C.G., 1995. Gratuitous overexpression of genes in Escherichia coli leads to growth inhibition and ribosome destruction. J. Bacteriol. 177, 1497–1504.
Drepper, T., Eggert, T., Circolone, F., Heck, A., Krauss, U., Guterl, J.-K., Wendorff, M., Losi, A., Gärtner, W., Jaeger, K.-E., 2007. Reporter proteins for in vivo fluorescence without oxygen. Nat. Biotechnol. 25, 443–445. http://dx.doi.org/10.1038/nbt1293.
Drepper, T., Gensch, T., Pohl, M., 2013. Advanced in vivo applications of blue light photoreceptors as alternative fluorescent proteins. Photochem. Photobiol. Sci. 12, 1125–1134. http://dx.doi.org/10.1039/c3pp50040c.
Drepper, T., Huber, R., Heck, A., Circolone, F., Hillmer, A.-K., Büchs, J., Jaeger, K.-E., 2010. Flavin mononucleotide-based fluorescent reporter proteins outperform green fluorescent protein-like proteins as quantitative in vivo real-time reporters. Appl. Environ. Microbiol. 76, 5990–5994. http://dx.doi.org/10.1128/AEM.00701-10.
Dusny, C., Grünberger, A., Probst, C., Wiechert, W., Kohlheyer, D., Schmid, A., 2015. Technical bias of microcultivation environments on single-cell physiology. Lab Chip 15, 1822–1834. http://dx.doi.org/10.1039/c4lc01270d.
Dusny, C., Schmid, A., 2016. The MOX promoter in Hansenula polymorpha is ultra-sensitive to glucose-mediated carbon catabolite repression. FEMS Yeast Res. 16, 1–15. http://dx.doi.org/10.1093/femsyr/fow067.
Eldar, A., Elowitz, M.B., 2010. Functional roles for noise in genetic circuits. Nature 467, 167–173. http://dx.doi.org/10.1038/nature09326.
Fowler, C.C., Li, Y., 2014. Construction and application of riboswitch-based sensors that detect metabolites within bacterial cells. In: Lafontaine, D., Dubé, A. (Eds.), Therapeutic Applications of Ribozymes and Riboswitches. Humana Press, Totowa, NJ, pp. 177–197. http://dx.doi.org/10.1007/978-1-62703-730-3.
Fritz, G., Megerle, J.A., Westermayer, S.A., Brick, D., Heermann, R., Jung, K., Rädler, J.O., Gerland, U., 2014. Single cell kinetics of phenotypic switching in the arabinose utilization system of E. coli. PLoS One 9, e89532. http://dx.doi.org/10.1371/journal.pone.0089532.
Frommer, W.B., Davidson, M.W., Campbell, R.E., 2009. Genetically encoded biosensors based on engineered fluorescent proteins. Chem. Soc. Rev. 38, 2833–2841. http://dx.doi.org/10.1039/b907749a.
Frunzke, J., Bramkamp, M., Schweitzer, J.-E., Bott, M., 2008. Population Heterogeneity in Corynebacterium glutamicum ATCC 13032 caused by prophage CGP3. J. Bacteriol. 190, 5111–5119. http://dx.doi.org/10.1128/JB.00310-08.
Gibson, D.G., Glass, J.I., Lartigue, C., Noskov, V.N., Chuang, R.-Y., Algire, M.A., Benders, G.A., Montague, M.G., Ma, L., Moodie, M.M., Merryman, C., Vashee, S., Krishnakumar, R., Assad-garcia, N., Andrews-Pfannkoch, C., Denisova, E.A., Young, L., Qi, Z.-Q., Segall-Shapiro, T.H., Calvey, C.H., Parmar, P.P., Hutchison, C.A., Smith, H.O., Venter, J.C., 2010. Creation of a bacterial cell controlled by a chemically synthesized genome. Science 329, 52–56. http://dx.doi.org/10.1126/science.1190719.
Glass, J.I., Assad-Garcia, N., Alperovich, N., Yooseph, S., Lewis, M.R., Maruf, M., Hutchison, C.A., Smith, H.O., Venter, J.C., 2006. Essential genes of a minimal bacterium. Proc. Natl. Acad. Sci. USA 103, 425–430. http://dx.doi.org/10.1073/pnas.0510013103.
Gough, A.H., Chen, N., Shun, T.Y., Lezon, T.R., Boltz, R.C., Reese, C.E., Wagner, J., Vernetti, L.A., Grandis, J.R., Lee, A.V., Stern, A.M., Schurdak, M.E., Taylor, D.L., 2014. Identifying and quantifying heterogeneity in high content analysis: application of heterogeneity indices to drug discovery. PLoS One 9, e102678. http://dx.doi.org/10.1371/journal.pone.0102678.
Grimbergen, A.J., Siebring, J., Solopova, A., Kuipers, O.P., 2015. Microbial bet-hedging: the power of being different. Curr. Opin. Microbiol. 25, 67–72. http://dx.doi.org/10.1016/j.mib.2015.04.008.
Gruenberger, A., Probst, C., Heyer, A., Wiechert, W., Frunzke, J., Kohlheyer, D., 2013. Microfluidic picoliter bioreactor for microbial single-cell analysis: fabrication, system setup, and operation. J. Vis. Exp. (82), e50560. http://dx.doi.org/10.3791/50560.
Grünberger, A., Paczia, N., Probst, C., Schendzielorz, G., Eggeling, L., Noack, S., Wiechert, W., Kohlheyer, D., 2012. A disposable picolitre bioreactor for cultivation and investigation of industrially relevant bacteria on the single cell level. Lab Chip 12, 2060–2068. http://dx.doi.org/10.1039/c2lc40156h.
Grünberger, A., Probst, C., Helfrich, S., Nanda, A., Stute, B., Wiechert, W., von Lieres, E., Nöh, K., Frunzke, J., Kohlheyer, D., 2015. Spatiotemporal microbial single-cell analysis using a high-throughput microfluidics cultivation platform. Cytometry A 87, 1101–1115. http://dx.doi.org/10.1002/cyto.a.22779.
Grünberger, A., van Ooyen, J., Paczia, N., Rohe, P., Schiendzielorz, G., Eggeling, L., Wiechert, W., Kohlheyer, D., Noack, S., 2013. Beyond growth rate 0.6: Corynebacterium glutamicum cultivated in highly diluted environments. Biotechnol. Bioeng. 110, 220–228. http://dx.doi.org/10.1002/bit.24616.
Grünberger, A., Wiechert, W., Kohlheyer, D., 2014. Single-cell microfluidics: opportunity for bioprocess development. Curr. Opin. Biotechnol. 29, 15–23. http://dx.doi.org/10.1016/j.copbio.2014.02.008.
Guiziou, S., Sauveplane, V., Chang, H.-J., Clerté, C., Declerck, N., Jules, M., Bonnet, J., 2016. A part toolbox to tune genetic expression in Bacillus subtilis. Nucleic Acids Res. 44, 7495–7508. http://dx.doi.org/10.1093/nar/gkw624.
Healey, D., Axelrod, K., Gore, J., 2016. Negative frequency-dependent interactions can underlie phenotypic heterogeneity in a clonal microbial population. Mol. Syst. Biol. 12, 877. http://dx.doi.org/10.15252/msb.20167033.
Hebisch, E., Knebel, J., Landsberg, J., Frey, E., Leisner, M., 2013. High variation of fluorescence protein maturation times in closely related Escherichia coli strains. PLoS One 8, e75991. http://dx.doi.org/10.1371/journal.pone.0075991.
Helfrich, S., Azzouzi, C.E., Probst, C., Seiffarth, J., Grünberger, A., Wiechert, W., Kohlheyer, D., Nöh, K., 2015. Vizardous: interactive analysis of microbial populations with single cell resolution. Bioinformatics 31, 3875–3877. http://dx.doi.org/10.1093/bioinformatics/btv468.
Hewitt, C.J., Nebe-Von Caron, G., Axelsson, B., McFarlane, C.M., Nienow, A.W., 2000. Studies related to the scale-up of high-cell-density E. coli fed-batch fermentations using multiparameter flow cytometry: effect of a changing microenvironment with respect to glucose and dissolved oxygen concentration. Biotechnol. Bioeng. 70, 381–390.
Hewitt, C.J., Onyeaka, H., Lewis, G., Taylor, I.W., Nienow, A.W., 2007. A comparison of high cell density fed-batch fermentations involving both induced and non-induced recombinant Escherichia coli under well-mixed small-scale and simulated poorly mixed large-scale conditions. Biotechnol. Bioeng. 96, 495–505. http://dx.doi.org/10.1002/bit.21127.
Hodgman, C.E., Jewett, M.C., 2012. Cell-free synthetic biology: thinking outside the cell. Metab. Eng. 14, 261–269. http://dx.doi.org/10.1016/j.ymben.2011.09.002.
Huang, S., 2009. Non-genetic heterogeneity of cells in development: more than just noise. Development 136, 3853–3862. http://dx.doi.org/10.1242/dev.035139.
Hutchison, C.A., Chuang, R.-Y., Noskov, V.N., Assad-Garcia, N., Deerinck, T.J., Ellisman, M.H., Gill, J., Kannan, K., Karas, B.J., Ma, L., Pelletier, J.F., Qi, Z., Richter, R.A., Strychalski, E.A., Sun, L., Suzuki, Y., Tsvetanova, B., Wise, K.S., Smith, H.O., Glass, J.I., Merryman, C., Gibson, D.G., Venter, J.C., 2016. Design and synthesis of a minimal bacterial genome. Science 351. http://dx.doi.org/10.1126/science.aad6253.
Jahn, M., Vorpahl, C., Türkowsky, D., Lindmeyer, M., Bühler, B., Harms, H., Müller, S., 2014. Accurate determination of plasmid copy number of flow-sorted cells using droplet digital PCR. Anal. Chem. 86, 5969–5976. http://dx.doi.org/10.1021/ac501118v.
Jang, Sungho, Lee, B., Jeong, H., Jin, S.H., Jang, Sungyeon, Kim, S.G., Jung, G.Y., Lee, C., 2016. On-chip analysis, indexing and screening for chemical producing bacteria in a microfluidic static droplet array. Lab Chip 16, 1909–1916. http://dx.doi.org/10.1039/C6LC00118A.
Jõers, A., Kaldalu, N., Tenson, T., 2010. The frequency of persisters in Escherichia coli reflects the kinetics of awakening from dormancy. J. Bacteriol. 192, 3379–3384. http://dx.doi.org/10.1128/JB.00056-10.
Kaminski, T.S., Scheler, O., Garstecki, P., 2016. Droplet microfluidics for microbiology: techniques, applications and challenges. Lab Chip 16, 2168–2187. http://dx.doi.org/10.1039/c6lc00367b.
Käß, F., Junne, S., Neubauer, P., Wiechert, W., Oldiges, M., 2014a. Process inhomogeneity leads to rapid side product turnover in cultivation of Corynebacterium glutamicum. Microb. Cell Fact. 13, 6. http://dx.doi.org/10.1186/1475-2859-13-6.
Käß, F., Prasad, A., Tillack, J., Moch, M., Giese, H., Büchs, J., Wiechert, W., Oldiges, M., 2014b. Rapid assessment of oxygen transfer impact for Corynebacterium glutamicum. Bioprocess Biosyst. Eng. 37, 2567–2577. http://dx.doi.org/10.1007/s00449-014-1234-1.
Khlebnikov, A., Datsenko, K.A., Skaug, T., Wanner, B.L., Keasling, J.D., 2001. Homogeneous expression of the P(BAD) promoter in Escherichia coli by constitutive expression of the low-affinity high-capacity AraE transporter. Microbiology 147, 3241–3247. http://dx.doi.org/10.1099/00221287-147-12-3241.
Khlebnikov, A., Risa, O., Skaug, T., Carrier, T.A., Keasling, J.D., 2000. Regulatable arabinose-inducible gene expression system with consistent control in all cells of a culture. J. Bacteriol. 182, 7029–7034. http://dx.doi.org/10.1128/JB.182.24.7029-7034.2000.Updated.
Kiviet, D.J., Nghe, P., Walker, N., Boulineau, S., Sunderlikova, V., Tans, S.J., 2014. Stochasticity of metabolism and growth at the single-cell level. Nature 514, 376–379. http://dx.doi.org/10.1038/nature13582.
Kortmann, M., Kuhl, V., Klaffl, S., Bott, M., 2015. A chromosomally encoded T7 RNA polymerase-dependent gene expression system for Corynebacterium glutamicum: construction and comparative evaluation at the single-cell level. Microb. Biotechnol.

8, 253–265. http://dx.doi.org/10.1111/1751-7915.12236.
Kussell, E., Leibler, S., 2005. Phenotypic diversity, population growth, and information in fluctuating environments. Science 309, 2075–2078. http://dx.doi.org/10.1126/science.1114383.
Lapin, A., Müller, D., Reuss, M., 2004. Dynamic behavior of microbial populations in stirred bioreactors simulated with Euler–Lagrange methods: traveling along the lifelines of single cells. Ind. Eng. Chem. Res. 43, 4647–4656. http://dx.doi.org/10.1021/ie030786k.
Lapin, A., Schmid, J., Reuss, M., 2006. Modeling the dynamics of E. coli populations in the three-dimensional turbulent field of a stirred-tank bioreactor—a structured–segregated approach. Chem. Eng. Sci. 61, 4783–4797. http://dx.doi.org/10.1016/j.ces.2006.03.003.
Lara, A.R., Galindo, E., Ramírez, O.T., Palomares, L.A., 2006. Living with heterogeneities in bioreactors: understanding the effects of environmental gradients on cells. Mol. Biotechnol. 34, 355–381. http://dx.doi.org/10.1385/MB:34:3:355.
Lasken, R.S., McLean, J.S., 2014. Recent advances in genomic DNA sequencing of microbial species from single cells. Nat. Rev. Genet. 15, 577–584. http://dx.doi.org/10.1038/nrg3785.Recent.
Lemoine, A., Martinez-Iturralde, N.M., Spann, R., Neubauer, P., Junne, S., 2015. Response of Corynebacterium glutamicum exposed to oscillating cultivation conditions in a two- and a novel three-compartment scale-down bioreactor. Biotechnol. Bioeng. 112, 1220–1231. http://dx.doi.org/10.1002/bit.25543.
Lidstrom, M.E., Konopka, M.C., 2010. The role of physiological heterogeneity in microbial population behavior. Nat. Chem. Biol. 6, 705–712. http://dx.doi.org/10.1038/nchembio.436.
Lino, R., Matsumoto, Y., Nishino, K., Yamaguchi, A., Noji, H., 2013. Design of a large-scale femtoliter droplet array for single-cell analysis of drug-tolerant and drug-resistant bacteria. Front. Bioeng. Biotechnol. 4, 300. http://dx.doi.org/10.3389/fmicb.2013.00300.
Löffler, M., Simen, J.D., Jäger, G., Schäferhoff, K., Freund, A., Takors, R., 2016. Engineering E. coli for large-scale production – strategies considering ATP expenses and transcriptional responses. Metab. Eng. 38, 73–85. http://dx.doi.org/10.1016/j.ymben.2016.06.008.
Luidalepp, H., Jõers, A., Kaldalu, N., Tenson, T., 2011. Age of inoculum strongly influences persister frequency and can mask effects of mutations implicated in altered persistence. J. Bacteriol. 193, 3598–3605. http://dx.doi.org/10.1128/JB.00085-11.
Mahr, R., Frunzke, J., 2016. Transcription factor-based biosensors in biotechnology: current state and future prospects. Appl. Microbiol. Biotechnol. 100, 79–90. http://dx.doi.org/10.1007/s00253-015-7090-3.
Mahr, R., Gätgens, C., Gätgens, J., Polen, T., Kalinowski, J., Frunzke, J., 2015. Biosensor-driven adaptive laboratory evolution of L-valine production in Corynebacterium glutamicum. Metab. Eng. 32, 184–194. http://dx.doi.org/10.1016/j.ymben.2015.09.017.
Maloney, P.C., Rotman, B., 1973. Distribution of suboptimally induces -D-galactosidase in Escherichia coli. The enzyme content of individual cells. J. Mol. Biol. 73, 77–91.
Marbach, A., Bettenbrock, K., 2012. lac operon induction in Escherichia coli: systematic comparison of IPTG and TMG induction and influence of the transacetylase LacA. J. Biotechnol. 157, 82–88. http://dx.doi.org/10.1016/j.jbiotec.2011.10.009.
Martins, B.M.C., Locke, J.C.W., 2015. Microbial individuality: how single-cell heterogeneity enables population level strategies. Curr. Opin. Microbiol. 24, 104–112. http://dx.doi.org/10.1016/j.mib.2015.01.003.
Mazutis, L., Gilbert, J., Ung, W.L., Weitz, D.A., Griffiths, A.D., Heyman, J.A., 2013. Single-cell analysis and sorting using droplet-based microfluidics. Nat. Protoc. 8, 870–891. http://dx.doi.org/10.1038/nprot.2013.046.
Medema, M.H., Breitling, R., Bovenberg, R., Takano, E., 2011. Exploiting plug-and-play synthetic biology for drug discovery and production in microorganisms. Nat. Rev. Microbiol. 9, 131–137. http://dx.doi.org/10.1038/nrmicro2478.
Michener, J.K., Thodey, K., Liang, J.C., Smolke, C.D., 2012. Applications of genetically-encoded biosensors for the construction and control of biosynthetic pathways. Metab. Eng. 14, 212–222. http://dx.doi.org/10.1016/j.ymben.2011.09.004.
Moffitt, J.R., Lee, J.B., Cluzel, P., 2012. The single-cell chemostat: an agarose-based, microfluidic device for high-throughput, single-cell studies of bacteria and bacterial communities. Lab Chip 12, 1487–1494. http://dx.doi.org/10.1039/c2lc00009a.
Morgan-Kiss, R.M., Wadler, C., Cronan, J.E., 2002. Long-term and homogeneous regulation of the Escherichia coli araBAD promoter by use of a lactose transporter of relaxed specificity. Proc. Natl. Acad. Sci. USA 99, 7373–7377. http://dx.doi.org/10.1073/pnas.122227599.
Moussa, R., Baierl, A., Steffen, V., Kubitzki, T., Wiechert, W., Pohl, M., 2014. An evaluation of genetically encoded FRET-based biosensors for quantitative metabolite analyses in vivo. J. Biotechnol. 191, 250–259. http://dx.doi.org/10.1016/j.jbiotec.2014.07.007.
Müller, S., Nebe-von-Caron, G., 2010. Functional single-cell analyses: flow cytometry and cell sorting of microbial populations and communities. FEMS Microbiol. Rev. 34, 554–587. http://dx.doi.org/10.1111/j.1574-6976.2010.00214.x.
Münch, K.M., Müller, J., Wienecke, S., Bergmann, S., Heyber, S., Biedendieck, R., Münch, R., Jahn, D., 2015. Polar fixation of plasmids during recombinant protein production in Bacillus megaterium results in population heterogeneity. Appl. Environ. Microbiol. 81, 5976–5986. http://dx.doi.org/10.1128/AEM.00807-15.
Mustafi, N., Grünberger, A., Kohlheyer, D., Bott, M., Frunzke, J., 2012. The development and application of a single-cell biosensor for the detection of L-methionine and branched-chain amino acids. Metab. Eng. 14, 449–457. http://dx.doi.org/10.1016/j.ymben.2012.02.002.
Mustafi, N., Grünberger, A., Mahr, R., Helfrich, S., Nöh, K., Blombach, B., Kohlheyer, D., Frunzke, J., 2014. Application of a genetically encoded biosensor for live cell imaging of L-valine production in pyruvate dehydrogenase complex-deficient Corynebacterium glutamicum strains. PLoS One 9, e85731. http://dx.doi.org/10.1371/journal.pone.0085731.
Nanda, A.M., Thormann, K., Frunzke, J., 2015. Impact of spontaneous prophage induction on the fitness of bacterial populations and host-microbe interactions. J. Bacteriol. 197, 410–419. http://dx.doi.org/10.1128/JB.02230-14.
Neubauer, P., Cruz, N., Glauche, F., Junne, S., Knepper, A., Raven, M., 2013. Consistent development of bioprocesses from microliter cultures to the industrial scale. Eng. Life Sci. 13, 224–238. http://dx.doi.org/10.1002/elsc.201200021.
Neubauer, P., Junne, S., 2010. Scale-down simulators for metabolic analysis of large-scale bioprocesses. Curr. Opin. Biotechnol. 21, 114–121. http://dx.doi.org/10.1016/j.copbio.2010.02.001.
Neumeyer, A., Hübschmann, T., Müller, S., Frunzke, J., 2013. Monitoring of population dynamics of Corynebacterium glutamicum by multiparameter flow cytometry. Microb. Biotechnol. 6, 157–167. http://dx.doi.org/10.1111/1751-7915.12018.
Noorman, H., 2011. An industrial perspective on bioreactor scale-down: what we can learn from combined large-scale bioprocess and model fluid studies. Biotechnol. J. 6, 934–943. http://dx.doi.org/10.1002/biot.201000406.
Ozbudak, E.M., Thattai, M., Kurtser, I., Grossman, A.D., van Oudenaarden, A., 2002. Regulation of noise in the expression of a single gene. Nat. Genet. 31, 69–73. http://dx.doi.org/10.1038/ng869.
Ozbudak, E.M., Thattai, M., Lim, H.N., Shraiman, B.I., Van Oudenaarden, A., 2004. Multistability in the lactose utilization network of Escherichia coli. Nature 427, 737–740. http://dx.doi.org/10.1038/nature02298.
Paige, J.S., Nguyen-duc, T., Song, W., Jaffrey, S.R., 2012. Fluorescence imaging of cellular metabolites with RNA. Science 335, 1194. http://dx.doi.org/10.1126/science.1218298.
Pátek, M., Nesvera, J., Guyonvarch, A., Reyes, O., Leblon, G., 2003. Promoters of Corynebacterium glutamicum. J. Biotechnol. 104, 311–323. http://dx.doi.org/10.1016/S0168-1656(03)00155-X.
Ploss, T.N., Reilman, E., Monteferrante, C.G., Denham, E.L., Piersma, S., Lingner, A., Vehmaanperä, J., Lorenz, P., van Dijl, J.M., 2016. Homogeneity and heterogeneity in amylase production by Bacillus subtilis under different growth conditions. Microb. Cell Fact. 15, 57. http://dx.doi.org/10.1186/s12934-016-0455-1.
Potzkei, J., Kunze, M., Drepper, T., Gensch, T., Jaeger, K.-E., Buechs, J., 2012. Real-time determination of intracellular oxygen in bacteria using a genetically encoded FRET-based biosensor. BMC Biol. 10, 28. http://dx.doi.org/10.1186/1741-7007-10-28.
Rollin, J.A., Tam, T.K., Zhang, Y.-H.P., 2013. New biotechnology paradigm: cell-free biosystems for biomanufacturing. Green Chem. 15, 1708–1719. http://dx.doi.org/10.1039/c3gc40625c.
Rosano, G.L., Ceccarelli, E.A., 2014. Recombinant protein expression in Escherichia coli: advances and challenges. Front. Microbiol. 5, 172. http://dx.doi.org/10.3389/fmicb.2014.00172.
Saïda, F., Uzan, M., Odaert, B., Bontems, F., 2006. Expression of highly toxic genes in E. coli: special strategies and genetic tools. Curr. Protein Pept. Sci. 7, 47–56.
Saliba, A.-E., Westermann, A.J., Gorski, S.A., Vogel, J., 2014. Single-cell RNA-seq: advances and future challenges. Nucleic Acids Res. 42, 8845–8860. http://dx.doi.org/10.1093/nar/gku555.
Santana, M.P., Aburjaile, F.F., Parise, M.T.D., Tiwari, S., Silva, A., Azevedo, V., Pinto, A.C., 2016. RNA-seq – revealing biological insights in bacteria. In: Kulski, J.K. (Ed.), Biochemistry, Genetics and Molecular Biology. Next Generation Sequencing - Advances, Applications and Challenges, pp. 205–228.
Scripture, J.B., Voelker, C., Miller, S., O'Donnell, R.T., Polgar, L., Rade, J., Horazdovsky, B.F., Hogg, R.W., 1987. High-affinity L-arabinose transport operon. Nucleotide sequence and analysis of gene products. J. Mol. Biol. 197, 37–46.
Shaner, N.C., Steinbach, P.A., Tsien, R.Y., 2005. A guide to choosing fluorescent proteins. Nat. Methods 2, 905–909. http://dx.doi.org/10.1038/nmeth819.
Siegele, D.A., Hu, J.C., 1997. Gene expression from plasmids containing the araBAD promoter at subsaturating inducer concentrations represents mixed populations. Proc. Natl. Acad. Sci. USA 94, 8168–8172.
Silander, O.K., Nikolic, N., Zaslaver, A., Bren, A., Kikoin, I., Alon, U., Ackermann, M., 2012. A genome-wide analysis of promoter-mediated phenotypic noise in Escherichia coli. PLoS Genet. 8, e1002443. http://dx.doi.org/10.1371/journal.pgen.1002443.
Smits, W.K., Kuipers, O.P., Veening, J.-W., 2006. Phenotypic variation in bacteria: the role of feedback regulation. Nat. Rev. Microbiol. 4, 259–271. http://dx.doi.org/10.1038/nrmicro1381.
Solopova, A., van Gestel, J., Weissing, F.J., Bachmann, H., Teusink, B., Kok, J., Kuipers, O.P., 2014. Bet-hedging during bacterial diauxic shift. Proc. Natl. Acad. Sci. USA 111, 7427–7432. http://dx.doi.org/10.1073/pnas.1320063111.
Stewart, M.K., Cookson, B.T., 2012. Non-genetic diversity shapes infectious capacity and host resistance. Trends Microbiol. 20, 461–466. http://dx.doi.org/10.1016/j.tim.2012.07.003.
Strack, R.L., Jaffrey, S.R., 2013. New approaches for sensing metabolites and proteins in live cells using RNA. Curr. Opin. Chem. Biol. 17, 651–655. http://dx.doi.org/10.1016/j.cbpa.2013.05.014.
Takors, R., 2012. Scale-up of microbial processes: impacts, tools and open questions. J. Biotechnol. 160, 3–9. http://dx.doi.org/10.1016/j.jbiotec.2011.12.010.
Tracy, B.P., Gaida, S.M., Papoutsakis, E.T., 2010. Flow cytometry for bacteria: enabling metabolic engineering, synthetic biology and the elucidation of complex phenotypes. Curr. Opin. Biotechnol. 21, 85–99. http://dx.doi.org/10.1016/j.copbio.2010.02.006.
Uhlendorf, J., Miermont, A., Delaveau, T., Charvin, G., Fages, F., Bottani, S., Batt, G., Hersen, P., 2012. Long-term model predictive control of gene expression at the population and single-cell levels. Proc. Natl. Acad. Sci. USA 109, 14271–14276. http://dx.doi.org/10.1073/pnas.1206810109.
Unthan, S., Grünberger, A., van Ooyen, J., Gätgens, J., Heinrich, J., Paczia, N., Wiechert, W., Kohlheyer, D., Noack, S., 2013. Beyond growth rate 0.6: what drives Corynebacterium glutamicum to higher growth rates in defined medium. Biotechnol. Bioeng. 111, 359–371. http://dx.doi.org/10.1002/bit.25103.

Vasdekis, A.E., Silverman, A.M., Stephanopoulos, G., 2015. Origins of cell-to-cell bioprocessing diversity and implications of the extracellular environment revealed at the single-cell level. Sci. Rep. 5, 17689. http://dx.doi.org/10.1038/srep17689.

Vasdekis, A.E., Stephanopoulos, G., 2015. Review of methods to probe single cell metabolism and bioenergetics. Metab. Eng. 27, 115–135. http://dx.doi.org/10.1016/j.ymben.2014.09.007.

Veening, J.-W., Murray, H., Errington, J., 2009. A mechanism for cell cycle regulation of sporulation initiation in Bacillus subtilis. Genes Dev. 23, 1959–1970. http://dx.doi.org/10.1101/gad.528209.

Veening, J.-W., Smits, W.K., Kuipers, O.P., 2008a. Bistability, epigenetics, and bet-hedging in bacteria. Annu. Rev. Microbiol. 62, 193–210. http://dx.doi.org/10.1146/annurev.micro.62.081307.163002.

Veening, J.-W., Stewart, E.J., Berngruber, T.W., Taddei, F., Kuipers, O.P., Hamoen, L.W., 2008b. Bet-hedging and epigenetic inheritance in bacterial cell development. Proc. Natl. Acad. Sci. USA 105, 4393–4398. http://dx.doi.org/10.1073/pnas.0700463105.

Wakamoto, Y., Dhar, N., Chait, R., Schneider, K., Signorino-Gelo, F., Leibler, S., McKinney, J.D., 2013. Dynamic persistence of antibiotic-stressed mycobacteria. Science 339, 91–95.

Wandrey, G., Bier, C., Binder, D., Hoffmann, K., Jaeger, K.-E., Pietruszka, J., Drepper, T., Büchs, J., 2016. Light-induced gene expression with photocaged IPTG for induction profiling in a high-throughput screening system. Microb. Cell Fact. 15, 63. http://dx.doi.org/10.1186/s12934-016-0461-3.

Westerwalbesloh, C., Grünberger, A., Stute, B., Weber, S., Wiechert, W., Kohlheyer, D., von Lieres, E., 2015. Modeling and CFD simulation of nutrient distribution in picoliter bioreactors for bacterial growth studies on single-cell level. Lab Chip 15, 4177–4186. http://dx.doi.org/10.1039/c5lc00646e.

Xiao, Y., Bowen, C.H., Liu, D., Zhang, F., 2016. Exploiting nongenetic cell-to-cell variation for enhanced biosynthesis. Nat. Chem. Biol. 12, 339–344. http://dx.doi.org/10.1038/nchembio.2046.

Young, D.D., Deiters, A., 2007. Photochemical activation of protein expression in bacterial cells. Angew. Chem. Int. Ed. Engl. 46, 4290–4292. http://dx.doi.org/10.1002/anie.200700057.

Young, J.W., Locke, J.C.W., Altinok, A., Rosenfeld, N., Bacarian, T., Swain, P.S., Mjolsness, E., Elowitz, M.B., 2012. Measuring single-cell gene expression dynamics in bacteria using fluorescence time-lapse microscopy. Nat. Protoc. 7, 80–88. http://dx.doi.org/10.1038/nprot.2011.432.

Zemella, A., Thoring, L., Hoffmeister, C., Kubick, S., 2015. Cell-free protein synthesis: pros and cons of prokaryotic and eukaryotic systems. Chembiochem 16, 2420–2431. http://dx.doi.org/10.1002/cbic.201500340.

Zenobi, R., 2013. Single-cell metabolomics: analytical and biological perspectives. Science 342, 1243259. http://dx.doi.org/10.1126/science.1243259.

Zhang, Y., Shang, X., Lai, S., Zhang, G., Liang, Y., Wen, T., 2012. Development and application of an arabinose-inducible expression system by facilitating inducer uptake in Corynebacterium glutamicum. Appl. Environ. Microbiol. 78, 5831–5838. http://dx.doi.org/10.1128/AEM.01147-12.

II.3 Establishing of light-controlled expression systems

II.3.1 Light-responsive control of bacterial gene expression

Light-responsive control of bacterial gene expression: Precise triggering of the *lac* promoter activity using photocaged IPTG

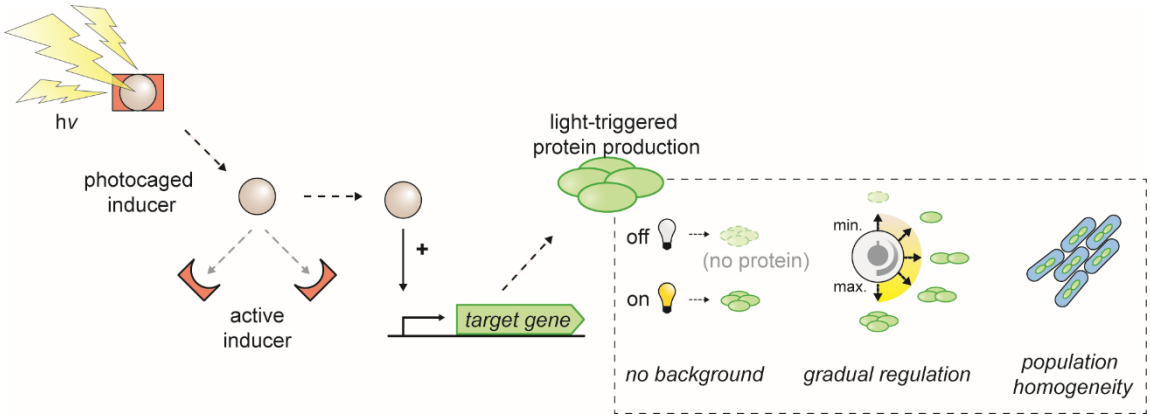

Dennis Binder, Alexander Grünberger, Anita Loeschcke, Christopher Probst, Claus Bier, Jörg Pietruszka, Wolfgang Wiechert, Dietrich Kohlheyer, Karl-Erich Jaeger and Thomas Drepper

Integr Biol (Camb). 2014;6: 755–65.

The full online version may be found at:
http://dx.doi.org/10.1039/c4ib00027g.

For the complete supporting information see Appendix (**Chapter V.2**) turn to page **195.**

Integrative Biology

PAPER

View Article Online
View Journal | View Issue

Light-responsive control of bacterial gene expression: precise triggering of the *lac* promoter activity using photocaged IPTG†

Cite this: *Integr. Biol.*, 2014, 6, 755

Dennis Binder,‡[a] Alexander Grünberger,‡[b] Anita Loeschcke,[a] Christopher Probst,[b] Claus Bier,[c] Jörg Pietruszka,[bc] Wolfgang Wiechert,[b] Dietrich Kohlheyer,[b] Karl-Erich Jaeger*[ab] and Thomas Drepper*[a]

Received 7th February 2014,
Accepted 15th May 2014

DOI: 10.1039/c4ib00027g

www.rsc.org/ibiology

Light can be used to control numerous cellular processes including protein function and interaction as well as gene expression in a non-invasive fashion and with unprecedented spatiotemporal resolution. However, for chemical phototriggers tight, gradual, and homogeneous light response has never been attained in living cells. Here, we report on a light-responsive bacterial T7 RNA polymerase expression system based on a photocaged derivative of the inducer molecule isopropyl-β-D-thiogalactopyranoside (IPTG). We have comparatively analyzed different *Escherichia coli lac* promoter-regulated expression systems in batch and microfluidic single-cell cultivation. The *lacY*-deficient *E. coli* strain Tuner(DE3) harboring additional plasmid-born copies of the *lacI* gene exhibited a sensitive and defined response to increasing IPTG concentrations. Photocaged IPTG served as a synthetic photo-switch to convert the *E. coli* system into an optogenetic expression module allowing for precise and gradual light-triggering of gene expression as demonstrated at the single cell level.

Insight, innovation, integration

Optogenetic approaches aim to trigger biological processes by light. For the establishment of a light-responsive *E. coli* expression system, we validate different *lac* promoter-controlled, T7 RNA polymerase-dependent expression modules. Using microfluidic techniques we were able to pin down and abolish bottlenecks of inducer-dependent regulatory response. By implementing a derivative of the synthetic inducer IPTG, which is coupled to the light-sensitive photocaging group 6-nitropiperonal, we assembled a precise photoswitch that can be controlled by UV-A light.

Introduction

Synthetic biology requires the development of regulatory switches that facilitate dynamic regulation of target gene expression.[1–4] In this context, optogenetic approaches demonstrated precise control over cellular functions by light.[5–7] The unique variability of the stimulus light, including its color and intensity, allows for a specific triggering of cellular events in a non-invasive and highly resolving spatiotemporal fashion.[5] Light-mediated control over gene expression basically relies on two principles which use either genetically encoded biological photoreceptors or chemically photocaged biomolecules.[6–9] Recombinant photoreceptors, for example, have been successfully employed for light-mediated *in vivo* signal transduction in synthetic biological applications.[10–12] The principle of photocaging poses an alternative approach to achieve light-mediated control over gene expression. Photocaged molecules are rendered biologically inactive through the addition of a photo-removable protection group, the so-called photocaging group or photocage. Functionality can be restored, both *in vitro* and *in vivo*, by the light-mediated release (uncaging) of the bioactive molecule.[13] Plenty of biomolecules were subjected to photocaging, including proteins or small inducer molecules,[7,14] *e.g.* isopropyl β-D-thiogalactopyranoside (IPTG)[15] and a doxycycline analog,[16] which were able to activate *lac* and *tet* promoter-controlled microbial expression systems upon UV-A light exposure.

[a] *Institute of Molecular Enzyme Technology, Heinrich-Heine-University Düsseldorf, Research Center Jülich, Germany. E-mail: k.-e.jaeger@fz-juelich.de, t.drepper@fz-juelich.de*
[b] *Institute of Bio- and Geosciences, IBG-1: Biotechnology, Systems Biotechnology, Research Center Jülich, Germany*
[c] *Institute for Bioorganic Chemistry, Heinrich-Heine-University Düsseldorf, Research Center Jülich, Germany*

† Electronic supplementary information (ESI) available. See DOI: 10.1039/c4ib00027g

‡ These authors contributed equally to this work.

Induction of *lac* promoter-dependent gene expression by sugar analogs with light-responsive photocaging was first described using 6-nitropiperonal (NP) photocaged IPTG.[15] Here, the NP-photocaged IPTG was unable to bind the repressor LacI, while its biological activity was restored upon UV-A light exposure, leading to LacI binding and therefore to derepression of gene expression.[15] However, currently available light-controlled systems, which operate with photocaged molecules (caged T7RP; caged IPTG; caged doxycycline),[15–17] have not yet been employed for precise and homogeneous *in vivo* regulation of microbial gene expression.

The *Escherichia coli* T7-RNA polymerase (T7RP)-dependent expression system is regarded as the most widely used system for high-level gene expression.[18–20] It consists of a lambda DE3 lysogenic *E. coli* strain carrying a chromosomally integrated copy of the T7RP gene whose expression is tightly controlled by the *lac* promoter[20] and an appropriate expression plasmid allowing target gene expression from a T7 promoter. The highly processive phage polymerase exclusively targets its own promoter and therefore operates decoupled from other cellular processes.[21] For this reason, the *E. coli* T7 system is recommended as a 'what to try first' system for the expression of pro- and eukaryotic proteins.[20,22]

One of the most prominent T7RP expression strains is *E. coli* BL21(DE3).[19] However, this common system harbors the wild-type *E. coli lac* operon including the lactose permease-encoding *lacY* gene, whose expression is also lactose-dependent and causes a positive feedback loop by actively translocating inducer molecules into the cell.[23] Thereby, it generates a non-gradual and also inhomogeneous induction behavior over a bacterial population, especially for low amounts of inducer molecules.[24] Therefore, the precise fine regulation of gene expression using common T7RP- and *lac*-based expression modules appears to be difficult.

The expression of a target gene is usually analyzed within an entire bacterial population; however, to gain insights into exact regulation processes, the expression needs to be studied at the single cell level. Currently, batch cultivation is combined with reporter-imaging technologies such as single cell photography[25] or flow cytometry analysis.[26] A profound drawback of these methods is the system-inherent discontinuous environment.[27] For instance, nutrient depletion and accumulation of metabolic products result in discontinuity over time within the cultivation vessel.[28] Therefore, those methods are unable to distinguish between environmental or biological heterogeneity or even determine the origin of depicted heterogeneities.[27,29] Furthermore, the above mentioned single cell analyses such as fluorescence-activated cell sorting (FACS) only provide a snapshot of cellular states rather than full information about ongoing behavior and could additionally produce artificial results as cells are analyzed "off-line" outside the cultivation device.

The challenge of understanding cellular heterogeneity resulted in an increasing amount of different devices and protocols for investigating single cells "on-line". Systems range from basic agar-pads[30] to advanced microfluidic single cell set-ups.[31–33] The latter include single cell traps,[34] single cell channels[35,36] and monolayer growth chambers.[37,38] Recently, a picoliter bioreactor for the investigation of single cell processes over many generations under constant conditions was developed.[39] Since cells are cultured in a monolayer, the genealogical analysis of clonal colonies can be performed,[40,41] allowing for the reconstruction of lineage trees and thus for accurately assessing population heterogeneity under constant environmental conditions in contrast to common agar-pad-based technologies.[42]

With this advanced microfluidic technology at hand, we characterized different *E. coli* T7RP expression systems in order to establish an efficient and light-responsive expression system in *E. coli*.

Materials and methods

Bacterial strains and plasmids

Escherichia coli strains DH5α,[43] BL21(DE3)[18] and Tuner(DE3) (Novagen) were grown in Luria–Bertani (LB) medium[44] supplemented with kanamycin (50 μg ml^{-1}) or chloramphenicol (50 μg ml^{-1}) at 37 °C under constant agitation.

The construction of expression vectors and recombinant DNA techniques were carried out in *E. coli* DH5α as described by Sambrook *et al.*[44]

The derivative of the pRhotHi-2[45] expression vector pRhotHi-2-LacI was constructed by excising the *aphII* gene from pBSL15[46] with restriction enzyme *Bam*HI. The resulting fragment was subsequently cloned into the *Bgl*II-site of pBBR22b,[47] harboring a copy of the *lacI* gene. As the final expression vector, the variant was chosen, where *aphII* and T7 promoters were oriented in opposite directions. The EYFP-encoding reporter gene,[48] which was isolated by hydrolyzing pRhotHi-2-EYFP with *Nde*I and *Xho*I, was cloned into pRhotHi-2-LacI resulting in pRhotHi-2-LacI-EYFP.

All bacterial strains and plasmids used in this study are listed in Table S1 (ESI†).

NP-photocaged IPTG synthesis modified according to Young & Deiters 2007[15]

IPTG (100 mg, 0.42 mmol) and 6-nitropiperonal (245 mg, 1.26 mmol, for synthesis see ESI,† Methods) were dissolved in 1 ml of dimethylsulfoxide (DMSO). At 0 °C concentrated sulfuric acid (0.15 ml) was carefully added and the reaction was allowed to warm up to room temperature. After 24 h the reaction mixture was quenched with water and extracted with ethyl acetate. The combined organic layer was dried over magnesium sulfate and concentrated under reduced pressure. The residue was purified by flash-column chromatography on SiO_2 (EtOAc/pentane 7 : 3) to receive (122.5 mg, 0.29 mmol, 72%) of a light yellow solid. After an additional cleaning step *via* MPLC we had (31.4 mg, 0.08 mmol) of a colorless pure product, with a yield of 18% in our hands. Analytical data are shown in the ESI,† Methods.

Deep well plate cultivation and off-line measurement of *in vivo* fluorescence

Expression cultures were grown in 96 deep well plates (Master Block, Greiner Bio One) by shaking at 600 rpm. After inoculation

with a cell density corresponding to an OD_{580} of 0.1 in a volume of 950 µl, expression cultures were incubated for 2 h until cells reached an OD_{580} of 0.4–0.6. The target gene expression was induced with 50 µl of inducer solution leading to final inducer concentrations in a range from 0 to 100 µM IPTG in a final volume of 1 ml.

Cultures (1 ml) pre-supplemented with 40 µM NP-photocaged IPTG were grown in the dark for 1, 1.5 or 2 h and subsequently exposed to UV-A light for 0.25 to 10 minutes (hand lamp VL-315.BL, Vilber Lourmat, France; placed at a distance of 2.5 cm over the deep well plate). After 6 and 20 h of cultivation in the dark, respectively, *in vivo* fluorescence and cell densities (OD_{580}) were measured in 96 flat bottom transparent polystyrene microplates (Thermo scientific-Nunclon) using a fluorescence microplate-reader (Tecan Infinite M1000 Pro). Prior to measurements samples were diluted 5-fold in 0.1 M Tris-HCl buffer (pH 8.0) resulting in a final volume of 100 µl. Emission of YFP was determined at 527 nm after excitation with blue light (λ_{max} = 488 nm). Fluorescence units of diluted samples were normalized to a cell density of OD_{580} = 1.0.

Microfluidic cultivation

A single-use polydimethylsiloxane (PDMS) microfluidic chip fabricated as previously described[39,49] was utilized to cultivate single cells and isogenic microcolonies (Fig. 1). A single chip used in this study (Fig. 1A) contained several hundred monolayer growth chambers (Fig. 1B and C) (dimensions: 1 µm × 40 µm × 40 µm) facilitating high-throughput single cell analysis. Each growth chamber was interconnecting two parallel 10-fold deeper supply channels, as illustrated in Fig. 1D. Throughout the operation both supply channels were infused with identical volume flow rates. This resulted in solely diffusion-based mass transport across the shallow cultivation chambers, permitting reliable single cell tracking for genealogical studies inside growing microcolonies.

Cell suspensions for chip perfusion were prepared by inoculating fresh cultures from a preculture to an OD_{580} of 0.05 and cultivated until the mid-logarithmic growth phase was reached.

This cell suspension was infused at 200 nl min^{-1} using 1 ml disposable syringes and high precision syringe pumps (neMESYS, Cetoni, Germany) to randomly inoculate single mother cells into the growth chambers. After sufficient single cells were trapped, the cell suspension was replaced with fresh LB medium infused at 100 nl min^{-1}. After 1 h cultivation, cells were induced by IPTG supplemented LB cultivation media.

During cultivation at 37 °C the chip was continuously perfused with fresh medium to maintain constant environmental culture conditions. If desired, the perfusion of fresh medium was manually stopped to induce batch equivalent conditions inside the chambers (with nutrition depletion and byproduct accumulation). Media supplemented with NP-photocaged IPTG were exposed to UV-A light prior to use.

Time-lapse microscopy and image analysis

The microfluidic chip was mounted onto a motorized microscope (Nikon Eclipse Ti) equipped with an in-house developed incubator and a heated Nikon Apo TIRF 100× Oil DIC N objective (ALA OBJ-Heater, Ala Scientific Instruments, USA) for temperature control. Furthermore, the microscope was equipped with a Nikon perfect focus system compensating for thermal drift, an ANDOR LUCA R DL604 EMCCD camera (Andor Technology plc., Belfast, UK), a 300 W Xenon light source for fluorescence excitation (Lambda DG4, Sutter Instruments, USA), and YFP fluorescence filters (AHF Analysentechnik, Germany) (excitation: 500 nm/20, dichroic: 500 nm and emission: 535 nm/30). If not stated different, the fluorescence and camera exposure was 200 ms for EYFP, at zero camera gain and 100% lamp intensity. Fluorescence exposure times were minimized to avoid the impact on cellular growth or viability.

Phase contrast and fluorescence microscopy images of multiple colonies were captured in a sequence every 10 min by automated time-lapse microscopy thereby facilitating image-based single cell analysis with spatiotemporal resolution. Final image sequences were analyzed using the Nikon NIS Elements AR software package to determine cell length and fluorescence intensity. The mean fluorescence intensity of each cell was determined by measuring the fluorescence values of each cell and subtracting the background fluorescence value obtained from an empty position of the cultivation chamber. The visualization of the lineage tree was realized using in-house developed Python-based software.

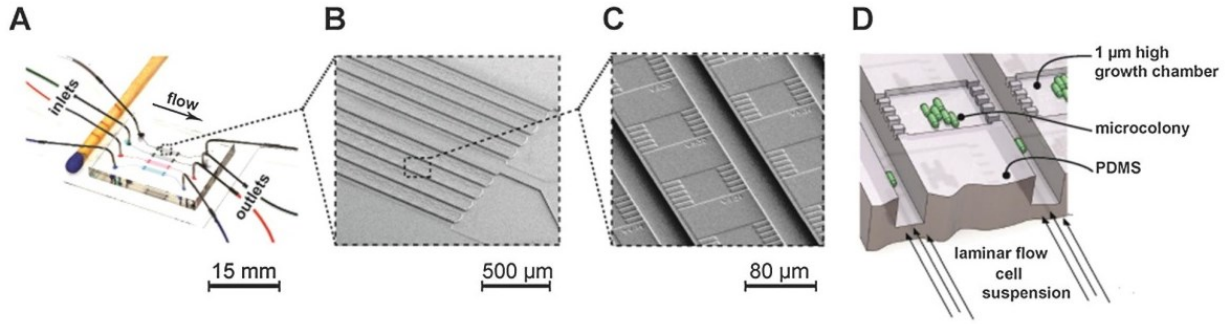

Fig. 1 Microfluidic PDMS single cell cultivation devices. (A) Photograph of a PDMS cultivation chip next to a match. (B) SEM of monolayer cultivation sections containing several hundreds of single cultivation chambers (C). (D) Schematic illustration of microscale growth chamber that is perfused with cell suspensions and media for cultivation of trapped cells.

Results and discussion

We aimed to establish an optogenetic expression system in bacteria that provides minimal background activity as well as a gradual and homogenous light response within the entire cell population (Fig. 2A). Hence, we constructed a *lac* promoter-based *E. coli* T7RP expression system that provides exact controllability *via* photocaged inducer molecules (Fig. 2B). The characteristics and functions of all regulatory and metabolic elements involved in the control of *lac* promoter/operator activity in *E. coli* are well described.[19,50,51] In this context, the repressor LacI, the lactose permease LacY and the diffusible artificial inducer IPTG play key roles in triggering *lac* gene expression. Firstly, the impact of LacY and LacI on the stringency and regulatory dynamics of *lac* promoter/operator-based gene expression was analyzed by characterization of different *E. coli* T7RP-based expression systems (Table 1) at both population and single cell level. The applied expression systems constitute combinations of *E. coli* strains and plasmids differing in their *lacY* and *lacI* configurations, whereas the expression of the genes encoding the T7 polymerase and the *in vivo* fluorescence reporter YFP is always controlled by the same *lac* promoter and operator, respectively.

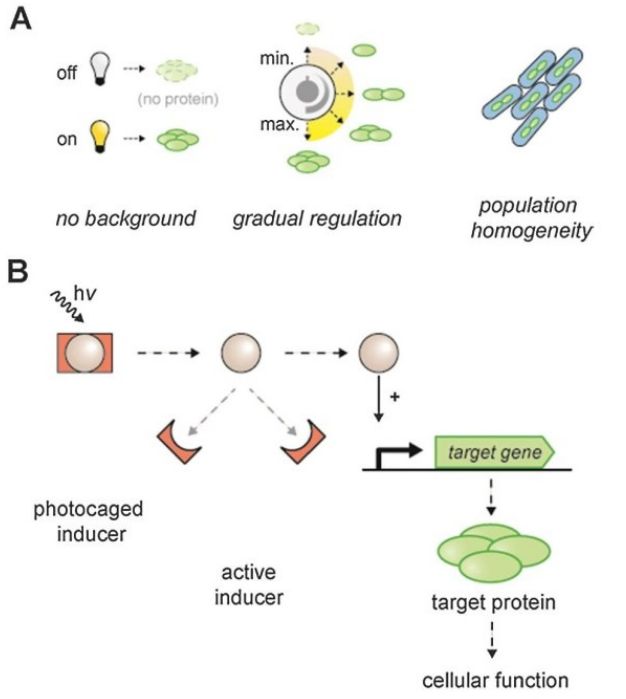

Fig. 2 Principal characteristics of the aimed *lac* promoter-based optogenetic expression system. (A) Low background activity will ensure a defined switch from a clear OFF state to an ON state with high gene expression levels. A gradual induction response will allow a direct correlation between defined irradiation times and protein accumulation levels. Simultaneous and identical induction behavior of all cells will produce a homogeneous population. (B) Concept of exerting light-dependent control over gene expression using the photocaged inducer IPTG. NP-photocaged IPTG is released upon UV-A light irradiation. The decaged inducer activates the *lac* promoter and induces gene expression allowing for a light-responsive control of cellular behavior.

Table 1 *E. coli* expression systems characterized in this study

E. coli strain/plasmid	*lacY*[a]	*lacI*[a]
BL21(DE3)/pRhotHi-2-EYFP	chr	chr
Tuner(DE3)/pRhotHi-2-EYFP	—	chr
Tuner(DE3)/pRhotHi2-LacI-EYFP	—	chr/pl

[a] chr: chromosome, pl: plasmid.

The role of lactose permease was studied by comparing IPTG-dependent responsiveness of YFP expression in the commonly used *E. coli* T7RP expression strain BL21(DE3)[19,20,22] (*lacY*$^+$, *lacI*$^+$) to the so far rarely used permease-deficient *E. coli* T7RP expression strain Tuner(DE3) (*lacY*$^-$, *lacI*$^+$). *E. coli* Tuner(DE3) is suitable for inducer-dependent adjustment of gene expression levels[52] and assumed to show homogeneous induction behavior that, however, has not been verified in a scientific study so far. The mid-copy T7RP expression plasmids pRhotHi-2 (*lacI*$^-$)[45] and pRhotHi-2-LacI (*lacI*$^+$) additionally allowed us to adjust the intracellular levels of the repressor LacI.

Strict regulation of *lac* operator-controlled gene expression is impeded in *E. coli* standard expression host BL21(DE3)

Properties of *lac* regulation were first investigated in *E. coli* BL21(DE3) carrying the expression vector pRhotHi-2-EYFP. Cells were initially grown in a common batch cultivation set-up (Fig. 3A) using IPTG concentrations ranging from 0 to 100 μM. YFP *in vivo* fluorescence was quantified 6 and 20 h (representing the late logarithmic and stationary phase, respectively) after induction of gene expression (Fig. 3B). The results clearly demonstrated a high background expression level in non-induced cultures (0 μM IPTG). In all cases, the addition of IPTG led to a moderate increase of YFP-mediated *in vivo* fluorescence (a two-fold increase after 6 h and a three-fold increase after 20 h), irrespective of the applied inducer concentration. The results thus show that the first strain/vector system, where LacY is present and the amount of LacI is low, neither exhibits low background activity nor allows gradual induction of gene expression. Subsequently, homogeneity of the induction behavior was tested for the chosen expression system in a microfluidic perfusion set-up (Fig. 3C), which allows us to keep *E. coli* in the logarithmic growth phase under persistent cultivation conditions until the growth chamber is completely filled with cells. To this end, cells were trapped in microscale growth chambers and incubated for 1 h before YFP expression was induced applying media supplemented with different IPTG concentrations. To analyze the mean fluorescence during the development of microcolonies, single cell fluorescence values were monitored for a cultivation time of up to 500 min (Fig. 3D).

Low inducer concentrations (10 μM IPTG) resulted in a highly heterogeneous expression response of individual cells, as reflected by large error bars. With 40 μM IPTG, cells exhibited a homogeneously strong fluorescence. Apparently, the expression response was saturated at this concentration, as supplementation with 100 μM IPTG produced the same results (see Fig. S1, ESI†). Interestingly, evaluable time periods (*i.e.* the

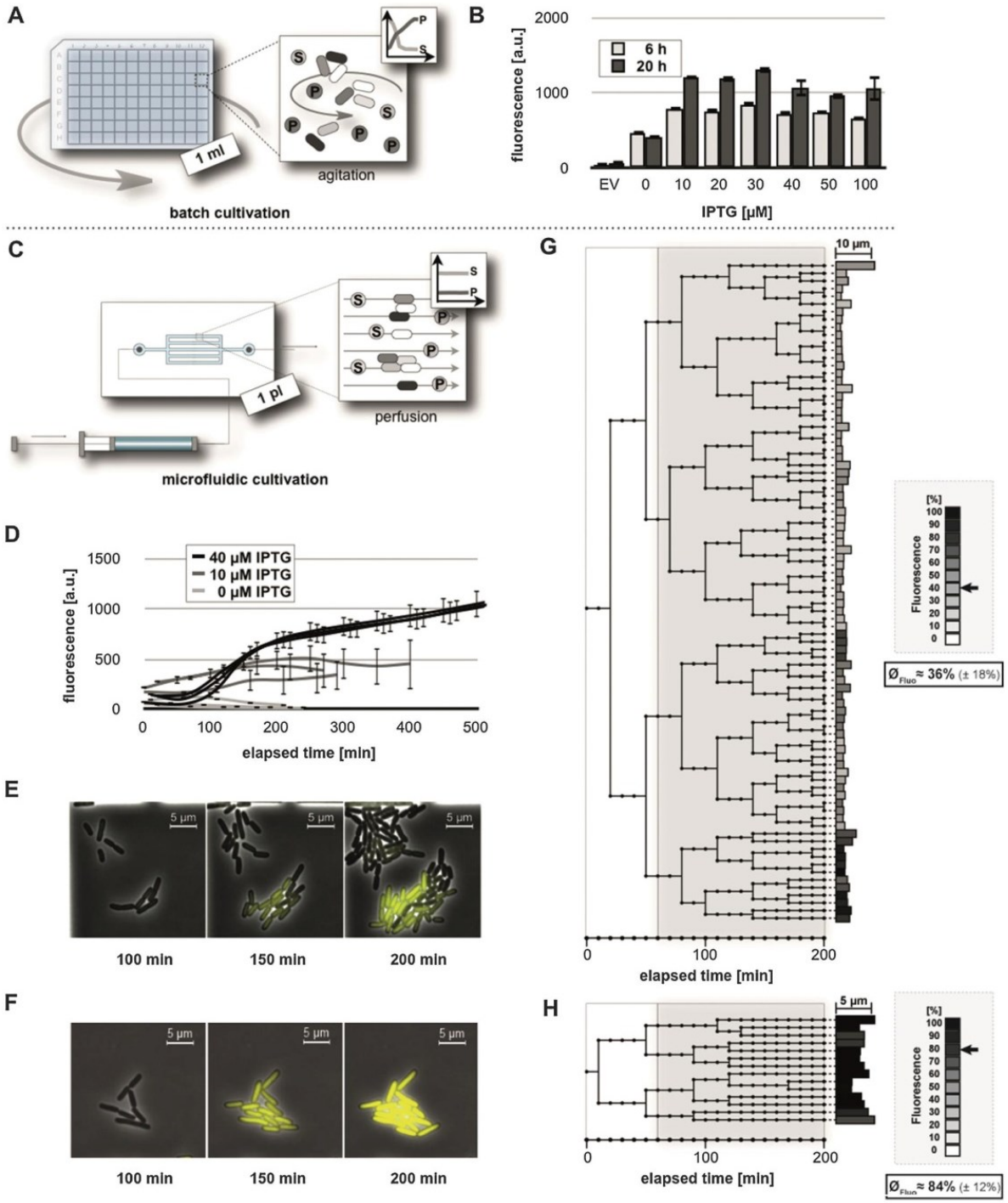

Fig. 3 Analysis of IPTG-induced expression in *E. coli* BL21(DE3)/pRhotHi-2-EYFP. (A) Schematic diagram of *E. coli* batch cultivation in deep well plates, where cells were agitated in a defined volume of cultivation medium. Metabolizable media components (Ⓢ) are consumed while metabolic products (Ⓟ) accumulate over time. (B) *In vivo* fluorescence of batch cultures at different IPTG concentrations. EV: empty vector control. Values are means of triplicate measurements. Error bars indicate the respective standard deviations. a.u.: arbitrary units. (C) Schematic diagram of microfluidic perfusion cultivation, where medium is constantly flushed through growth chambers. Here, both media components (Ⓢ) and metabolic products (Ⓟ) are maintained at constant levels. (D) Fluorescence of developing microcolonies during differently supplemented microfluidic cultivation. For each IPTG concentration, single cell fluorescence values were monitored for three independent microcolonies until the bacteria fully colonized the growth chambers. (E, F) Selected photographs from time lapse microscopy during microfluidic cultivation with 10 µM (E) and 40 µM IPTG (F). (G, H) Lineage trees of single cells, where YFP expression (grey highlighted) was induced with 10 µM (G) and 40 µM IPTG (H) after 1 h of precultivation. Lineage trees were generated from data of representative microcolonies over a period of 200 minutes. End point fluorescence (grayscale) and individual cell size (bar length) are plotted. In the box, the fluorescence mean value and standard deviation normalized to the highest value achieved in all microfluidic experiments is depicted. This fluorescence value is also marked by an arrow.

cultivation time needed by a microcolony to fully occupy the micro-incubation chamber) indicated an inverse correlation between *lac* induction and cellular growth (Fig. 3D). This was likewise observed for single cell traces of differently induced *E. coli* BL21(DE3)/pRhotHi-2-EYFP cells (see Fig. S3, ESI†).

Remarkably, in contrast to the observations made in batch cultures (Fig. 3B), cells in the microfluidic set-up (Fig. 3D) showed that very low YFP fluorescence intensities could be observed where YFP expression was induced with 40 instead of 10 μM IPTG. These observations might result from elementary differences in applied cultivation technologies, as in batch cultivation, media components such as glucose that are involved in carbon catabolite repression of the *lac* promoter are consumed over time, whereas in the microfluidic perfusion system cells are continuously supplied with fresh media. Therefore, media components relevant for catabolite repression may be maintained at 'repressing' concentrations without additional IPTG and also might impair full induction of YFP expression at intermediate inducer concentrations (*i.e.* 10 μM) during microfluidic but not batch cultivation.

To further analyze the fluorescence development at the single cell level during microfluidic cultivation, lineage trees were generated from data of representative microcolonies, each of which developed from a single cell, supplemented with 10 or 40 μM IPTG over a time-period of 200 minutes (Fig. 3G and H).

In a microcolony supplemented with 10 μM IPTG (Fig. 3G) variably fluorescing (the mean value of normalized YFP fluorescence: 36% ± 18%) and differentially growing sub-populations developed from the initial cell (see also Video S1, ESI†). At the time of induction, four cells gave rise to explicitly different branches. In the three upper branches where cells showed only low fluorescence, the bacteria divided 23 times on average. In contrast, in the lower branch, where cells showed relatively high fluorescence, bacteria divided only 11 times. As expected from the results shown in Fig. 3D and F, the tree ended with uniformly strong fluorescing cells (84% in average with a standard deviation of ±12%) when the medium was supplemented with 40 μM IPTG (Fig. 3H). Here, the correlation of *lac* induction with cellular growth becomes evident in an altogether drastically smaller tree. On average, cells divided only 2.5 times after induction. The observed inconsistency of growth rates at lower inducer concentrations may promote overgrowth of cells with lower expression levels and displacement of cells with higher expression levels during cultivation, yielding a rather unfavorable overall expression and unpredictable regulatory response.

In summary, applying microfluidic cultivation with time lapse microscopy allowed for the first time to demonstrate differences in the induction response in cells of the standard expression host *E. coli* BL21(DE3). In combination with pRhotHi-2-EYFP this strain does not allow precise control of gene expression as required for systems biology and optogenetic approaches. It exhibits a high expression background in the absence of IPTG, a non-gradual expression response to increasing inducer concentrations as well as an inhomogeneous and unpredictable behavior of individual cells at intermediate inducer concentrations. In another study, these characteristics have also been observed for expression of a reporter gene which was under direct control of the *lac* promoter.[53] We show here that these same observations also hold for the T7RP expression system.

LacY-deficiency and elevated amounts of the LacI repressor enable precise control of T7RP-dependent gene expression

Deletion of *lacY* eliminates permease-mediated IPTG import and thus prevents the positive feedback loop.[24] As a consequence, IPTG can only enter the cells *via* diffusion processes which thereby enables strict dependency of *lac* gene expression on supplemented inducer concentrations.[23]

Hence, we next examined IPTG-responsiveness of the lactose permease-deficient strain *E. coli* Tuner(DE3) ($lacY^-$, $lacI^+$) in the absence or presence of an additional copy of the plasmid-born *lacI* gene. First, expression of the YFP reporter gene was analyzed in *E. coli* Tuner(DE3) carrying pRhotHi-2-EYFP ($lacI^-$) at increasing inducer concentrations (0–100 μM) in a batch cultivation set-up (Fig. 4A). As expected, this strain showed a gradual expression response for low amounts of inducer up to 20 μM. Moreover, a lower background expression of YFP was observed compared to the expression in *E. coli* BL21(DE3), leading to a 5-fold (6 h) to 8-fold (20 h) increase of *in vivo* fluorescence intensities. These results confirm the characteristics of the T7RP expression strain *E. coli* Tuner(DE3) described before[52] and corroborate that *lacY*-deficiency allows a gradual induction of *lac* promoter-dependent gene expression in response to increasing inducer concentrations.[24] Notably, in our system the *lac* promoter-controlled expression is conveyed *via* T7RP to the fluorescence output. However, basal expression of this system was still too high for aspired optogenetic applications. In order to overcome this leaky basal expression observed in *E. coli* Tuner(DE3) with pRhotHi-2-EYFP, an additional copy of the *lac* repressor gene *lacI* was introduced. To this end, the new expression vector pRhotHi-2-LacI was constructed, harboring a copy of the *lacI* gene under the control of its natural constitutive promoter. Subsequently, *E. coli* Tuner(DE3)/pRhotHi-2-LacI-EYFP was subjected to expression studies applying inducer concentrations from 0 to 100 μM (Fig. 4B). Compared to both afore conducted expression studies (Fig. 3B and 4A), a clearly reduced background expression under non-induced conditions was observed. Furthermore, expression response strictly depended on inducer concentrations enabling a gradual response for IPTG concentrations up to 30 μM and 40 μM after 6 and 20 hours, respectively. Maximal induction of reporter gene expression finally resulted in a 15-fold (6 h) and 23-fold (20 h) increase of YFP-mediated fluorescence (Fig. 4B). Moreover, with an exception for induction with 100 μM IPTG, the ratio of the fluorescence signal detected after 6 and 20 hours of cell cultivation remained remarkably constant and is thus largely independent of the growth phase. The homogeneity of expression response within a cell population of *E. coli* Tuner(DE3) harboring expression plasmid pRhotHi-2-LacI-EYFP was tested by monitoring the fluorescence development of single cells using microfluidic

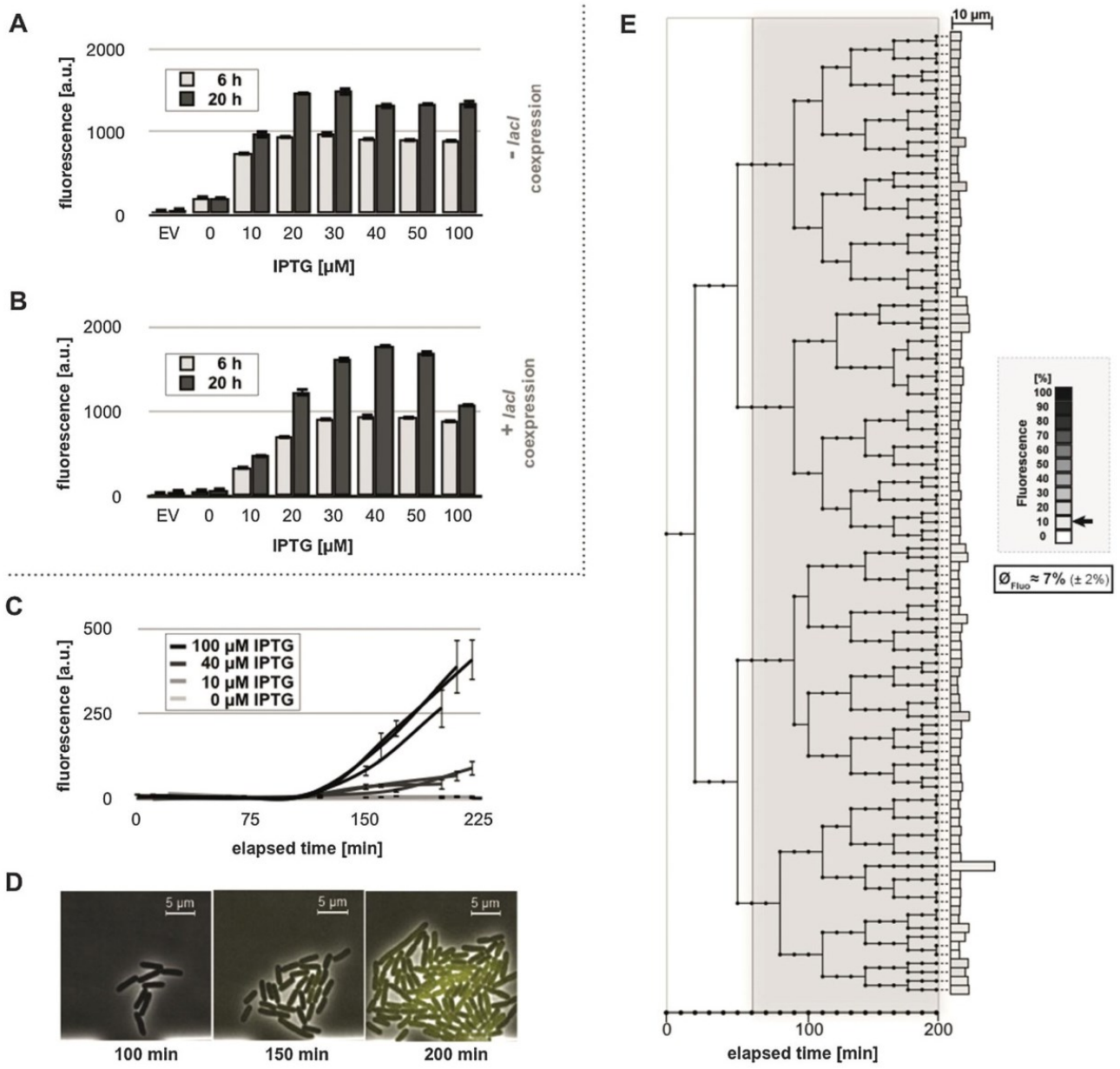

Fig. 4 Analysis of IPTG-induced expression in *E. coli* Tuner (DE3)/pRhotHi-2-EYFP (A) and Tuner(DE3)/pRhotHi-2-LacI-EYFP (B–E). (A, B) Development of *in vivo* fluorescence during batch cultivations of *E. coli* Tuner(DE3) with pRhotHi-2-eYFP (A) and pRhotHi-2-LacI-EYFP (B) after addition of increasing concentrations of IPTG. EV: empty vector control. Values are means of triplicate measurements. Error bars indicate the respective standard deviations. a.u.: arbitrary units. (C) Fluorescence development of microcolonies during microfluidic cultivation. Single cell fluorescence values were monitored for three independent microcolonies. For each IPTG concentration, fluorescence development of three microcolonies is plotted. Data points represent mean fluorescence values of all cells with the standard deviation as error bars. (D) Selected photographs from time lapse microscopy during microfluidic cultivation with 40 µM IPTG. (E) Lineage tree of a single cell, where YFP expression (grey highlighted) was induced with 40 µM IPTG after 1 h of precultivation. Lineage trees were generated from data of representative microcolonies over a period of 200 minutes. End point fluorescence (grayscale) and individual cell size (bar length) are plotted. Furthermore, the fluorescence mean value and standard deviation normalized to the highest value obtained in all microfluidic experiments are depicted. This fluorescence value is also marked by an arrow.

techniques (Fig. 4C–E). Traces of representative microcolonies displayed a gradual (Fig. 4C) and homogeneous (Fig. 4D) fluorescence increase. However, final fluorescence values were much weaker than those previously observed in *E. coli* BL21(DE3) with pRhotHi-2-EYFP (Fig. 3D and 4C). Therefore, fluorescence development of cultures that were supplemented with 10 µM IPTG showed no significant increase in YFP *in vivo* fluorescence as also observed for uninduced cells. The generally lower fluorescence values of Tuner(DE3) might be explained by the faster growth that restricted the evaluable time period to 225 minutes. This assumption was corroborated by long-term microfluidic cultivation that revealed comparable final *in vivo* fluorescence values for both investigated strains (Fig. S4, ESI†). To analyze the fluorescence development of an initial single cell

during repeated cell division, a lineage tree was generated over a time period of 200 minutes from a representative microcolony where target gene expression was induced by adding 40 μM IPTG (Fig. 4E). In contrast to *E. coli* BL21(DE3)/pRhotHi-2-EYFP, this tree branches to cells with equal end point fluorescence values of 7% ± 2% (see also additional histograms in Fig. S2B, ESI†). Moreover, no distinctive growth impairment occurred (also elucidated by additional single cell traces shown in Fig. S5, ESI†), as indicated by a high cell division rate after induction of gene expression (26 times on average). The detailed characterization of the *E. coli* T7RP expression strain Tuner(DE3) demonstrates that *lac* permease deficiency and elevated *lacI* copy numbers enable the precise control of gene expression levels. The respective strain showed low background expression and a gradual induction response to different inducer concentrations. Furthermore, this expression system exhibits a superior homogeneity in both expression behavior and cellular growth, which is independent of the applied cultivation conditions.

Precise triggering of T7RP-dependent gene expression by light

The expression system composed of *E. coli* Tuner(DE3) and pRhotHi-2-LacI-EYFP was used to implement light-responsive gene expression. To this end, we synthesized an NP-photocaging group which was subsequently coupled to IPTG as described before[15] (see Methods, ESI†), yielding NP-photocaged IPTG (Fig. 5A). After UV-A exposure, the resulting regioisomeric NP-nitrosocarbonyl esters are hydrolyzed in *E. coli* releasing IPTG (Fig. 5A).

The light-responsiveness of this expression system was tested with *E. coli* Tuner(DE3) cells carrying plasmid pRhotHi-2-LacI-EYFP that were batch cultivated in LB medium supplemented with 40 μM NP-photocaged IPTG for two hours in the dark. T7RP-dependent YFP expression was induced by exposure

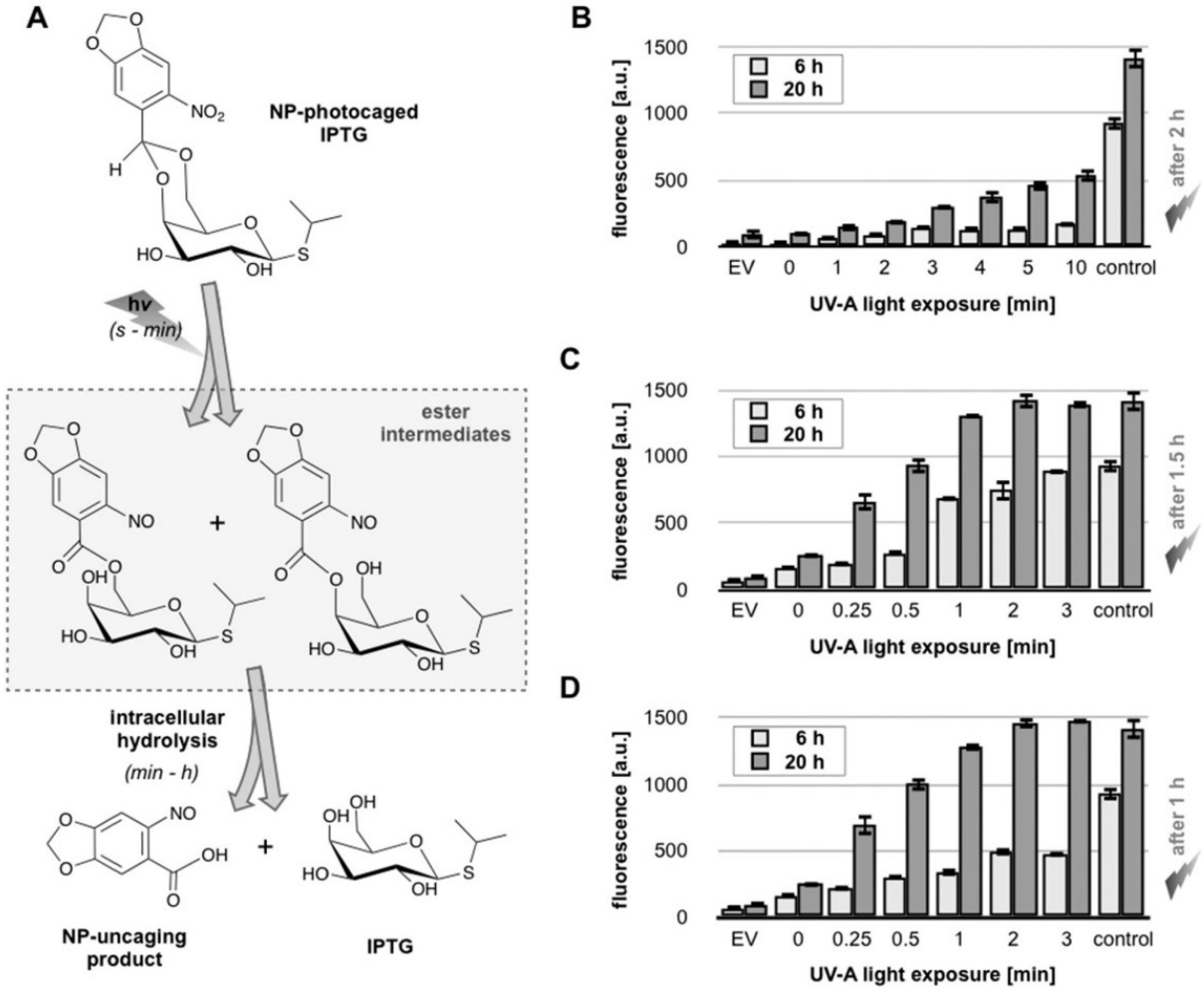

Fig. 5 UV-A light-controlled regulation of gene expression in *E. coli* Tuner(DE3)/pRhotHi-2-LacI-EYFP using NP-photocaged IPTG. (A) Two-step release of NP-photocaged IPTG by UV-A light exposure and intracellular hydrolysis as described by Young & Deiters (2007).[15] The reaction times ranging from seconds (s) over minutes (min) to hours (h) are given in brackets. (B–D) *In vivo* fluorescence of *E. coli* cultures supplemented with 40 μM NP-photocaged IPTG. Gene expression was specifically induced by increasing periods of UV-A light exposure. Cultures were induced after 2 h (B), 1.5 h (C) or 1 h (D) of pre-cultivation where cells were kept in darkness. Corresponding control cultures were supplemented with 40 μM uncaged IPTG. EV: empty vector control. Values are means of triplicate measurements. Error bars indicate the respective standard deviations. a.u.: arbitrary units.

to UV-A light (λ_{max} = 365 nm) with increasing times ranging from 0 to 10 minutes (Fig. 5B). As shown in Fig. S6 (ESI†), UV-A illumination did not lead to phototoxic effects since exposure times of up to 30 minutes are not affecting cellular fitness. Subsequently, YFP *in vivo* fluorescence was recorded 6 and 20 hours after UV-A illumination and compared to results obtained with conventionally induced cultures (Fig. 5B). These first results clearly demonstrated that the increase of light exposure time provoked a gradual expression response with NP-photocaged IPTG. However, neither 6 nor 20 hours of YFP expression after light induction were sufficient to achieve *in vivo* fluorescence values comparable to IPTG-induced cultures (Fig. 5B, control). This observation can either be explained by a decreased stability of NP-photocaged IPTG molecules in comparison to IPTG or it could be speculated that a deferred intracellular hydrolysis of photo-cleaved ester intermediates (Fig. 5A) might result in a delayed release of IPTG and thus prevented fully efficient induction of gene expression. However, since the comparison of different time-points of NP-IPTG supplementation did not lead to enhanced YFP expression levels (Fig. S7, ESI†), *in vivo* instability of NP-photocaged IPTG can be neglected. Next, the time of *E. coli* precultivation was shortened in order to increase the efficiency of *E. coli*-mediated hydrolysis of its ester intermediate. As shown in Fig. 5C and D, earlier UV-A light exposure indeed yielded higher YFP expression levels: under these conditions, the *in vivo* fluorescence gradually increased in response to prolonged duration of light exposure and, finally, levels of conventionally induced cells were reached after 2 minutes of UV-A light excitation. The light-response of the novel expression system was also analyzed at the single cell level. Therefore, *E. coli* Tuner(DE3)/pRhotHi-2-LacI-EYFP was subjected to microfluidic cultivation in LB medium containing 40 μM NP-photocaged IPTG, which was pre-exposed to UV-A light for 1 minute (data not shown). Surprisingly, no light-induced YFP expression could be detected in the microfluidic set-up over the entire cultivation time, even when the concentration of caged inducer molecules was increased to 100 μM (Fig. 6A).

Two aspects might be considered to explain this observation: (1) IPTG molecules are intracellularly hydrolysed and immediately washed out of the cells due to free bidirectional diffusion over the cell membrane. (2) The results shown in Fig. 5D suggested that hydrolase levels in the early logarithmic growth phase were too low to promptly release IPTG in the cytoplasm. In the microfluidic cultivation set-up, exactly this growth phase seems to be mimicked due to persistent nutrient supply.[54] To overcome these specific limitations during microfluidic cultivation, the same experimental set-up was chosen as before with the subtle difference that media flow was turned off after rinsing trapped cells with light-exposed medium. Fig. 6B clearly shows that microscale batch cultivation indeed resulted in a light-induced expression response. Furthermore, at the end of the experiment (*i.e.* after 450 min), UV-A light-induced YFP expression was comparable to that of conventionally induced cells (Fig. 6C). Online monitoring of the fluorescence development of microcolonies further revealed that the expression

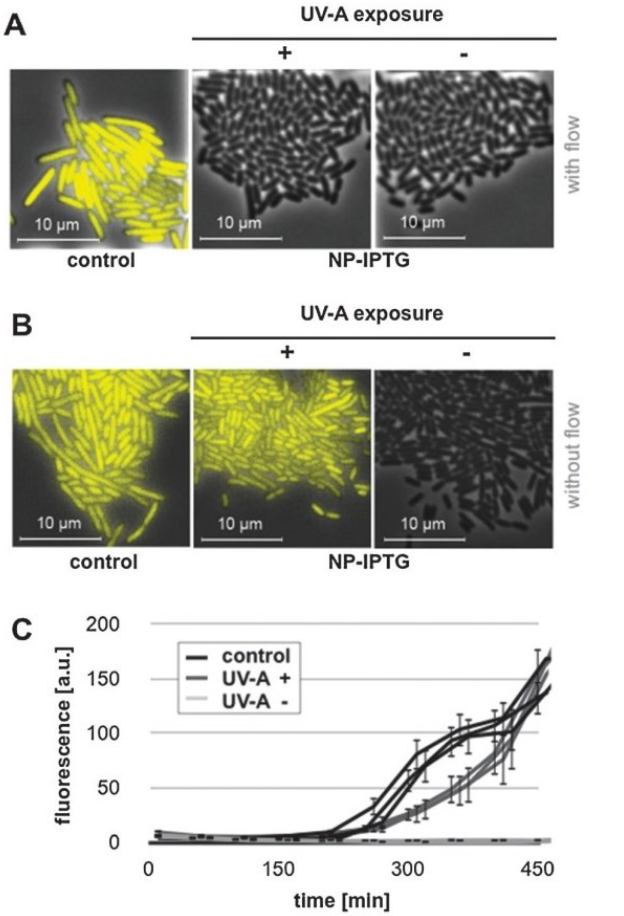

Fig. 6 Light-controlled YFP expression in microcolonies of *E. coli* Tuner(DE3) cells carrying expression vector pRhotHi-2-LacI-EYFP. Photographs were taken from time lapse microscopy during microfluidic perfusion cultivation (A) and microscale batch cultivation (B) using LB medium supplemented with 100 μM (A) or 40 μM (B) of NP-photocaged IPTG and applied with (+) or without (–) pre-exposure to UV-A light. Control: LB medium supplemented with equivalent concentrations of conventional IPTG. (C) Fluorescence development of microcolonies during microscale batch cultivation. Single cell fluorescence values were monitored for three representative microcolonies. Control: medium supplemented with 40 μM conventional IPTG; UV-A+: NP-photocaged IPTG supplemented medium that was UV-A exposed for 1 min prior to cultivation. UV-A–: unexposed NP-photocaged IPTG supplemented medium.

response upon UV-A light exposure was decelerated in comparison to conventionally induced cultures (Fig. 6C). Moreover, these data clearly document the remarkable homogeneity of light-dependent expression response. Thus, the combination of tightly controlled *lac* promoter-based T7RP-dependent gene expression with the use of photocaged IPTG molecules allowed a non-invasive and precise light control over gene expression in *E. coli*.

To finally elucidate the role of LacY in NP-photocaged IPTG-dependent triggering of *lac*-based gene expression, light responsiveness was monitored in the *E. coli lacY*$^+$ strain BL21(DE3)/pRhotHi-2-EYFP (Fig. S8, ESI†). Surprisingly, a gradual light response during batch cultivation was observed, suggesting a diffusion-based instead of a LacY-mediated uptake of the caged

inducer molecule before photo-cleavage (Fig. S8A, ESI†). However, microscale batch cultivation clearly revealed a distinctive heterogeneity of expression at the single cell level (Fig. S8B, ESI†) demonstrating that LacY indeed conveyed a positive feedback loop due to the specific uptake of decaged IPTG after light-mediated cleavage.

To the best of our knowledge the here presented optogenetic set-up, consisting of the *lacY*-deficient *E. coli* strain Tuner(DE3) and NP-photocaged IPTG, represents the first gradually light-regulated T7RP-dependent expression system in bacteria. The NP-photocaged IPTG-based system exhibits several outstanding features including precise and gradual regulation, high population homogeneity and low background expression. Moreover, the implementation of T7RP allows the expression of large and complex gene clusters[55] and enables broad applicability to various alternative expression hosts,[56] that is, however, clearly dependent on the actual growth phase (compare Fig. 5C and D and Fig. 6A and B), the corresponding expression host and the applied cultivation approach.

In contrast, photoreceptor-based light control is often hampered by their high basal activities[10] and their extremely sharp transitions from inactive to active signaling states.[57] Furthermore, the use of photoreceptors as light switches is usually restricted to certain hosts, as they specifically interact with corresponding signal transduction proteins and/or promoters.

Nevertheless, novel caged inducer molecules that are directly activated in a one-step photocleavage reaction are required to ensure high temporal resolution of light-regulated gene expression that is mostly independent of growth conditions. Furthermore, the establishment of advanced single cell batch cultivation systems seems to be vitally important,[58] as it was shown within this study that environmental discontinuity is a crucial limitation for some synthetic biology approaches.

Conclusions

Exact control of gene expression by light allows the regulation of simple to complex cellular functions in living microorganisms with high spatial and temporal resolution. The results presented here clearly demonstrate that well characterized expression modules can be easily converted into a versatile photo-switch by implementing photo-caged effector molecules, such as NP-photocaged IPTG. The here described light switch is a valuable optogenetic tool applicable for biomedicine, systems biology, functional genomics, and biotechnology. Moreover, this optogenetic module can be implemented as a "photo-biobrick" into light-controlled higher-order artificial networks useful for a variety of synthetic biology approaches.

Acknowledgements

Special thanks go to Vera Ophoven and Thomas Classen for valuable assistance during NP-photocaged IPTG synthesis. Further, we thank Stefan Helfrich and Katharina Nöh for Phyton-based lineage tree visualization. This work was partly performed at the Helmholtz Nanoelectronic Facility (HNF) of Research Center Jülich and supported by grants from Federal Ministry of Education and Research (OptoSys, FKZ 031A16).

References

1 S. Mukherji and A. van Oudenaarden, *Nat. Rev. Genet.*, 2009, **10**, 859–871.
2 K. D. Bhalerao, *Trends Biotechnol.*, 2009, **27**, 368–374.
3 M. H. Medema, R. Breitling, R. Bovenberg and E. Takano, *Nat. Rev. Microbiol.*, 2011, **9**, 131–137.
4 G. Stephanopoulos, *ACS Synth. Biol.*, 2012, **1**, 514–525.
5 J. M. Christie, J. Gawthorne, G. Young, N. J. Fraser and A. J. Roe, *Mol. Plant*, 2012, **5**, 533–544.
6 T. Drepper, U. Krauss, S. Meyer zu Berstenhorst, J. Pietruszka and K.-E. Jaeger, *Appl. Microbiol. Biotechnol.*, 2011, **90**, 23–40.
7 C. Brieke, F. Rohrbach, A. Gottschalk, G. Mayer and A. Heckel, *Angew. Chem., Int. Ed.*, 2012, **51**, 8446–8476.
8 U. Krauss, T. Drepper and K.-E. Jaeger, *Chem. – Eur. J.*, 2011, **17**, 2552–2560.
9 C. W. Riggsbee and A. Deiters, *Trends Biotechnol.*, 2010, **28**, 468–475.
10 J. J. Tabor, A. Levskaya and C. A. Voigt, *J. Mol. Biol.*, 2011, **405**, 315–324.
11 R. Ohlendorf, R. R. Vidavski, A. Eldar, K. Moffat and A. Möglich, *J. Mol. Biol.*, 2012, **416**, 534–542.
12 J. Melendez, M. Patel, B. L. Oakes, P. Xu, P. Morton and M. N. McClean, *Integr. Biol.*, 2014, **6**, 366–372.
13 A. Deiters, *ChemBioChem*, 2010, **11**, 47–53.
14 D. D. Young and A. Deiters, *Org. Biomol. Chem.*, 2007, **5**, 999–1005.
15 D. D. Young and A. Deiters, *Angew. Chem., Int. Ed.*, 2007, **46**, 4290–4292.
16 S. B. Cambridge, D. Geissler, S. Keller and B. Cürten, *Angew. Chem., Int. Ed.*, 2006, **45**, 2229–2231.
17 C. Chou, D. D. Young and A. Deiters, *ChemBioChem*, 2010, **11**, 972–977.
18 F. W. Studier and B. A. Moffatt, *J. Mol. Biol.*, 1986, **189**, 113–130.
19 K. Terpe, *Appl. Microbiol. Biotechnol.*, 2006, **72**, 211–222.
20 J. C. Samuelson, in *Methods in molecular biology*, ed. T. C. Evans and M.-Q. Xu, Humana Press, Totowa, NJ, 1st edn, 2011, vol. 705, pp. 195–209.
21 I. Iost, J. Guillerez and M. Dreyfus, *J. Bacteriol.*, 1992, **174**, 619–622.
22 S. Gräslund, P. Nordlund, J. Weigelt, B. M. Hallberg, J. Bray, O. Gileadi, S. Knapp, U. Oppermann, C. Arrowsmith, R. Hui, J. Ming, S. Dhe-Paganon, H. Park, A. Savchenko, A. Yee, A. Edwards, R. Vincentelli, C. Cambillau, R. Kim, S.-H. Kim, Z. Rao, Y. Shi, T. C. Terwilliger, C.-Y. Kim, L.-W. Hung, G. S. Waldo, Y. Peleg, S. Albeck, T. Unger, O. Dym, J. Prilusky, J. L. Sussman, R. C. Stevens, S. A. Lesley, I. A. Wilson, A. Joachimiak, F. Collart, I. Dementieva, M. I. Donnelly, W. H. Eschenfeldt, Y. Kim, L. Stols, R. Wu,

M. Zhou, S. K. Burley, J. S. Emtage, J. M. Sauder, D. Thompson, K. Bain, J. Luz, T. Gheyi, F. Zhang, S. Atwell, S. C. Almo, J. B. Bonanno, A. Fiser, S. Swaminathan, F. W. Studier, M. R. Chance, A. Sali, T. B. Acton, R. Xiao, L. Zhao, L. C. Ma, J. F. Hunt, L. Tong, K. Cunningham, M. Inouye, S. Anderson, H. Janjua, R. Shastry, C. K. Ho, D. Wang, H. Wang, M. Jiang, G. T. Montelione, D. I. Stuart, R. J. Owens, S. Daenke, A. Schütz, U. Heinemann, S. Yokoyama, K. Büssow and K. C. Gunsalus, *Nat. Methods*, 2008, **5**, 135–146.

23 A. Fernández-Castané, C. E. Vine, G. Caminal and J. López-Santín, *J. Biotechnol.*, 2012, **157**, 391–398.

24 A. Marbach and K. Bettenbrock, *J. Biotechnol.*, 2012, **157**, 82–88.

25 I. G. de Jong, J.-W. Veening and O. P. Kuipers, *Environ. Microbiol.*, 2012, **14**, 3110–3121.

26 S. Müller and G. Nebe-von-Caron, *FEMS Microbiol. Rev.*, 2010, **34**, 554–587.

27 A. R. Lara, E. Galindo, O. T. Ramírez and L. A. Palomares, *Mol. Biotechnol.*, 2006, **34**, 355–381.

28 S. Unthan, A. Grünberger, J. van Ooyen, J. Gätgens, J. Heinrich, N. Paczia, W. Wiechert, D. Kohlheyer and S. Noack, *Biotechnol. Bioeng.*, 2013, **111**, 359–371.

29 S. Huang, *Development*, 2009, **136**, 3853–3862.

30 J. W. Young, J. C. W. Locke, A. Altinok, N. Rosenfeld, T. Bacarian, P. S. Swain, E. Mjolsness and M. B. Elowitz, *Nat. Protoc.*, 2012, **7**, 80–88.

31 B. Lin and A. Levchenko, *Curr. Opin. Chem. Biol.*, 2012, **16**, 307–317.

32 A. Grünberger, W. Wiechert and D. Kohlheyer, *Curr. Opin. Biotechnol.*, 2014, **29**, 15–23.

33 F. S. O. Fritzsch, K. Rosenthal, A. Kampert, S. Howitz, C. Dusny, L. M. Blank and A. Schmid, *Lab Chip*, 2013, **13**, 397–408.

34 C. Probst, A. Grünberger, W. Wiechert and D. Kohlheyer, *J. Microbiol. Methods*, 2013, **95**, 470–476.

35 P. Wang, L. Robert, J. Pelletier, W. L. Dang, F. Taddei, A. Wright and S. Jun, *Curr. Biol.*, 2010, **20**, 1099–1103.

36 G. Schendzielorz, M. Dippong, A. Grünberger, D. Kohlheyer, A. Yoshida, S. Binder, C. Nishiyama, M. Nishiyama, M. Bott and L. Eggeling, *ACS Synth. Biol.*, 2014, **3**, 21–29.

37 W. Mather, O. Mondragón-Palomino, T. Danino, J. Hasty and L. S. Tsimring, *Phys. Rev. Lett.*, 2010, **104**, 208101.

38 G. Ullman, M. Wallden, E. G. Marklund, A. Mahmutovic, I. Razinkov and J. Elf, *Philos. Trans. R. Soc. London, Ser. B*, 2013, **368**, 20120025.

39 A. Grünberger, N. Paczia, C. Probst, G. Schendzielorz, L. Eggeling, S. Noack, W. Wiechert and D. Kohlheyer, *Lab Chip*, 2012, **12**, 2060–2068.

40 N. Mustafi, A. Grünberger, D. Kohlheyer, M. Bott and J. Frunzke, *Metab. Eng.*, 2012, **14**, 449–457.

41 N. Mustafi, A. Grünberger, R. Mahr, S. Helfrich, K. Nöh, B. Blombach, D. Kohlheyer and J. Frunzke, *PLoS One*, 2014, **9**, e85731.

42 L. Robert, G. Paul, Y. Chen, F. Taddei, D. Baigl and A. B. Lindner, *Mol. Syst. Biol.*, 2010, **6**, 1–12.

43 D. Hanahan, *J. Mol. Biol.*, 1983, **166**, 557–580.

44 J. Sambrook, E. F. Fritsch and T. Maniatis, *Molecular cloning: a laboratory manual*, Cold Spring Harbor Laboratory Press, New York City, USA, 2nd edn, 1989.

45 N. Katzke, S. Arvani, R. Bergmann, F. Circolone, A. Markert, V. Svensson, K.-E. Jaeger, A. Heck and T. Drepper, *Protein Expression Purif.*, 2010, **69**, 137–146.

46 M. F. Alexeyev, *Biotechniques*, 1995, **18**, 52–56.

47 F. Rosenau and K. Jaeger, in *Enzyme functionality: design, engineering and screening*, ed. A. Svendson, Dekker, Marcel Inc, New York, 1st edn, 2004, pp. 617–630.

48 J. Potzkei, M. Kunze, T. Drepper, T. Gensch, K.-E. Jaeger and J. Buechs, *BMC Biol.*, 2012, **10**, 28.

49 A. Gruenberger, C. Probst, A. Heyer, W. Wiechert, J. Frunzke and D. Kohlheyer, *J. Visualized Exp.*, 2013, (82), e50560.

50 C. J. Wilson, H. Zhan, L. Swint-Kruse and K. S. Matthews, *Cell. Mol. Life Sci.*, 2007, **64**, 3–16.

51 M. Santillán and M. C. Mackey, *J. R. Soc., Interface*, 2008, **5**, 29–39.

52 D. Hartinger, S. Heinl, H. E. Schwartz, R. Grabherr, G. Schatzmayr, D. Haltrich and W.-D. Moll, *Microb. Cell Fact.*, 2010, **9**, 62.

53 E. M. Ozbudak, M. Thattai, H. N. Lim, B. I. Shraiman and A. Van Oudenaarden, *Nature*, 2004, **427**, 737–740.

54 A. Grünberger, J. van Ooyen, N. Paczia, P. Rohe, G. Schiendzielorz, L. Eggeling, W. Wiechert, D. Kohlheyer and S. Noack, *Biotechnol. Bioeng.*, 2013, **110**, 220–228.

55 A. Loeschcke, A. Markert, S. Wilhelm, A. Wirtz, F. Rosenau, K.-E. Jaeger and T. Drepper, *ACS Synth. Biol.*, 2013, **2**, 22–33.

56 S. C. Troeschel, S. Thies, O. Link, C. I. Real, K. Knops, S. Wilhelm, F. Rosenau and K.-E. Jaeger, *J. Biotechnol.*, 2012, **161**, 71–79.

57 A. Levskaya, A. A. Chevalier, J. J. Tabor, Z. B. Simpson, L. A. Lavery, M. Levy, E. A. Davidson, A. Scouras, A. D. Ellington, E. M. Marcotte and C. A. Voigt, *Nature*, 2005, **438**, 441–442.

58 J. Dai, S. H. Yoon, H. Y. Sim, Y. S. Yang, T. K. Oh, J. F. Kim and J. W. Hong, *Anal. Chem.*, 2013, **85**, 5892–5899.

II.3.2 Photocaged Arabinose

Photocaged Arabinose – A Novel Optogenetic Switch for Rapid and Gradual Control of Microbial Gene Expression

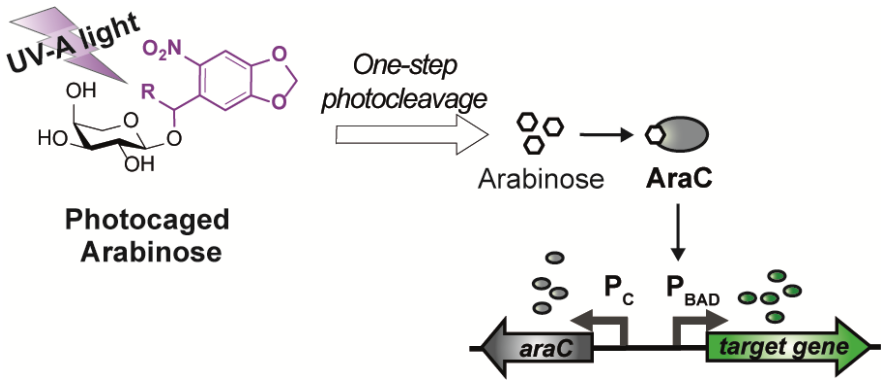

Dennis Binder, Claus Bier, Alexander Grünberger, Dagmar Drobietz, Jennifer Hage-Hülsmann, Georg Wandrey, Jochen Büchs, Dietrich Kohlheyer, Anita Loeschcke, Wolfgang Wiechert, Karl-Erich Jaeger, Jörg Pietruszka and Thomas Drepper

ChemBioChem 2016; 17: 296–300.

The full online version may be found at:
http://dx.doi.org/10.1002/cbic.201500609.

For the complete supporting information see Appendix (**Chapter V.3**) turn to page **207.**

ChemPubSoc Europe

DOI: 10.1002/cbic.201500609

CHEMBIOCHEM Communications

Photocaged Arabinose: A Novel Optogenetic Switch for Rapid and Gradual Control of Microbial Gene Expression

Dennis Binder,[a] Claus Bier,[b] Alexander Grünberger,[c] Dagmar Drobietz,[b] Jennifer Hage-Hülsmann,[a] Georg Wandrey,[d] Jochen Büchs,[d] Dietrich Kohlheyer,[c] Anita Loeschcke,[a] Wolfgang Wiechert,[c] Karl-Erich Jaeger,[a, c] Jörg Pietruszka,[b, c] and Thomas Drepper*[a]

Controlling cellular functions by light allows simple triggering of biological processes in a non-invasive fashion with high spatiotemporal resolution. In this context, light-regulated gene expression has enormous potential for achieving optogenetic control over almost any cellular process. Here, we report on two novel one-step cleavable photocaged arabinose compounds, which were applied as light-sensitive inducers of transcription in bacteria. Exposure of caged arabinose to UV-A light resulted in rapid activation of protein production, as demonstrated for GFP and the complete violacein biosynthetic pathway. Moreover, single-cell analysis revealed that intrinsic heterogeneity of arabinose-mediated induction of gene expression was overcome when using photocaged arabinose. We have thus established a novel phototrigger for synthetic bio(techno)logy applications that enables precise and homogeneous control of bacterial target gene expression.

In recent years, optogenetic tools have evolved as key players in controlling cellular functions.[1] The advantage of light as an exogenous stimulus is based on its unique physical properties, such as high variability and selectivity, and it allows triggering of biological processes in a non-invasive fashion and with unprecedented spatiotemporal resolution. In order to employ light for the control of cellular functions, both sophisticated chemical and genetically encoded phototriggers (photocaged compounds and recombinant photoreceptors) have been developed over the last decade.[1] For instance, light-controlled histidine kinases,[2] photocaged inducers,[3] antibiotics,[4] oligonucleotides,[5] and even plasmids[6] have been shown to trigger cellular functions with high precision and ease.

Accurate and tight control of bacterial gene expression is of the utmost importance for synthetic bio(techno)logy. However, in most microbial expression setups, precise, rapid, and straightforward induction of gene expression is still a challenge, especially if gene expression needs to be induced in multiple expression cultures grown in parallel and if inducer concentrations are varied (e.g., for high-throughput screening and bioprocess engineering). As a consequence, low spatiotemporal resolution and invasive supplementation of inducers greatly limit parallelization and monitoring of conventional protein production processes.

These challenges were recently addressed by employing photocaged isopropyl β-D-thiogalactopyranoside (IPTG), which was able to activate *lac* promoter-driven gene expression upon UV-A light exposure.[7] However, full release of bioactive IPTG is a two-step process that involves hydrolytic cleavage of the photosensitive protection group nitropiperonal by a cellular esterase, because light exposure only yields accumulation of nonfunctional ester intermediates.[7] The applicability of photocaged IPTG is therefore restricted in terms of temporal resolution. In addition, a sophisticated riboswitch for activation of protein production was developed with caged theophylline, the functionality of which was strictly dependent on target gene region, though.[8]

In this work, we developed, for the first time, one-step photocleavable inducers to drive arabinose-inducible bacterial gene expression upon short light exposure, without the requirement for additional factors such as specific cellular enzymes or target gene sequence (Figure 1). Two photocaged arabinose compounds were synthesized in a three-step reac-

[a] D. Binder, J. Hage-Hülsmann, Dr. A. Loeschcke, Prof. Dr. K.-E. Jaeger, Dr. T. Drepper
Institute of Molecular Enzyme Technology
Heinrich-Heine-University Düsseldorf, Forschungszentrum Jülich
Stetternicher Forst, 52426 Jülich (Germany)
E-mail: t.drepper@fz-juelich.de

[b] C. Bier, D. Drobietz, Prof. Dr. J. Pietruszka
Institute of Bioorganic Chemistry, Heinrich-Heine-University Düsseldorf
Forschungszentrum Jülich
Stetternicher Forst, 52426 Jülich (Germany)

[c] Dr. A. Grünberger, Prof. Dr. D. Kohlheyer, Prof. Dr. W. Wiechert, Prof. Dr. K.-E. Jaeger, Prof. Dr. J. Pietruszka
Institute of Bio- and Geosciences (IBG-1), Forschungszentrum Jülich
Stetternicher Forst, 52426 Jülich (Germany)

[d] G. Wandrey, Prof. Dr. J. Büchs
AVT—Biochemical Engineering, RWTH Aachen University
Worringer Weg 1, 52074 Aachen (Germany)

Supporting information for this article is available on the WWW under http://dx.doi.org/10.1002/cbic.201500609.

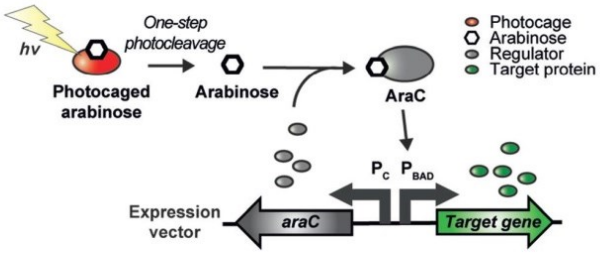

Figure 1. UV-A light-mediated optogenetic control over AraC/P_{BAD}-regulated gene expression by photocaged arabinose. Photoreleased arabinose activates P_{BAD}-regulated gene expression upon binding to the P_C promoter-controlled AraC regulator protein.

ChemPubSoc Europe

CHEMBIOCHEM Communications

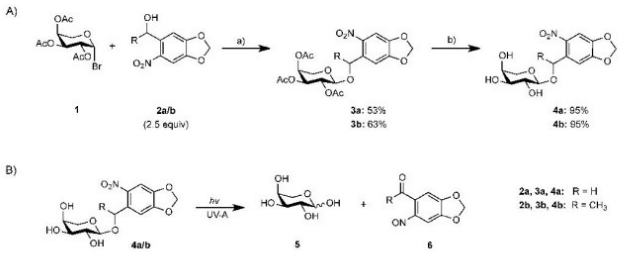

Scheme 1. Synthesis of NP and NBE photocaged arabinose **4a/b**, and light-mediated one-step photocleavage. A) Synthesis of **4a** and **4b**: a) Ag_2CO_3 (0.6 equiv), AgOTf (0.6 equiv), CH_2Cl_2, RT; b) NaOMe (0.23 M in MeOH), Dowex 650C. B) Light-controlled release of inducer **5** and additional nitroso photoproduct **6** from **4a** or **4b** upon UV-A light exposure.

tion from arabinose donor **1** by using 6-nitropiperonylalcohol (NP; **2a**) and 1-(6-nitrobenzo[d][1,3]dioxol-5-yl)ethanol (NBE; **2b**) caging groups (Scheme 1 A; yield over two steps via glycoside **3**: **4a**, 48%; **4b**, 60%; see Methods and Figures S1–11 in the Supporting Information). In an efficient one-step photocleavage reaction, both photocaged arabinose compounds released L-(+)-arabinose (**5**) as well as the corresponding nitroso compound (**6**) upon short UV-A light exposure (Scheme 1 B).

As expected from similar caged compounds,[9] in vitro analysis (Tables 1, S2, and S3; Figures S12 and S13) revealed that the NBE moiety of **4b** showed slightly improved photorelease and uncaging quantum yield compared to the NP compound (**4a**). The compounds are non-toxic and stable in vivo and in vitro in the dark (Figure S14; Supporting Information). Furthermore, **4a** and **4b** displayed adequate absorptivity and solubility in aqueous solution for in vivo applications (Table 1).

Table 1. (Photo-)chemical properties of photocaged arabinose **4a/b**.

Compound	λ_{max} [nm] (ε [$M^{-1}cm^{-1}$])[a]	$t_{0.5}$ [min][b]	s [mM][c]	s^* [mM][d]	ϕ_u[e]
4a	246 (12200) 353 (6000)	19.1	8.1	174.1	0.11
4b	246 (9500) 358 (4600)	13.7	6.9	162.8	0.29

[a] ε = extinction coefficient at λ_{max}, [b] $t_{0.5}$ = uncaging half-life time, [c] s = solubility in deionized and degassed water, [d] s^* = solubility in DMSO, and [e] ϕ_u = uncaging quantum yield.

In order to characterize the light-responsiveness of the novel system in vivo, an *Escherichia coli* expression setup was established based on the P_{BAD} promoter[11] and an improved AraC regulator protein[12] (Supporting Information). Thus, expression of genes from P_{BAD} is inducible with L-arabinose, which is imported by a complex transport system (involving the genes *araEFGH*) upon binding to the AraC regulator protein (Figure 1).[12]

Light-induced expression of the GFPmut3 reporter gene[13] was tested in microtiter expression cultures after adding **4a** or **4b.** Light-induced decaging of both **4a** and **4b** in vivo resulted in fast and strong expression responses, and slightly outperformed conventional induction with equimolar amounts (25 μM) of arabinose (**5**; Figure 2A, Figure S17). Bacterial gene expression was fully induced after 10 min of UV-A light exposure. Rapid responsiveness of the novel phototriggers was further characterized by comparing to the previously established photocaged IPTG[7] (Figure 2B). Besides superior induction to that with conventional arabinose ($t_{0.5}$ = 2.1 h), **4a/b** ($t_{0.5}$ = 1.6/1.4 h) distinctly outperformed light induction with photocaged IPTG ($t_{0.5}$ = 3.8 h; Table S5, Figure S19).

In contrast, in non-exposed cultures gene expression was tightly inhibited (for low concentrations see Figures S15 and S16) during the complete cultivation process, as indicated by the absence of GFP fluorescence. Exposure of cultures to light of increasing intensity was achieved by varying the layers of diffusion foils between the UV-A light source and the cultivation device (for attained intensities see Table S4). It was possible to stepwise upregulate GFP expression by stepwise increasing the UV-A light intensity (Figure 2C). As the compounds were almost equally suited for in vivo applications (Figure 2A), **4a** was applied in subsequent experiments because of its superior solubility. GFP expression using both **5** and NP-photocaged arabinose **4a** induction was monitored at the single-cell level in microfluidic cultivation devices[14] (Figure 2D). Former studies revealed fluctuations in arabinose uptake as decisive for cell-to-cell variations;[15] thus, conventional induction (without extensive modification of the native arabinose uptake system)[16] showed heterogeneous expression. Induction with **4a**, however, produced a much faster and homogeneous response (Figure S18, Videos S1 and S2), which might be explained by passive diffusion of photocaged arabinose into the cell. Single-cell analysis further demonstrated that non-invasive light induction is highly suited for spatiotemporal control in nano-scale cultivation devices, or when inducer supplementation is technically difficult, for example, during high-throughput cultivation or in closed cultivation systems for strictly anaerobic bacteria.

Next, **4a** was used to induce production of the secondary metabolite violacein (**11**), which has antitumor and antibiotic properties.[17] The enzymes that catalyse the synthesis of **11** from tryptophan (**7**; via **8**–**10**; Figure 3A) are encoded by a 7.4-kb gene cluster (*vioABCDE)* from *Chromobacterium violaceum* ATCC 12472.[18] For expression in *E. coli*, the *vio* gene cluster was amplified from the *C. violaceum* genome and introduced into the pAra (see the Supporting Information) expression vector. Concerted expression of all *vio* genes in the presence of **4a** was upregulated with increasing UV-A light intensity, as visualized by the increasingly dark violet color of ethanol extracts (Figure 3B). Spectroscopic analysis (Figure 3C) further revealed substantial violacein production, with yields of up to 270 mg L^{-1} (Figure S20; Table S6), notably without any further metabolic engineering of the expression host. Hence, the applicability of the phototrigger in a biotechnological context was proven with light control of the large and complex *vio* gene cluster from *C. violaceum*.

In summary, photocaged arabinose represents the first example of a one-step photocleavable inducer that allows fast and accurate control of target gene expression in *E. coli*. In

ChemPubSoc Europe

CHEMBIOCHEM Communications

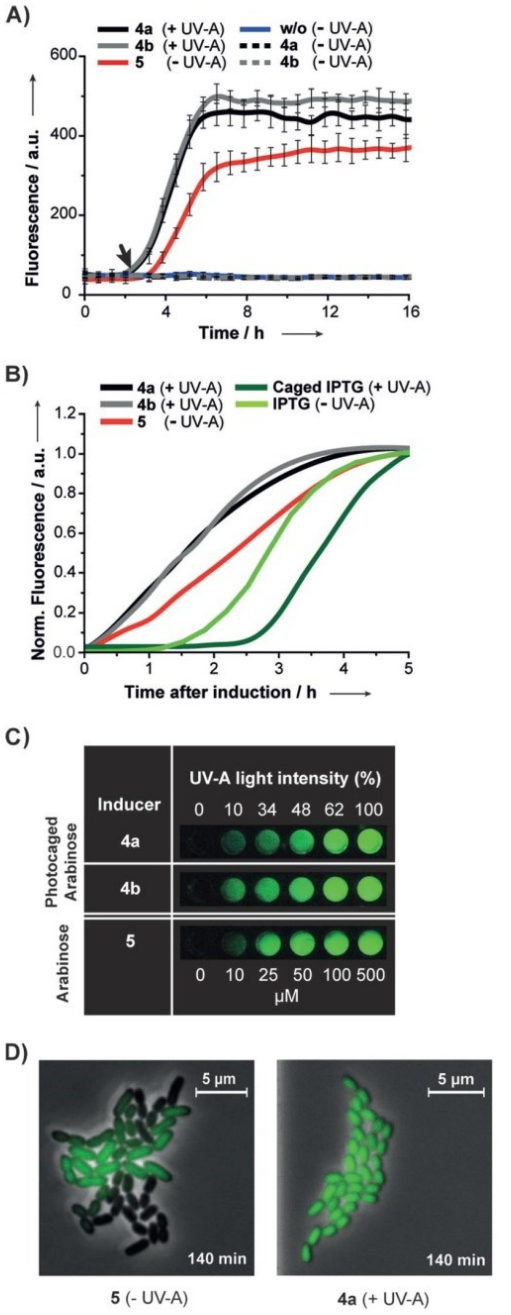

Figure 2. Rapid, gradual, and homogeneous light activation of AraC/P_{BAD}-regulated gene expression in *E. coli*. A) Biomass-normalized GFP in vivo fluorescence for differently treated expression cultures. Light induction (365 nm; 10 min; time of induction indicated by arrow) with **4a** or **4b** was compared to equimolar induction (25 µM) by the conventional inducer **5**, and without (w/o) inducer. B) Comparison with caged IPTG-based induction[7] of gene expression by light. Half-maximal fluorescence was attained after 1.6 (**4a**), 1.4 (**4b**), 2.1 (**5**), 2.9 (IPTG), and 3.8 h (caged IPTG). C) Gradual up-regulation of GFP expression (in vivo fluorescence after 20 h of cultivation; cell densities adjusted to $OD_{580} = 20$) with step-wise incrementing of UV-A light intensity (10 min, 0–0.9 mW cm^{-2}) by using **4a** and **4b** (100 µM), as well as increasing concentrations of **5**. D) Isogenic colonies showing homogeneous fluorescence profile for light induction (**4a**; 365 nm; 1 min), and a heterogeneous fluorescence response for equimolar conventional induction (**5**; 25 µM).

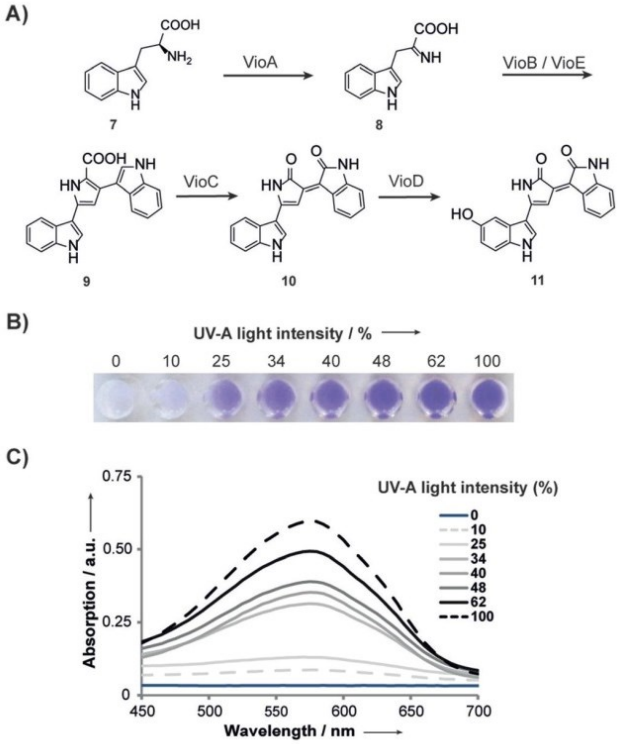

Figure 3. Light-controlled violacein production using **4a**. A) Biosynthesis of violacein (**11**) from tryptophan (**7**), mediated by enzymes encoded in the *vioABCDE* cluster from *C. violaceum* ATCC 12472. B) Deepening color of 100-fold diluted ethanol extracts from differently exposed expression cultures (UV-A: 0–0.9 mW cm^{-2}). C) Absorption spectra of tenfold diluted ethanol extracts indicate up-regulation of violacein production with increasing UV-A exposure.

contrast to similarly sophisticated setups using photocaged theophylline[8] or IPTG,[7] this optogenetic tool performs independently of the target DNA downstream of the promoter (unlike caged theophylline) or secondary cellular reactions (unlike caged IPTG). As light control through photocaged arabinose is basically transferable to other microbes, this system might prove beneficial for setting up tight, gradual, homogenous, and temporally highly resolved gene expression in various biotechnologically relevant pro- and eukaryotes as well as archaea.[19] Future applications range from light-mediated synchronization of biosynthetic pathways[20] to spatiotemporally precise triggering of special applications where induction through supplementation is unfavorable (e.g., in anaerobic, closed, or microfluidic cultivation systems).[21] Moreover, in combination with currently developed photomicrobioreactors and single-cell cultivation platforms,[13] the photocaged arabinose-regulated system will contribute to fully automatized control and optimization of microbial production processes.

Acknowledgements

Supported by grants from Federal Ministry of Education and Research (OptoSys, FKZ 031A16), Ministry of Innovation, Science

ChemPubSoc Europe

CHEMBIOCHEM Communications

and Research of North-Rhine Westphalia and German Research Foundation (INST 208/654-1 FUGG). Work was partly performed at Helmholtz Nanoelectronic Facility (HNF) of Forschungszentrum Jülich. We thank Stephan Thies for fruitful discussions and advise on violacein biosynthesis.

Keywords: caged compounds · gene expression · optogenetics · photochemistry · synthetic biology

[1] a) C. Brieke, F. Rohrbach, A. Gottschalk, G. Mayer, A. Heckel, *Angew. Chem. Int. Ed.* **2012**, *51*, 8446 – 8476; *Angew. Chem.* **2012**, *124*, 8572 – 8604; b) T. Drepper, U. Krauss, S. Meyer zu Berstenhorst, J. Pietruszka, K.-E. Jaeger, *Appl. Microbiol. Biotechnol.* **2011**, *90*, 23 – 40; c) L. Gardner, A. Deiters, *Curr. Opin. Chem. Biol.* **2012**, *16*, 292 – 299; d) A. Deiters, *Curr. Opin. Chem. Biol.* **2009**, *13*, 678 – 686.

[2] a) J. J. Tabor, A. Levskaya, C. A. Voigt, *J. Mol. Biol.* **2011**, *405*, 315 – 324; b) R. Ohlendorf, R. R. Vidavski, A. Eldar, K. Moffat, A. Möglich, *J. Mol. Biol.* **2012**, *416*, 534 – 542.

[3] a) S. B. Cambridge, D. Geissler, S. Keller, B. Cürten, *Angew. Chem. Int. Ed.* **2006**, *45*, 2229 – 2231; *Angew. Chem.* **2006**, *118*, 2287 – 2289; b) S. B. Cambridge, D. Geissler, F. Calegari, K. Anastassiadis, M. T. Hasan, A. F. Stewart, W. B. Huttner, V. Hagen, T. Bonhoeffer, *Nat. Methods* **2009**, *6*, 527 – 531.

[4] a) W. A. Velema, J. P. van der Berg, M. J. Hansen, W. Szymanski, A. J. M. Driessen, B. L. Feringa, *Nat. Chem.* **2013**, *5*, 924 – 928; b) W. A. Velema, J. P. van der Berg, W. Szymanski, A. J. M. Driessen, B. L. Feringa, *ACS Chem. Biol.* **2014**, *9*, 1969 – 1974.

[5] S. Yamazoe, Q. Liu, L. E. McQuade, A. Deiters, J. K. Chen, *Angew. Chem. Int. Ed.* **2014**, *53*, 10114 – 10118; *Angew. Chem.* **2014**, *126*, 10278 – 10282.

[6] J. Hemphill, J. Govan, R. Uprety, M. Tsang, A. Deiters, *J. Am. Chem. Soc.* **2014**, *136*, 7152 – 7158.

[7] a) D. D. Young, A. Deiters, *Angew. Chem. Int. Ed.* **2007**, *46*, 4290 – 4292; *Angew. Chem.* **2007**, *119*, 4368 – 4370; b) D. Binder, A. Grünberger, A. Loeschcke, C. Probst, C. Bier, J. Pietruszka, W. Wiechert, D. Kohlheyer, K.-E. Jaeger, T. Drepper, *Integr. Biol.* **2014**, *6*, 755 – 765.

[8] S. Walsh, L. Gardner, A. Deiters, G. J. Williams, *ChemBioChem* **2014**, *15*, 1346 – 1351.

[9] D. D. Young, A. Deiters, *Bioorg. Med. Chem. Lett.* **2006**, *16*, 2658 – 2661.

[10] F. Bley, K. Schaper, H. Görner, *Photochem. Photobiol.* **2008**, *84*, 162 – 171.

[11] a) L.-M. Guzman, D. Belin, M. J. Carson, J. Beckwith, *J. Bacteriol.* **1995**, *177*, 4121 – 4130; b) T. Brautaset, R. Lale, S. Valla, *Microb. Biotechnol.* **2009**, *2*, 15 – 30; c) S. Balzer, V. Kucharova, J. Megerle, R. Lale, T. Brautaset, S. Valla, *Microb. Cell Fact.* **2013**, *12*, 26.

[12] S. K. Lee, H. H. Chou, B. F. Pfleger, J. D. Newman, Y. Yoshikuni, J. D. Keasling, *Appl. Environ. Microbiol.* **2007**, *73*, 5711 – 5715.

[13] B. P. Cormack, R. H. Valdivia, S. Falkow, *Gene* **1996**, *173*, 33 – 38.

[14] A. Grünberger, W. Wiechert, D. Kohlheyer, *Curr. Opin. Biotechnol.* **2014**, *29*, 15 – 23.

[15] a) J. Mäkelä, M. Kandhavelu, S. M. D. Oliveira, J. G. Chandraseelan, J. Lloyd-Price, J. Peltonen, O. Yli-Harja, A. S. Ribeiro, *Nucleic Acids Res.* **2013**, *41*, 6544 – 6552; b) G. Fritz, J. A. Megerle, S. A. Westermayer, D. Brick, R. Heermann, K. Jung, J. O. Rädler, U. Gerland, *PLoS One* **2014**, *9*, e89532.

[16] A. Khlebnikov, Ø. Risa, T. Skaug, T. A. Carrier, J. D. Keasling, *J. Bacteriol.* **2000**, *182*, 7029 – 7034.

[17] P. Vaishnav, A. L. Demain, *Biotechnol. Adv.* **2011**, *29*, 223 – 229.

[18] T. Morohoshi, M. Kato, K. Fukamachi, N. Kato, T. Ikeda, *FEMS Microbiol. Lett.* **2008**, *279*, 124 – 130.

[19] a) D. Qiu, F. H. Damron, T. Mima, H. P. Schweizer, H. D. Yu, *Appl. Environ. Microbiol.* **2008**, *74*, 7422 – 7426; b) K. Ben-Samoun, G. Leblon, O. Reyes, *FEMS Microbiol. Lett.* **1999**, *174*, 125 – 130; c) J. Zhang, Y.-J. Liu, G.-Z. Cui, Q. Cui, *Biotechnol. Biofuels* **2015**, *8*, 36; d) E. Bode, A. O. Brachmann, C. Kegler, R. Simsek, C. Dauth, Q. Zhou, M. Kaiser, P. Klemmt, H. B. Bode, *ChemBioChem* **2015**, *16*, 1115 – 1119; e) N. Peng, L. Deng, Y. Mei, D. Jiang, Y. Hu, M. Awayez, Y. Liang, Q. She, *Appl. Environ. Microbiol.* **2012**, *78*, 5630 – 5637; f) A. Bottin, J. Kämper, R. Kahmann, *Mol. Gen. Genet.* **1996**, *253*, 342 – 352.

[20] M. H. Medema, R. Breitling, R. Bovenberg, E. Takano, *Nat. Rev. Microbiol.* **2011**, *9*, 131 – 137.

[21] C. Tan, S.-J. Lo, P. R. LeDuc, C.-M. Cheng, *Lab Chip* **2012**, *12*, 3654 – 3665.

Manuscript received: November 13, 2015

Accepted article published: December 16, 2015

Final article published: January 19, 2016

II.3.3 Photocaged Carbohydrates

Photo-caged carbohydrates – versatile tools for controlling gene expression by light

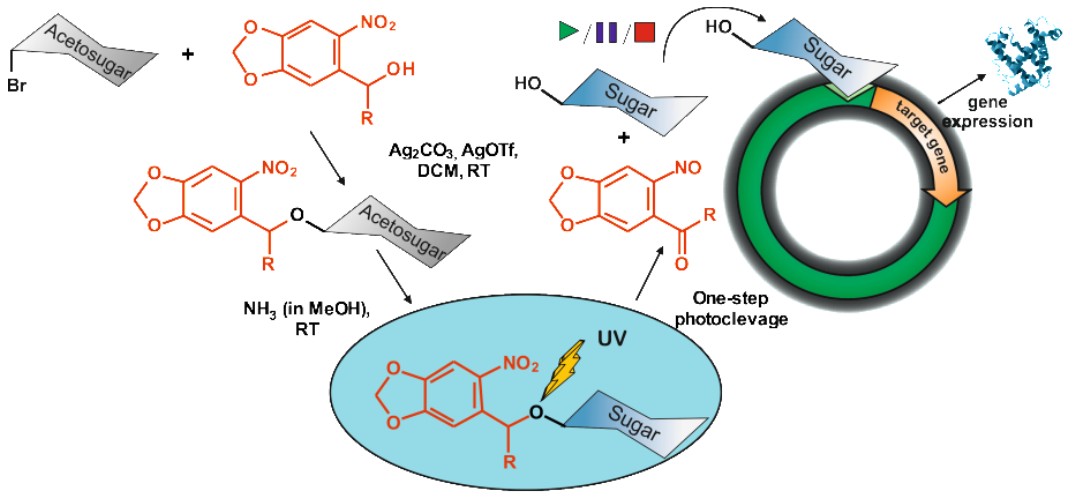

Claus Bier, Dennis Binder, Dagmar Drobietz, Anita Loeschcke, Thomas Drepper, Karl-Erich Jaeger and Jörg Pietruszka

Synthesis 2016; doi:10.1055/s-0035-1562617.

For the complete supporting information see Appendix (**Chapter V.4**) turn to page **239.**

Photocaged carbohydrates – versatile tools for controlling gene expression by light

Claus Bier[a]
Dennis Binder[b]
Dagmar Drobietz[a]
Anita Loeschcke[b]
Thomas Drepper[b]
Karl-Erich Jaeger[b,c]
Jörg Pietruszka[a,c]*

[a]* Institute of Bioorganic Chemistry, Heinrich-Heine-Universität Düsseldorf, Forschungszentrum Jülich, Stetternicher Forst, 52426 Jülich, Germany. Email: j.pietruszka@fz-juelich.de

[b] Institute of Molecular Enzyme Technology, Heinrich-Heine-Universität Düsseldorf, Forschungszentrum Jülich, Stetternicher Forst, 52426 Jülich, Germany.

[c] Institute of Bio- and Geosciences (IBG-1): Biotechnology, Forschungszentrum Jülich, Wilhelm-Johnen-Straße, 52428 Jülich, Germany,

Dedicated to Prof. Dr. Dieter Enders on the occasion of his 70th birthday

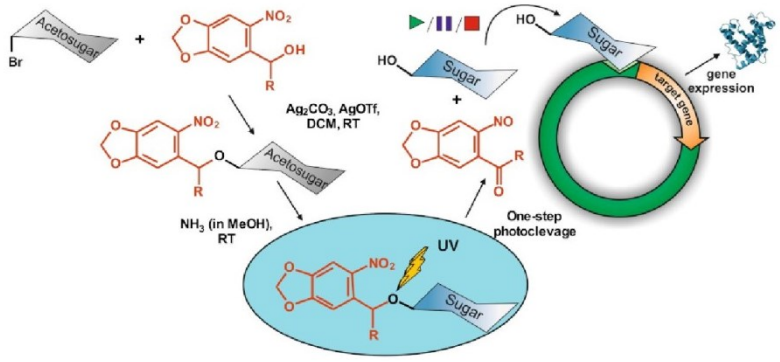

Received:
Accepted:
Published online:
DOI:

Abstract The control of biological processes plays a central role in life science, especially the tight regulation of gene expression for biotechnological systems. In this context, optogenetic tools have emerged as an important instrument for controlling gene expression by light with high spatiotemporal resolution in a non-invasive way. Here, we present the syntheses and characterization of biofunctional photocaged carbohydrates, on the basis of the biologically most relevant carbohydrates glucose, galactose, rhamnose and lactose. The single-step cleavage of these compounds allows both, to rapidly activate and temporary or permanently repress the transcription in *E. coli* after short UV-A light exposure. This study thus presents a versatile toolbox of photocaged carbohydrates for the light-triggered-regulation and control of cellular processes useful for synthetic bio(techno)logy applications.

Key words caged compounds, carbohydrates, optogenetics, bacterial gene expression, photo-removable protection group, biotechnology.

Introduction

Optogenetic tools are playing an increasingly important role in controlling biological and biotechnological processes by light.[1-3] Especially at the cellular scale, photocaged inducers are often used for photo-triggering cellular functions as for instance gene expression.[1,4] To this end, photocaged inducer molecules are regularly applied, e.g. caged antibiotics, nucleotides, and amino acids.[2,5,6,7]

Photocaged inducers offer considerable advantages as compared to classical inducers because they allow the non-invasive and disturbance-free manipulation of a biological system by light. Such systems can also be used to trigger anaerobic cell systems without distracting their atmosphere. In comparison to classical induction, photocaged inducers are therefore convenient to control cell systems with high temporal resolution.[2,8]

Carbohydrates and carbohydrate-derivatives are the most important inducers used for triggering biological cell systems. For example, transcription of the well-known *lac*-operon is controlled by carbohydrates (activation by lactose and allolactose; temporary repression by glucose). Recently it has been shown that it is possible to activate a *lac* promoter-driven gene expression system with photocaged isopropyl β-D-1-thiogalactopyranoside (IPTG) upon UV-A light exposure in a two-step process.[9,10] This article focusses on the synthesis of photocaged carbohydrates that are suitable to develop light-responsive gene expression systems.

Microorganisms are complex and sensitive biological systems, thus, photocaged compounds should not be toxic in any way; otherwise, they would lead to cell death or inhibit cellular growth. Furthermore, the photoproducts should not influence the viability of the cells. The caged inducer has to be inactivated by the photo-removable protecting group and become active after photo-release. Consequently, it has to be hydrolytically stable, since otherwise a tight and gradual control of cellular functions would not be possible. The solubility has to be adequate, in order to have sufficient amounts of photocaged inducer available inside the cell. The irradiation wavelength that causes the cleavage should not be too short, because this would lead to cell damage, in particular upon elongated irradiation. A wavelength that is too long would make the handling quite difficult, because all experiments would have to take place at an even higher wavelength, to prevent the cleavage of the photo inducer beforehand. Few photocaged carbohydrates and derivatives have been synthesized so far, primarily as tools for protecting group strategy in natural product synthesis.[11] Due to photocleavage at wavelengths below 300 nm, these compounds are not well suited for biological *in vivo* applications. At these wavelengths, cell damage can be expected.

Results and Discussion

With these requirements for photocaged inducers in mind, we aimed at synthesizing a purposive toolbox of photocaged carbohydrates that are readily accessible in a short reaction sequence and well applicable for a broad range of carbohydrate inducible expression systems. Therefore, we decided to photocage the biologically most relevant carbohydrates (glucose, galactose, rhamnose, lactose) with the following strategy: To be able to link carbohydrates to a photo-labile protecting group we chose to utilize the well-established peracetylated glycosyl bromides **1a-e** as donors. For their syntheses they have to be protected and selectively activated.[12,13]

Depending on the carbohydrate used, the protection and the activation was performed over route A or B (Scheme 1).[14]

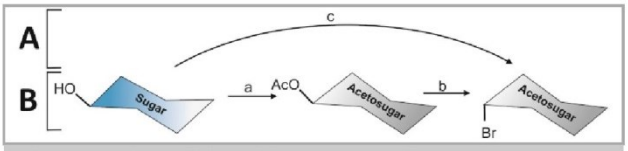

Scheme 1 Synthesis of glycosyl donors; route A: a) NaOAc, Ac2O, 140 °C -> 20 °C, b) 33% HBr in CH3COOH, 0 °C -> 20 °C, ~2 h; route B: c) 33% HBr in CH3COOH, Ac2O, r.t., 2-5 h.

Table 1 Synthesised protected and activated glycosyl donors **1**

Name	Structure	Route[a]	Yield
2,3,4,6-Tetra-O-acetyl-α-D-galactopyranosyl bromide (**1a**)	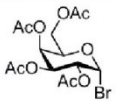	A	85%
2,3,4,6-Tetra-O-acetyl-α-D-glucopyranosyl bromide (**1b**)	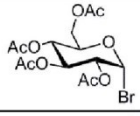	A	86%
2,3,4-Tri-*O*-acetyl-α-L-rhamnopyranosyl bromide (**1c**)	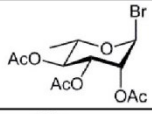	B	74%
2,3,4-Tri-*O*-acetyl-β-L-arabinopyranosyl bromide (**1d**)	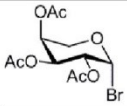	B	72%[13]
2,3,6,2',3',4',6'-Hepta-O-acetyl-α-D-lactosyl bromide (**1e**)	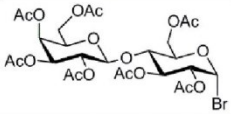	A	87%

In most cases, route B was preferred. Only for L-rhamnose and L-arabinose, where the protected and activate carbohydrates are highly sensitive to hydrolysis, route A gave superior yields. However, all activated and protected carbohydrates (**1a-e**) could be obtained with yields exceeding 72% (Table 1).

The activated and protected carbohydrate is then coupled to 6-nitropiperonylalcohol (**2**) (NP) or 1-(6-nitrobenzo[d][1,3]dioxol-5-yl)ethanol (***3***) (NBE), which have been synthesized by the literature known procedure.[13] The glycosylation proceeds *via* a Koenigs-Knorr type reaction (Table 2).[15] In our case, we used a one-to-one mixture of silver triflate and silver carbonate. Silver triflate is better soluble in organic solvents than silver carbonate making it more accessible for the reaction. It has the disadvantage that it lowers the pH value of the reaction, which can cause the cleavage of the freshly formed glycosylic bond. For this reason, we add silver carbonate to adjust the pH from neutral to slightly basic conditions. Because of the neighbouring group participation (NGP) β-configured glycosides were expected.[16] In case of D-galactose, L-rhamnose and L-arabinose the influence of the neighbouring group is strong enough. In case of D-lactose and D-glucose, however, a mixture of α- and β-configured glycosides is formed (α:β, 21:79). Due to the NGP the main product is the β-configured glycoside.

After glycosylation, the acetate-protecting groups were removed under basic conditions. At first, we performed the deprotection reaction in a solution of sodium methoxide in methanol.[13] While deprotection was achieved, the photo-labile protecting group proved to be sensitive to prolonged exposure to strong basic conditions. Hence, milder conditions were applied (ammonia in methanol). Purification of the final products is most challenging within the sequence: Since the acetals formed are relatively labile towards acidic conditions, a standard normal phase column chromatography of the acetate products **4/5** was not feasible. The products **4/5** degrade on the column even in the presence of one percent triethylamine. Taking the crude product forward yielding the deprotected caged carbohydrate **6/7** proved to be superior: After removal of the solvent, the remaining solid was purified by sequential extraction of side-products. The final product was freeze-dried.

L-Rhamnose was protected not only with NP **2**, but also with NBE **3**, both ultimately having different properties: NBE protected caged carbohydrates are about 15% less soluble in water than NP-caged carbohydrates potentially leading to problems in biological systems that need a higher amount of carbohydrates permanently available. (Table 3) However, NBE protected caged carbohydrates have a higher quantum yield than NP, thus the NBE group is more readily cleaved under irradiation conditions than the corresponding NP protected carbohydrates. (Table 3) For the synthesis of NBE caged L-rhamnose, we used a 2.5-fold access of an enantiomeric mixture of NBE. We expected to receive a one-to-one diastereomeric mixture of the *R*- and *S*-NBE caged L-rhamnose. However, surprisingly we received only one diastereomer in a kinetic resolution (Table 2).

Table 2 Synthesis of photocaged carbohydrates.

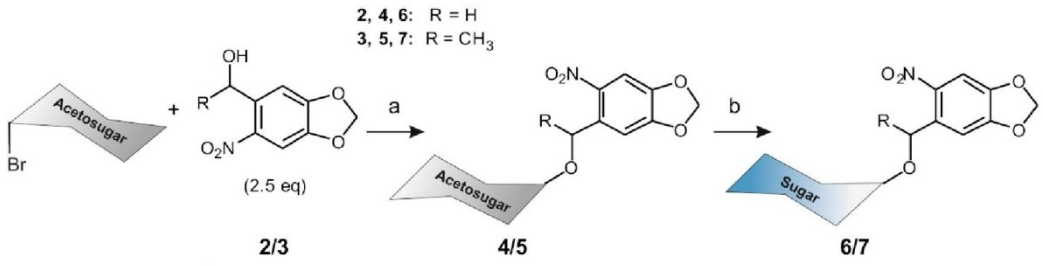

Name	Structure	Yield over 2 steps; diastereomeric ratio β:α
cGalactose 6a 6-nitropiperonyl β-D-galactopyranosid	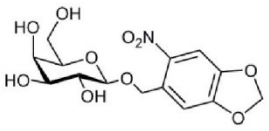	54
cGlucose 6b 6-nitropiperonyl β- D-glucopyranosid 6-nitropiperonyl α- D-glucopyranosid	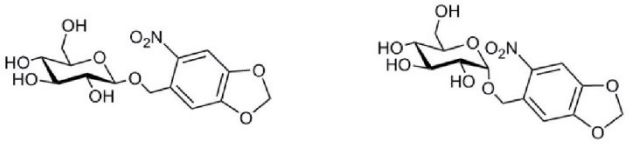	45; 79:21
cRhamnose 6c 6-nitropiperonyl β-L-rhamnopyranosid	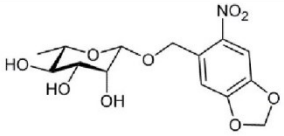	48
cMeRhamnose 7c 1-(6-nitrobenzo[*d*][1,3]dioxol)-5-yl)ethyl β- L-rhamnopyranosid	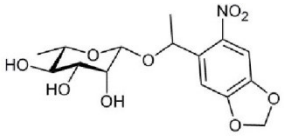	55
cArabinose 6d 6-nitropiperonyl-β- L-arabinopyranosid	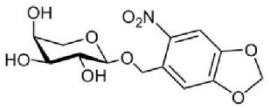	51[13]
cLactose 6e 6-nitropiperonyl-β- D-lactopyranosid 6-nitropiperonyl-α- D-lactopyranosid	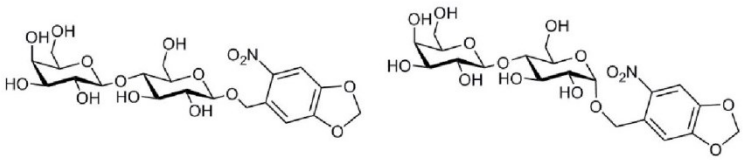	50; 74:26

a) Ag_2CO_3 (0.6eq), AgOTf (0.6 eq), CH_2Cl_2, r.t., 12 h; **b)** NH_3, CH_3OH, r.t., 5-24 h

Important properties for biological utilization of the products were collected: (Table 3). The measured absorption spectra provided information about the excitation wavelength (maximum: 356 nm in water). Although photolysis could be possible at wavelength up to roughly 400 nm (Figures S7, S10, S13, S16, S19; Supporting information), all in vitro cleavage experiments described were performed at 375 nm. Furthermore, the solubility is a key feature that restricts the working range in aqueous biological systems. As pointed out above, NP-photocaged carbohydrates are in general better soluble in water then their NBE-photocaged analogs. As expected, depending on the number of free hydroxyl-groups a trend in their solubility is observable. To appraise light quantities and exposure times for later *in vivo* photo-release applications, the quantum yield was determined in water: The cleavage of all photo-release systems was analysed *via* HPLC as a function of the irradiation time. The decay followed a first order kinetic for all studied caged carbohydrates; complete cleavage was achieved in one-step (Scheme 2 A /Figure 1), irradiation of a 1 mmol/L solution in water led to the expected amount of free carbohydrate (Figure 2). This also proves that for the photo-release of the carbohydrate no additional hydrolase activity is required, in contrast to photocaged IPTG 8, which is known to photolyze in a two-step cleavage reaction (Scheme 2 B).[9,13]

Table 3: Photochemical properties of photocaged carbohydrates[a]

compound	λ_{max}[nm] (ε [$M^{-1}cm^{-1}$])	$t_{0.5}$ [min]	s [mM]	Φ_u
cGalactose 6a	245 (10561) 356 (5757)	8.3	11.2	0.25
cGlucose 6b	245 (4077) 356 (2340)	7.9	32.0	0.45
cRhamnose 6c	245 (12775), 356 (6642)	7.9	4.9	0.19
cMeRhamnose 7c	245 (6794) 356 (3295).	5.47	4,2	0.48
cArabinose 6d[13]	246 (12200) 353 (6000)	19.1	8.1	0.11
cMeArabinose 7d[13]	246 (9 500) 358 (4 600)	13.7	6.9	0.29
cLactose 6e	245 (9206), 356 (4962)	9.5	58.2	0.22

[a] Extinction coefficient ε at λ_{max}, uncaging half-life time $t_{0.5}$, solubility s in water and uncaging quantum yield ϕ_u were measured in deionized and degassed water.

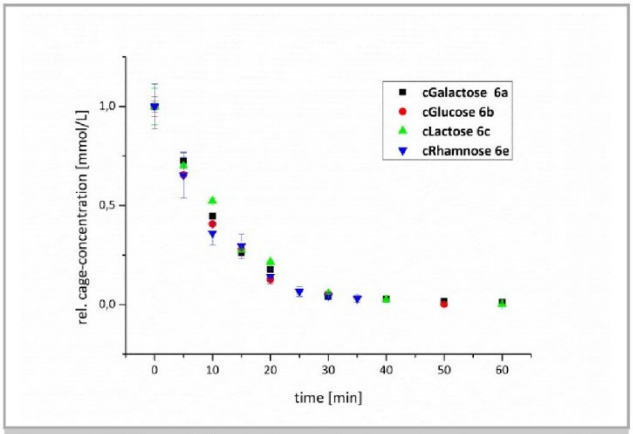

Figure 1 HPLC analysis of the photo-cleavage and -release of the carbohydrates depending on the irradiation time; 1mmol/L in H_2O; 375 nm 6.4 mW/cm^2, r.t..

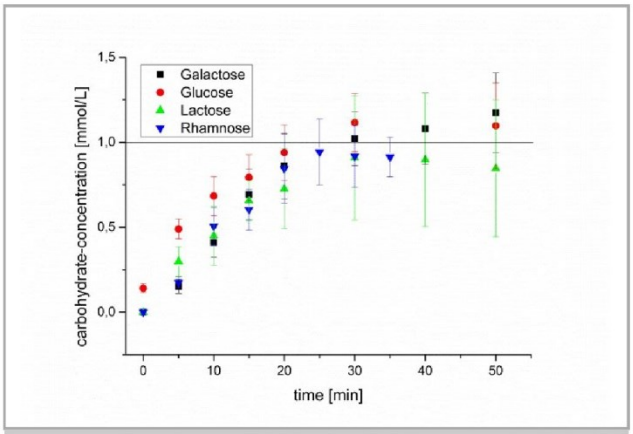

Figure 2 Molar amount of released carbohydrate depending on the irradiation time; 1mmol/L in H_2O; 375 nm 6.4 mW/cm^2, r.t..

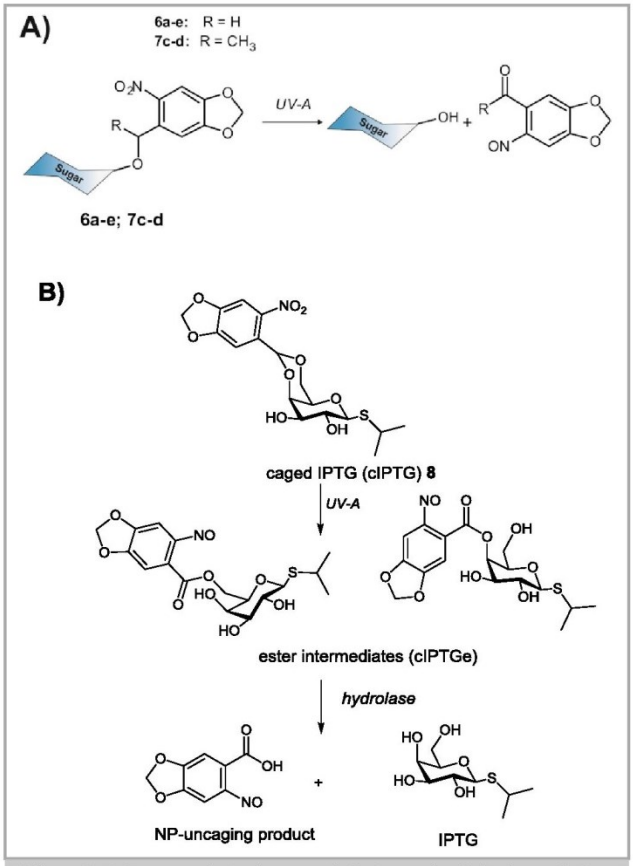

Schema 2: A One-step photo cleavage of photocaged carbohydrates. B Two-step photo cleavage of photocaged Isopropyl β-D-1-thiogalactopyranoside (IPTG) [9,17]

With this versatile toolbox of light-responsible inducer molecules at hand, we next tested their biological applicability. In particular, we aimed at controlling bacterial gene expression with light as shown schematically in (Scheme 3). Both, activating ('Play') as well as temporary ('Pause') or permanent repressing ('Stop') bacterial expression systems were tested.

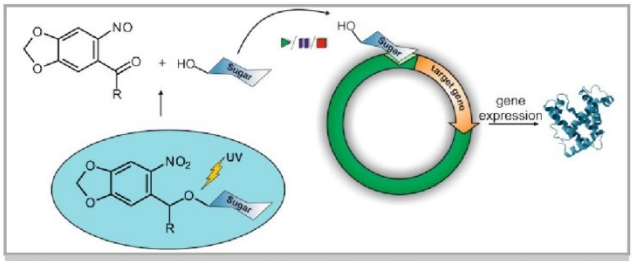

Scheme 3 Schematic representation of bacterial gene expression system controlled by photocaged carbohydrates (activate 'Play'; temporary repress 'Pause'; permanently repress 'Stop').

To this end, a set of different carbohydrate-sensitive *E. coli* expression systems was recruited based on the most common biotechnological expression strain BL21(DE3) and its derivative Tuner(DE3).[10,18] Furthermore, for arabinose-inducible gene expression the *E. coli* strain LMG194 was chosen which does not metabolize arabinose.[19] The promoter/regulator expression

systems included IPTG-, D-galactose-, and lactose-inducible PT7lac/LacI systems,[10] an arabinose-inducible PBAD/AraC system[13] as well as a L-rhamnose-repressible PrhaBAD/RhaRS system.[20] Furthermore, D-glucose was tested for its ability to repress PT7lac/LacI based gene expression *via* catabolite repression. The strain/plasmid systems used in this study are listed in Table 4.

Table 4 Light-controlled expression systems and conditions.

Caged inducer	*E. coli* strain (plasmid(s))	Working concen-tration	UV-A light exposure times	Expres-sion time [h]	Feature Action
cIPTG 8	Tuner(DE3) (pRhotHi-2-LacI-EYFP)	40 µM	2 min	16	Two-step P_{lac} activation
cArabinose 6d	LMG194 (pAra-GFP)	25 µM	10 min	16	Fast one-step P_{BAD} activation
cMeArabinose 7d	LMG194 (pAra-GFP)	25 µM	10 min	16	Fast one-step P_{BAD} activation
cGalactose 6a	BL21(DE3) (pRhotHi-2-LacI-EYFP)	0.4 mM	30 min	16	One-step P_{lac} activation
cLactose 6e	BL21(DE3) (pRhotHi-2-LacI-EYFP)	2 mM	30 min	16	Alternative chemical inducer for strong induction (dark activity)
cRhamnose 6c	Tuner(DE3) (pRhotHi-2-LacI-EYFP) + (pLemo)	0.1 mM	20 min	20	Permanent repression, T7RP based gene expression
cGlucose 6b	Tuner(DE3) (pRhotHi-2-LacI-EYFP)	5 mM	30 min	4	Temporary catabolite repression

Light induction of gene expression in *E. coli* (Figure 3) could be demonstrated for both cArabinose **6d** and cMeArabinose **7d**[13] as well as for cGalactose **6a** and even slightly outperformed induction using equimolar amounts of conventional inducers galactose (PT7lac/LacI) and arabinose (PBAD/AraC). Whereas for these three caged carbohydrates dark control cultures indicated *in vivo* stability, the cLactose **6e** derivative revealed strong induction of gene expression in both presence and absence of UV-A light. Here, it can be presumed that cLactose 6e is not stable *in vivo* due to enzymatic hydrolysis in terms of glycosidase or especially β-galactosidase activity. In a rhamnose-repressible PrhaBAD/RhaRS expression setup,[20] photo-release of cRhamnose **6c** was able to effectively downregulate IPTG-induced gene expression due to rhamnose induced expression of the T7 RNA polymerase inhibitor protein T7LysY. Finally, cGlucose **6b** was shown to slightly downregulate IPTG-induced gene expression *via* glucose-mediated catabolite repression. Notably, for cGlucose **6b** the dark control already significantly reduced gene expression responses. Hence, prior to application of cGlucose **6b** an in-depth characterization and optimization regarding crucial parameters such as the working concentration might be reasonable.

In conclusion, photocaged arabinose, galactose and rhamnose directly proved highly applicable to control bacterial gene expression by light and will inevitably provide the basis for sophisticated optogenetic control of microbial gene expression in the future. cGlucose-based regulation of gene expression might require optimization to function properly, and could further be employed for other catabolite repression sensitive expression systems such as PBAD/AraC or PrhaBAD/RhaRS setups. However, cLactose highlights that despite well applicable photolysis and stability *in vitro*, caged compounds might behave dissimilar in biological systems. The wealth of hydrolyzing microbial enzymes is thus a key feature that dictates *in vivo* applicability. Compared to previously described cIPTG-based light induction,[9,13] the presented photocaged carbohydrates release their effector molecules in a one-step photocleavage fashion, without being dependent on additional secondary reactions such as enzymatic hydrolysis. Hence, the temporal resolution of control is significantly increased. (Figures 3 and 4)

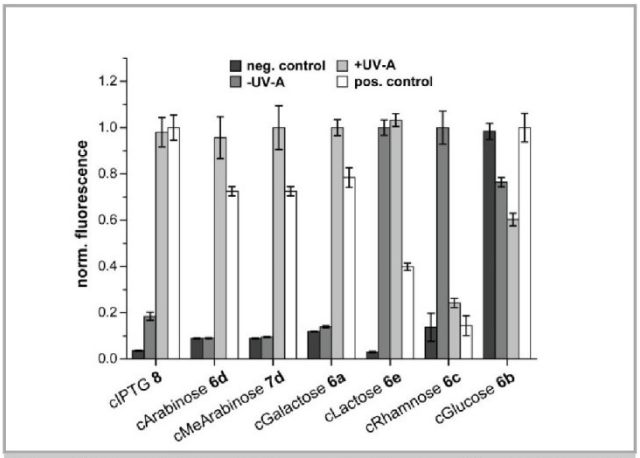

Figure 3 Light-control of bacterial gene expression using different photocaged carbohydrates. *E. coli* expression cultures were supplemented with the respective caged effector prior to cultivation. Dark-control cultures (-UV-A; grey bars) were constantly kept in the dark, whereas light-induced cultures (+UV-A; light grey bars) were subjected to short UV-A light exposure during exponential growth. Corresponding positive control cultures (white bars) were simultaneously supplemented with equimolar amounts of uncaged carbohydrates, whereas negative controls (dark grey bars) were cultivated without inducers. Gene expression was quantified *via* EYFP or GFP *in vivo* fluorescence reporters 4 h after induction (for cGlucose **6b** due to transient repression) or after overnight expression. Values are means of triplicate measurements. Error bars indicate the respective standard deviations.

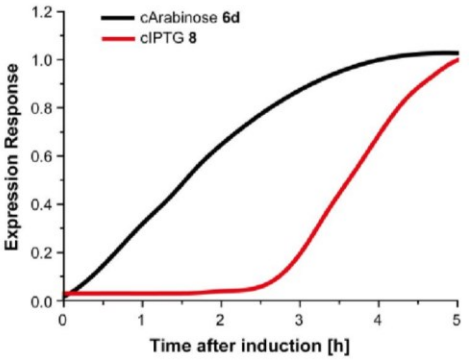

Figure 4 Comparison of temporal resolutions using one- and two-step photo-release inducers. One-step cArabinose **6d** based light induction (black curve) significantly outperforms the two-step cIPTG-based **8** induction of gene expression. Expression response is given as relative values indicating GFP production levels after induction of target gene expression (modified from Binder et al. 2016[13])

This study shows that nitropiperonyl photocaging is in principle applicable to a broad range of carbohydrates applicable for controlling gene expression in bacteria. Moreover, further relevant carbohydrates such as fructose, xylose or ribose could be made accessible for light control in a similar fashion. Established phototriggers will significantly expand the optogenetic toolbox with respect to light-controlled microbial gene expression. Further conceivable applications include light-controlled carbon source feeding. Together with novel photo-microbioreactors[17] and single-cell cultivation platforms,[21] photocaged carbohydrates will empower a higher-order control and automatization of microbial productions.

The experimental section has no title; please leave this line here.

All chemicals for synthesis were obtained from commercial sources and used as received unless stated otherwise. Solvents were reagent grade. Solvents were dried and purified by common methods. Thin-layer chromatography (TLC) was performed using pre-coated (Polygram® SIL G/UV, Macherey-Nagel) silica gel plates, and components were visualized *via* staining with cerium molybdenum solution [phosphomolybdic acid (25 g), $Ce(SO_4)_2 \cdot H_2O$ (10 g), conc. H_2SO_4 (60 mL), H_2O (940 mL)], or UV-light. Flash chromatography was performed on silica gel (Merck silica gel 60 (0.063–0.200 µm). Solvents for flash chromatography (petroleum ether/ EtOAc/ n-pentane/ CH_2Cl_2) were distilled prior to use. Petroleum ether refers to a fraction with a boiling point between 40–60 °C. The NMR spectra (^1H and ^{13}C) were measured at 20 °C on a Bruker Avance/DRX 600 spectrometer in deuterated solvents ($CDCl_3$, DMSO-d_6, CD_3OD). Chemical shifts are given in ppm relative to the resonance of the solvent (^1H: $CDCl_3$= 7.26 ppm, ^1H: CD_3OD = 2.50 ppm or ^1H: DMSO-d_6 = 3.31 ppm/ ^{13}C: $CDCl_3$= 77.16 ppm, ^{13}C: CD_3OD = 49.00 ppm or ^{13}C: DMSO-d_6 = 39.52 ppm). The IR spectra were measured with a Perkin Elmer SpectrumOne IR-spectrometer ATR. Optical rotation was determined at 20 °C on a Perkin Elmer Polarimeter 241 MC against sodium D-line. HRMS (ESI) spectra were recorded by the ZEA 3 of the Forschungszentrum Jülich. Melting points were recorded using a Büchi melting point B-545 apparatus. UV-Vis absorption spectra were recorded on Genesys 10S UV/VIS Spectrophotometer (Thermo Scientific). In addition, UV-Vis absorption was quantified using a Tecan infinite M1000Pro microplate reader. Uncaging experiments were performed with the LUMOS 43® from Atlas Photonics at 375 nm. The freed sugar was separated and detected by a Jasco HPLC system [column: Hyperclone 5 µ ODS (C18) 120 (Phenomenex)] combined with the light scattering detector ELSD ZAM 3000 from AlphaCrom. UV-A light exposure was performed using VL-315.BL 45 W hand lamp from Vilber Lourmat. Light intensity was quantified using a Thermal Power Sensor (S302C, Thorlabs Inc, USA).

Procedures:

General procedure A for the two-step synthesis of peracetylated pyranosyl bromides **1a; 1b; 1e**

A suspension of dry sodium acetate (1.1 eq) in acetic anhydride (13.1 eq) was heated to reflux (~140° C). The heater was removed and the carbohydrate (1 eq) was added in small portion to the hot solution so that the reaction mixture starts to reflux on its own. After this, the reaction mixture was cooled to room temperature, and then poured on ice. After crystallization, the formed solid was separated by filtration and washed with ice water. The product was vacuum-dried.

The acetylated carbohydrate was added to a stirring solution of hydrobromic acid 33 wt. % in acetic acid at 0 °C in small portions. After full conversion (45 min-4 h), the reaction was poured on ice water and extracted with CH_2Cl_2 three times. The combined organic phase was washed with a saturated sodium bicarbonate solution and dried over anhydrous magnesium sulfate. The solvent was removed under reduced pressure.[12]

General procedure B for the one-pot synthesis of peracetylated pyranosyl bromides **1c; 1d**

The carbohydrate (1.00 g) was dissolved in 5 mL acetic anhydride at r.t. 1.5 mL hydrobromic acid solution 33 wt. % in acetic acid was added to this solution. After the solid was completely dissolved additional 7.5 mL hydrobromic acid solution 33 wt. % in acetic acid were added. The reaction mixture was stirred for additional 2 h. Afterwards it was concentrated under reduced pressure. Twice 20 mL toluene were added and then removed under reduced pressure. The crude product was recrystallized twice from diethyl ether.[13]

General procedure C for the synthesis of photocaged carbohydrates **6a-e**; **7c**

All glassware was dried prior use. One *Schlenk* tube was charged with 1 g (per mmol carbohydrate) molecular sieve 3 Å and the peracetylated pyranosyl bromide (1 eq) dissolved in dry dichloromethane. A second flask was charged with 1 g (pro mmol carbohydrate) molecular sieve 3 Å and 6-nitropiperonylalcohol NP **2** or 1-(6-nitrobenzo[*d*][1,3]di-oxol-5-yl)ethanol NBE **3** (2.5 eq) dissolved in dry dichloromethane. After one hour of stirring they were combined. Next, silver carbonate (0.6 eq) and silver triflate (0.6 eq) were added. The reaction was stirred at r.t. until full conversion (as detected by tlc) was observed. The molecular sieve was removed *via* filtration. The filtrate was washed with a saturated sodium bicarbonate solution and brine. The combined organic layer was dried with anhydrous magnesium sulfate and concentrated under reduced pressure.

The crude product **4/5** (500mg) was dissolved in 4.5 mL methanol and 2.5 mL of a 7 N solution of ammonia in methanol was added. The reaction was stirred at r.t. until tlc confirmed complete deprotection. The solvent was removed under reduced pressure. The remaining solid was suspended in methyl *tert*-butyl ether and treated with ultrasonic. Afterwards the mixture was centrifuged and the solvent was transfused. This procedure is repeated. Then the solid is suspended in a small amount of deionized water and centrifuged. This is repeated three times. The remaining solid is freeze-dried

General determination of the quantum yield

The quantum yield of **2/3** was determined in comparison to the quantum yield of 5-acetoxymethyl-6-nitro-benzo[1,3]dioxole (NPA-Ac), because this substance is quite similar to **2/3**.[22] The procedure was followed as described in literature.[13,22,23]

General determination of the solubility

The solubility was measured photometrically. The concentration is proportional to absorption at high dilutions. With the Beer–Lambert law it is possible to calculate the concentration of a saturated solution referring to the absorption of solutions with the concentration of 20, 10 and 5 µmol/L at 356 nm.[5]

Expression cultures and light induction

Expression cultures were grown in sterile 48-well flowerplates (m2p-labs GmbH, Aachen, Germany) at 37°C and 1500 rpm using a deep-well plate incubator (Thermomixer C; Eppendorf, Hamburg, Germany) and appropriate antibiotic selection (50 µg/ml kanamycin for all strains and additionally 35 µg/ml chloramphenicol when applying the pLemo plasmid). Overnight precultures were inoculated from a fresh LB-Agar transformation plate in 0.8 ml of Lysogeny Broth (LB) medium (Luria / Miller from Carl Roth, Karlsruhe, Germany;[24]). After 16 h of precultivation, main cultures were inoculated in again 0.8 ml of LB medium to a cell density corresponding to an optical density of 0.01 at a wavelength of 580 nm (OD_{580}) and directly supplemented with respective caged compounds prior to cultivation. Final working concentrations were as follows: 40 µM (c)IPTG, 25 µM (c) arabinose or (cMe)arabinose, 100 µM (c)rhamnose, 2 mM (c)lactose, 5 mM glucose. Rhamnose-and glucose-controlled cultures were further supplemented with 100 and 25 µM IPTG simultaneous to rhamnose or glucose supplementation / light exposure, respectively. During the exponential growth phase (OD_{580} of 0.4 – 0.6), gene expression was induced /repressed once *via* supplementing 20-fold stock solution of the conventional inducer or *via* short UV-A light-induction (VL-315.BL hand lamp 45 W, Vilber Lourmat, France; distance to flowerplate: 1.5 cm, approx. 0.9 mW cm^{-2}) using respective photocaged carbohydrates. After intended expression periods in the dark, *in vivo* fluorescence ($\lambda_{ex}/\lambda_{em}$: 488/527 nm for EYFP; 485/520 nm for GFP) and cell densities (OD_{580}) of 5-fold diluted samples (0.1 M Tris-HCl buffer; pH 8.0; 100 µl final volume) were measured in 96 flat bottom transparent polystyrene microplates using a fluorescence microplate-reader (Tecan Infinite M1000 Pro). Relative fluorescence units of diluted samples were normalized to a cell density of OD_{580} =1.0 and to respective maxima.[13]

Syntheses

2,3,4,6-Tetra-O-acetyl-α-D-galactopyranosyl bromide (1a)

Compound **1a** was synthesized according to the general procedure **A** from D-galactose (2.00g, 11.10 mmol). Yield: 3.03 g (8.58 mmol,85%) colorless syrup. ^{1}H and ^{13}C NMR data were consistent with Literature.[25]

^{1}H NMR (600 MHz, Chloroform-*d*): δ = 6.69 (d, $^3J_{1/2}$ = 4.0 Hz, 1H, 1-CH), 5.54 – 5.49 (m, 1H, 4-CH), 5.39 (dd, $^3J_{3/2}$ = 10.6, $^3J_{3/4}$ = 3.3 Hz, 1H, 3-CH), 5.04 (dd, $^3J_{2/3}$ = 10.7, $^3J_{2/1}$ = 4.1 Hz, 1H, 2-CH), 4.48 (t, $^3J_{5/4}$ = 6.5 Hz, $^3J_{5/6a/b}$ = 6.5 Hz, 1H, 5-CH), 4.18 (dd, $^2J_{6a/b}$ = 11.5 Hz, $^3J_{6a/b/5}$ = 6.4 Hz, 1H, $6_{a/b}$–CH_2), 4.10 (dd, $^2J_{6a/b}$ = 11.4, 6.7 Hz, 1H, $6_{a/b}$–CH_2), 2.14 (s, 3H, -CH_3) 2.10 (s, 3H, -CH_3), 2.05 (s, 3H, -CH_3), 2.00 (s, 3H, -CH_3).

^{13}C NMR (151 MHz, Chloroform-*d*): δ = δ 170.43 (C=O), 170.18 (C=O), 170.01 (C=O), 169.87 (C=O), 88.24 (C-1), 71.18 (C-5), 68.11 (C-3), 67.89 (C-2), 67.10 (C-4), 60.95 (C-$6_{a/b}$), 20.87 (-CH_3), 20.76 (-CH_3), 20.71 (-CH_3), 20.68 (-CH_3).

2,3,4,6-Tetra-O-acetyl-α-D-glucopyranosyl bromide (1b)

Compound **1b** was synthesized according to the general procedure **A** from D-glucose (2.00g, 11.10 mmol). Yield: 3.07 g (8.68 mmol, 84%) colorless syrup. ^{1}H and ^{13}C NMR data were consistent with literature data.[25,26]

^{1}H NMR (600 MHz, Chloroform-*d*): δ = 6.60 (d, $^3J_{1/2}$ = 4.0 Hz, 1H, 1-CH), 5.54 (t, $^3J_{3/2}$ = 9.7 Hz, $^3J_{3/4}$ = 9.7 Hz 1H, 3-CH), 5.15 (t, $^3J_{4/3}$ = 9.8 Hz, $^3J_{4/5}$ = 9.8 Hz, 1H, 4-CH), 4.83 (dd, $^3J_{2/3}$ = 10.0 Hz, $^3J_{2/1}$ = 4.1 Hz, 1H, 2-CH), 4.38 – 4.24 (m, 2H, 5-CH, $6_{a/b}$-CH_2), 4.12 (dd, $^2J_{6a/b}$ = 12.5 Hz, $^3J_{6a/b/5}$ = 1.9 Hz, 1H, $6_{a/b}$-CH_2), 2.09 (s, 3H, -CH_3), 2.08 (s, 3H, -CH_3),2.04 (s, 3H, -CH_3), 2.02 (s, 3H, -CH_3).

^{13}C NMR (151 MHz, Chloroform-*d*): δ = 170.60 (C=O), 169.95 (C=O), 169.89 (C=O), 169.56 (C=O), 86.68 (C-1), 72.25 (C-5), 70.71 (C-2), 70.28 (C-3), 67.29 (C-4), 61.07 (C-$6_{a/b}$), 20.79 (-CH_3), 20.77 (-CH_3), 20.74 (-CH_3), 20.67 (-CH_3).

2,3,4-Tri-*O*-acetyl-α-L-rhamnopyranosyl bromide (1c)

Compound **1c** was synthesized according to general procedure **B** from L-rhamnose (1.00g, 5.49 mmol). Yield: 1,44g (4.06 mmol, 74%) colorless syrup. ^{1}H and ^{13}C NMR data were consistent with Literature.[26]

^{1}H NMR (600 MHz, Chloroform-*d*): δ = 6.24 (m, 1H, 1-H), 5.65 (dd, $^3J_{3,4}$ = 10.2 Hz, $^3J_{3,2}$ = 3.4 Hz, 1H, 3-H), 5.43 (dd, $^3J_{2,3}$ = 3.4 Hz, $^3J_{2,1}$ = 1.6 Hz, 1H, 2-H), 5.14 (t, $^3J_{4,3}$ = 10.1 Hz, $^3J_{4,5}$ = 10.1 Hz 1H, 4-H), 4.09 (dq, $^3J_{5,4}$ = 10.0 Hz, $^3J_{5,6}$ = 6.3 Hz, 1H, 5-H), 2.15 (s, 3H, -CH_3), 2.06 (s, 3H, -CH_3), 1.99 (s, 3H, -CH_3), 1.27 (d, *J* = 6.2 Hz, 3H, 6-H_3).

^{13}C NMR (151 MHz, Chloroform-*d*): δ = 169.93 (C=O), 169.84 (C=O), 169.70 (C=O), 83.82 (C-1), 72.55 (C-2), 71.22 (C-5), 70.40(C-4), 68.02 (C-3), 20.89 (-CH_3), 20.85 (-CH_3), 20.72 (-CH_3), 17.08 (C-6).

2,3,6,2',3',4',6'-Hepta-O-acetyl-α-D-lactosyl bromide (1e)

Compound **1e** was synthesized according to the general procedure **A** from D-galactose (2.00 g, 5.84 mmol). Yield: 3.56 g (5.08 mmol, 87%) colorless syrup.

^{1}H NMR (600 MHz, Chloroform-*d*): δ = 6.53 (d, $^3J_{1/2}$ = 4.0 Hz, 1H, 1-CH), 5.56 (t, $^3J_{3/2}$ = 9.6 Hz, $^3J_{2/3}$ = 9.6 Hz 1H, 3-CH), 5.36 (dd, $^3J_{4'/3'}$= 3.6, $^3J_{4'/5'}$= 1.2 Hz, 1H, 4´-CH), 5.13 (dd, $^3J_{2'/3'}$ = 10.4, $^3J_{2'/1'}$7.9 Hz, 1H, 2´-CH), 4.96 (dd, $^3J_{3'/2'}$= 10.4, $^3J_{3'/4'}$= 3.4 Hz, 1H, 3´-CH), 4.76 (dd, $^3J_{2/3}$= 9.9, $^3J_{2/1}$= 4.1 Hz, 1H, 2-CH), 4.56 – 4.47 (m, 2H, 1´-CH, 6-CH), 4.25 – 4.12 (m, 3H, 5-CH, 6-CH, 6´-CH), 4.08 (dd, $^3J_{6'/6'}$= 11.2, $^3J_{6'/5'}$= 7.2 Hz, 1H, 6´-CH), 3.91 – 3.82 (m, 2H, 5´-CH, 4-CH).

^{13}C NMR (151 MHz, Chloroform-*d*): δ = 170.50 (C=O), 170.33 (C=O), 170.29 (C=O), 170.22 (C=O), 170.13 (C=O), 169.37 (C=O), 169.11 (C=O), 100.98 (C-1´), 86.54 (C-1), 75.14 (C-4), 73.14 (C-5), 71.17 (C-3´), 71.03 (C-2), 70.97 (C-5´), 69.77 (C-4´), 69.20 (C-2´), 66.77 (C-4´), 61.21 (C-6), 61.03 (C-6´), 20.97 (-CH_3), 20.96 (-CH_3), 20.84 (-CH_3), 20.82 (2*-CH_3), 20.81 (-CH_3), 20.66 (-CH_3).

Photocaged Carbohydrates

6-Nitropiperonyl β-D-galactopyranosid (6a) [cGalactose]

Compound **6a** was synthesized according to the general procedure **C** over two steps from **1a** (500 mg, 1.22 mmol). Yield: 236 mg (0.66 mmol, 54%) light-yellow solid.

IR (ATR): $\tilde{\nu}_{max}$ = 3344, 2927, 1651, 1516, 1504, 1486, 1441, 1421, 1379, 1318, 1258, 1155, 1116, 1091, 1071, 1027, 974, 928, 888, 865, 818, 756, 665.cm^{-1}.

^{1}H NMR (600 MHz, DMSO-d_6): δ = 7.71 (s, 1H, 7´-H), 7.61 (s, 1H, 4´-H), 6.25 (d, $^2J_{2'}$ = 4.8 Hz, 2H, 2´-H), 5.20 (d, $^3J_{2\text{-}OH\text{-}2}$ = 5.0 Hz, 1H, 2-OH), 5.06 (d, $^2J_{1''a\text{-}1''b}$ = 16.2 Hz, 1H, 1´´a-H), 4.92 (d, $^2J_{1''b\text{-}1''a}$ = 16.3 Hz, 1H, 1´´b-H), 4.74 (d, $^3J_{4\text{-}OH\text{-}4}$ = 5.0 Hz, 1H, 4-OH), 4.59 (t, 1H, $6_{a/b}$-OH), 4.41 (d, $^3J_{3\text{-}OH;3}$ = 4.6 Hz, 1H, 3-OH), 4.22 (d, *J* = 7.7 Hz, 1H, 1-H), 3.64(m, 1H, H-3), 3.51

(dtd, J = 22.3 Hz, J = 11.1 Hz, J = 5.8 Hz, 2H, $6_{a/b}$-H), 3.44 (ddd, J = 9.6 Hz, J = 7.7 Hz, J = 4.9 Hz, 1H, 2-H), 3.37 (m, 1H, 5-H), 3.31(m, 1H, 4-H).

^{13}C NMR (151 MHz, DMSO-d_6): δ = 152.54 (C-7a), 146.56 (C-3a), 140.19 (C-6´), 133.16 (C-5´), 107.24 (C-4´), 105.00 (C-7´), 103.37 (C-2´), 103.05 (C-1), 75.35 (C-5), 73.22 (C-4), 70.69 (C-2), 68.18 (C-3), 66.43 (C-1´´), 60.45 (C-6).

HRMS (ESI, positiv mode): m/z [M+Na]$^+$ calcd for $C_{14}H_{17}NO_{10}Na$: 382,0750; found:382.0747.

UV/Vis (H_2O): λ_{max} (ε) = 245 nm (10561), 356 nm (5757).

mp: 191 °C

optical rotatory power:$[\alpha]_D^{20}$ = -17 (c =0.3 in DMSO)

6-Nitropiperonyl β-D-glucopyranosid and 6-nitropiperonyl α- D-glucopyranosid (6b) [cGlucose]

Compound **6b** was synthesized according to the general procedure **C** over two steps from **1b** (500 mg, 1.22 mmol). Yield: 197 mg (0.55 mmol, 45%) light-yellow solid.

α/β-IR (ATR): $\tilde{\nu}_{max}$ = 3336, 2921, 1617, 1505, 1482, 1482, 1448, 1423, 1382, 1325, 1258, 1197, 1166, 1056, 1024, 925, 894, 818, 776, 756, 725 cm^{-1}.

β-^{1}H NMR (600 MHz, DMSO-d_6): δ = 7.70 (s, 1H, 7´-H), 7.60 (s, 1H, 4´-H), 6.24 (s, 2H, 2´-H), 5.36 (d, J = 4.9 Hz, 1H ,3,4 -OH), 5.08 (d, J = 16.2 Hz, 1H,1´´a-H), 4,95 (m, 3H, 1´´b-H,2-OH, 3,4-OH), 4.53 (t, $^3J_{6\text{-}OH/6a}$ = 5.8 Hz, $^3J_{6\text{-}OH/6b}$ = 5.8 Hz, 1H, 6-OH), 4.27 (d, $^3J_{1/2}$ = 7.6 Hz, 1H, 1-H), 3.68 (dd, $^2J_{6a/6b}$ = 11.5 Hz, $^3J_{6a/5}$ = 5.9 Hz, 1H, 6_a-H), 3.45 (m, 1H, 6_b-H), 3.16 (m, 1H, 5-H), 3.11 (m, 3H, 2-H, 3-H, 4-H,).

β- ^{13}C NMR (151 MHz, DMSO-d_6): δ = 152.59 (C-7a), 146.58 (C-3a), 140.18 (C-6´), 133.11 (C-5´), 107.18 (C-4´), 105.02 (C-7´), 103.41 (C-2´), 102.43 (C-1), 76.94 (C-3/4), 76.52 (C-5), 73.61 (C-3/4), 69.99 (C-2), 66.54 (C-1´´), 60.97 (C-6).

α-^{1}H NMR (600 MHz, DMSO-d_6): δ = 7.70 (s, 1H, 7´-H), 7.57 (s, 1H, 4´-H), 6.24 (s ,2H, 2´-H), 5.03 (d, J = 6.0 Hz, 1H ,3,4 -OH), 4,95 (m, 1H, 1´´a-H,), 4.81 (m, 4H, 1´´b-H,1-H, 2-OH, 3,4-OH) 4.49 (t, $^3J_{6\text{-}OH/6a}$ = 5.5 Hz, $^3J_{6\text{-}OH/6b}$ = 5.8 Hz, 1H, 6-OH), 3.62 (dd, $^2J_{6a/6b}$ = 11.5 Hz, $^3J_{6a/5}$ = 5.9 Hz, 1H, 6_a-H), 3.54 (td, J = 9.3, 5.0 Hz, 1H, 3-H)), 3.39 (dd, J = 10.2, 5.5 Hz, 1H, 4-H), 3.27 (m, 1H, 2-H), 3.16 (m, 2H, 6_b-H, 5-H).

α-^{13}C NMR (151 MHz, DMSO-d_6) : δ = 152.59 (C-7a), 146.58 (C-3a), 140.25(C-6´), 133.11 (C-5´), 107.13(C-4´), 104.90 (C-7´), 103.29 (C-2´), 98.55 (C-1), 73.34 (C-4), 73.32 (C-3), 71.97 (C-2), 70.28 (C-5), 65.00 (C-1´´), 60.90 (C-6).

HRMS (ESI, positiv mode): m/z [M+Na]$^+$ =calcd for $C_{14}H_{17}NO_{10}Na$: 382.07502 found: 382.07457.

β/α: UV/Vis (H_2O): λ_{max} (ε) = 245 nm (4078), 356 nm (2340).

β/α: mp: 153°C

β/α: optical rotatory power:$[\alpha]_D^{20}$ = -4,1 (c = 0.4 in DMSO)

6-Nitropiperonyl β-L-rhamnopyranosid (6c) [cRhamnose]

Compound **6c** was synthesized according to the general procedure **C** over two steps from **1c** (500 mg, 2.83 mmol). Yield: 233 mg (0.68 mmol, 48%) light-yellow solid.

IR (ATR): $\tilde{\nu}_{max}$ =3283, 2917, 1617, 1542, 1517, 1506, 1486, 1447, 1425, 1407, 1323, 1259, 1109, 1127, 1072, 1052, 1022, 979, 927, 915, 870, 815, 755, 686 cm^{-1}.

^{1}H NMR (600 MHz, DMSO-d_6) δ [ppm]: 7.68 (s, 1H, 7´-H), 7.20 (s, 1H, 4´-H), 6.24 (dd, J = 3.5, 1.0 Hz, 2H, 2´-H), 4.84 (m, 2H, 1´´a-H, 2-OH), 4.74 (m, 2H, 1´´b-H, 4-OH), 4.67 (d, $^3J_{1,2}$ = 1.6 Hz, 1H, 1-H), 4.58 (d, $^3J_{3\text{-}OH,3}$ = 5.9 Hz, 1H, 3-OH), 3.68 (td, $^3J_{2,3}$ = 3.9 Hz, $^3J_{2,1}$ = 1.7 Hz, 1H, 2-H), 3.47 (ddd, $^3J_{3,4}$ = 9.4 Hz, $^3J_{3,3\text{-}OH}$ = 5.9 Hz, $^3J_{3,2}$ = 3.4 Hz, 1H, 3-H), 3.39 (dq, $^3J_{5,4}$ = 9.5, $^3J_{5,6}$ = 6.2 Hz, 1H, 5-H), 3.20 (td, $^3J_{4,5}$ = 9.3 Hz, $^3J_{4,3}$ = 9.3 Hz, $^3J_{4,4\text{-}OH}$ =5.6 Hz, 1H,4-H), 1.13 (d, $^3J_{6,5}$ = 6.1 Hz, 3H, 6-H).

^{13}C NMR (151 MHz, DMSO-d_6) : δ = 152.02 (C-7a), 146.89 (C-3a), 141.14 (C-6´), 131.20 (C-5´), 107.49 (C-4´), 105.21 (C-7´), 103.44 (C-2´), 100.05 (C-1), 71.87 (C-4), 70.73 (C-3), 70.28 (C-2), 68.98 (C-5), 65.14 (C-1´´), 17.90 (C-6).

HRMS (ESI, positiv mode): m/z [M+Na]$^+$ calcd for $C_{15}H_{19}NO_9Na$: 380.09575; found: 380.09516.

UV/Vis (MeOH): λ_{max} (ε) = 242 nm (9301), 293 nm (2365), 344 nm (4377).

mp: 157 °C

optical rotatory power:$[\alpha]_D^{20}$ = 20 (c = 0.2 in MeOH)

1-(6-Nitrobenzo[*d*][1,3]dioxol)-5-yl)ethyl β-L-rhamnopyranosid (7c) [cMeRhamnose]

Compound **7c** was synthesized according to the general procedure **C** over two steps from **1c** (500 mg, 2.83 mmol). Yield: 278 mg (0.78 mmol, 55%) light-yellow-brownish solid.

IR (ATR): $\tilde{\nu}_{max}$ =3436, 2976, 2935, 1619, 1516, 1502, 1483, 1424, 1397, 1362, 1339, 1255, 1136, 1122, 1109, 1090,1064,1029, 999, 933, 904, 882, 857, 844, 807, 767, 757, 663.

1H NMR (600 MHz, DMSO-d6) : δ = 7.53 (s, 1H, 7´-H), 7.19 (s, 1H, 4´-H), 6.23 (d, $^2J_{2',2'}$ = 20.7 Hz, 2H, 2´-H), 5.12 (q, $^3J_{1'',2''}$ = 6.3 Hz, 1H, 1´´-H), 4.77 (d, $^3J_{2\text{-}OH,2}$ = 4.4 Hz, 1H, 2-OH), 4.72 (m, 2H, 1-H, 4-OH), 4.53 (m, 1H, 3-OH), 3.64 (m, 1H, 2-H), 3.36 (m, 1H, 3-H), 3.11 (m, , 1H, 4-H), 2.89 (dq, $^3J_{5,4}$ = 12.2Hz, $^3J_{5,6}$ =6.5 Hz, 1H, 5-H), 1.43 (d, $^3J_{2'',1''}$ = 6.4 Hz, 3H, 2´´-H), 0.84 (d, $^3J_{6,5}$ = 6.2 Hz, 3H, 6-H).

^{13}C NMR (151 MHz, DMSO-d_6): δ = 151.67 (C-7a), 146.63 (C-3a), 141.07 (C-6´), 136.17 (C-5´), 106.58 (C-4´), 104.08 (C-7´), 103.27 (C-2´), 99.63 (C-1), 71.61 (C-4), 70.62 (C-3), 70.55 (C-2), 69.29 (C-5), 69.18 (C-1´´), 22.12 (C-2´´), 17.47 (C-6).

HRMS (ESI, positiv mode): m/z [M+Na]$^+$ calcd for $C_{14}H_{17}NO_9Na$: 366.0801; found: 366.0795

UV/Vis (H_2O): λ_{max} (ε) = 248 nm (6794), 355 nm (3295).

mp: 112 °C

6-Nitropiperonyl-β-D-lactopyranosid and 6-nitropiperonyl-α- D -lactopyranosid (6e) [cLactose]

Compound **6e** was synthesized according to the general procedure **C** over two steps from **1e** (500 mg, 0.71 mmol). Yield: 186 mg (0.36 mmol, 50%) light-yellow solid.

IR (ATR): $\tilde{\nu}_{max}$ = 3367, 1617, 1506, 1487, 1448, 1381, 1323, 1262, 1027, 927, 878, 782, 756.

β-^{1}H NMR (600 MHz, DMSO-d_6) : δ = 7.71 (s, 1H, 7´´-H), 7.60 (s, 1H, 4´´-H), 6.24 (s, 2H, 2´´-H), 5,52 (d, J = 5.1 Hz, 1H, 2, 3, 4, 2´, 3´, 4´, 5´-OH), 5.07 (m, 2H, 1´´´a-H, 2, 3, 4, 2´, 3´, 4´, 5´-OH), 4.94 (m, 1H, 1´´´b-H), 4,78 (m, 1H, 6´-OH), 4.72 – 4.69 (m,1H, 2, 3, 4, 2´, 3´, 4´, 5´ -OH), 4.67 (t, J = 5.2 Hz, 1H, 2, 3, 4, 2´, 3´, 4´, 5´-OH) 4.61 (t, J = 6.0 Hz, 1H, 6-OH), 4.52 (d, J = 4.6 Hz,1H, 2, 3, 4, 2´, 3´, 4´, 5´-OH) 4.36 (d, J = 4.3 Hz,1H, 1-H), 4.21 (d, J = 6.9 Hz,1H, 1´-H), 3.75-3.62 (m,2H, 6a-H, 4´-H), 3.51 (m, 1H, 6b-H), 3.45 (dq, J = 10.9, 5.6 Hz, 1H, 3´-H), 3.34 – 3.28 (m, 6H, 4-H, 5-H, 5´-H, 3-H, 2´-H, 6´a-H), 3.18 (m, 2H, 6´b-H, 2-H).

β-^{13}C NMR (151 MHz, DMSO-d_6): δ = 152.64 (C-7a), 146.65 (C-3a), 140.23 (C-6´´), 133.07 (C-5´´), 107.18 (C-4´´), 105.38 (C-7´´), 103.87 (C-2´´), 103.44(C-1´), 102.11 (C-1), 80.57 (C-4), 75.56 (C-3´), 74.89 (C-5), 74.79 (C-5´), 73.39 (C-2), 73.26 (C-3), 70.80 (C-2´), 68.19 (C-4´), 66.67 (C-1´´´) 60.46 (C-6), 60.34 (C-6´).

α-^{1}H NMR (600 MHz, DMSO-d_6) : δ = 7.70 (s, 1H, 7´´-H), 7.08 (s, 1H, 4´´-H), 6.24 (s, 2H, 2´´-H), 5.07 (m, 3H, ,1´´´a-H, 2x OH), 4.94 (m, 1H, 1´´´b-H), 4,78 (m, 3H, 6´-OH, 2x OH), 4.72 – 4.69 (m, 1H, OH), 4.52 (d, *J* = 4.6 Hz,1H, OH), 4.36 (d, *J* = 4.3 Hz,1H, 1-H), 4.14 (d, *J* = 7.6 Hz, 1H, 1´-H), 3.75-3.62 (m, 2H, 6a-H, 4´-H), 3.53 (m,1H, 6b-H), 3.45 (dq, *J* = 10.9, 5.6 Hz, 1H, 3´-H) 3.34 – 3.28 (m, 6H, 4-H, 5-H, 5´-H, 3-H, 2´-H, 6´a-H), 3.18 (m, 2H, 6´b-H, 2-H).

α-^{13}C NMR (151 MHz, DMSO-d_6): δ = 152.28 (C-7a), 147.00 (C-3a), 140.77 (C-6´´), 131.24 (C-5´´), 106.90 (C-4´´), 105.10 (C-7´´), 103.78 (C-2´´), 103.59 (C-1´), 99.15 (C-1), 80.61 (C-4), 75.42 (C-3´), 75.25 (C-5), 75.01 (C-5´), 72.57 (C-2), 71.52 (C-3), 70.57 (C-2´), 67.79 (C-4´), 67.13 (C-1´´´), 60.34 (C-6), 60.23 (C-6´).

HRMS (ESI, positive mode): m/z $[M+Na]^+$ calcd for $C_{20}H_{27}NO_{15}Na$: 544.12784; found: 544.12736.

β/α mixture: UV/Vis (H_2O): λ_{max} (ε) = 245 nm (9206)*, 356 nm (4962).

β/α mixture: mp: 203 °C

β/α mixture: optical rotatory power:$[\alpha]_D^{20}$ = -16 (c = 0.2 in MeOH)

Acknowledgments

We gratefully acknowledge the support by grants from the Federal Ministry of Education and Research (OptoSys, FKZ 031A167) and Andreas Klein for taking the group picture.

Supporting Information

YES (this text will be updated with links prior to publication)

Primary Data

YES (this text will be updated with links prior to publication)

References

1) Drepper, T.; Krauss, U.; Meyer zu Berstenhorst, S.; Pietruszka, J.; Jaeger, K.-E. *Appl. Microbiol. Biotechnol.* **2011,** 90, 23-40.

2) Brieke, C.; Rohrbach, F.; Gottschalk, A.; Mayer, G.; Heckel, A. *Angew. Chem.* **2012,** 124, 8572-8604.

3) Gardner, L.; Deiters, A. *Curr. Opin. Chem. Biol.* **2012,** 16, 292-299.

4) Deiters, A. *Curr. Opin. Chem. Biol.* **2009,** 13, 678-686.

5) Cambridge, S. B.; Geissler, D.; Calegari, F.; Anastassiadis, K.; Hasan, M. T.; Stewart, A. F.; Huttner, W. B.; Hagen, V.; Bonhoeffer, T. *Nat Meth* **2009,** 6, 527-531.

6) (a) Cambridge, S. B.; Geissler, D.; Keller, S.; Cürten, B. *Angew. Chem., Int. Ed. Engl.* **2006,** 45, 2229-2231; (b) Velema, W. A.; van der Berg, J. P.; Szymanski, W.; Driessen, A. J. M.; Feringa, B. L. *ACS Chem. Biol.* **2014,** 9, 1969-1974; (c) Yamazoe, S.; Liu, Q.; McQuade, L. E.; Deiters, A.; Chen, J. K. *Angew. Chem., Int. Ed. Engl.* **2014,** 53, 10114-10118.

(7) (a) Klán, P.; Šolomek, T.; Bochet, C. G.; Blanc, A.; Givens, R.; Rubina, M.; Popik, V.; Kostikov, A.; Wirz, J. *Chem. Rev.* **2012,** 113, 119-191; (b) Mayer, G.; Heckel, A. *Angew. Chem., Int. Ed. Engl.* **2006,** 45, 4900-4921.

(8) Deiters, A. *ChemBioChem* **2010,** 11, 47-53.

(9) Young, D. D.; Deiters, A. *Angew. Chem.* **2007,** 119, 4368-4370.

(10) Binder, D.; Grunberger, A.; Loeschcke, A.; Probst, C.; Bier, C.; Pietruszka, J.; Wiechert, W.; Kohlheyer, D.; Jaeger, K.-E.; Drepper, T. *Integr. Biol.* **2014,** 6, 755-765.

(11) (a) Nicolaou, K. C.; Hummel, C. W.; Nakada, M.; Shibayama, K.; Pitsinos, E. N.; Saimoto, H.; Mizuno, Y.; Baldenius, K. U.; Smith, A. L. *J. Am. Chem. Soc.* **1993,** 115, 7625-7635; (b) Zehavi, U.; Patchornik, A. *J. Org. Chem.* **1972,** 37, 2285-2288; (c) Zehavi, U.; Amit, B.; Patchornik, A. *J. Org. Chem.* **1972,** 37, 2281-2285.

(12) Meo, P.; Osborn, H., Best Synthetic Methods: Carbohydrates. In Elsevier Science Ltd.: New York: 2003.

(13) Binder, D.; Bier, C.; Grünberger, A.; Drobietz, D.; Hage-Hülsmann, J.; Wandrey, G.; Büchs, J.; Kohlheyer, D.; Loeschcke, A.; Wiechert, W.; Jaeger, K.-E.; Pietruszka, J.; Drepper, T. *ChemBioChem* **2016,** 17, 296-299.

(14) (a) Weygand, F.; Ziemann, H.; Bestmann, H. J. *Chem. Ber.* **1958,** 91, 2534-2537; (b) Franchimont, A. P. N. *Ber. Dtsch. Chem. Ges.* **1879,** 12, 1938-1942; (c) Fischer, E. *Ber. Dtsch. Chem. Ges.* **1916,** 49, 584-585; Kartha, K. P. R.; Jennings, H. J. *J. Carbohydr. Chem.* **1990,** 9, 777-781.

(15) Koenigs, W.; Knorr, E. *Ber. Dtsch. Chem. Ges.* **1901,** 34, 957-981.

(16) Paulsen, H. *Angew. Chem.* **1982,** 94, 184-201.

(17) Wandrey, G.; Bier, C.; Binder, D.; Hoffmann, K.; Jaeger, K.-E.; Pietruszka, J.; Drepper, T.; Büchs, J. *Microb Cell Fact.* **2016,** 15, 1.

(18) Terpe, K. *Appl. Microbiol. Biotechnol.* **2006,** 72, 211-222.

(19) Guzman, L. M.; Belin, D.; Carson, M. J.; Beckwith, J. *J. Bacteriol.* **1995,** 177, 4121-30.

(20) Wagner, S.; Klepsch, M. M.; Schlegel, S.; Appel, A.; Draheim, R.; Tarry, M.; Högbom, M.; van Wijk, K. J.; Slotboom, D. J.; Persson, J. O.; de Gier, J.-W. *Proc. Natl. Acad.* **2008,** 105, 14371-14376.

(21) Grünberger, A.; Wiechert, W.; Kohlheyer, D. *Curr. Opin. Biotechnol.* **2014,** 29, 15-23.

(22) Bley, F.; Schaper, K.; Görner, H. *Photochem. Photobiol.* **2008,** 84, 162-171.

(23) Bier, B. A. *Optische Schalter und Fluoreszenzsonden-Design*. HHU (Düsseldorf, Germany), Düsseldorf, **2011**.

(24) Sambrook, J.; Fritsch, E. F.; Maniatis, T., *Molecular cloning*. ed.; Cold spring harbor laboratory press New York: 1989; Vol. 2.

(25) Tojino, M.; Hirose, Y.; Mizuno, M. *Tetrahedron Lett.* **2013,** 54, 7124-7126.

(26) Zhao, Y.; Biggins, J. B.; Thorson, J. S. *J. Am. Chem. Soc.* **1998,** 120, 12986-12987.

Biographical sketches

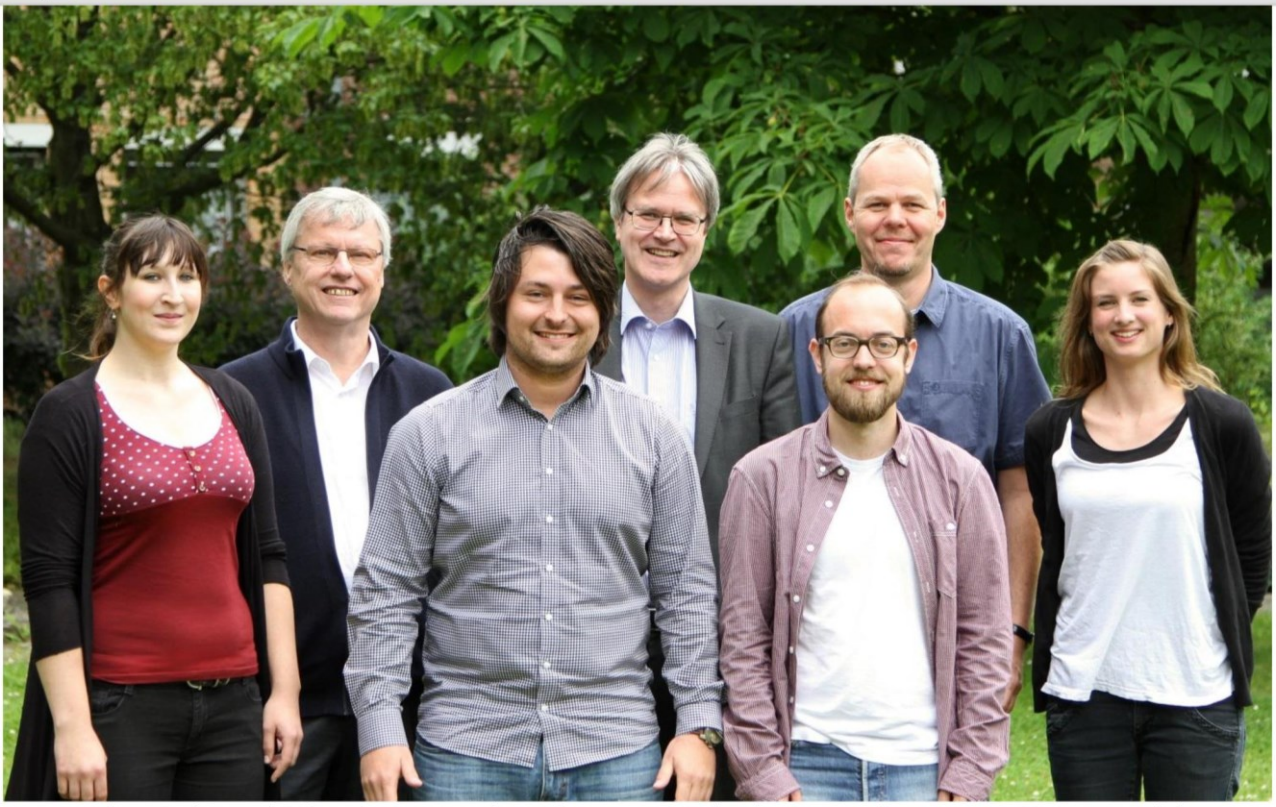

Dagmar Drobietz, Prof. Dr. Karl-Erich Jaeger, Dennis Binder; Prof. Dr. Jörg Pietruszka, Claus Bier, Dr. Thomas Drepper, Dr. Anita Loeschcke (from right to left).

Dagmar Drobietz was trained as a chemical laboratory technician at the Forschungszentrum Jülich until June 2013. After the successful finish, she was first employed at the Forschungszentrum Jülich and later at the Institute for Bioorganic Chemistry within the framework of the OptoSys-project. In October 2015, she joined WFK cleaning Technology Institute e.v. as laboratory technician.

Prof. Dr. Karl-Erich Jaeger studied biology and chemistry at Ruhr-University Bochum and obtained the degree of Dr. rer. nat. in 1982. From 1988 to 1989 he worked as a postdoc at the Department of Microbiology of the University of British Columbia in Vancouver, Canada, with Prof. Robert E.W. Hancock. After his habilitation in Microbiology at Ruhr-University Bochum he received a call to the Chair of Microbiology at University of Stuttgart and in 2002, he accepted the call as head of the Institute of Molecular Enzyme Technology of Heinrich-Heine-Universität Düsseldorf. In 2013, he was also appointed as director at the Institute of Bio- and Geosciences IBG-1: Biotechnology of Forschungszentrum Jülich. In 2002, Karl-Erich Jaeger joined the existing and very successful Collaborative Research Centre SFB 380 funded by the German Research Association (DFG) and coordinated by RWTH Aachen University with Dieter Enders as the speaker. In 2007, the monograph "Asymmetric Synthesis with Chemical and Biological Methods" appeared which was co-edited by Dieter Enders and Karl-Erich Jaeger and summarized the most important results obtained within SFB 380.

Dennis Binder studied biochemistry at the Heinrich-Heine University in Düsseldorf. In 2013 he obtained his master degree in biochemistry after working under the supervision of Prof. Karl-Erich Jaeger on the topic of light-regulated gene expression in *E. coli*. Since then, he is pursuing his PhD at the institute of Molecular Enzyme Technology at the Forschungszentrum Jülich in the group of Dr. Thomas Drepper and under supervision of Prof. Karl-Erich Jaeger. His work focusses on microbial expression systems, single-cell analysis and especially photocaged compound based light control of biological systems.

Prof. Dr. Jörg Pietruszka studied chemistry at the University of Hamburg where he also obtained his doctorate in 1993 with Prof. Dr. W. A. König. After two years in Cambridge/UK with Prof. Dr. S. V. Ley, he started his independent career at the University of Stuttgart fulfilling the requirement for his 'Habilitation' in 2001. The endeavor was supported by Liebig fellowships and a DFG grant. In 2000/2001 he was a visiting lecturer at the University of Freiburg (Germany), 2001/2002 a guest professor at the University of Cardiff (Wales), and 2003/2003 a substitute professor at the University of Tübingen (Germany). In 2004, a professorship at the University of Gießen was declined; since 2004, he holds a position as full professor at the Heinrich-Heine-Universität of Düsseldorf; he is also director of IBG-1 at the Forschungszentrum Jülich since 2013. His research interests include the development of new synthetic methods from organoboron compounds to biocatalysis as well as natural product synthesis.

Claus Bier studied chemistry at the Rheinische Friedrich Wilhelm Universität Bonn. In 2011 he obtained his diploma in chemistry under the supervision of Prof. Dr. Kubitscheck . Since 2012, he is working on his Dissertation under the guidance of Prof. Dr. J. Pietruszka at the institute for bioorganic chemistry at the Heinrich-Heine-Universität Düsseldorf, located at the Forschungszentrum Jülich. His work focusses on the synthesis of photocaged compounds for biotechnological and synthetic biological applications.

Dr. Thomas Drepper studied biology at the Ruhr-University Bochum and since 2004, he is head of the Bacterial Photobiotechnology group at the Institute for Molecular Enzyme Technology, Heinrich-Heine-University Düsseldorf, Germany. His scientific interests lie in the analysis and application of light-dependent processes. In particular, his group developed synthetic biology tools to use photosynthetic bacteria for biotechnological applications. In addition his lab established novel optogenetic tools for controlling and monitoring biological processes in bacteria, including photo-responsive expression systems as well as fluorescent reporter proteins and biosensors based on bacterial blue-light photoreceptors.

Dr. Anita Loeschcke studied biology at the University of Cologne where she graduated receiving her diploma in 2009. She joined Dr. T. Drepper's group of Bacterial Photobiotechnology at Prof. Dr. K.-E. Jaegers Institute of Molecular Enzyme Technology for a PhD scholarship obtaining her doctorate in 2012. Since then, she is further pursuing her studies on microbial synthetic biology as a Postdoc at Prof. Dr. K.-E. Jaeger's institute.

II.4 Technical setup and optimization of light exposure

II.4.1 DMNB Actinometry

Using 1,2-dimethoxy-4-nitrobenzene actinometry to monitor UV-A light exposure in photobiotechnological setups

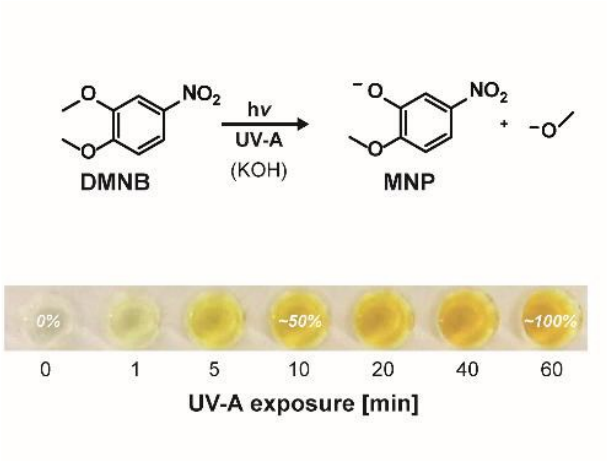

Dennis Binder, Claus Bier, Oliver Klaus, Jörg Pietruszka, Karl-Erich Jaeger, and Thomas Drepper

Manuscript in preparation

For the complete supporting information see Appendix (**Chapter V.5**) turn to page **261.**

Using 1,2-dimethoxy-4-nitrobenzene actinometry to monitor UV-A light exposure in photobiotechnological setups

Dennis Binder,*[a] Claus Bier,[b] Oliver Klaus,[a] Jörg Pietruszka,[b,c] Karl-Erich Jaeger,[a,c] and Thomas Drepper*[a]

ABSTRACT

Photocaged compounds are sophisticated optogenetic switches that can be used for controlling cellular functions by light. Although non-invasive light-control can be simply implemented into bioprocesses *via* UV-A-mediated uncaging of bioactive compounds, the adaption of illumination conditions to novel cultivation setups is often an intricate task. In particular, up- or down-scaling of microbial cultures often require the reevaluation of light intensity and exposure times. Here, we report on a spectroscopic method that allows direct monitoring of UV-A light doses inside of different lab-scale cultivation vessels using 1,2-dimethoxy-4-nitrobenzene (DMNB) as a chemical actinometer. By monitoring light-triggered photoconversion of DMNB, we were able to analyze sample illumination that is affected by different cultivation vessel geometries and process parameters that are relevant for microbial cultivation. In the future, this method can help to analyze and calibrate light regimes for the reliable application of light-responsive bioprocesses.

KEYWORDS: DMNB Actinometry, Photocaged Compounds, UV-A Light Exposure, Flowerplate Cultivation, Cultivation Parameters, Up- / Downscaling

INTRODUCTION

1,2-Dimethoxy-4-nitrobenzene (DMNB) exhibits broad absorptivity in the entire UV range. Thus, it is commonly used in various photochemical and photobiological applications as UV-light-responsive photo-removable protecting group. This way it offers a straightforward and quantitative photorelease of various leaving groups bound at its C5 position.[1–3] Photocaged compounds as such fail to monitor light exposure appropriately, as their photolysis or the entailed biological response is often interconnected with additional cellular factors such as pH and oxygen as well as metabolic or growth states. For instance, photocaged isopropyl-β-D-thiogalactopyranoside (IPTG)[4] is converted into biologically inactive ester intermediates upon light exposure, which require further enzymatic hydrolysis to release the IPTG inducer for *lac* promoter-mediated gene expression.[5] Apparently, in this case the effector molecule release is not solely dependent on the applied UV-A light exposure conditions. Thus, there is a need to monitor light exposure in different experimental setups *in vitro* and thus irrespective of cellular factors.

To tackle these challenges, different actinometers have been developed to quantify UV light exposure *in vitro* by chemical means.[6–10] Interestingly, in alkaline aqueous solution the sole DMNB caging group, lacking an effector group in the C5 position, undergoes a full conversion into 2-methoxy-5-nitrophenolate (MNP) upon UV-A light exposure together with significant spectroscopic changes.[11,12]

In this study, we evaluated DMNB as a chemical actinometer for analyzing the basic impact of different common cultivation vessel geometries and setups on sample illumination under authentic cultivation conditions.

RESULTS AND DISCUSSION

DMNB exhibits similar absorption properties to conventional UV-A light-responsive photocaged compounds,[4,13] and allows to monitor its photoconversion spectroscopically.[12] To prove that DMNB actinometry is suitable to monitor light exposure of samples under conditions that resemble standard laboratory cultivation setups,[14,15] the UV-A-induced photoreaction was first monitored in shaken baffled microplates, so-called Flowerplates (m2p labs, Germany).[16,17] Here, 60 min of UV-A light exposure (λ_{max}= 365 nm, 5.4 mW/cm^2) sufficed to fully convert DMNB to MNP (Fig. 1 A, Fig. S1–2) with significant spectroscopic changes (Fig. 1 B). In particular, absorption in the violet to blue spectral range increased during photoconversion, yielding a distinct yellow coloring (Fig. 1 C) of the exposed solution (ΔA_{max}=262, 351 and 422 nm; see Fig. S3). Spectroscopic changes at a wavelength of 422 nm (Fig. 1 B) showed a direct correlation to exposure times.

For subsequent experiments, we choose the long-wavelength absorption difference maximum to monitor UV-A light exposure. Initially, we analyzed the impact of the reaction volume and geometric shape of different commonly used cultivation vessels on DMNB conversion. Therefore, translucent and black microtiter plates (MTP) were used for small-volume cultivations (0.1 mL), black Flowerplates for mid-volume cultivations (1 mL) and flasks for high-volume cultivations (10 and 100 mL) (**Fig. 2 A**). Small-volumes of 0.1 mL in both translucent and black MTPs led to a fast conversion of DMNB into MNP that was complete after at most 15 min of mid-power UV-A light exposure (5.4 mW/cm^2). Interestingly, mid-volume conversions in Flowerplates led to a significantly decelerated conversion that took up to 45 min of light exposure and was even slightly outperformed by high-volume conversion using 100 mL of DMNB solution. The conversion of 10 mL DMNB solution in flasks was strikingly fast and fully completed after 15 min of light exposure. Half-value times $t_{0.5}$ (exposure times required for 50% conversion) that were calculated from exponential decay fitting (**Fig. 2 B**) of conversion curves indicated that photoreactions in translucent MTPs ($t_{0.5}$ = 1.0 min) were significantly improved as compared to those in black MTPs ($t_{0.5}$ = 2.8 min). Here, it can be assumed that despite highly similar plate geometries (Table S1), the translucency of the MTP enabled a higher light-

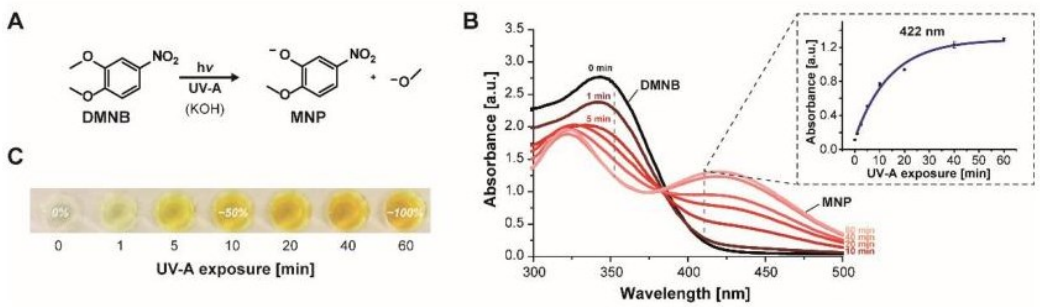

Figure 1. Photochemical monitoring of UV-A light exposure in Flowerplates using DMNB actinometry. A) Photochemical formation of 2-methoxy-5-nitrophenolate (MNP) from DMNB using UV-A light in aqueous potassium hydroxide solution.[11] **B)** Light-mediated conversion of DMNB (1.25 mM) after 0, 1, 5, 10, 20, 40 and 60 min of mid-power UV-A light exposure (5.4 mW/cm²). Grey dashed lines indicate respective maximal absorption differences of ΔA_{max}= 351 and 422 nm in the UV-A to blue range; the insert shows the relation between absorbance at 422 nm and the duration of UV-A exposure. **C**) Colorimetric changes of DMNB solution upon increased UV-A exposure. Values are means of triplicate measurements. Error bars indicate the respective standard deviations. a.u.: arbitrary units.

exposed surface-to-volume ratio (> 0.48 mm^{-1}; for a detailed calculation see Table S1) than the black MTP (0.50 mm^{-1}) due to additional lateral light exposure that in turn accelerates DMNB conversion. This was in full accordance with the observation that the flask with 10 mL DMNB solution (surface-to-volume ratio: >0.41 mm^{-1}) yielded significantly improved DMNB conversions ($t_{0.5}$ = 2.2 min) as compared to 1 mL ($t_{0.5}$ = 10.2 min) and 100 mL conversions ($t_{0.5}$ = 8.4 min) with reduced surface-to-volume ratios (0.10 and > 0.17 mm^{-1}, respectively). Thus, we could observe that UV-A light exposure required for DMNB conversion rather depended on the exposed surface-to-volume ratio (**Fig. 2 B**) than on the reaction volume.

Next, we intended to evaluate the variation of process parameters that are known to be critical during microbial cultivation approaches using a Flowerplate-based cultivation setup.[14,15] As longest conversion times were observed for this vessel type, we further assumed that the variation of standard parameters would here be most noticeable. We thus systematically analyzed the impact of deviations from standard parameters (1.25 mM DMNB, no plate cover, RT, 1000 rpm, 800 µL, 1.5 cm distance to light source) on DMNB photoconversions.

During biological applications, photocaged compounds are applied in various concentrations ranging from the lower micromolar, e.g. for photocaged antibiotics [18] or inducers,[5,14] to the lower millimolar range, e.g. for photocaged amino acids.[19] In this context, we evaluated the impact of DMNB concentration on the velocity of UV-A light mediated conversion. The light conversion decelerated with increasing DMNB concentrations (**Fig. 3 A**), ranging from 10 (0.1 mM) to 60 minutes (1 mM) until complete conversion and $t_{0.5}$ values of 1.6 to 8.5 minutes, respectively.

Since for common microplate-based cultivation setups, different sterile barriers are applied to reduce contamination as well as liquid evaporation and e.g. plastic covers can be used to mount diffusion foils onto a plate to create a light gradient,[14,15] we next evaluated the impact of different plate covers on UV-A light-mediated DMNB conversion (Fig. 3 B). A conventional plastic cover just slightly decelerated the photoreaction, yielding 1.3-fold increased half-value times ($t_{0.5}$ = 11.5 min) compared to DMNB conversions without cover ($t_{0.5}$ = 8.7 min), whereas an Airsheet cover already slowed down light conversions 2.2-fold ($t_{0.5}$ = 19.4 min). Both covers together finally reduced UV-A light mediated DMNB conversion 2.9-fold ($t_{0.5}$ = 25.4 min).

Next, we further analyzed the effect of shaking frequencies and sample volumes on DMNB photoconversion as variable parameters in common microbial cultivation setups (**Fig. 3 C**). For unshaken culture vessels, half-value times for DMNB photoconversion increased with ascending filling volumes from 125 µL ($t_{0.5}$ = 2.0 min) to 1500 µL ($t_{0.5}$ = 27.1 min). Interestingly, further increments of filling volumes up to 3000 µL ($t_{0.5}$ = 15.8 min) led to reduced half-value times. Here, it can be assumed that for filling volumes above 1500 µL the reduction of the actual distance to the light source outpaced

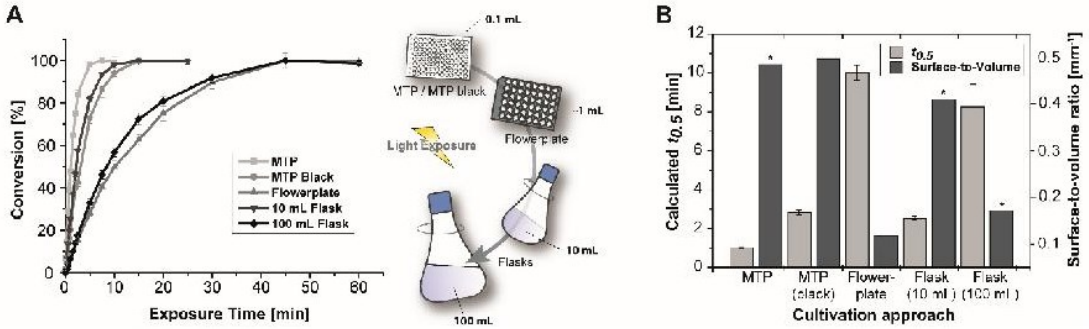

Figure 2. Impact of different sample volumes and cultivation vessel geometries on UV-A light mediated DMNB conversion. A) Conversions of DMNB in different cultivation vessels containing different volumes of DMNB solution (1.25 mM) volumes. **B**) Half-value times ($t_{0.5}$) calculated from exponential decay fits (light grey) are presented together with the light-exposed surface-to-volume ratios (light-accessible liquid surface per total liquid volume in mm^{-1}) of analyzed cultivation vessels (dark grey). Asterisks (*) indicate the underestimation of light-exposed surface-to-volume ratio due to translucent cultivation vessels. Here, lateral light exposure is expected to account for enlarged exposed surfaces. Values are means of triplicate measurements. Error bars indicate the respective standard deviations.

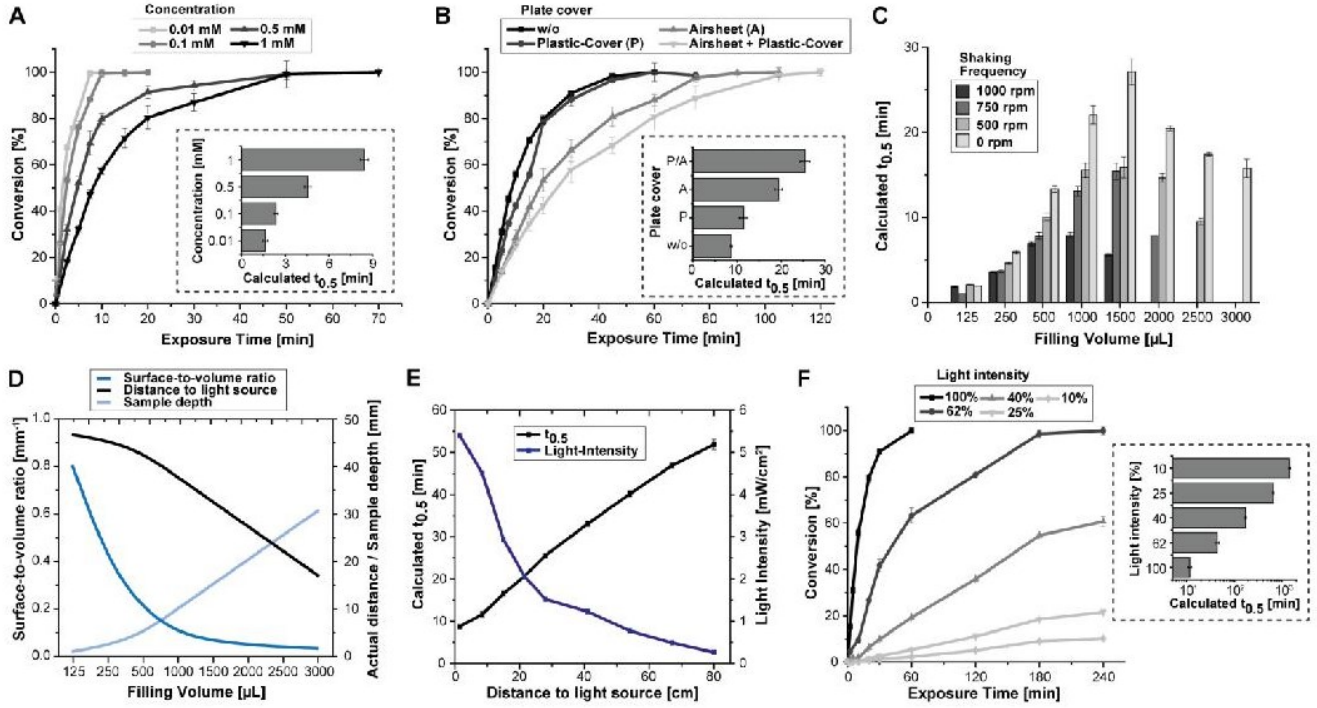

Figure 3. Impact of process parameter variation on UV-A light mediated DMNB conversion in a Flowerplate-based experimental setup. The following parameters were varied: **A**) DMNB concentration, **B**) plate covers, **C**) shaking frequency and filling volumes, **E**) distance to light source and **F**) light intensity. Standard parameters were: 1000 rpm, 1.25 mM DMNB, RT, 800 µL, 1.5 cm distance, 100 % light intensity (5.4 or 2.5 mW/cm² for Fig. 3 F), no cover. Insets in dotted-line boxes indicate $t_{0.5}$ calculations from respective exponential decays. **D**) Surface-to-volume ratios (blue line) and sample depth (light blue line) are plotted together with the actual distance from the liquid surface to the light source (black line) for different filling volumes in a Flowerplate using the vessel specifications depicted in Tab. S1. Values are means of triplicate measurements. Error bars indicate the respective standard deviations.

the effects of a decreasing exposed surface-to-volume ratio as well as an increasing depth of the reaction liquid (**Fig. 3 D**).

These effects were likewise observed for different shaking frequencies, yet the turning point for the slow decrease of $t_{0.5}$ values was shifted from 1500 to 1000 µL for highest shaking frequencies (1000 rpm).

In general, increasing shaking frequencies led to a stepwise reduction of DMNB conversion times that can be attributed to both increased stirring efficiencies and liquid surface enlargement (**Fig. 3 C**). Hence, the variation of the shaking frequency significantly accelerated DMNB photoconversion up to 4.8 fold. This was, for instance, observed for 1500 µL and the shift of shaking frequency from 0 ($t_{0.5}$ = 27.1 min) to 1000 rpm ($t_{0.5}$ = 5.6 min), whereas frequencies above 1000 rpm just merely improved conversion (data not shown). As the actual light source distance was generally assumed to be crucial for DMNB conversion with respect to different filling volumes (**Fig. 3 C,D**), we further analyzed the impact of enlarged light source distances (as one way to decrease light intensity) in detail (**Fig. 3 E**).

The variation of light source distance proved highly suited to reduce light intensity from 5.4 mW/cm² (1.5 cm) to 0.3 mW/cm² (80 cm) and thus about 20.8-fold. The impact of light source distance variation on DMNB photoconversion was likewise significant as it decelerated the half-value times $t_{0.5}$ from 8.7 (for 1.5 cm) to 51.9 minutes (for 80 cm), and thus about 5.9-fold.

In addition to reduce light intensities by means of increasing the light source distance, we finally observed UV-A light mediated DMNB conversions for different light intensities that were dimmed using different layers of diffusion foils mounted on a plastic cover (**Fig. 3 F**). The corresponding light intensities (due to the plastic cover 100% here corresponds to 2.5 mW/cm²) could be successfully dimmed to 62, 40, 25 and 10% applying 1, 3, 5 and 6 layers of diffusion foils, respectively.[14]

Dimmed light-intensities showed the most striking impact on DMNB photoconversions of all analyzed parameters. Here, the reduction to 62% light-intensity (1.5 mW/cm²) already led to a 3.8-fold deceleration ($t_{0.5}$ = 43.5 min) of half-value times from initially 11.5 min (100% with plastic cover), and prolonged durations until total conversion from about 60 to 240 min. Extended reduction of light-intensity to 40, 25 and 10% further decelerated the half-value times to 174 (15.2-fold), 656 (57.1-fold) and 1450 min (126.3-fold), respectively. Further parameters such as temperature and liquid turbidity showed only negligible impact on DMNB conversion and were thus omitted from our evaluation (data not shown).

CONCLUSIONS

DMNB actinometry was established as a straightforward method to appropriately evaluate the sample illumination inside of different cultivation vessels and upon variation of crucial process parameters. Initial analysis of DMNB conversion in different common lab-scale cultivation vessels revealed that the light-exposed surface-to-volume ratio was of utmost importance for the velocity of the observed photoreaction, whereas the total liquid volume played an inferior role. For the Flowerplate, shaking frequency and applied plate covers showed appreciable influences on DMNB

photoconversion. These effects were more pronounced for different filling volumes and thus for the surface-to-volume ratio as well as for the respective compound concentration (**Table 1**).

Table 1. Impact of different setup parameters on half-conversion times $t_{0.5}$ in a Flowerplate. Percentages in brackets indicate the deviation from the standard $t_{0.5}$ value that was set to 100%.

Parameter	Low	Mid	High	Impact
Shaking frequency [rpm]	0 (233%)	500 (188%)	1000 (100%)	+
Cover*	w/o (100%)	A (222%) P (131%)	A/P (290%)	+
Surface-to-volume [mm^{-1}]	0.1 (100%)	0.4 (45%)	0.8 (23%)	++
Filling Volume [µL]	125 (21%)	800 (100%)	1500 (64%)	++
Concentration [mM]	0.01 (19%)	0.1 (28%)	1 (100%)	++
Light source distance [cm]	1.5 (100%)	41 (379%)	80 (593%)	+++
Light intensity [%]	10 (12634%)	40 (1520%)	100 (100%)	++++

* A: Airsheet, P: Plastic Cover, A/P: Airsheet and Plastic Cover applied

The reduction of light intensity had the most significant impact on photoconversion, operated either by enlargement of the light source distance or by dimming, as one-tenth of light intensity increased half-conversion times about 126-fold.

The presented actinometer approach will prospectively facilitate quick and straightforward calibration of UV-A light-irradiance for photobio(techno)logical processes and gives a first estimation of expected efficiency and speed of photoreactions in the chosen cultivation setup. Finally, a multitude of chemical actinometers[20] based on, for instance, meso-diphenylhelianthrene[21] or bisaryl-pyridazinone[22] compounds exists, which would be highly suited to report longer wavelength light exposure appropriately.

EXPERIMENTAL

DMNB conversion was monitored using both absorption spectra and the change of absorption at a wavelength of 422 nm (100 µL, Tecan Infinite M1000 Pro microplate reader) using 1.25 mM DMNB in aqueous KOH solution (0.5 M) at RT (22 °C). To improve DMNB solubility (Fig. S4), 10% (v/v) DMSO was supplemented. UV-A exposure was carried out using a UV-A hand lamp (VL-315.BL 45 W, Vilber Lourmat, France; 5.4 mW/cm^2 at 365 nm for 1.5 cm distance to light source). Light intensity quantifications were conducted using a Thermal Power Sensor (S302C, Thorlabs Inc, USA). Specifications of all cultivation vessels and exact experimental setups are summarized in Tables S1 and S2. All plates were shaken in a deep-well plate incubator (Thermomixer C; Eppendorf, Germany) at 1000 rpm (3 mm shaking diameter), whereas flasks were shaken at 150 rpm (3 mm shaking diameter). Plate covers were gas-permeable Airsheets (Exel Scientific, USA) and standard clear polystyrene lids (Greiner Bio-One, Germany). Light intensities were dimmed with varying layers of diffusion foils (White Diffusion LEE216, LEE Filters, USA) mounted onto a polystyrene lid.

Exponential decay fitting (unweighted functions with $R^2 > 0.985$) was conducted using OriginPro 9.0G® (OriginLab Corporation, USA) assuming the following condition: Compound concentration $c(t)$ exponentially decays with increasing exposure times t in dependenence of the time constant k, according to equation (1): $c(t) = c_0 * e^{-k*t}$ (1).
Consequential the time-constants τ and $t_{0.5}$ were calculated according to equation (2): $t_{0.5} = ln(2) * k$ (2).

ACKNOWLEDGEMENTS

This work was supported by grants from the Federal Ministry of Education and Research (OptoSys, FKZ 031A16).

NOTES AND REFERENCES

1. A. P. Pelliccioli and J. Wirz, *Photochem. Photobiol. Sci.*, 2002, **1**, 441–458.
2. C. Brieke, F. Rohrbach, A. Gottschalk, G. Mayer, and A. Heckel, *Angew. Chem. Int. Ed. Engl.*, 2012, **51**, 8446–76.
3. K. Nakayama, I. Heise, H. Görner, and W. Gärtner, *Photochem. Photobiol.*, 2011, **87**, 1031–5.
4. D. D. Young and A. Deiters, *Angew. Chem. Int. Ed. Engl.*, 2007, **46**, 4290–2.
5. D. Binder, A. Grünberger, A. Loeschcke, C. Probst, C. Bier, J. Pietruszka, W. Wiechert, D. Kohlheyer, K.-E. Jaeger, and T. Drepper, *Integr. Biol. (Camb).*, 2014, **6**, 755–65.
6. H. G. Heller and J. R. Langan, *J. Chem. Soc., Perkin Trans. 2*, 1981, 341–343.
7. J. M. Allen, S. K. Allen, and S. W. Baertschi, *J. Pharm. Biomed. Anal.*, 2000, **24**, 167–78.
8. A. Ribeiro Santos, R. Ballardini, P. Belser, M. T. Gandolfi, V. M. Iyer, and L. Moggi, *Photochem. Photobiol. Sci.*, 2009, **8**, 1734–42.
9. T. Lehóczki, É. Józsa, and K. Ősz, *J. Photochem. Photobiol. A Chem.*, 2013, **251**, 63–68.
10. S. Goldstein and J. Rabani, *J. Photochem. Photobiol. A Chem.*, 2008, **193**, 50–55.
11. H. C. H. A. Van Riel, G. Lodder, and E. Havinga, *J. Am. Chem. Soc.*, 1981, **103**, 7257–7262.
12. J.-Y. Zhang, H. Esrom, and I. W. Boyd, *Appl. Surf. Sci.*, 1999, **138-139**, 315–319.
13. C. Bier, D. Binder, D. Drobietz, A. Loeschcke, T. Drepper, K.-E. Jaeger, and J. Pietruszka, *Synthesis (Stuttg).*, 2017, **49**, 42–52.
14. D. Binder, C. Bier, A. Grünberger, D. Drobietz, J. Hage-Hülsmann, G. Wandrey, J. Büchs, D. Kohlheyer, A. Loeschcke, W. Wiechert, K.-E. Jaeger, J. Pietruszka, and T. Drepper, *Chembiochem*, 2016, **17**, 296–299.
15. D. Binder, J. Frohwitter, R. Mahr, C. Bier, A. Grünberger, A. Loeschcke, P. Peters-Wendisch, D. Kohlheyer, J. Pietruszka, J. Frunzke, K.-E. Jaeger, V. F. Wendisch, and T. Drepper, *Appl. Environ. Microbiol.*, 2016, **82**, 6141–6149.
16. M. Funke, S. Diederichs, F. Kensy, C. Müller, and J. Büchs, *Biotechnol. Bioeng.*, 2009, **103**, 1118–28.
17. T. Schlepütz and J. Büchs, *J. Biosci. Bioeng.*, 2014, **117**, 485–96.
18. W. A. Velema, J. P. van der Berg, W. Szymanski, A. J. M. Driessen, and B. L. Feringa, *ACS Chem. Biol.*, 2014, **9**, 1969–74.
19. R. Uprety, J. Luo, J. Liu, Y. Naro, S. Samanta, and A. Deiters, *Chembiochem*, 2014, **15**, 1793–9.
20. H. Kuhn, S. Braslavsky, and R. Schmidt, *Pure Appl. Chem.*, 1989, **61**, 187–210.
21. H.-J. Adick, R. Schmidt, and H.-D. Brauer, *J. Photochem. Photobiol. A Chem.*, 1989, **49**, 311–316.
22. E. Orhan, L. Gundogdu, M. Kose, and Y. Yokoyama, *J. Photochem. Photobiol. A Chem.*, 2016, **314**, 164–170.

II.4.2 Light-induced induction profiling

Light-induced gene expression with photocaged IPTG for induction profiling in a high-throughput screening system

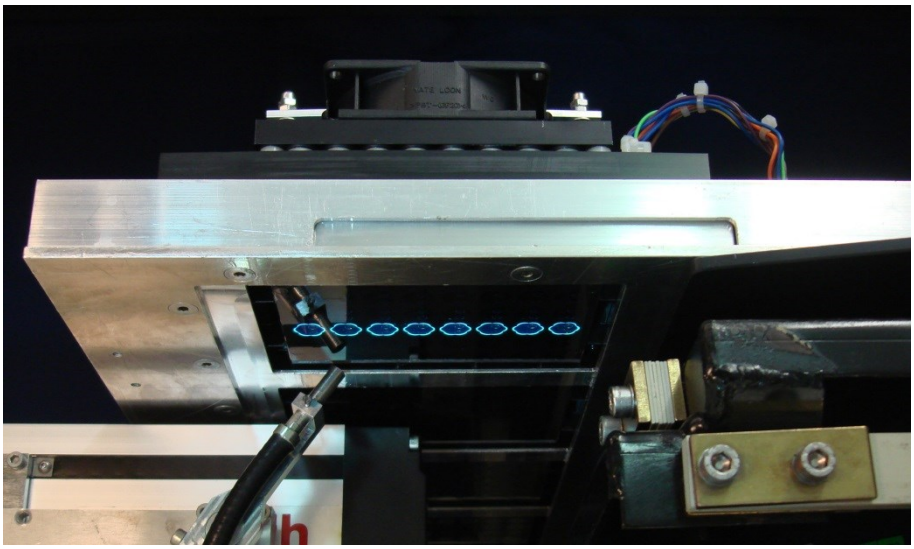

Georg Wandrey, Claus Bier, Dennis Binder, Kyra Hoffmann, Karl-Erich Jaeger, Jörg Pietruszka, Thomas Drepper and Jochen Büchs

Microb Cell Fact 2016, 15:63.

The full online version may be found at:
http://dx.doi.org/10.1186/s12934-016-0461-3.

For the complete supporting information see Appendix (**Chapter V.6**) turn to page **263.**

Wandrey et al. Microb Cell Fact (2016) 15:63
DOI 10.1186/s12934-016-0461-3

Microbial Cell Factories

RESEARCH

Open Access

Light-induced gene expression with photocaged IPTG for induction profiling in a high-throughput screening system

Georg Wandrey[1], Claus Bier[2], Dennis Binder[3], Kyra Hoffmann[1], Karl-Erich Jaeger[3,4], Jörg Pietruszka[2,4], Thomas Drepper[3] and Jochen Büchs[1*]

Abstract

Background: Inducible expression systems are frequently used for the production of heterologous proteins. Achieving maximum product concentrations requires induction profiling, namely the optimization of induction time and inducer concentration. However, the respective experiments can be very laborious and time-consuming. In this work, a new approach for induction profiling is presented where induction in a microtiter plate based cultivation system (BioLector) is achieved by light using photocaged isopropyl β-D-1-thiogalactopyranoside (cIPTG).

Results: A flavin mononucleotide-based fluorescent reporter protein (FbFP) was expressed using a T7-RNA-polymerase dependent *E. coli* expression system which required IPTG as inducer. High power UV-A irradiation was directed into a microtiter plate by light-emitting diodes placed above each well of a 48-well plate. Upon UV irradiation, IPTG is released (uncaged) and induces product formation. IPTG uncaging, formation of the fluorescent reporter protein and biomass growth were monitored simultaneously in up to four 48-well microtiter plates in parallel with an in-house constructed BioLector screening system. The amount of released IPTG can be gradually and individually controlled for each well by duration of UV-A exposure, irradiance and concentration of photocaged IPTG added at the start of the cultivation. A comparison of experiments with either optical or conventional IPTG induction shows that product formation and growth are equivalent. Detailed induction profiles revealed that for the strain and conditions used maximum product formation is reached for very early induction times and with just 6–8 s of UV-A irradiation or 60–80 µM IPTG.

Conclusions: Optical induction and online monitoring were successfully combined in a high-throughput screening system and the effect of optical induction with photocaged IPTG was shown to be equivalent to conventional induction with IPTG. In contrast to conventional induction, optical induction is less costly to parallelize, easy to automate, non-invasive and without risk of contamination. Therefore, light-induced gene expression with photocaged IPTG is a highly advantageous method for the efficient optimization of heterologous protein production and has the potential to replace conventional induction with IPTG.

Keywords: Caged compounds, Photocaged IPTG, LED array, Optical induction, Automatization, High-throughput screening, Recombinant protein expression, *Escherichia coli*, FbFP, Induction profiling, BioLector, Shaken microtiter plate

*Correspondence: jochen.buechs@avt.rwth-aachen.de
[1] AVT-Biochemical Engineering, RWTH Aachen University, Worringerweg 1, Aachen 52074, Germany
Full list of author information is available at the end of the article

Background

High productivity in heterologous protein production is achieved by optimization of strains, culture conditions and process related parameters. Inducible expression systems are applied to separate the cultivation into an initial growth phase for unimpeded biomass formation and a subsequent production phase where growth is impeded while metabolic resources are shifted towards product formation. The switch from growth to production phase (induction of target gene expression) can be achieved by addition of small chemical inducer molecules among which isopropyl β-D-1-thiogalactopyranoside (IPTG) is the most popular choice and widely applied, especially in lab scale. The amount of IPTG and the time when it is added during cultivation are crucial parameters for process performance [1, 2]. If induction is performed too early, biomass concentration is insufficient for reasonable protein production; if it is performed too late, not enough substrate is left for product formation. If IPTG concentration is not sufficiently high, cells may not reach their full expression potential; however, if IPTG concentration exceeds a critical limit, a balanced metabolism cannot be maintained and toxic effects might be observed [3–5].

The induction optimum depends on the respective strain, expression plasmid and target gene [2, 6]. Although general recommendations (i.e. 'induce with 1000 µM IPTG at OD 0.6-1.2' [1, 2]) commonly yield decent results and mathematical models for induction parameters have been described [5, 7, 8], the optimum parameters for each process still have to be verified in time-consuming experiments. Hence, microtiter plate based screening systems that allow parallelized and cost-effective experiments in small scale have successfully been applied [9, 10]. However, the addition of IPTG solution to small scale cultures is associated with some drawbacks which are usually not discussed in literature. For induction, either cumbersome manual intervention at each time of induction or cost-intensive investment into an automatized liquid handling system is required. Before addition of IPTG, the microtiter plate shaking is usually stopped which can result in an oxygen limitation [9]. Then, the sterile barrier on top of the microtiter plate is pierced or removed which necessitates precautions to avoid contamination [10]. The addition of an IPTG containing solution dilutes the cultures and additional pipetting is required if different amounts of IPTG have to be added to different wells but the dilution effect is to be kept constant. If the sterile barrier is pierced for pipetting, the barrier might not seal the well completely anymore once the pipettes or syringes are retracted. This can result in increased evaporation which affects results. If the sterile barrier is instead removed for pipetting, it has to be replaced either manually or by additional automated equipment, once a pipetting step is completed.

This complex procedure of adding IPTG solution is especially problematic when different clones of a clone library are to be compared regarding heterologous protein production. The clones should not be induced at the same time but when they reach the same optical density. Each time a single clone reaches the induction criterion the invasive induction procedure is activated which interrupts the measurement and affects the growth of all clones [9]. With ever increasing numbers of parallel cultivations individual induction with IPTG solution reaches its limits even with automated pipetting systems. Instead, a parallelized and less invasive induction method for small scale cultivations is highly desirable.

Non-invasive optical measuring techniques have already been applied extensively for online monitoring [11–13]. In this study, it was investigated whether non-invasive optical induction could be practical as well [14]. In 2007, Young and Deiters attached the photoremovable group 6-nitropiperonal to IPTG yielding a photocaged IPTG derivative (cIPTG) which serves as a dormant IPTG reservoir [15]. As long as the photocage is attached, cIPTG cannot bind to the *lac* repressor and no target gene is expressed. Upon UV-A irradiation IPTG is uncaged and can act as an inducer. Based on this concept, a device for individual optical induction of each well in a microtiter plate was constructed. A high-throughput screening system was then used for detailed induction profiling and to test whether optical induction with cIPTG could replace conventional induction with IPTG.

Results and discussion

LED array for optical induction

To achieve optical induction, UV-A irradiation has to be introduced into the culture broth containing cIPTG to release uncaged IPTG from its photocage. We constructed an LED array with 48 UV-A LEDs ($\lambda_{max} = 368$ nm, Fig. 1). A high-performance UV-A LED is positioned directly above each corresponding well. Once an LED is switched on, UV-A irradiation passes the transparent sterile barrier on top of the microtiter plate and reaches the culture. There, the intense UV-A irradiation (52 mW/cm^2) leads to cIPTG uncaging and subsequently expression of target genes is induced. A mask positioned between LEDs and microtiter plate ensures that per LED only one well is illuminated. Cross-illumination through the walls of neighbouring wells can be excluded because plates with black walls are used. The LED array can quickly be mounted on top of the microtiter plate where it is positioned by a notch and fixed by two screws. Due to its robust design the LED

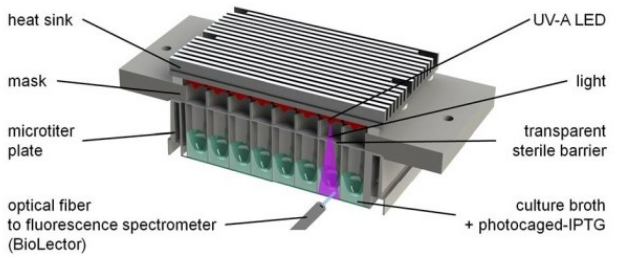

Fig. 1 LED array for individual illumination of 48 wells in a microtiter plate. High performance UV-A LEDs are mounted onto a heat sink. Emitted light passes a transparent gas-permeable sterile barrier and reaches the subjacent well containing the culture and photocaged-IPTG (cIPTG). A mask ensures that no stray light can enter adjacent wells. IPTG is uncaged and induces formation of a fluorescent reporter protein. Protein and biomass concentrations are monitored through the transparent bottom of the microtiter plate using an in-house constructed BioLector setup. A robotic arm moves an optical fiber which is connected to a fluorescence spectrometer from well to well in rapid succession to allow quasi-continuous and non-invasive measurements during continuous orbital shaking for cultivation

array can be used for illumination during cultivation under typical shaking conditions which are required for sufficient oxygen transfer and mixing [16].

Online monitoring with BioLector screening system

The space below the microtiter plate is not affected by the illumination from above. Therefore, non-invasive online fluorescence measurements according to the BioLector design [11, 17] were performed through the transparent bottom using an in-house constructed BioLector prototype. A fluorescence excitation wavelength is chosen from the white spectrum of a xenon lamp by an excitation monochromator inside the fluorescence spectrometer and the light is guided to the microtiter plate through one branch of a Y-shaped optical fibre bundle. Through the other branch the resulting scattered light and fluorescence emission is guided back to the spectrometer where the light passes the emission monochromator and reaches the detector. The optical fibre bundle is moved by a robotic arm which allows measuring each culture in rapid succession without stopping the shaking movement of the well plate. Up to four microtiter plates in parallel can be monitored with an acquisition rate of one to two data points per second. In the most basic setup this device is used to gather quasi-continuous data on biomass growth and fluorescent protein formation by monitoring suitable excitation/emission wavelength combinations.

Suitable excitation/emission wavelength combinations for online monitoring can either be taken from literature or can also be extracted from 2D fluorescence scans obtained using the method described by Siepert et al. [18]. Fig. 2 shows 2D fluorescence spectra obtained at three time points during a cultivation of *E. coli* Tuner(DE3)/pRhotHi-2-LacI-EcFbFP. This strain was chosen for optical induction experiments in this work because it was already shown that the T7-RNA polymerase expression host *E. coli* Tuner(DE3) is well-suited for tight and gradual regulation of homogenous gene expression in combination with cIPTG [19]. At the beginning of the cultivation, cIPTG was added to a concentration of 400 µM. The first 2D fluorescence spectrum obtained right before optical induction (Fig. 2a) shows no fluorescence of the flavin mononucleotide-based fluorescent reporter protein (FbFP). Then, expression of FbFP reporter gene was induced by uncaging of cIPTG with UV-A irradiation using the LED array. The 2D fluorescence spectrum obtained 5 h after optical induction (Fig. 2c) shows a strong fluorescence signal with the spectral characteristics of FbFP [20]. This demonstrates successful optical induction with cIPTG and the constructed UV-A LED array. As reported previously, FbFP formation can be monitored at an excitation wavelength of 450 nm and an emission wavelength of 495 nm (Fig. 2c, white cross) [20].

Identification of additional fluorescence signal

Besides the FbFP signal an additional fluorescence signal ($\lambda_{ex,max} = 335$ nm, $\lambda_{em,max} = 405$ nm) appeared in the 2D fluorescence spectrum measured ten minutes after UV-A irradiation for optical induction (Fig. 2b). Five hours after UV-A irradiation (Fig. 2c) this signal is still visible but its intensity is lowered by about 60 %. Due to the appearance of this signal immediately after UV-A irradiation and its later decay, it was suspected that the signal might result from caged IPTG ester intermediates (cIPTGe, Fig. 3a) which are the photoproducts of cIPTG as described by Young and Deiters [15]. According to these authors, the ester intermediates are hydrolysed by intracellular esterases to yield the nitropiperonal uncaging product and free IPTG.

The fluorescence emission spectrum of caged IPTG ester intermediates that were isolated by HPLC and identified by NMR (Additional files 1, 2) are shown in Fig. 3b. The normalized emission spectrum with maximum emission at 417 nm ($\lambda_{ex} = 330$ nm) fits in well with the emission spectrum observed in vivo after photo-cleavage. Besides the ester intermediates the isolated nitropiperonal uncaging product showed a similar emission spectrum. Therefore, the observed fluorescence might be caused by the caged IPTG ester intermediates, the nitropiperonal uncaging product or a combination of both. Fluorescence intensities are not compared directly since the emission spectra were obtained with different devices and the recovery rate of the HPLC method for caged

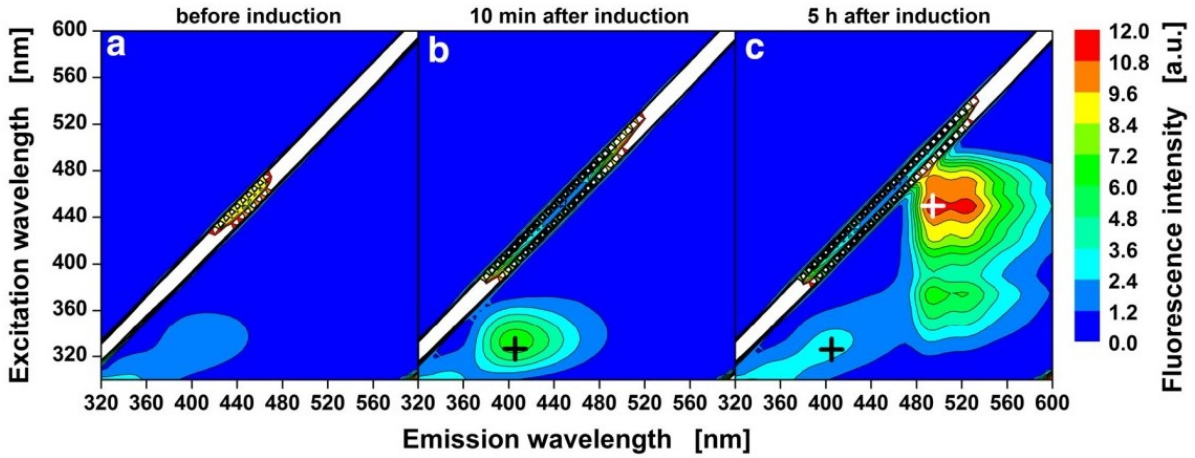

Fig. 2 Fluorescence spectrum of an *E. coli* Tuner(DE3)/pRhotHi-2-LacI-EcFbFP culture before and after optical induction. 2D fluorescence scan with excitation wavelengths from 300–600 nm and emission wavelengths from 320–600 nm before (**a**) and after optical induction (**b**: 10 min, **c**: 5 h). Ten minutes after UV-A irradiation for optical induction a fluorescence signal with an excitation maximum at 335 nm and an emission maximum at 405 nm is detected (**b**). Five hours later this signal is reduced by about 60 % and a strong fluorescence signal of the target protein FbFP with an excitation maximum at 450 nm and an emission maximum at 495 nm is detected (**c**). Biomass autofluorescence was detected but is not visible in this plot because other fluorescence signals are much stronger. Cultivation conditions: 800 µL Wilms-MOPS mineral medium (20 g/L glucose, 0.2 M MOPS) per well in a 48-FlowerPlate, 30 °C, shaking frequency: 1000 rpm, shaking diameter: 3 mm, 400 µM cIPTG added at the start of cultivation, optical induction with LED array after 10 h of cell cultivation for 6 s (λ_{max} = 368 nm, I = 52 mW/cm^2)

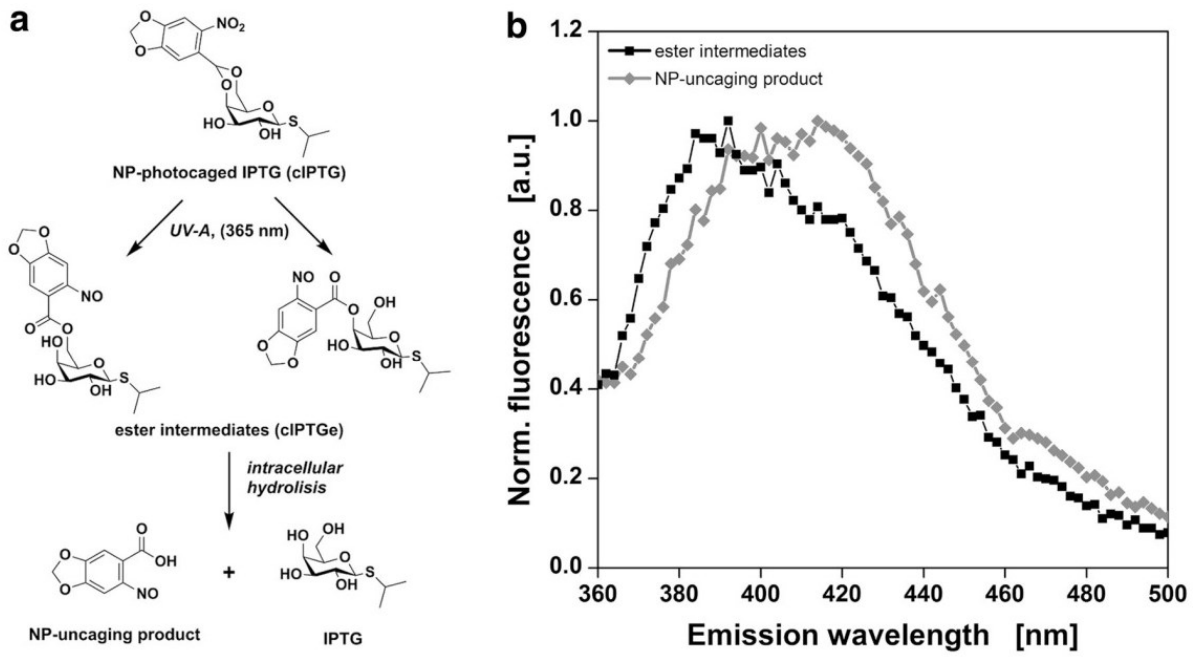

Fig. 3 cIPTG uncaging mechanism and fluorescence emission spectra of caged IPTG ester intermediates and NP-uncaging product. The two-step cIPTG uncaging mechanism as described by Young and Deiters [15] **a** and normalized fluorescence emission spectra (λ_{ex} = 330 nm) of cIPTG ester intermediates isolated via HPLC (*black*) and nitropiperonal uncaging product (*grey*) in H_2O (**b**)

IPTG ester intermediate isolation was not determined. However, the course of the fluorescence intensity during the cultivation can still be valuable to characterize the uncaging reaction.

For 12 cultures the duration of UV-A irradiation for optical induction was varied from 0–60 s (Fig. 4a). As a consequence of UV-A irradiation, the fluorescence signal rises instantly. Then, the fluorescence intensities

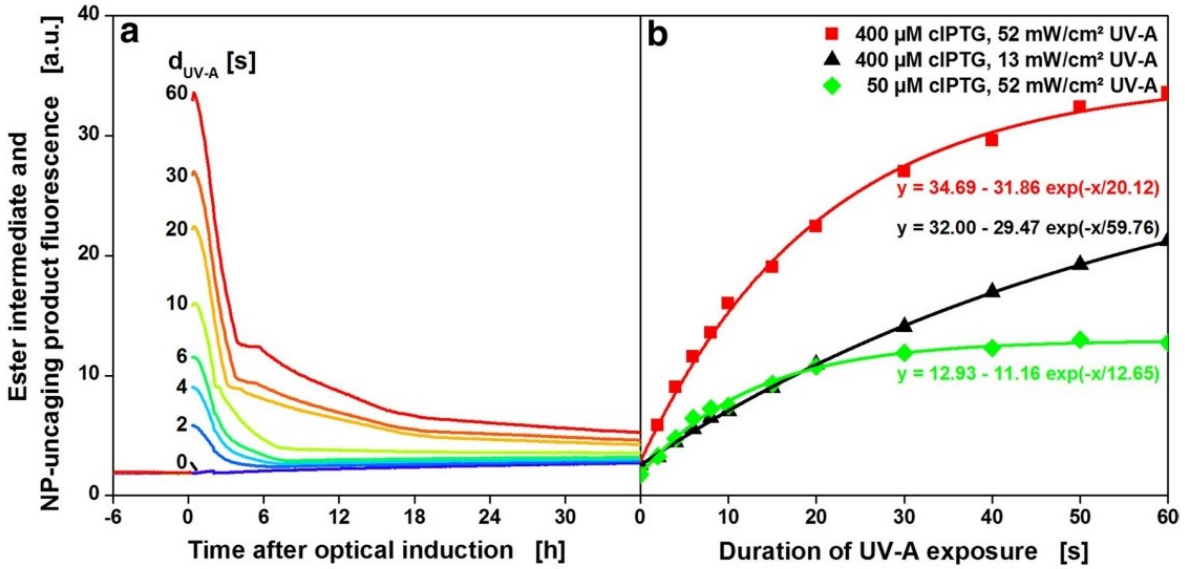

Fig. 4 Online measurement of cIPTG ester intermediates and NP-uncaging product. Fluorescence intensity ($\lambda_{Ex} = 326$ nm, $\lambda_{Em} = 407$ nm, *black cross* in Fig. 2) of 12 *E. coli* cultures before and after UV-A irradiation for 0–60 s (**a**) and fluorescence intensity measured directly after irradiation as a function of duration of UV-A exposure (**b**). At the beginning of the cultivation, 400 µM cIPTG were added to the medium. After 10 h, optical induction was performed with the LED array ($\lambda_{max} = 368$ nm, $I = 52 mW/cm^2$). The amount of ester intermediates increases with increasing duration of UV-A exposure and can be fitted with first-order kinetics (*solid lines* and equations in B, $R^2 > 0.995$). Reduced irradiance leads to lower rate constants (*black triangles*, $I = 13 mW/cm^2$) and reduced cIPTG concentration to lower amplitude (*green diamonds*, 50 µM cIPTG). Cultivation conditions: 800 µL Wilms-MOPS mineral medium (20 g/L glucose, 0.2 M MOPS) per well in a 48-FlowerPlate, 30 °C, shaking frequency: 1000 rpm, shaking diameter: 3 mm. Not all data shown in **a** (complete set provided in Additional file 8)

quickly decrease over the course of the following 2–3 h (Fig. 4a). HPLC measurements confirmed that cIPTG ester intermediates were formed after UV-A irradiation. They were stable for at least 24 h when no cells were present, but fully degraded when lipase PL from *Alcaligenes sp.* was added (Additional file 3). This fits in well with previous reports where cIPTG ester intermediates are obtained within seconds to minutes of UV-A irradiation and are subsequently hydrolysed to the nitropiperonal uncaging product and IPTG within minutes to hours ($t_{1/2} = 63$ min) [15]. Possibly, the nitropiperonal uncaging product shows weaker fluorescence than the cIPTG ester intermediates and the fast decline of the fluorescence intensity in the first 2–3 h after irradiation indicates the conversion of cIPTG ester intermediates to the nitropiperonal uncaging product. The following slower signal decay over the remaining cultivation time could be caused by cell growth masking the fluorescence signal or subsequent reactions, e.g. dimerization, of the nitropiperonal uncaging product [21].

Characterization of optical induction with cIPTG

Online fluorescence spectroscopy is already a method frequently applied to investigate other uncaging processes [22]. In Fig. 4b the ester intermediate and NP-uncaging product fluorescence measured directly after irradiation is given as a function of duration of exposure ($d_{UV-A} = 0–60$ s). With longer duration of exposure more cIPTG is uncaged and higher ester intermediate concentrations are detected. Since the substrate of the uncaging reaction (cIPTG) is depleted during the reaction the reaction rate decreases accordingly. The data are in very good accordance with first-order kinetics (equations and solid lines in Fig. 4b, $R^2 > 0.995$). HPLC measurements confirmed the photo-uncaging of cIPTG as a function of UV-A exposure duration (Additional file 4). As to be expected for a photochemical reaction, the reaction rate constant is dependent on irradiance. This is shown by a reduction of irradiance by 75 % from 52 to 13 mW/cm^2, resulting in a 66 % slower reaction (black triangles, Fig. 4b). The ester intermediate concentration is also influenced by the amount of cIPTG added at the beginning of the cultivation. A reduction of the initial cIPTG concentration by 87.5 % from 400 µM to 50 µM cIPTG reduces the ester intermediate signal by 63 % (green diamonds, Fig. 4b). These experiments show that three parameters can be used to control the amount of IPTG that is uncaged by optical induction: duration of UV-A exposure, irradiance and initial concentration of cIPTG. In the following experiments only duration of UV-A exposure ($d_{UV-A} = 0–60$ s) is used to control the amount of released IPTG while irradiance and initial cIPTG concentration are kept constant (52 mW/cm^2, 400 µM cIPTG).

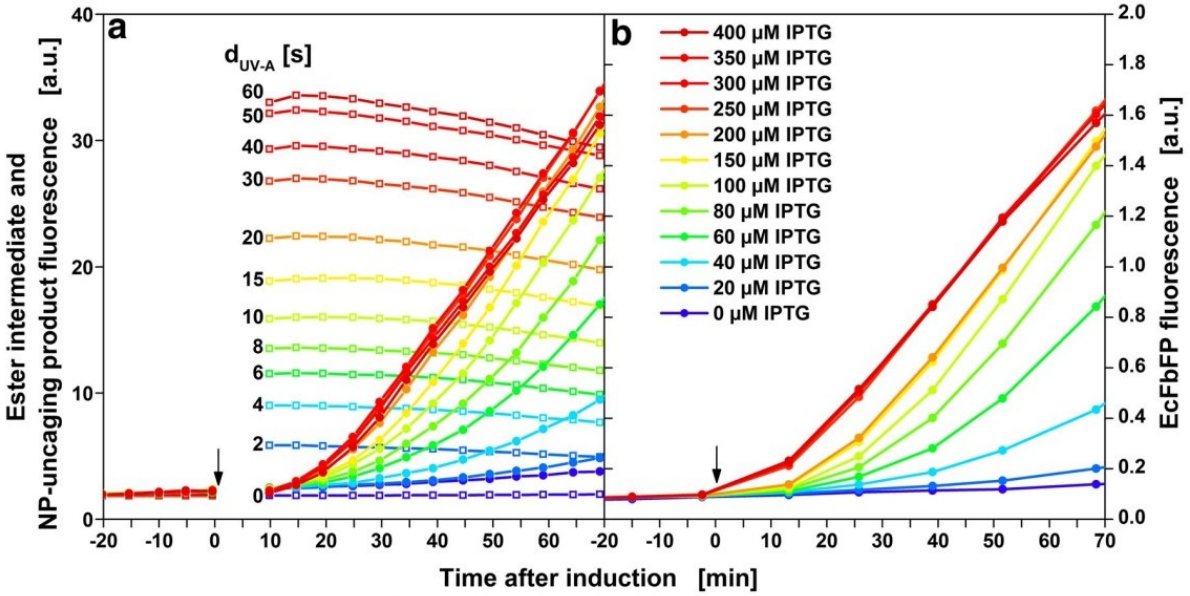

Fig. 5 Onset of heterologous protein production after induction with cIPTG or IPTG. Fluorescence intensity of ester intermediate and NP-uncaging product (*open squares*, $\lambda_{Ex} = 326$ nm, $\lambda_{Em} = 407$ nm) and FbFP fluorescence intensity (*circles*, $\lambda_{Ex} = 450$ nm, $\lambda_{Em} = 495$ nm) immediately before and after induction with either cIPTG (**a**) or IPTG (**b**). Induction is performed with 0–60 s of UV-A irradiation or 0–400 µM IPTG after 10 h of cultivation. In **a** more data points per time are shown because fewer wells were monitored in parallel

For a comparison of optical induction with cIPTG to conventional induction with manually added IPTG solution, it is interesting to know how much of a delay is caused by the two-step uncaging mechanism. A significant delay would complicate a direct comparison of the two induction methods and would make a faster one-step uncaging mechanism more desirable. Figure 5a shows the development of fluorescence signal mediated by the formation of ester intermediates and FbFP immediately after optical induction. FbFP fluorescence before induction (black arrow) is very low which indicates that the expression system is tightly regulated so that, if at all, only minor amounts of target protein are produced. This furthermore substantiates that cIPTG added at the start of the cultivation does indeed not induce the cells prior to UV-A irradiation. After UV-A irradiation, the ester intermediate and NP-uncaging product signal increases instantly. Depending on the duration of UV-A exposure, an increase in FbFP fluorescence can be detected 15–25 min after optical induction (Fig. 5a). About the same delay is observed for conventional induction with IPTG solution (Fig. 5b). The observed response time after optical induction is much faster than reported in literature [23]. This means that under high irradiance conditions (52 mW/cm^2) and with high initial cIPTG concentrations (400 µM cIPTG), used in this investigation, the uncaging mechanism of cIPTG is not the rate limiting step preceding transcription. Onset of protein formation seems to be equivalent for both methods of induction.

The FbFP signal also shows that the rate of product formation can be increased gradually with either increasing duration of UV-A exposure or increasing IPTG concentration. Both induction methods allow fine-tuning the initial product formation rate in the same range and to the same maximum. In this experiment, the maximum initial product formation rate is reached with either about 30 s UV-A or 250 µM IPTG.

A distinct advantage of the constructed UV-A LED array is that optical induction can obviously be achieved within seconds where previously several minutes of irradiation were required for uncaging [15, 19]. The very short induction times are most probably a result of the high irradiance of 52 mW/cm^2. Since the strong UV-A irradiation applied in our design could be potentially phototoxic we tested the influence on non-induced cultures. For exposure durations of up to 60 s, no influence on biomass growth was observed during the exponential phase and only minute deviations were detected in the stationary phase (Additional file 5). Therefore, phototoxicity due to UV-A irradiation is of no concern for the short UV-A exposure times ($d_{UV-A} = 0–40$ s) applied in the subsequent experiments.

Induction profiling

So far, optical induction with cIPTG was shown to be a robust method that allows gradual inducer release, very fast onset of protein synthesis and fine-tuning of protein formation. Since protein formation was essentially equal

to conventional induction the optical induction method was applied for detailed induction profiling with variation of time of induction and duration of UV-A exposure to maximize product formation. For comparison, conventional induction profiling with manual addition of IPTG solution was conducted as well. Online signals for biomass (scattered light) and FbFP fluorescence are given in Fig. 6. Induced cultures differ from non-induced cultures in growth and product formation after the respective time of induction (indicated by arrows). A number of trends can be deduced from the experiments as discussed below.

Firstly, increasing inducer concentrations reduce growth rates and delay the time to reach final biomass concentration (Fig. 6a, e). For example, a non-induced culture reaches the maximum biomass signal (scattered light intensity) after 18 h while a culture induced with 400 µM IPTG reaches the maximum 19 h later (Fig. 6a, time of induction: 7.5 h). A growth delay of about 17 h is observed when 400 µM of cIPTG are irradiated with UV-A light for 40 s at the same time point (Fig. 6e).

Secondly, a delay in growth is also observed when inductions are performed earlier rather than later (Fig. 6b, f). For example, the highest biomass signal is reached after about 40 h if the induction is performed 1.5 h into the cultivation with either 400 µM IPTG (Fig. 6b) or 400 µM cIPTG and 40 s of UV-A light (Fig. 6f). For later inductions this effect is gradually less pronounced because the cultivation has already progressed further. Decreased growth rates are caused by the drain of metabolites into heterologous protein formation ("metabolic burden") and models to correlate growth rate and heterologous protein formation have been developed [4, 24, 25].

Thirdly, initial product formation is faster with higher inducer concentrations (Fig. 6c, g; a more detailed view is provided in Additional file 6). However, over the course of the following production phase the rate decreases slightly with more pronounced decreases for higher IPTG concentration (150–1000 µM). This decrease might be attributed to overloading protein synthesis capabilities with gratuitous mRNA coding for the target protein and thereby, in the long run, decreasing synthesis capability. In contrast, cultures induced with less IPTG (25–100 µM) and lower initial product formation rates are less strained and (as visible from the biomass signal) still exhibit growth. Therefore, their production rates can still increase and eventually surpass those of more strongly induced cultures. High product concentrations at the end of the cultivation are not reached with high IPTG concentrations, but rather with moderate values of e.g. 75 to 100 µM (Fig. 6c) or 8–10 s UV-A light (Fig. 6g) (when the induction is preformed 7.5 h after the start of the cultivation).

Fourthly, product formation is also influenced by the time of induction. If, for example, the induction is performed with rather high IPTG concentrations (400 µM, Fig. 6d) or long exposures (40 s, Fig. 6h), product concentration is highest, if the induction is performed 9 h after inoculation. For earlier induction times not enough cells are present to produce high amounts of protein, for later induction times not enough substrate is left.

In summary, the microtiter plate-based approach allowed to collect not just end-point but quasi-continuous data of high resolution and over a broad range of induction conditions. Thereby, it could be shown that the observed effects of conventional and optical induction on growth and product formation are equivalent under the applied conditions. This is demonstrated even more clearly in Fig. 7 which exclusively shows end-point fluorescence measured after 42 h of cultures induced either conventionally (red) or optically (blue). For a constant inducer concentration (400 µM IPTG or 40 s UV-A exposure) the impact of induction time is shown in Fig. 7a. Vice versa, for a constant induction time (5.5 h) the impact of inducer concentration is shown in Fig. 7b. The trends and maxima of target protein concentration are once again very similar for both induction methods. Further studies are needed to explain the slight shift of about 30 min to earlier induction times for optical induction shown in Fig. 7a. It may result from either the two-step uncaging mechanism or from experimental deviations between consecutive cultivations. As already demonstrated in Fig. 5, the hydrolysis of the caged IPTG ester intermediates by intracellular esterases does not represent the rate limiting step under the conditions applied in this work.

(See figure on next page.)

Fig. 6 Online measurement data for conventional induction profiling with manual addition of IPTG solution and optical induction profiling with cIPTG. Scattered light and FbFP fluorescence of cultures induced with IPTG (**a**–**d**) and cultures induced with cIPTG (**e**–**h**). Time of induction and inducer strength (IPTG concentration or duration of UV-A exposure) were varied in full factorial design. Colors from *blue* to *red* mark later induction times (0.5–16 h), dull to bright colors mark increasing inducer strength (0–1000 µM IPTG or 0–40 s duration of UV-A exposure). In total, 304 cultures were induced conventionally and 96 cultures were induced optically. The first column (**a**, **c**, **e**, **g**) shows a subset of cultivations with a fixed induction time of 7.5 h and the second column (**b**, **d**, **f**, **h**) shows a subset of cultivations with a fixed inducer strength of 400 µM IPTG or 400 µM cIPTG and 40 s UV-A exposure. The online signals for all 400 cultivations are provided in Additional file 9. *Small colored down-pointing arrows* illustrate the time of induction (not all shown). *Long horizontal arrows in black* illustrate general trends, e.g. impact of increasing inducer concentration on growth (**a**). Cultivation conditions: 800 µL Wilms-MOPS mineral medium per well in a 48-FlowerPlate, 400 µM cIPTG added to cultures induced with the LED array (λ_{max} = 368 nm, I = 52 mW/cm^2), 30 °C, shaking frequency: 1000 rpm, shaking diameter: 3 mm

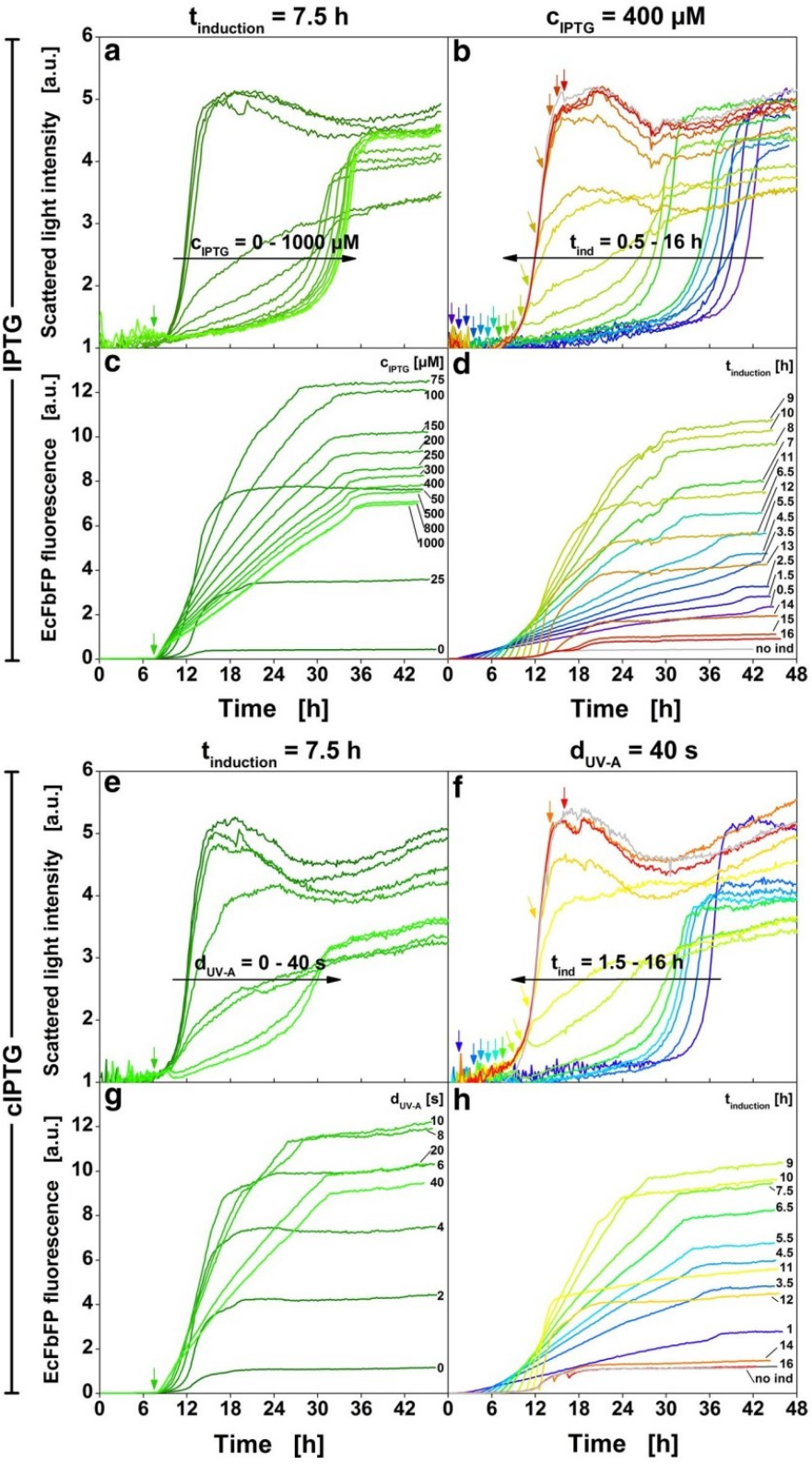
t induction = 7.5 h
c IPTG = 400 µM
a
b
c IPTG = 0 - 1000 µM
t ind = 0.5 - 16 h
IPTG
Scattered light intensity [a.u.]
EcFbFP fluorescence [a.u.]
c IPTG [µM]
75
100
150
200
250
300
400
50
500
800
1000
25
0
t induction [h]
9
10
8
7
11
6.5
12
5.5
4.5
3.5
13
2.5
1.5
0.5
14
15
16
no ind
Time [h]
t induction = 7.5 h
d UV-A = 40 s
e
f
d UV-A = 0 - 40 s
t ind = 1.5 - 16 h
cIPTG
g
h
d UV-A [s]
10
8
20
6
40
4
2
0
t induction [h]
9
10
7.5
6.5
5.5
4.5
11
3.5
12
1
14
16
no ind
Time [h]

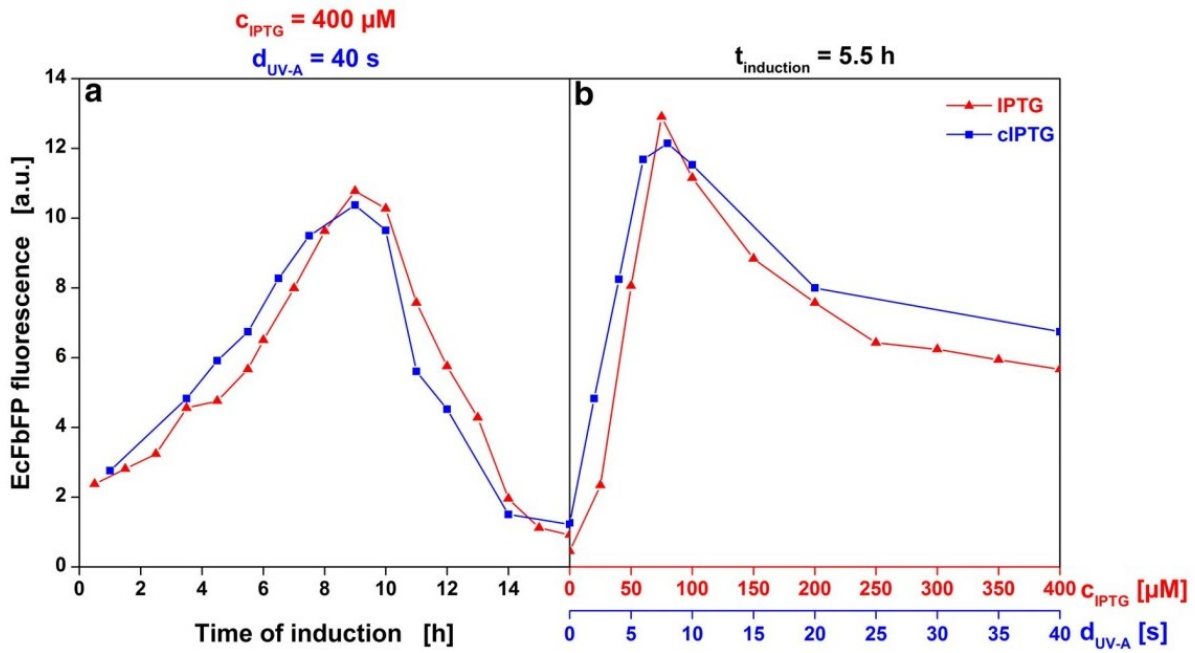

Fig. 7 Comparison of end-point FbFP fluorescence after induction with IPTG or cIPTG. FbFP fluorescence after 42 h of individual cultures induced at varied time points (0.5–16 h) with either 400 µM IPTG (*red curve*) or cIPTG after 40 s UV-A exposure (*blue curve*) (**a**) and of cultures induced after 5.5 h with either 0–400 µM IPTG or 0–40 s UV-A exposure (**b**)

Figure 7 demonstrates that induction conditions optimized with either method can be applied interchangeably. The transfer of an optimized operation point including time of induction and inducer concentration or duration of UV-A exposure, respectively, is straight-forward: Time of induction is about equivalent and duration of UV-A exposure is, in first approximation, linearly correlated to IPTG concentration with 10 s of UV-A irradiation being equivalent to 100 µM IPTG under the applied conditions (52 mW/cm^2, 400 µM cIPTG). HPLC–UV measurements confirmed that 116.2 µM (±29.4 µM) cIPTG were uncaged under these conditions (Additional file 4). However, a direct quantification of the subsequently released IPTG was not possible due the detection being more difficult. Based on the reaction scheme by Young and Deiters the amount of cIPTG uncaged to ester intermediates and the amount of subsequently released IPTG are expected to be equivalent (Fig. 3a). Further experiments are required to independently verify the amount of released IPTG. Fernández et al. developed an HPLC–MS method for the direct quantification of intracellular IPTG in the required µM range [26]. Further experiments would also be required to construct a more detailed model that describes the amount of released IPTG as a function of all optical parameters (UV-A exposure duration, irradiance, cIPTG concentration) and first-order kinetics should be considered for the impact of UV-A exposure duration as presented in the fits in Fig. 4b and Additional file 4.

The operating point for highest target protein concentration can be chosen from Fig. 8 which shows FbFP fluorescence at the end of all induction profiling cultivations. This plot reveals the existence of two general induction regimes that can be applied to achieve high target protein concentrations. If the time of induction is set to 9 h, a broad range of IPTG concentrations (100–400 µM) or UV-A exposure durations (10–40 s) leads to good product formation represented by yellow to red colors in a vertical zone. A second zone with slightly higher protein concentrations is oriented horizontally and represents the optimum IPTG concentration (60–80 µM) or UV-A exposure duration (6–8 s) for early induction. Within this region, time of induction only has a minor influence (1–6 h).

The presented induction profiles are in accordance with data on a closely related strain (*E. coli* BL21(DE3)/pRhotHi-2-EcFbFP) cultivated in the same medium, previously published by Huber et al. [9]. Since in this work four microtiter plates were monitored in parallel instead of just one, induction profiles with more data points and higher resolution could be obtained. The importance of detailed induction profiling with high resolution can be exemplified by deviations from the optimum IPTG concentration in the horizontal regime. Inductions with 50 or 150 µM IPTG at 2.5 h yield only 60 % of the protein that is produced after induction with 75 µM IPTG. The still prevalent induction with 1000 µM IPTG in the early

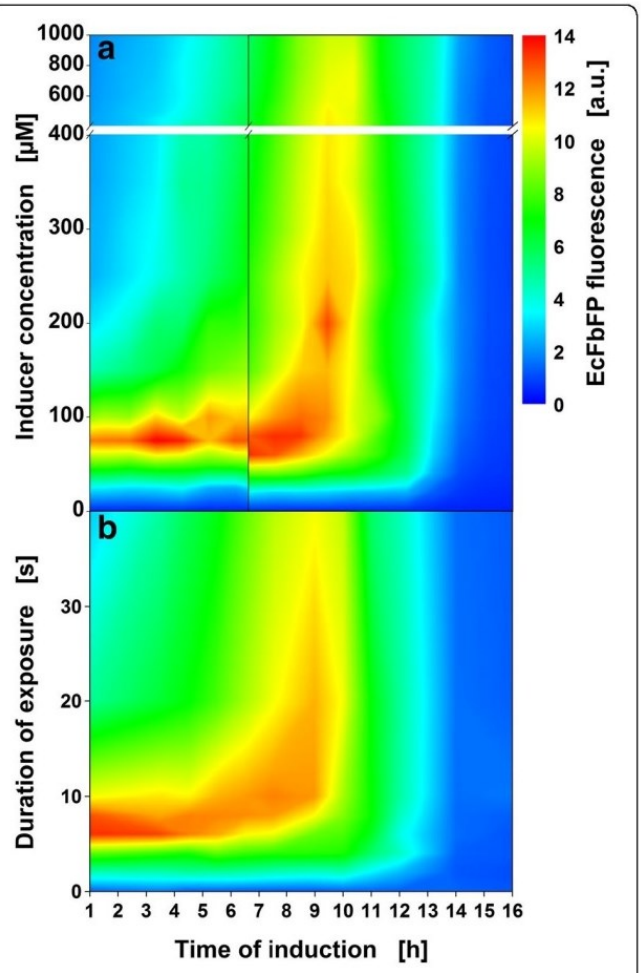

Fig. 8 Induction profiles for conventional induction with manual addition of IPTG solution and optical induction with cIPTG. End-point FbFP fluorescence of cultures conventionally induced with IPTG (**a**) or optically induced with cIPTG upon UV-A exposure (**b**). Colors from *blue* to *red* indicate induction conditions that lead to increasing FbFP concentrations. For optical induction 400 µM cIPTG was added at the start of the cultivation. Note the axis break at 400 µM IPTG in so that both induction profiles are scaled equally in the range of 0–400 µM IPTG and 0–40 s UV-A exposure to facilitate comparison (**a**). Results for higher IPTG concentrations (400–1000 µM) are still shown but do not yield higher FbFP concentrations. Also note the vertical black line at an induction time of 6.5 h that highlights a change in microtiter plate lot. IPTG induction experiments with induction times of 1–6.5 h were performed in 48-FlowerPlates of lot 14xx, all other experiments were performed with plates of lot 15xx. The normalization procedure is described in Additional file 7. Cultivation conditions for *E. coli* Tuner(DE3)/pRhotHi-2-LacI-EcFbFP: 800 µL Wilms-MOPS mineral medium per well in a 48-FlowerPlate, 30 °C, shaking frequency: 1000 rpm, shaking diameter: 3 mm

exponential growth phase [2] (in our case after approx. 9–10 h) is also far from ideal to achieve high target protein concentrations with the strain used in this work. The highest protein concentration after an induction with 1000 µM IPTG is achieved when the culture is induced after 10 h. It yields only 70 % of the target protein that is achieved when the culture is induced with 75 µM IPTG after 2.5 h. Thus, overinduction with too much IPTG not only wastes a cost-intensive chemical but also reduces product concentration. An efficient process with high product concentration can only be reached when induction parameters are optimized for each individual strain and target protein. Light-induced gene expression with photocaged IPTG applied in a high-throughput system allows performing this optimization much more easily than before.

Conclusions

An LED array allowing for individual illumination of each well of a 48-well microtiter plate was constructed and successfully applied for light-induced gene expression based on photocaged IPTG. The fluorescence of the reporter protein FbFP was measured online in up to four microtiter plates in parallel. Irradiating photocaged IPTG resulted in an additional distinct fluorescence signal which could be assigned to photocaged IPTG ester intermediates and the nitropiperonal uncaging product. This signal was subsequently applied to characterize the uncaging reaction. In the future, it might also be utilized to control more advanced induction strategies. As an example, the IPTG concentration profile over time which usually follows a step function (addition or release at one time point) could be replaced by fine-tuned profiles with continuous inducer release depending on current biomass concentration or growth rate [27–29]. The combination of an LED array and a BioLector screening system could also be used to study gene expression and protein production controlled by chemically distinct photocaged compounds or by photoreceptors [30–32].

In this study, we compared optical induction with photocaged IPTG to conventional induction with manual addition of IPTG solutions and showed that both methods yield essentially equivalent results under the applied conditions. This means that induction parameters which can be optimized easily with optical induction can later be transferred to conventional induction protocols for e.g. stirred tank bioreactors. Optical induction can be parallelized easily as well and it has the distinct advantage of being less invasive as the shaking motion of the microtiter plate is not stopped. This is of great importance since even short oxygen limitation influences expression of genes involved in central metabolism and can lead to a complete loss of productivity in organisms sensitive to sudden oxygen limitation [33, 34]. Also, optical measurements which are affected by a change in the shaking motion can be continued throughout the induction. Furthermore, the sterile barrier is not compromised by optical induction which might prove very convenient for strictly anaerobic cultivations or cell culture applications

[35]. In conclusion, light-induced induction shows several advantages and can readily replace conventional induction for screening purposes in microtiter plates.

Methods

Microorganism and target protein

The strain *Escherichia coli* Tuner(DE3)/pRhotHi-2-LacI-EcFbFP was used for all experiments. Except for the target protein it is identical to a strain previously used to study light-induced gene expression by Binder et al. [19]. It offers several advantageous characteristics for this study: Because of the permease deficiency (*lacY*$^-$) of *E. coli* Tuner(DE3) IPTG can only enter the cell via concentration dependent diffusion. Therefore, an unimodal induction response homogenously distributed over the entire population can be expected [19, 36]. The low-copy number plasmid pRhotHi-2 carrying a T7 promoter offers potential for high-level expression [37]. Additional expression of the repressor LacI reduces the basal expression which allows easier quantification at low induction levels [19]. The flavin-based fluorescent protein FbFP was chosen as the target protein because its fluorescence develops immediately after translation and no maturation step depending on intracellular oxygen concentration is required as for proteins of the GFP-family [38]. For better expression, a sequence optimized for *E. coli* codon bias was used [20].

The construction of expression vectors and recombinant DNA techniques were carried out in *E. coli* DH5α [39] as described by Sambrook et al. [40]. The EcFbFP reporter gene was isolated from pRhotHi-2-EcFbFP [37, 41] and inserted into target vector pRhotHi-2-LacI via *Nde*I/*Xho*I restriction, yielding the final construct pRhotHi-2-LacI-EcFbFP.

Precultivations

Prior to induction experiments two sequential precultivation steps were performed. The first precultivation step was done with 10 mL complex TB medium (5 g/L glycerol, 24 g/L yeast extract, 12 g/L tryptone, 12.54 g/L K_2HPO_4, 2.3 g/L KH_2PO_4; all ingredients from Roth, Germany) in 250 mL shake flasks. Shake flasks were inoculated to an initial optical density of 0.1 (OD_{600}) from cryogenically preserved cultures and cultivated on an orbital shaker (LS-X, Kuhner, Switzerland) at 350 rpm with a shaking diameter of 50 mm for 5 h at 37 °C. For the second precultivation step 10 mL of a modified Wilms-MOPS minimal medium [42] (20 g/L glucose, 6.98 g/L $(NH_4)_2SO_4$, 3 g/L K_2HPO_4, 2 g/L Na_2SO_4, 41.85 g/L (N-morpholino)-propanesulfonic acid (MOPS), 0.5 g/L MgSO4·$7H_2O$, 0.01 g/L thiamine hydrochloride, 1 mL/L trace element solution [0.54 g/L $ZnSO_4·7H_2O$, 0.48 g/L $CuSO_4·5H_2O$, 0.3 g/L $MnSO_4·H_2O$, 0.54 g/L $CoCl_2·6H_2O$, 41.76 g/L $FeCl_3·6H_2O$, 1.98 g/L $CaCl_2·2H_2O$, 33.4 g/L Na_2EDTA (Titriplex III)]) were used. The pH-value was adjusted to 7.5 with NaOH. Shake flasks were again inoculated to an initial optical density of 0.1 (OD_{600}) and placed on an orbital shaker at 350 rpm with a shaking diameter of 50 mm. After cultivation for 9 h at 30 °C the second precultures reached the early exponential growth phase and the main culture in microtiter plates was inoculated. In all cultivation steps 50 µg/mL kanamycin sulfate was added.

Microtiter plate cultivations

Microtiter plate cultivations for induction experiments were conducted in 48-well FlowerPlates (MTP-48-B, lot 1404 & 1509, m2p-labs, Germany). As in the second precultivation step Wilms-MOPS mineral medium was used. Wilms-MOPS medium is suited to achieve high cell densities and high heterologous protein concentrations [42]. As demonstrated elsewhere, optical induction with cIPTG is not restricted to mineral media and can also be performed in complex media like LB [15, 19]. LB medium was not used here because it is restricted to low cell densities since its nitrogen-containing complex compounds are used as energy source which results in the formation of ammonium and alkalization [43]. Other complex media like TB were not used because lot-to-lot variations in raw materials have been reported to effect reproducibility in induced cultures [44]. Each well was filled with 800 µL Wilms-MOPS medium from a master mix inoculated to an initial optical density of 0.1 (OD_{600}). Plates were sealed with an autoclaved self-adhesive transparent polyolefin sealing foil (900371, HJ-Bioanalytik, Germany) as sterile barrier. The foil reduces evaporation while still allowing sufficient gas transfer. Up to four microtiter plates in parallel were placed on an orbital shaker (ES-X, Kuhner, Switzerland) with a shaking frequency of 1000 rpm and a shaking diameter of 3 mm at 30 °C.

Optical induction with LED array

Nitropiperonal-photocaged IPTG (cIPTG) was synthesized from IPTG and 6-nitropiperonal as previously described [19]. At the beginning of microtiter plate cultivations for optical induction 400 µM cIPTG was added from a 40 mM stock solution in DMSO stored in the dark at −20 °C. An in-house constructed array of 48 high-power UV-A LEDs (LZ1-3x, LED Engin, USA) attached to a heat sink was mounted on top of a microtiter plate resulting in one LED per well to be positioned at a distance of 14 mm in coaxial position (Fig. 1). A mask with cylindrical holes with 11 mm diameter ensures that only the corresponding well is illuminated and no stray light can enter adjacent wells. No induction was observed in wells that were adjacent to illuminated wells but not

illuminated themselves. Between heat sink and mask a 3 mm gap is left to allow sufficient gas transfer to and from the wells. When an LED is switched on, UV-A irradiation passes the transparent sterile barrier and reaches the culture where IPTG is uncaged. LEDs are wired in a matrix layout and switched using 14 metal oxide semiconductor field-effect transistors on a driver stage fixed onto the shaking tray next to the microtiter plate. The driver stage is connected to a microcontroller (Arduino Uno R3, Arduino LLC, USA) and controlled via a PC running LabVIEW (LabVIEW v14, National Instruments, USA). LEDs are operated at 700 mA resulting in a high irradiance of at the well bottom (52.7 mW/cm^2, $\lambda_{max} = 368$ nm) with low well-to-well deviation (SD 3.2 mW/cm^2). Irradiance at the position of the well bottom was determined on bottomless microtiter plates with a thermal power sensor (S302C, Thorlabs, Germany). For optical induction experiments cultures were irradiated for 2–60 s. During irradiation a temperature increase of 0.7 K/min occurred which was measured using a rhodamin-based fluorescence method [45, 46] (data not shown). Since uncaging was achieved within 1 min, the temporary temperature increase (<0.7 K) was considered to be within acceptable limits. For one of the experiments performed to characterize photo-uncaging a lower effective irradiance (13 mW/cm^2) was used. This was achieved by placing a strip of diffuser foil (White Diffusion LEE216, LEE Filters, USA) directly below the LEDs.

Fluorescence spectroscopy

Fluorescence measurements were performed through the transparent bottom of the microtiter plates during cultivation, according to the established BioLector setup [11, 17]. A quartz/quartz multi-mode fiber (LUV 105 µM, LEONI, Germany) is moved sequentially below the wells of four microtiter plates by a Cartesian motion system (CMS, Bosch Rexroth, Germany) to allow quasi-continuous fluorescence measurements on all wells without stopping the shaking movement which might otherwise result in cell sedimentation or oxygen limitation. In contrast to commercially available designs, a spectrofluorometer with excitation/emission monochromators (Fluoromax-4, HORIBA Jobin–Yvon GmbH, Germany) was applied. It enables variation and optimization of excitation/emission wavelength in a range of 200–950 nm. During cultivation cIPTG ester intermediates were excited at a wavelength of $\lambda_{Ex} = 326$ nm and therefore below the maximum excitation wavelength of $\lambda_{Ex.max} = 335$ nm to reduce NADH fluorescence cross-talk. cIPTG ester intermediate fluorescence was measured at $\lambda_{Em} = 407$ nm. FbFP fluorescence ($\lambda_{Ex} = 450$ nm, $\lambda_{Em} = 495$ nm) and biomass formation (scattered light at 650 nm) were monitored as well. When measuring the cIPTG ester intermediate fluorescence the excitation and emission slits were set to a bandwidth of 8 nm. The raw intensities measured for FbFP fluorescence and biomass (scattered light) were higher and therefore the slit bandwidth could be reduced to 4 nm. Integration time was set to 600 ms for fluorescence signals and 900 ms for scattered light (biomass). 2D fluorescence spectra of cultures before and after uncaging with UV-A irradiation were obtained by scanning the excitation wavelength from 300 to 600 nm and the emission wavelength from 320 to 600 nm (stepsize: 5 nm) according to a previously published setup [18]. As reference, cIPTG ester intermediates and the nitropiperonal-uncaging product were isolated by HPLC (Additional file 1), identified by NMR (Additional file 2) and fluorescence spectra from 360 to 500 nm were obtained with a plate reader ($\lambda_{Ex} = 330$ nm, Infinite M1000 Pro, Tecan, Switzerland).

Induction profiling

Conventional induction with IPTG and optical induction with uncaging of cIPTG were compared in induction experiments. A culture well was either conventionally induced by manually adding IPTG solution with a pipette or optically induced by illumination with the LED array. The two parameters varied were time of induction (in relation to the start of the cultivation, 0.5–16 h) and either IPTG concentration (0–1000 µM) in case of conventional induction or duration of UV-A exposure (0–40 s) in case of optical induction. Conventional induction was achieved by pausing the measurement, stopping the shaker, removing the sealing foil and manually adding 20 µL IPTG solution from a set of sterile stock solutions with a multichannel pipette (Eppendorf, Germany). Then, the sealing foil was replaced and the shaker was started again. For optical induction a cIPTG concentration of 400 µM and a high irradiance of 52.7 mW/cm^2 were used. No manual interference was required at all since the LED array was automatically controlled by a LabVIEW script during shaking.

During the induction profiling experiments the microtiter plate supplier (m2p-labs, Germany) changed the manufacturing of the plates' transparent bottom. According to the supplier, for FlowerPlates with lot numbers 14xx and earlier a 150 µM thin polystyrene foil (158 K, BASF, Germany) was used. In contrast, a 700 µM thick polystyrene foil (Styron 678E, Dow Chemical, USA) was used for plates with lot number 15xx and later. The thicker foil reduced fluorescence and scattered light intensities. Also, the plates with higher lot numbers feature two small opaque spots (intended to take up pH- and oxygen sensor dyes) which increase the scattered light baseline. To allow comparison of cultures on different microtiter plates, data was normalized to the biomass

signal (scattered light) of non-induced reference cultures (Additional file 7).

Abbreviations

IPTG: isopropyl β-D-1-thiogalactopyranoside; cIPTG: 6-nitropiperonal-photocaged isopropyl β-D-1-thiogalactopyranoside; FbFP: flavin-mononucleotide-based fluorescent reporter protein; T7-RNA-polymerase: ribonucleic acid polymerase from bacteriophage T7; *E. coli*: *Escherichia coli*; UV-A: ultraviolet A radiation with a wavelength of 315–400 nm; LED: light-emitting diode; 2D: two-dimensional; EcFbFP: *E. coli* codon bias-optimized FbFP; HPLC: high-performance liquid chromatography; NMR: nuclear magnetic resonance spectroscopy; GFP: green fluorescent protein; DNA: deoxyribonucleic acid; TB: terrific broth; MOPS: (*N*-morpholino)-propanesulfonic acid; EDTA: ethylenediaminetetraacetic acid; DMSO: dimethyl sulfoxide; SD: standard deviation; NADH: reduced form of nicotinamide adenine dinucleotide; NP: 6-nitropiperonal; cIPTGe: ester intermediate in the cIPTG photouncaging reaction.

List of symbols

λ_{max}: wavelength with maximum intensity; OD_{600}: optical density at a wavelength of 600 nm; $\lambda_{ex,max}$: excitation wavelength resulting in maximum fluorescence emission; $\lambda_{em,max}$: wavelength with maximum fluorescence emission; λ_{ex}, λ_{em}: fluorescence excitation and emission wavelength; $t_{1/2}$: half-life; $d_{UV\text{-}A}$: duration of UV-A exposure; I: irradiance; $t_{induction}$: time of induction; c_{IPTG}: IPTG concentration.

Additional files

Additional file: 1. cIPTG was dissolved in isopropanol/n-heptan 50/50. (8.3 mg in 2.5 mL) and irradiated for 10 min (375 nm; 6.2 mW/cm^2). cIPTG and its ester intermediates (cIPTGe1 and cIPTGe2) were then separated via HPLC (column: Chiralpak IC, 250·10 mm, Daicel, Japan; solvent: n-heptan:2-propanol (30:70); flow rate: 0.5 mL/min; detection: UV 258 nm)

Additional file: 2. NMR-measurement of ester intermediates. cIPTGe1 (A) and cIPTGe2 (B) were identified via NMR. **cIPTGe1 (A):** 1H-NMR (600 MHz, CDCl3), δ [ppm]: 7.35 (s, 1 H, 4´-CH), 6.01 (s, 1 H, 7´-CH), 6.14 (s, 2 H, 2´-CH2), 4.75 (dd, 2J6a, 6b = 11.5 Hz, 2J6a, 5 = 6.0 Hz, 1 H, 6-CH2), 4.66 (dd, 2J6b, 6a = 11.4 Hz, 2J6b, 5 = 6.6 Hz, 1 H, 6-CH2), 4.39 (m, 1 H, 1-CH), 3.98 (m, 1 H, 4-CH), 3.87 (m, 1 H, 5-CH), 3.63 (m, 2 H, 2-CH, 3-CH), 3.17 (septet, 3JSCH, CH3a/b = 6.70 Hz, 1 H, -SCH), 2.73 (s, 1 H, OH), 2.59 (s, 1 H, OH), 2.45 (s, 1 H, OH), 1.31 (d, 3JCH3a, SCH = 1.70 Hz, 3H, -CH3a), 1.30 (d, 3JCH3b, SCH = 1.80 Hz, 3H,-CH3b). 13C-NMR (151 MHz, CDCl3), δ [ppm]: 166.94 (C-7), 160.67 (C-6´), 153.16 (C-7a´), 150.80 (C-3a´), 133.61 (C-5´), 108.72 (C-4´), 103.36 (C-2´), 89.36 (C-7´), 86.00 (C-1), 75.66 (C-5), 74.34 (C-3), 70.51 (C-2), 68.47 (C-4), 64.69 (C-6), 35.92 (SCH), 24.22 (C- CH3a), 23.99 (C- CH3b). **cIPTGe2 (B):** 1H-NMR (600 MHz, CDCl3), δ [ppm]: 7.42 (s, 1 H, 4´-CH), 6.19 (s, 2 H, 2´-CH2), 6.01 (s, 1 H, 7´-CH), 5.69 (dd, 3J4,3 = 3.6 Hz, 3J4,5 = 1.1 Hz 1 H, 4–CH), 4.47 (d, 3J1,2 = 9.7 Hz, 1 H, 1-CH), 3.86 (m, 1 H, 5-CH), 3,78 (m, 2 H, 6a-CH2, 3-CH), 3.70 (dd, 3J6b, 6a = 11.9 Hz, 3J6b, 5 = 7.1 Hz, 1H, 6-CH2), 3.30 (t, 3J2,1 = 9.4 Hz, 3J2,3 = 9.4 Hz, 1 H, 2-CH2)), 3.18 (m, 1 H, -SCH), 1.31 (d, 3JCH3a/b, SCH = 1.6 Hz, 3H,-CH3a), 1.30 (d, 3JCH3a/b, SCH = 1.5 Hz, 3H,-CH3b)

Additional file: 3. Relative amount of cIPTG ester intermediates over time. No ester intermediates are detected without UV-A irradiation (-UV-A). After UV-A irradiation (+UV-A) ester intermediates are detected. They were stable for at least 24 h (+24 h). Addition of lipase PL from *Alcaligenes sp.* fully degrades the ester intermediates (+lipase). HPLC (Jasco HPLC system, column: Hyperclone 5 µ ODS (C18) 120 (Phenomenex), solvent: MeOH:H2O 30:70, flow rate: 1 mL/min, 25 °C, 30 µL, detection: UV 258 nm at 11.46 min). 1000 µM cIPTG in H_2O, irradiation with 6.4 mW/cm^2 at 375 nm for 10 min and storage at RT for 24 h, addition of 1 mg lipase PL (Alcaligenes sp. lipase 100000 U/g) to 910 µL at 38 °C for 24 h

Additional file: 4. Photo-uncaging of cIPTG as a function of UV-A exposure duration. In vitro decomposition of 400 µM cIPTG in H_2O by UV-A irradiation (λ_{max} = 368 nm, I = 52 mW/cm^2, n = 4) monitored via HPLC–UV. HPLC (Jasco HPLC system, column: Hyperclone 5 µ ODS (C18) 120 (Phenomenex), solvent: MeOH:H2O 30:70, flow rate: 1 mL/min, 25 °C, 30 µL, detection: UV 258 nm at 19.04 min)

Additional file: 5. Effect of UV-A irradiation on cell growth. Scattered light intensity of non-induced cultures irradiated with UV-A LEDs for 0–120 s (λ_{max} = 368 nm, I = 52 mW/cm^2). No cIPTG was added to the medium. The black arrow indicates the time of UV-A exposure in the exponential phase. For up to 60 s of UV-A exposure only minute deviations are detected in the scattered light signal. Exposure for 120 s leads to a slightly lower scattered light signal in the stationary phase. Since exposure durations of up to 40 s were sufficient for optical induction, negative effects of UV-A irradiation are of no concern for the bacteria used in this work. Cultivations were performed in triplicates; standard deviation is shown in the same color as the mean value but at 50 % transparency

Additional file: 6. Initial product formation after induction. Zoomed view of Fig. 6c and Fig. 6g. FbFP fluorescence of *E. coli* cultures induced after 7.5 h with 0–1000 µM IPTG (A) or 400 µM of cIPTG and 0–40 s of UV-A irradiation (B). The initial product formation gradually increases with increasing IPTG concentrations (0–400 µM) and is saturated for higher concentrations (400–1000 µM) (A). However, the highest product fluorescence at the end of the cultivation after 42 h is reached with 75–100 µM IPTG (A, right side). For optical induction, initial product formation rate is highest for 20–40 s of UV-A irradiation and the highest product concentrations after 42 h are reached with 8–10 s (B). Note the axis scaling and breaks for increased readability. Additionally, note that only 400 µM of cIPTG are available for uncaging in B. Cultivation conditions: 800 µL Wilms-MOPS mineral medium per well in a 48-FlowerPlate, 400 µM cIPTG added to cultures induced with the LED array (λ_{max} = 368 nm, I = 52 mW/cm^2), 30 °C, shaking frequency: 1000 rpm, shaking diameter: 3 mm

Additional file: 7. Data normalization. Raw scattered light signals are influenced by the microtiter plate lot (A). For normalization the raw signals of cultivations in one lot can be multiplied with a correction factor to match the course of the other cultivation (B). The correction factor is determined by dividing the scattered light intensities at the end of the cultivation after 42 h. This correction factor can also be applied to correct EcFbFP fluorescence signals (C). The normalized signals of cultures induced with 0, 100 or 200 µM IPTG are in good agreement. This demonstrates that reproducible results can be obtained even when different microtiter plate lots are used. Cultivation conditions: 800 µL Wilms-MOPS mineral medium per well in a 48-FlowerPlate, 30 °C, shaking frequency: 1000 rpm, shaking diameter: 3 mm. Error bars in A and B indicate the standard deviation of six reference cultures. Induction in C after 6 h. Data for 0 µM IPTG and lot 14xx is not visible in C because it is almost identical to lot 15xx

Additional file: 8. Online measurement of cIPTG ester intermediates and NP-uncaging product. This figure shows the full data set of the measurement presented in Fig. 4 where measurements for 8, 15, 40 and 50 s of UV-A irradiation were not shown to increase readability. Fluorescence intensity (λ_{Ex} = 326 nm, λ_{Em} = 407 nm, black cross in Fig. 2) of 12 *E. coli* cultures before and after UV-A irradiation for 0–60 s (A) and fluorescence intensity measured directly after irradiation as a function of duration of UV-A exposure (B). At the beginning of the cultivation, 400 µM cIPTG were added to the medium. After 10 h, optical induction was performed with the LED array (λ_{max} = 368 nm, I = 52 mW/cm^2). The amount of

ester intermediates increases with increasing duration of UV-A exposure and can be fitted with first-order kinetics (solid lines and equations in B, $R^2 > 0.995$). Reduced irradiance leads to lower rate constants (black triangles, I = 13 mW/cm²) and reduced cIPTG concentration to lower amplitude (green diamonds, 50 µM cIPTG). Cultivation conditions: 800 µL Wilms-MOPS mineral medium (20 g/L glucose, 0.2 M MOPS) per well in a 48-FlowerPlate, 30 °C, shaking frequency: 1000 rpm, shaking diameter: 3 mm

Additional file: 9. Online measurement data for conventional induction profiling with manual addition of IPTG solution and optical induction profiling with cIPTG. This figure shows the full data set of induction profiling experiment presented in Fig. 6. Scattered light and FbFP fluorescence of 304 E. coli cultures induced with IPTG (A-F) and of 96 E. coli cultures induced with cIPTG (G-L). Time of induction and inducer strength (IPTG concentration or duration of UV-A exposure) are varied in full factorial design. Colors from blue to red mark later induction times (0.5–16 h), dull to bright colors mark increasing inducer strength (0–1000 µM IPTG or 0–40 s duration of UV-A exposure). The first column (A,D,G,J) shows the full data set while the second column (B,E,H,K) shows a subset at a fixed induction time of 7.5 h and the third column (C,F,I,L) shows a subset at a fixed inducer strength of 400 µM IPTG or 40 s UV-A exposure. Small colored down-pointing arrows illustrate the time of induction (not all shown). Long horizontal arrows in black illustrate general trends, e.g. impact of increasing inducer concentration on growth (B). Cultivation conditions: 800 µL Wilms-MOPS mineral medium per well in a 48-FlowerPlate, 400 µM cIPTG added to cultures induced with the LED array (λ_{max} = 368 nm, I = 52 mW/cm²), 30 °C, shaking frequency: 1000 rpm, shaking diameter: 3 mm

Authors' contributions

GW designed the study, constructed the LED array and BioLector, performed the cultivation experiments and data analysis and drafted the manuscript. CB synthesized the cIPTG, performed the HPLC and NMR experiments and analysis and participated in drafting the manuscript. DB performed the cloning as well as some of the offline fluorescence emission scans and participated in data analysis and drafting the manuscript. KH participated in the cultivation experiments and data analysis. KEJ, JP, TD and JB supervised the study, participated in data interpretation and assisted in drafting the manuscript. All authors read and approved the final manuscript.

Author details

[1] AVT-Biochemical Engineering, RWTH Aachen University, Worringerweg 1, Aachen 52074, Germany. [2] Institute of Bioorganic Chemistry, Heinrich-Heine-University Düsseldorf, Forschungszentrum Jülich, Jülich 52426, Germany. [3] Institute of Molecular Enzyme Technology, Heinrich-Heine-University Düsseldorf, Forschungszentrum Jülich, Jülich 52426, Germany. [4] Institut für Bio- und Geowissenschaften (IBG-1: Biotechnologie), Forschungszentrum Jülich, Jülich 52428, Germany.

Acknowledgements

The Federal Ministry of Education and Research is gratefully acknowledged for financial support (031A167A-C).

Competing interests

The authors declare that they have no competing interests.

Received: 4 December 2015 Accepted: 13 April 2016
Published online: 23 April 2016

References

1. Donovan RS, Robinson CW, Glick BR. Review: optimizing inducer and culture conditions for expression of foreign proteins under the control of the *lac* promoter. J Ind Microbiol. 1996;16:145–54.
2. Berrow NS, Büssow K, Coutard B, Diprose J, Ekberg M, Folkers GE, Levy N, Lieu V, Owens RJ, Peleg Y, et al. Recombinant protein expression and solubility screening in *Escherichia coli*: a comparative study. Acta Crystallogr D Biol Crystallogr. 2006;62:1218–26.
3. Shitu JO, Woodley JM, Wnek R, Chartrain M, Hewitt CJ. Induction studies with *Escherichia coli* expressing recombinant interleukin-13 using multiparameter flow cytometry. Biotechnol Lett. 2009;31:577–84.
4. Bentley WE, Mirjalili N, Andersen DC, Davis RH, Kompala DS. Plasmid-encoded protein—the principal factor in the metabolic burden associated with recombinant bacteria. Biotechnol Bioeng. 1990;35:668–81.
5. Miao F, Kompala DS. Overexpression of cloned genes using recombinant *Escherichia coli* regulated by a T7-promoter. 1. Batch cultures and kinetic modeling. Biotechnol Bioeng. 1992;40:787–96.
6. Rahmen N, Fulton A, Ihling N, Magni M, Jaeger KE, Büchs J. Exchange of single amino acids at different positions of a recombinant protein affects metabolic burden in *Escherichia coli*. Microb Cell Fact. 2015;14:10.
7. Dreisigmeyer DW, Stajic J, Nemenman I, Hlavacek WS, Wall ME. Determinants of bistability in induction of the *Escherichia coli lac* operon. IET Syst Biol. 2008;2:293–303.
8. Noel JT, Pilyugin SS, Narang A. The diffusive influx and carrier efflux have a strong effect on the bistability of the *lac* operon in *Escherichia coli*. J Theor Biol. 2009;256:14–28.
9. Huber R, Ritter D, Hering T, Hillmer AK, Kensy F, Müller C, Wang L, Büchs J. Robo-Lector—a novel platform for automated high-throughput cultivations in microtiter plates with high information content. Microb Cell Fact. 2009;8:42.
10. Rohe P, Venkanna D, Kleine B, Freudl R, Oldiges M. An automated workflow for enhancing microbial bioprocess optimization on a novel microbioreactor platform. Microb Cell Fact. 2012;11:144.
11. Samorski M, Müller-Newen G, Büchs J. Quasi-continuous combined scattered light and fluorescence measurements: a novel measurement technique for shaken microtiter plates. Biotechnol Bioeng. 2005;92:61–8.
12. Baumann P, Bluthardt N, Renner S, Burghardt H, Osberghaus A, Hubbuch J. Integrated development of up- and downstream processes supported by the cherry-tag (TM) for real-time tracking of stability and solubility of proteins. J Biotechnol. 2015;200:27–37.
13. Höpfner T, Bluma A, Rudolph G, Lindner P, Scheper T. A review of non-invasive optical-based image analysis systems for continuous bioprocess monitoring. Bioprocess Biosyst Eng. 2010;33:247–56.
14. Drepper T, Krauss U, Berstenhorst SMZ, Pietruszka J, Jaeger KE. Lights on and action! controlling microbial gene expression by light. Appl Microbiol Biotechnol. 2011;90:23–40.
15. Young DD, Deiters A. Photochemical activation of protein expression in bacterial cells. Angewandte Chemie. 2007;46:4290–2.
16. Funke M, Diederichs S, Kensy F, Müller C, Büchs J. The baffled microtiter plate: increased oxygen transfer and improved online monitoring in small scale fermentations. Biotechnol Bioeng. 2009;103:1118–28.
17. Kensy F, Zang E, Faulhammer C, Tan RK, Büchs J. Validation of a high-throughput fermentation system based on online monitoring of biomass and fluorescence in continuously shaken microtiter plates. Microb Cell Fact. 2009;8:31.
18. Siepert EM, Gartz E, Tur MK, Delbruck H, Barth S, Buchs J. Short-chain fluorescent tryptophan tags for on-line detection of functional recombinant proteins. BMC Biotechnol. 2012;12:65.
19. Binder D, Grünberger A, Loeschcke A, Probst C, Bier C, Pietruszka J, Wiechert W, Kohlheyer D, Jaeger KE, Drepper T. Light-responsive control of bacterial gene expression: precise triggering of the *lac* promoter activity using photocaged IPTG. Integr Biol. 2014;6:755–65.
20. Drepper T, Eggert T, Circolone F, Heck A, Krauss U, Guterl JK, Wendorff M, Losi A, Gärtner W, Jaeger KE. Reporter proteins for in vivo fluorescence without oxygen. Nat Biotechnol. 2007;25:443–5.
21. Bley F, Schaper K, Gorner H. Photoprocesses of molecules with 2-nitrobenzyl protecting groups and caged organic acids. Photochem Photobiol. 2008;84:162–71.
22. Klán P, Šolomek T, Bochet CG, Blanc A, Givens R, Rubina M, Popik V, Kostikov A, Wirz J. Photoremovable protecting groups in chemistry and biology: reaction mechanisms and efficacy. Chem Rev. 2013;113:119–91.
23. Binder D, Bier C, Grünberger A, Drobietz D, Hage-Hülsmann J, Wandrey G, Büchs J, Kohlheyer D, Loeschcke A, Wiechert W et al. Photocaged arabinose—a novel optogenetic switch for rapid and gradual control

of microbial gene expression. ChemBioChem. 2015;. doi:10.1002/cbic.201500609.
24. Bienick MS, Young KW, Klesmith JR, Detwiler EE, Tomek KJ, Whitehead TA. The interrelationship between promoter strength, gene expression, and growth rate. PLoS One. 2014;9:e109105.
25. Perfeito L, Ghozzi S, Berg J, Schnetz K, Lässig M. Nonlinear fitness landscape of a molecular pathway. PLoS Genet. 2011;7:e1002160.
26. Fernández A, Ruiz J, Caminal G, López-Santín J. Development and validation of a liquid chromatography–mass spectrometry assay for the quantitation of IPTG in *E. Coli* fed-batch cultures. Anal Chem. 2010;82:5728–34.
27. Striedner G, Cserjan-Puschmann M, Pötschacher F, Bayer K. Tuning the transcription rate of recombinant protein in strong *Escherichia coli* expression systems through repressor titration. Biotechnol Prog. 2003;19:1427–32.
28. Pinsach J, de Mas C, Lopez-Santín J. Induction strategies in fed-batch cultures for recombinant protein in *Escherichia coli*: application to rhamnulose 1-phosphate aldolase. Biochem Eng J. 2008;41:181–7.
29. Altenbach-Rehm J, Nell C, Arnold M, Weuster-Botz D. Parallel bubble columns with fed-batch technique for microbial process development on a small scale. Chem Eng Technol. 1999;22:1051–8.
30. Ziegler T, Möglich A. Photoreceptor engineering. Front Mol Biosci. 2015;2:30.
31. Brieke C, Rohrbach F, Gottschalk A, Mayer G, Heckel A. Light-Controlled Tools. Angewandte Chemie. 2012;51:8446–76.
32. Heo J, Cho D-H, Ramanan R, Oh H-M, Kim H-S. PhotoBiobox: a tablet sized, low-cost, high throughput photobioreactor for microalgal screening and culture optimization for growth, lipid content and CO_2 sequestration. Biochem Eng J. 2015;103:193–7.
33. Gyamerah MH. Oxygen requirement and energy relations of itaconic acid fermentation by *Aspergillus terreus* NRRL 1960. Appl Microbiol Biotechnol. 1995;44:20–6.
34. Tolla DA, Savageau MA. Regulation of aerobic-to-anaerobic transitions by the FNR cycle in *Escherichia coli*. J Mol Biol. 2010;397:893–905.
35. Duetz WA. Microtiter plates as mini-bioreactors: miniaturization of fermentation methods. Trends Microbiol. 2007;15:469–75.
36. Marbach A, Bettenbrock K. *lac* operon induction in *Escherichia coli*: systematic comparison of IPTG and TMG induction and influence of the transacetylase LacA. J Biotechnol. 2012;157:82–8.
37. Katzke N, Arvani S, Bergmann R, Circolone F, Markert A, Svensson V, Jaeger KE, Heck A, Drepper T. A novel T7 RNA polymerase dependent expression system for high-level protein production in the phototrophic bacterium *Rhodobacter capsulatus*. Protein Expr Purif. 2010;69:137–46.
38. Drepper T, Huber R, Heck A, Circolone F, Hillmer AK, Büchs J, Jaeger KE. Flavin mononucleotide-based fluorescent reporter proteins outperform green fluorescent protein-like proteins as quantitative in vivo real-time reporters. Appl Environ Microbiol. 2010;76:5990–4.
39. Hanahan D. Studies on transformation of *Escherichia-Coli* with plasmids. J Mol Biol. 1983;166:557–80.
40. Sambrook J, Fritsch EF, Maniatis T, Laboratory CS. Molecular cloning: a laboratory manual. 2nd ed. New York: Cold Spring Harbor Laboratory Press; 1989.
41. Wingen M, Potzkei J, Endres S, Casini G, Rupprecht C, Fahlke C, Krauss U, Jaeger KE, Drepper T, Gensch T. The photophysics of LOV-based fluorescent proteins–new tools for cell biology. Photochem Photobiol Sci. 2014;13:875–83.
42. Wilms B, Hauck A, Reuss M, Syldatk C, Mattes R, Siemann M, Altenbuchner J. High-cell-density fermentation for production of L-N-carbamoylase using an expression system based on the *Escherichia coli rhaBAD* promoter. Biotechnol Bioeng. 2001;73:95–103.
43. Losen M, Frolich B, Pohl M, Buchs J. Effect of oxygen limitation and medium composition on Escherichia coli fermentation in shake-flask cultures. Biotechnol Prog. 2004;20:1062–8.
44. Diederichs S, Korona A, Staaden A, Kroutil W, Honda K, Ohtake H, Buchs J. Phenotyping the quality of complex medium components by simple online-monitored shake flask experiments. Microb Cell Fact. 2014;13(1):1.
45. Sakakibara J, Adrian RJ. Whole field measurement of temperature in water using two-color laser induced fluorescence. Exp Fluids. 1999;26:7–15.
46. Kunze M, Lattermann C, Diederichs S, Kroutil W, Büchs J. Minireactor-based high-throughput temperature profiling for the optimization of microbial and enzymatic processes. J Biol Eng. 2014;8:22.

II.5 Versatility of light-control

II.5.1 Light-controlled Corynebacterium cell factories

Light-controlled cell factories – Employing photocaged IPTG for light-mediated optimization of *lac*-based gene expression and valencene biosynthesis in *Corynebacterium glutamicum*

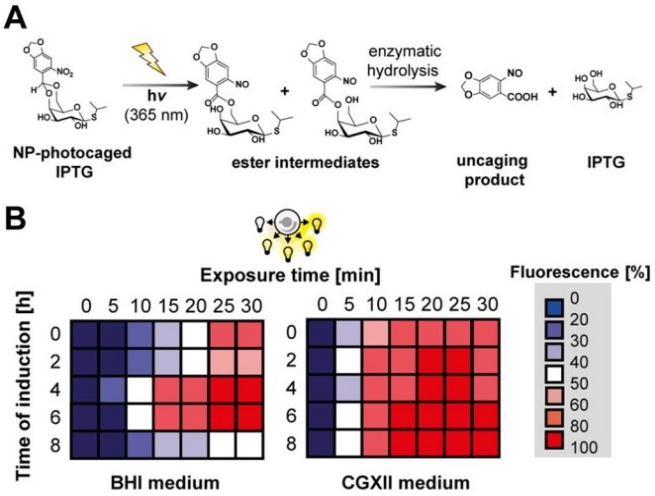

Dennis Binder, Jonas Frohwitter, Regina Mahr, Claus Bier, Alexander Grünberger, Anita Loeschcke, Petra Peters-Wendisch, Dietrich Kohlheyer, Jörg Pietruszka, Julia Frunzke, Karl-Erich Jaeger, Volker Wendisch and Thomas Drepper

Appl Env Microbiol 2016; doi: 10.1128/AEM.01457-16

The full online version may be found at:
http://dx.doi.org/10.1128/AEM.01457-16

For the complete supporting information see Appendix (**Chapter V.7**) turn to page **270.**

AMERICAN SOCIETY FOR MICROBIOLOGY | Applied and Environmental Microbiology

Parales | Biotechnology | T

Light-Controlled Cell Factories: Employing Photocaged Isopropyl-β-D-Thiogalactopyranoside for Light-Mediated Optimization of *lac* Promoter-Based Gene Expression and (+)-Valencene Biosynthesis in *Corynebacterium glutamicum*

Dennis Binder,[a] Jonas Frohwitter,[b] Regina Mahr,[c] Claus Bier,[d] Alexander Grünberger,[c] Anita Loeschcke,[a] Petra Peters-Wendisch,[b] Dietrich Kohlheyer,[c] Jörg Pietruszka,[c,d] Julia Frunzke,[c] Karl-Erich Jaeger,[a,c] Volker F. Wendisch,[b] Thomas Drepper[a]

Institute of Molecular Enzyme Technology, Heinrich-Heine-University D sseldorf, Forschungszentrum J lich, J lich, Germany[a]; Chair of Genetics of Prokaryotes, Faculty of Biology & CeBiTec, Bielefeld University, Bielefeld, Germany[b]; Institute of Bio- and Geosciences, IBG-1: Biotechnology, Forschungszentrum J lich, J lich, Germany[c]; Institute for Bioorganic Chemistry, Heinrich-Heine-University D sseldorf, Forschungszentrum J lich, J lich, Germany[d]

ABSTRACT

Precise control of microbial gene expression resulting in a defined, fast, and homogeneous response is of utmost importance for synthetic bio(techno)logical applications. However, even broadly applied biotechnological workhorses, such as *Corynebacterium glutamicum*, for which induction of recombinant gene expression commonly relies on the addition of appropriate inducer molecules, perform moderately in this respect. Light offers an alternative to accurately control gene expression, as it allows for simple triggering in a noninvasive fashion with unprecedented spatiotemporal resolution. Thus, optogenetic switches are promising tools to improve the controllability of existing gene expression systems. In this regard, photocaged inducers, whose activities are initially inhibited by light-removable protection groups, represent one of the most valuable photoswitches for microbial gene expression. Here, we report on the evaluation of photocaged isopropyl-β-D-thiogalactopyranoside (IPTG) as a light-responsive control element for the frequently applied *tac*-based expression module in *C. glutamicum*. In contrast to conventional IPTG, the photocaged inducer mediates a tightly controlled, strong, and homogeneous expression response upon short exposure to UV-A light. To further demonstrate the unique potential of photocaged IPTG for the optimization of production processes in *C. glutamicum*, the optogenetic switch was finally used to improve biosynthesis of the growth-inhibiting sesquiterpene (+)-valencene, a flavoring agent and aroma compound precursor in food industry. The variation in light intensity as well as the time point of light induction proved crucial for efficient production of this toxic compound.

IMPORTANCE

Optogenetic tools are light-responsive modules that allow for a simple triggering of cellular functions with unprecedented spatiotemporal resolution and in a noninvasive fashion. Specifically, light-controlled gene expression exhibits an enormous potential for various synthetic bio(techno)logical purposes. Before our study, poor inducibility, together with phenotypic heterogeneity, was reported for the IPTG-mediated induction of *lac*-based gene expression in *Corynebacterium glutamicum*. By applying photocaged IPTG as a synthetic inducer, however, these drawbacks could be almost completely abolished. Especially for increasing numbers of parallelized expression cultures, noninvasive and spatiotemporal light induction qualifies for a precise, homogeneous, and thus higher-order control to fully automatize or optimize future biotechnological applications.

Corynebacterium glutamicum represents one of the most important biotechnological platform organisms and massively contributes to the industrial production of amino acids (1–5), but it has also been engineered, for instance, for the production of lower alcohols (6–9), organic acids (10–13), diamines (14, 15), and carotenoids (16–18). However, currently applied expression setups show only moderate performance regarding both precise control and expression homogeneity. Population heterogeneity affecting both growth and expression may strongly impact biotechnological processes (19). For instance, a distinct population heterogeneity has recently been described for *C. glutamicum* cultures producing L-valine (20, 21). While cell-to-cell variations within isogenic populations may constitute an overall fitness advantage over cohabiting competitors (22, 23) in natural environments, such heterogeneity is highly unfavorable in biotechnological production processes (19).

Therefore, an emerging need for novel synthetic expression tools exists that enable homogeneous and higher-order control

Received 14 May 2016 **Accepted** 28 July 2016

Accepted manuscript posted online 12 August 2016

Citation Binder D, Frohwitter J, Mahr R, Bier C, Gr nberger A, Loeschcke A, Peters-Wendisch P, Kohlheyer D, Pietruszka J, Frunzke J, Jaeger K-E, Wendisch VF, Drepper T. 2016. Light-controlled cell factories: employing photocaged isopropyl-β-D-thiogalactopyranoside for light-mediated optimization of *lac*-based gene expression and (+)-valencene biosynthesis in *Corynebacterium glutamicum*. Appl Environ Microbiol 82:000–000. doi:10.1128/AEM.01457-16.

Editor: R. E. Parales, University of California—Davis

Address correspondence to Volker F. Wendisch, volker.wendisch@uni-bielefeld.de, or Thomas Drepper, t.drepper@fz-juelich.de.

D.B. and J.F. contributed equally to this study.

Supplemental material for this article may be found at http://dx.doi.org/10.1128/AEM.01457-16.

over gene expression. Optogenetics, originally devised to control cells, typically neurons in living tissue, that have been genetically modified to express light-sensitive ion channels, now also include the light-mediated control and specific triggering of gene expression in a noninvasive and highly resolving spatiotemporal fashion (24). In contrast to other induction signals, light involves a seemingly homogeneous signal perception for both photosensory modules (25, 26) and chemically synthesized phototriggers, such as photocaged compounds (27, 28), given that cultures are uniformly exposed. Photocaged molecules are rendered biologically inactive through the addition of a photoremovable protection group, also designated a photocaging group or photocage. Specific functionality can be restored easily and noninvasively (i.e., without exerting manipulations that may alter the physiology of cells during ongoing cultivation) by light-mediated release (uncaging) of the bioactive molecule (29, 30).

By means of photocaged isopropyl-β-D-thiogalactopyranoside (IPTG), a conventional *lac* promoter-based gene expression system was recently redirected to enable accurately controlled and homogeneous gene expression by UV-A light in *Escherichia coli* (27). Traditional *lac*-based gene regulation in *C. glutamicum*, however, has limitations, e.g., due to the absence of a lactose uptake system and poor permeability of the *C. glutamicum* membrane for IPTG (31). Therefore, derepression of the *lac* or *tac* promoter using IPTG is often conducted during inoculation (32–34), which prohibits tight and temporally accurate regulation, so that the precise control of toxic gene products or metabolic fluxes is distinctly impeded. In a recent study, for instance, the IPTG-induced production of (+)-valencene, a natural constituent of the essential oils of citrus fruits, faced serious growth impairment in *C. glutamicum* (34). Here, only moderate production could be obtained of this bicyclic sesquiterpenoid, which is used as an additive by the food and beverage industry, due to its pleasant orange-like odor (35, 36).

Within this work, we demonstrate the limitations of IPTG induction in *C. glutamicum* and how to circumvent them during *tac*-based gene expression by using light-responsive photocaged inducer molecules. The established optogenetic expression setup was finally applied to improve production of the sesquiterpene (+)-valencene, despite its growth-impeding properties.

MATERIALS AND METHODS

DNA manipulation and construction of plasmids. DNA techniques and molecular biology methods were performed basically as described previously (37).

Bacterial strains, plasmids, and media. All bacterial strains, plasmids, and oligonucleotides used in this study are listed in Table 1. *E. coli* strains were cultured at 37°C under constant agitation in lysogeny broth (LB) (Luria/Miller; Carl Roth, Karlsruhe, Germany) (37) and supplemented with kanamycin (50 $\mu g \cdot ml^{-1}$) and spectinomycin (250 $\mu g \cdot ml^{-1}$), if required. *C. glutamicum* ATCC 13032 was used as the wild-type strain (38). Cultivations were performed using brain heart infusion (BHI) complex medium (Difco; BD, Heidelberg, Germany) or CGXII minimal medium (39, 40). If appropriate, media were supplemented with 25 $\mu g \cdot ml^{-1}$ kanamycin and 100 $\mu g \cdot ml^{-1}$ spectinomycin.

***C. glutamicum* EYFP expression cultures.** Enhanced yellow fluorescent protein (EYFP) expression cultures were cultivated (800 μl at 1,500 rpm, 85% relative humidity, and 30°C) in a BioLector microbioreactor system (m2p-labs, Germany) under constant monitoring of biomass accumulation and EYFP fluorescence development. Expression cultures were inoculated to cell densities corresponding to an optical density at 600 nm (OD_{600}) of 1.0 for CGXII medium and 0.05 for BHI medium.

Chemical synthesis of NP-photocaged IPTG. 6-Nitropiperonyl (NP)-photocaged IPTG was synthesized in a one-step reaction from IPTG and 6-nitropiperonal, as previously described (27).

Conventional and light induction of gene expression. Conventional IPTG induction was conducted after 0, 2, 4, 6, or 8 h of cultivation via small-volume pipetting. Light-induced expression cultures were directly supplemented with photocaged IPTG (from dimethyl sulfoxide [DMSO] stock solutions, just as for IPTG) prior to cultivation and noninvasively exposed to UV-A light (VL-315.BL hand lamp, 45 W; Vilber Lourmat, France; distance to FlowerPlate, 1.5 cm, approximately 0.9 $mW \cdot cm^{-2}$) at desired time points. Light exposure was varied by using different exposure times (0 to 30 min) or different light intensities experimentally created by dimming the reaction wells with various layers of diffusion foils (White Diffusion Lee 216; Lee Filters, USA). Here, an exposure time of 30 min resulted in full induction. Light intensities were quantified using a thermal power sensor (S302C; Thorlabs, Inc., USA).

(+)-Valencene production cultures. Seed cultures for (+)-valencene production and growth experiments with *C. glutamicum* were performed in 10 ml of LB supplemented with 50 mM glucose at 30°C and 120 rpm in 100-ml nonbaffled flasks. For adaptation of the cells to production conditions, a second seed culture in CGXII minimal medium with 4% glucose monohydrate was inoculated from the LB seed culture and grown for 5 to 6 h (50 ml of CGXII, 500-ml baffled flasks, 30°C, 120 rpm). Both the second seed and the main cultures were inoculated to an OD_{600} of 1. Production and growth experiments were conducted in 48-well FlowerPlates (m2p-labs, Germany) in 800 μl of CGXII medium with 4% glucose monohydrate as the source of carbon at 30°C and 1,200 rpm offline for production or in a BioLector system (m2p-labs) for online monitoring of growth. Production was induced with IPTG 0, 2, 4, and 6 h after inoculation and for NP-photocaged IPTG (cIPTG)-based light induction (see above) 4 and 6 h after inoculation using either 0.1 or 0.25 mM each compound, respectively. After induction, 200 μl of *n*-dodecane was added aseptically to the cultures, which were grown for additional 24 h. After cultivation, the *n*-dodecane layer was harvested by centrifugation at 4°C for 1 to 2 h at 24,000 × *g*. Subsequently, the (+)-valencene content of the *n*-dodecane phase was determined by gas chromatography-mass spectrometry (GC-MS) measurements.

Flow cytometry analysis. Flow cytometry analyses of *C. glutamicum* (43) were performed with a FACSAria II flow cytometer (Becton Dickinson, Heidelberg, Germany) using a blue solid-state laser (Sapphire 488-20) with an excitation wavelength of 488 nm. Cytometer setup and performance tracking were performed with Cytometer Setup 0026 and Tracking Beads (bright [3 mm], mid [3 mm], and dim [2 mm] beads) labeled with a mixture of fluorochromes (Becton Dickinson). Forward-scatter characteristics (FSC) and side-scatter characteristics were detected as small-angle and orthogonal scatters of the 488-nm laser, respectively. EYFP fluorescence was detected using a 502-nm long-pass and a 530/30-nm band-pass filter set. FACSDiva software 6.0 was used to record the measurements. During analyses, thresholding on FSC was applied to remove background noise. Data were analyzed with the FlowJo version 10.0.8 analysis software (Tree Star, Ashland, OR, USA). To stain dead cells, cells with an OD_{600} of approximately 0.05 were incubated with 20 μM propidium iodide (PI) (stock solution, 20 mM in DMSO) (Molecular Probes, Leiden, The Netherlands) for 15 min at room temperature (RT). For validation of the protocol, intact cells and cells with injured membranes (treated with 70% isopropyl alcohol for 30 min) were mixed in different ratios. Afterwards, cells were stained as described above. For the detection of the fluorescent dye PI, a 595-nm long-pass and a 610/20-nm band-pass filter set was used.

Strain construction. The genes *dxs* and *idi* coding for 1-deoxy-D-xylulose-5-phosphate synthase and isopentenyl pyrophosphate (IPP) isomerase, respectively, were PCR amplified using oligonucleotides 1 to 4 (Table 1) from genomic DNA of *C. glutamicum* ATCC 13032, which was isolated as previously described (44). For improved expression, the (+)-valencene synthase gene *CnVS* of *Callitropsis nootkatensis* was codon

TABLE 1 Strains, plasmid, and oligonucleotides used in this study

Strain, plasmid, or oligonucleotide	Relevant characteristics or sequence (5′ →3′)[a]	Reference or source
Strains		
E. coli DH5α	F⁻ *thi-1 endA1 hsdR17*(r⁻ m⁻) *supE44* Δ*lacU169* (Φ80*lacZ*ΔM15) *recA1 gyrA96 relA1*	41
C. glutamicum ATCC 13032	Biotin auxotroph, wild-type strain	38, 42
C. glutamicum EYFP	ATCC 13032(pEKEx2-EYFP)	32
C. glutamicum VLC3	ATCC 13032 Δ*crtE* Δ*idsA*(pVWEx1-*CnVS*)(pEKEx3-*ispA*)	34
C. glutamicum VLC4	ATCC 13032 Δ*crtE* Δ*idsA*(pVWEx1-o*CnVS*)(pEKEx3-*ispA*)	This study
C. glutamicum VLC5	ATCC 13032 Δ*crtE* Δ*idsA*(pVWEx1)(pEKEx3-*ispA-oCnVS*)	This study
C. glutamicum VLC6	ATCC 13032 Δ*crtE* Δ*idsA*(pVWEx1-*dxs-idi*)(pEKEx3-*ispA-oCnVS*)	This study
Plasmids		
pEKEx2-EYFP	Km^r; pEKEx2 containing EYFP with an artificial RBS under the control of P_{tac}	32
pVWEx1	Km^r; *E. coli*/*C. glutamicum* shuttle vector for regulated gene expression (P_{tac}, *lacI*^{q}, pCG1 *ori*V_{Cg})	45
pVWEx1-CnVS	pVWEx1 derivative for IPTG-inducible expression of (+)-valencene synthase gene *CnVS* of *Callitropsis nootkatensis* containing an artificial ribosome binding site	34
pVWEx1-oCnVS	pVWEx1 derivative for IPTG-inducible expression of codon optimized (+)-valencene synthase gene *oCnVS* from *Callitropsis nootkatensis* containing an artificial ribosome binding site	This work
pVWEx1-*dxs-idi*	pVWEx1 derivative for IPTG-inducible expression of 1-deoxy-D-xylulose 5-phosphate synthase (*dxs*) and the isopentenyl pyrophosphate isomerase (*idi*) genes of *Corynebacterium glutamicum*	This work
pEKEx3	Spec^r; *E. coli*/*C. glutamicum* shuttle vector for regulated gene expression (P_{tac}, *lacI*^{q}, pBL1 *ori*V_{Cg})	46
pEKEx3-*ispA*	pEKEx3 derivative for IPTG-inducible expression of FPP synthase gene *ispA* from *E. coli* containing an artificial ribosome binding	34
pEKEx3-*ispA-oCnVS*	pEKEx3 derivative for IPTG-inducible expression of FPP synthase gene *ispA* from *E. coli* and the codon-optimized (+)-valencene synthase gene *oCnVS* from *Callitropsis nootkatensis*	This work
Oligonucleotides		
(1) dxs_fwd	CCTGCAGGTCGACTCTAGAG**AGGAGG**CCCTTCAGATGGGAATTCTGAACAG	
(2) dxs_rev	CCCTAAGCTTAGACATCTGAAGGG**CCTCCT**TTATTCCCCGAACAGGG	
(3) idi_fwd	CCCTGTTCGGGGAATAA**AGGAGG**CCCTTCAGATGTCTAAGCTTAGGG	
(4) idi_rev	CGAGCTCGGTACCCGGGGATCTTACTCTGCGTCAAACGCTTCC	
(5) ispA_fwd	CCTGCAGGTCGACTCTAGAG**AGGAGG**CCCTTCAGATGGACTTTCCGCAGC	
(6) ispA_rev	CGTTGAACATTTCCGCCATATGAAGGG**CCTCCT**TTATTTATTACGCTGGATGATG	
(7) oCnVS_fwd	CATCATCCAGCGTAATAAATAA**AGGAGG**CCCTTCATATGGCGGAAATGTTCAACG	
(8) oCnVS_rev	CGAGCTCGGTACCCGGGGATCTTACGGGATGATCGGTTCCACG	

[a] Artificial ribosome binding site sequences are in bold type within oligonucleotide sequences. Km^r, kanamycin resistance; Spec^r, spectinomycin resistance; RBS, ribosome binding site.

optimized for *C. glutamicum* ATCC 13032 using a codon usage protocol provided by http://www.kazusa.or.jp/codon/ and synthesized by GeneArt/Life Technologies (Darmstadt, Germany), yielding the gene *oCnVS* (see the supplemental material). The farnesyl pyrophosphate synthase gene *ispA* was PCR amplified from genomic DNA of *E. coli* as described previously (34). All genes were cloned into the expression vector pVWEx1 (45) or pEKEx3 (46) by Gibson assembly (47) using the BamHI restriction site and the respective oligonucleotides shown in Table 1. Primers were constructed such that an artificial ribosomal binding site (AGGAGG) was added 8 bp upstream of the translational start codon of each gene. The integrity of all inserts was confirmed by sequencing (Sequencing Core Facility, Bielefeld University).

GC-MS measurements. The harvested *n*-dodecane phases of the production cultures were analyzed using a Thermo Scientific Trace GC Ultra connected to a Thermo Scientific ISQ single quadrupole mass spectrometer using a TG-5MS column (length, 30 m; inside diameter [i.d.], 0.25 mm; film thickness, 0.25 μm) (Thermo Scientific, Waltham, MA, USA). After splitless injection of 1 μl, the initial temperature of 40°C was increased by 10°C/min to 160°C and then by 15°C/min to 300°C, with a 2-min ramp at 300°C at the end of the measurement and a constant helium gas flow rate of 1 ml/min. The MS operating parameters were ionization voltage, 70 eV (electron impact ionization); and ion source and interface temperature, 230°C. (+)-Valencene was identified by the comparison of retention time and mass spectrum to technical (+)-valencene (Sigma-Aldrich, Steinheim, Germany). For quantitative analysis of (+)-valencene, a calibration curve with technical (+)-valencene was used.

RESULTS

Establishing NP-photocaged IPTG-based light induction in *C. glutamicum*. In a previous study, NP-photocaged IPTG (cIPTG) was employed in *E. coli* to noninvasively control gene expression by light in a gradual and homogeneous fashion (27). Here, we aimed to transfer the photoswitch to the biotechnological workhorse *C. glutamicum* to generate an easily light-addressable induction system applicable for various biotechnological purposes. The frequently applied IPTG-inducible *tac* promoter-based pEKEx expression vector (44, 48) was chosen as a target system for cIPTG-mediated light induction. To characterize the light responsiveness of gene expression in *C. glutamicum*, the pEKEx2-EYFP (32) expression vector was employed, allowing online monitoring of induction processes in batch cultures, as well as at the single-cell level by means of EYFP reporter fluorescence.

We first determined key system specifications, namely, (i) the inducibility of the *tac* promoter at different time points during cultivation, (ii) the maximum expression levels, and (iii) the respective dynamic range of induction. cIPTG, which efficiently re-

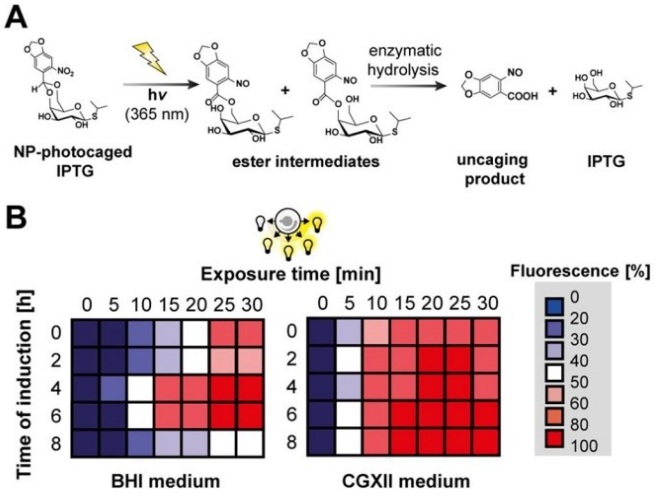

FIG 1 Light-controlled gene expression in *C. glutamicum* using cIPTG as a photoswitch. (A) Two-step release of IPTG from cIPTG by UV-A light-mediated photocleavage and enzymatic hydrolysis of photoproduct esters as described by Young and Deiters (49). (B) Gradual upregulation of EYFP expression in *C. glutamicum* ATCC 13032 (pEKEx2-EYFP) depending on the time of UV-A light exposure (λ_{max} = 365 nm, 0.9 mW · cm^{-2}) using BHI complex (left) or CGXII-glucose minimal medium (right) supplemented with 100 μM cIPTG. Relative EYFP fluorescence values originate from biomass-normalized triplicates and depict low (blue) to high (red) EYFP fluorescence intervals after 20 h of overexpression. Color gradations represent differential expression outputs obtained by variation of induction time or UV-A light exposure. Maximum biomass-normalized fluorescence values obtained in both media are means of triplicates and were arbitrarily set to 100%. h*v*, light energy.

leases IPTG in a two-step photocleavage reaction (49) upon short UV-A light exposure and subsequent enzymatic hydrolysis of the photoproduct esters (Fig. 1A), was added to EYFP expression cultures. To test the light induction of EYFP expression at different growth phases of *C. glutamicum*, cultures were illuminated at different time points of cell growth (0 to 8 h) during cultivation in BHI complex and CGXII minimal medium. Moreover, the irradiation dose was increased stepwise by extending the time of light exposure (0 to 30 min) in order to evaluate the gradual responsiveness of the chosen expression system. The EYFP production profiles clearly demonstrated that cIPTG can be used as a photoswitch enabling light induction of gene expression in *C. glutamicum* in a gradual manner and over a long period of cultivation (Fig. 1B). In BHI complex medium, full inducibility and maximal dynamic range (i.e., an expression range of 0 to 100%) were obtained by increasing the exposure time after 4 to 6 h of cultivation (corresponding to the mid-exponential-growth phase; see Fig. S1 in the supplemental material). Induction in the lag or early exponential phase (0 to 2 h; 0 to 80% expression output) as well as in the late-exponential phase (8 h; 0 to 50% expression output) still resulted in a gradual light response of EYFP expression but impaired the dynamic range. In CGXII minimal medium, light induction produced expression outputs corresponding properly to the exposure time at all monitored induction time points. UV-A light exposure times of 20 to 25 min at moderate intensities (0.9 mW · cm^{-2}) were sufficient to fully induce gene expression in BHI and CGXII medium.

Comparative analysis of EYFP expression in *C. glutamicum* using conventional IPTG and cIPTG-based light induction. In a next step, cIPTG-based light induction of gene expression was compared to conventional IPTG induction using the same EYFP reporter system (pEKEx2-EYFP). EYFP output signals were measured depending on different induction time points (0 to 8 h) over the course of a following overexpression period (0 to 20 h) in both BHI and CGXII media. To directly compare conventional and light induction, the EYFP fluorescence ratios determined after cIPTG (30-min light exposure, 100 μM) and IPTG induction (100 μM) are shown as heat maps (Fig. 2). In BHI medium (Fig. 2A), IPTG induction was similar to or slightly outperformed light-dependent cIPTG induction in the lag and early exponential-growth phases (0 to 2 h). In contrast, upon induction in the mid- or late-exponential phase (4 to 8 h), cIPTG outperformed conven-

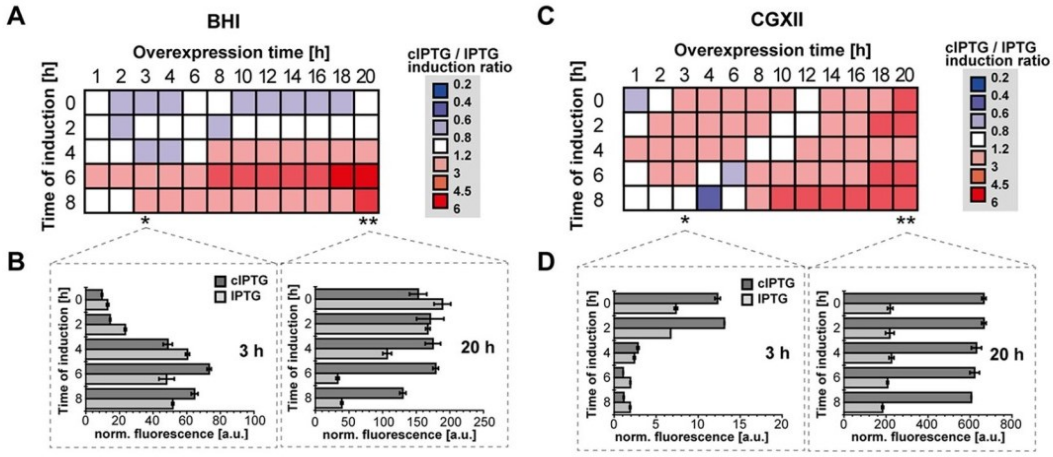

FIG 2 Comparative analysis of IPTG and cIPTG induction of *tac* promoter-mediated EYFP expression in *C. glutamicum* ATCC 13032 (pEKEx2-EYFP). Fluorescence ratio intervals of cIPTG- (30 min UV-A, 100 μM) and IPTG-induced (100 μM) EYFP fluorescence are shown during cultivation in BHI complex (A) and CGXII-glucose minimal medium (C) depending on the time of induction and on overexpression times. Fluorescence ratios originate from biomass-normalized triplicates and depict low (blue, superior IPTG induction) to high (red, superior cIPTG induction) ratio intervals in color gradations. Bar plots indicate individual biomass-normalized (norm.) fluorescence values (in arbitrary units [a.u.]) as means of triplicates after 3 h (left) and 20 h (right) of IPTG- (gray) and cIPTG-induced (dark gray) EYFP expression in BHI complex (B) and CGXII-glucose minimal medium (D). Error bars indicate the respective standard deviations.

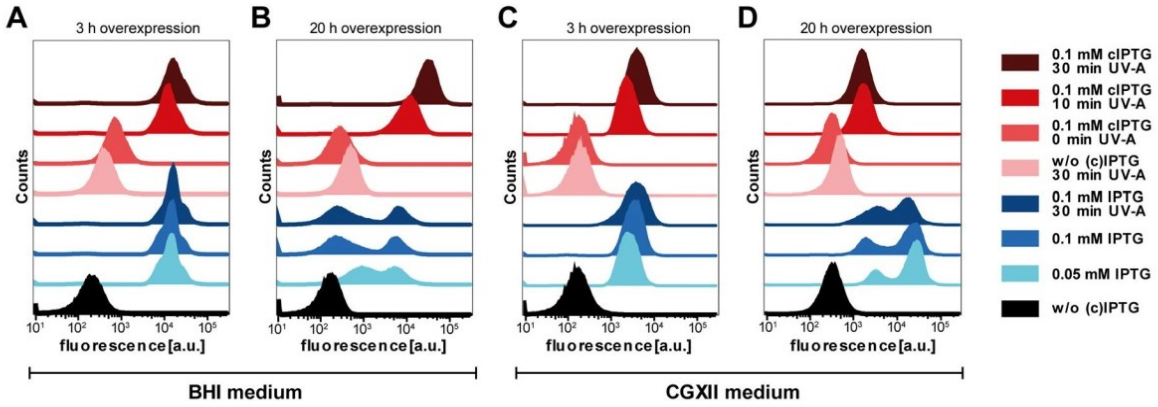

FIG 3 Flow cytometric single-cell analysis of gene expression induced by IPTG and cIPTG in *C. glutamicum* ATCC 13032 (pEKEx2-EYFP). Distribution of EYFP fluorescence intensities was plotted against the number of cells (counts). Expression cultures were compared in BHI complex (A and B) and CGXII-glucose minimal medium (C and D), and fluorescence was measured after 3 h (A and C) and 20 h (B and D) of EYFP overexpression and induction with IPTG and light after 5 h of cultivation. For light induction, cells were exposed to UV-A light (λ_{max} = 365 nm) for 10 and 30 min, respectively, with a light intensity of 0.9 mW · cm^{-2}.

tional IPTG, particularly after overexpression periods longer than 8 h. Significant effects were observed for induction after 6 h of cultivation, where light induction produced an expression output up to 6-fold higher than induction with conventional IPTG after 18 h of overexpression. Besides the evaluation of relative effects, a description of individual absolute fluorescence outputs provides insights into system-inherent specifications. In this sense, the initial inducibility of the *tac* promoter in *C. glutamicum* cultures during early to late-logarithmic-growth phases, which was determined 3 h after induction (Fig. 2B, left), showed that the velocity of induction increases with ongoing cultivation time for both IPTG and cIPTG. Here, only a slight improvement in light induction could be observed for mid- to late-logarithmic-growth phases (6 to 8 h). For longer expression times (in particular after 20 h of target gene expression), however, light-mediated induction of mid- to late-logarithmic *C. glutamicum* cultures (6 to 8 h) using cIPTG resulted in much higher EYFP expression than that with conventional induction (Fig. 2B, right).

In CGXII medium (Fig. 2C), light induction can effectively be applied for a broad range of induction time points from early to late-exponential phases and outperformed conventional IPTG induction up to 4-fold for overexpression periods greater than 12 h. For late-exponential induction (6 to 8 h), IPTG initially performed well but was outpaced by cIPTG with increasing cultivation times. In contrast to BHI medium, the expression response in CGXII medium is significantly slower for both IPTG and cIPTG, as depicted by low fluorescence levels after 3 h of EYFP overexpression (Fig. 2D, left). After 20 h of overexpression (Fig. 2D, right), however, considerable EYFP fluorescence was observed especially for light induction, which outperformed conventional IPTG induction up to 3-fold. Strikingly, expression outputs for both cIPTG- and IPTG-mediated induction were, contrary to cultivations in BHI medium and irrespective of the time of induction, highest at the end of the experiment (Fig. 2D, right).

Basal background levels (see Fig. S2 in the supplemental material) using nonexposed cIPTG were found to be moderate in BHI medium (up to 1.5-fold increase in comparison to control strains) and CGXII medium (up to 2.2-fold). As reported in the literature (50), basal expression levels of the system used here were found to be elevated in CGXII minimal medium and increased with ongoing cultivation times. The dynamic range of induction, however, was high and comparable in BHI medium (63-fold for cIPTG and 61-fold for IPTG). In CGXII minimal medium, light induction was higher than conventional IPTG induction (239-fold compared to 46-fold, respectively; see Fig. S3 in the supplemental material).

In summary, the comparative analysis of cIPTG and IPTG induction in BHI and CGXII media showed that noninvasive light induction is broadly applicable in *C. glutamicum*. Particularly, light induction during mid- to late-exponential growth significantly outperformed conventional IPTG induction up to 6-fold. Moreover, for long overexpression periods of up to 20 h, cIPTG persistently proved to be as efficient as equimolar amounts of IPTG. Interestingly, despite a slightly delayed induction response caused by the essential enzymatic cleavage of the photoproducts (Fig. 1A), cIPTG-based light induction was comparable to IPTG induction in *C. glutamicum* and temporally even outperformed the conventional induction response for late induction in BHI and early induction in CGXII medium.

Single-cell analysis of EYFP expression after induction with IPTG and cIPTG. As cIPTG-dependent light induction was successfully demonstrated for standard bulk cultivations in both BHI complex and CGXII minimal media, light- and IPTG-induced gene expression was next analyzed at the single-cell level in order to analyze the homogeneity of expression behavior within *C. glutamicum* batch cultures. To this end, the fluorescence of single cells from conventional and light-induced cultures was monitored by flow cytometry. Single-cell EYFP fluorescence values for cultures induced with light after 5 h of cultivation (light- to deep-red-colored histograms) showed a homogeneous distribution after both 3 h (Fig. 3A and C) and 20 h (Fig. 3B and D) of overexpression in BHI (Fig. 3A and B) and CGXII media (Fig. 3C and D). For IPTG induction (light- to deep-blue-colored histograms), however, a heterogeneous fluorescence distribution was observed with increasing expression time in both media. Surprisingly, the two media differently influenced the expression phenotype of the IPTG-induced *C. glutamicum* expression strain. In BHI medium, a second population with lower fluorescence intensity occurred

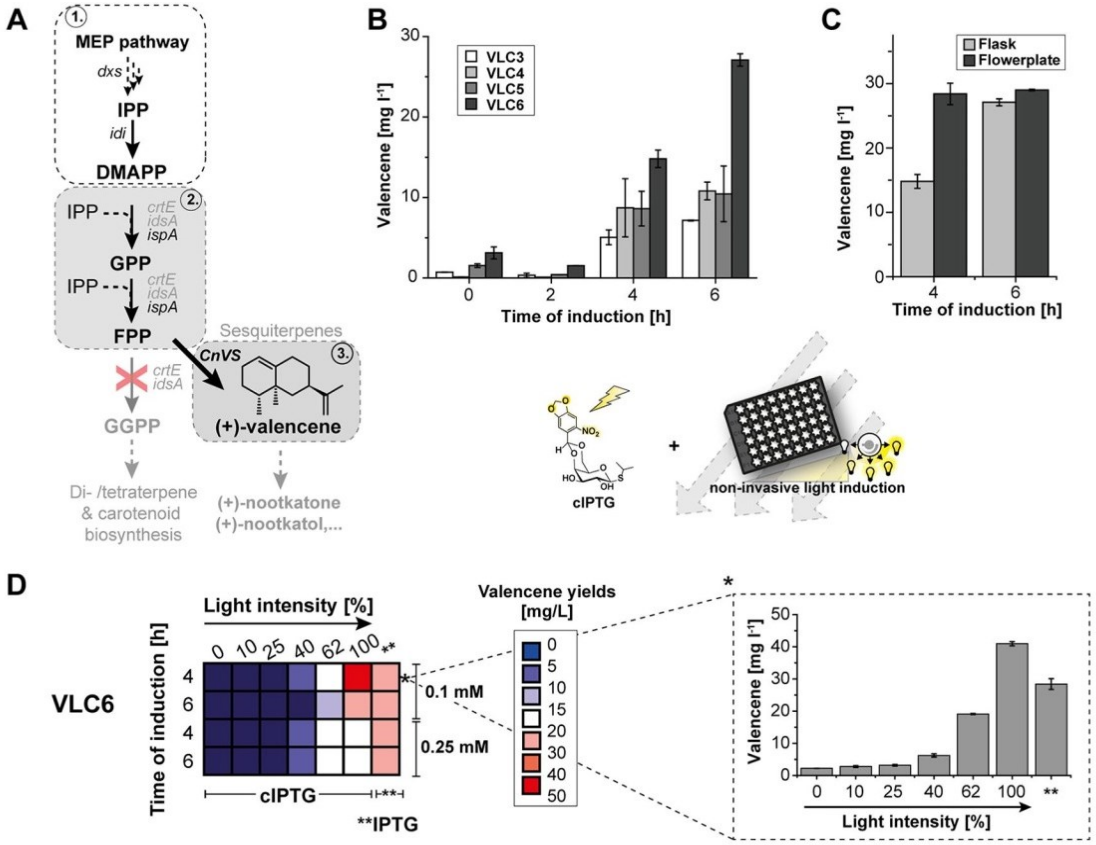

FIG 4 Light-controlled (+)-valencene production in *C. glutamicum* using CGXII-glucose medium. (A) Biosynthetic route for (+)-valencene production (3) based on the MEP pathway (1) and appropriate isoprenoid pathway gene deletions for improved FPP precursor supply (2). To improve the metabolic flux toward FPP, the heterologous gene *ispA* and, at a later stage, the endogenous genes *dxs* and *idi*, were overexpressed. (B) Screening of engineered *C. glutamicum* strains VLC3 to VLC6 for (+)-valencene productivity upon IPTG induction (0.1 mM) after different induction time points. (C) (+)-Valencene production upon IPTG induction (0.1 mM) by strain VLC6 grown for 24 h in a flask (light gray) and FlowerPlate (dark gray). (D) (+)-Valencene productivity profiles (left) indicating valencene titer intervals from low (blue) to high (red) in milligrams per liter after 24 h of production with VLC6 using different times of induction as well as different (c)IPTG concentrations (0.1 and 0.25 mM). Light intensities were incremented in a stepwise manner (100% here correlates to 0.9 mW · cm^{-2}). The results obtained for induction after 4 h with 0.1 mM cIPTG marked with an asterisk are shown in more detail on the right. Double asterisks indicate control experiments with IPTG induction. All averaged data originated from the results of at least three independent biological triplicates. MEP, methylerythritol phosphate; IPP, isopentenyl pyrophosphate; DMAPP, dimethylallyl pyrophosphate; GPP, geranyl pyrophosphate; FPP, farnesyl pyrophosphate; GGPP, geranylgeranyl pyrophosphate. Error bars indicate the respective standard deviations.

after 20 h of overexpression, whereas prolonged expression in CGXII medium obviously resulted in the formation of a second population with increased YFP accumulation. In principle, expression heterogeneity has recently been described for a similar expression setup in *C. glutamicum* (50). Notably, flow cytometric single-cell analysis using propidium iodide-based LIVE/DEAD staining (43) further suggested that light induction did not affect membrane integrity and thus cell viability (see Fig. S4 in the supplemental material).

In summary, cIPTG-based light control of gene expression in *C. glutamicum* was shown to distinctly outperform conventional IPTG induction with respect to maximum expression levels, responsiveness, homogeneity, and inducibility, especially for longer expression periods.

Employing cIPTG for the production of the toxic sesquiterpene (+)-valencene. As a challenging task, we tried to apply the light-controlled expression setup to improve the biosynthesis of the bacterial growth-inhibiting terpenoid (+)-valencene. A *C. glutamicum* strain producing (+)-valencene was recently constructed by metabolic engineering (34). Here, we first analyzed whether (+)-valencene production could be further elevated via metabolic engineering (Fig. 4A). The initial strain *C. glutamicum* VLC3 carries deletions of the *crtE* and *idsA* genes to preclude formation of the undesired geranylgeranyl pyrophosphate (GGPP). Farnesyl pyrophosphate (FPP) was synthesized by the FPP synthase IspA from *E. coli*. FPP, in turn, is converted to (+)-valencene via the (+)-valencene synthase CnVS from *Callitropsis nootkatensis* (35). In the newly constructed (+)-valencene producer strain VLC4, the CnVS-encoding gene was expressed after its adaptation to the codon usage of *C. glutamicum*. In strain VLC6, the genes coding for IspA and CnVS were combined on a single vector, allowing the introduction of a second IPTG-inducible vector for overexpression of the genes encoding the 1-deoxy-D-xylulose 5-phosphate synthase (*dxs*) and isopentenyl pyrophosphate isomerase (*idi*) to enhance the supply of the precursors isopentenyl pyrophosphate (IPP) and dimethylallyl pyrophosphate (DMAPP) (18), and consequently, of FPP. Since CnVS gene expression perturbed growth, we presumed that the optimization

and timing of CnVS expression would be one key aspect to elevate (+)-valencene production (Fig. 4A) and hence, an appealing target for cIPTG-based light control. Therefore, (+)-valencene accumulation was first monitored in flask cultivations using the primary VLC3 producer strain, as well as our newly constructed producers VLC4 to -6 (Table 1) upon conventional induction of gene expression after different cultivation times (0 to 6 h). Cultivation in shake flasks revealed that the time of induction was crucial for (+)-valencene productivity, as the (+)-valencene titers in all four tested strains were largely improved when induced after 4 and 6 h (Fig. 4B). Moreover, after 6 h of induction, VLC4 with the codon-optimized valencene synthase (oCnVS) showed slightly increased production of (+)-valencene up to 1.5-fold (10.8 ± 1.1 mg · liter^{-1}) compared to that with VLC3 (7.2 ± 0.6 mg · liter^{-1}). In contrast, the coexpression of *ispA* and oCnVS genes from a single plasmid in VLC5 showed only a negligible influence on titer (10.5 ± 3.5 mg · liter^{-1}).

Notably, additional overexpression of *dxs* and *idi* in VLC6 led to 3.8-fold-improved (+)-valencene production (27.1 ± 0.6 mg · liter^{-1}). The production of (+)-valencene by VLC6 was further characterized at a microtiter plate scale using 48-well FlowerPlates (51, 52). With this approach, (+)-valencene production was further enhanced when induced after 4 h and slightly after 6 h (Fig. 4C). Here, improved valencene titers could be attributed to the fact that oxygen-unlimited FlowerPlate cultivations yielded up to 2-fold-higher biomass formation (see Table S1 in the supplemental material). Next, we analyzed whether light-mediated induction with cIPTG could further optimize the (+)-valencene production level by applying different light regimes, cIPTG concentrations, and induction time points (Fig. 4D, left).

Variable light control of (+)-valencene production led to 1.4-fold elevated (+)-valencene titers compared to those with conventional IPTG induction. Optimal productivity was found for full light induction (i.e., 100% light intensity = 0.9 mW · cm^{-2}) after 4 h of cultivation using 0.1 mM cIPTG (Fig. 4D, left) and yielded final titers of 41.0 ± 0.1 mg · liter^{-1}. During (+)-valencene production, IPTG-induced *dxs-idi* overexpression in VLC6 was found to significantly lower growth rates up to 30% (μ_{max} = 0.29 ± 0.01 · h^{-1}) compared to those with noninduced cultures (μ_{max} = 0.42 ± 0.01 · h^{-1}). Compared to expression cultures that have been induced by IPTG, growth impairment could partly be abolished using cIPTG (μ_{max} = 0.34 ± 0.01 · h^{-1}). However, cell growth was still hampered by cIPTG induction, since noninduced cultures still exhibited an approximately 20% higher growth rate (see Fig. S5 in the supplemental material). Much larger growth differences in light and IPTG-induced production cultures were observed for early induction (see Fig. S6 in the supplemental material).

By applying cIPTG-based light-controlled screening for optimized expression parameters, we were able to significantly elevate (+)-valencene titers in *C. glutamicum* approximately 6-fold, from an initial 7.2 mg · liter^{-1} to 41.0 mg · liter^{-1}. The combination of metabolic engineering and light-controlled expression resulted in an about 17-fold improved (+)-valencene production compared to a titer of 2.4 mg · liter^{-1} reported in our previous study.

DISCUSSION

This study demonstrates optogenetic control of microbial gene expression as a valuable tool for synthetic bio(techno)logical applications. Photocaged carbohydrates (27, 28), for instance, can be readily transferred to different biotechnological production hosts and employed to precisely control gene expression in a straightforward and spatiotemporal fashion. Moreover, photocaged carbohydrate inducers seem to abrogate native expression heterogeneity because their increased membrane permeability may supersede uptake by specific transport systems or by poor diffusion. A homogeneous expression response was shown here for NP-photocaged IPTG in *C. glutamicum*, as well as in a recent study employing photocaged arabinose in *E. coli* (28). Furthermore, the fact that the strong light induction response was independent of cellular states enables appropriate biomass production, which is essential for several complex biosynthetic procedures and especially those leading to the production of toxic compounds. Noninvasive and gradual upregulation of gene expression by light, moreover, provides a fast and easy option to screen for optimized expression conditions, rendering time-consuming and invasive inducer supplementation obsolete. The established optogenetic expression modules can thus be applied in novel photomicrobioreactors (53) and single-cell cultivation platforms (19) to precisely control the expression of target genes and thereby fully automatize the optimization of microbial production processes in a high-throughput fashion. Notably, cIPTG-based light induction requires elevated expenditures of costs and labor and is further unsuited for large-scale fermentations where light exposure poses an additional challenge. However, especially for closed (e.g., anaerobic) systems and increasing numbers of parallelized expression cultures, noninvasive and spatiotemporal light induction will provide a higher-order control.

For the light-controlled (+)-valencene production in this study, light induction facilitated the optimal balance between growth and production (see Fig. S6 in the supplemental material) and provided stronger gene expression levels in CGXII (Fig. 2D) and thus efficient gene expression for late induction. Noteworthy, those improvements could not be reproduced by optimizing conventional IPTG induction with respect to inducer concentration (see Fig. S7 in the supplemental material). Finally, for the light-controlled expression system using the best (+)-valencene-producing strain, *C. glutamicum* VLC6, a titer of 41.0 mg · liter^{-1} and volumetric productivity of 1.46 mg · liter^{-1} · h^{-1} were obtained (see Table S1 in the supplemental material). These values are in the same range as those obtained with other bacteria and higher than those obtained with eukaryotic microorganisms. To the best of our knowledge, the highest titers and volumetric (+)-valencene productivities so far were described for *Rhodobacter sphaeroides* expressing the mevalonate operon from *Paracoccus zeaxanthinifaciens* and the codon-optimized (+)-valencene synthase CnVS, which reached a titer of 352 mg · liter^{-1} and a productivity of 4.88 mg · liter^{-1} · h^{-1} (35). The yeasts *Saccharomyces cerevisiae* (titer, 1.36 mg · liter^{-1}; productivity, 18 μg · liter^{-1} · h^{-1}), *Schizophyllum commune* (titer, 16.6 mg · liter^{-1}; productivity, 115 μg · liter^{-1} · h^{-1}), and *Pichia pastoris* (titer, 51 mg · liter^{-1}; productivity, 1 mg · liter^{-1} · h^{-1}), however, proved suitable for the *in situ* conversion of (+)-valencene to more valuable products, such as (+)-nootkatone (35, 54, 55).

Future improvements in (+)-valencene production by *C. glutamicum* might include further engineering of FPP biosynthesis and process optimization by, e.g., fed-batch cultivation with glucose or alternative carbon sources feeding directly into the methylerythritol phosphate (MEP) pathway. Moreover, the temporal decoupling and thus independent regulation of FPP and (+)-va-

lencene biosynthetic pathways, e.g., by means of multichromatic optogenetic control (26, 56, 57), might offer potential for debottlenecking, further optimizing the metabolic flux toward (+)-valencene biosynthesis. To realize future metabolic flux engineering and uncoupled just-in-time gene expression, novel molecular tools have to be developed (58, 59). Here, alternative *C. glutamicum* expression systems based on anhydrotetracycline, arabinose, or propionate might be interesting targets for future light-controlled expression setups (60–62).

ACKNOWLEDGMENTS

This work was supported by grants from the Federal Ministry of Education and Research (OptoSys, FKZ 031A167) and the Ministry of Innovation, Science and Research of North-Rhine Westphalia and German Research Foundation (INST 208/654-1 FUGG).

We thank Nadine Katzke and Katrin Troost for advice on the initial GC measurements and terpenoid biosynthesis.

FUNDING INFORMATION

This work, including the efforts of Karl-Erich Jaeger, was funded by Deutsche Forschungsgemeinschaft (DFG) (INST 208/654-1 FUGG). This work, including the efforts of Dennis Binder, Regina Mahr, and Claus Bier, was funded by Bundesministerium für Bildung und Forschung (BMBF) (OptoSys FKZ 031A167).

REFERENCES

1. **Park SH, Kim HU, Kim TY, Park JS, Kim S-S, Lee SY.** 2014. Metabolic engineering of *Corynebacterium glutamicum* for L-arginine production. Nat Commun **5**:4618. http://dx.doi.org/10.1038/ncomms5618.
2. **Mahr R, Gätgens C, Gätgens J, Polen T, Kalinowski J, Frunzke J.** 2015. Biosensor-driven adaptive laboratory evolution of L-valine production in *Corynebacterium glutamicum*. Metab Eng **32**:184–194. http://dx.doi.org/10.1016/j.ymben.2015.09.017.
3. **Wendisch VF.** 2014. Microbial production of amino acids and derived chemicals: synthetic biology approaches to strain development. Curr Opin Biotechnol **30**:51–58. http://dx.doi.org/10.1016/j.copbio.2014.05.004.
4. **Eggeling L, Bott M.** 2015. A giant market and a powerful metabolism: L-lysine provided by *Corynebacterium glutamicum*. Appl Microbiol Biotechnol **99**:3387–3394. http://dx.doi.org/10.1007/s00253-015-6508-2.
5. **Jensen JVK, Wendisch VF.** 2013. Ornithine cyclodeaminase-based proline production by *Corynebacterium glutamicum*. Microb Cell Fact **12**:63. http://dx.doi.org/10.1186/1475-2859-12-63.
6. **Blombach B, Riester T, Wieschalka S, Ziert C, Youn J-W, Wendisch VF, Eikmanns BJ.** 2011. *Corynebacterium glutamicum* tailored for efficient isobutanol production. Appl Environ Microbiol **77**:3300–3310. http://dx.doi.org/10.1128/AEM.02972-10.
7. **Niimi S, Suzuki N, Inui M, Yukawa H.** 2011. Metabolic engineering of 1,2-propanediol pathways in *Corynebacterium glutamicum*. Appl Microbiol Biotechnol **90**:1721–1729. http://dx.doi.org/10.1007/s00253-011-3190-x.
8. **Siebert D, Wendisch VF.** 2015. Metabolic pathway engineering for production of 1,2-propanediol and 1-propanol by *Corynebacterium glutamicum*. Biotechnol Biofuels **8**:91. http://dx.doi.org/10.1186/s13068-015-0269-0.
9. **Jojima T, Noburyu R, Sasaki M, Tajima T, Suda M, Yukawa H, Inui M.** 2015. Metabolic engineering for improved production of ethanol by *Corynebacterium glutamicum*. Appl Microbiol Biotechnol **99**:1165–1172. http://dx.doi.org/10.1007/s00253-014-6223-4.
10. **Litsanov B, Brocker M, Bott M.** 2012. Toward homosuccinate fermentation: metabolic engineering of *Corynebacterium glutamicum* for anaerobic production of succinate from glucose and formate. Appl Environ Microbiol **78**:3325–3337. http://dx.doi.org/10.1128/AEM.07790-11.
11. **Wieschalka S, Blombach B, Bott M, Eikmanns BJ.** 2013. Bio-based production of organic acids with *Corynebacterium glutamicum*. Microb Biotechnol **6**:87–102. http://dx.doi.org/10.1111/1751-7915.12013.
12. **Zahoor A, Otten A, Wendisch VF.** 2014. Metabolic engineering of *Corynebacterium glutamicum* for glycolate production. J Biotechnol **192**:366–375.
13. **Otten A, Brocker M, Bott M.** 2015. Metabolic engineering of *Corynebacterium glutamicum* for the production of itaconate. Metab Eng **30**:156–165. http://dx.doi.org/10.1016/j.ymben.2015.06.003.
14. **Kind S, Jeong WK, Schröder H, Wittmann C.** 2010. Systems-wide metabolic pathway engineering in *Corynebacterium glutamicum* for bio-based production of diaminopentane. Metab Eng **12**:341–351. http://dx.doi.org/10.1016/j.ymben.2010.03.005.
15. **Schneider J, Wendisch VF.** 2010. Putrescine production by engineered *Corynebacterium glutamicum*. Appl Microbiol Biotechnol **88**:859–868. http://dx.doi.org/10.1007/s00253-010-2778-x.
16. **Heider SAE, Peters-Wendisch P, Wendisch VF.** 2012. Carotenoid biosynthesis and overproduction in *Corynebacterium glutamicum*. BMC Microbiol **12**:198. http://dx.doi.org/10.1186/1471-2180-12-198.
17. **Heider SAE, Peters-Wendisch P, Netzer R, Stafnes M, Brautaset T, Wendisch VF.** 2013. Production and glucosylation of C50 and C40 carotenoids by metabolically engineered *Corynebacterium glutamicum*. Appl Microbiol Biotechnol **98**:1223–1235.
18. **Heider SAE, Wolf N, Hofemeier A, Peters-Wendisch P, Wendisch VF.** 2014. Optimization of the IPP precursor supply for the production of lycopene, decaprenoxanthin and astaxanthin by *Corynebacterium glutamicum*. Front Bioeng Biotechnol **2**:28.
19. **Grünberger A, Wiechert W, Kohlheyer D.** 2014. Single-cell microfluidics: opportunity for bioprocess development. Curr Opin Biotechnol **29**:15–23. http://dx.doi.org/10.1016/j.copbio.2014.02.008.
20. **Mustafi N, Grünberger A, Kohlheyer D, Bott M, Frunzke J.** 2012. The development and application of a single-cell biosensor for the detection of L-methionine and branched-chain amino acids. Metab Eng **14**:449–457. http://dx.doi.org/10.1016/j.ymben.2012.02.002.
21. **Mustafi N, Grünberger A, Mahr R, Helfrich S, Nöh K, Blombach B, Kohlheyer D, Frunzke J.** 2014. Application of a genetically encoded biosensor for live cell imaging of L-valine production in pyruvate dehydrogenase complex-deficient *Corynebacterium glutamicum* strains. PLoS One **9**:e85731. http://dx.doi.org/10.1371/journal.pone.0085731.
22. **Veening J-W, Smits WK, Kuipers OP.** 2008. Bistability, epigenetics, and bet-hedging in bacteria. Annu Rev Microbiol **62**:193–210. http://dx.doi.org/10.1146/annurev.micro.62.081307.163002.
23. **Eldar A, Elowitz MB.** 2010. Functional roles for noise in genetic circuits. Nature **467**:167–173. http://dx.doi.org/10.1038/nature09326.
24. **Drepper T, Krauss U, Meyer zu Berstenhorst S, Pietruszka J, Jaeger K-E.** 2011. Lights on and action! Controlling microbial gene expression by light. Appl Microbiol Biotechnol **90**:23–40. http://dx.doi.org/10.1007/s00253-011-3141-6.
25. **Ohlendorf R, Vidavski RR, Eldar A, Moffat K, Möglich A.** 2012. From dusk till dawn: one-plasmid systems for light-regulated gene expression. J Mol Biol **416**:534–542. http://dx.doi.org/10.1016/j.jmb.2012.01.001.
26. **Tabor JJ, Levskaya A, Voigt CA.** 2011. Multichromatic control of gene expression in *Escherichia coli*. J Mol Biol **405**:315–324. http://dx.doi.org/10.1016/j.jmb.2010.10.038.
27. **Binder D, Grünberger A, Loeschcke A, Probst C, Bier C, Pietruszka J, Wiechert W, Kohlheyer D, Jaeger K-E, Drepper T.** 2014. Light-responsive control of bacterial gene expression: precise triggering of the *lac* promoter activity using photocaged IPTG. Integr Biol (Camb) **6**:755–765. http://dx.doi.org/10.1039/C4IB00027G.
28. **Binder D, Bier C, Grünberger A, Drobietz D, Hage-Hülsmann J, Wandrey G, Büchs J, Kohlheyer D, Loeschcke A, Wiechert W, Jaeger K-E, Pietruszka J, Drepper T.** 2016. Photocaged arabinose–a novel optogenetic switch for rapid and gradual control of microbial gene expression. Chembiochem **17**:296–299. http://dx.doi.org/10.1002/cbic.201500609.
29. **Deiters A.** 2009. Light activation as a method of regulating and studying gene expression. Curr Opin Chem Biol **13**:678–686. http://dx.doi.org/10.1016/j.cbpa.2009.09.026.
30. **Brieke C, Rohrbach F, Gottschalk A, Mayer G, Heckel A.** 2012. Light-controlled tools. Angew Chem Int Ed Engl **51**:8446–8476. http://dx.doi.org/10.1002/anie.201202134.
31. **Pátek M, Nesvera J, Guyonvarch A, Reyes O, Leblon G.** 2003. Promoters of *Corynebacterium glutamicum*. J Biotechnol **104**:311–323. http://dx.doi.org/10.1016/S0168-1656(03)00155-X.
32. **Hentschel E, Will C, Mustafi N, Burkovski A, Rehm N, Frunzke J.** 2013. Destabilized eYFP variants for dynamic gene expression studies in *Corynebacterium glutamicum*. Microb Biotechnol **6**:196–201. http://dx.doi.org/10.1111/j.1751-7915.2012.00360.x.
33. **Binder S, Schendzielorz G, Stäbler N, Krumbach K, Hoffmann K, Bott M, Eggeling L.** 2012. A high-throughput approach to identify genomic

variants of bacterial metabolite producers at the single-cell level. Genome Biol **13:**R40. http://dx.doi.org/10.1186/gb-2012-13-5-r40.

34. **Frohwitter J, Heider SAE, Peters-Wendisch P, Beekwilder J, Wendisch VF.** 2014. Production of the sesquiterpene (+)-valencene by metabolically engineered *Corynebacterium glutamicum*. J Biotechnol **191:**205–213. http://dx.doi.org/10.1016/j.jbiotec.2014.05.032.
35. **Beekwilder J, van Houwelingen A, Cankar K, van Dijk ADJ, de Jong RM, Stoopen G, Bouwmeester H, Achkar J, Sonke T, Bosch D.** 2014. Valencene synthase from the heartwood of Nootka cypress (*Callitropsis nootkatensis*) for biotechnological production of valencene. Plant Biotechnol J **12:**174–182. http://dx.doi.org/10.1111/pbi.12124.
36. **Fraatz MA, Berger RG, Zorn H.** 2009. Nootkatone–a biotechnological challenge. Appl Microbiol Biotechnol **83:**35–41. http://dx.doi.org/10.1007/s00253-009-1968-x.
37. **Sambrook J, Fritsch EF, Maniatis T.** 1989. Molecular cloning: a laboratory manual, 2nd ed. Cold Spring Harbor Laboratory Press, Cold Spring Harbor, NY.
38. **Kalinowski J, Bathe B, Bartels D, Bischoff N, Bott M, Burkovski A, Dusch N, Eggeling L, Eikmanns BJ, Gaigalat L, Goesmann A, Hartmann M, Huthmacher K, Krämer R, Linke B, McHardy AC, Meyer F, Möckel B, Pfefferle W, Pühler A, Rey DA, Rückert C, Rupp O, Sahm H, Wendisch VF, Wiegräbe I, Tauch A.** 2003. The complete *Corynebacterium glutamicum* ATCC 13032 genome sequence and its impact on the production of L-aspartate-derived amino acids and vitamins. J Biotechnol **104:**5–25. http://dx.doi.org/10.1016/S0168-1656(03)00154-8.
39. **Keilhauer C, Eggeling L, Sahm H.** 1993. Isoleucine Synthesis in *Corynebacterium glutamicum*: molecular analysis of the ilvB-ilvN-ilvC operon. J Bacteriol **175:**5595–5603.
40. **Unthan S, Grünberger A, van Ooyen J, Gätgens J, Heinrich J, Paczia N, Wiechert W, Kohlheyer D, Noack S.** 2013. Beyond growth rate 0.6: what drives *Corynebacterium glutamicum* to higher growth rates in defined medium. Biotechnol Bioeng **111:**359–371.
41. **Hanahan D.** 1983. Studies on transformation of *Escherichia coli* with plasmids. J Mol Biol **166:**557–580. http://dx.doi.org/10.1016/S0022-2836(83)80284-8.
42. **Abe S, Takayama K-I, Kinoshita S.** 1967. Taxonomical studies on glutamicum acid-producing bacteria. J Gen Appl Microbiol **13:**279–301. http://dx.doi.org/10.2323/jgam.13.279.
43. **Neumeyer A, Hübschmann T, Müller S, Frunzke J.** 2013. Monitoring of population dynamics of *Corynebacterium glutamicum* by multiparameter flow cytometry. Microb Biotechnol **6:**157–167. http://dx.doi.org/10.1111/1751-7915.12018.
44. **Eikmanns BJ, Thum-Schmitz N, Eggeling L, Lüdtke KU, Sahm H.** 1994. Nucleotide sequence, expression and transcriptional analysis of the *Corynebacterium glutamicum gltA* gene encoding citrate synthase. Microbiology **140:**1817–1828. http://dx.doi.org/10.1099/13500872-140-8-1817.
45. **Peters-Wendisch PG, Schiel B, Wendisch VF, Katsoulidis E, Möckel B, Sahm H, Eikmanns BJ.** 2001. Pyruvate carboxylase is a major bottleneck for glutamate and lysine production by *Corynebacterium glutamicum*. J Mol Microbiol Biotechnol **3:**295–300.
46. **Stansen C, Uy D, Delaunay S, Eggeling L, Goergen J-L, Wendisch VF.** 2005. Characterization of a *Corynebacterium glutamicum* lactate utilization operon induced during temperature-triggered glutamate production. Appl Environ Microbiol **71:**5920–5928. http://dx.doi.org/10.1128/AEM.71.10.5920-5928.2005.
47. **Gibson DG, Young L, Chuang R, Venter JC, Hutchison CA, III, Smith HO.** 2009. Enzymatic assembly of DNA molecules up to several hundred kilobases. Nat Methods **6:**343–345. http://dx.doi.org/10.1038/nmeth.1318.
48. **Eikmanns BJ, Kleinertz E, Liebl W, Sahm H.** 1991. A family of *Corynebacterium glutamicum/Escherichia coli* shuttle vectors for cloning, controlled gene expression, and promoter probing. Gene **102:**93–98. http://dx.doi.org/10.1016/0378-1119(91)90545-M.
49. **Young DD, Deiters A.** 2007. Photochemical activation of protein expression in bacterial cells. Angew Chem Int Ed Engl **46:**4290–4292. http://dx.doi.org/10.1002/anie.200700057.
50. **Kortmann M, Kuhl V, Klaffl S, Bott M.** 2014. A chromosomally encoded T7 RNA polymerase-dependent gene expression system for *Corynebacterium glutamicum*: construction and comparative evaluation at the single-cell level. Microb Biotechnol **8:**253–265.
51. **Funke M, Diederichs S, Kensy F, Müller C, Büchs J.** 2009. The baffled microtiter plate: increased oxygen transfer and improved online monitoring in small scale fermentations. Biotechnol Bioeng **103:**1118–1128. http://dx.doi.org/10.1002/bit.22341.
52. **Schlepütz T, Büchs J.** 2014. Scale-down of vinegar production into microtiter plates using a custom-made lid. J Biosci Bioeng **117:**485–496. http://dx.doi.org/10.1016/j.jbiosc.2013.10.007.
53. **Wandrey G, Bier C, Binder D, Hoffmann K, Jaeger K-E, Pietruszka J, Drepper T, Büchs J.** 2016. Light-induced gene expression with photocaged IPTG for induction profiling in a high-throughput screening system. Microb Cell Fact **15:**63. http://dx.doi.org/10.1186/s12934-016-0461-3.
54. **Scholtmeijer K, Cankar K, Beekwilder J, Wösten HA, Lugones BLG, Bosch D.** 2014. Production of (+)-valencene in the mushroom-forming fungus *S. commune*. Appl Microbiol Biotechnol **98:**5059–5068. http://dx.doi.org/10.1007/s00253-014-5581-2.
55. **Wriessnegger T, Augustin P, Engleder M, Leitner E, Müller M, Kaluzna I, Schürmann M, Mink D, Zellnig G, Schwab H, Pichler H.** 2014. Production of the sesquiterpenoid (+)-nootkatone by metabolic engineering of *Pichia pastoris*. Metab Eng **24:**18–29. http://dx.doi.org/10.1016/j.ymben.2014.04.001.
56. **Velema WA, van der Berg JP, Szymanski W, Driessen AJM, Feringa BL.** 2014. Orthogonal control of antibacterial activity with light. ACS Chem Biol **9:**1969–1974. http://dx.doi.org/10.1021/cb500313f.
57. **Hansen MJ, Velema WA, Lerch MM, Szymanski W, Feringa BL.** 2015. Wavelength-selective cleavage of photoprotecting groups: strategies and applications in dynamic systems. Chem Soc Rev **44:**3358–3377. http://dx.doi.org/10.1039/C5CS00118H.
58. **Medema MH, Breitling R, Bovenberg R, Takano E.** 2011. Exploiting plug-and-play synthetic biology for drug discovery and production in microorganisms. Nat Rev Microbiol **9:**131–137. http://dx.doi.org/10.1038/nrmicro2478.
59. **Wendisch VF, Jorge JMP, Pérez-García F, Sgobba E.** 2016. Updates on industrial production of amino acids using *Corynebacterium glutamicum*. World J Microbiol Biotechnol **32:**105. http://dx.doi.org/10.1007/s11274-016-2060-1.
60. **Lausberg F, Chattopadhyay AR, Heyer A, Eggeling L, Freudl R.** 2012. A tetracycline inducible expression vector for *Corynebacterium glutamicum* allowing tightly regulable gene expression. Plasmid **68:**142–147. http://dx.doi.org/10.1016/j.plasmid.2012.05.001.
61. **Zhang Y, Shang X, Lai S, Zhang G, Liang Y, Wen T.** 2012. Development and application of an arabinose-inducible expression system by facilitating inducer uptake in *Corynebacterium glutamicum*. Appl Environ Microbiol **78:**5831–5838. http://dx.doi.org/10.1128/AEM.01147-12.
62. **Plassmeier JK, Busche T, Molck S, Persicke M, Pühler A, Rückert C, Kalinowski J.** 2013. A propionate-inducible expression system based on the *Corynebacterium glutamicum prpD2* promoter and PrpR activator and its application for the redirection of amino acid biosynthesis pathways. J Biotechnol **163:**225–232. http://dx.doi.org/10.1016/j.jbiotec.2012.08.009.

II.6 Uncovering future perspectives

II.5.1 Cage me if you can!

Cage me if you can! – From assembly to application of photocaged compounds in microbial biotechnology

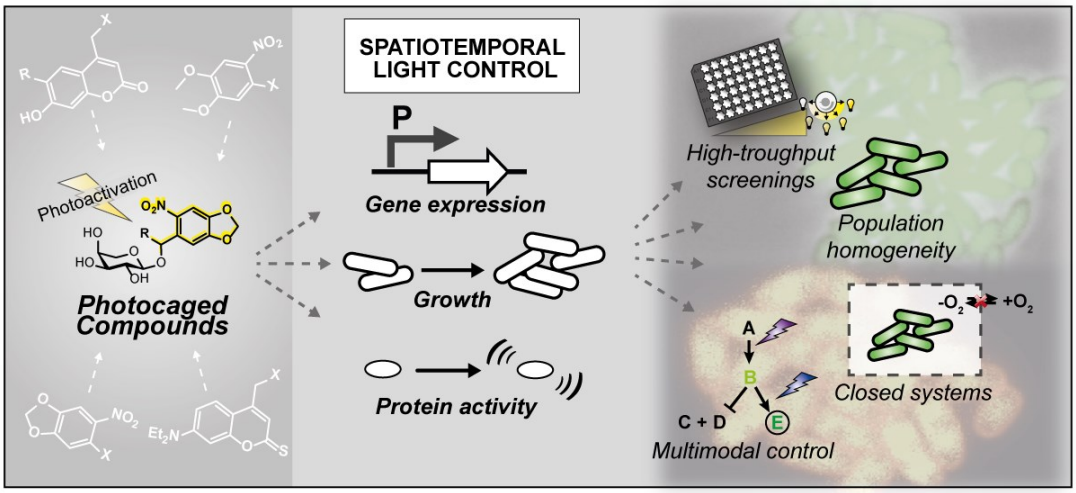

Dennis Binder, Jörg Pietruszka, Karl-Erich Jaeger and Thomas Drepper

Manuscript in preparation

REVIEW ARTICLE

Cage me if you can! – From assembly to application of photocaged compounds in microbial biotechnology

Dennis Binder [a]
Jörg Pietruszka [b,c]
Karl-Erich Jaeger [a,c]
Thomas Drepper [a]

[a] Institute of Molecular Enzyme Technology, Heinrich-Heine-University Düsseldorf, Forschungszentrum Jülich, 52425 Jülich, Germany
[b] Institute for Bioorganic Chemistry, Heinrich-Heine-University Düsseldorf, Forschungszentrum Jülich, , 52425 Jülich, Germany
[c] Institute of Bio- and Geosciences, IBG-1: Biotechnology, Forschungszentrum Jülich, , 52425 Jülich, Germany

GRAPHICAL ABSTRACT

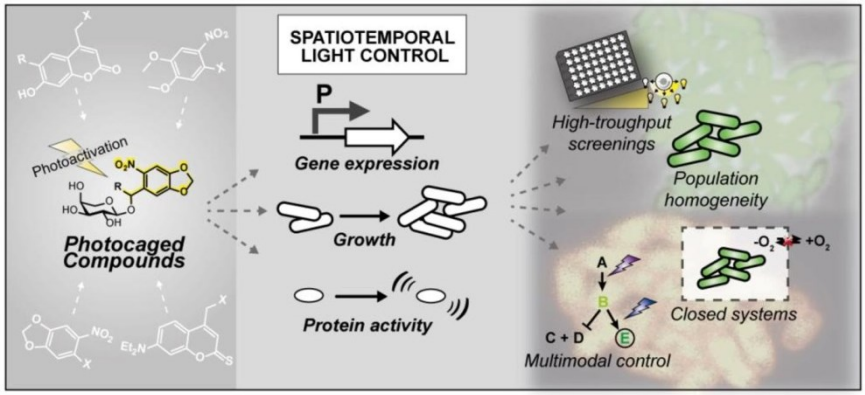

Highlights

- A vast variety of auspicious photocages offers versatile UV-C to IR excitation feasibility
- Growth, gene expression or protein activity can be controlled in a spatiotemporal fashion
- Membrane-permeable photocaged inducers provide outstanding population homogeneity
- Photouncaging is highly suited to exert a higher-order control in single-cell cultivations
- Prospective applications include high-throughput screenings, closed or multimodal processes

KEYWORDS

(Photo)caged compounds • Spatiotemporal Control • Optogenetics • Photocaging • Synthetic Bio(techno)logy • Single-Cell Analysis Applications • High-Throughput Screening

ABSTRACT

Optogenetic switches are light-responsive regulatory components that enable simple and straightforward triggering of biological functions with unprecedented spatiotemporal resolution. Here, the unique stimulus light offers utmost flexibility, specificity, and precision. In this context, photocaged compounds qualify as valuable tools to accomplish such higher-order light control over cellular functions in a non-invasive fashion.

In this mini review, we depict recent advances on novel photocaging groups and photocaged biomolecules for the employment in microbial biotechnology. Further, we highlight current light-controlled *in vivo* applications using photocaged compounds. Here, biological functions such as cellular growth, protein activity or especially gene expression are favorable targets for light-mediated control.

Finally, we illustrate future perspectives for light-triggered applications in synthetic biology and biotechnology. Especially, single-cell applications seem to benefit from spatiotemporal, high-throughput-feasible and non-invasive light control,

where photouncaging can be implemented to trigger microbes with unimagined population homogeneity. Conclusively, photochemical triggering of biological functions entails several beneficial features that will be discussed to unravel the yet uncharted biotechnological potential of light-controlled microbial cell factories.

INTRODUCTION

In nature, biological key processes such as growth, gene expression or protein function are arranged with utmost precision and accuracy to fulfill fundamental functions within a cell. For numerous synthetic biology and biotechnological applications, a strong demand for external control exists to trigger synthetically engineered processes in a similarly elaborate fashion. To cope with those demands, light is currently evolving as a key player in providing a higher-order control over cellular functions [1,2]. The advantages of light control comprise an unprecedented spatiotemporal resolution together with high variability and selectivity, which jointly empower the triggering of biological functions in a precise and non-invasive fashion. In this context, photocaged compounds, which are rendered biologically inactive through the fusion to a photo-labile protection group and can regain their primal function upon short light exposure, emerged as valuable tools for studying and regulating cellular functions. Although photocaged compounds are established as so-called optogenetic tools in neuroscience [3] or pharmacology [4,5], their beneficial features were rather tentatively perceived in microbial biotechnology.

Here, we review current and most feasible photocaged compounds for microbial applications and highlight their strengths and deficiencies in terms of *in vivo* feasibility. Furthermore, we uncover fields of application that would hugely benefit from spatiotemporal light control using photocaged compounds and finally unravel challenges that have to be tackled in the future.

Chromatic and feature diversity of novel and established photocaging groups

Over the last decades, a vast multitude of different photocaging groups was established providing a remarkable chromatic diversity that enables excitation ranging from UV-C to IR light [1,6] (**Figure 1**). Prior to *in vivo* application of photocaged compounds, the assembly and functionality has to be realized *in vitro*. Thus, the respective photocaging groups should be readily synthesized in a straightforward and stable fashion and offer easy coupling to alternative effector molecules. In this context, especially *o*-nitrobenzyl-photocaging groups (NB) and their derivatives such as nitroveratryl- (NV), or nitropiperonyl- (NP) photocages are commonly used to mediate an adequate and well-characterized UV-light triggered release [1,7]. Whereas NB shows significant absorptivity in the UV-C to UV-B range, absorption spectra of NV and NP photocages are bathochromically shifted towards sufficient UV-A absorption, that is much more applicable for *in vivo* photolysis. To tackle manifold applications, an efficient photolysis, i.e. a high product of absorptivity ε and uncaging quantum yield Φ, both *in vitro* and *in vivo* is an essential key feature. In addition to an efficient photorelease upon conventional one-photon excitation, two-photon uncaging (TPU) poses a valuable alternative to conduct the photorelease using two photons of approximately twice the usual wavelength [1,8]. TPU seems a powerful tool to implement light impulses into applications with utmost precision in the lower femtoliter-scale [1,8,9]. The feasibility of different photocages for TPU has been reviewed elsewhere in further detail [8]. Moreover, it allows employing much higher wavelengths that are commonly well applicable for diverse purposes such as deep-tissue penetration as well as multichromatic or generally bathochromic regulation. For example, *p*-hydroxyphenacyl photocages (*p*HP), which are usually less suited for biological applications due to main absorptivity in the UV-B to UV-C range [10], were recently recruited for TPU to provide excitation

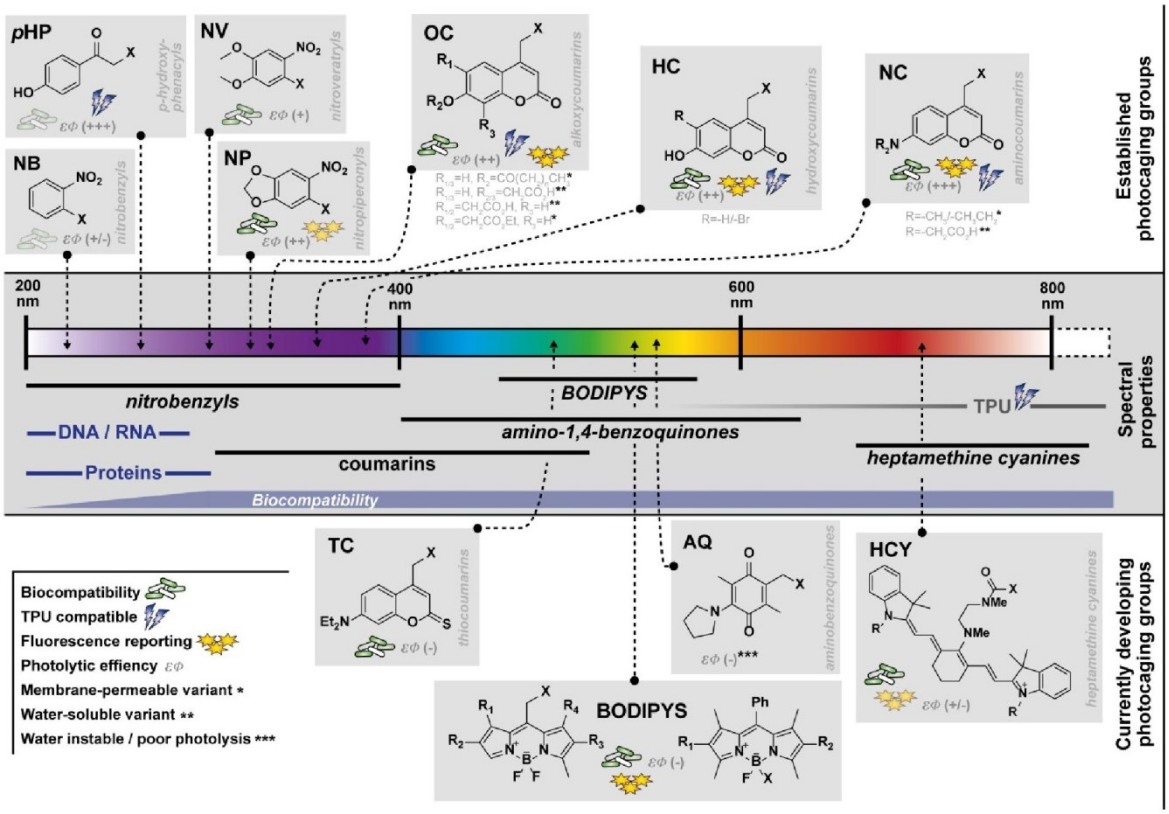

Figure 1. Features of selected photocaging groups for microbial *in vivo* applications. Arrows indicate respective absorption maxima within the schematic UV-Vis spectrum, whereas bars above the respective compound class display the approximate range of absorption. Caging groups at the top have been successfully applied in *in vivo* applications, while recently developing compounds at the bottom panel have to be fully evaluated in the near future. Beneficial features such as biocompatibility (cells), TPU compatibility (flashes) or fluorescent reporting (stars) are highlighted and membrane-permeability (*) and solubility (**) is indicated for selected compounds. Caging groups are further evaluated regarding photolytic efficiency ($\varepsilon\Phi$). Abbreviations: NB: *o*-nitrobenzyl; *p*HP: *p*-hydroxyphenacyl; NV: 6-nitroveratryl; NP: 6-nitropiperonyl; OC: alkoxycoumarin; HC: hydroxycoumarin; NC: aminocoumarin; TC: (amino-)thiocoumarin; AQ: amino-1,4-benzoquinone; HCY: heptamethine cyanine

with visible light at 550 nm and thus largely improved biological compatibility [11].

Furthermore, coumarin-4-ylmethyl (CM) derivatives are highly applicable photocages, that are significantly red-shifted compared to nitrobenzyl-cages [1,12]. Here, different moieties in the C6, C7 and C8-position are able to decisively shift the absorptivity into the visible range and to improve water-solubility or membrane-permeability, respectively [6,12–16]. Established coumarin classes include alkoxycoumarins (OC), aminocoumarins (NC) and hydroxycoumarins (HC). Promising CM derivatives are, for instance, the established 6-bromo-HC (BHC) or the novel 7-diethylamino-4-thiocoumarinmethyl- (TC) that were shown to be well-suited for UV-A, blue and two-photon as well as green light uncaging, respectively [17–19]. For biological applications, the highly promising chromatic diversity of CM photocages that spans from the UV-A to the IR range provides a solid foundation to trigger different cellular events independently with different light colors [6,13,16].

Moreover, heptamethine cyanine (HCY) photocages enable red to IR light uncaging without the need for TPU, yet their photocleavage was shown to occur in dependency on singlet oxygen [20,21].

For many caging derivatives, biocompatibility with respect to crucial features such as solubility, toxicity or *in vivo* photolysis has been shown at least in mammalian cells, whereas others are merely applicable *in vitro* and would require extensive reengineering prior to be feasible for microbial *in vivo* applications. To specifically modulate compound solubility hydro- or rather amphiphilic groups can be introduced to existing photocages as depicted for carboxy-derivatives of NB or HC compounds [22,23].

Whereas most photocages offer adequate solubility in aqueous solution that commonly extends to the lower millimolar range e.g. for NP [24], some compounds do not work in water due to degradation, poor solubility or reduced photolysis. Red light-absorbing amino-1,4-benzoquinones (AQ), for instance, revealed water incompatibility due to chromophore degradation and poor photorelease in aqueous solution [25,26]. Water-dispersible compound-conjugated nanoparticles, however, proved suited to release AQ-photocaged drugs efficiently into aqueous medium [27].

During *in vivo* applications, direct online-monitoring of photocleavage processes, preferably in form of in- or decreasing photocaged compound or increasing photo-product fluorescence, is a valuable tool in spatial and precise triggering. This way, the photorelease can be traced prior to and thus independent of biological responses. Here, strongly fluorescing CM or BODIPY photocages are favored, although Wandrey *et al.* showed that also the transient nitroso-photoproducts qualify for fluorescence-based online monitoring of NP-compound photouncaging [28].

Conclusively, a broad variety of versatile photocaging groups emerged over the last years, whereof just well-established and quite recent ones were highlighted beforehand. Earlier photocages and those, which are less commonly applied for microbial applications, have been reviewed elsewhere [1,6,7].

Photocaged compounds as versatile tools for microbial biotechnology

The versatility of photocaging groups led to numerous achievements especially in neurobiology [3], photopharmacology [4,5,29], material sciences [30], biomedicine [21,31] and generally in mammalian cell biology [1], where photouncaging has established as a valuable tool for quite some time. Lately, however, photouncaging experiences a kind of renaissance in microbial biotechnology. Here, recent advances in controlling microbial key proccesses such as growth, protein function and gene expression will be reviewed.

Recent advances in photocaged amino acid based control of protein function

Light control of protein functions bears several benefits over natural control mechanisms. Whereas, for instance, the up- or down-regulation of protein production is time- and energy-consuming and allosteric protein regulation can further depend on cellular metabolization or uptake processes, light can provide a spatiotemporal and independent control of protein function. In this context, photocaged amino acids have established as valuable tools to implement light control into macromolecular proteins [32,33]. To incorporate photocaged amino acids into cellular proteins, genetic code expansion is required. Here, the application of an orthogonal translational machinery with specifically engineered tRNA / tRNA synthetase pairs for the incorporation of sterically demanding amino acids allows for the site-specific delivery of the photocaged amino acids in response to an TAG amber stop codon [19,33].

To study and control protein and especially enzyme functionality, numerous photocaged amino acids have been developed over the past years. Favored target amino acids are those, which are involved in catalytic activity, protein folding or post-translational modifications. A broader overview of light-controlled protein functions has been reviewed elsewhere [33] and thus just recent examples and tools will be considered in the context of microbial applications hereafter.

A key protein for numerous synthetic gene expression setups in microbial biotechnology, that is commonly included into gene circuits to elevate overall expression levels, poses the recombinant bacteriophage T7 RNA polymerase (T7RP). Accordingly, an NB-photocaged tyrosine (**Figure 2A**) was incorporated into the recombinantly produced polymerase to mediate protein activity and thus high-level gene expression in both bacterial and mammalian cells upon light exposure [34]. In *Escherichia coli*, the light activation of the photocaged T7RP yielded a more than five-fold increase in luciferase reported gene expression [34]. In a more recent approach, the NB-photocaged

tyrosine was exchanged by NP-photocaged tyrosine to yield a more rapid uncaging together with an improved solubility, yet the photo-functionality of the T7RP was just shown in mammalian cells [35].

Besides those indirect approaches to control luciferase gene expression, two different HC-photocaged lysines (**Figure 2A**) were directly incorporated into the firefly luciferase, enabling the photocontrol with three different light colors [19]. Furthermore, the two photocaged lysines were introduced into recombinant EGFP proteins to control chromophore maturation by light. Whereas the BHC and the HC derivative allowed the excitation with both UV-A and blue light, the BHC-photocaged lysine was further feasible for two-photon-uncaging in the near IR range [19]. Moreover, Uprety *et al.* further presented NP-photocaged cysteine, homocysteine and lysine (**Figure 2A**) for the efficient incorporation into both bacterial and mammalian proteins [32].

Earlier photocaged amino acids include NB-fluorotyrosines [36], NP-lysine [37], or NV-serine [38] and complement the group of available photocaged amino acids. Together with above mentioned genetic code expansion tools a solid basis is established to successfully mask and unmask most miscellaneous proteins. Since recent and early advances in controlling protein function by light, was strikingly pinpointed for proteins such as T7RP [34,35], luciferase [19,32], EGFP [19] or β-galactosidase [39], numerous auspicious microbial applications for controlling protein or enzyme functionality can be presumed in the future.

Recent advances in controlling microbial gene expression by light

Transcription factor-based control of gene expression in microbes exhibits a valuable target for photouncaging applications, since the linkage of respective effector molecules and photolabile protecting groups mostly results in a tremendous decrease of their binding affinity or rather ligand recognition. The first photocaged inducer that was employed to drive bacterial gene expression is NP-photocaged IPTG (**Figure 2B**) [40]. Here, IPTG is efficiently released in a two-step photocleavage process upon short UV-A light exposure and subsequent enzymatic hydrolysis of the photoproduct esters. Whereas the initial setup proved light-activation of *lac* promoter based gene expression in *E. coli* in principle [40], a more recent redesign implemented the recombinant T7RP for high-level gene expression with NP-photocaged IPTG [41]. Despite the fact that the redesign worked well in a gradual and homogeneous fashion with low micromolar inducer concentrations, the essential two-step-photo-cleavage reaction impeded the temporal resolution of light control. In contrast, one-step-photocleavable NP-photocaged arabinose (**Figure 2B**) was shown to trigger P_{BAD} promoter based gene expression in *E. coli* in more rapid, strong and homogeneous fashion as compared to conventional arabinose induction [42].

Analogous to NP-photocaged arabinose, different carbohydrates, namely NP-photocaged galactose, rhamnose and glucose (**Figure 2B**) were synthesized and proven to be suited for controlling, i.e. inducing or repressing, bacterial gene expression by light [24]. NP-photocaged rhamnose, for instance, was applied to drive the P_{rhaBAD} promoter-controlled expression of *T7Lys* that encodes the T7 Lysozyme, a natural and strong inhibitor of the T7RP. This way, it was possible to almost completely repress T7RP based gene expression upon short light exposure [24].

Besides exerting light-control of promoter activity using photocaged inducers, it is further feasible to obtain photocontrol of riboswitches (**Figure 2B**). In this context, a synthetic theophylline-sensing riboswitch [43] was recently employed in combination with NP-photocaged theophylline [44] to photoactivate gene expression in *E. coli* [45]. Here, light-activation was able to 276-fold upregulate *lacZ*-reported gene expression, which was strictly dependent on the target gene region, though.

For the moment, this poor versatile deployment of different promoter-target gene combinations clearly restricts the application of NP-photocaged

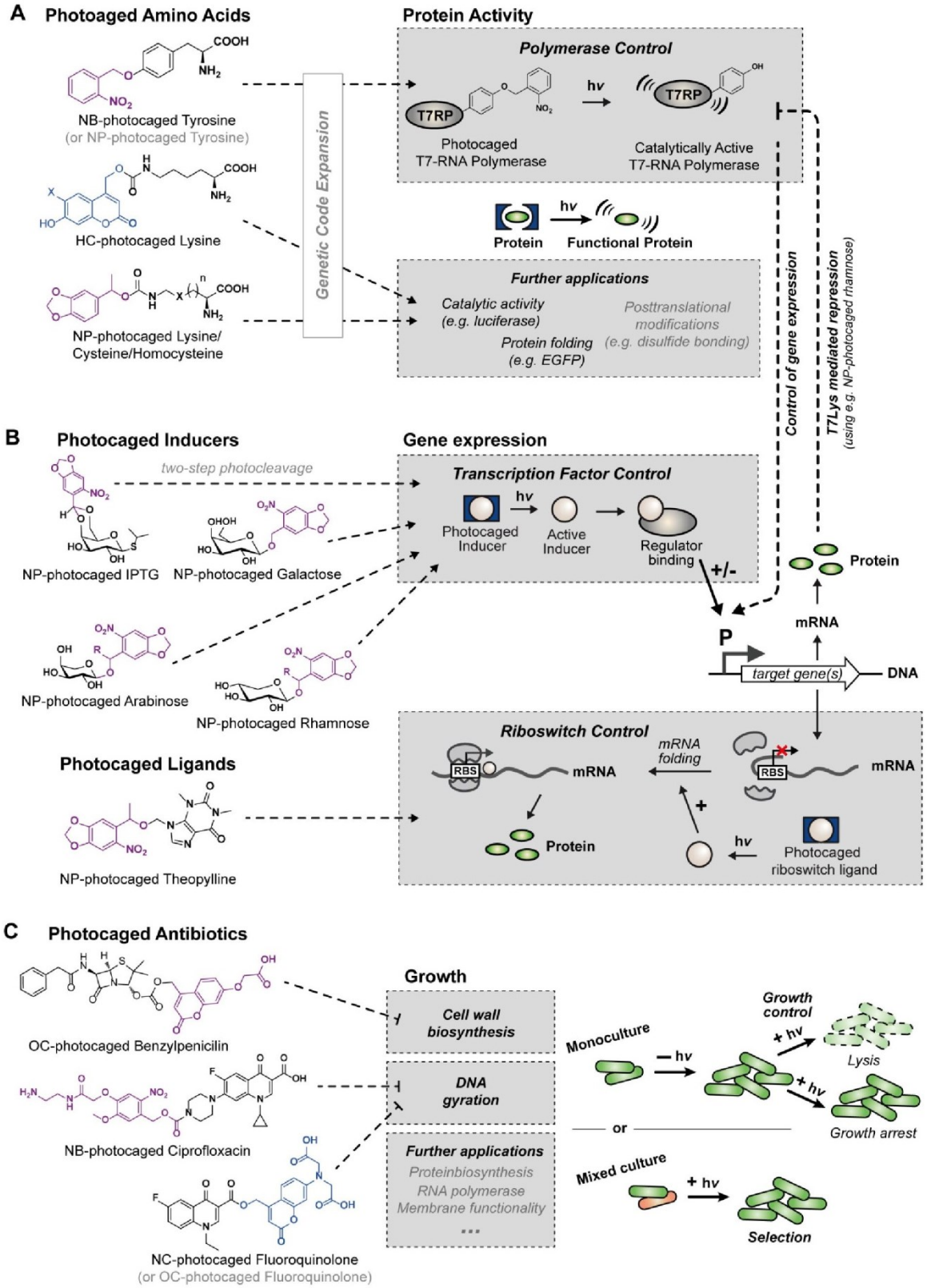

Figure 2. Recent advances in photocaged compound based light-control of microbial cellular functions. A) Photocaged amino acid based control of protein functions such as catalytic activity, protein folding or posttranslational modifications. **B)** Photocaged inducer or ligand based light control of transcription factors or riboswitches, respectively. **C)** Photocaged antibiotics based light control of microbial growth and selection in mono- and mixed cultures.

theophylline and illustrates the need for further extensive riboswitch engineering in the future

Recent advances in microbial growth control using photocaged antibiotics

As light allows selectively triggering activities in living microbes with high spatiotemporal resolution, microbial growth is an appealing target for photocaged compounds. Firstly, in microbial monocultures a single photocaged antibiotic can adjust cellular growth and thus balance growth and production processes. Secondly, the growth of different microbial species can be precisely balanced by means of photocaged antibiotics in mixed cultures (**Figure 2C**).

In a monoculture, NB-photocaged ciprofloxacin (**Figure 2C**) was shown to efficiently reduce cell viability of *E. coli* upon light exposure. Here, the selectivity of light-controlled antibiotic activity was enhanced using LPS-targeting nanoparticles that were conjugated to the NB-photocaged ciprofloxacin to provide cell-wall targeted drug delivery [46]. Similarly, an OC-photocaged fluoroquinolone was shown to specifically decrease *E. coli* growth rates upon UV-B light exposure in a mixed culture of *E. coli* and *Micrococcus luteus* [47]. Moreover, for a mixture of *E. coli* and *Staphylococcus aureus* two photocaged antibiotics (**Figure 2C**) were applied in a chromatically orthogonal fashion to mediate conditional species selection upon exposure to UV-B or white light, respectively [48]. Specifically, OC-photocaged benzylpenicillin exhibited a narrow absorption spectrum in the UV-A range, whereas light absorption of NC-photocaged fluoroquinolone was rather broad and extended to the blue range. This way, photouncaging had to be conducted primarily using blue or white light exposure to trigger both compounds independently in a chronological fashion. Interestingly, the microbial antibiotics puromycin [49], erythromycin [50] and doxycycline [51,52] were photocaged in another context, yet might emerge as appealing tools for controlling microbial growth in the future.

In summary, photocaged antibiotics are valuable means to control microbial growth and selection in various biotechnological applications. Particularly, for microbial consortia light-control is well suited to implement the selection for specific strains. Conceivable applications include light-controlled shared biotechnological productions or the selective mediation of growth arrest or cell death for different microbes and microbial communities.

Further applications of photocaged compounds

Besides amino acids, inducers, ligands and antibiotics, numerous other biomolecules have been subjected to photocaging that are beneficial for special applications such as *in vitro* DNA synthesis, gene editing or protein biochemistry. In this context, notable photocaged compounds were employed to mediate light-control of plasmids [53], CRISPR/Cas9 systems [54], ions such as protons [55] or cooper [56], selenocysteine [57], dimerizers [58], or enzymatic substrates such as caged luciferin [59]. Moreover, the large field of photocaged oligonucleotides was not reviewed in detail since applications are primarily in the field of *in vitro* DNA synthesis and mammalian cell biology [60].

In the near future, one has to evaluate if and to what extent those compounds can be employed to control cellular functions in microbial biotechnology.

Future light-controlled application in synthetic bio(techno)logy

Numerous beneficial features arise from the application of light control by means of photocaged compounds (**Box 1**). Of all natural stimuli light entails the utmost spatiotemporal precision, that can be exploited for numerous synthetic bio(techno)logy applications. For microsystems such as microfluidic or agar pad-based cultivations, the high spatial resolution of electromagnetic radiation could enable the triggering of single colonies or even cells (e.g. within a microbial biofilm) in the future. The unique spatial potential of light was highlighted recently using one- and two-photon uncaging of NC-photocaged oligonucleotides in hydrogels to mediate light-controlled DNA hybridization [9]. Here,

Box 1: Key features of photocaged compounds for microbial biotechnology

Light control is well suited for numerous **lab-scale applications** from picoliter to liter scale.

Spatial	Especially microscale applications such as microfluidic and agar-pad based cultivations benefit from light control as single compartments or even cells (using TPU) can be triggered specifically.
Temporal	While conventional chemical inducers /compounds underlie diffusion, uptake and conversion processes, photocaged compounds provide instantaneous intracellular control.
Gradual	The variation of light intensity, exposure times or wavelengths allows for fine-tuned response levels.
Non-invasive	External control enables triggering special applications such as picoliter or closed (e.g. anaerobic) systems with minimal invasion and thus negligible process perturbation (e.g. dilution, contamination or oxygenation).
Homogeneous	Uniform cell penetration of photocaged compounds irrespective of transport systems frequently involves unexpected population homogeneity (often in contrast to conventional chemical induction).
Multi-chromatic	For multimodal bioprocesses light control by means of photocaged compounds provides a straightforward strategy to implement multiple stimuli in a selective and spatiotemporal fashion.

two-photon uncaging produced excitation volumes down to one femtoliter (Figure 3A).

Especially, for the control over numerous parallelized microsystems, light is a valuable tool to trigger single compartments with adequate spatial precision and in an appropriate amount of time.

The temporal benefit of light-regulation becomes most evident if hundreds or thousands of parallelized cultures have to be induced at the same time. Whereas light induction works simultaneously, implying an appropriate light source, conventional chemical induction requires invasive time- and labor-intensive pipetting or pricey liquid handling systems. In addition, the actual induction process can be much faster as, in contrast to conventional chemical induction processes where uptake, diffusion and conversion may claim a significant amount of time, photocaged compounds usually accumulate inside the cells prior to light induction. Using NP-photocaged arabinose, for instance, the conventional equimolar arabinose induction response was outperformed approximately 1.5-fold with respect to velocity (Figure 3B).

Besides the spatiotemporal features of light, the high variability of electromagnetic radiation in color (wavelength), intensity and dosage (time of exposure) entails the benefit of readily and precisely leveling the photo-release in a gradual manner. This gradual control can be applied to screen for optimal gene expression levels and would be much more challenging for chemical induction where concentration gradients have to be adjusted manually. Here, again NP-photocaged arabinose proved well suited to gradually upregulate the production of the secondary metabolite violacein in response to an increasing light intensity [42] (Figure 3C).

To achieve a higher-order control of cellular functions, not only fast, precise and gradual control is of interest, it is also desirable that all cells behave in exactly the same manner. Thus, population homogeneity is a valuable feature that is often neglected in case of appropriate overall yields on bulk level. Strikingly, for different light-controlled *in vivo* applications we recently found that population homogeneity seems inherent for photocaged compounds such as photocaged IPTG [41,61] and photocaged arabinose [42]. Due to the application of hydrophobic photocaging moieties, compounds are able to passively enter the cells, bypassing complex transport systems that are known to play a pivotal role in phenotypic heterogeneity as shown for GFP production in *E. coli* (Figure 3D) [42]. Moreover, the non-invasive properties of light entail unique beneficial features that allow the external triggering of closed biological systems. For instance, nanoscale batch cultivations, where small volumes hamper process-unaffecting supplementation, or hermetically sealed anaerobic systems can be non-invasively triggered by light in a straightforward manner (Figure 3E).

Here, chemical supplementation, media exchange or triggering with alternative stimuli such as temperature would result in unreasonably high technical and time-consuming efforts. Non-invasive light induction further minimizes sample contamination that can occur during chemical supplementation.

In addition, chemical induction clearly falls behind with respect to high-throughput feasibility and fully automated microbial cultivations (**Figure 3F**). Automated light control can fully exploit temporal, non-invasive and gradual features, whereas conventional chemical supplementation would necessitate costly liquid handling systems or labor- and time-intensive manual pipetting. Thus, light-mediated screenings for optimal production conditions were just recently shown to fully characterize fluorescent reporter based gene expression [28] or elevate terpenoid biosynthetic procedures using NP-photocaged IPTG [61].

A higher-order control of complex biological processes can be achieved using multiparameter light control. To trigger multiple events by light, two main principles are pursued, namely sequential

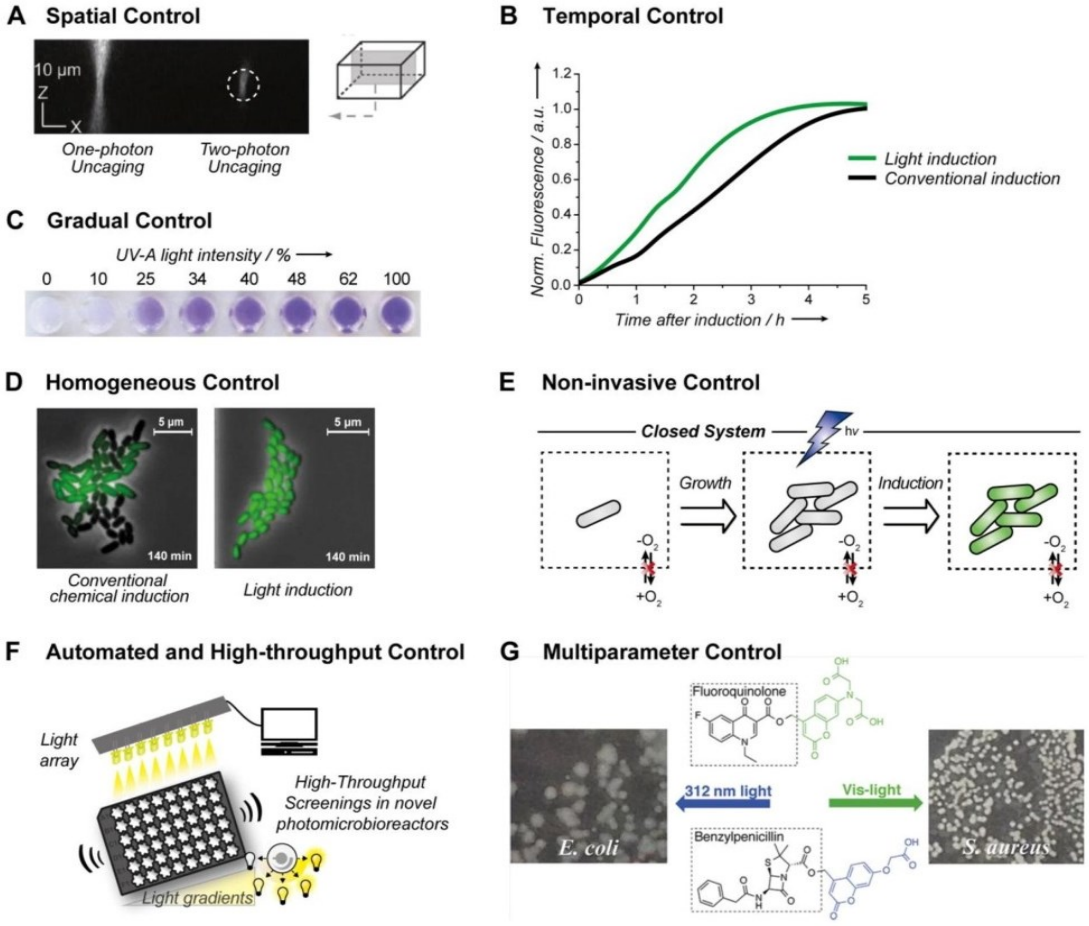

Figure 3. Key features of current and future applications for photocaged compound based light control in microbial biotechnology. A) High spatial uncaging resolution demonstrated in a hydrogel-based assay for one- and two-photon excitation of NC-photocaged oligonucleotides. The dotted circle highlights the TPU area (below 4 µm in diameter; excitation volumes down to 1 fl). Reproduced with permission from [9]. **B)** Light induction using NP-photocaged arabinose temporally outperforms induction of GFP monitored gene expression with conventional arabinose. **C)** Upregulation of light-intensity gradually increases NP-photocaged arabinose controlled production of violacein. **D)** Isogenic colonies showing homogeneous GFP expression for light induction using NP-photocaged arabinose, in contrast to a heterogeneous population response for equimolar conventional induction. Fig. 3 B-D were reproduced and adapted with permission from [42]. **E)** Non-invasive triggering of micro-scale applications (e.g. micro-batch or anaerobic cultivations) that can be triggered by light with minimal oxygenation- or dilution-effects and thus minimal process perturbation. **F)** In advanced photomicrobioreactors light-control can assist to fully automatize cultivation control in a high throughput fashion. **G)** Multiparameter light control using NC- and OC-photocaged antibiotics to mediate bacterial selection in mixed cultures upon UV or white light exposure. Reproduced with permission from [48].

uncaging and chromatically orthogonal uncaging [7]. Simple sequential uncaging can be obtained despite a spectral overlap, if photolytic efficiencies of applied compounds differ adequately. This was recently demonstrated for different *p*HP-photocaged deoxythymidines *in vitro* [62]. More effort, however, is put on the development of chromatically orthogonal photocaged compounds that bear minimal spectral overlap and can be sequentially activated upon excitation with two different wavelengths. One such example poses the aforementioned application of OC- and NC-photocaged benzylpenicillin and fluoroquinilone to mediate bacterial selection upon UV or white light exposure in mixed cultures of *E. coli* and *S. aureus* [48] (**Figure 3G**).

Highly advantageous for the endeavor of chromatic orthogonal uncaging is the principle of two-photon uncaging [1], and the involved development of two-photon excitable photocaged derivatives such as HCs [19]. Two-photon uncaging provides a novel range of excitation as wavelengths of twice the absorption maximum are applied for the respective photo-release, currently ranging from 550 to 900 nm. Though, the required experimental setup increases the intricacy of straightforward light-control, two-photon uncaging (**Figure 3A**) involves unprecedented spatial resolution of below one femtoliter as well as deepest tissue penetration [1,7].

Key challenges and future directions / Conclusions

Recent advances on photouncaging applications have corroborated the feasibility in attaining a high-level light control of microbial key processes such as protein function, gene expression or growth. Besides the generally expedient features of light in controlling microbial cellular functions (**Box 1**), several special applications such as high-throughput screenings, closed or multimodal processes were insinuated to hugely benefit from light-control.

To cope with such upcoming applications in the future, novel photo(micro)bioreactors [28] need to be developed. Here, light-control might assist to fully automatize the optimization of microbial production processes in a high-throughput fashion. Moreover, for light-controlled high-throughput screenings at the single-cell level, light control elements such as gradient generators [63] have to be implemented into existing cultivation platforms [64] in order to enable a differential light exposure in thousands of micro-cultivation chambers.

Photocaged carbohydrates, for instance, have recently emerged as valuable alternatives for inducing microbial gene expression [24,28,41,42,61], implicating a straightforward, spatiotemporal and non-invasive control that frequently supersedes conventional chemical induction especially at the level of population heterogeneity, expression strengths and temporal resolution. A versatile toolbox consisting of multi-chromatic photocaged antibiotics, inducers or amino acids needs to be developed, to tackle prospective and complex multi-modal applications in the future. Furthermore, two photon uncaging can be a sophisticated accessory tool for light control at the single-cell level and has to be elucidated in-depth for future applications.

In summary, to fully exploit all key features of the unique and auspicious stimulus light, further extensive research and development on the field of chemical photocaging seems necessary.

Probably, those numerous benefits might be fully harnessed only in a joint venture of photocaged compounds, chemical photoswitches [65] and genetically-encoded photoreceptors [66] for an enlightened future in synthetic biology and biotechnology.

ACKNOWLEDGEMENTS

We gratefully acknowledge the support by grants from the Federal Ministry of Education and Research (OptoSys, FKZ 031A167).

RECOMMENDED READING REFERENCES

• of special interest

Binder et al. 2014
This article presents the reengineering of *lac*-based gene expression using photocaged IPTG to yield improved expression features such as high-level gene expression and population

homogeneity, yet uncovers specific drawbacks of photocaged IPTG with respect to temporal resolution.

Walsh et al. 2014
The combination of photocaged theophylline together with a tailor-made synthetic theophylline-responsive riboswitch yielded a spatiotemporal control of bacterial gene expression, whose functionality was closely interrelated to the target gene and thus the downstream region of the promoter, though.

Hansen et al. 2015
This review provides an extensive overview of valuable photocaging groups with a focus on strategies to provide wavelength-selective and chromatically orthogonal photouncaging.

Baker & Deiters 2014
This review article summarized recent developments and applications of light control using genetically encoded unnatural amino acids to optically trigger protein function.

Binder et al. 2016b
This study demonstrates straightforward applicability of photocaged IPTG in the biotechnological platform organism *C. glutamcium* and reveals clear benefits in contrast to conventional IPTG induction such as population homogeneity and superior expression strengths that are largely independent of growth phases.

•• of outstanding interest

Velema et al. 2014
This article impressively describes the first chromatically orthogonal and selective growth control of single bacterial strains in microbial consortia using photocaged antibiotics.

Luo et al. 2014
Different coumarinyl photocaged lysines are described to provide fluorescence reported spatiotemporal control in *E. coli* and mammalian cells over a broad spectral range including UV-A, blue- and IR-light (TPU).

Fournier et al. 2013, 2014
A novel blue- to green-light absorbing 7-diethylamino-4-thiocoumarinylmethyl photocaging group with low UV-A absorptivity is presented as highly applicable for photorelease of bioactive compounds in living zebrafish embryos.

Bier et al. 2016
This article describes the plug-and-play synthesis of diverse photocaged carbohydrates together with their photochemical properties and further highlights selected compounds as highly prospective for future biotechnological applications.

Wandrey et al. 2016
In this study photocaged IPTG based light regulation was successfully combined with a high-throughput screening system based on a novel photomicrobioreactor to control, monitor and optimize heterologous protein production by optical means.

Binder et al. 2016
This study highlights photocaged arabinose as the first one-step photocleavable bacterial inducer for fast, accurate and homogeneous control of target gene expression that works independently of target genes or secondary cellular reactions.

REFERENCES

1 Brieke, C. *et al.* (2012) Light-controlled tools. *Angew. Chem. Int. Ed. Engl.* 51, 8446–76

2 Drepper, T. *et al.* (2011) Lights on and action! Controlling microbial gene expression by light. *Appl. Microbiol. Biotechnol.* 90, 23–40

3 Ellis-Davies, G.C.R. (2007) Caged compounds: photorelease technology for control of cellular chemistry and physiology. *Nat. Methods* 4, 619–28

4 Fan, N.-C. *et al.* (2012) Photocontrolled targeted drug delivery: photocaged biologically active folic acid as a light-responsive tumor-targeting molecule. *Angew. Chem. Int. Ed. Engl.* 51, 8806–10

5 Lerch, M.M. *et al.* (2016) Emerging Targets in Photopharmacology. *Angew. Chem. Int. Ed. Engl.* 55, 10978-99.

6 Klán, P. *et al.* (2013) Photoremovable protecting groups in chemistry and biology: reaction mechanisms and efficacy. *Chem. Rev.* 113, 119–91

7 Hansen, M.J. *et al.* (2015) Wavelength-selective cleavage of photoprotecting groups: strategies and applications in dynamic systems. *Chem. Soc. Rev.* 44, 3358–77

8 Bort, G. *et al.* (2013) From one-photon to two-photon probes: "caged" compounds, actuators, and photoswitches. *Angew. Chem. Int. Ed. Engl.* 52, 4526–37

9 Fichte, M.A.H. *et al.* (2016) Three-Dimensional Control of DNA Hybridization by Orthogonal Two-Color Two-Photon Uncaging. *Angew. Chem. Int. Ed. Engl.* 55, 8948-52.

10 Givens, R.S. *et al.* (2012) Applications of *p*-hydroxyphenacyl (*p*HP) and coumarin-4-ylmethyl photoremovable protecting groups. *Photochem. Photobiol. Sci.* 11, 472–88

11 Houk, A.L. *et al.* (2016) Two-Photon Activation of *p*-Hydroxyphenacyl Phototriggers: Toward Spatially Controlled Release of Diethyl Phosphate and ATP. *J. Phys. Chem. B* 120, 3178–86

12 Goeldner, M. and Givens, R.S. (2005) *Dynamic Studies in Biology*, 1999 Wiley- VCH: Weinheim, Germany.

13 Furuta, T. *et al.* (1999) Brominated 7-hydroxycoumarin-4-ylmethyls: photolabile protecting groups with biologically useful cross-sections for two photon photolysis. *Proc. Natl. Acad. Sci. U. S. A.* 96, 1193–200

14 Eckardt, T. *et al.* (2002) Deactivation behavior and excited-state properties of (coumarin-4-yl)methyl derivatives. 2. Photocleavage of selected (coumarin-4-yl)methyl-caged adenosine cyclic 3',5'-monophosphates with fluorescence enhancement. *J. Org. Chem.* 67, 703–10

15 Hagen, V. *et al.* (2003) [7-(Dialkylamino)coumarin-4-yl]methyl-Caged Compounds as Ultrafast and Effective Long-Wavelength Phototriggers of 8-Bromo-Substituted Cyclic Nucleotides. *Chembiochem* 4, 434–42

16 Amatrudo, J.M. *et al.* (2014) Wavelength-selective one- and two-photon uncaging of GABA. *ACS Chem. Neurosci.* 5, 64–70

17 Fournier, L. *et al.* (2013) Coumarinylmethyl Caging Groups with Redshifted Absorption. *Chem. - A Eur. J.* 19, 17494–17507

18 Fournier, L. *et al.* (2013) A blue-absorbing photolabile protecting group for *in vivo* chromatically orthogonal photoactivation. *ACS Chem. Biol.* 8, 1528–36

19 Luo, J. *et al.* (2014) Genetically encoded optochemical probes for simultaneous fluorescence reporting and light activation of protein function with two-photon excitation. *J. Am. Chem. Soc.* 136, 15551–8

20 Gorka, A.P. *et al.* (2014) A near-IR uncaging strategy based on cyanine photochemistry. *J. Am. Chem. Soc.* 136, 14153–9

21 Nani, R.R. *et al.* (2015) Near-IR Light-Mediated Cleavage of Antibody-Drug Conjugates Using Cyanine Photocages. *Angew. Chem. Int. Ed. Engl.* 54, 13635–8

22 Schaper, K. *et al.* (2010) The α,5-dicarboxy-2-nitrobenzyl caging group, a tool for biophysical applications with improved hydrophilicity: synthesis, photochemical properties and biological characterization. *Photochem. Photobiol.* 86, 1247–54

23 Hagen, V. *et al.* (2001) Highly Efficient and Ultrafast Phototriggers for cAMP and cGMP by Using Long-Wavelength UV/Vis-Activation. *Angew. Chemie Int. Ed.* 40, 1045–1048

24 Bier, C. *et al.* (2016) Photocaged carbohydrates – versatile tools for controlling gene expression by light. *Synthesis (Stuttg).* DOI: 10.1055/s-0035-1562617.

25 Chen, Y. and Steinmetz, M.G. (2005) Photochemical cyclization with release of carboxylic acids and phenol from pyrrolidino-substituted 1,4-benzoquinones using visible light. *Org. Lett.* 7, 3729–32

26 Chen, Y. and Steinmetz, M.G. (2006) Photoactivation of amino-substituted 1,4-benzoquinones for release of carboxylate and phenolate leaving groups using visible light. *J. Org. Chem.* 71, 6053–60

27 Carling, C.-J. *et al.* (2015) Efficient Red Light Photo-Uncaging of Active Molecules in Water Upon Assembly into Nanoparticles. *Chem. Sci.* 7, 2392–2398

28 Wandrey, G. *et al.* (2016) Light-induced gene expression with photocaged IPTG for induction profiling in a high-throughput screening system. *Microb. Cell Fact.* 15, 63

29 Velema, W.A. *et al.* (2014) Photopharmacology: beyond proof of principle. *J. Am. Chem. Soc.* 136, 2178–91

30 San Miguel, V. *et al.* (2011) Wavelength-selective caged surfaces: how many functional levels are possible? *J. Am. Chem. Soc.* 133, 5380–8

31 Bao, C. *et al.* (2015) Building biomedical materials using photochemical bond cleavage. *Adv. Mater.* 27, 1647–62

32 Uprety, R. *et al.* (2014) Genetic encoding of caged cysteine and caged homocysteine in bacterial and mammalian cells. *Chembiochem* 15, 1793–9

33 Baker, A.S. and Deiters, A. (2014) Optical control of protein function through unnatural amino acid mutagenesis and other optogenetic approaches. *ACS Chem. Biol.* 9, 1398–407

34 Chou, C. *et al.* (2010) Photocaged t7 RNA polymerase for the light activation of transcription and gene function in pro- and eukaryotic cells. *Chembiochem* 11, 972–7

35 Hemphill, J. *et al.* (2013) Genetically encoded light-activated transcription for spatiotemporal control of gene expression and gene silencing in mammalian cells. *J. Am. Chem. Soc.* 135, 13433–9

36 Wilkins, B.J. *et al.* (2010) Site-specific incorporation of fluorotyrosines into proteins in *Escherichia coli* by photochemical disguise. *Biochemistry* 49, 1557–9

37 Gautier, A. *et al.* (2010) Genetically encoded photocontrol of protein localization in mammalian cells. *J. Am. Chem. Soc.* 132, 4086–8

38 Lemke, E. a *et al.* (2007) Control of protein phosphorylation with a genetically encoded photocaged amino acid. *Nat. Chem. Biol.* 3, 769–72

39 Deiters, A. *et al.* (2006) A genetically encoded photocaged tyrosine. *Angew. Chem. Int. Ed. Engl.* 45, 2728–31

40 Young, D.D. and Deiters, A. (2007) Photochemical activation of protein expression in bacterial cells. *Angew. Chem. Int. Ed. Engl.* 46, 4290–2

41 Binder, D. *et al.* (2014) Light-responsive control of bacterial gene expression: precise triggering of the *lac* promoter activity using photocaged IPTG. *Integr. Biol. (Camb).* 6, 755–65

42 Binder, D. *et al.* (2016) Photocaged Arabinose - A Novel Optogenetic Switch for Rapid and Gradual Control of Microbial Gene Expression. *Chembiochem* 17, 296–299

43 Lynch, S.A. and Gallivan, J.P. (2009) A flow cytometry-based screen for synthetic riboswitches. *Nucleic Acids Res.* 37, 184–92

44 Young, D.D. and Deiters, A. (2006) Photochemical hammerhead ribozyme activation. *Bioorg. Med. Chem. Lett.* 16, 2658–61

45 Walsh, S. *et al.* (2014) Intracellular light-activation of riboswitch activity. *Chembiochem* 15, 1346–51

46 Wong, P.T. *et al.* (2016) Light-controlled active release of photocaged ciprofloxacin for lipopolysaccharide-targeted drug delivery using dendrimer conjugates. *Chem. Commun. (Camb).* 52, 10357-60.

47 Velema, W. a *et al.* (2015) Bacterial patterning controlled by light exposure. *Org. Biomol. Chem.* 13, 1639–42

48 Velema, W.A. *et al.* (2014) Orthogonal control of antibacterial activity with light. *ACS Chem. Biol.* 9, 1969–74

49 Buhr, F. *et al.* (2015) Design of photocaged puromycin for nascent polypeptide release and spatiotemporal monitoring of translation. *Angew. Chem. Int. Ed. Engl.* 54, 3717–21

50 Gardner, L. *et al.* (2011) Photochemical control of bacterial signal processing using a light-activated erythromycin. *Mol. Biosyst.* 7, 2554–7

51 Cambridge, S.B. *et al.* (2006) A caged doxycycline analogue for photoactivated gene expression. *Angew. Chem. Int. Ed. Engl.* 45, 2229–31

52 Cambridge, S.B. *et al.* (2009) Doxycycline-dependent photoactivated gene expression in eukaryotic systems. *Nat. Methods* 6, 527–31

53 Hemphill, J. *et al.* (2014) Site-specific promoter caging enables optochemical gene activation in cells and animals. *J. Am. Chem. Soc.* 136, 7152–8

54 Hemphill, J. *et al.* (2015) Optical Control of CRISPR/Cas9 Gene Editing. *J. Am. Chem. Soc.* 137, 5642–5

55 Barth, A. and Corrie, J.E.T. (2002) Characterization of a new caged proton capable of inducing large pH jumps. *Biophys. J.* 83, 2864–71

56 Mbatia, H.W. *et al.* (2012) CuproCleav-1, a first generation photocage for Cu+. *Chem. Commun. (Camb).* 48, 5331–3

57 Rakauskaitė, R. *et al.* (2015) Biosynthetic selenoproteins with genetically-encoded photocaged selenocysteines. *Chem. Commun. (Camb).* 51, 8245–8

58 Ballister, E.R. *et al.* (2014) Localized light-induced protein dimerization in living cells using a photocaged dimerizer. *Nat. Commun.* 5, 5475

59 Shao, Q. *et al.* (2009) Photoactivable bioluminescent probes for imaging luciferase activity. *Chem. Commun. (Camb).* 27, 4028–30

60 Gardner, L. and Deiters, A. (2012) Light-controlled synthetic gene circuits. *Curr. Opin. Chem. Biol.* 16, 292–9

61 Binder, D. *et al.* (2016) Light-controlled cell factories - Employing photocaged IPTG for light-mediated optimization of *lac*-based gene expression and (+)-valencene biosynthesis in *Corynebacterium glutamicum*. *Appl. Environ. Microbiol.* DOI: 10.1128/AEM.01457-16.

62 Rodrigues-Correia, A. *et al.* (2014) Selective uncaging of DNA through reaction rate selectivity. *Org. Lett.* 16, 5128–31

63 Kim, H.S. *et al.* (2014) A microfluidic photobioreactor array demonstrating high-throughput screening for microalgal oil production. *Lab Chip* 14, 1415–25

64 Grünberger, A. *et al.* (2014) Single-cell microfluidics: opportunity for bioprocess development. *Curr. Opin. Biotechnol.* 29, 15–23

65 Szymański, W. *et al.* (2013) Reversible photocontrol of biological systems by the incorporation of molecular photoswitches. *Chem. Rev.* 113, 6114–78

66 Ziegler, T. and Möglich, A. (2015) Photoreceptor engineering. *Front. Mol. Biosci.* 2, 30

III. General Discussion

Within the framework of this thesis, a set of different universally applicable light-controlled expression systems was established in *E. coli*, transferred to alternative expression hosts and applied in first biotechnological applications. Here, the established optogenetic expression tools will be shortly summarized (**III.1**) and compared to existing photocaged compound and photoreceptor-based approaches to control bacterial gene expression by light (**III.2**). Furthermore, prospective and future targets for light-controlled expression setups in different biotechnological key microbes will be discussed (**III.3**). Besides the obvious advantages arising from light-control, special future applications (**III.4**) will be elucidated in-depth that might hugely benefit from photo-uncaging concepts. Conclusively, light-control using photocaged compounds will be critically assessed in terms of future applicability, feasibility and transfer to industrial applications (**III.5**).

III.1 Summary of within this work established light-controlled expression systems

Different light-controlled expression systems based on photocaged compounds were established during this work, and within associated and co-supervised bachelor or master projects. In the following, these will be briefly capitulated under consideration of individual highlight findings, with key aspects summarized in **Table III.1**.

Initially, the previously described photocaged IPTG (Young and Deiters 2007b) was applied in a redirected and optimized T7RP-based high-level gene expression circuit (**Chapter II.3.1**) (Binder et al. 2014). Here, the expression response showed several improved features, which will be elucidated in the next chapter. In this study, the two-step-photocleavage reaction and the involved delay of gene expression response were uncovered as clear bottlenecks of photocaged IPTG-based light induction. In a more recent approach (**Chapter II.4.2**), the loss of temporal resolution was circumvented by means of extensive process optimization including the application of higher working concentrations, higher light-intensities, higher cell densities or synthetic cultivation media (Wandrey et al. 2016). Cultivation and light parameters could thus be modified accordingly to produce an immediate expression response, which was comparable to IPTG induction.

Similarly, during the application of photocaged IPTG in *C. glutamicum* (**Chapter II.5.1**) the loss of temporal resolution due to the two-step-photocleavage was negligible under applied conditions and even outperformed the generally poor induction with conventional IPTG slightly (Binder et al. 2016b).

Furthermore, light-controlled gene expression using photocaged IPTG was transferred to the alternative expression hosts *P. putida* and *B. subtilis* within the framework of two associated bachelor theses of Sonja Kubicki and Nora Bitzenhofer (Bitzenhofer 2016; Kubicki 2015). In *P. putida*, light induction using photocaged IPTG was found to exhibit a moderate inductivity and would need further process optimization prior to a straightforward application (Kubicki 2015). Here, the impact of two-step-photocleavage is not yet fully elucidated. Moreover, light induction using photocaged IPTG, in *B. subtilis*, provided an efficient induction (Bitzenhofer 2016) of P_{T7lac} promoter based gene expression (Püth 2015; Troeschel et al. 2012). Even though comparable expression results could be obtained for both IPTG and light induction, the two-step-photocleavage was found to delay the gene expression response significantly.

TABLE III.1 | Summary of established light-controlled expression systems.

Compound	Expression host	Induction / Repression [x-fold]	Advantages	Applicability* (Bottlenecks)	Reference
Photocaged IPTG	*E. coli* Tuner(DE3)	50	Homogeneity, gradual regulation	**++** (Two-step-photocleavage / Temporal resolution)	(Binder et al. 2014; Wandrey et al. 2016)
Photocaged IPTG	*C. glutamicum* ATCC13032	240	Homogeneous, gradual & strong induction (> IPTG)	**+++** (Two-step-photocleavage)	(Binder et al. 2016b)
Photocaged Arabinose	*E. coli* LMG(DE3)	60	Homogeneous, gradual & rapid regulation	**+++** (n.d.)	(Binder et al. 2016a)
Photocaged IPTG	*P. putida* KT2440	10	Gradual regulation	**+/-** (high working concentrations, low expression levels)	(Kubicki 2015)
Photocaged IPTG	*B. subtilis* DB430-T7	12	Gradual regulation	**+/-** (Two-step-photocleavage / moderate dynamic range)	(Bitzenhofer 2016)
Photocaged Galactose	*E. coli* BL21(DE3)	3.5	First one-step photocleavable *lac* inducer	**+** (low dynamic range)	(Bier et al. 2016)
Photocaged Rhamnose	*E. coli* Tuner(DE3)	4	One-step photocleavable	**++** (no full repression)	(Bier et al. 2016)
Photocaged Glucose	*E. coli* BL21(DE3)	1.6	One-step photocleavable, High solubility	**+/-** (high working concentrations, growth impairments)	(Bier et al. 2016)
Photocaged Lactose	*E. coli* BL21(DE3)	34**	Much stronger and faster induction than Lactose	**--** (enzymatic hydrolysis *in vivo*)	(Bier et al. 2016)

* Rough estimation of applicability for precise regulation of gene expression with regard to presented (dis-)advantages.
** For UV-A light exposed and unexposed cultures.
Grey lines highlight the results of two bachelor projects that were concerned with setting up NP-photocaged IPTG based light-control in the alternative expression hosts *P. putida* and *B. subtilis*.

In contrast, instantaneous light-control was demonstrated applying photocaged arabinose (**Chapter II.3.2**), which is released in an efficient one-step photolysis (Binder et al. 2016a). Under standard lab conditions in *E. coli,* photocaged arabinose was found

to temporally outperform the induction response of photocaged IPTG up to 2.1-fold and enabled the up-to-date most rapid regulation of bacterial gene expression by light.
Furthermore, the NP-photocaging that was applied for arabinose is highly versatile (**Chapter II.3.3**), and thus led to the development of further photolabile carbohydrates (Bier et al. 2016). In this study, *in vivo* functionality of photocaged derivatives of galactose, rhamnose and glucose was in principle approved in *E. coli*. Here, in-depth characterization and optimization has to be conducted and will lead to highly applicable photoswitches for microbial gene expression in the near future, though.
Lastly, photocaged lactose (**Chapter II.3.3**) showed highly favorable expression characteristics in terms of rapid and strong induction of gene expression that can probably be attributed to significantly improved resorption kinetics in terms of membrane permeability. However, the compound was found to be not stable in *E. coli* (Bier et al. 2016), which presumably leads back to enzymatic hydrolysis e.g. by intrinsic glycosidases or especially by the *β*-galactosidase. Here, it might be interesting to review light control in novel hosts with poor glycosidase activity or *lacZ*-deficient strains such as *E. coli* Tuner(DE3). Notably, the example of photocaged lactose illustrates that the wealth of hydrolyzing microbial enzymes is a crucial aspect that dictates *in vivo* applicability of photocaged compounds.
The summary of all presented light-controlled expression systems based on photocaged compounds demonstrates that light induction of gene expression is, in principle, highly applicable for different biotechnological key microbes (**Tab. III.1**).

III.2 Comparison to existing optogenetic switches

In the following chapter, the established light-controlled expression systems, which were developed within the framework of this thesis, will be compared to existing approaches of controlling bacterial gene expression by light. To this end, both photo-uncaging applications (**III.2.1**) and genetically-encoded photoreceptors (**III.2.2**) will be appraised.

III.2.1 Comparison to photo-uncaging applications

First of all, with **NP-photocaged IPTG** a highly sophisticated approach of controlling gene expression by light was described in 2007. This work was a milestone for light-activated bacterial gene expression using caged compounds (Young and Deiters 2007b). Here, the application of 0.5 mM of photocaged IPTG in a pUC19 plasmid-based *E. coli* BL21(DE3) expression system yielded an about 10-fold light activation of P_{lac}-

derived *lacZ* expression, which corresponded to approximately 85% of the expression response obtained with conventional, equimolar IPTG induction.

Based on this approach, photocaged IPTG mediated light-control was within this work (**Chapter II.3.1**) transferred to alternative expression systems in order to establish more applicable biotechnological expression setups (Binder et al. 2014). In detail, T7RP-based high-level gene expression systems were applied to realize stronger overall expression levels than those achieved with simple P_{lac} promoters. Furthermore, cultivation conditions were optimized to obtain expression outputs that were fully comparable to conventional IPTG induction. Here, it was crucial to light-induce gene expression in time to allow sufficient intracellular hydrolysis of released photoproduct esters. Moreover, the novel expression setup allowed the application of up to 12.5-fold reduced working concentrations of 40 µM and a highly gradual regulation that is known to be impeded for common *lac*-based gene expression systems (Hartinger et al. 2010; Ozbudak et al. 2004; Samuelson 2011). Lastly, the single-cell responses of photocaged IPTG-based light induction were tuned towards homogeneity by applying the *lac* permease-deficient *E. coli* Tuner(DE3) expression host, yielding an overall high degree of precise light regulation down to the single-cell level. Notably, the relatively low temporal resolution due to the essential two-step-photocleavage reaction remained as one distinct bottleneck of photocaged IPTG based light regulation.

In a further study (**Chapter II.4.2**), however, also this drawback could be abolished *via* extensive process optimization in a novel photomicrobioreactor setup (Wandrey et al. 2016). Here, 10-fold elevated working concentrations as well as the application of a synthetic cultivation medium and about 40-fold higher UV-A light intensities yielded an instantaneous expression response that was highly comparable to conventional IPTG induction. Although the exact reasons of the improved temporal resolution are not yet fully elucidated, the study illustrates that rapid regulation of gene expression is also feasible using photocaged IPTG. Moreover, it demonstrated that the transient nitroso-photoproducts, which emerge upon photolysis of photocaged IPTG, are well suited for fluorescence-based online monitoring of the photouncaging reaction.

In addition to photocaged IPTG-driven induction of gene expression, which displays a low-molecular photocaged compound, a different approach was developed by Chou *et al*. presenting **NB-photocaged T7RP**. Here, the introduction of NB-photocaged tyrosine into a protein was realized *via* orthogonal tRNA synthase-tRNA pairs from *Methanococcus jannaschii* (Chou et al. 2010). Through the replacement of a catalytically active tyrosine by NB-photocaged tyrosine, photo-functionality of recombinant T7RP proteins could be attained to trigger T7RP-derived gene expression in both *E. coli* and mammalian cells. Although the sophisticated application of photocaged amino acids to

gain light-regulation of protein activities is quite elaborated and was shown in principle for a multitude of amino acids and proteins (Baker and Deiters 2014), labor input and quantity of required functional elements still restrict unconfined application.

Another, valuable approach of controlling gene expression by light is concerned with riboswitch regulation and was recently exemplified by means of photocaged theophylline (Walsh et al. 2014). Here, light-activation of **NP-photocaged theophylline** (Walsh et al. 2014; Young and Deiters 2006) was able to 276-fold upregulate *lacZ*-reported gene expression using a synthetic theophylline riboswitch (Lynch and Gallivan 2009), which was strictly dependent on the target gene region, though. For the moment, this poor versatile deployment of different promoter-reporter or rather promoter-target gene combinations clearly restricts the application of NP-photocaged theophylline and illustrates the need for further extensive riboswitch engineering in the future (Berens and Suess 2015).

Ultimately, the photocaged arabinose constructed within this work (**Chapter II.3.2**) represents the first example of a one-step photocleavable inducer that allows fast, accurate and independent control of target gene expression in *E. coli*. In contrast to similarly sophisticated setups using photocaged theophylline or IPTG, photocaged arabinose performs independently of the target DNA downstream of the promoter (unlike caged theophylline) or secondary cellular reactions (unlike caged IPTG) (Binder et al. 2016a). Besides the more prevalent **NP-photocaged arabinose** derivative, a 1-(6-nitrobenzo[d][1,3]dioxol-5-yl)ethanol (NBE) photocage was able to improve the uncaging quantum yield about 2.6-fold (Binder et al. 2016a). Hence, **NBE-photocaged arabinose** further illustrates that simple modifying groups can play a major role in improving photochemical or physicochemical properties such as quantum yields or solubility. The so far uncharted potential of specifically tailoring photocaged compounds towards the respective application particularly in terms of solubility, photolysis, wavelength or membrane-permeability definitely has to be fully elucidated in the future.

Besides the here presented photocaged compounds to control bacterial gene expression, several other sophisticated approaches exist that approved light-control either *in vitro* or in eukaryotic systems (Deiters 2010; Gardner et al. 2011; Young and Deiters 2007a). It will be interesting to see if some of those photoswitches can be recruited for bacterial light-regulation.

III.2.2 Comparison to photoreceptor-based applications

In addition to elaborately designed chemical photoswitches, a recent research field is engaged in controlling gene expression in bacterial cells by means of genetically encoded photoreceptors (Drepper et al. 2011; Möglich and Moffat 2010; Ziegler and Möglich 2015). Here, both naturally occurring and artificially engineered photoreceptors are employed to control bacterial gene expression (Schmidt and Cho 2015; Shcherbakova et al. 2015; Ziegler and Möglich 2015). Three most relevant examples will be discussed hereafter.

The first recombinant photoreceptor for light-controlled gene expression in *E. coli* is the phytochrome-based **Cph8**, which comprises the cyanobacterial red-light sensing Cph1 domain from *Synechocystis* PCC6803 and the EnvZ histidine kinase domain from *E. coli* (Levskaya et al. 2005). Furthermore, the *Synechocystis* PCC6803 genes *ho1* and *pcyA* genes were introduced into the system to convert heme into the essential phytochrome chromophore phycocyanobilin. Upon red-light exposure, gene expression could be successfully repressed about 18-fold *via* the OmpR regulator in initial setups (Levskaya et al. 2005; Tabor et al. 2011). Further extensive optimization and expression level adjustments of this system yielded a compressed and highly applicable light-switch with 72-fold dynamic range that was efficiently activated or repressed upon excitation with light around 740 or 650 nm, respectively (Schmidl et al. 2014).

Similar to Cph8, another *Synechocystis* photosystem was employed, this time in its natural form, as a green light responsive photoswitch to control bacterial gene expression (Hirose et al. 2008; Tabor et al. 2011). The cyanobacterial two-component system comprises of the green-light sensing histidine kinase **CcaS** and its response regulator CcaR. Initial CcaS-based light-control of gene expression in *E. coli* was able to induce gene expression 2-fold (Tabor et al. 2011). Extensive redesign of the two-component system, however, achieved to tremendously enlarge the dynamic range of light-regulation up to 112-fold and finally yielded a green light sensor that is efficiently activated or repressed upon green and red irradiation around 520 and 650 nm, respectively (Schmidl et al. 2014).

Another prominent approach of light-controlled gene expression is based on the blue-light sensing recombinant LOV histidine kinase **YF1** (Möglich et al. 2009). Here, the YtvA LOV sensing-domain from *B. subtilis* was fused to the FixL kinase effector-domain of *Bradyrhizobium japonicum* to yield a blue-light repressed two-component system. In an initial setup, the artificial two component system YF1/FixJ was able to repress gene expression approximately 70-fold upon continuous blue-light exposure. Moreover, a redesign using an inversion cassette based on the lambda cI repressor yielded additional

blue-light activated expression setups that were capable to induce gene expression up to 460-fold in a highly dynamic fashion (Ohlendorf et al. 2012).

Compared to photocaged compounds, the application of genetically encoded photoreceptors generally bears both clear advantages and distinct bottlenecks (**Tab. III.2**). While photo-uncaging applications are usually activated upon **short light exposure** (seconds to minutes), photoreceptor-based applications often require either **continuous or pulsed irradiation** due to the commonly fast dark-recovery kinetics (Davidson et al. 2013; Ziegler and Möglich 2015). Although a fast dark-recovery might thus involve a more cost- and labor-intense light irradiation (e.g. temperature effects within the culture), it bears the considerable advantage of **reversibility**. For irreversible photoswitching, however, one can use photoreceptors with extended dark recoveries (Circolone et al. 2012). **Responsiveness** of light-regulation using photoreceptors lies in the same range as compared to those obtained with photocaged compounds, yet strictly depends on the respective photoreceptor setup. It can range from several minutes (Olson et al. 2014) to two hours (Ohlendorf et al. 2012) of delay for the protein production onset.

TABLE III.2 | Comparison of crucial light-control features for photocaged compounds and photoreceptors.

Feature	Photocaged compounds	Photoreceptors
Exposure	Short	Continuous or pulsed
Reversibility	None*	Full
Responsiveness	Fast	Fast
Spatial specificity	Moderate (Diffusion-limited)	Usually high
Reaction selectivity	Moderate	Cross-talk can occur
Stability	Usually stable	Usually stable
Toxicity	Can occur at high concentrations	Usually low
Homogeneity	Good	Usually good
Versatile applicability	Good	Restricted

*reversible chemical photoswitches such as azobenzenes (Szymański et al. 2013) are not discussed within this work.

The **specificity** of photoreceptor-based applications is expected to be high as photoreceptor proteins may be tagged or fused for specific localization, whereas photo-uncaging applications are usually subject to free diffusion. Here, however, caged proteins should bear a comparable specificity. Photoreceptor **selectivity** might be negatively affected by cross-talk between endogenous proteins, which is especially observed for bacterial sensor kinases (Krell et al. 2010). Such cross-talk, for instance, necessitated the deletion of the endogenous *E. coli* EnvZ histidine kinase in Cph8-based applications to prohibit the cross-talk with the shared response regulator OmpR (Levskaya et al. 2005; Olson et al. 2014; Tabor et al. 2011). Likewise, for some individual photocaged compounds, side-reactions have been reported (Pelliccioli and Wirz 2002; San Miguel et al. 2011).

In terms of **stability**, photoreceptors show slight benefits as compared to photocaged compounds. While photoreceptors might face problems regarding oligomerization or protein stability, photocaged molecules are challenged to resist partially harsh cellular environments as well as a multitude of modifying and degrading enzymes. This was, for instance, exemplified within this thesis by means of photocaged lactose (**Chapter II.3.3**), which significantly hydrolyzed *in vivo* even under dark conditions (Bier et al. 2016). Especially ester-moiety comprising photocaged compounds are prone to enzymatic degradation and beyond that are even in charge for the full release of some effector molecules like photocaged IPTG (Young and Deiters 2007b). By chemical means, however, it should be possible to provide sufficient *in vivo* stability of photocaged compounds using, for instance, bulky esters, modifying groups or simply an alternative photocaging derivative (Brieke et al. 2012; Goeldner and Givens 2005; Klán et al. 2013; Szymański et al. 2014).

The same is true for overcoming potential **toxicity** issues with individual photocaging derivatives and photocaged compounds. In the rare cases of compound toxicity, a variety of well-established photo-protection groups is available to choose from for reducing toxicity (Brieke et al. 2012; Hansen et al. 2015).

Both photocaged compounds (Binder et al. 2016a; Binder et al. 2016b; Binder et al. 2014) and photoreceptors (Ohlendorf et al. 2012; Olson et al. 2014) affect unexpected **population homogeneity** if applied for light-controlled gene expression. Conventional chemical induction, however, is commonly known to depict distinct cell-to-cell-variations (Balzer et al. 2013; Fritz et al. 2014; Marbach and Bettenbrock 2012).

One key advantage of photocaged compounds seems to be their **transferability** to alternative expression strains or hosts, as no heterologous expression (e.g. of photoreceptor genes) and the involved fine-adjustment of genetically encoded components (e.g. the balance between photoreceptor and response regulator) is required. Hence, given that an expression system is already applicable in a desired expression host, the implementation of light-control by means of photocaged inducers is quite feasible, as demonstrated within this work *via* application of photocaged IPTG in alternative expression hosts (Binder et al. 2016b; Bitzenhofer 2016; Kubicki 2015). Common photoreceptor based systems such as YF1-, Cph8 or CcaS-setups, however, were precisely tailored and mutagenized for *E. coli* (Gleichmann et al. 2013; Ohlendorf et al. 2012; Schmidl et al. 2014), thus neglecting the light-control in alternative auspicious biotechnological workhorses so far.

Conclusively, each approach of controlling cellular functions by light exhibits considerable advantages over the other. Probably, the power of light might be fully

harnessed only in a joint venture of photocaged compounds and photoreceptors for a bright future in synthetic biology and biotechnology (Brieke et al. 2012).

III.3 Prospective optogenetic expression systems

In the previous chapter, the versatile interspecies-transfer was highlighted as a key benefit of photocaged compounds. In this regard, alternative biotechnological workhorses (Liebl et al. 2014; Terpe 2006) such as *Bacilli* should be made accessible for light-control to tackle manifold photobiotechnological applications in the future (**Chapter III.4**). Moreover, novel expression systems have to be developed for already accessed organisms in order to achieve a higher-order control of gene cascades in a multimodal or multi-chromatic fashion. In this context, the triggering of different promotor/regulator systems by means of different light colors or light intensities poses a valuable tool to control complex gene sets and will be further appraised in a following chapter (**see Chapter III.4.3**). Beforehand, some prospective expression setups that qualify for setting up **future optogenetic switches** based on photocaged compounds will be discussed in the following (**Tab. III.3**, **Fig. III.1**).

For *E. coli,* additional expression tools exist, whereof the aTc-inducible P_{tet}/TetR, the L-rhamnose inducible P_{rhaBAD}/RhaRS and the propionate-inducible P_{prpR}/PrpR system are established systems for inducible gene expression (Terpe 2006).

The P_{tet}/TetR system (**Fig. III.1 A**) is well established for high-level gene expression in *E. coli* (Skerra 1994; Terpe 2006) and is commonly applying **aTc** as an inducer, due to its significantly improved TetR binding affinity and a distinctly lower antibiotic activity (Berens and Hillen 2003). Consequentially, extremely low working concentrations of about 200 nM can suffice for full induction. Thus, aTc-inducible gene expression represents an appealing target for a light-inductive system. Interestingly, for photoactivation of mammalian gene expression, the structural analogue doxycycline was already successfully subjected to photocaging (Cambridge et al. 2009; Cambridge et al. 2006; Sauers et al. 2010). Thus, it may be assumed that aTc could be readily photocaged in a similar manner.

Another established expression system in *E. coli* poses the P_{rhaBAD}/RhaRS system (**Fig. III.1 B**), which is highly similar to the P_{BAD}/AraC system (Brautaset et al. 2009; Haldimann et al. 1998). As photocaged **L-rhamnose** was already proven functional (**Chapter II.3.3**) in a repressible expression setup (Bier et al. 2016), light-activated gene expression using P_{rhaBAD}/RhaRS based gene expression poses an auspicious alternative that should be established in the future. Interestingly, a modified *rhaBAD* expression system solely

consisting of the RhaS regulator was just recently shown to provide efficient induction by means of alternative sugars such as L-mannose or L-lyxose (Kelly et al. 2016).

TABLE III.3 | Prospective targets for light-controlled expression setups *via* photocaging.

Host	System (Inducer)	Chemically accessibility of the inducer	x-fold induction (concentration)	Features	Reference
E. coli	P_{tet}/TetR (aTc)	+/-*	5000 0.4 µM	Low working concentrations	(Skerra 1994; Lutz and Bujard 1997)
	P_{rhaBAD}/RhaRS (Rhamnose)	++ (Bier et al. 2016)	7800 (2 -12 mM)	Large regulatory range	(Haldimann et al. 1998; Wagner et al. 2008)
	P_{prpB}/PrpR (Propionate)	+*	1500 (50 mM)	Cheap inducer, homogeneous, leaky but CCR-sensitive	(Lee and Keasling 2005)
	P_{T7lac}/LacI (Galactose)	++ (Bier et al. 2016)	10 (0.4 mM)	Moderate dynamic range	(Xu et al. 2012)
	P_{T7betO}/BetI (Choline)	++ (Peng and Goeldner 1996; Specht and Goeldner 2004)	20 / 130** (100 mM)	Inducible and Repressible, low basal expression	(Ike et al. 2015)
	Pm/XylS (Salicylate/ Anthranilate)	++*	30*** (1.5 mM)	Rapid and strong expression response but very leaky	(Binder et al. 2016c)
P. putida	P_{nagAa}/NagR (Salicylate)	++*	n.d. (0.1 -1 mM)	low basal expression & working concentration	(Schmitz et al. 2015; Wierckx et al. 2005)
	P_{sal}/NahR (Salicylate)	++*	175 (1 mM)	Tight & gradual regulation	(Calero et al. 2016)
	P_{rhaB}/RhaRS (Rhamnose)	++ (Bier et al. 2016)	750 (10 mM)	High regulatory range	(Calero et al. 2016)
	P_{araB}/AraC (Arabinose)	++ (Binder et al. 2016a)	n.d. (1 mM****)	Significantly lowered working concentration	(Calero et al. 2016)
C. glutamicum	P_{BAD}/AraC (Arabinose)	++ (Binder et al. 2016a)	>400 (4 mM)	Homogeneous	(Zhang et al. 2012)
	P_{prpD2}/PrpR (Propionate)	+*	120 (10 µM)	Low working concentrations, Reversible induction	(Plassmeier et al. 2013)
	P_{tet}/TetR (aTc)	+/-*	50 (0.5 µM)	Low working concentrations, Low basal expression	(Lausberg et al. 2012)
B. subtilis / B. megaterium	P_{xylA}/XylR (Xylose)	++*	>200 (30 mM)	Low basal expression, High-level but heterogeneous expression	(Bitzenhofer 2016; Stammen et al. 2010)

aTc: anhydrotetracycline. * Rough estimation. ** Repression. CCR: carbon catabolite repression. Leakiness can be reduced *via* glucose. *** Alternative promoter variants for reduced leakiness and thus improved dynamic ranges available. **** Using AraE overexpression.

Another prospective photocaging target seems to be **propionate** as it is highly applicable for controlling gene expression in *E. coli* (**Fig. III.1 C**) (Lee and Keasling 2005). Despite the simple structure of propionate it could be in some degree challenging to cage this inducer since ester-mediated photocaging of carboxyl moieties is commonly observed to readily undergo intracellular hydrolysis in bacteria.

In addition to those established expression systems, more recently a galactose-inducible P_{T7lac}/LacI (Xu et al. 2012), a choline-inducible P_{T7betO}/BetI system (Ike et al. 2015) and a salicylate-inducible Pm/XylS system (Binder et al. 2016c) were identified as valuable expression tools for *E. coli* and might pose appealing targets for photocaged inducers.

D-Galactose was a long time neglected as a valuable inducer for *lac* expression circuits (**Fig. III.1 D**), yet recent studies show strong galactose induction of *lac* based gene expression, especially in strains lacking the galactose kinase GalK, thus providing the inability to metabolize the inducer (Xu et al. 2012). In this context, synthesis and basic functionality of photocaged galactose (**Chapter II.3.3**) could be already proven within the framework of this thesis (Bier et al. 2016). However, further optimization seems essential to produce a more applicable expression setup in terms of expression strength and dynamic range of regulation for this first one-step-photocleavable *lac* inducer. Using *galK*$^+$ strains, it would be further conceivable to produce light-controlled reversible expression tools based on the metabolization of galactose.

As mentioned, novel **choline** inducible and repressible expression systems implementing the T7RP for high-level gene expression were established recently for *E. coli* (**Fig. III.1 E**) (Ike et al. 2015). Interestingly, in another context photocaged choline derivatives were already synthesized (Peng and Goeldner 1996; Specht and Goeldner 2004) and might empower future light-control of those choline-regulated expression tools.

Moreover, benzoate inducible Pm/XylS expression systems pose sophisticated tools for recombinant protein production (Balzer et al. 2013; Brautaset et al. 2009). While photocaging of the conventional inducer *m*-toluic acid might face similar problems as propionate due to its carboxyl moiety, alternative benzoate inducers like salicylic or anthranilic acid could be much more chemically accessible *via* their hydroxyl- or amino-functionalities, respectively. In this respect, the XylS regulator protein of the conventional Pm/XylS system was in the framework of this thesis (**Chapter II.1.1**) mutagenized to improve **salicylate** and anthranilate inducibility in *E. coli* significantly (Binder et al. 2016c).

In ***P. putida***, further salicylate-inducible expression systems have also been applied for gene expression control and were based on the P_{nagAa}/NagR (Schmitz et al. 2015; Wierckx et al. 2005) or the P_{sal}/NahR regulon (Calero et al. 2016). All three salicylate-inducible expression systems (**Fig. III.1 F**) would thus be highly attractive targets for novel light-controlled expression setups using either photocaged salicylate or anthranilate (for the novel Pm/XylS system) derivatives.

In general, *P. putida* qualifies as a highly versatile workhorse especially for natural product biosynthesis with vast intrinsic metabolic and enzymatic capacities (Loeschcke

and Thies 2015). Future light-controlled expression tools for *P. putida* might further target the L-rhamnose-inducible P_{rhaB}/RhaSR (**Fig. III.1 B**) or the L-arabinose-inducible P_{BAD}/AraC system (**Fig. III.1 G**) (Calero et al. 2016).

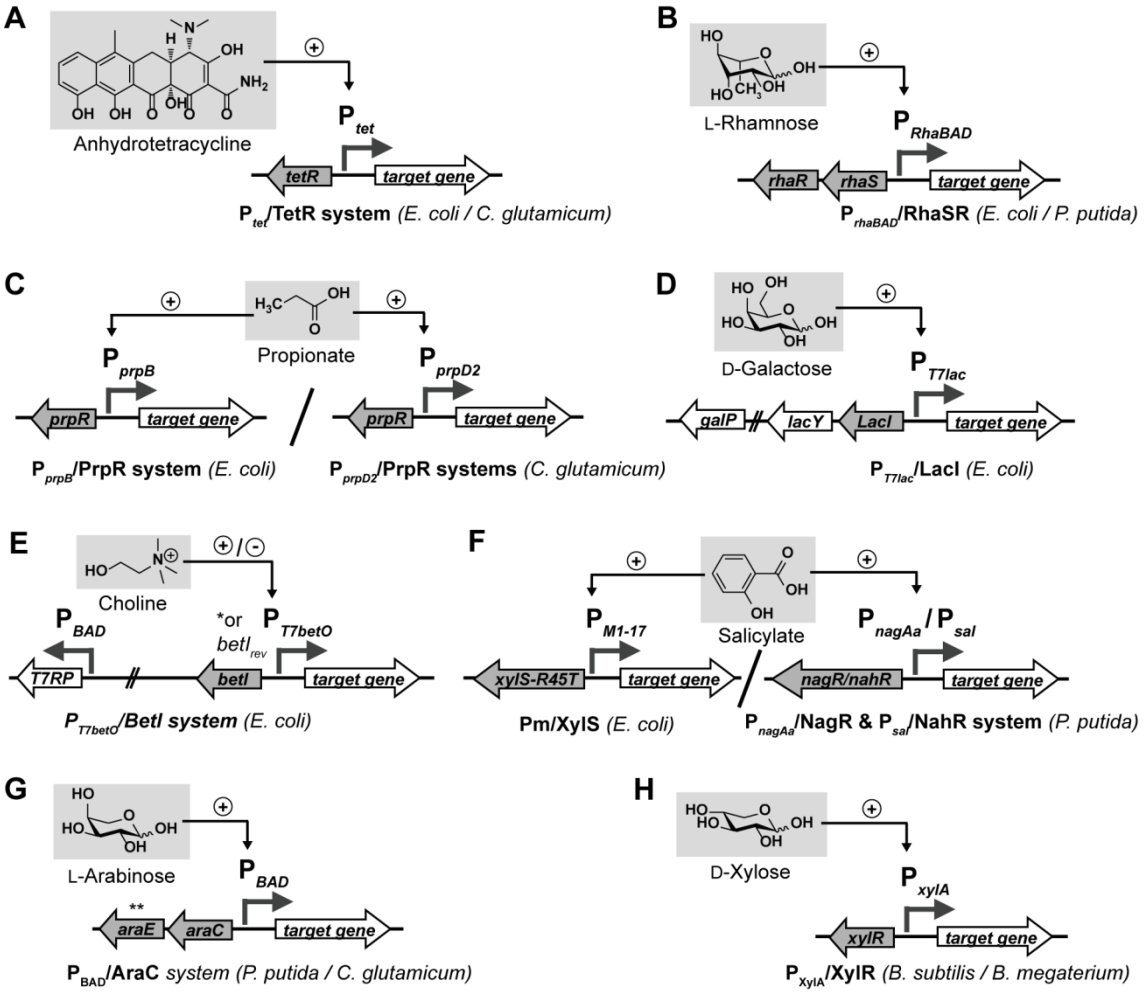

FIGURE III.1 | Putative targets for future light-controlled promoter / regulator systems.

(**A**) aTc-inducible gene expression in *E. coli* or *C. glutamicum* based on the P_{tet}/TetR-system. (**B**) L-rhamnose-inducible gene expression in *E. coli* or *P. putida* based on the P_{rhaBAD}/RhaRS-system. (**C**) Propionate-inducible gene expression in *E. coli* or *C. glutamicum* based on the $P_{prpB/D2}$/PprR-system. (**D**) Galactose-inducible gene expression in *E. coli* based on the P_{T7lac}/LacI-system. (**E**) Choline-inducible gene expression in *E. coli* based on the P_{T7betO}/BetI-system. Here, the T7RP drives choline-inducible gene expression in the presence of arabinose. BetI regulator mutants are available that reverse the choline response (*), producing choline-repressible setups. (**F**) Salicylate-inducible gene expression in *E. coli* or *P. putida* based on the Pm/XylS^{R45T}, the P_{nagAa}/NagR or the P_{sal}/NahR system. (**G**) L-Arabinose-inducible gene expression in *P. putida* or *C. glutamicum* based on the P_{BAD}/AraC system. The coexpression of *araE* (**), which encodes the arabinose transporter AraE, is optional, yet mediates both increased sensitivity and population homogeneity. (**H**) D-Xylose-inducible gene expression in *B. subtilis* or *B. megaterium* based on the P_{xylA}/XylR system.

Notably, for the P_{BAD}-based expression setup the coexpression of the AraE transporter gene yielded about 100-fold reduced and thus principally applicable working concentrations of 1 mM for photouncaging (Calero et al. 2016).

Several elaborated expression tools exist as well for the biotechnological workhorse ***C. glutamicum***, which represents one of the most important biotechnological platform organisms, particularly in regard to its contributions to the industrial amino acid production (Eggeling and Bott 2015; Jensen and Wendisch 2013; Mahr et al. 2015; Park et al. 2014; Wendisch 2014).

Here, analogous to *P. putida* and *E. coli,* a promising arabinose-inducible expression system was established recently that produced a homogeneous expression response upon constitutive *araE* coexpression (Zhang et al. 2012). A further prospective photocaging target seems to be propionate as it is highly applicable for controlling gene expression in *C. glutamicum* in a reversible fashion (**Fig. III.1 C**) (Plassmeier et al. 2013). Moreover, a P_{tet}/TetR system exists for *C. glutamicum*, which exhibits well-titratable gene expression with extremely low working concentrations in the nanomolar range (Lausberg et al. 2012).

Furthermore, Gram-positive ***Bacillus*** strains such as *B. subtilis* or *B. megaterium* are popular hosts for recombinant protein production due to their excellent protein secretion capacity (Korneli et al. 2013; Terpe 2006; Troeschel et al. 2012). Here, especially the **D-xylose**-inducible P_{xylA}/XylR system (**Fig. III.1 H**) is a highly attractive expression tool for both *B. subtilis* (Troeschel et al. 2012) and *B. megaterium* (Stammen et al. 2010). NP-photocaging is also conceivable for xylose, and could thus pave the way for future light-controlled gene expression in *Bacilli* based on photocaged xylose.

The here presented expression systems highlight the variety of inducible expression setups, which are yet un-accessed for light-control. For photocaged derivatives of rhamnose, galactose or arabinose, photocaging has been initiated and was already proven in principle (Bier et al. 2016; Binder et al. 2016a). Moreover, photocaged choline was already fully established for a quantitative release upon UV-A light exposure (Peng and Goeldner 1996; Specht and Goeldner 2004). Hence, novel light-controlled expression setups based on these compounds will most definitely emerge in the near future. In this context, the success of setting up novel photocaged compound-based photoswitches for *E. coli* and diverse alternative biotechnological key organisms will mainly depend on the successful synthesis, the compatibility of the respective host to light exposure or the necessary working concentrations.

Concerning aTc, propionate, salicylate or possibly anthranilate, chemical synthesis seems challenging, yet feasible and the multitude of accessible expression hosts with such inducers should provide a further incentive to realize their photocaging.

Notably, some bacteria are under reasonable suspicion to be more sensible or rather vulnerable for light exposure than others, taking into account that elaborate photo-sensing systems have evolved to protect the respective organism against excessive light exposure (Gomelsky and Hoff 2011). However, regarding *E. coli* (Binder et al. 2014), *P. putida* (Kubicki 2015), *C. glutamicum* (Binder et al. 2016b), *B. subtilis* or *B. megaterium* (Bitzenhofer 2016), at least UV-A light exposure, even in excessive amounts, appeared not to be harmful.

Lastly, the working concentration is a key aspect for the functionality of light-control. In this context, concentrations above 2 mM were found to impede bacterial growth (**Chapter II.3.3**) in individual cases to a certain extent (Bier et al. 2016). Moreover, the required UV-A light exposure increases proportionally with elevated working concentrations as well (**Chapter II.4.1**). This was, for instance, observed for the transfer of photocaged IPTG from *E. coli* to *C. glutamicum* (**Chapter II.5.1**), where the 2.5-fold increase in concentrations led to about 10-fold enlarged, yet still manageable, exposure times for full conversion (Binder et al. 2016b).

Conclusively, future work on novel light-controlled expression setups using photocaged compounds will surely benefit from the wealth of different sophisticated expression tools. Here, different alternative expression platforms such *P. putida*, *C. glutamicum*, *B. subtilis* or *B. megaterium* should play a major role to tackle versatile photobiotechnological applications such as natural compound or recombinant protein productions as well as high-throughput screenings appropriately.

III.4 Future photouncaging applications

Upon establishing a broad variety of light-controlled expression setups in various biotechnological key microbes, a multitude of future applications discloses, which will be subsequently discussed in further detail.

III.4.1 High-throughput light-control of micro-cultivations

Diverse bio(techno)logical questions require a **high-throughput** in the assessment of experimental parameters. For instance, microbial production processes are crucially dependent on parameters such as expression levels or time of induction. In this context, light is a valuable tool to implement precisely controlled parameter modifications into the respective application. Especially for picoliter scale cultivations such as monolayer

chambers (Grünberger et al. 2014), droplets (Kaminski et al. 2016; Mazutis et al. 2013) or agar pad-based setups (Young et al. 2012), the high **spatial resolution** of light provides considerable advantages that are scarcely complied with conventional chemical induction.

In this sense, two-photon-excitation seems a powerful tool to introduce light impulses into single-cell applications with utmost precision in the lower femtoliter-scale (Bort et al. 2013; Brieke et al. 2012; Fichte et al. 2016) and thus to empower the triggering of single populations or even cells. The concept of two-photon uncaging will later be elucidated in further detail (**Chapter III.4.2**). However, even focused one-photon excitation was shown to enable spatial control on the 20 µm-scale i.e. for areas with 20 µm in diameter (Ohlendorf et al. 2012) and hence outperforms conventional chemical induction distinctly.

In particular, for the control of numerous parallelized microsystems, optogenetic tools qualify for triggering single compartments with adequate spatial precision and in an appropriate amount of time. The additional **temporal benefit** of light-regulation becomes most evident if hundreds or thousands of parallelized cultures e.g. in 3456-well microtiter plates have to be induced at the same time and in a diversified fashion. Light induction can be easily implemented simultaneously, implying an appropriate light source, whereas conventional chemical induction requires invasive, time- and labor-intensive pipetting or pricey automated liquid handling systems (Huber et al. 2009; Rohe et al. 2012).

High-throughput screening is currently accompanied with elevated expenditures of work and time in pico- to nanoliter cultivations. The microfluidic perfusion setups that were applied in this study (**e.g. Chapter II.1.1**), for instance, bear four separately perfused nutrient channels, so that merely four different environmental conditions, e.g. inducer concentrations, may be applied (Gruenberger et al. 2013; Grünberger et al. 2015; Grünberger et al. 2014). Likewise, in microfluidic droplet cultivations (Mazutis et al. 2013) the high-throughput variation or temporal definition of different stimuli involves tremendous efforts. To this end, external and variable control of different events and especially at any given time-point would significantly facilitate the screening of e.g. expression parameters such as induction time points or strengths in current micro-cultivations (**Fig. III.2 A**). High-throughput light-control of microfluidic or droplet microfluidic single-cell applications might be implemented to existing setups *via* non-invasive and spatiotemporal triggering of defined zones. In this sense, light-gradients could be introduced with high temporal flexibility by means of miniaturized graduated neutral-density filters or light-impermeability gradients.

The later concept was just recently exemplified in a light-mediated high-throughput screening of microalgal growth using novel microfluidic photo-bioreactors by creation of up to 64 different light conditions *via* a black dye gradient (Kim et al. 2014). This study properly demonstrates how light-control can assist in setting up high-throughput single-cell applications in the future.

Moreover, standard micro- to milliliter scale high-throughput cultivations could experience a higher degree of throughput applying optogenetic tools.

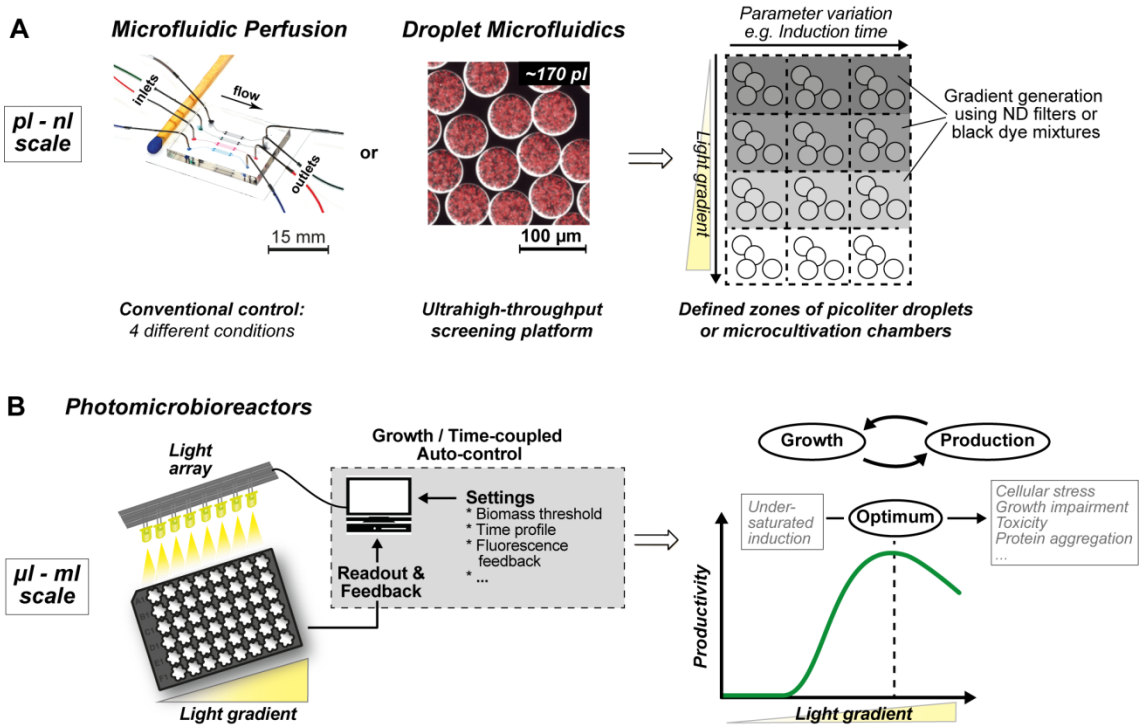

FIGURE III.2 | Prospective high-throughput light-control of micro-cultivations.

(**A**) Light-control of pico- to nanoliter-scale micro-cultivations. While conventional microfluidic perfusion (left) or droplet microfluidic setups (center) enable cultivations under only few different conditions, the implementation of light-control in terms of e.g. gradually increased light intensities alongside the microchips would allow varying a much broader range of parameters upon spatiotemporal light induction (using e.g. photocaged inducers for induction). Modified from Binder *et al.* (2014) *Integr Biol (Camb)* 6: 755–65; doi: 10.1039/c4ib00027g (Fig. III.2 A left) and Mahler *et al.* (2015) *RSC Adv* 5:101871–101878; doi: 10.1039/C5RA20118G (Fig. III.2 A middle), under the terms of the Creative Commons Attribution-Non Commercial 3.0 Unported Licence. (**B**) In advanced photomicrobioreactors (µl–ml scale cultivations) light-control can assist to fully automatize cultivation control (left), where online-monitoring of biomass production and fluorescent feedback is implemented to conditionally (e.g. upon achieving certain thresholds) trigger single-well cultivations, and, for instance, pursues the superior goal of finding optimal induction levels and time points as well as a perfect balance between growth and production (right).

For microbial productions, conventional chemical induction is frequently applied to vary induction levels and thus optimize recombinant protein production. Here, applied conventional chemical induction discloses obvious bottlenecks as high-throughput would necessitate costly automated liquid handling systems (Huber et al. 2009; Rohe et al.

2012) or labor- and time-consuming manual pipetting that entails considerably elevated contamination risks.

Light induction, however, can fully exploit spatiotemporal, non-invasive and gradual features of electromagnetic radiation and thusly qualifies for high-throughput and full automation of microbial cultivations (**Fig. III.2 B**). High-throughput feasibility was illustrated in this work (**Chapter II.4.2**) by means of photocaged IPTG based induction profiling (Wandrey et al. 2016). Moreover, future bioprocesses could be fully automatized by time- or growth-coupled light induction to serve the superior goal of optimizing microbial cultivations with respect to optimal productivity or a perfect balance between growth and production.

III.4.2 Light-controlled special applications

Besides the employment of spatiotemporal light-control to elevate the high-throughput of microbial cultivations, electromagnetic radiation bears additional benefits for several special synthetic bio(techno)logical applications.

The **non-invasive fashion** of light would enable to trigger **closed applications** from the outside, thus providing minimal process perturbation (**Fig. III.3 A**). Evidently, **anaerobic or small volume batch cultivations** could benefit from non-invasive light control since supplementation of, for example, chemical inducers during the process would entail oxygenation, dilution or at least tremendous technical efforts to minimize such customary interferences. In this context, the non-invasive and spatiotemporal triggering of different anaerobes such as *Chlostridium*, *Actinomyces, Bacteroides* or *Rhodobacter*, could provide a higher degree of regulation to tackle various aspiring anaerobic biotechnological applications (Cueto-Rojas et al. 2015). For instance, the phototrophic Gram-negative bacterium *R. capsulatus* displays tremendous membrane storage and unique metabolic capacities only under anaerobic conditions that qualify for prospective applications such as high-level membrane protein production (Katzke et al. 2012; Katzke et al. 2010; Özgür 2015, Heck & Drepper 2016). Nonetheless, sophisticated expression tools for temporal and external control of gene expression or growth lack to a large extent and should be established in the future based on optogenetic approaches.

Furthermore, the **high selectivity and specificity** together with its excellent **spatiotemporal precision**, empowers electromagnetic radiation to control complex tasks such as specific events in **multicellular environments** (**Fig. III.3 B**). Hence, light can provide precise control of microbial consortia to gain so far uncharted insights into the complexity of a multicellular microbial world and to tackle prospective multi-species

applications (Brenner et al. 2008; Hays et al. 2015; Song et al. 2014). In this context, diverse applications have been explored and can be anticipated in the future.

For instance, the growth of different microbial species can be precisely balanced by means of photocaged or photoswitchable antibiotics (Velema et al. 2015; Velema et al. 2014a; Velema et al. 2013). This was recently exemplified for a mixture of *E. coli* and *Staphylococcus aureus* using photocaged derivatives of fluoroquinolone and benzylpenicillin in an orthogonal fashion (Velema et al. 2014a). Here, a light-triggered conditional species selection was conducted by exposure to UV-B or white light, respectively.

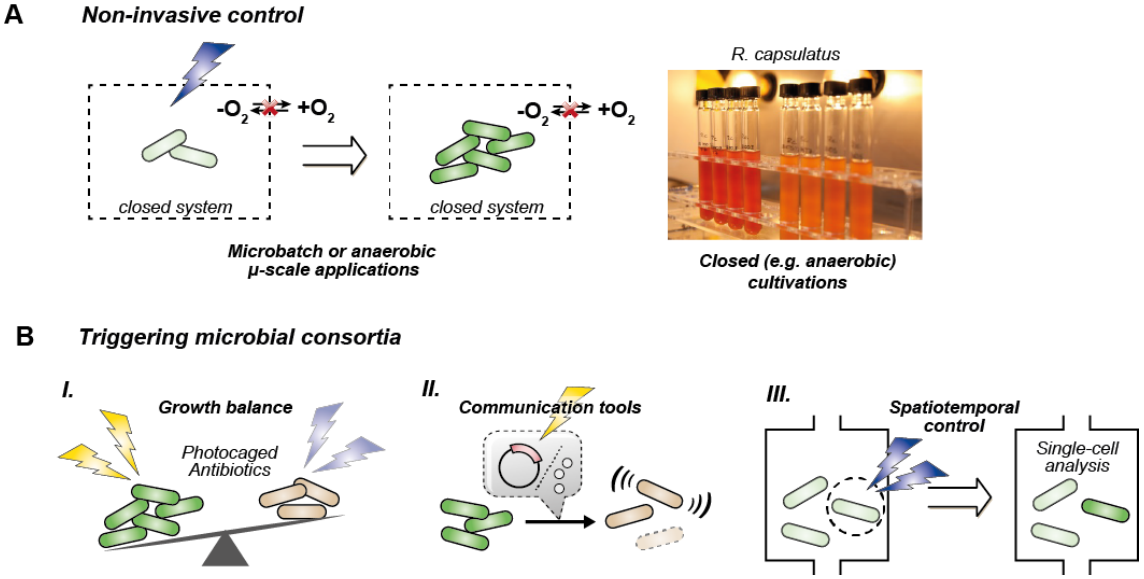

FIGURE III.3 | Potential of light-control for special synthetic bio(techno)logical applications.
(**A**) Non-invasive triggering of micro-scale applications (e.g. micro-batch or anaerobic cultivations) that can be triggered by light with minimal oxygenation- or dilution-effects and thus minimal process perturbation (left). Also anaerobic lab-scale cultivations such as those with *R. capsulatus* (picture generously provided by Dr. Achim Heck) might benefit from additional external light-control using optogenetic switches (right). (**B**) Especially at the single-cell level, spatiotemporal light-control of microbial consortia would enable (*I.*) a convenient species balance between two microorganisms *via* photocaged antibiotics, (*II.*) a precisely coordinated inter-species communication and (*III.*) the excitation of single-cells in isogenic populations *via* two-photon excitation.

Furthermore, inter-cellular communication tools (Hays et al. 2015; Song et al. 2014) might be subjected to light-control in order to gain spatiotemporal regulation of processes that are crucial for the entire consortium. This way, otherwise constitutively or randomly executed processes like horizontal gene transfer, plasmid replication, predation or simple metabolite exchange could be specifically light-programmed to design and optimize synthetic microbial consortia for biotechnological or biomedical purposes. In this context, precisely timed shared productions or bacterial ‘physicians’ that selectively

deliver therapeutics or rather antibiotics to pathogenic cells would be valuable targets for light-control (Claesen and Fischbach 2015; Medema et al. 2011; Smanski et al. 2016).
Lastly, spatiotemporal light-control of single-cells e.g. by means of **two-photon-excitation** can disclose yet uncharted insights into single-cell dynamics as well as signal perception and propagation. The specific implementation of a light impulse to a single-cell would allow gaining novel insights on signal perception and propagation that are otherwise perturbed in complex populations. Here, single-cell triggering could unravel the impact of surrounding microbes on phenotypic heterogeneity in isogenic or multi-species microbial consortia more clearly.
However, it will be of pivotal interest to see how highly diffusive caged and uncaged compounds might limit the spatial resolution of a light impulse. To this end, the commonly reported intracellular accumulation and the bidirectional diffusion of caged biomolecules has to be subject to future studies. Specifically, further extensive work is needed on cell-permeability and intracellular accumulation of caged and uncaged compounds to finally elucidate the question to what extent photocaged compound based light control can be applied at low picoliter-scale spatial resolution in the future.
Irrespective of the yet unanswered exact impact of two-photon-uncaging (TPU) on the spatial resolution of light control, the approach involves a novel mode of regulation in the red to IR range. Given that respective compounds exhibit convenient TPU cross sections, also UV-B and UV-C absorbing compounds can be readily recommitted for biological applications as TPU drives them at twice the wavelength applied for conventional excitation (Houk et al. 2016). Furthermore, using TPU it will be possible to discriminate between compounds absorbing in the same range if they considerably differ in their TPU cross-section i.e. the efficiency of TPU. Generally, photocaged compounds are considered as TPU compatible for *in vivo* applications for TP cross-sections above 0.1 GM. Here, one GM (Göppert-Mayer) unit corresponds to 10^{-50} cm^4 s $photon^{-1}$ and characterizes the product of the two photon-areas and a time, in which the two photons have to be applied to drive the photoreaction (Bort et al. 2013; Brieke et al. 2012).
Inevitably, TPU can be a sophisticated accessory tool for light control at the single-cell level and has to be elucidated in-depth for future applications.

III.4.3 Multi-modal light-control of gene cascades

As already insinuated for TPU, driving biotechnological applications in a multi-modal fashion bears pivotal advantages of concerting complex processes in a higher degree of control. Specifically, an effectively controlled orchestration of multiple cellular processes is desired in diverse contexts, such as complex gene or protein networks or effective end

product biosynthesis from a complex multi-modular biosynthetic pathway (Medema et al. 2011; Smanski et al. 2016).

To implement such **multi-parameter light regulation** (**Fig. III.4 A**) generally three main principles are conceivable: Chromatically orthogonal, sequential and simultaneous photouncaging. The most evident form of multi-modal photocaged compound based light control poses **chromatically orthogonal regulation** (Brieke et al. 2012; Hansen et al. 2015; Klán et al. 2013). Here, two different bioactive molecules are caged with two different photocages that absorb at different wavelengths. For a minimal spectral overlap of both photocaged compounds, light regulation can be obtained in any chosen order, thus providing utmost flexibility. For conventional photocages, e.g. NB- and CM-derived photoprotection groups, however, a spectral overlap does exist, which often limits the chronological sequence of photouncaging. This was, for instance, observed during the application of different CM-caged antibiotics for orthogonal light control of mixed bacterial populations (Velema et al. 2014a). While the OC-caged benzylpenicillin derivative exhibited a narrow absorption spectrum in the UV-A range, light absorption of the NC-caged fluoroquinolone derivative was rather broad and extended to the blue range. Since both compounds showed distinct UV light absorptivity, photouncaging had to be conducted primarily using blue or white light exposure to trigger both compounds independently in a chronological fashion.

A sequence restriction is likewise observed for the approach of **sequential photouncaging** using two compounds that absorb in the same range, yet vary distinctly in their photochemical properties. In detail, the photolytically highly efficient and fast uncaging reaction can be triggered upon short irradiation prior to uncaging compounds with a much less efficient photorelease by applying increased light exposure times or intensities. Notably, the success and especially the selectivity of sequential photouncaging will clearly depend on a sufficiently different uncaging efficiency. For instance, different levels of regulation were achieved for sequential photouncaging of different *p*HP-caged deoxythymidines *in vitro* (Rodrigues-Correia et al. 2014). Here, the product of extinction coefficient and uncaging quantum yield differed up to 470-fold, thus providing an excellent basis for this sequential uncaging approach.

Besides the application of different light qualities and quantities to exert light control in a multi-modal fashion, it is further possible to **photoactivate different photocaged compounds simultaneously**. In this context, one may benefit from clearly different features of the triggered biological response such as expression strength, activation kinetics, or opposed regulatory mechanisms e.g. the simultaneous activation of one reaction together with the repression of another. Most evidently, the within the framework of this study uncovered significant temporal delay of the photocaged IPTG mediated

gene expression (Chapter II.3.1) may pose a sophisticated tool, e.g. in combination with fast phototriggers such as photocaged arabinose (Chapter II.3.2), to initiate different cellular events chronologically. Here, a simultaneous light activation of both compounds would create two expression responses with a sequential i.e. temporal offset.

Irrespective of the chosen approach for multi-modal light control, orthogonal triggering of cellular events ingeniously enables to **reengineer regulatory cascades or metabolic pathways** towards the desired productivity and functionality.

Firstly, differential expression of separate genes or gene units is a useful tool to debottleneck metabolic fluxes towards a product (Cress et al. 2016; Medema et al. 2011; Wendisch et al. 2016). While the homologous expression of a complete gene cluster may be evolutionary adapted for required productivity by means of codon usage or host-specific control mechanisms, heterologous expression of gene clusters will most likely benefit from reengineering (Liebl et al. 2014; Loeschcke et al. 2013). The exact temporal, sequential and spatial arrangement of gene expression can reveal benefits during microbial production processes, not only with respect to end product yields but also regarding side-product formation (Medema et al. 2011).

Most evident conveniences of precise control over gene expression are manifested for toxic gene products. For simple single-gene expression setups, both late and tightly regulated gene expression is commonly found to be a key aspect in dealing with toxic metabolites or proteins (Miroux and Walker 1996; Saïda et al. 2006; Wagner et al. 2008). Likewise, for complex gene cascades with toxic intermediates or end-products, differential control in a multi-modal fashion might be suitable. In this sense, in a first step the precursor supply could be triggered, whereas upon sufficient biomass accumulation the production of a toxic end-product could be initiated in a second and delayed step. This approach was corroborated within this thesis using the example of (+)-valencene biosynthesis (Chapter II.5.1), where a yet unimodal delay of toxic (+)-valence production was able to elevate overall productivity significantly (Binder et al. 2016b). It may be speculated that the temporal decoupling and thus completely independent triggering of FPP and (+)-valencene biosynthetic procedures, e.g. by means of multi-chromatic optogenetic control, might offer tremendous potential for further debottlenecking the metabolic flux towards (+)-valencene biosynthesis in *C. glutamicum*.

Moreover, by means of multi-modal light regulation, the irreversibility of photouncaging can be bypassed if inhibitory compounds such as glucose are released or repressing proteins such as the T7 lysozyme inhibitor are produced as a result of a second light activation.

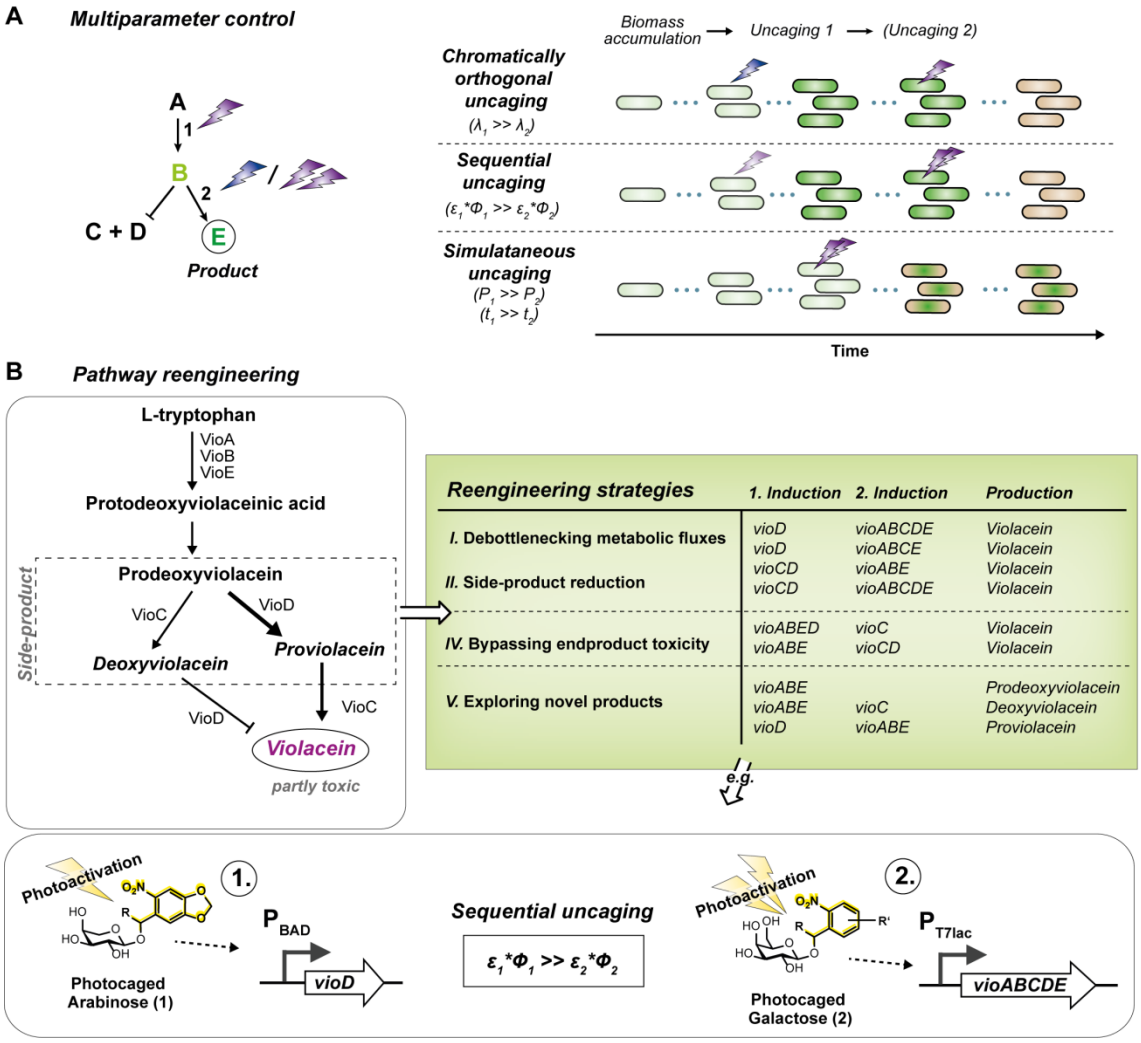

FIGURE III.4 | Prospective multiparameter light-control of gene cascades to redirect or debottleneck metabolic fluxes towards the end-product.

(**A**) Ways of multiparameter light control: Chromatically orthogonal uncaging using two different-colored photocaged compounds, sequential uncaging using photocaged compounds with highly dissimilar photochemical properties and simultaneous uncaging of two different photocaged compounds with e.g. antagonistic responses or delayed induction kinetics. (**B**) The five enzyme violacein biosynthetic pathway is depicted together with conceivable reengineering strategies to produce optimized metabolic fluxes, a reduction of side-product formation or end-product toxicity as well as novel metabolites. Abbreviations: *λ*: maximal absorption wavelength; *ε*: extinction coefficient; *Φ*: uncaging quantum yield; *P*: promoter strength; *t*: induction kinetics.

Finally, the differential expression of genes may not only assist in elevating end-product yields but also in creating so far uncharted metabolite diversity with novel target compounds of e.g. medical relevance in a single production strain in an ‘on-demand’ fashion.

A concrete example for a prospective metabolic pathway that would hugely benefit from extensive reengineering in this sense, poses the violacein biosynthesis (Cress et al. 2016; Hilgers 2016; Hoshino 2011; Vaishnav and Demain 2010). The production of the

secondary metabolite violacein is mediated by five enzymes that catalyze the synthesis of violacein from L-tryptophan and are encoded by *vioABCDE* gene cluster (**Fig. III.4 B**). Even though the recombinant production of violacein, which has promising antitumor and antibiotic properties (Hoshino 2011; Subramaniam et al. 2014; Vaishnav and Demain 2010), led to substantial yields in *E. coli* (**Chapter II.3.2**), a considerable side-product formation was observed (Binder et al. 2016a). These side-products, essentially consisting of deoxyviolacein, might be reduced by simple pathway reengineering. In this context, the initial induction of *vioD* expression prior to the actual expression of the whole gene cluster could debottleneck the metabolic flux towards a higher overall violacein productivity by minimizing deoxyviolacein side-products (**Fig. III.4 B**).

Furthermore, it would be interesting to express the violacein cluster in elaborately designed tryptophan-overproducing *C. glutamicum* strains that deliver the violacein precursor L-tryptophan at the gram scale (Ikeda 2006; Ikeda and Katsumata 1999). Here, however, it might be essential to express the precursor accumulating genes *vioABE* prior to end-product biosynthetic *vioDE* genes, since the (deoxy-)violacein end-products were be shown to be toxic for *C. glutamicum* (Sun et al. 2016).

Finally, the violacein pathway depicts how differential gene expression can be used to exploit nature's wealthy variety of natural compounds and their inherently vast antimicrobial potential. In initial production experiments, that were conducted in a, with this work associated, master thesis of Fabienne Hilgers, the expression of different *vio* genes yielded considerable metabolite diversity (Hilgers 2016). For instance, the alternative violacein pathway derivatives deoxyviolacein, proviolacein and prodeoxyviolacein could be produced *via* expression of *vioABCE*, *vioABDE* and *vioABE*, respectively (Hilgers 2016).

For introduced stages of violacein pathway reengineering, multi-modal light control represents a highly promising tool. Based on the photoswitches established within this thesis, essentially the combination of photocaged arabinose and photocaged galactose (**Chapter II.3.3**) would be feasible for sequential photouncaging due to different working concentrations (25 µM as compared to 400 µM) and thus different exposure times (10 min as compared to 30 min). Furthermore, the application of NB photocaging derivatives instead of NP compounds could contribute to increase differences in photochemical properties and thus to enable sequential photouncaging (**Fig. III.4 B**).

In future synthetic bio(techno)logical applications, multi-modal light control will certainly assist in redirecting metabolic pathways and gaining a higher order control of complex gene cascades.

III.5 Final and critical evaluation of photouncaging applicability

To apply photocaged compounds for high-throughput, spatiotemporal or multi-modal light control in a broad range of biotechnological applications, several specific requirements have to be fulfilled, apart from the general prerequisites for successful photocaging (see Chapter I.5.2.1). These will be critically assessed hereafter (**III.5.1**) and finally the industrial applicability of photocaged compound based light control will be questioned in detail (**III.5.2**).

III.5.1 Critical factors for successful photouncaging

Besides the initially presented prerequisites for successful photouncaging, further parameters were highlighted during this thesis as crucial for setting up light control appropriately.

Predominantly, the **light intensity** was found to be a key parameter for the uncaging process (Chapter II.4.1). In this context, the application of high-power UV-A LEDs (53 mW/cm^2) instead of the conventional low-power UV-A hand lamp (~1 mW/cm^2) corroborated a crucial significance of light intensities in reducing overall light exposure times (Chapter II.3.1 & II.4.2), as they achieved an up to 45-fold elevated photolysis (Binder et al. 2014; Wandrey et al. 2016). Thus, light intensities were able to further improve the temporal resolution of light induction from a technical point of view down to the lower second scale (**Fig. III.5 A**).

Besides that, also the photocaged compound **working concentration** is under reasonable suspicion to elevate temporal resolution distinctly. In the same study (Chapter II.4.2) ten-fold increased working concentrations of photocaged IPTG were found to provide an instantaneous expression response, which contravened initial studies (Chapter II.3.1 & II.3.2) on photocaged IPTG based light-responsiveness (Binder et al. 2016a; Binder et al. 2014). Notably, this concentration dependent acceleration was likewise observed (Chapter II.4.2) for increasing concentrations of conventional IPTG (Wandrey et al. 2016). Here, IPTG concentrations above 250 µM evoked most rapid induction of gene expression, although an overall saturation was already observed for 75 µM IPTG at the end of the whole cultivation. Despite the fact that elevated working concentrations are presumed to provide faster *in vivo* expression responses, one has to note that an increased working concentration entails the elongation of exposure times for complete uncaging. This became most evident for low UV-A light intensities, as for instance the photorelease of 40 µM and 100 µM of caged IPTG required exposure times of 2 and 20 minutes (Chapter II.3.1 & II.5.1), respectively (Binder et al. 2014). Elevated

working concentrations in the millimolar range are further assumed to provide more growth impairments than those in the lower micromolar range. This was, for instance, observed for photocaged glucose that was found to be slightly toxic in the lower millimolar range (Bier et al. 2016). Here, the supplementation of 20 mM photocaged glucose (Chapter II.3.3) in combination with light exposure reduced cellular growth by about 50%. In this context, applicability is further restricted by the compound solubility, which lay in the range between 2 and 60 mM for respective photocaged carbohydrates (Chapter II.3.3) in aqueous solution (Bier et al. 2016).

Conclusively, high working concentrations partly confine the applicability of photocaged compounds *in vivo* with respect to required exposure times or compound solubility and toxicity.

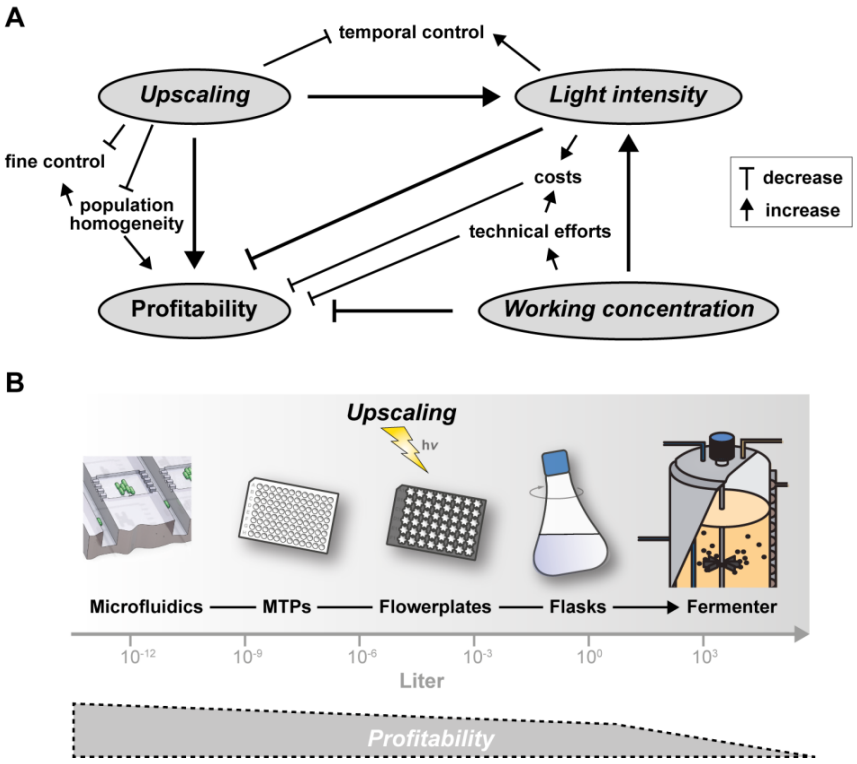

FIGURE III.5 | Critical factors influencing photouncaging applications and estimated profitability for upscaling of photocaged compound based light control.

(**A**) Critical factors affecting successful photouncaging applications. (**B**) Upscaling of light controlled cultivations using photocaged compounds. With increasing culture volumes, profitability of photouncaging starts to decrease.

Moderate to low working concentrations, however, exhibited a straightforward applicability and were even suited for the opulent production of toxic gene products (Chapter II.5.1) (Binder et al. 2016b). In this context, it was beneficial that most light-controlled expression setups depicted a broad range of inducibility (Chapter II.4.2 & II.5.1) from early exponential to early stationary growth phases (Binder et al. 2016b; Wandrey et al. 2016). Notably, standard *E. coli* expression cultures using photocaged

IPTG were clearly dependent on early induction time points to provide a decent induction of gene expression, though. Here, a systematic evaluation of light-inducibility in terms of different cultivation conditions, working concentrations, light intensities and induction time points will probably unravel underlying mechanisms more clearly.

Fortunately, photocaged compound based applications were found to be noticeably independent of conventional carbohydrate transport systems (**Chapter II.3.2 & II.5.1**). Most probably due to the improved membrane permeability of photocaged compounds, quite favorable features arose, namely outstanding **population homogeneity** and partly elevated expression strengths compared to equimolar conventional induction (**Fig. III.5 A**).

Additional parameters that exhibited appreciable influence on photocleavage reactions during µl- to ml-scale cultivations setups in different microtiter plates generally included shaking frequencies, surface-to-volume ratios, plate covers and the distance to the light source as shown by DMNB actinometry (**Chapter II.4.1**). Shaking frequencies and plate covers showed more severe influences than filling volumes and the therewith interrelated surface-to-volume ratio. Nonetheless, the highest impact on photoconversion exhibited still the reduction of light intensity, either *via* light source distance enlargement or actual dimming of the respective light source.

Taking into account this complex interplay between all those critical factors, photouncaging will be conclusively evaluated with respect to economic and large-scale feasibility (**Fig. III.5 B**).

III.5.2 Economic and large-scale feasibility of photouncaging

To evaluate **economic applicability** of photocaged compound based light control in more detail, a raw estimation of costs that incur during chemical synthesis has to be conducted. To this end, conventional purchasable chemical inducers were compared to selected self-synthesized photocaged inducers from a financial point of view.

Strikingly, a cost calculation for conventional chemical inducers including current market prices and common working concentrations revealed a broad price range relating to the price of a one liter expression culture (**Tab. III.4**). While inducers such as salicylate, arabinose, galactose, lactose and propionate represent rather cheap inducers in the lower cent (€) range, especially synthetic inducer molecules such as aTc and TMG exhibit up to 7000-fold increased and thus strikingly high costs per liter. Moderate costs, however, can be estimated for inducers such as xylose, rhamnose, IPTG and choline.

Interestingly, price calculations for photocaged inducers that were during this thesis synthesized and provided by our academic collaboration partner at small scales are

within the same moderate range. In this sense, the application of photocaged IPTG or photocaged arabinose should produce costs in the range of 0.3 to 1.7 € per liter expression culture, respectively. Here, the actual costs are strongly dependent on the precursors applied for the synthesis. For instance, the self-synthesis of 6-nitropiperonal instead of purchasing it, would produce more efforts, yet could reduce overall costs about 17%. Although, costs for the 2-step photocaged IPTG (Binder et al. 2014) and the 3-step NP-photocaged arabinose synthesis (Binder et al. 2016a) are estimated to be roughly the same, the application of NP-photocaged arabinose appears even more cost-effective due to the 1.6-fold reduced working concentrations of 25 µM for full induction. Furthermore, the omission of column chromatography purification procedures (**Chapter II.3.3**) can further account for reduced processing costs (Bier et al. 2016).

TABLE III.4 | Raw estimation of costs and economic feasibility for conventional (purchased) and photocaged inducer (self-synthesized) applications.

	Inducer	Molecular Weight [g/mol]	Working concentrations	Price* / kg	Price / l	Economic feasibility
Conventional inducers	Salicylate	138.12	1 mM	48.3	< 0.01 €	+++
	Arabinose	150.13	0.1 mM	670 €	0.01 €	+++
	Galactose	180.16	0.4 mM	315 €	0.02 €	+++
	Lactose	360.31 (xH_2O)	5 mM	35 €	0.06 €	+++
	Propionate	74.08	50 mM	26.3 €	< 0.09 €***	+++
	Xylose	150.13	30 mM	54 €	0.24 €	++
	Rhamnose	164.16	10 mM	190 €	0.31 €	++
	IPTG	238.30	0.1 mM	37500 €	0.89 €	+
	Choline	139.62 (Cl^-)	100 mM	85.7	1.20 €	+ / -
	aTC	462.88 (HCl)	0.5 µM	226600000 €	52.44 €	- -
	TMG	210.25	1 mM	333000 €	70.01 €	- - -
Photocaged inducers	Photocaged IPTG	415.41	40 – 100 µM	~ 41000 € (1-step synthesis)	~ 0.7 - 1.7 €	(+)
				~ 34000 € (2-step synthesis)	~ 0.6 - 1.4 €	(+)
	NP-Photocaged Arabinose	329.26	25 – 100 µM**	~ 34000 € (3-step synthesis)	~ 0.3 - 1.1 €	(++)

Light-grey highlighted columns do not include expenses for labor and time expenditures.
* calculated from the Carl Roth website in May 2016 for 1 kg supply and > 98% purity
** for *araBAD*-deletion strains
*** the price for propionate induction in *C. glutamicum* would be further decreased about 5000-fold.

Notably, extensive modifications were implemented in order to realize full induction of gene expression at such low concentrations for the expression systems applied in this work. For instance, the initial study on photocaged IPTG applied 0.5 mM of the compound (Young and Deiters 2007b), whereas in the redesign using a lower plasmid copy number and the implementation of the T7RP (**Chapter II.3.1**) 12.5-fold reduced concentrations sufficed for full induction (Binder et al. 2014). Substantially, the here

applied P_{BAD}-based expression setup was reengineered by means of *araBAD*-deficiency (Guzman et al. 1995) and a mutagenized AraC regulator (Lee et al. 2007) to provide full induction at 25 µM of arabinose (Binder et al. 2016a) and therefore 2680-fold reduced concentrations (**Chapter II.3.2**) compared to conventional setups using up to 67 mM (Terpe 2006). Admittedly, just by applying expression systems that were reengineered towards high inducer sensitivity, photocaged compound based light control appears economically feasible to such extent.

Conclusively, the application of photocaged compounds discloses manageable costs. Particularly for the production of high-value products, photocaged compound based light control is justifiable if the production process profits hereof, for instance, due to population homogeneity or stronger overall expression levels. The actual costs of about 1 € per liter for photocaged compound synthesis (**Tab. III.4**) appear negligible if the profits for the final products are comparatively large. For example, (+)-valencene and violacein productivities of 41 and 270 mg per liter that were obtained in this study, could produce incomes in the regions of 160 and 88,000 €, respectively. Notably, all these calculations are based on actual market prices (Sigma Aldrich) and do not include any downstream processing. Nevertheless, the calculations highlight that photocaged compound-based light control can be economically feasible, if their benefits outbalance conventional control procedures in a high-value biotechnological application.

Quite obviously, the economic feasibility was found to be strongly correlated to the applied working concentration (**Tab. III.4**). For instance, propionate induction in *C. glutamicum* (Plassmeier et al. 2013) would present an inducible expression setup with utmost cost-efficiency as considerably low costs of 0.09 € per liter for *E. coli* (Lee and Keasling 2005) might be further decreased 5000-fold due to the reduction of working concentrations from 50 mM to 10 µM. Accordingly, from an economic point of view, the synthesis of photocaged propionate can be strongly suggested and would probably outperform most of the conventionally applied inducers with respect to running costs.

However, also with respect to functionality and general applicability the inducer concentration is of utmost importance. Specifically, high photocaged compounds working concentrations led to a significant enlargement of required light intensities. As mentioned earlier, the 2.5-fold increase of the photocaged IPTG concentration from 40 µM (in *E. coli;* **Chapter II.3.1**) to 100 µM (in *C. glutamicum;* **Chapter II.5.1**) produced about 10-fold extended exposure times for full photo-conversion (Binder et al. 2016b; Binder et al. 2014). These observations are in good accordance with *in vitro* results using DMNB actinometry (**Chapter II.4.1**), where the increment of DMNB concentration from 0.1 mM to 1 mM, likewise resulted in roughly 6-fold increased times until complete conversion and 5.2-fold elevated half-conversion times, respectively.

Moreover, biocompatibility of excessive amounts of photocaged inducers has to be further elucidated in the future. For initial tests using individual photocaged carbohydrates (unpublished and preliminary results), for instance, concentrations above 2 mM were already found to fully impede cellular growth, whereas for photocaged glucose 2.5-fold amounts of the photocaged compound (**Chapter II.3.3**) showed minor impacts on biomass formation (Bier et al. 2016). Notably, at such high concentrations also the high purity of synthesized compounds might be of elevated importance.

Another interesting question for the future of photocaged compounds will be to what extent an **upscaling** of current light-controlled applications is feasible. Whereas lower liter-scale cultivations should work more or less readily for photouncaging applications, larger-scale photobioreactors such as sunlight-driven 25000 liter microalgae reactors (Olaizola 2000) could face significant difficulties. Here, the requirement of an artificial high-power light source, an appropriate surface-to-volume ratio, and eligible mixing efficacies will definitely restrict photouncaging applications to several hundred liter cultivations at most (**Fig. III.5 B**).

Furthermore, accessory issues traditionally occurring during the upscaling of microbial productions such as poor aeration (Garcia-Ochoa and Gomez 2009) or environmental heterogeneities (Lara et al. 2006) will come along. More than for usual microbial production processes (Takors 2012; Xia et al. 2016), the upscaling of photobiotechnological applications and especially those using photocaged compounds faces serious challenges and will require tremendous work in the future.

Yet, for lab-scale cultivations photouncaging has emerged as a sophisticated and well applicable tool to achieve a high-throughput feasible, spatiotemporal and non-invasive control over various synthetic bio(techno)logical applications. Here, current photouncaging in the picoliter to liter scale provides a versatile plug-and-play control over bacterial gene expression in a rapid, homogeneous and tight fashion. Thus, plenty of challenges can be tackled in various biotechnological key microbes in future applications.

IV. References

Acar M, Mettetal JT, van Oudenaarden A (2008) Stochastic switching as a survival strategy in fluctuating environments. Nat Genet 40:471–5.

Ahn JH, Jang Y-S, Lee SY (2016) Production of succinic acid by metabolically engineered microorganisms. Curr Opin Biotechnol 42:54–66.

Amann E, Brosius J, Ptashne M (1983) Vectors bearing a hybrid *trp-lac* promoter useful for regulated expression of cloned genes in *Escherichia coli*. Gene 25:167–78.

Amatrudo JM, Olson JP, Lur G, Chiu CQ, Higley MJ, Ellis-Davies GCR (2014) Wavelength-selective one- and two-photon uncaging of GABA. ACS Chem Neurosci 5:64–70.

Andrews KJ, Lin EC (1976) Thiogalactoside transacetylase of the lactose operon as an enzyme for detoxification. J Bacteriol 128:510–3.

Arvani S, Markert A, Loeschcke A, Jaeger K-E, Drepper T (2012) A T7 RNA polymerase-based toolkit for the concerted expression of clustered genes. J Biotechnol 159:162–71.

Baeshen MN, Al-Hejin AM, Bora RS, Ahmed MMM, Ramadan HAI, Saini KS, Baeshen NA, Redwan EM (2015) Production of Biopharmaceuticals in *E. coli*: Current Scenario and Future Perspectives. J Microbiol Biotechnol 25:953–62.

Baker AS, Deiters A (2014) Optical control of protein function through unnatural amino acid mutagenesis and other optogenetic approaches. ACS Chem Biol 9:1398–407.

Bakke I, Berg L, Aune TEV, Brautaset T, Sletta H, Tøndervik A, Valla S (2009) Random mutagenesis of the *Pm* promoter as a powerful strategy for improvement of recombinant-gene expression. Appl Environ Microbiol 75:2002–11.

Balzer S, Kucharova V, Megerle J, Lale R, Brautaset T, Valla S (2013) A comparative analysis of the properties of regulated promoter systems commonly used for recombinant gene expression in *Escherichia coli*. Microb Cell Fact 12:26.

Baneyx F (1999) Recombinant protein expression in *Escherichia coli*. Curr Opin Biotechnol 10:411–21.

Bao C, Zhu L, Lin Q, Tian H (2015) Building biomedical materials using photochemical bond cleavage. Adv Mater 27:1647–62.

Barth A, Corrie JET (2002) Characterization of a new caged proton capable of inducing large pH jumps. Biophys J 83:2864–71.

Beales N (2004) Adaptation of Microorganisms to Cold Temperatures, Weak Acid Preservatives, Low pH, and Osmotic Stress: A Review. Compr Rev Food Sci Food Saf 3:1–20.

Berens C, Hillen W (2003) Gene regulation by tetracyclines. Constraints of resistance regulation in bacteria shape TetR for application in eukaryotes. Eur J Biochem 270:3109–21.

Berens C, Suess B (2015) Riboswitch engineering - making the all-important second and third steps. Curr Opin Biotechnol 31:10–5.

Bier C, Binder D, Drobietz D, Loeschcke A, Drepper T, Jaeger K-E, Pietruszka J (2016) Photocaged carbohydrates – versatile tools for controlling gene expression by light. Synthesis (Stuttg). doi: 10.1055/s-0035-1562617.

Binder D, Bier C, Grünberger A, Drobietz D, Hage-Hülsmann J, Wandrey G, Büchs J, Kohlheyer D, Loeschcke A, Wiechert W, Jaeger K-E, Pietruszka J, Drepper T (2016a) Photocaged Arabinose - A Novel Optogenetic Switch for Rapid and Gradual Control of Microbial Gene Expression. Chembiochem 17:296–299.

Binder D, Frohwitter J, Mahr R, Bier C, Grünberger A, Loeschcke A, Peters-Wendisch P, Kohlheyer D, Pietruszka J, Frunzke J, Jaeger K-E, Wendisch VF, Drepper T (2016b) Light-controlled cell factories - Employing photocaged IPTG for light-mediated optimization of *lac*-based gene expression and (+)-valencene biosynthesis in *Corynebacterium glutamicum*. Appl Environ Microbiol. doi: 10.1128/AEM.01457-16

Binder D, Grünberger A, Loeschcke A, Probst C, Bier C, Pietruszka J, Wiechert W, Kohlheyer D, Jaeger K-E, Drepper T (2014) Light-responsive control of bacterial gene expression: precise triggering of the *lac* promoter activity using photocaged IPTG. Integr Biol (Camb) 6:755–65.

Binder D, Probst C, Grünberger A, Hilgers F, Loeschcke A, Jaeger K-E, Kohlheyer D, Drepper T (2016c) Comparative Single-Cell Analysis of Different *E. coli* Expression Systems during Microfluidic Cultivation. PLoS One 11:e0160711.

Bitzenhofer NL (2016) Verwendung von photocaged compounds zur Licht-gesteuerten Expression in *Bacillus* (Bachelor Thesis). Heinrich-Heine University Düsseldorf (Germany), *in preparation*.

Blatny JM, Brautaset T, Winther-Larsen HC, Karunakaran P, Valla S (1997) Improved broad-host-range RK2 vectors useful for high and low regulated gene expression levels in gram-negative bacteria. Plasmid 38:35–51.

Blattner FR, Plunkett G, Bloch CA, Perna NT, Burland V, Riley M, Collado-Vides J, Glasner JD, Rode CK, Mayhew GF, Gregor J, Davis NW, Kirkpatrick HA, Goeden MA, Rose DJ, Mau B, Shao Y (1997) The complete genome sequence of *Escherichia coli* K-12. Science 277:1453–62.

Bley F, Schaper K, Görner H (2008) Photoprocesses of molecules with 2-nitrobenzyl protecting groups and caged organic acids. Photochem Photobiol 84:162–71.

Blombach B, Riester T, Wieschalka S, Ziert C, Youn J-W, Wendisch VF, Eikmanns BJ (2011) *Corynebacterium glutamicum* tailored for efficient isobutanol production. Appl Environ Microbiol 77:3300–10.

De Boer HA, Comstock LJ, Vasser M (1983) The *tac* promoter: a functional hybrid derived from the *trp* and *lac* promoters. Proc Natl Acad Sci U S A 80:21–5.

Boezi JA, Cowie DB (1961) Kinetic Studies of *β*-Galactosidase Induction. Biophys J 1:639–647.

Bort G, Gallavardin T, Ogden D, Dalko PI (2013) From one-photon to two-photon probes: "caged" compounds, actuators, and photoswitches. Angew Chem Int Ed Engl 52:4526–37.

Brautaset T, Lale R, Valla S (2009) Positively regulated bacterial expression systems. Microb Biotechnol 2:15–30.

Brehm-Stecher BF, Johnson EA (2004) Single-cell microbiology: tools, technologies, and applications. Microbiol Mol Biol Rev 68:538–59.

Brenner K, You L, Arnold FH (2008) Engineering microbial consortia: a new frontier in synthetic biology. Trends Biotechnol 26:483–9.

Brieke C, Rohrbach F, Gottschalk A, Mayer G, Heckel A (2012) Light-controlled tools. Angew Chem Int Ed Engl 51:8446–76.

Busby S, Ebright RH (1999) Transcription activation by catabolite activator protein (CAP). J Mol Biol 293:199–213.

Byrgazov K, Vesper O, Moll I (2013) Ribosome heterogeneity: another level of complexity in bacterial translation regulation. Curr Opin Microbiol 16:133–9.

Calero P, Jensen SI, Nielsen AT (2016) Broad host range ProUSER vectors enable fast characterization of inducible promoters and optimization of *p*-coumaric acid production in *Pseudomonas putida* KT2440. ACS Synth Biol. 5:741-53.

Cambridge SB, Geissler D, Calegari F, Anastassiadis K, Hasan MT, Stewart AF, Huttner WB, Hagen V, Bonhoeffer T (2009) Doxycycline-dependent photoactivated gene expression in eukaryotic systems. Nat Methods 6:527–31.

Cambridge SB, Geissler D, Keller S, Cürten B (2006) A caged doxycycline analogue for photoactivated gene expression. Angew Chem Int Ed Engl 45:2229–31.

Chamberlin M, McGrath J, Waskell L (1970) New RNA polymerase from *Escherichia coli* infected with bacteriophage T7. Nature 228:227–31.

Chou C, Young DD, Deiters A (2010) Photocaged t7 RNA polymerase for the light activation of transcription and gene function in pro- and eukaryotic cells. Chembiochem 11:972–7.

Christie JM, Arvai AS, Baxter KJ, Heilmann M, Pratt AJ, O'Hara A, Kelly SM, Hothorn M, Smith BO, Hitomi K, Jenkins GI, Getzoff ED (2012a) Plant UVR8 photoreceptor senses UV-B by tryptophan-mediated disruption of cross-dimer salt bridges. Science 335:1492–6.

Christie JM, Gawthorne J, Young G, Fraser NJ, Roe AJ (2012b) LOV to BLUF: flavoprotein contributions to the optogenetic toolkit. Mol Plant 5:533–44.

Circolone F, Granzin J, Jentzsch K, Drepper T, Jaeger K-E, Willbold D, Krauss U, Batra-Safferling R (2012) Structural basis for the slow dark recovery of a full-length LOV protein from *Pseudomonas putida*. J Mol Biol 417:362–74.

Claesen J, Fischbach MA (2015) Synthetic microbes as drug delivery systems. ACS Synth Biol 4:358–64.

Cohn M (1957) Contributions of studies on the beta-galactosidase of *Escherichia coli* to our understanding of enzyme synthesis. Bacteriol Rev 21:140–68.

Cress BF, Jones JA, Kim DC, Leitz QD, Englaender A, Collins SM, Linhardt RJ, Koffas MAG (2016) Rapid generation of CRISPR/dCas9-regulated, orthogonally repressible hybrid T7-*lac* promoters for modular, tuneable control of metabolic pathway fluxes in *Escherichia coli*. Nucleic Acids Res. 2016;44: 4472–85.

Cruz FG, Koh JT, Link KH (2000) Light-Activated Gene Expression. J Am Chem Soc 122:8777–8778.

Cueto-Rojas HF, van Maris AJA, Wahl SA, Heijnen JJ (2015) Thermodynamics-based design of microbial cell factories for anaerobic product formation. Trends Biotechnol 33:534–46.

Daber R, Stayrook S, Rosenberg A, Lewis M (2007) Structural analysis of *lac* repressor bound to allosteric effectors. J Mol Biol 370:609–19.

Davidson E a, Basu AS, Bayer TS (2013) Programming microbes using pulse width modulation of optical signals. J Mol Biol 425:4161–6.

Deiters A (2009) Light activation as a method of regulating and studying gene expression. Curr Opin Chem Biol 13:678–86.

Deiters A (2010) Principles and applications of the photochemical control of cellular processes. Chembiochem 11:47–53.

Delvigne F, Goffin P (2014) Microbial heterogeneity affects bioprocess robustness: dynamic single-cell analysis contributes to understanding of microbial populations. Biotechnol J 9:61–72.

Delvigne F, Pêcheux H, Tarayre C (2015) Fluorescent Reporter Libraries as Useful Tools for Optimizing Microbial Cell Factories: A Review of the Current Methods and Applications. Front Bioeng Biotechnol 3:147.

Deutscher J, Francke C, Postma PW (2006) How phosphotransferase system-related protein phosphorylation regulates carbohydrate metabolism in bacteria. Microbiol Mol Biol Rev 70:939–1031.

Drepper T, Gensch T, Pohl M (2013) Advanced in vivo applications of blue light photoreceptors as alternative fluorescent proteins. Photochem Photobiol Sci 12:1125–34.

Drepper T, Huber R, Heck A, Circolone F, Hillmer A-K, Büchs J, Jaeger K-E (2010) Flavin mononucleotide-based fluorescent reporter proteins outperform green fluorescent protein-like proteins as quantitative *in vivo* real-time reporters. Appl Environ Microbiol 76:5990–4.

Drepper T, Krauss U, Meyer zu Berstenhorst S, Pietruszka J, Jaeger K-E (2011) Lights on and action! Controlling microbial gene expression by light. Appl Microbiol Biotechnol 90:23–40.

Dubendorff JW, Studier FW (1991) Controlling basal expression in an inducible T7 expression system by blocking the target T7 promoter with *lac* repressor. J Mol Biol 219:45–59.

Dumon-Seignovert L, Cariot G, Vuillard L (2004) The toxicity of recombinant proteins in *Escherichia coli*: a comparison of overexpression in BL21(DE3), C41(DE3), and C43(DE3). Protein Expr Purif 37:203–6.

Dunaway M, Olson JS, Rosenberg JM, Kallai OB, Dickerson RE, Matthews KS (1980) Kinetic studies of inducer binding to *lac* repressor.operator complex. J Biol Chem 255:10115–9.

Dusny C, Grünberger A, Probst C, Wiechert W, Kohlheyer D, Schmid A (2015) Technical bias of microcultivation environments on single-cell physiology. Lab Chip 15:1822–34.

Dusny C, Schmid A (2015) Microfluidic single-cell analysis links boundary environments and individual microbial phenotypes. Environ Microbiol 17:1839–56.

Eckardt T, Hagen V, Schade B, Schmidt R, Schweitzer C, Bendig J (2002) Deactivation behavior and excited-state properties of (coumarin-4-yl)methyl derivatives. 2. Photocleavage of selected (coumarin-4-yl)methyl-caged adenosine cyclic 3',5'-monophosphates with fluorescence enhancement. J Org Chem 67:703–10.

Eggeling L, Bott M (2015) A giant market and a powerful metabolism: L-lysine provided by *Corynebacterium glutamicum*. Appl Microbiol Biotechnol 99:3387–94.

Eikmanns BJ, Kleinertz E, Liebl W, Sahm H (1991) A family of *Corynebacterium glutamicum/Escherichia coli* shuttle vectors for cloning, controlled gene expression, and promoter probing. Gene 102:93–8.

Eldar A, Elowitz MB (2010) Functional roles for noise in genetic circuits. Nature 467:167–73.

Ellis-Davies GCR (2007) Caged compounds: photorelease technology for control of cellular chemistry and physiology. Nat Methods 4:619–28.

Engels J, Schlaeger E (1977) Synthesis, Structure, and Reactivity of Adenosine Cyclic 3',5'-Phosphate Benzyl Triesters. J Med Chem 20:7–11.

Fan N-C, Cheng F-Y, Ho JA, Yeh C-S (2012) Photocontrolled targeted drug delivery: photocaged biologically active folic acid as a light-responsive tumor-targeting molecule. Angew Chem Int Ed Engl 51:8806–10.

Fenno L, Yizhar O, Deisseroth K (2011) The development and application of optogenetics. Annu Rev Neurosci 34:389–412.

Ferrer M, Chernikova TN, Yakimov MM, Golyshin PN, Timmis KN (2003) Chaperonins govern growth of *Escherichia coli* at low temperatures. Nat Biotechnol 21:1266–7.

Fichte MAH, Weyel XMM, Junek S, Schäfer F, Herbivo C, Goeldner M, Specht A, Wachtveitl J, Heckel A (2016) Three-Dimensional Control of DNA Hybridization by Orthogonal Two-Color Two-Photon Uncaging. Angew Chem Int Ed Engl 55:8948-52.

Fournier L, Aujard I, Le Saux T, Maurin S, Beaupierre S, Baudin J-B, Jullien L (2013a) Coumarinylmethyl Caging Groups with Redshifted Absorption. Chem Eur J 19:17494–17507.

Fournier L, Gauron C, Xu L, Aujard I, Le Saux T, Gagey-Eilstein N, Maurin S, Dubruille S, Baudin J-B, Bensimon D, Volovitch M, Vriz S, Jullien L (2013b) A blue-absorbing photolabile protecting group for *in vivo* chromatically orthogonal photoactivation. ACS Chem Biol 8:1528–36.

Fowler CC, Li Y (2014) Construction and Application of Riboswitch-Based Sensors That Detect Metabolites Within Bacterial Cells. In: Lafontaine D, Dubé A, editors. Therapeutic Applications of Ribozymes and Riboswitches. Totowa, NJ: Humana Press; 2014. pp. 177–197.

Fritz G, Megerle JA, Westermayer SA, Brick D, Heermann R, Jung K, Rädler JO, Gerland U (2014) Single cell kinetics of phenotypic switching in the arabinose utilization system of *E. coli*. PLoS One 9:e89532.

Furuta T, Wang SS, Dantzker JL, Dore TM, Bybee WJ, Callaway EM, Denk W, Tsien RY (1999) Brominated 7-hydroxycoumarin-4-ylmethyls: photolabile protecting groups with biologically useful cross-sections for two photon photolysis. Proc Natl Acad Sci U S A 96:1193–200.

Garcia-Ochoa F, Gomez E (2009) Bioreactor scale-up and oxygen transfer rate in microbial processes: an overview. Biotechnol Adv 27:153–76.

Gardner L, Deiters A (2012) Light-controlled synthetic gene circuits. Curr Opin Chem Biol 16:292–9.

Gardner L, Zou Y, Mara A, Cropp TA, Deiters A (2011) Photochemical control of bacterial signal processing using a light-activated erythromycin. Mol Biosyst 7:2554–7.

Gilbert W, Müller-Hill B (1966) Isolation of the *lac* repressor. Proc Natl Acad Sci U S A 56:1891–8.

Givens RS, Rubina M, Wirz J (2012) Applications of *p*-hydroxyphenacyl (*p*HP) and coumarin-4-ylmethyl photoremovable protecting groups. Photochem Photobiol Sci 11:472–88.

Gleichmann T, Diensthuber RP, Moglich A (2013) Charting the Signal Trajectory in a Light-Oxygen-Voltage Photoreceptor by Random Mutagenesis and Covariance Analysis. J Biol Chem 288:29345-55.

Goeldner M, Givens RS (2005) Dynamic Studies in Biology. Weinheim (Germany): Wiley- VCH: Weinheim, Germany; 2005. pp. 1–94.

Gomelsky M, Hoff WD (2011) Light helps bacteria make important lifestyle decisions. Trends Microbiol 19:441–8.

Gorka AP, Nani RR, Zhu J, Mackem S, Schnermann MJ (2014) A near-IR uncaging strategy based on cyanine photochemistry. J Am Chem Soc 136:14153–9.

Görner H (2005) Effects of 4,5-dimethoxy groups on the time-resolved photoconversion of 2-nitrobenzyl alcohols and 2-nitrobenzaldehyde into nitroso derivatives. Photochem Photobiol Sci 4:822–8.

Gräslund S, Nordlund P, Weigelt J, Hallberg BM, Bray J, et al. (2008) Protein production and purification. Nat Methods 5:135–46.

Grossman TH, Kawasaki ES, Punreddy SR, Osburne MS (1998) Spontaneous cAMP-dependent derepression of gene expression in stationary phase plays a role in recombinant expression instability. Gene 209:95–103.

Gruenberger A, Probst C, Heyer A, Wiechert W, Frunzke J, Kohlheyer D (2013) Microfluidic picoliter bioreactor for microbial single-cell analysis: fabrication, system setup, and operation. J Vis Exp (82):e50560.

Grünberger A, Probst C, Helfrich S, Nanda A, Stute B, Wiechert W, von Lieres E, Nöh K, Frunzke J, Kohlheyer D (2015) Spatiotemporal microbial single-cell analysis using a high-throughput microfluidics cultivation platform. Cytometry A 87:1101–15.

Grünberger A, Wiechert W, Kohlheyer D (2014) Single-cell microfluidics: opportunity for bioprocess development. Curr Opin Biotechnol 29:15–23.

Guan L, Kaback HR (2006) Lessons from lactose permease. Annu Rev Biophys Biomol Struct 35:67–91.

Guzman LM, Belin D, Carson MJ, Beckwith J (1995) Tight regulation, modulation, and high-level expression by vectors containing the arabinose P_{BAD} promoter. J Bacteriol 177:4121–30.

Hagen V, Frings S, Wiesner B, Helm S, Kaupp UB, Bendig J (2003) [7-(Dialkylamino)coumarin-4-yl]methyl-Caged Compounds as Ultrafast and Effective Long-Wavelength Phototriggers of 8-Bromo-Substituted Cyclic Nucleotides. Chembiochem 4:434–42.

Haldimann A, Daniels LL, Wanner BL (1998) Use of new methods for construction of tightly regulated arabinose and rhamnose promoter fusions in studies of the *Escherichia coli* phosphate regulon. J Bacteriol 180:1277–86.

Hansen MJ, Velema WA, Lerch MM, Szymanski W, Feringa BL (2015) Wavelength-selective cleavage of photoprotecting groups: strategies and applications in dynamic systems. Chem Soc Rev 44:3358–77.

Hartinger D, Heinl S, Schwartz HE, Grabherr R, Schatzmayr G, Haltrich D, Moll W-D (2010) Enhancement of solubility in *Escherichia coli* and purification of an aminotransferase from *Sphingopyxis sp*. MTA144 for deamination of hydrolyzed fumonisin B(1). Microb Cell Fact 9:62.

Harwood CR, Cranenburgh R (2008) *Bacillus* protein secretion: an unfolding story. Trends Microbiol 16:73–9.

Hays SG, Patrick WG, Ziesack M, Oxman N, Silver PA (2015) Better together: engineering and application of microbial symbioses. Curr Opin Biotechnol 36:40–49.

Heck A, Drepper T (2016) Engineering Photosynthetic α-Proteobacteria for the Production of Recombinant Proteins and Terpenoids. In: Hallenbeck P (ed) Adv Exp Med Biol, Modern topics in phototrophic prokaryotes. Springer International Publishing, in press

Helfrich S, Azzouzi CE, Probst C, Seiffarth J, Grünberger A, Wiechert W, Kohlheyer D, Nöh K (2015) Vizardous: interactive analysis of microbial populations with single cell resolution. Bioinformatics 31:3875–7.

Hemphill J, Govan J, Uprety R, Tsang M, Deiters A (2014) Site-specific promoter caging enables optochemical gene activation in cells and animals. J Am Chem Soc 136:7152–8.

Hemphill J, Liu Q, Uprety R, Samanta S, Tsang M, Juliano RL, Deiters A (2015) Conditional control of alternative splicing through light-triggered splice-switching oligonucleotides. J Am Chem Soc 137:3656–62.

Hilgers F (2016) Light-controlled production of bacterial secondary metabolites (Master Thesis). Heinrich-Heine University Düsseldorf (Germany)

Hiltner JK, Hunter IS, Hoskisson PA (2015) Tailoring specialized metabolite production in *streptomyces*. Adv Appl Microbiol 91:237–55.

Hirose Y, Shimada T, Narikawa R, Katayama M, Ikeuchi M (2008) Cyanobacteriochrome CcaS is the green light receptor that induces the expression of phycobilisome linker protein. Proc Natl Acad Sci U S A 105:9528–33.

Holmes WM, Platt T, Rosenberg M (1983) Termination of transcription in *E. coli*. Cell 32:1029–32.

Hoshino T (2011) Violacein and related tryptophan metabolites produced by *Chromobacterium violaceum*: biosynthetic mechanism and pathway for construction of violacein core. Appl Microbiol Biotechnol 91:1463–1475.

Houk AL, Givens RS, Elles CG (2016) Two-Photon Activation of *p*-Hydroxyphenacyl Phototriggers: Toward Spatially Controlled Release of Diethyl Phosphate and ATP. J Phys Chem B 120:3178–86.

Huang C-J, Lin H, Yang X (2012) Industrial production of recombinant therapeutics in *Escherichia coli* and its recent advancements. J Ind Microbiol Biotechnol 39:383–99.

Huber R, Ritter D, Hering T, Hillmer A-K, Kensy F, Müller C, Wang L, Büchs J (2009) Robo-Lector - a novel platform for automated high-throughput cultivations in microtiter plates with high information content. Microb Cell Fact 8:42.

Ike K, Arasawa Y, Koizumi S, Mihashi S, Kawai-Noma S, Saito K, Umeno D (2015) Evolutionary Design of Choline-Inducible and -Repressible T7-Based Induction Systems. ACS Synth Biol 4: 1352-60.

Ikeda M (2006) Towards bacterial strains overproducing L-tryptophan and other aromatics by metabolic engineering. Appl Microbiol Biotechnol 69:615–26.

Ikeda M, Katsumata R (1999) Hyperproduction of tryptophan by *Corynebacterium glutamicum* with the modified pentose phosphate pathway. Appl Environ Microbiol 65:2497–502.

Ikeuchi M, Ishizuka T (2008) Cyanobacteriochromes: a new superfamily of tetrapyrrole-binding photoreceptors in cyanobacteria. Photochem Photobiol Sci 7:1159–67.

Il'ichev Y V, Schwörer MA, Wirz J (2004) Photochemical reaction mechanisms of 2-nitrobenzyl compounds: methyl ethers and caged ATP. J Am Chem Soc 126:4581–95.

Imshenetsky AA, Lysenko S V, Kazakov GA (1978) Upper boundary of the biosphere. Appl Environ Microbiol 35:1–5.

Inui M, Kawaguchi H, Murakami S, Vertès AA, Yukawa H (2004) Metabolic engineering of *Corynebacterium glutamicum* for fuel ethanol production under oxygen-deprivation conditions. J Mol Microbiol Biotechnol 8:243–54.

Iost I, Guillerez J, Dreyfus M (1992) Bacteriophage T7 RNA polymerase travels far ahead of ribosomes *in vivo*. J Bacteriol 174:619–22.

Jacob F, Monod J (1961) Genetic regulatory mechanisms in the synthesis of proteins. J Mol Biol 3:318–356.

Jana S, Deb JK (2005) Strategies for efficient production of heterologous proteins in *Escherichia coli*. Appl Microbiol Biotechnol 67:289–98.

Jensen JVK, Wendisch VF (2013) Ornithine cyclodeaminase-based proline production by *Corynebacterium glutamicum*. Microb Cell Fact 12:63.

Jobe A, Bourgeois S (1972) *lac* repressor-operator interaction. J Mol Biol 69:397–408.

Kaminski TS, Scheler O, Garstecki P (2016) Droplet microfluidics for microbiology: techniques, applications and challenges. Lab Chip 16:2168–2187.

Kandori H (2015) Ion-pumping microbial rhodopsins. Front Mol Biosci 2:52.

Kaplan JH, Forbush B, Hoffman JF (1978) Rapid photolytic release of adenosine 5'-triphosphate from a protected analogue: utilization by the Na:K pump of human red blood cell ghosts. Biochemistry 17:1929–35.

Katzke N, Arvani S, Bergmann R, Circolone F, Markert A, Svensson V, Jaeger K-E, Heck A, Drepper T (2010) A novel T7 RNA polymerase dependent expression system for high-level protein production in the phototrophic bacterium *Rhodobacter capsulatus*. Protein Expr Purif 69:137–46.

Katzke N, Bergmann R, Jaeger K-E, Drepper T (2012) Heterologous high-level gene expression in the photosynthetic bacterium *Rhodobacter capsulatus*. Methods Mol. Biol. pp 251–69

Keasling JD (1999) Gene-expression tools for the metabolic engineering of bacteria. Trends Biotechnol 17:452–460.

Kelly CL, Liu Z, Yoshihara A, Jenkinson SF, Wormald MR, Otero J, Estévez A, Kato A, Marqvorsen MHS, Fleet GWJ, Estévez RJ, Izumori K, Heap JT (2016) Synthetic Chemical Inducers and Genetic Decoupling Enable Orthogonal Control of the *rhaBAD* Promoter. ACS Synth Biol doi: 10.1021/acssynbio.6b00030.

Khlebnikov A, Datsenko KA, Skaug T, Wanner BL, Keasling JD (2001) Homogeneous expression of the P(BAD) promoter in *Escherichia coli* by constitutive expression of the low-affinity high-capacity AraE transporter. Microbiology 147:3241–7.

Khlebnikov A, Risa O, Skaug T, Carrier TA, Keasling JD (2000) Regulatable arabinose-inducible gene expression system with consistent control in all cells of a culture. J Bacteriol 182:7029–34.

Klán P, Šolomek T, Bochet CG, Blanc A, Givens R, Rubina M, Popik V, Kostikov A, Wirz J (2013) Photoremovable protecting groups in chemistry and biology: reaction mechanisms and efficacy. Chem Rev 113:119–91.

Korneli C, David F, Biedendieck R, Jahn D, Wittmann C (2013) Getting the big beast to work—systems biotechnology of *Bacillus megaterium* for novel high-value proteins. J Biotechnol 163:87–96.

Kortmann M, Kuhl V, Klaffl S, Bott M (2014) A chromosomally encoded T7 RNA polymerase-dependent gene expression system for *Corynebacterium glutamicum*: construction and comparative evaluation at the single-cell level. Microb Biotechnol 8: 253–65.

Krämer CEM, Singh A, Helfrich S, Grünberger A, Wiechert W, Nöh K, Kohlheyer D (2015) Non-Invasive Microbial Metabolic Activity Sensing at Single Cell Level by Perfusion of Calcein Acetoxymethyl Ester. PLoS One 10:e0141768.

Krauss U, Drepper T, Jaeger K-E (2011) Enlightened enzymes: strategies to create novel photoresponsive proteins. Chem Eur J 17:2552–60.

Krell T, Lacal J, Busch A, Silva-Jiménez H, Guazzaroni M-E, Ramos JL (2010) Bacterial sensor kinases: diversity in the recognition of environmental signals. Annu Rev Microbiol 64:539–59.

Kubicki S (2015) Licht-gesteuerte Genexpression in industriell relevanten Bakterien (Bachelor Thesis). Heinrich-Heine University Düsseldorf (Germany)

Kussell E, Leibler S (2005) Phenotypic diversity, population growth, and information in fluctuating environments. Science 309:2075–8.

Lara AR, Galindo E, Ramírez OT, Palomares LA (2006) Living with heterogeneities in bioreactors: understanding the effects of environmental gradients on cells. Mol Biotechnol 34:355–81.

Lausberg F, Chattopadhyay AR, Heyer A, Eggeling L, Freudl R (2012) A tetracycline inducible expression vector for *Corynebacterium glutamicum* allowing tightly regulable gene expression. Plasmid 68:142–7.

Lee SK, Chou HH, Pfleger BF, Newman JD, Yoshikuni Y, Keasling JD (2007) Directed evolution of AraC for improved compatibility of arabinose- and lactose-inducible promoters. Appl Environ Microbiol 73:5711–5.

Lee SK, Keasling JD (2006) Effect of glucose or glycerol as the sole carbon source on gene expression from the Salmonella *prpBCDE* promoter in *Escherichia coli*. Biotechnol Prog 22:1547–51.

Lee SK, Keasling JD (2005) A propionate-inducible expression system for enteric bacteria. Appl Environ Microbiol 71:6856–62.

Lerch MM, Hansen MJ, van Dam GM, Szymanski W, Feringa BL (2016) Emerging Targets in Photopharmacology. Angew Chem Int Ed Engl 55:10978-99.

Levskaya A, Chevalier AA, Tabor JJ, Simpson ZB, Lavery LA, Levy M, Davidson EA, Scouras A, Ellington AD, Marcotte EM, Voigt CA (2005) Synthetic biology: engineering *Escherichia coli* to see light. Nature 438:441–2.

Lewis M, Chang G, Horton NC, Kercher MA, Pace HC, Schumacher MA, Brennan RG, Lu P (1996) Crystal structure of the lactose operon repressor and its complexes with DNA and inducer. Science 271:1247–54.

Li W, Zhou X, Lu P (2004) Bottlenecks in the expression and secretion of heterologous proteins in *Bacillus subtilis*. Res Microbiol 155:605–10.

Lidstrom ME, Konopka MC (2010) The role of physiological heterogeneity in microbial population behavior. Nat Chem Biol 6:705–12.

Liebl W, Angelov A, Juergensen J, Chow J, Loeschcke A, Drepper T, Classen T, Pietruszka J, Ehrenreich A, Streit WR, Jaeger K-E (2014) Alternative hosts for functional (meta)genome analysis. Appl Microbiol Biotechnol 98:8099–109.

Lin W, Albanese C, Pestell RG, Lawrence DS (2002) Spatially discrete, light-driven protein expression. Chem Biol 9:1347–53.

Link KH, Shi Y, Koh JT (2005) Light activated recombination. J Am Chem Soc 127:13088–9.

Litsanov B, Brocker M, Bott M (2012) Toward homosuccinate fermentation: metabolic engineering of *Corynebacterium glutamicum* for anaerobic production of succinate from glucose and formate. Appl Environ Microbiol 78:3325–37.

Liu Q, Deiters A (2014) Optochemical control of deoxyoligonucleotide function *via* a nucleobase-caging approach. Acc Chem Res 47:45–55.

Loeschcke A, Markert A, Wilhelm S, Wirtz A, Rosenau F, Jaeger K-E, Drepper T (2013) TREX: A Universal Tool for the Transfer and Expression of Biosynthetic Pathways in Bacteria. ACS Synth Biol 2:22–33.

Loeschcke A, Thies S (2015) *Pseudomonas putida*-a versatile host for the production of natural products. Appl Microbiol Biotechnol 99:6197–214.

De Lorenzo V, Eltis L, Kessler B, Timmis KN (1993a) Analysis of *Pseudomonas* gene products using *lacIq*/P*trp-lac* plasmids and transposons that confer conditional phenotypes. Gene 123:17–24.

De Lorenzo V, Fernández S, Herrero M, Jakubzik U, Timmis KN (1993b) Engineering of alkyl- and haloaromatic-responsive gene expression with mini-transposons containing regulated promoters of biodegradative pathways of *Pseudomonas*. Gene 130:41–6.

Losi A, Gärtner W (2012) The evolution of flavin-binding photoreceptors: an ancient chromophore serving trendy blue-light sensors. Annu Rev Plant Biol 63:49–72.

Luo J, Uprety R, Naro Y, Chou C, Nguyen DP, Chin JW, Deiters A (2014) Genetically encoded optochemical probes for simultaneous fluorescence reporting and light activation of protein function with two-photon excitation. J Am Chem Soc 136:15551–8.

Lusic H, Deiters A (2006) A New Photocaging Group for Aromatic N -Heterocycles. Synthesis (Stuttg) 13:2147–2150.

Lutz R, Bujard H (1997) Independent and tight regulation of transcriptional units in *Escherichia coli via* the LacR/O, the TetR/O and AraC/I1-I2 regulatory elements. Nucleic Acids Res 25:1203–10.

Lynch SA, Gallivan JP (2009) A flow cytometry-based screen for synthetic riboswitches. Nucleic Acids Res 37:184–92.

Mahler L, Tovar M, Weber T, Brandes S, Rudolph MM, Ehgartner J, Mayr T, Figge MT, Roth M, Zang E (2015) Enhanced and homogeneous oxygen availability during incubation of microfluidic droplets. RSC Adv 5:101871–101878.

Mahr R, Frunzke J (2016) Transcription factor-based biosensors in biotechnology: current state and future prospects. Appl Microbiol Biotechnol 100:79–90.

Mahr R, Gätgens C, Gätgens J, Polen T, Kalinowski J, Frunzke J (2015) Biosensor-driven adaptive laboratory evolution of L-valine production in *Corynebacterium glutamicum*. Metab Eng 32:184–94.

Marbach A, Bettenbrock K (2012) *lac* operon induction in *Escherichia coli*: Systematic comparison of IPTG and TMG induction and influence of the transacetylase LacA. J Biotechnol 157:82–8.

Mazutis L, Gilbert J, Ung WL, Weitz DA, Griffiths AD, Heyman JA (2013) Single-cell analysis and sorting using droplet-based microfluidics. Nat Protoc 8:870–91.

Medema MH, Breitling R, Bovenberg R, Takano E (2011) Exploiting plug-and-play synthetic biology for drug discovery and production in microorganisms. Nat Rev Microbiol 9:131–7.

Menzella HG, Ceccarelli EA, Gramajo HC (2003) Novel *Escherichia coli* strain allows efficient recombinant protein production using lactose as inducer. Biotechnol Bioeng 82:809–17.

Miroux B, Walker JE (1996) Over-production of Proteins in *Escherichia coli* : Mutant Hosts that Allow Synthesis of some Membrane Proteins and Globular Proteins at High Levels. Mol Biol 260:289–298.

Miyada CG, Stoltzfus L, Wilcox G (1984) Regulation of the *araC* gene of *Escherichia coli* : Catabolite repression , autoregulation, and effect on *araBAD* expression. Proc Natl Acad Sci U S A 81:4120–4124.

Möglich A, Ayers RA, Moffat K (2009) Design and signaling mechanism of light-regulated histidine kinases. J Mol Biol 385:1433–44.

Möglich A, Moffat K (2010) Engineered photoreceptors as novel optogenetic tools. Photochem Photobiol Sci 9:1286–300.

Mohammed Y, Lee B, Kang Z, Du G (2014) Development of a two-step cultivation strategy for the production of vitamin B12 by *Bacillus megaterium*. Microb Cell Fact 13:102.

Moore SJ, Mayer MJ, Biedendieck R, Deery E, Warren MJ (2014) Towards a cell factory for vitamin B12 production in *Bacillus megaterium*: bypassing of the cobalamin riboswitch control elements. N Biotechnol 31:553–61.

Moussa R, Baierl A, Steffen V, Kubitzki T, Wiechert W, Pohl M (2014) An evaluation of genetically encoded FRET-based biosensors for quantitative metabolite analyses *in vivo*. J Biotechnol 191:250–259.

Müller S, Nebe-von-Caron G (2010) Functional single-cell analyses: flow cytometry and cell sorting of microbial populations and communities. FEMS Microbiol Rev 34:554–87.

Münch KM, Müller J, Wienecke S, Bergmann S, Heyber S, Biedendieck R, Münch R, Jahn D (2015) Polar Fixation of Plasmids during Recombinant Protein Production in *Bacillus megaterium* Results in Population Heterogeneity. Appl Environ Microbiol 81:5976–86.

Mustafi N, Grünberger A, Mahr R, Helfrich S, Nöh K, Blombach B, Kohlheyer D, Frunzke J (2014) Application of a Genetically Encoded Biosensor for Live Cell Imaging of L-Valine Production in Pyruvate Dehydrogenase Complex-Deficient *Corynebacterium glutamicum* Strains. PLoS One 9:e85731.

Nani RR, Gorka AP, Nagaya T, Kobayashi H, Schnermann MJ (2015) Near-IR Light-Mediated Cleavage of Antibody-Drug Conjugates Using Cyanine Photocages. Angew Chem Int Ed Engl 54:13635–8.

Neumeyer A, Hübschmann T, Müller S, Frunzke J (2013) Monitoring of population dynamics of *Corynebacterium glutamicum* by multiparameter flow cytometry. Microb Biotechnol 6:157–67.

Ni J, Auston DA, Freilich DA, Muralidharan S, Sobie EA, Kao JPY (2007) Photochemical gating of intracellular Ca^{2+} release channels. J Am Chem Soc 129:5316–7.

Niimi S, Suzuki N, Inui M, Yukawa H (2011) Metabolic engineering of 1,2-propanediol pathways in *Corynebacterium glutamicum*. Appl Microbiol Biotechnol 90:1721–9.

Novick A, Weiner M (1957) Enzyme induction as an all-or-none phenomenon. Proc Natl Acad Sci 43:553–566.

Ohlendorf R, Vidavski RR, Eldar A, Moffat K, Möglich A (2012) From Dusk till Dawn: One-Plasmid Systems for Light-Regulated Gene Expression. J Mol Biol 416:534–42.

Olaizola M (2000) Commercial production of astaxanthin from *Haematococcus pluvialis* using 25,000-liter outdoor photobioreactors. J Appl Phycol 12:499–506.

Olson EJ, Hartsough LA, Landry BP, Shroff R, Tabor JJ (2014) Characterizing bacterial gene circuit dynamics with optically programmed gene expression signals. Nat Methods 11:449-55.

Otten A, Brocker M, Bott M (2015) Metabolic engineering of *Corynebacterium glutamicum* for the production of itaconate. Metab Eng 30:156–65.

Ozbudak EM, Thattai M, Lim HN, Shraiman BI, Van Oudenaarden A (2004) Multistability in the lactose utilization network of *Escherichia coli*. Nature 427:737–40.

Özgür AY (2015) Evaluation of a *Rhodobacter capsulatus nif* promoter- based system for the heterologous expression of therapeutically relevant membrane proteins (PhD Thesis). Heinrich-Heine University Düsseldorf (Germany)

Papageorgiou G, Ogden D, Corrie JET (2005) Synthetic and photochemical studies of substituted 1-acyl-7-nitroindolines. Photochem Photobiol Sci 4:887–96.

Park SH, Kim HU, Kim TY, Park JS, Kim S-S, Lee SY (2014) Metabolic engineering of *Corynebacterium glutamicum* for L-arginine production. Nat Commun 5:4618.

Pathak GP, Vrana JD, Tucker CL (2013) Optogenetic control of cell function using engineered photoreceptors. Biol Cell 105:59–72.

Patton RA, Hristov AN, Lapierre H (2014) Protein feeding and balancing for amino acids in lactating dairy cattle. Vet Clin North Am Food Anim Pract 30:599–621.

Pelliccioli AP, Wirz J (2002) Photoremovable protecting groups: reaction mechanisms and applications. Photochem Photobiol Sci 1:441–458.

Peng L, Goeldner M (1996) Synthesis and Characterization of Photolabile Choline Precursors as Reversible Inhibitors of Cholinesterases : Release of Choline in the Microsecond Time Range. J Org Chem 61:185–191.

Plassmeier JK, Busche T, Molck S, Persicke M, Pühler A, Rückert C, Kalinowski J (2013) A propionate-inducible expression system based on the *Corynebacterium glutamicum prpD2* promoter and PrpR activator and its application for the redirection of amino acid biosynthesis pathways. J Biotechnol 163:225–32.

Poblete-Castro I, Becker J, Dohnt K, dos Santos VM, Wittmann C (2012) Industrial biotechnology of *Pseudomonas putida* and related species. Appl Microbiol Biotechnol 93:2279–90.

Polisky B, Bishop RJ, Gelfandt DH (1976) A plasmid cloning vehicle allowing regulated expression of eukaryotic DNA in bacteria. Proc Natl Acad Sci U S A 73:3900–4.

Ponomarova O, Patil KR (2015) Metabolic interactions in microbial communities : untangling the Gordian knot. Curr Opin Microbiol 27:37–44.

Porro D, Gasser B, Fossati T, Maurer M, Branduardi P, Sauer M, Mattanovich D (2011) Production of recombinant proteins and metabolites in yeasts: when are these systems better than bacterial production systems? Appl Microbiol Biotechnol 89:939–48.

Püth N (2015) Vergleichende Charakterisierung verschiedener Expressionssysteme in *Bacillus subtilis* (Bachelor Thesis). Heinrich-Heine University Düsseldorf (Germany)

Ramos JL, Gonzalez-Carrero M, Timmis KN (1988) Broad-host range expression vectors containing manipulated meta-cleavage pathway regulatory elements of the TOL plasmid. FEBS Lett 226:241–6.

Ramos JL, Michan C, Rojo F, Dwyer D, Timmis K (1990) Signal-regulator interactions. Genetic analysis of the effector binding site of XylS, the benzoate-activated positive regulator of *Pseudomonas* TOL plasmid meta-cleavage pathway operon. J Mol Biol 211:373–82.

Ramos JL, Stolz A, Reineke W, Timmis KN (1986) Altered effector specificities in regulators of gene expression: TOL plasmid *xylS* mutants and their use to engineer expansion of the range of aromatics degraded by bacteria. Proc Natl Acad Sci U S A 83:8467–71.

Robert L, Paul G, Chen Y, Taddei F, Baigl D, Lindner AB (2010) Pre-dispositions and epigenetic inheritance in the *Escherichia coli* lactose operon bistable switch. Mol Syst Biol 6:1–12.

Rockwell NC, Lagarias JC (2010) A brief history of phytochromes. Chemphyschem 11:1172–80.

Rockwell NC, Su Y-S, Lagarias JC (2006) Phytochrome structure and signaling mechanisms. Annu Rev Plant Biol 57:837–58.

Roderick SL (2005) The *lac* operon galactoside acetyltransferase. C R Biol 328:568–75.

Rodrigues-Correia A, Knapp-Bühle D, Engels JW, Heckel A (2014) Selective uncaging of DNA through reaction rate selectivity. Org Lett 16:5128–31.

Rohe P, Venkanna D, Kleine B, Freudl R, Oldiges M (2012) An automated workflow for enhancing microbial bioprocess optimization on a novel microbioreactor platform. Microb Cell Fact 11:144.

Rosano GL, Ceccarelli EA (2014) Recombinant protein expression in *Escherichia coli*: advances and challenges. Front Microbiol 5:172.

Saïda F, Uzan M, Odaert B, Bontems F (2006) Expression of highly toxic genes in *E. coli*: special strategies and genetic tools. Curr Protein Pept Sci 7:47–56.

Saier MH (2013) Microcompartments and protein machines in prokaryotes. J Mol Microbiol Biotechnol 23:243–69.

Saliba A-E, Westermann AJ, Gorski SA, Vogel J (2014) Single-cell RNA-seq: advances and future challenges. Nucleic Acids Res 42:8845–60.

Samuelson JC (2011) Recent developments in difficult protein expression: a guide to *E. coli* strains, promoters, and relevant host mutations. In: Evans, TC, Xu M-Q (eds) Methods Mol. Biol., 1st ed. Humana Press, Totowa, NJ, pp 195–209

San Miguel V, Bochet CG, del Campo A (2011) Wavelength-selective caged surfaces: how many functional levels are possible? J Am Chem Soc 133:5380–8.

Sánchez S (2005) Microbial diversity--the bright and promising future of microbial manufacturing. Curr Opin Microbiol 8:229–33.

Sanchez-Garcia L, Martín L, Mangues R, Ferrer-Miralles N, Vázquez E, Villaverde A (2016) Recombinant pharmaceuticals from microbial cells: a 2015 update. Microb Cell Fact 15:33.

Sauers DJ, Temburni MK, Biggins JB, Ceo LM, Galileo DS, Koh JT (2010) Light-activated gene expression directs segregation of co-cultured cells *in vitro*. ACS Chem Biol 5:313–20.

Schaper K, Etinski M, Fleig T (2009) Theoretical investigation of the excited states of 2-nitrobenzyl and 4,5-methylendioxy-2-nitrobenzyl caging groups. Photochem Photobiol 85:1075–81.

Schaper K, Madani Mobarekeh SA, Doro P, Maydt D (2010) The α,5-dicarboxy-2-nitrobenzyl caging group, a tool for biophysical applications with improved hydrophilicity: synthesis, photochemical properties and biological characterization. Photochem Photobiol 86:1247–54.

Schleif R (2010) AraC protein, regulation of the L-arabinose operon in *Escherichia coli*, and the light switch mechanism of AraC action. FEMS Microbiol Rev 34:779–96.

Schmidl SR, Sheth RU, Wu A, Tabor JJ (2014) Refactoring and optimization of light-switchable *Escherichia coli* two-component systems. ACS Synth Biol 3:820–31.

Schmidt D, Cho YK (2014) Natural photoreceptors and their application to synthetic biology. Trends Biotechnol 33:80–91.

Schmidt FR (2004) Recombinant expression systems in the pharmaceutical industry. Appl Microbiol Biotechnol 65:363–72.

Schmitz S, Nies S, Wierckx N, Blank LM, Rosenbaum MA (2015) Engineering mediator-based electroactivity in the obligate aerobic bacterium *Pseudomonas putida* KT2440. Front Microbiol 6:284.

Scripture JB, Voelker C, Miller S, O'Donnell RT, Polgar L, Rade J, Horazdovsky BF, Hogg RW (1987) High-affinity L-arabinose transport operon. Nucleotide sequence and analysis of gene products. J Mol Biol 197:37–46.

Sender R, Fuchs S, Milo R (2016) Are We Really Vastly Outnumbered? Revisiting the Ratio of Bacterial to Host Cells in Humans. Cell 164:337–40.

Shaner NC, Steinbach PA, Tsien RY (2005) A guide to choosing fluorescent proteins. Nat Methods 2:905–9.

Shcherbakova DM, Shemetov AA, Kaberniuk AA, Verkhusha VV (2015) Natural photoreceptors as a source of fluorescent proteins, biosensors, and optogenetic tools. Annu Rev Biochem 84:519–50.

Siegele DA, Hu JC (1997) Gene expression from plasmids containing the *araBAD* promoter at subsaturating inducer concentrations represents mixed populations. Proc Natl Acad Sci U S A 94:8168–72.

Skerra A (1994) Use of the tetracycline promoter for the tightly regulated production of a murine antibody fragment in *Escherichia coli*. Gene 151:131–5.

Smanski MJ, Zhou H, Claesen J, Shen B, Fischbach MA, Voigt CA. (2016) Synthetic biology to access and expand nature's chemical diversity. Nat Rev Microbiol 14:135–149.

Smits WK, Kuipers OP, Veening J-W (2006) Phenotypic variation in bacteria: the role of feedback regulation. Nat Rev Microbiol 4:259–71.

Song H, Ding M, Jia X, Ma Q, Yuan Y (2014) Synthetic microbial consortia: from systematic analysis to construction and applications. Chem Soc Rev 43:6954–81.

Specht A, Goeldner M (2004) 1-(*o*-Nitrophenyl)-2,2,2-trifluoroethyl ether derivatives as stable and efficient photoremovable alcohol-protecting groups. Angew Chem Int Ed Engl 43:2008–12.

Stammen S, Müller BK, Korneli C, Biedendieck R, Gamer M, Franco-Lara E, Jahn D (2010) High-yield intra- and extracellular protein production using *Bacillus megaterium*. Appl Environ Microbiol 76:4037–46.

Studier FW (1991) Use of bacteriophage T7 lysozyme to improve an inducible T7 expression system. J Mol Biol 219:37–44.

Studier FW (2005) Protein production by auto-induction in high density shaking cultures. Protein Expr Purif 41:207–34.

Studier FW, Daegelen P, Lenski RE, Maslov S, Kim JF (2009) Understanding the Differences between Genome Sequences of *Escherichia coli* B Strains REL606 and BL21 (DE3) and Comparison of the *E . coli* B and K-12 Genomes. J Mol Biol 394:653–680.

Studier FW, Moffatt BA (1986) Use of bacteriophage T7 RNA polymerase to direct selective high-level expression of cloned genes. J Mol Biol 189:113–30.

Subramaniam S, Ravi V, Sivasubramanian A (2014) Synergistic antimicrobial profiling of violacein with commercial antibiotics against pathogenic micro-organisms. Pharm Biol 52:86–90.

Sun H, Zhao D, Xiong B, Zhang C, Bi C (2016) Engineering *Corynebacterium glutamicum* for violacein hyper production. Microb Cell Fact 15:148.

Szymański W, Beierle JM, Kistemaker HAV, Velema WA, Feringa BL (2013) Reversible photocontrol of biological systems by the incorporation of molecular photoswitches. Chem Rev 113:6114–78.

Szymański W, Velema WA, Feringa BL (2014) Photocaging of Carboxylic Acids: A Modular Approach. Angew Chem Int Ed Engl 53:8682-6.

Tabor JJ, Levskaya A, Voigt CA (2011) Multichromatic control of gene expression in *Escherichia coli*. J Mol Biol 405:315–24.

Tabor S, Richardson CC (1985) A bacteriophage T7 RNA polymerase/promoter system for controlled exclusive expression of specific genes. Proc Natl Acad Sci U S A 82:1074–8.

Tahirov TH, Temiakov D, Anikin M, Patlan V, McAllister WT, Vassylyev DG, Yokoyama S (2002) Structure of a T7 RNA polymerase elongation complex at 2.9 Å resolution. Nature 420:43–50.

Takors R (2012) Scale-up of microbial processes: impacts, tools and open questions. J Biotechnol 160:3–9.

Terpe K (2006) Overview of bacterial expression systems for heterologous protein production: from molecular and biochemical fundamentals to commercial systems. Appl Microbiol Biotechnol 72:211–22.

Thattai M, van Oudenaarden A (2004) Stochastic gene expression in fluctuating environments. Genetics 167:523–30.

Troeschel SC, Thies S, Link O, Real CI, Knops K, Wilhelm S, Rosenau F, Jaeger K-E (2012) Novel broad host range shuttle vectors for expression in *Escherichia coli*, *Bacillus subtilis* and *Pseudomonas putida*. J Biotechnol 161:71–9.

Umeda N, Takahashi H, Kamiya M, Ueno T, Komatsu T, Terai T, Hanaoka K, Nagano T, Urano Y (2014) Boron dipyrromethene as a fluorescent caging group for single-photon uncaging with long-wavelength visible light. ACS Chem Biol 9:2242–6.

Vaishnav P, Demain AL (2010) Unexpected applications of secondary metabolites. Biotechnol Adv 29:223–9.

Velema WA, van der Berg JP, Hansen MJ, Szymanski W, Driessen AJM, Feringa BL (2013) Optical control of antibacterial activity. Nat Chem 5:924–8.

Velema WA, van der Berg JP, Szymanski W, Driessen AJM, Feringa BL (2015) Bacterial patterning controlled by light exposure. Org Biomol Chem 13:1639–42.

Velema WA, van der Berg JP, Szymanski W, Driessen AJM, Feringa BL (2014a) Orthogonal control of antibacterial activity with light. ACS Chem Biol 9:1969–74.

Velema WA, Szymanski W, Feringa BL (2014b) Photopharmacology: beyond proof of principle. J Am Chem Soc 136:2178–91.

Wagner S, Klepsch MM, Schlegel S, Appel A, Draheim R, Tarry M, Högbom M, van Wijk KJ, Slotboom DJ, Persson JO, de Gier J-W (2008) Tuning *Escherichia coli* for membrane protein overexpression. Proc Natl Acad Sci U S A 105:14371–6.

Walsh G (2010) Biopharmaceutical benchmarks 2010. Nat Biotechnol 28:917–24.

Walsh S, Gardner L, Deiters A, Williams GJ (2014) Intracellular light-activation of riboswitch activity. Chembiochem 15:1346–51.

Wandrey G, Bier C, Binder D, Hoffmann K, Jaeger K-E, Pietruszka J, Drepper T, Büchs J (2016) Light-induced gene expression with photocaged IPTG for induction profiling in a high-throughput screening system. Microb Cell Fact 15:63.

Wanner BL, Kodaira R, Neidhardt FC (1977) Physiological regulation of a decontrolled *lac* operon. J Bacteriol 130:212–22.

Wanner BL, Kodaira R, Neidhardt FC (1978) Regulation of *lac* Operon Expression : Reappraisal of the Theory of Catabolite Repression. J Bacteriol 136:947–954.

Wendisch VF (2014) Microbial production of amino acids and derived chemicals: synthetic biology approaches to strain development. Curr Opin Biotechnol 30:51–8.

Wendisch VF, Jorge JMP, Pérez-García F, Sgobba E (2016) Updates on industrial production of amino acids using *Corynebacterium glutamicum*. World J Microbiol Biotechnol 32:105.

Westers L, Westers H, Quax WJ (2004) *Bacillus subtilis* as cell factory for pharmaceutical proteins : a biotechnological approach to optimize the host organism. Biochim Biophys Acta 1694:299–310.

Whitman WB, Coleman DC, Wiebe WJ (1998) Prokaryotes: the unseen majority. Proc Natl Acad Sci U S A 95:6578–83.

Wierckx NJP, Ballerstedt H, de Bont JAM, Wery J (2005) Engineering of Solvent-Tolerant *Pseudomonas putida* S12 for Bioproduction of Phenol from Glucose. Appl Environ Microbiol 71:8221–8227.

Wieschalka S, Blombach B, Bott M, Eikmanns BJ (2013) Bio-based production of organic acids with *Corynebacterium glutamicum*. Microb Biotechnol 6:87–102.

Wilson CJ, Zhan H, Swint-Kruse L, Matthews KS (2007) The lactose repressor system: paradigms for regulation, allosteric behavior and protein folding. Cell Mol Life Sci 64:3–16.

Xia J, Wang G, Lin J, Wang Y, Chu J, Zhuang Y, Zhang S (2016) Advances and Practices of Bioprocess Scale-up. Adv Biochem Eng Biotechnol 152:137–51.

Xiao Y, Bowen CH, Liu D, Zhang F (2016) Exploiting nongenetic cell-to-cell variation for enhanced biosynthesis. Nat Chem Biol 12:339–44.

Xu J, Banerjee A, Pan S-H, Li ZJ (2012) Galactose can be an inducer for production of therapeutic proteins by auto-induction using *E. coli* BL21 strains. Protein Expr Purif 83:30–6.

Yamazoe S, Liu Q, McQuade LE, Deiters A, Chen JK (2014) Sequential Gene Silencing Using Wavelength-Selective Caged Morpholino Oligonucleotides. Angew Chemie 126:10278–10282.

Young DD, Deiters A (2007a) Photochemical control of biological processes. Org Biomol Chem 5:999–1005.

Young DD, Deiters A (2007b) Photochemical activation of protein expression in bacterial cells. Angew Chem Int Ed Engl 46:4290–2.

Young DD, Deiters A (2006) Photochemical hammerhead ribozyme activation. Bioorg Med Chem Lett 16:2658–61.

Young DD, Garner RA, Yoder JA, Deiters A (2009) Light-activation of gene function in mammalian cells via ribozymes. Chem Commun (Camb) (5):568–70.

Young JW, Locke JCW, Altinok A, Rosenfeld N, Bacarian T, Swain PS, Mjolsness E, Elowitz MB (2012) Measuring single-cell gene expression dynamics in bacteria using fluorescence time-lapse microscopy. Nat Protoc 7:80–8.

Zenobi R (2013) Single-cell metabolomics: analytical and biological perspectives. Science 342:1243259.

Zhang Y, Shang X, Lai S, Zhang G, Liang Y, Wen T (2012) Development and application of an arabinose-inducible expression system by facilitating inducer uptake in *Corynebacterium glutamicum*. Appl Environ Microbiol 78:5831–8.

Zhao J, Lin S, Huang Y (2013) Mechanism-based design of a photoactivatable firefly luciferase. J Am Chem Soc 135:7410–3.

Ziegler T, Möglich A (2015) Photoreceptor engineering. Front Mol Biosci 2:30.

Ziegler T, Schumacher CH, Möglich A (2016) Guidelines for Photoreceptor Engineering. Methods Mol Biol 1408:389–403.

V. Appendix

V.1 Supporting Information for Chapter II.1.1 – Microfluidic Analysis of *E. coli* expression systems

Comparative single-cell analysis of different *E. coli* expression systems during microfluidic cultivation

Dennis Binder,* Christopher Probst,* Alexander Grünberger,* Fabienne Hilgers, Anita Loeschcke, Karl-Erich Jaeger, Dietrich Kohlheyer, Thomas Drepper

PLoS One 2016; 11:e0160711.

S1 Appendix. Supporting methods.

Exact LB growth media recipes and quantification of galactose, lactose and glucose.

doi:10.1371/journal.pone.0160711.s001

Supporting Methods

LB Growth Media

For initial cultivations four different lysogeny broth (LB) cultivation media were employed that were constituted as follows: LB1 (25 g l^{-1} ready-to-use mix Luria/Miller; Carl Roth, Karlsruhe, Germany); LB2 (10 g l^{-1} tryptone/peptone from casein (Carl Roth, Karlsruhe, Germany), 10 g l^{-1} NaCl, 5 g l^{-1} yeast extract (type KAT, Ohly, Hamburg Germany); LB3 (10 g l^{-1} peptone from casein (Carl Roth, Karlsruhe, Germany), 10 g l^{-1} NaCl, 5 g l^{-1} yeast extract (Carl Roth, Karlsruhe, Germany); LB4 (10 g l^{-1} Bacto™ peptone (BD Biosciences, Franklin Lakes, NJ, USA), 10 g l^{-1} NaCl, 5 g l^{-1} Bacto™ yeast extract (BD Biosciences, Franklin Lakes, NJ, USA).

Quantification of galactose, lactose and glucose

Galactose and lactose were quantified *via* photometric detection of NADH using a β-galactosidase, galactose mutarotase and β-galactose dehydrogenase based enzyme assay (Rapid Kit K-LACGAR; Megazyme, Ireland). For glucose measurements a hexokinase/glucose-6-phosphate dehydrogenase based assay for NADPH detection was performed as previously described [58].

Supporting Reference

58. Richhardt J, Bringer S, Bott M. Role of the pentose phosphate pathway and the Entner-Doudoroff pathway in glucose metabolism of *Gluconobacter oxydans* 621H. Appl Microbiol Biotechnol. 2013; 97: 4315–23.

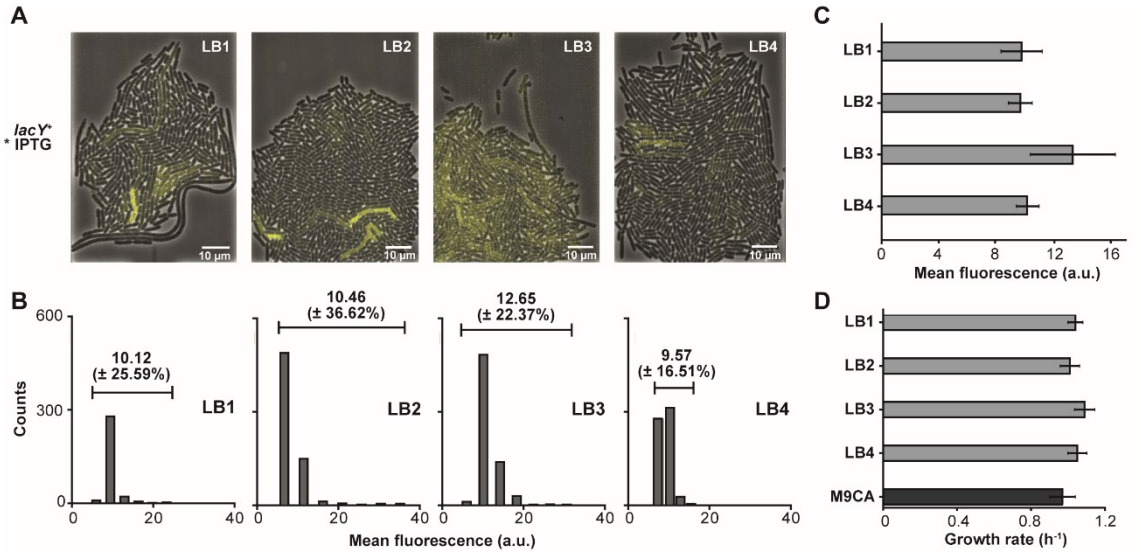

S1 Fig. Expression responses and growth of *E. coli* BL21(DE3) with (A-C) and without (D) the pRhotHi-2-EYFP expression vector in different complex LB cultivation. (A) Representative micro-colonies, weakly induced (2.5 µM) with IPTG after approximately 4 h of cultivation in four different LB media. (B) Mean fluorescence distribution for the representative microcolonies shown above. Mean values and coefficient of variations are plotted above the bar, indicating the complete spread. (C) Mean fluorescence for ten EYFP-expressing colonies cultivated in the four different media. (D) Comparison of maximum growth rates for non-induced cultivations in the different LB media (grey bars) with growth rates obtained for uninduced cultivation in the novel defined rich medium M9CA (dark grey bars).
doi:10.1371/journal.pone.0160711.s002

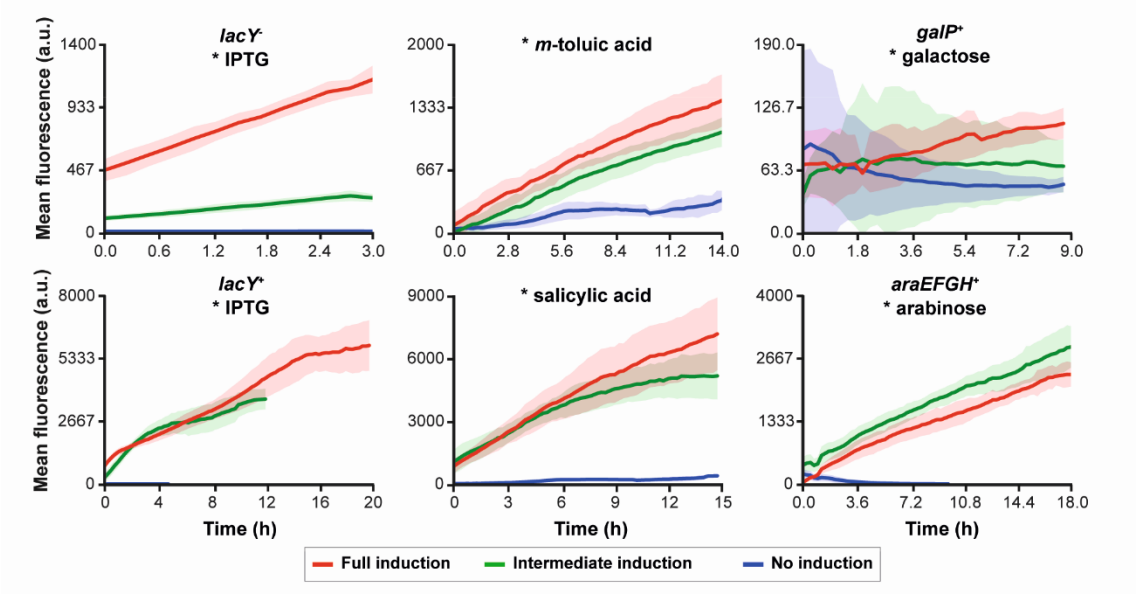

S2 Fig. Fluorescence profiles for conducted microfluidic expression setups. Averaged single-cell fluorescence development for at least ten populations cultivated without (blue), as well as using intermediate (green) and high inducer concentrations. Shaded areas indicate respective standard deviations. The end of the experiment corresponds to the time were cultivation chambers are almost fully loaded or where cells completely stopped growing.
doi:10.1371/journal.pone.0160711.s003

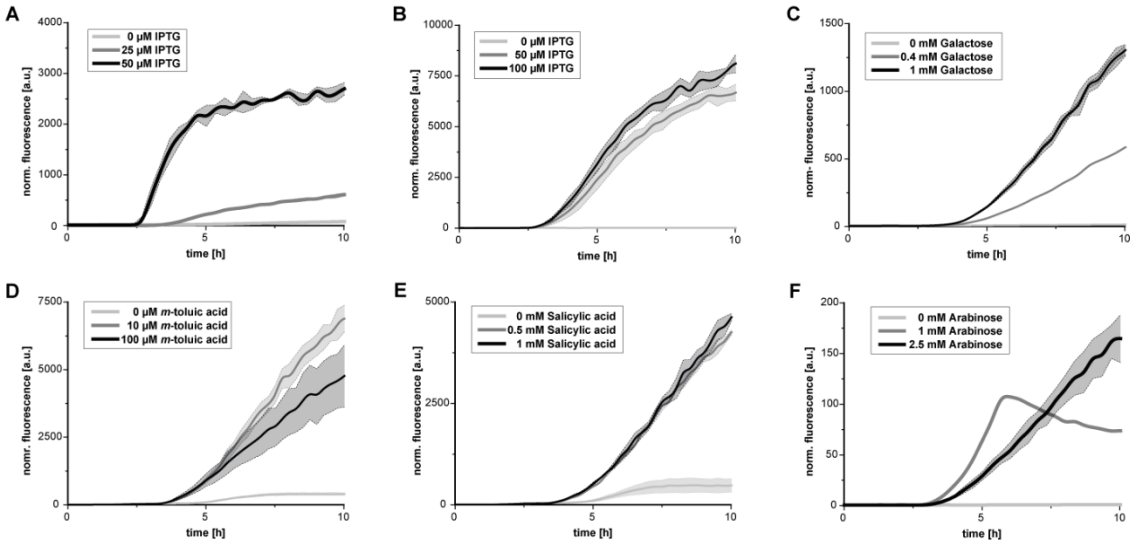

S3 Fig. Bulk fluorescence profiles for batch cultivations of different *E. coli* expression systems.

Expression response of the selected expression systems 1–6 (**A-F**) in a BioLector microbioreactor system (m2plabs, Germany) under constant monitoring of biomass accumulation and reporter fluorescence. Indicated fluorescence was biomass-normalized. Expression cultures were inoculated to cell densities corresponding to an optical density of 0.05 at 580 nm. Gene expression was induced when cell cultures reached the logarithmic growth phase (cell density of OD580 ~0.5). Cultures induced with 1 mM arabinose start to consume arabinose, while the are still growing, whereas induction with 2.5 mM arabinose leads to tremendous growth impairment and thus no arabinose consumption was observed during the observation period of 10 h. Expression cultures were performed at least in triplicates. Shaded areas indicate respective standard deviations. a.u.: arbitrary units.

doi:10.1371/journal.pone.0160711.s004

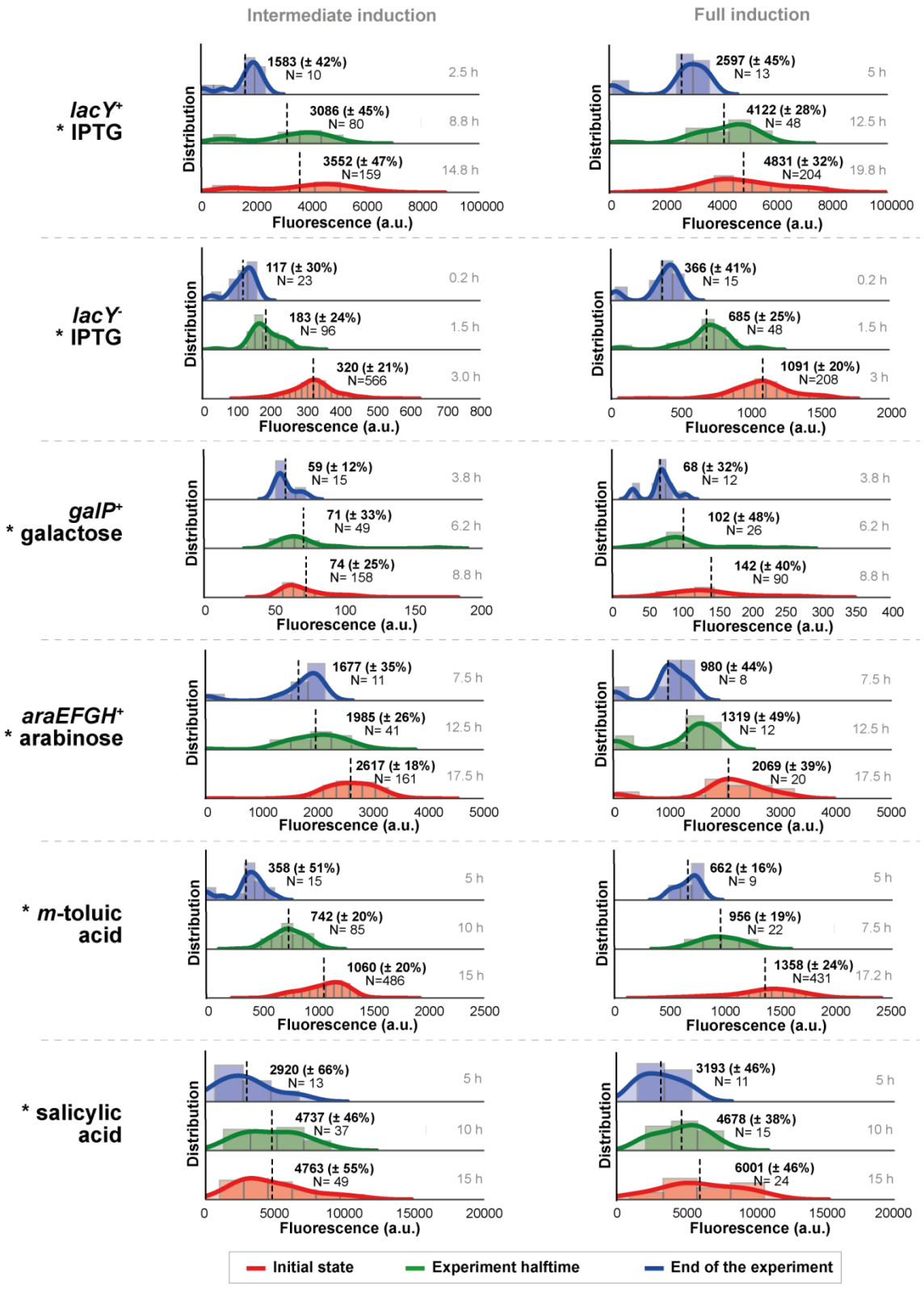

S4 Fig. Time-resolved fluorescence reporter expression patterns of microfluidic cultivations using intermediate and high inducer concentrations.

Histograms were plotted using single-cell fluorescence values obtained from representative populations at the initial (blue, N>8), intermediary (green, halftime of experiment) and end state (red, μ_{max} ~ 0) of conducted microfluidic cultivation experiments.

doi:10.1371/journal.pone.0160711.s005

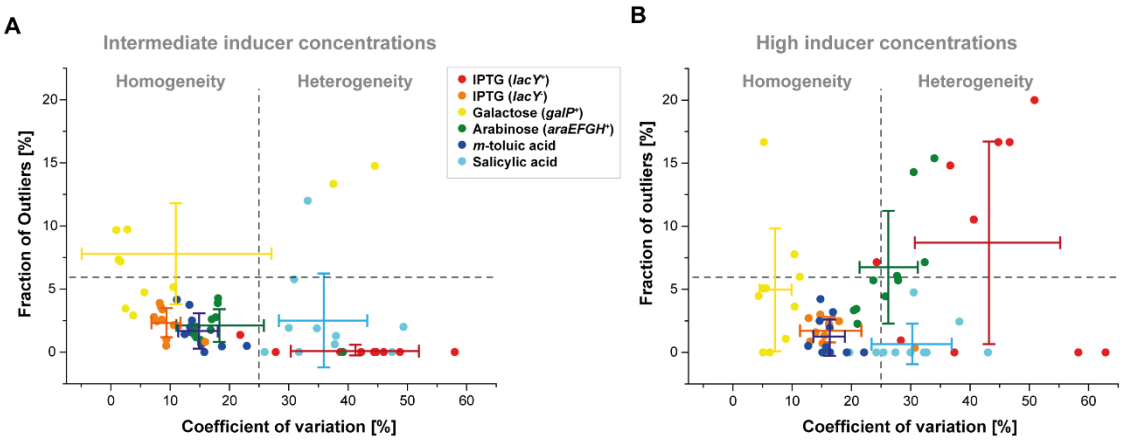

S5 Fig. Expression heterogeneity analysis of different *E. coli* expression systems during microfluidic cultivation using (A) intermediate and (B) high inducer concentrations for induction of target gene expression.

Percentaged coefficient of variation and fraction of outliers (outside the 1.5-fold IQR) are plotted as potential indicators of expression heterogeneity for ten individual microcolonies. Cross lines reveal respective means and standard deviations. Grey dotted lines show thresholds for expression heterogeneity (CV > 25%) or increased number of rare events (outliers > 6%) selected for the expressions systems at hand. The bottom left quadrant indicates the region of expression robustness and homogeneity.

doi:10.1371/journal.pone.0160711.s006

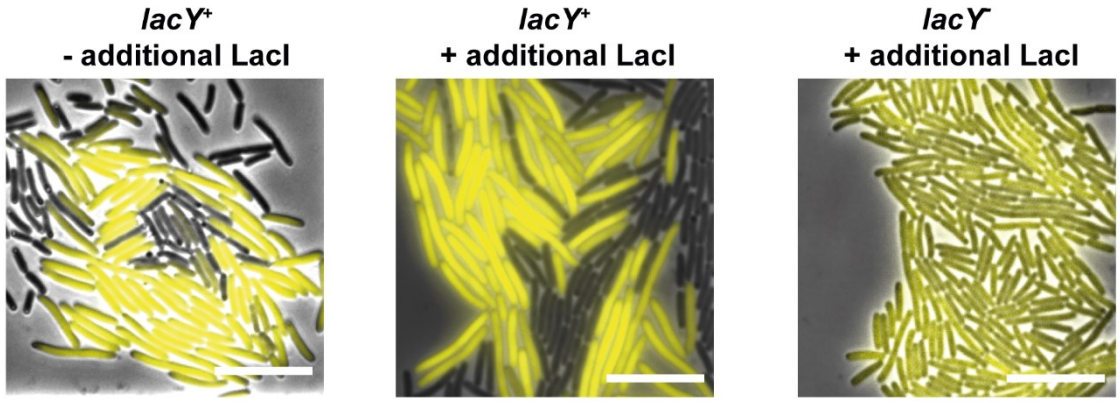

S6 Fig. Comparison of representative microcolonies from conducted microfluidic analyses, which differ in their *lacY* and *lacI* constitution.

lacY$^+$: *E. coli* BL21(DE3), *lacY*$^-$: *E. coli* Tuner(DE3),—additional LacI: pRhotHi-2 expression vector, + additional LacI: pRhotHi-2-LacI expression vector. The white scale bar corresponds to 10 µm.

doi:10.1371/journal.pone.0160711.s007

S1 Table. Bacterial strains, plasmids and oligonucleotides used in this study.

doi:10.1371/journal.pone.0160711.s008

Strain, plasmid, oligonucleotides	Relevant features, description or sequence*	Reference
Strains		
E. coli DH5α	*F⁻ Φ80lacZΔM15 Δ(lacZYA-argF) U169 recA1 endA1 hsdR17 (rk^-, mk^+) phoA supE44λ⁻ thi-1 gyrA96 relA1*	[56]
E. coli BL21(DE3)	*F⁻ ompT gal dcm lon $hsdS_B$(r_B^- m_B^-)λ(DE3 [lacI lacUV5 -T7 gene 1 ind1 sam7 nin5])*	[11]
E. coli Tuner(DE3)	*F⁻ ompT gal dcm lon $hsdS_B$ (r_B^- m_B^-) lacY1(DE3)*	Novagen
Plasmids		
pRhotHi-2-EYFP	pBBR1-MCS-derivative, P_{T7}-lacO-MCS, Km^R, Cm^R, EYFP	[57]
pRhotHi-2-LacI-EYFP	pBBR1-MCS-derivative, P_{T7}-lacO-MCS, Km^R, Cm^R, pBBR22b-lacI, EYFP	[14]
pAra-GFP	pSBM2g backbone, araC, Km^R, P_{BAD}-GFPmut3	[48]
pSB-M117-2g	pMB1 replicon, xylS, P_{M117}-GFPmut3	[6]
pM117-R45T-GFP	pSB-M117-2g with R45T mutation of XylS	This work
Oligonucleotides		
1 (XylS_SalI_for)	Binds upstream of *SalI*-site after *xylS*. Sequence: 5′ -GAGACACAACGTGGCTTTCC-3′	This work
2 (XylS_SacI_rev)	Binds upstream of *SacI*-site in front of *xylS*. Sequence: 5′ - ATCGACTTGGCGCCTTTCTAC-3′	This work
3 (XylS_R45T_rev)	Binds within *xylS*. Mediates R45T point mutation. Sequence: 5′ - CAGGCACGCTGCACCACAGAATC-3′	This work
4 (XylS_R45T_for)	Binds within *xylS*. Mediates R45T point mutation. Sequence: 5′ - GATTCTGTGGTGCAGCGTGCCTG-3′	This work

* Underlined sequence indicates point mutation used for XylS Mutagenesis (AGG → ACG).

S2 Table. Quantification of known inducing or repressing carbohydrates in different *E.coli* cultivation media.

doi:10.1371/journal.pone.0160711.s009

Medium	Reference	Glucose [mg l^{-1}]	Lactose [µg l^{-1}]	Galactose [µg l^{-1}]
LB medium 1	[48]	91.5 ± 1.3	5.3 ± 0.1	1.9 ± 0.3
LB medium 2	[14]	26.2 ± 0.7	5.3 ± 0.3	0.9 ± 0.3
LB medium 3	[59]	39.7 ± 1.9	6.4 ± 0.1	0.8 ± 0.1
LB medium 4	This study	52.1 ± 1.2	2.1 ± 0.3	n.d.
M9CA medium	This study	n.d.	n.d.	n.d.

n.d.: not detected

V.2 Supporting Information for Chapter II.3.1 – Light-responsive control of bacterial gene expression

Light-responsive control of bacterial gene expression: Precise triggering of the *lac* promoter activity using photocaged IPTG

Dennis Binder,* Alexander Grünberger,* Anita Loeschcke, Christopher Probst, Claus Bier, Jörg Pietruszka, Wolfgang Wiechert, Dietrich Kohlheyer, Karl-Erich Jaeger and Thomas Drepper. *Integr Biol (Camb).* 2014;6: 755–65.

Light-responsive control of bacterial gene expression: Precise triggering of the *lac* promoter activity using photocaged IPTG

Dennis Binder,*[a] Alexander Grünberger,*[b] Anita Loeschcke,[a] Christopher Probst,[b] Claus Bier,[c] Jörg Pietruszka,[b,c] Wolfgang Wiechert, [b] Dietrich Kohlheyer,[b] Karl-Erich Jaeger,[#a,b] and Thomas Drepper[#a]

[a] Institute of Molecular Enzyme Technology, Heinrich-Heine-University Dusseldorf, Research Center Jülich, Germany.

[b] Institute of Bio- and Geosciences, IBG-1: Biotechnology, Systems Biotechnology, Research Center Jülich, Germany

[c] Institute for Bioorganic Chemistry, Heinrich-Heine-University Düsseldorf, Research Center Jülich, Germany

[#] e-mail: k.-e.jaeger@fz-juelich.de or t.drepper@fz-juelich.de

* These authors contributed equally to this work.

The Supplementary material includes:

Supplementary table

Tab. S1 Strains and Plasmids applied in this work

Strains and plasmids	Relevant characteristics and genotype	References
***E. coli* strains**		
DH5α	*F⁻ Φ80lacZΔM15 Δ(lacZYA-argF) U169 recA1 endA1 hsdR17 (rk⁻, mk⁺) phoA supE44λ⁻ thi-1 gyrA96 relA1*	Hanahan 1983
BL21(DE3)	*F⁻ ompT gal dcm lon hsdS$_B$(r$_B^-$ m$_B^-$)λ(DE3 [lacI lacUV5-T7 gene 1 ind1 sam7 nin5])*	Studier & Moffatt 1986
Tuner(DE3)	*F⁻ ompT gal dcm lon hsdS$_B$ (r$_B^-$ m$_B^-$) lacY1(DE3)*	Novagen
Plasmids		
pRhotHi-2	pBBR1-MCS-derivative, P$_{T7}$-lacO-MCS, Km^R, Cm^R	Katzke *et al.* 2010
pRhotHi-2-EYFP	pBBR1-MCS-derivative, P$_{T7}$-lacO-MCS, Km^R, Cm^R, EYFP	Katzke *et al.* 2010
pBBR22b	pBBR1-MCS-derivative, P$_{T7}$-lacO-MCS, lacI, Cm^R	Rosenau & Jaeger, 2004
pBSL15	Km^R (*aphII*)	Alexeyev, 1985
pRhotHi-2-LacI	pBBR1-MCS-derivative, P$_{T7}$-lacO-MCS, Km^R, Cm^R, pBBR22b-lacI	this work
pRhotHi-2-LacI-EYFP	pBBR1-MCS-derivative, P$_{T7}$-lacO-MCS, Km^R, Cm^R, pBBR22b-lacI, EYFP	this work

Supplementary methods

Synthesis and analysis of 6-nitropiperonal [1]

Under absence of light, piperonal (10.0 g, 66.6mmol) was added to 70% nitric acid (56 mL) at 0 °C. During the addition the temperature should not rise above 0 °C. Afterwards the reaction mixture was stirred for 4h. The mixture was poured on ice. The precipitation was collected and washed with ice water. The product was recrystallized from ethanol to yield a yellow solid (12.35 g, 95%).

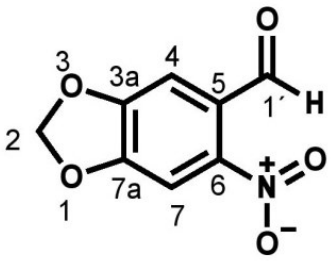

NMR data:

δ_H (600 MHz; $CDCl_3$) 6.24 (2 H, s, 2´-H), 7.34 (1 H, s, 7-H), 7.53 (1 H, s, 4-H), 10.30 (1 H, s, 1´-H).

δ_C (151 MHz; $CDCl_3$) 103.93 (2-C), 105.15 (7-C), 107.58 (4-C), 128.24 (5-C), 146.13 (6-C), 151.54 (3a-C/ *7a-C*), 152.26 (7a-C/ 3a-C), 186.87 (1´-C).

NMR spectra of 6-nitropiperonal:

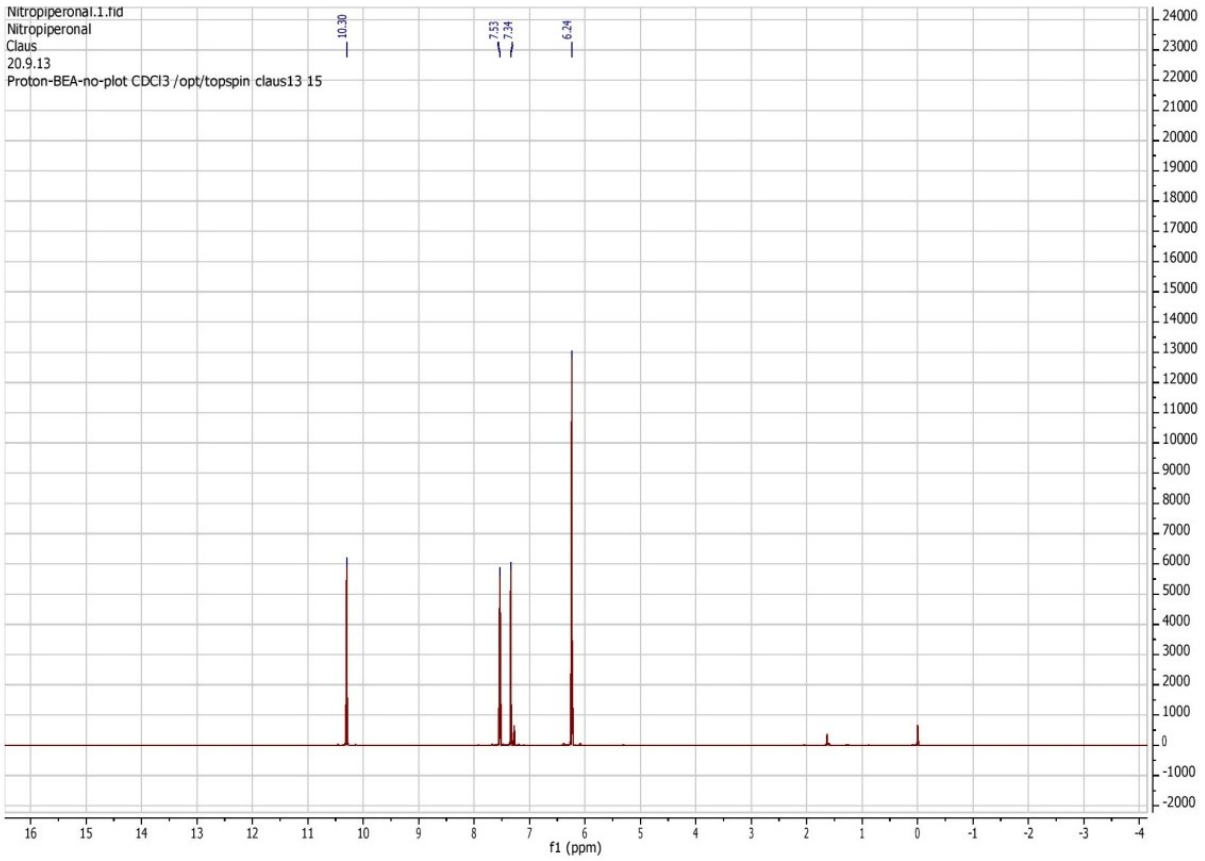

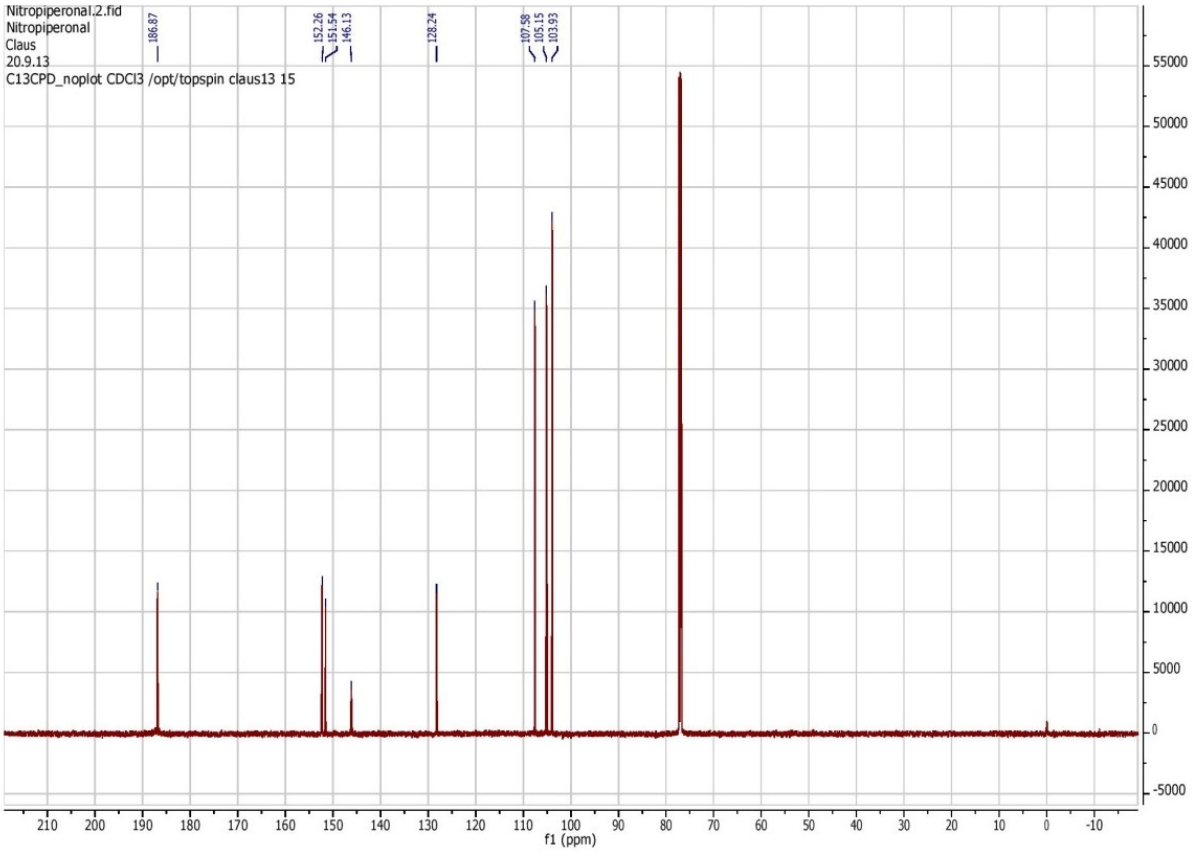

IR absorptions:

ν_{max} /cm^{-1} 3096, 3056, 2927, 1679, 1596, 1511, 1486, 1418, 1394, 1367, 1328, 1273, 1225, 1170, 1127, 1019, 922, 887, 880, 814, 790, 753, 725, 688.

Melting point:

95.6°C

UV-Vis absorptions:

λ_{max} ($CHCl_3$)/nm 260 (ε/dm^3 mol^{-1} cm^{-1} 2812), 308 (3125), 348 (18438).

Analytical data of NP-photocaged IPTG [2]

(4aR,6S,7R,8R,8aR)-6-(Isopropylthio)-2-(6-nitrobenzo[d][1,3]dioxol-5-yl)hexahydropyrano[3,2-d][1,3]dioxine-7,8-diol

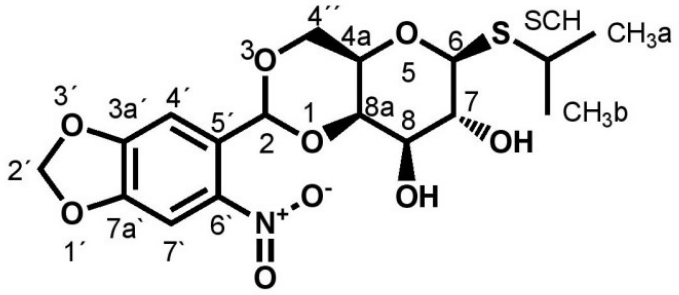

NMR data:

δ_H (600 MHz; $CDCl_3$) 1.35 (3 H, d, $^3J_{CH3a/b,\ SCH}$= 6.8 Hz, -CH_3a/b) 1.37 (3 H, d, $^3J_{CH3a/b,\ SCH}$= 6.8 Hz, -CH_3a/b), 2.54 (1 H, d, $^4J_{8,\ 7}$ = 7.4 Hz, 8-OH), 2.59 (1 H, d, $^4J_{7,\ 8}$ = 1.4 Hz, 7-OH), 3.26 (1 H, septet, $^3J_{SCH,\ CH3a/b}$ = 6.70 Hz, -SCH), 3.52 (1 H, s, 8a-CH), 3.71 (2 H, m, 7-CH, 8-CH), 4.07 (1 H, dd, $^2J_{4''a,\ 4''b}$ = 12.7 Hz, $^3J_{4''b,\ 4a}$ = 1.95 Hz, 4´´b-CH_2), 4.30 (2 H, m, 8a-CH,4´´a-CH_2), 4.41 (1 H, d,$^3J_{6,7}$ = 9.1 Hz, 6 –CH), 6.12 (2 H, s, 2´-CH_2), 6.18 (1 H, s, 2-CH), 7.35 (1 H, s, 4´-CH), 7.43 (1 H, s, 7´-CH).

δ_C (151 MHz; $CDCl_3$) 24.00 (C- CH_3a/CH_3b), 24.18 (C- CH_3a/CH_3b), 35.34 (SCH), 69.64 (C-4´´), 69.93 (C-4a), 70.13 (C-8), 73.78 (C-7), 75.97 (C-8a), 85.59 (C-6), 96.68 (C-2), 103.11 (C-2´),105.24 (C-7´), 107.56 (C-4´), 128.75 (C-6´), 142.32 (C-5´), 148.18 (C-3a´/7a´), 151.68 (C-3a´/7a´).

NMR spectra of NP-photocaged-IPTG:

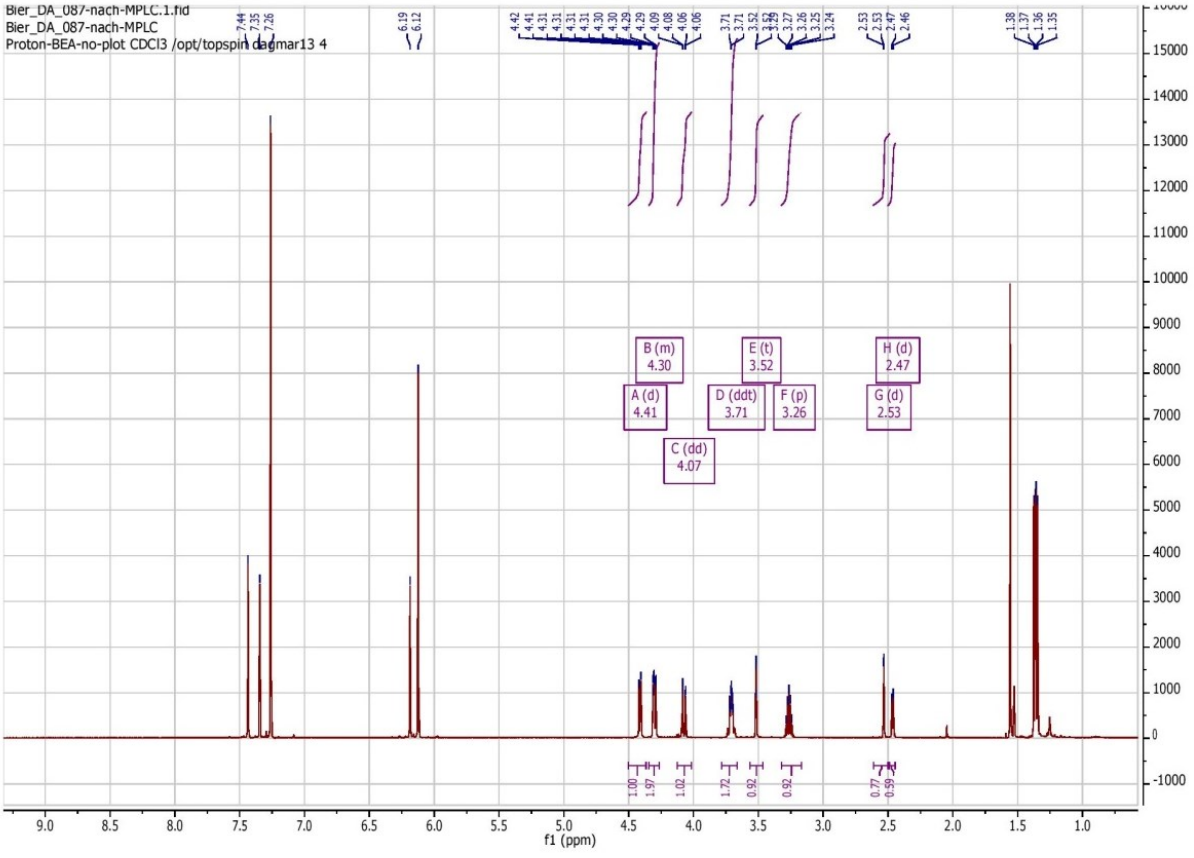

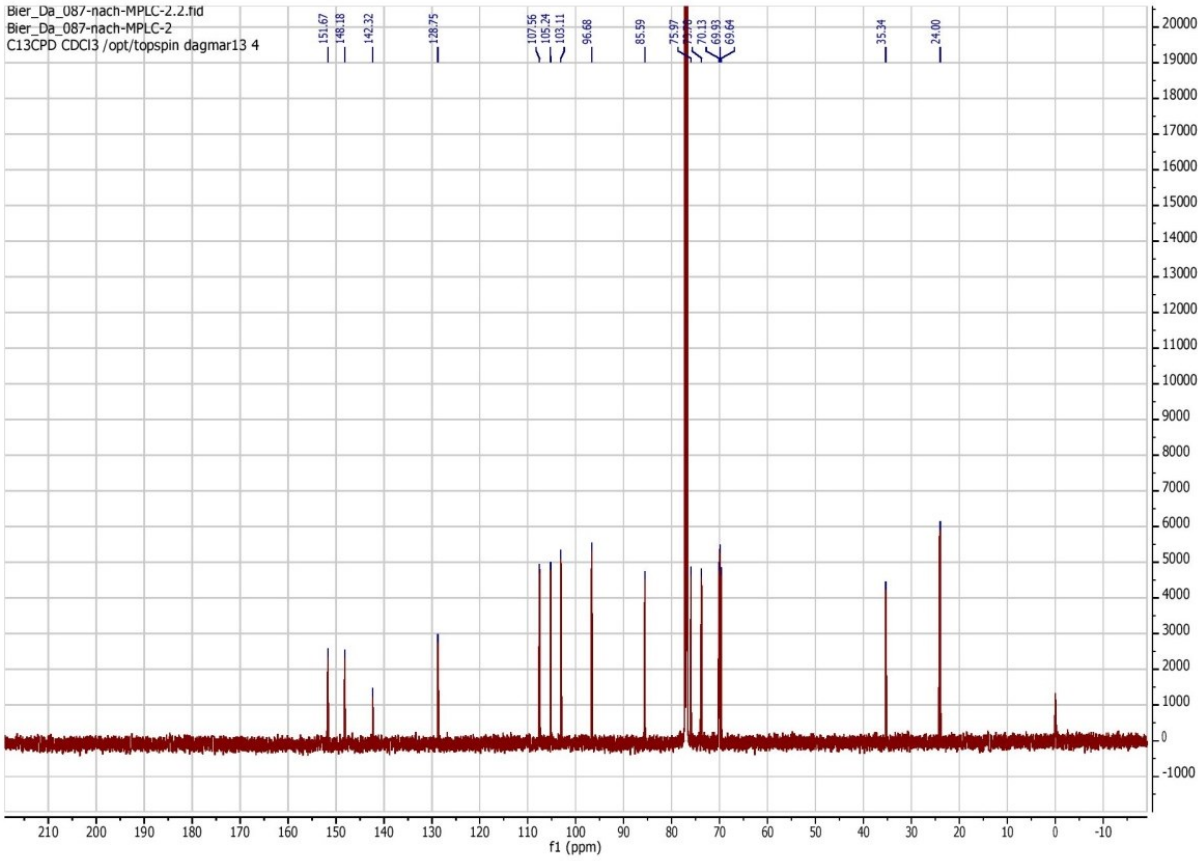

IR absorptions:

ν_{max} /cm^{-1} 3596, 3410,2967, 2916, 2866, 1639, 1615, 1522, 1506, 1486, 1431, 1408, 1363, 1342, 1268, 1240,1268, 1240, 1168, 1142, 1103,1051, 989, 964, 948, 929, 906, 888, 873,841,817, 799, 758, 727.

Melting point:

164.3°C

Mass spectrometry data:

HR-MS (ESI, positive mode):

m/z = 433.1275 (33 %, M+NH_4^+), 438.0829 (100 %, M+Na).

Optical rotation:

$[\alpha]_D^{20}$ -75.2° (c =0.2 in $CHCl_3$)

UV-Vis absorptions:

λ_{max} ($CHCl_3$)/nm 251 (ε/dm^3 mol^{-1} cm^{-1} 8333), 344 (3232).

Supplementary figures

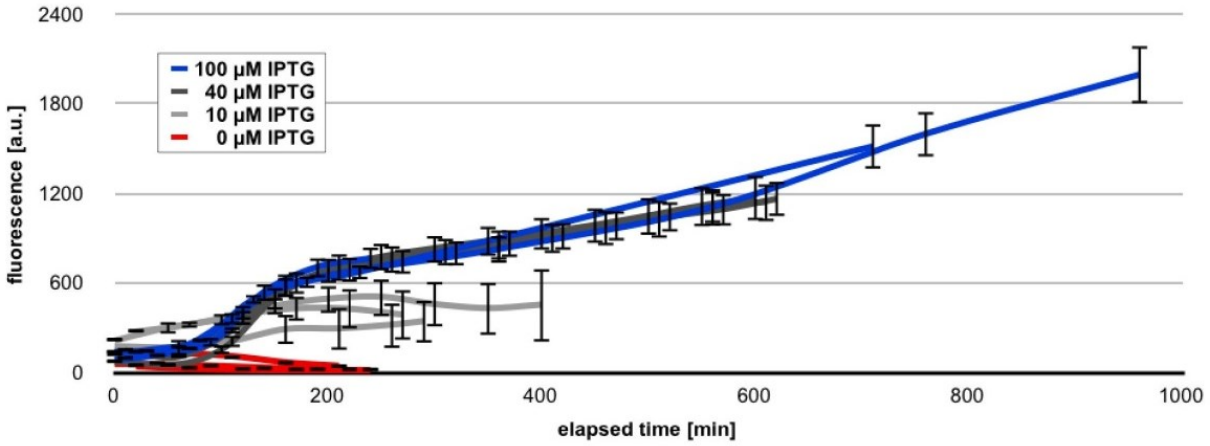

Fig. S1 Fluorescence development of *E.coli* BL21(DE3)/pRhotHi-2-EYFP microcolonies during differently supplemented microfluidic cultivation. For each concentration, fluorescence development of three independent microcolonies is plotted. Data points represent mean fluorescence values of all cells with the standard deviation as error bars. a.u.: arbitrary units

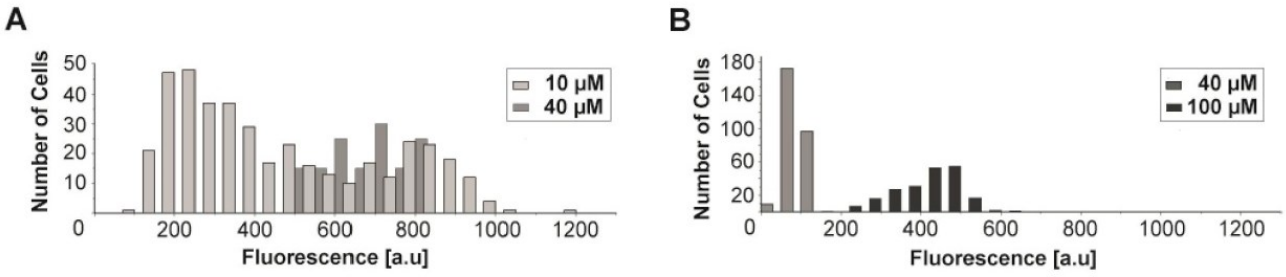

Fig. S2 Population histograms for representative microcolonies of differently induced *E. coli* BL21(DE3)/pRhotHi-2-EYFP (**A**) and Tuner(DE3)/pRhotHi-2-LacI-EYFP (**B**) populations after microfluidic cultivation for 100 min. a.u.: arbitrary units

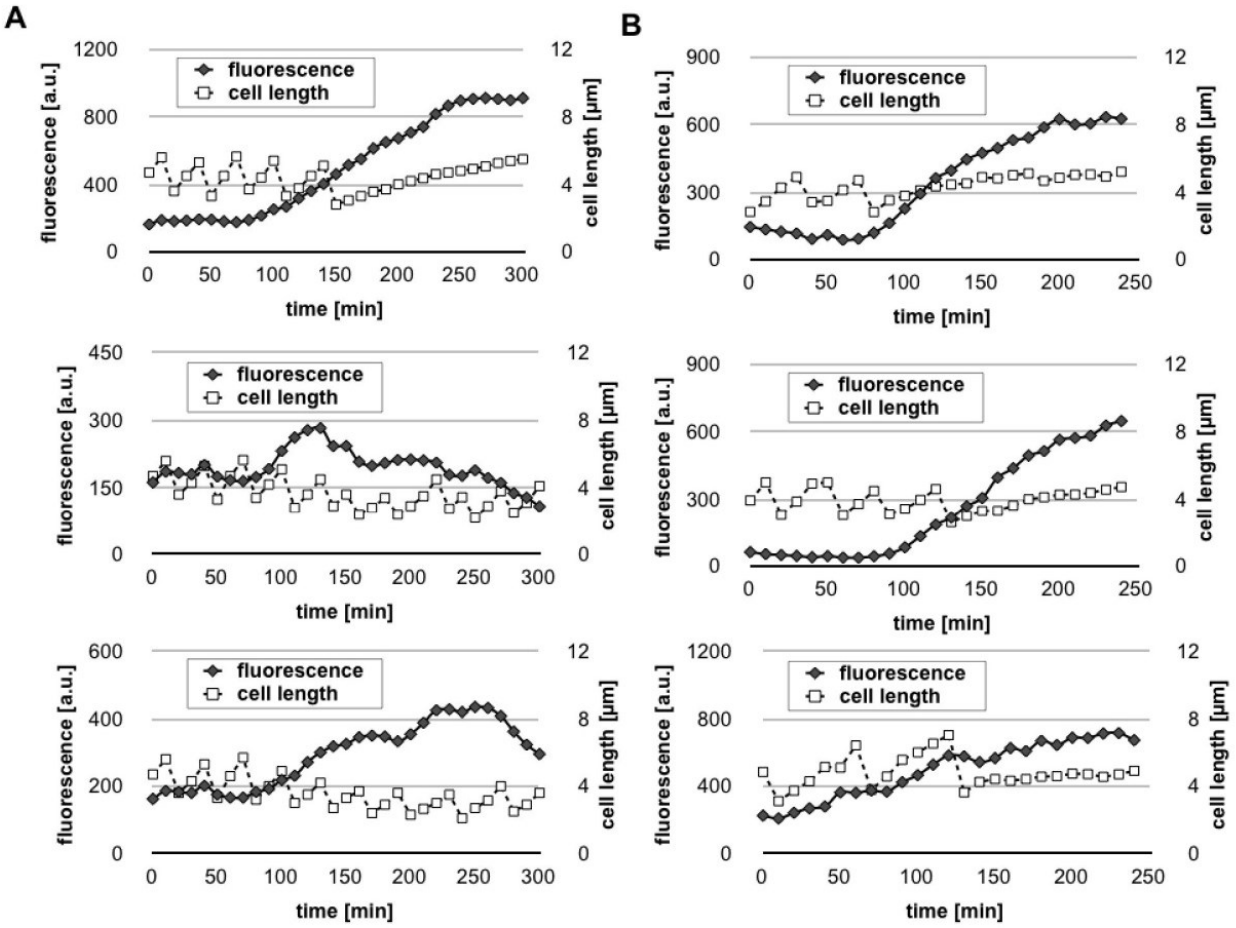

Fig. S3 Correlation between growth and fluorescence development of differently induced *E. coli* BL21(DE3)/pRhotHi-2-EYFP. Monitoring of single cell fluorescence (diamonds) and cell length (squares) as a measure for ongoing cell divisions during the induction with 10 µM (**A**) and 40 µM IPTG (**B**). a.u.: arbitrary units

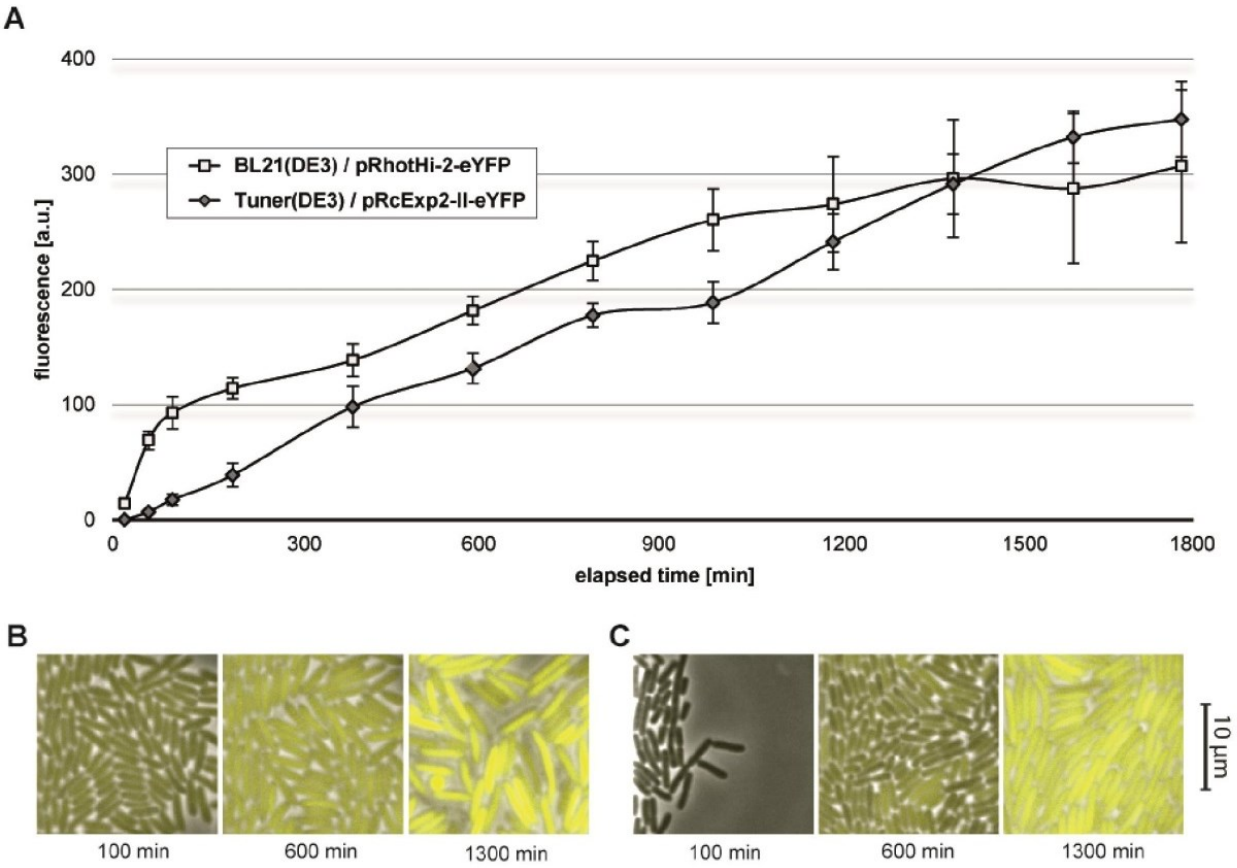

Fig. S4 **A** Long-term fluorescence development in *E. coli* BL21(DE3)/pRhotHi-2-EYFP (squares) and *E. coli* Tuner(DE3)/pRhotHi-2-LacI-EYFP (filled diamonds) during microfluidic perfusion cultivation upon full induction with 100 µM IPTG. Induction was performed after several hours of precultivation in cultivation chambers that were open at both sides [3,4] and therefore allowed for several cells to be monitored whereas others grew out of the cultivation device and were flushed away through the nutrient channel. Selected photographs of *E. coli* BL21(DE3)/pRhotHi-2-EYFP (**B**) and *E. coli* Tuner(DE3)/ pRhotHi-2-LacI-EYFP (**C**) show a delayed fluorescence in Tuner(DE3) that yields to comparable final levels at the end of the experiment. a.u.: arbitrary units

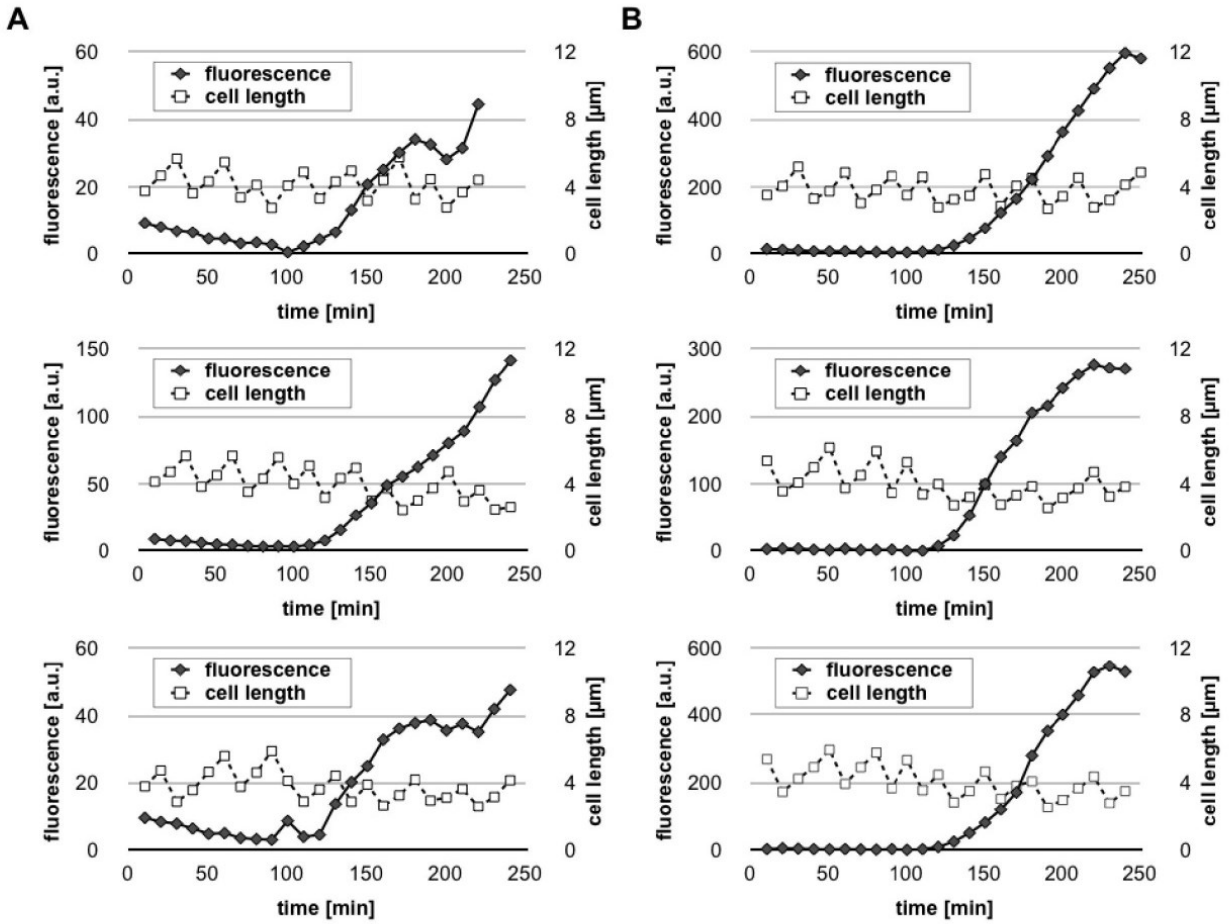

Fig. S5 Correlation between growth and fluorescence development of differently induced *E. coli* Tuner(DE3)/ pRhotHi-2-LacI-EYFP single cells. Monitoring of cell fluorescence (diamonds) and cell length (squares) as a measure for ongoing cell divisions during the induction with 40 µM (**A**) and 100 µM IPTG (**B**). a.u.: arbitrary units

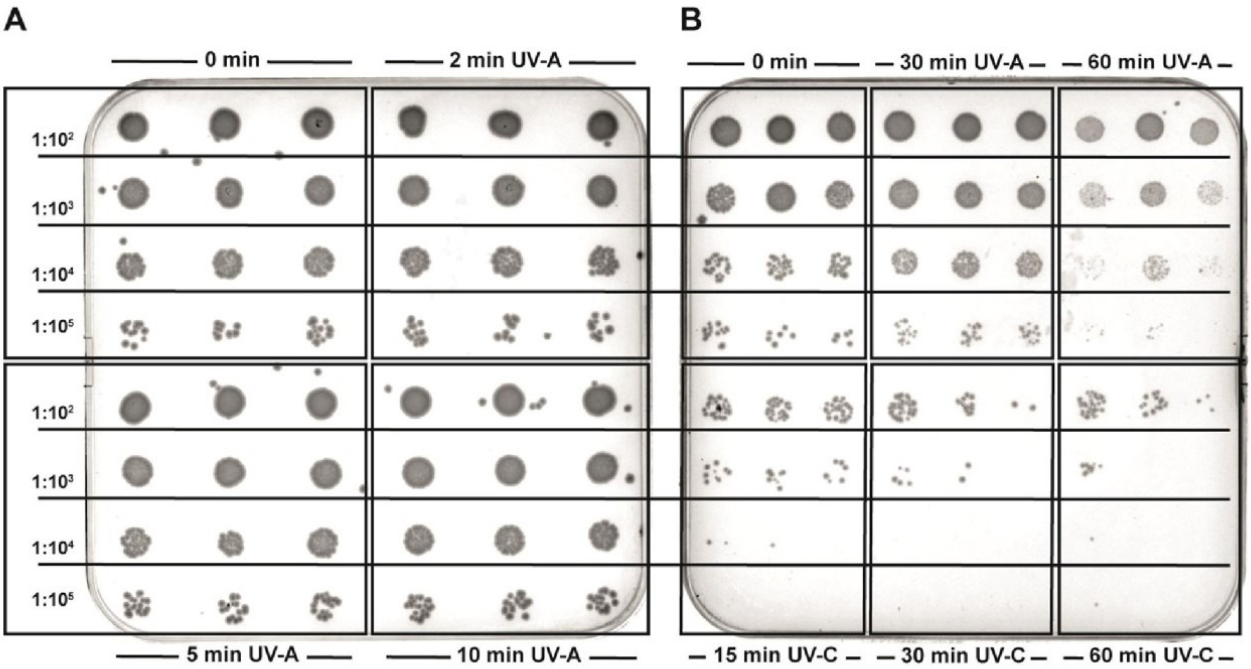

Fig. S6 Toxicity assay comparing colony forming of differently UV-exposed and serially diluted cell suspensions.
To exclude phototoxic effects caused by exposing *E. coli* cells with UV-A light, a phototoxicity assay was conducted. To analyze cell viability of differently UV-irradiated and serially diluted *E. coli* Tuner(DE3)/pRhotHi-2-LacI cells. Cultures were inoculated for 1.5 h and exposed for (**A**) 0, 2, 5 and 10 min to UV-A light and for (**B**) 0, 30 and 60 min to UV-A light (upper section) as well as 15, 30 and 60 min to UV-C light (lower section). Cultivation and exposure were performed exactly as described in the materials and methods section. UV-C exposure was realized using a low-intesity UV-C hand lamp (λ_{max}: 254 nm, 12 W, VL-6-LV from Vilber Lourmat, France). The cell cultures were diluted as indicated and 3 µl of diluted suspensions were placed on an LB-agar plate, which was cultivated over night (37°C, 50 µg/ml Kanamycin).

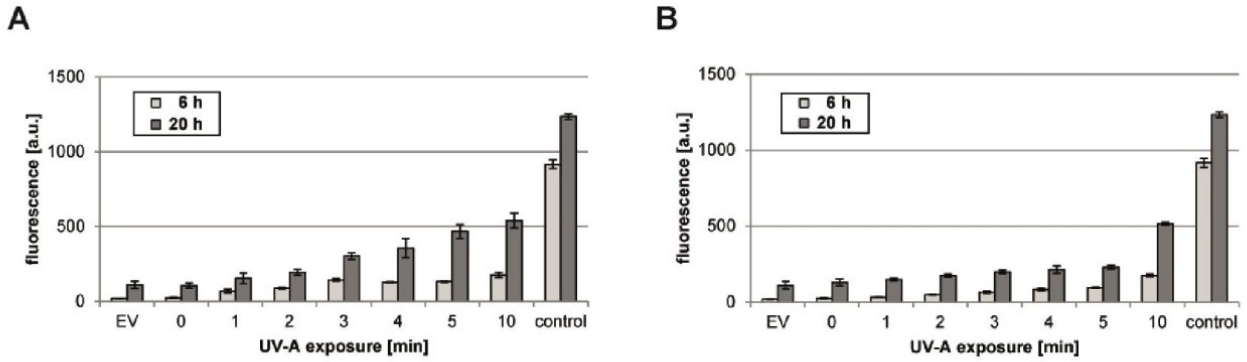

Fig. S7 Influence of NP-photocaged IPTG supplementation time on UV-A light-controlled regulation of gene expression in *E. coli* Tuner(DE3)/pRhotHi-2-LacI-EYFP.
In vivo fluorescence of *E. coli* cultures supplemented with 40 µM NP-photocaged IPTG either at the beginning of the cultivation (**A**) or directly before light induction (**B**). Gene expression was specifically induced by increasing periods of UV-A light exposure. Cultures were induced after 2 h of pre-cultivation where cells were kept in darkness. Corresponding control cultures were supplemented with 40 µM uncaged IPTG. EV: empty vector control. Values are means of triplicate measurements. Error bars indicate the respective standard deviations. a.u.: arbitrary units.

V.3 Supporting Information for Chapter II.3.2 – Photocaged Arabinose

Photocaged Arabinose – A Novel Optogenetic Switch for Rapid and Gradual Control of Microbial Gene Expression

Dennis Binder, Claus Bier, Alexander Grünberger, Dagmar Drobietz, Jennifer Hage-Hülsmann, Georg Wandrey, Jochen Büchs, Dietrich Kohlheyer, Anita Loeschcke, Wolfgang Wiechert, Karl-Erich Jaeger, Jörg Pietruszka, and Thomas Drepper. *ChemBioChem* 2016; 17: 296–300.

CHEMBIOCHEM

Supporting Information

Photocaged Arabinose: A Novel Optogenetic Switch for Rapid and Gradual Control of Microbial Gene Expression

Dennis Binder,[a] Claus Bier,[b] Alexander Grünberger,[c] Dagmar Drobietz,[b] Jennifer Hage-Hülsmann,[a] Georg Wandrey,[d] Jochen Büchs,[d] Dietrich Kohlheyer,[c] Anita Loeschcke,[a] Wolfgang Wiechert,[c] Karl-Erich Jaeger,[a, c] Jörg Pietruszka,[b, c] and Thomas Drepper*[a]

cbic_201500609_sm_miscellaneous_information.pdf
cbic_201500609_sm_arabinose.wmv
cbic_201500609_sm_Photocaged_arabinose.wmv

Supporting Information

Table of contents

1. General remarks

All chemicals for synthesis were obtained from commercial sources and used as received unless stated otherwise. Solvents were reagent grade. Solvents were dried and purified by common methods. Thin-layer chromatography (TLC) was performed using pre-coated (Polygram® SIL G/UV, Macherey-Nagel) silica gel plates, and components were visualized via staining with cerium molybdenum solution [phosphomolybdic acid (25 g), $Ce(SO_4)_2 \cdot H_2O$ (10 g), conc. H_2SO_4 (60 mL), H_2O (940 mL)], or UV-light. Flash chromatography was performed on silica gel (Merck silica gel 60 (0.063–0.200 µm). Solvents for flash chromatography (petroleum ether/ EtOAc/ n-pentane/ CH_2Cl_2) were distilled prior to use. Petroleum ether refers to a fraction with a boiling point between 40–60 °C. The NMR spectra (^1H and ^{13}C) were measured at 20 °C on a Bruker Avance/DRX 600 spectrometer in deuterated solvents ($CDCl_3$, DMSO-d_6, CD_3OD). Chemical shifts are given in ppm relative to the resonance of the solvent (^1H: $CDCl_3$= 7.26 ppm, ^1H: CD_3OD = 2.50 ppm or ^1H: DMSO-d_6 = 3.31 ppm/ ^{13}C: $CDCl_3$= 77.16 ppm, ^{13}C: CD_3OD = 49.00 ppm or ^{13}C: DMSO-d_6 = 39.52 ppm). The IR spectra were measured with a Perkin Elmer SpectrumOne IR-spectrometer ATR. Optical rotation was determined at 20 °C on a Perkin Elmer Polarimeter 241 MC against sodium D-line. HRMS (ESI) spectra were recorded by the ZEA 3 of the research center Jülich. Melting points were recorded using a Büchi melting point B-545 apparatus. UV-Vis absorption spectra were recorded on Genesys 10S UV/VIS Spectrophotometer (Thermo Scientific). In addition, UV-Vis absorption was quantified using a Tecan infinite M1000Pro microplate reader. Uncaging experiments were performed with the LUMOS 43® from Atlas Photonics at 375 nm. The freed sugar was separated and detected by a Jasco HPLC system [column: Hyperclone 5 µ ODS (C18) 120 (Phenomenex)] combined with the light scattering detector ELSD ZAM 3000 from AlphaCrom. UV-A light exposure was performed using VL-315.BL 45 W hand lamp from Vilber Lourmat. Light intensity was quantified using a Thermal Power Sensor (S302C, Thorlabs Inc, USA).

2. Supporting methods

2.1.1 Synthesis of 2,3,4-tri-O-acetyl-β-L-arabinopyranosyl bromide (1)

L-(+)-arabinose (1.00 g, 6.66 mmol) was dissolved in 5 mL acetic anhydride at room temperature. 1.5 mL HBr solution 33 wt. % in AcOH was added to this solution. After 1 h stirring, additional 7.5 mL HBr solution 33 wt. % in AcOH were added. The reaction mixture was stirred for additional 2 h. Afterwards, it was concentrated under reduced pressure. Twice 20 mL toluene were added and then removed under reduced pressure. The raw product was recrystallized twice from Et_2O to receive a colorless crystalline powder (1.63 g, 4.79 mmol, 72%).[1]

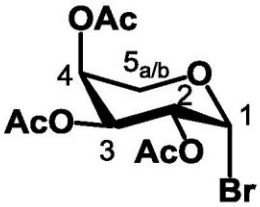

^1H NMR (600 MHz, [D_1]$CDCl_3$, RT) δ = 6.67 (d, $^3J_{1/2}$ = 3.9 Hz, 1H, 1-H), 5.37 (m, 2H, 3-H, 4-H), 5.06 (m, 1H, 2-H), 4.18 (d, $^2J_{5a/b}$ = 13.4 Hz, 1H, 5–H_a), 3.91 (dd, $^2J_{5a/b}$ = 13.4 Hz, $^3J_{5b/4}$ = 1.8 Hz, 1H, 5–H_b), 2.12 (s, 3H, -CH_3), 2.09 (s, 3H, -CH_3), 2.00 ppm (s, 3H, -CH_3).

^{13}C NMR (151 MHz, [D$_1$]CDCl$_3$, RT) δ = 170.1 (C=O), 170.1 (C=O), 169.8 (C=O), 89.8 (C-1), 68.0 (C-2), 67.9 (C-4), 67.7 (C-3), 64.8 (C-5), 20.9 (-CH$_3$), 20.8 (-CH$_3$), 20.7 ppm (-CH$_3$).

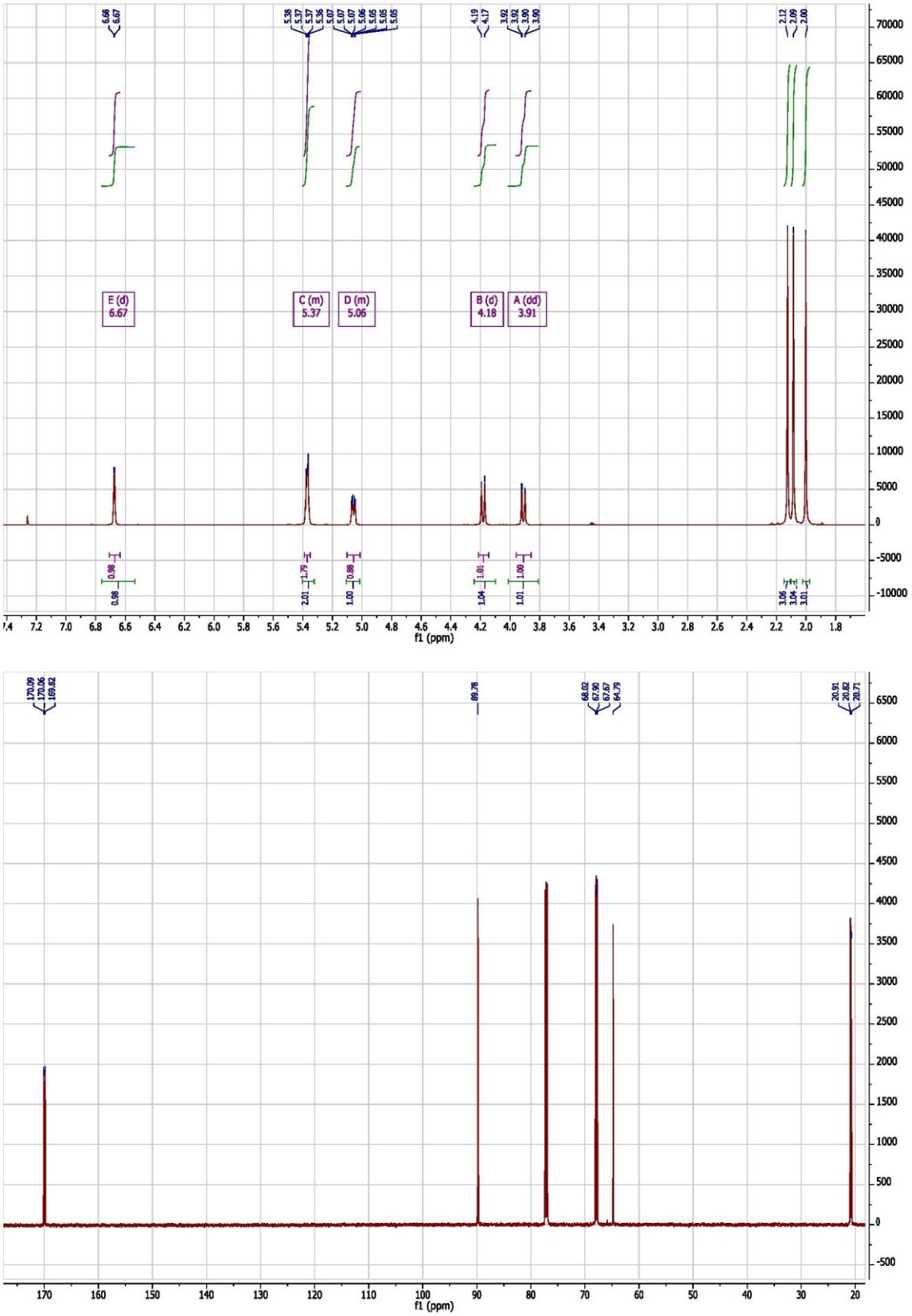

Figure S1. ^{1}H and ^{13}C NMR spectra of compound **1**.

IR (ATR): $\tilde{\nu}_{max}$ = 1734, 1375, 1206, 1126, 1097, 1070, 1043, 993, 929, 892, 857, 761, 684 cm^{-1}.

Melting point: 127 °C

optical rotatory power: $[\alpha]_D^{20}$ = 255° (c = 0.9 in $CHCl_3$)

2.1.2 Synthesis of 6-nitro-2-(1,3-benzodioxol-5-yl)-2-ethylalcohol (2b)

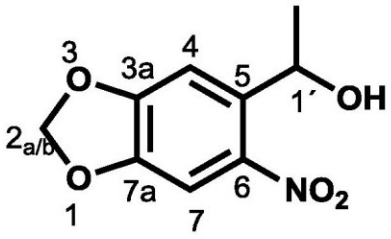

All glassware was dried prior to use. In a *Schlenk* tube 6-nitropiperonal (1.25 g, 6.41 mmol) was dissolved in 30 mL dry CH_2Cl_2. At 0 °C a solution of $Al(CH_3)_3$ in hexane (5.6 mL, 11.2 mmol, 2.00 M) was added dropwise over 20 min. The reaction mixture was stirred for additional 4 h until 6-nitropiperonal was fully converted. This was checked via TLC. Then the reaction mixture was poured on 20 mL of a mixture of ice and 1 M aqueous HCl (caution: evolution of CH_4). The aqueous phase was extracted twice with CH_2Cl_2. The combined organic phase was dried over anhydrous $MgSO_4$ and the solvent was removed under reduced pressure. The residue was purified by flash-column chromatography on SiO_2 (CH_2Cl_2/petroleum ether, 6:4) to yield a light yellow solid (1.05 g, 4.97 mmol, 84%).[2]

^{1}H NMR (600 MHz, $[D_4]CD_3OD$) δ = 7.45 (s, 1H, 7-H) 7.28 (s, 1H, 4-H), 6.14 (d, $J^2_{2a/2b}$ = 1.1 Hz, 1H, 2-H_a), 6.13 (d, $J^2_{2b/2a}$ = 1.1 Hz, 1H, 2-H_b), 5.36 (q, $J^3_{1´/CH3}$ = 6.3 Hz, 1H, 1'-H), 1.46 ppm (d, $J^3_{CH3/1´}$ = 6.3 Hz, 3H, -CH_3).

^{13}C NMR (151 MHz, $[D_1]CDCl_3$, RT) δ = 152.5 (C-6), 147.0 (C-7a), 141.5 (C-3a), 139.2 (C-5), 106.4 (C-4), 105.2 (C-7), 103.1 (C-2), 65.8 (C-1´), 24.3 ppm (-CH_3).

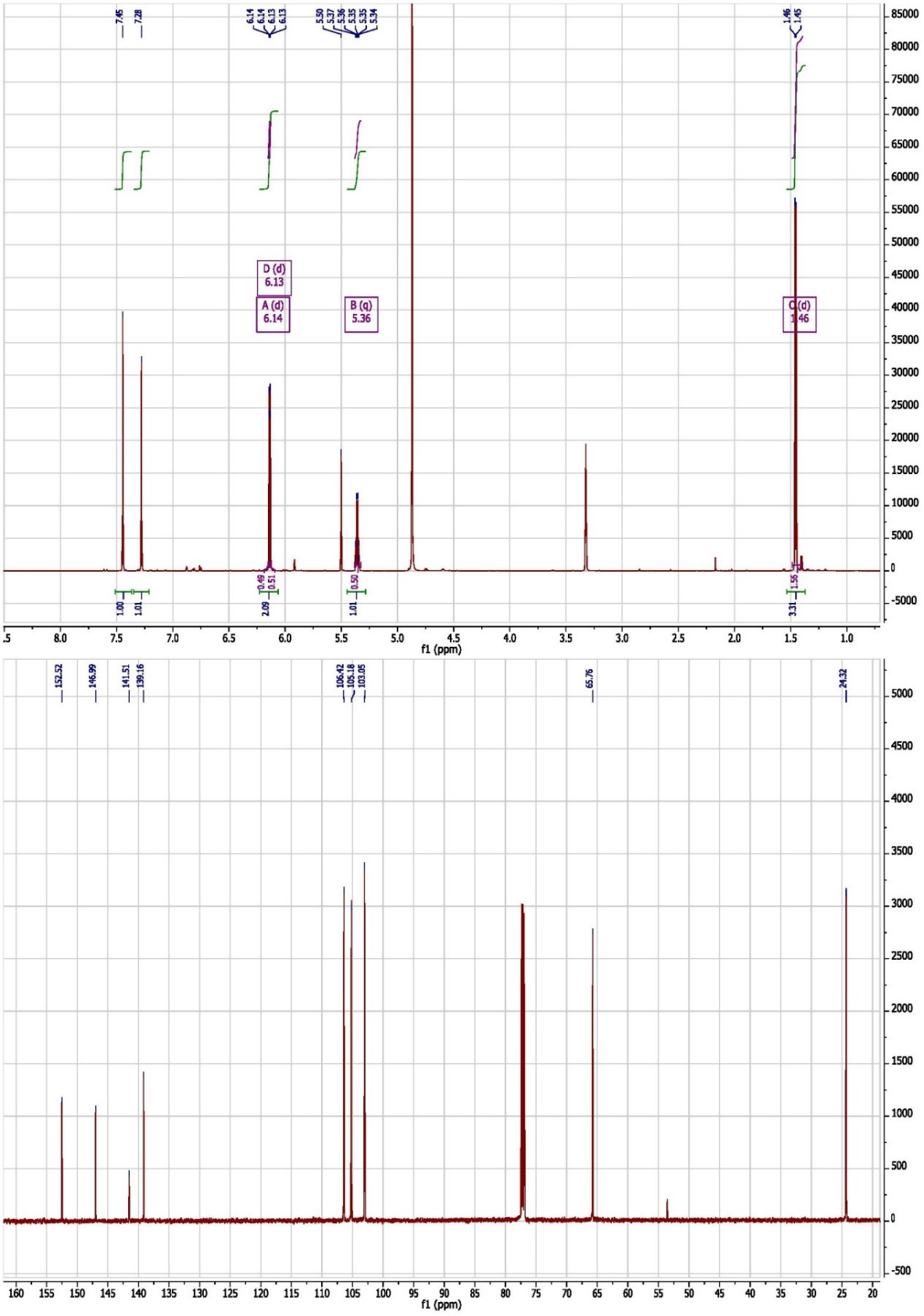

Figure S2. ^{1}H and ^{13}C NMR spectra of compound **2b**.

2.1.3 Synthesis of 6-nitropiperonyl-β-L-arabinopyranose triacetate (3a)

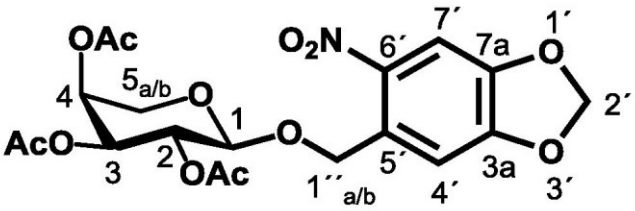

All glassware was dried prior to use. One *Schlenk* tube was charged with 1 g molecular sieve 5 Å and 2,3,4-Tri-O-acetyl-β-L-arabinopyranosyl bromide (400 mg, 1.18 mmol) dissolved in 0.5 mL dry CH_2Cl_2. A second one was charged with 1 g molecular sieve 5 Å and 6-nitropiperonylalcohol (581 mg, 2.95 mmol) dissolved in 1 mL of dry CH_2Cl_2. After one hour of stirring they were combined. Following $AgCO_3$ (195 mg, 0.71 mmol) and CF_3SO_3Ag (181 mg, 0.71 mmol) were added. The reaction was stirred at room temperature until full conversion. The molecular sieve was removed via filtration. The filtrate was washed with a saturated $NaHCO_3$ solution and brine. The combined organic layer was dried with anhydrous $MgSO_4$ and concentrated under reduced pressure. The residue was purified by flash-column chromatography on SiO_2 (CH_2Cl_2/ n-pentane; 8:2) to yield a light yellow solid (285 mg, 0.63 mmol, 53%).

^{1}H NMR (600 MHz, [D$_1$]CDCl$_3$, RT) δ = 7.62 (s, 1H, 7-H), 7.22 (s, 1H, 4´-H), 6.12 (s, 2H, 2´-H$_2$), 5.29 (m, 2H, 2-H, 3-H), 5.20 (d, $^2J_{1''a/1''b}$ = 15.3 Hz, 1H, 1´´-H$_a$), 5.10 (dd, $^3J_{4/3}$ = 9.1 Hz, $^3J_{4/5}$ = 3.6 Hz, 1H, 4-H), 4.98 (d, $^2J_{1''b/1''a}$ = 15.3 Hz, 1H, 1´´-H$_b$), 4.60 (d, $^3J_{1/2}$ = 6.6 Hz, 1H, 1-H), 4.04 (dd, $^2J_{5a/5b}$ = 13.0 Hz, $^3J_{5a/4}$ = 3.7 Hz, 1H, 5-H$_a$), 3.67 (dd, $^2J_{5b/a}$ = 13.0 Hz, $^3J_{5b/4}$ = 1.9 Hz, 1H, 5-H$_b$), 2.14 (s, 3H, -CH$_3$), 2.09 (s, 3H, -CH$_3$), 2.05 ppm (s, 3H, -CH$_3$).

^{13}C NMR (151 MHz, [D$_1$]CDCl$_3$, RT) δ = 170.4 (C=O), 170.2 (C=O), 169.7 (C=O), 152.9 (C-7a), 147.2 (C-3a), 140.8 (C-6´), 132.1 (C-5´), 107.4 (C-4´), 105.7 (C-7´), 103.2 (C-2´), 100.5 (C-1), 70.0 (C-4), 69.4 (C-2), 68.2 (C-1´´), 67.5 (C-3), 63.2 (C-5), 21.1 (-CH$_3$), 20.9 (-CH$_3$), 20.8 ppm (-CH$_3$).

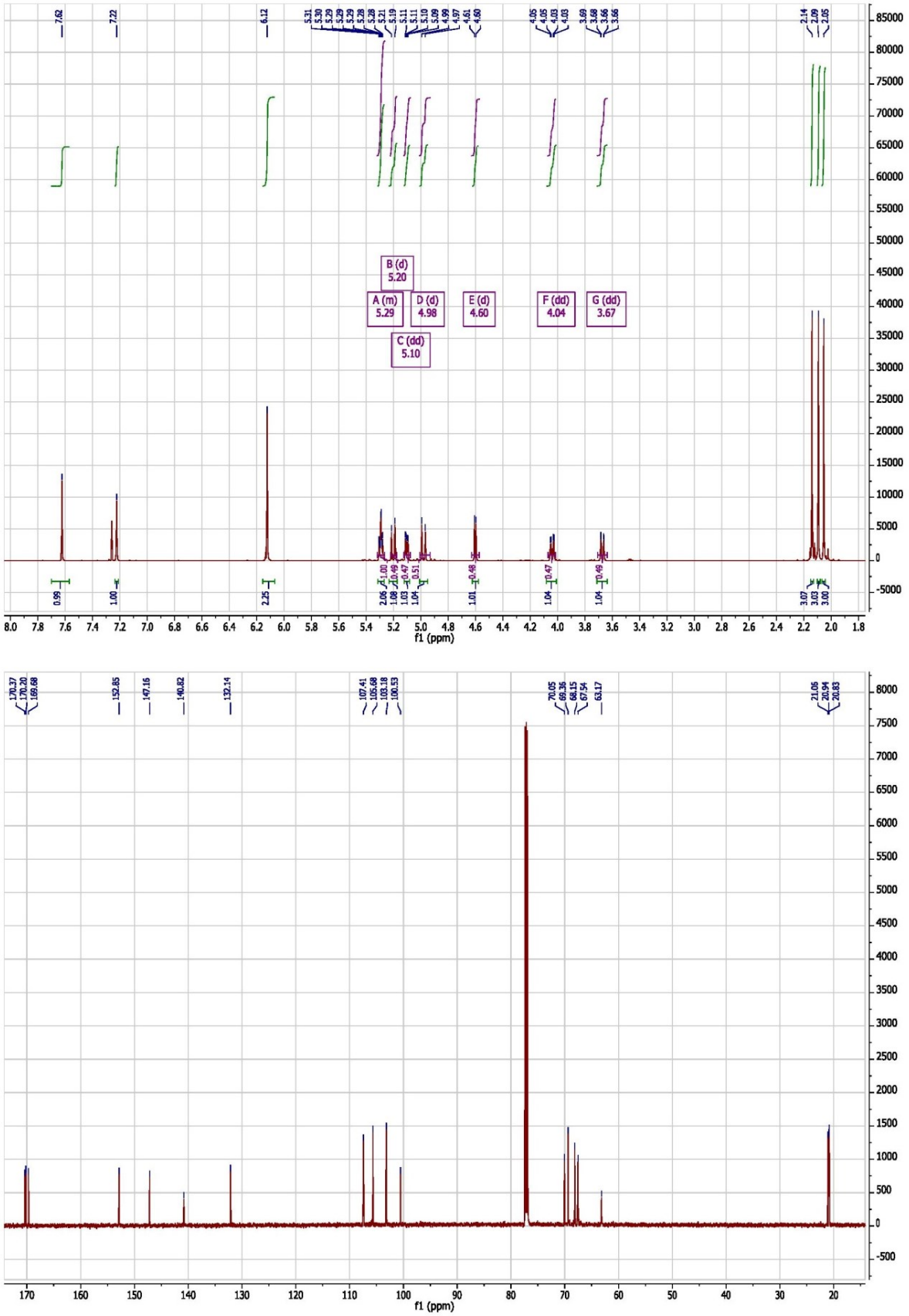

Figure S3. ^{1}H and ^{13}C NMR spectra of compound **3a**.

HRMS (ESI, positive mode): M = ($C_{19}H_{21}NO_{12}$), *m/z* =

calculated:	[M+Na]	478.09614	
found:	[M+Na]	478.09561	(100%)

IR (ATR): $\tilde{\nu}_{max}$ = 1740, 1521, 1506, 1485, 1370, 1324, 1252, 1213, 1104, 1055, 1026, 928, 877, 816, 756 cm^{-1}

Melting point: 64 °C

optical rotatory power: $[\alpha]_D^{20}$ = 11° (c = 0.08, in MeOH)

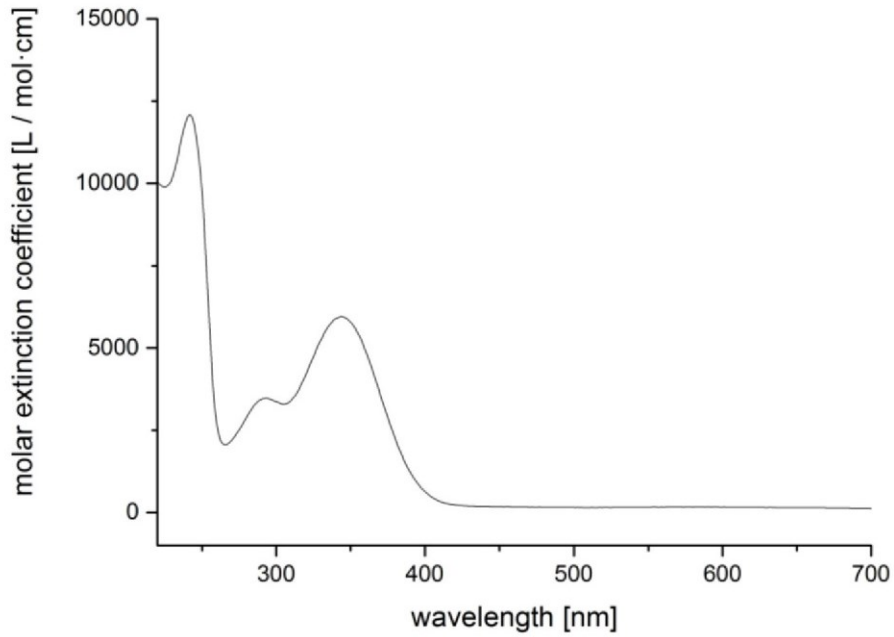

Figure S4. UV-Vis spectrum of compound **3a**. UV/Vis (MeOH): λ_{max} (ε) = 243 nm (12026), 295 nm (3470), 344 nm (5958).

2.1.4 Synthesis of 6-nitropiperonyl-β-L-arabinopyranose (4a)

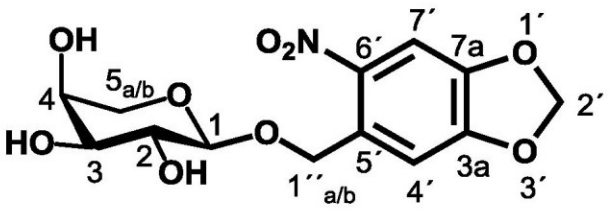

The product **3a** (200 mg, 0.43 mmol) was dissolved in 4 mL MeOH and 1 mL of a 0.23 M solution of NaOMe (in MeOH) was added. The reaction was stirred at room temperature until complete conversion. Afterwards, the reaction was neutralized with an ion exchanger (Dowex 650C). The mixture was filtrated. The filtrate was concentrated under reduced pressure. The residue was purified by flash-column chromatography on SiO_2 (EtOAc) to yield the product **4a** (134 mg, 0.41 mmol, 95%) as a light yellow solid.

^{1}H NMR (600 MHz, [D_6]DMSO, RT) δ = 7.71(s, 1H, 7-H), 7.57 (s, 1H, 4´-H), 6.25 (s, 2H, 2´-H_2), 5.21 (d, $^3J_{2\text{-OH}/2\text{-H}}$ = 4.7 Hz, 1H, 2-OH), 5.02 (d, $^2J_{1´´a/1´´b}$ = 16.0 Hz, 1H, 1´´$_a$-H_2), 4.86 (d, $^2J_{1´´b/1´´a}$ = 16.0 Hz, 1H, 1´´$_b$-H_2), 4.72 (d, $^3J_{4\text{-OH}/4\text{-H}}$ = 5.5 Hz, 1H, 4-OH), 4.57 (d, $^3J_{3\text{OH}/3\text{-H}}$ = 4.4 Hz, 1H, 3-OH), 4.24 (d, $^3J_{1\text{-H}/2\text{-H}}$ = 6.6 Hz, 1H, 1-H), 3.71 (dd, $^2J_{5a/5b}$ = 12.0 Hz, $^3J_{5a/4}$ = 3.4 Hz 1H, 5$_a$ -H_2), 3.64 (m, 1H, 3-H), 3.49 (m, 1H, 4-H), 3.41 (d, $^2J_{5b/a}$ = 12.0 Hz, 1H, 5$_b$-H_2) 3.37 ppm (m, 1H, 2-H).

^{13}C NMR *coupled* (151 MHz, [D_6]DMSO, RT) δ = 152.5 (s, C-7a), 146.6 (s, C-3a), 140.2 (s, C-6´), 133.1 (s, C-5´), 107.3 (d, J = 171.5 Hz, C-4´), 105.0 (d, J = 171.4 Hz, C-7´), 103.4 (t, J = 177.7 Hz, C-2´), 103.0 (d, J = 159.4 Hz, C-1), 72.4 (d, J = 138.5 Hz, C-4), 70.7 (d, J = 144.1 Hz, C-2), 67.5 (d, J = 142.9 Hz, C-3), 66.4 (t, J = 151.3 Hz, C-1´´a/b), 65.4 (t, J = 139.5 Hz, C-5).

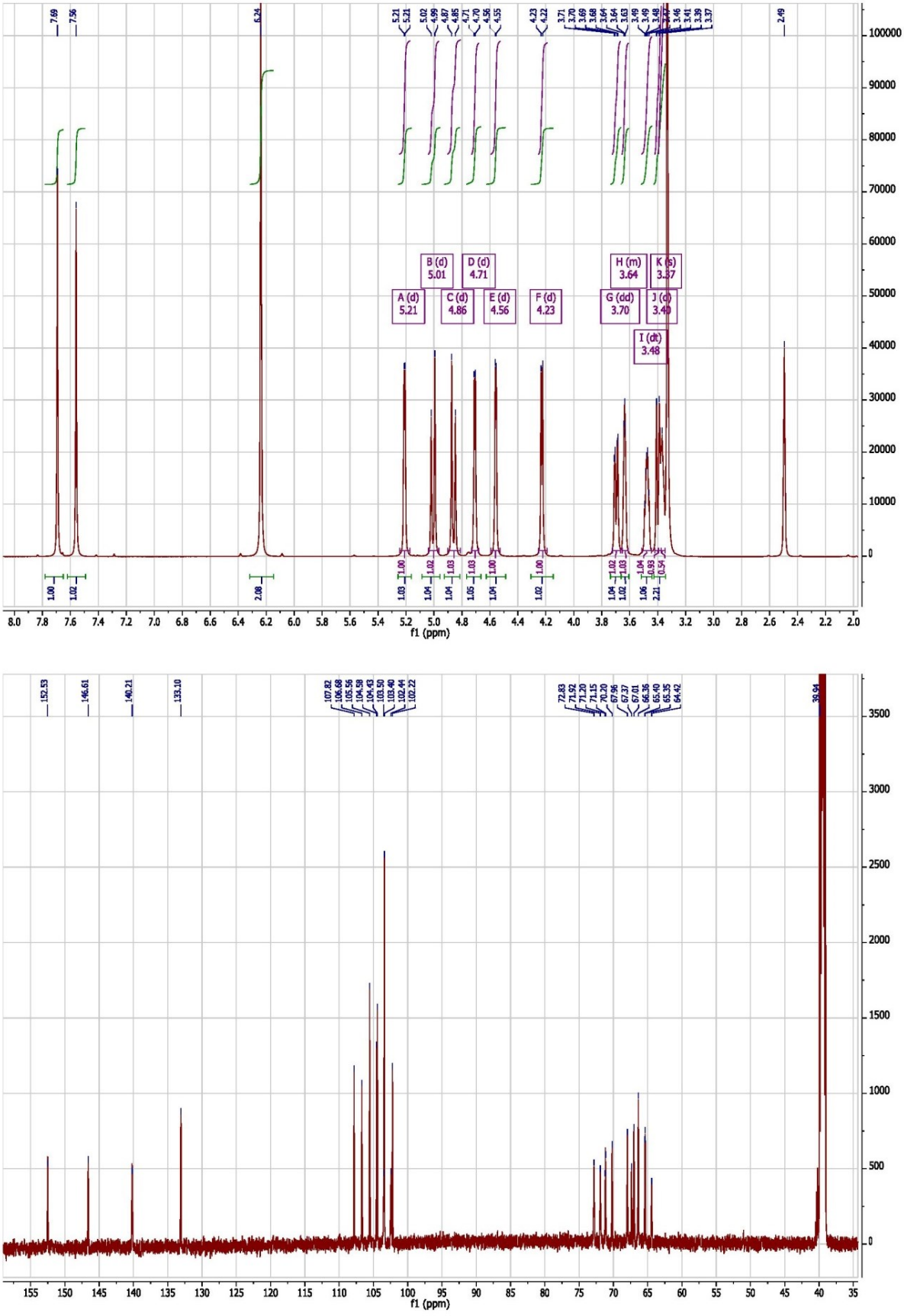

Figure S5. ^{1}H and ^{13}C NMR spectra of compound **4a**.

HRMS (ESI, positive mode): M = ($C_{13}H_{15}NO_9$), *m/z* =

calculated:	[M+Na]	352.0645	[2M+Na]	681.1391
found:	[M+Na]	352.0646 (66%)	[2M+Na]	681.1395 (100%)

IR (ATR): $\tilde{\nu}_{max}$ = 3544, 3343, 1614, 1515, 1506, 1475, 1444, 1374, 1318, 1255, 1198, 1153, 1136, 1062, 1037, 1013, 999, 933, 896, 868, 818, 788, 757, 698.

Melting point: 180°C

optical rotatory power: $[\alpha]_D^{20}$ = -3° (c = 0.08, in MeOH)

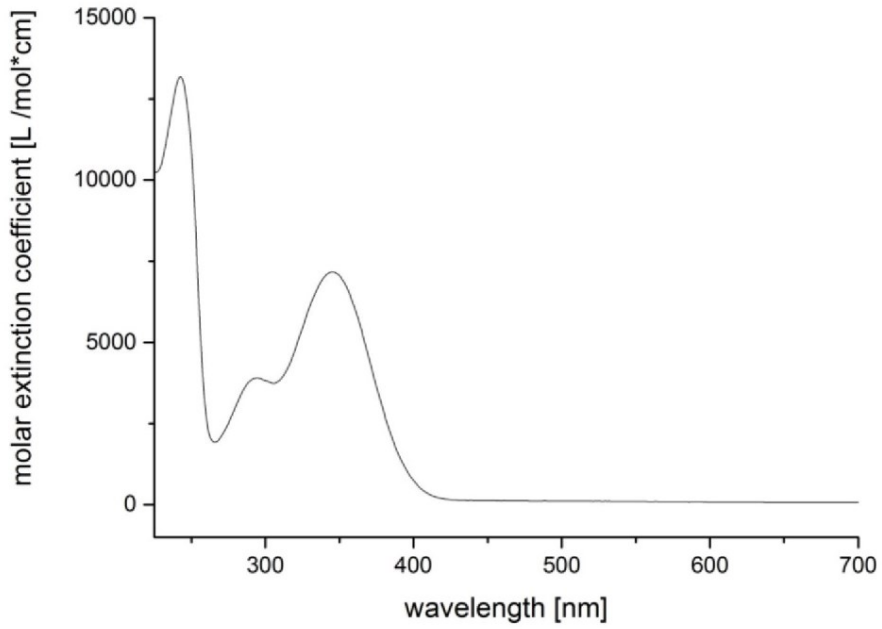

Figure S6. UV-Vis spectrum of compound **4a**. UV/Vis (MeOH): λ_{max} (ε) = 243 nm (13175), 295 nm (3909), 345 nm (7171).

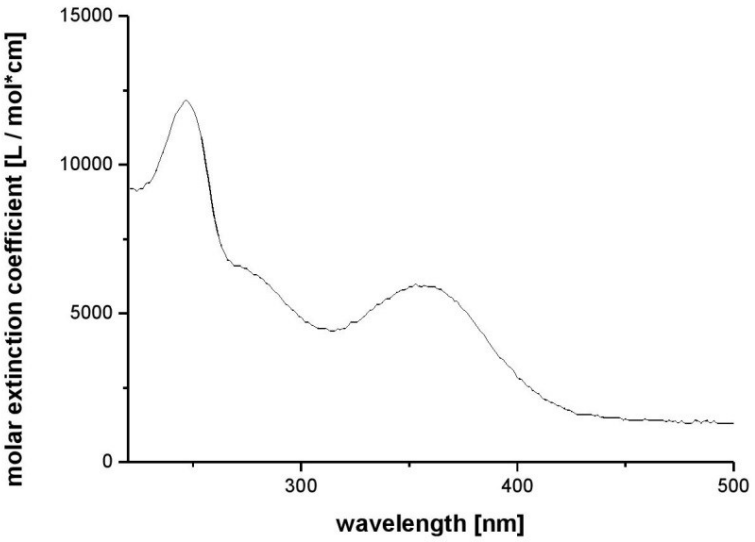

Figure S7. UV-Vis spectrum of compound **4a**. UV/Vis (H_2O): λ_{max} (ε) = 246 nm (12200), 271 nm (6600), 353 nm (6000).

2.1.5 Synthesis of (β-L -arabinopyranose triacetat)-((1-(6-nitro-1,3-benzodioxol)-5-yl)ethyl)-ether (3b)

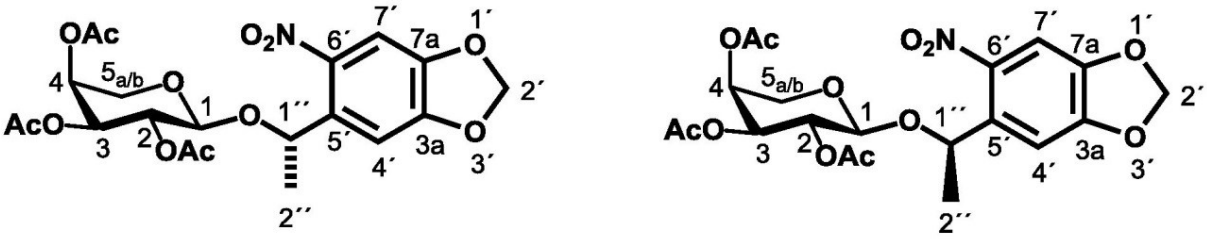

All glassware was dried prior to use. One *Schlenk* tube was charged with 1 g molecular sieve 5 Å and 2,3,4-Tri-O-acetyl-β-L-arabinopyranosyl bromide (**1**) (252 mg, 0.74 mmol) dissolved in 0.5 mL dry CH_2Cl_2. A second one was charged with 1 g molecular sieve 5 Å and 6-nitro-2-(1,3-benzodioxol-5-yl)-2-ethylalcohol (314 mg, 1.49 mmol) (**2b**) dissolved in 1 mL of dry CH_2Cl_2. After 1 hour of stirring, they were combined and silver carbonate (246 mg, 0.90 mmol) was added. The reaction was stirred at room temperature until full conversion. The molecular sieve was removed via filtration. The filtrate was washed with a saturated $NaHCO_3$ solution and brine. The combined organic layer was dried with anhydrous $MgSO_4$ and concentrated under reduced pressure. The residue was purified by flash-column

chromatography on SiO_2 (EtOAc/petroleum ether 1:1) to yield a light yellow solid (218 mg, 0.63 mmol, 63%).

^{1}H NMR (600 MHz[D_6]DMSO, RT) δ = 7.48 (s, 1H, 7-H), 7.47 (s, 1H, 7-H), 7.25 (s, 1H, 4´-H), 7.03 (s, 1H, 4´-H), 6.11 (m, 4H, 2´-H_2), 5.51 (q, $^{3}J_{1´´/2´´}$ = 6.3 Hz, 1H, 1´´-H), 5.46 (q, $^{3}J_{1´´/2´´}$ = 6.2 Hz, 1H, 1´´-H), 5.25 (m, 4H, 2-H, 3-H), 5.06 (dd, $^{3}J_{4/3}$ = 9.3 Hz, $^{3}J_{4/5}$ = 3.6 Hz, 1H, 4-H), 4.93 (dd, $^{3}J_{4/3}$ = 9.5 Hz, $^{3}J_{4/5}$ = 3.5 Hz, 1H, 4-H), 4.57 (d, $^{3}J_{1/2}$ = 6.8 Hz, 1H, 1-H), 4.20 (d, $^{3}J_{1/2}$ = 7.1 Hz, 1H, 1-H), 4.01 (dd, $^{2}J_{5a/5b}$ = 13.2, $^{3}J_{5a/4}$ = 3.1 Hz, 1H, 5a-H_2), 3.86 (dd, $^{2}J_{5a/5b}$ = 13.1 Hz, $^{3}J_{5a/4}$ = 3.4 Hz, 1H, 5a-H_2),3.54 (m, 2H, 5b-CH_2), 2.15 (s, 3H, -CH_3), 2.11 (s, 3H, -CH_3), 2.10 (s, 3H, -CH_3), 2.06 (s, 3H, -CH_3), 2.04 (s, 3H, -CH_3), 2.01 (s, 3H, -CH_3) 1.54 (d, $^{3}J_{2´´/1´´}$ = 6.3 Hz, 3H, 2´´H_3), 1.45 ppm (d, $^{3}J_{2´´/1´´-H}$ = 6.2 Hz, 3H, 2´´CH_3).

^{13}C NMR (151 MHz, [D_6]DMSO, RT) δ = 170.5 (C=O), 170.4 (C=O), 170.2 (C=O), 170.2 (C=O), 169.7 (C=O), 169.5 (C=O), 152.6 (C-7a), 152.5 (C-7a), 147.4 (C-3a), 147.1 (C-3a), 142.3 (C-6´), 140.6 (C-6´), 137.6 (C-5´), 136.5 (C-5´), 107.4 (C-4´), 106.7 (C-4´), 105.2 (C-7´), 105.1 (C-7´), 103.2 (C-2´), 103.0 (C-2´), 100.1 (C-1), 99.1 (C-1), 73.4(C-1´´), 71.7 (C-1´´), 70.5 (C-4), 70.1 (C-4), 69.5 (C-2), 69.5 (C-2), 67.8 (C-3), 67.6 (C-3), 63.7 (C-5), 63.3 (C-5), 24.0 (C-2´´), 23.0 (C-2´´), 21.0 (-CH_3), 21.1 (-CH_3), 21.0 (-CH_3), 20.9 (-CH_3), 20.9 (-CH_3), 20.8 ppm (-CH_3).

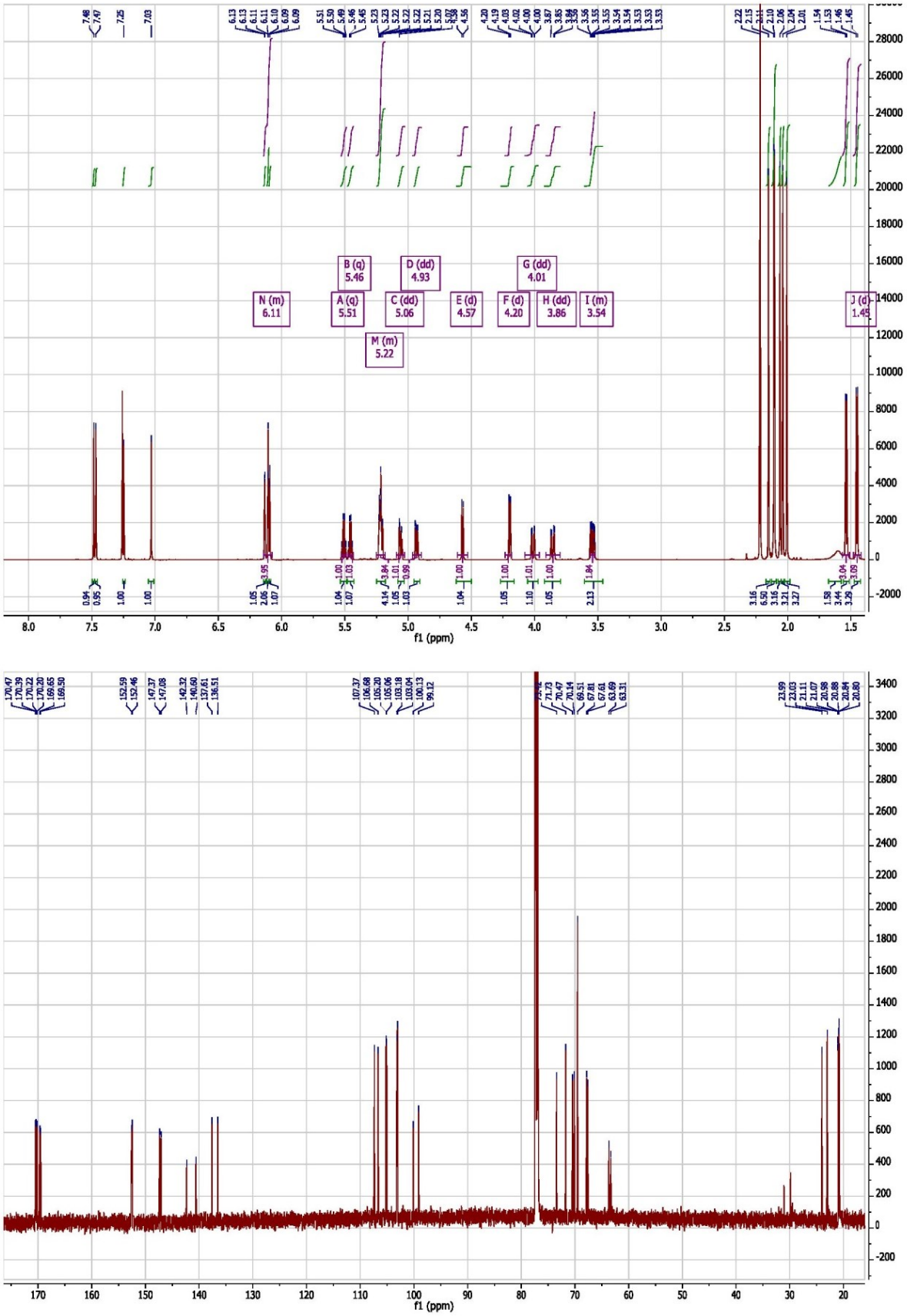

Figure S8. ^{1}H and ^{13}C NMR spectra of compound **3b**.

HRMS (ESI, positive mode): M = ($C_{20}H_{23}NO_{12}$), *m/z* =

calculated:	[M+Na]	492.11179	
found:	[M+Na]	492.11125	(100%)

IR (ATR): $\tilde{\nu}_{max}$ = 2924, 1740, 1522, 1483, 1370, 1252, 1216, 1105, 1025, 927, 876, 729, 601 cm^{-1}

2.1.6 Synthesis of β-L -arabinopyranosyl-((1-(6-nitro-1,3-benzodioxol)-5-yl)ethyl)-ether (4b)

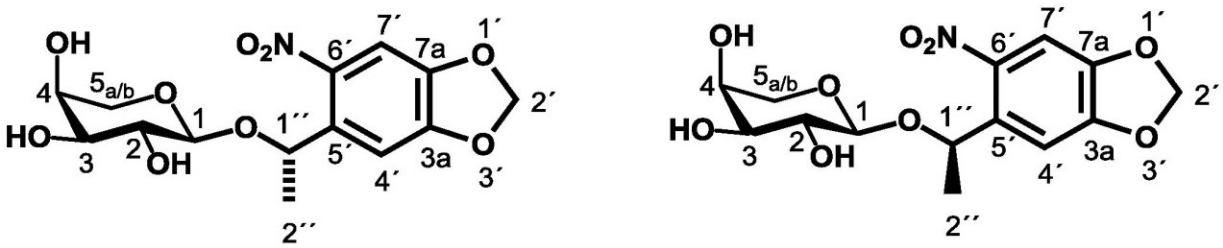

The product **4a** (500 mg, 1.07 mmol) was dissolved in 6 mL MeOH and 2.5 mL of a 0.23 M solution of NaOMe (in MeOH) was added. The reaction was stirred at room temperature until complete conversion. Afterwards, the reaction was neutralized with an ion exchanger (Dowex 650C). The mixture was filtrated. The filtrate was concentrated under reduced pressure. The residue was purified by flash-column chromatography on SiO_2 (EtOAc) to receive the product **(4a)** (348 mg, 1.01 mmol, 95%) as a light yellow solid.

For all analytical data, that was measured, the diastereomeric mixture (1:1 ratio) of compound **4b** was used**.**

Diastereomeric mixture of **4b** was partly separated *via* MPLC to distinguish the diastereomers by means of differential integration.

^{1}H NMR (600 MHz, [D_6]DMSO, RT) δ = 7.54 (s, 1H, 7´-H), 7.35 (s, 1H, 4´-H), 6.21 (m, 2H, 2´-H_2), 5.23 (q, $^{3}J_{1´´/2´´}$ = 6.2 Hz, 1H, 1´´-H), 5.01 (d, $^{3}J_{2\text{-}OH/2}$ = 3.8 Hz, 1H, 2-OH), 4.65 (d, $^{3}J_{4\text{-}OH/4}$ = 4.7 Hz, 1H, 4-OH), 4.49 (d, $^{3}J_{3\text{-}OH/3}$ = 4.3 Hz, 1H, 3-OH), 4.26 (d, $^{3}J_{1/2}$ = 5.6 Hz, 1H, 1-H), 3.58 (m, 1H, 3-H), 3.52 (dd, $^{2}J_{5a/5b}$ = 12.0 Hz, $^{3}J_{5a/4}$ 3.4 Hz, 1H, 5_b-H_2), 3.36 (m, 2H, 5-H, 3-H), 3.28 (d, $^{2}J_{5b/5a}$ = 12.0 Hz, 1H, 5_b-H_2), 1.40 ppm (d, $^{3}J_{2´´/1´´}$= 6.3 Hz, 3H, 2´´-H_3).

^{13}C NMR (151 MHz, [D_6]DMSO, RT) δ = 152.0 (C-7a),146.7 (C-3a), 140.4 (C-6´), 137.5 (C-5´), 107.0 (C-4´), 104.3 (C-7´), 103.3 (C-2´), 101.9 (C-1), 72.3 (C-2), 71.0 (C-1´´), 70.9 (C-4), 67.4 (C-3), 65.3 (C-5), 22.4 ppm (C-2´´).

^{1}H NMR (600 MHz, [D_6]DMSO, RT) δ = 7.59 (s, 1H, 7´-H), 7.49 (s, 1H, 4´-H), 6.21 (m, 2H, 2´-H_2), 5.35 (q, $^{3}J_{1´´/2´´}$ = 6.3 Hz, 1H, 1´´-H), 5.08 (d, $^{3}J_{2\text{-OH}/2}$ = 4.7 Hz, 1H, 2-OH), 4.61 (d, $^{3}J_{4\text{-OH}/4}$ = 5.7 Hz, 1H, 4-OH), 4.54 (d, $^{3}J_{3\text{-OH}/3}$ = 4.1 Hz, 1H, 3-OH), 3.80 (d, $^{3}J_{1\text{-H}/2}$ = 7 Hz, 1H, 1-H), 3.66 (dd, $^{2}J_{5a/5b}$ = 12.3 Hz, $^{3}J_{5a/4}$ 2.7 Hz, 1H, 5_a-H_2), 3.58 (m,1H, 3-H) 3.36 (m, 1H, 4-H), 3.22 (m, 1H, 2-H) 1.40 ppm (d, $^{3}J_{2´´/1´´}$ = 6.3 Hz, 3H, 2´´-CH_3).

^{13}C NMR (151 MHz, [D_6]DMSO, RT) δ = 152.3 (C-7a), 146.6 (C-3a), 141.8 (C-6´), 136.5 (C-5´), 107.0 (C-4´), 104.6 (C-7´), 103.4 (C-2´), 100.9 (C-1), 72.5 (C-2), 70.7 (C-1´´), 69.3 (C-4), 67.8 (C-3), 65.8 (C-5), 23.8 ppm (C-2´´).

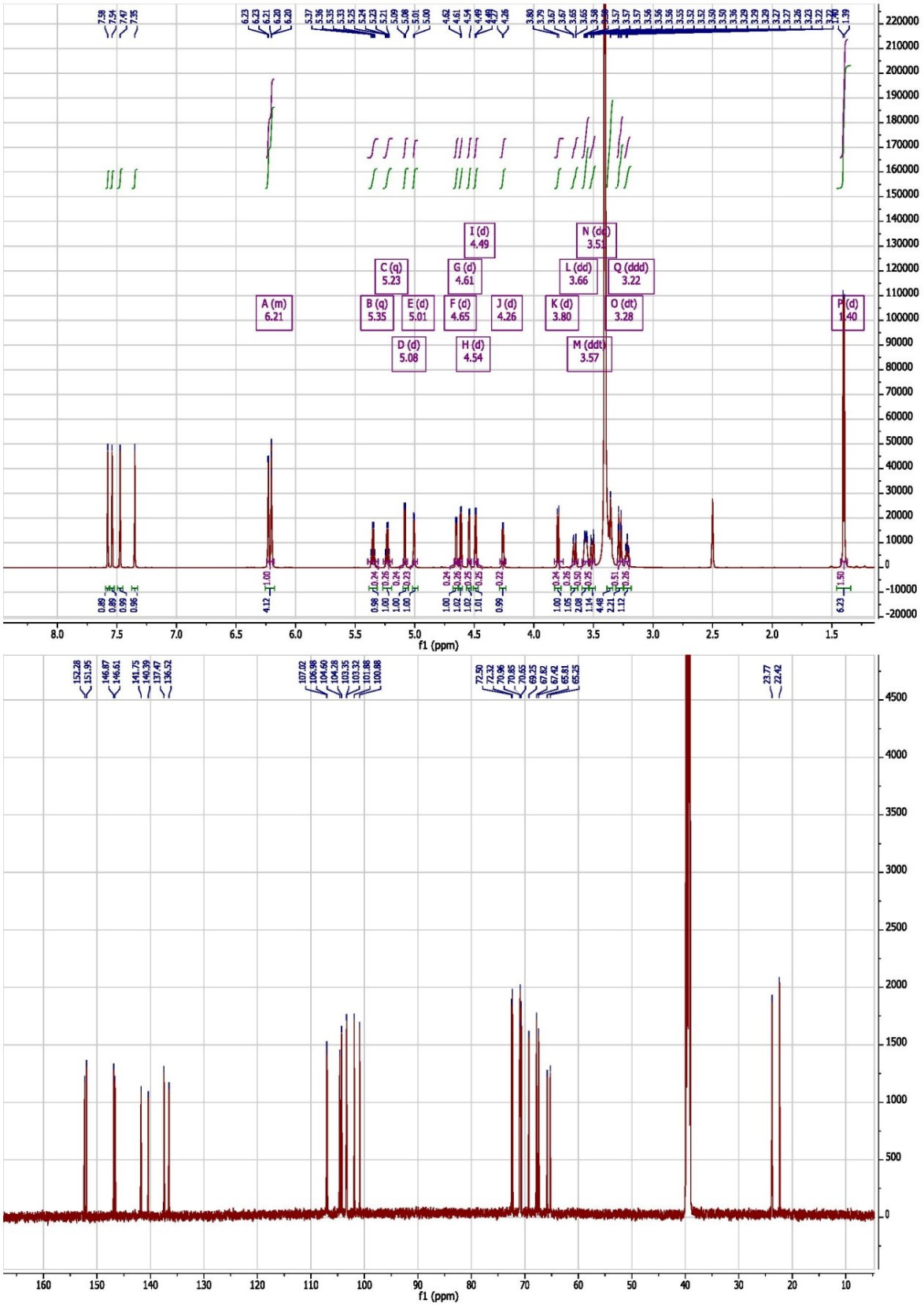

Figure S9. ^{1}H and ^{13}C NMR spectra of compound **4b**.

HRMS (ESI, positive mode): M = ($C_{14}H_{17}NO_9$), *m/z* =

calculated:	[M+Na]	366.08010	[M+K]	382.05404
found:	[M+Na]	366.07954 (100%)	[M+K]	382.05350 (24%)

IR (ATR): $\tilde{\nu}_{max}$ = 3354, 2922, 2476, 1617, 1515, 1504, 1484, 1323, 1257, 1135, 1033, 1068, 1007, 927, 883, 817, 774, 728 cm^{-1}.

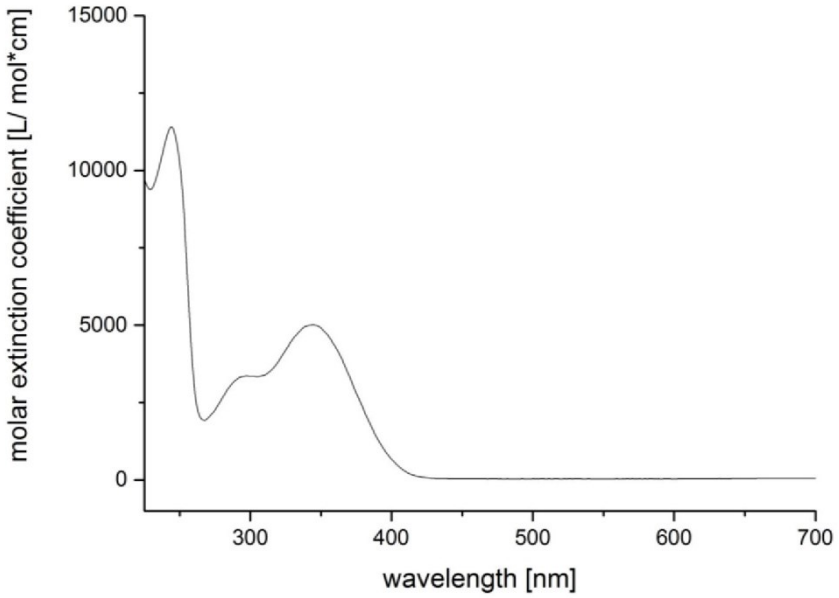

Figure S10. UV-Vis spectrum of compound **4b**. UV/Vis (MeOH): λ_{max} (ε) = 244 nm (11406), 297 nm (3460), 344 nm (5014).

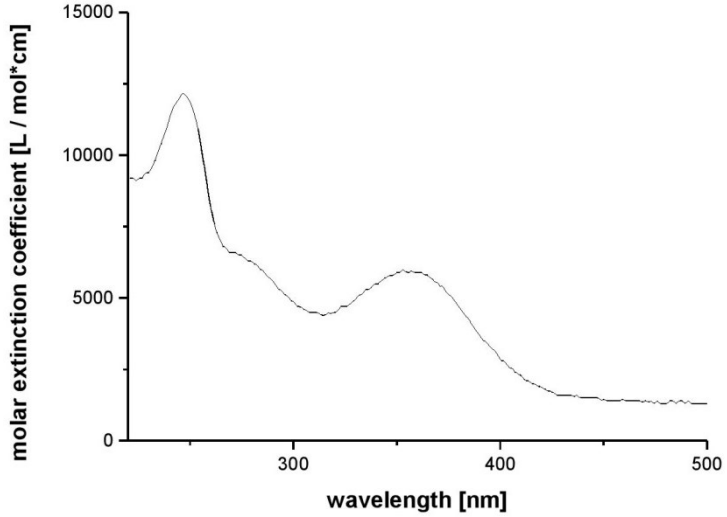

Figure S11. UV-Vis spectrum of compound **4b**. UV/Vis (H_2O): λ_{max} (ε) = 247 nm (9500), 312 nm (3000), 357 nm (4600).

optical rotatory power:$[\alpha]_D^{20}$ = 122° (c = 0.07, in MeOH)

2.2 Solubility analysis of 4a and 4b

The solubilities of **4a** and **4b** were determined photometrically at 25 °C using a Tecan M1000Pro microplate reader. Absorbances at 355 nm (approx. long-wavelength maximum for both compounds) of dilution series in both deionized and degased water and DMSO with known stock solutions were quantified und yielded highly linear calibration curves. Saturated solutions were centrifuged, filtrated and appropriately diluted (25 °C) to fit into the linear measuring range.

2.3 Bacterial strains and plasmids

Escherichia coli strains DH5α, Tuner(DE3) and LMG194 were grown in Luria–Bertani (LB) medium (Luria / Miller from Carl Roth, Karlsruhe, Germany; Sambrook *et al*. 1989) supplemented with kanamycin (50 µg/ml) and streptomycin (20 µg/ml, for *E. coli* LMG194 maintenance) at 37 °C under constant agitation.

Table S1. Bacterial strains, expression vectors and oligonucleotides used in this study.

	Name	Relevant characteristics	References
Bacterial strains	*E. coli* LMG194	*F⁻ ΔlacX74 galE galK thi rpsL ΔphoA Δara714 leu::Tn10*	[3]
	E. coli DH5α	*F⁻ Φ80lacZΔM15 Δ(lacZYA-argF) U169 recA1 endA1 hsdR17 (rk^-, mk^+) phoA supE44λ^- thi-1 gyrA96 relA1*	[4]
Expression vectors	pSB-M2g	pMB1 replicon, xylS, P_M-GFPmut3	[5]
	pAra-GFP	pSBM2g backbone, araC, Km^R, P_{BAD}-GFPmut3	This study
	pAra-vio	pSBM2g backbone, araC, Km^R, P_{BAD}-*vioABCDE*	This study
Oligonucleotides	1	Sequence: AGAG*ATTAAT*CGCGATGAAGCATTCTTCCG; Tm: 65 °C; *Ase*I-site (underlined and italicized nucleotides)	This study
	2	Sequence: ATAT*ATCGAT*TTTCTGCCCGATCCAGGC; Tm: 64 °C; *Bst*BI-site (underlined and italicized nucleotides)	This study

Construction of expression vectors and recombinant DNA techniques were carried out using *E. coli* DH5α as described by Sambrook *et al*.[6]

pAra-GFP was obtained by inserting a synthetic araC/P_{BAD}-based gene expression cassette (see Supporting Section 4; chemically synthesized by geneArt, Life Technologies, Darmstadt, Germany) into the pSB-M2g expression vector[5] in front of the GFPmut3 reporter gene[7] via *Nde*I and *Bgl*I restriction. The synthetic gene construct harbored an improved araC regulator variant (araC280*) for improved arabinose sensitivity[8], as well as the P_{BAD} promoter region from conventional pBAD vectors (Life Technologies, Darmstadt, Germany). For construction of pAra-vio the complete 7.4 kb violacein biosynthesis gene cluster from *Chromobacterium violaceum* ATCC 12472 was amplified using Primer 1 and 2 (Table S1). The obtained DNA fragment was hydrolyzed via *Ase*I / *Cla*I restriction and inserted into pAra-GFP that was hydrolyzed with *Nde*I and *Bst*BI, therefore replacing the GFPmut3 gene. All constructs were verified via sequencing. All bacterial strains and plasmids used in this study are listed in Table S1.

2.4 Expression cultures and light induction

GFP or violacein expression cultures were cultivated (800 µL, 1500 rpm, 85% rel. humidity, and 37 °C) in a BioLector microbioreactor system (m2plabs, Germany) under constant monitoring of biomass accumulation and GFP fluorescence development. Expression cultures were inoculated to cell density corresponding to an optical density of 0.05 at 580 nm and directly supplemented with **4a** or **4b** (from an 8 mM DMSO stock solution) prior to cultivation. Gene expression was induced once via supplementing 20-fold stock solution of arabinose **5** or UV-A light-induction (VL-315.BL hand lamp 45 W, Vilber Lourmat, France; distance to flowerplate: 1.5 cm, approx. 0.9 mW cm^{-2}) using photocaged arabinose **4a** or **4b**. Light gradients were created via dimming with varying layers of diffusion foils (White Diffusion LEE216, LEE Filters, USA). Light intensity was quantified using a Thermal Power Sensor (S302C, Thorlabs Inc, USA). Violacein expression cultures were in addition supplemented with 0.1 % (w/v) glucose in order to fully supress any basal expression.

2.5 Single cell analysis

Single cell analysis in microfluidic devices was performed exactly as previously described.[9] In order to conduct microbatch cultivations the flow was turned off after rinsing trapped cells with medium. To induce GFP expression the medium was supplemented with either arabinose **5** or photocaged arabinose **4a**. Light induction for cells supplemented with compound **4a** was achieved by exposing the microchips with UV-A light for 1 min (VL-315.BL hand lamp 45 W, Vilber Lourmat, France; distance to microchip: 26 cm).

2.6 Extraction of violacein

To extract violacein from *E. coli* LMG194/pAra-vio expression cultures, cells were pelleted by centrifugation (8000 g, 10 min, 4 °C), re-suspended in 500 µL of ethanol and incubated for 10 min at 75 °C to yield colorless cell residuals and a dark violet ethanol extract.

3. Supporting data

3.1 Quantification of uncaging half-life times

For quantification of uncaging half-life times, compound **4a** and **4b,** respectively, were dissolved in demineralized water using a defined concentration. 1 mL of this stock solution in a cuvette was illuminated at room temperature in the LUMOS 43 at 375 nm for a specific time period. Afterwards, the sample was measured on the HPLC (Jaso HPLC system (column: Hyperclone 5 µ ODS (C18) 120 (Phenomenex), MeOH:H_2O, 15:85; 1mL/min, 25 °C, 30 µL) and the amount of freed arabinose was detected via a light scattering detector (ELSD ZAM 3000 from AlphaCrom, 80 °C, gasflow 1.5 l_n/min). This procedure was carried out for different illumination durations. In order to quantify the specific amount of arabinose with the light scattering detector a calibration curve was measured. Saturation curves shown in the figure S12 (black squares) were fitted using a sigmoidal Boltzmann fit with OriginPro 9.0G®. The uncaging half-life time was calculated from fitting parameters (Table S2).

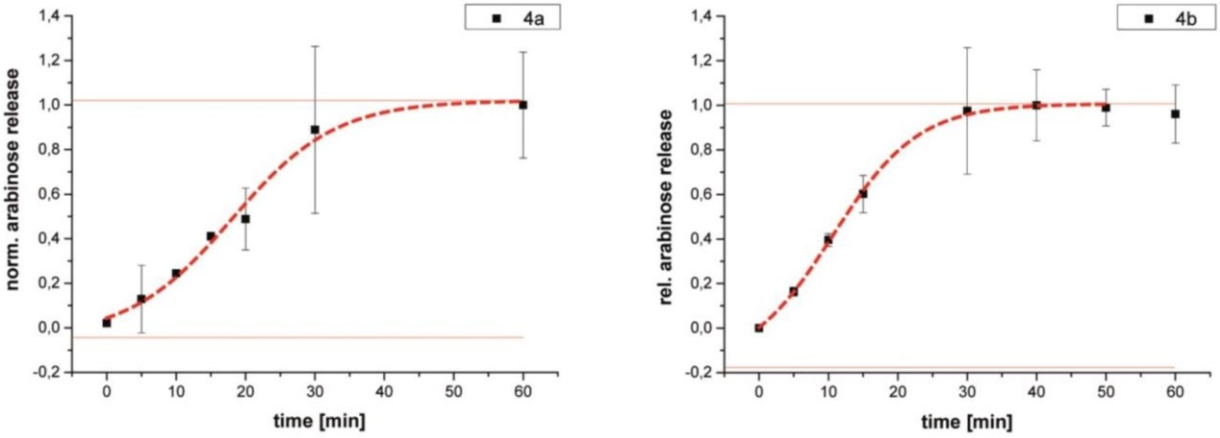

Figure S12. *In vitro* release of arabinose monitored via HPLC analysis, comparison of [6-nitropiperonyl-β-L-arabinopyranose] **4a** and [β-L -arabinopyranosyl-((1-(6-nitro-1,3-benzodioxol)-5-yl)ethyl)-ether] **4b. 4a:** 3 mmol in H_2O; 375 nm 6.4 mW/cm^2, RT, **4b:** 1.5 mmol in H_2O; 375 nm, RT,. Measurement (black squares) were performed in triplicates and fitted with a sigmoidal Boltzmann fit (red dotted line).

Table S2. Calculation of uncaging half-life times $t_{0.5}$ for photocaged arabinose **4a** and **4b** using fitting parameters from sigmoidal Boltzmann fits shown in Figure S1.

Inducer	$y_{0.5}$	A_1	A_2	x_0	dx	$t_{0.5}$ *[min]*
4a	0.57389	-0.04257	1.02007	18.04688	7.45321	**19.1**
4b	0.72202	-0.15073	0.99185	10.74436	5.81509	**13.7**

3.2 Determination of uncaging quantum yields

The quantum yield of **4a** and **4b** was determined in comparison to the quantum yield of nitropiperonylalcoholacetate (NPA-Ac), because this substance is quite similar to **4a** and **4b**[1]. The decomposition of NPA-Ac, **4a** and **4b** are first order reactions.

$$c(t) = c_0 \cdot e^{-k \cdot t}$$

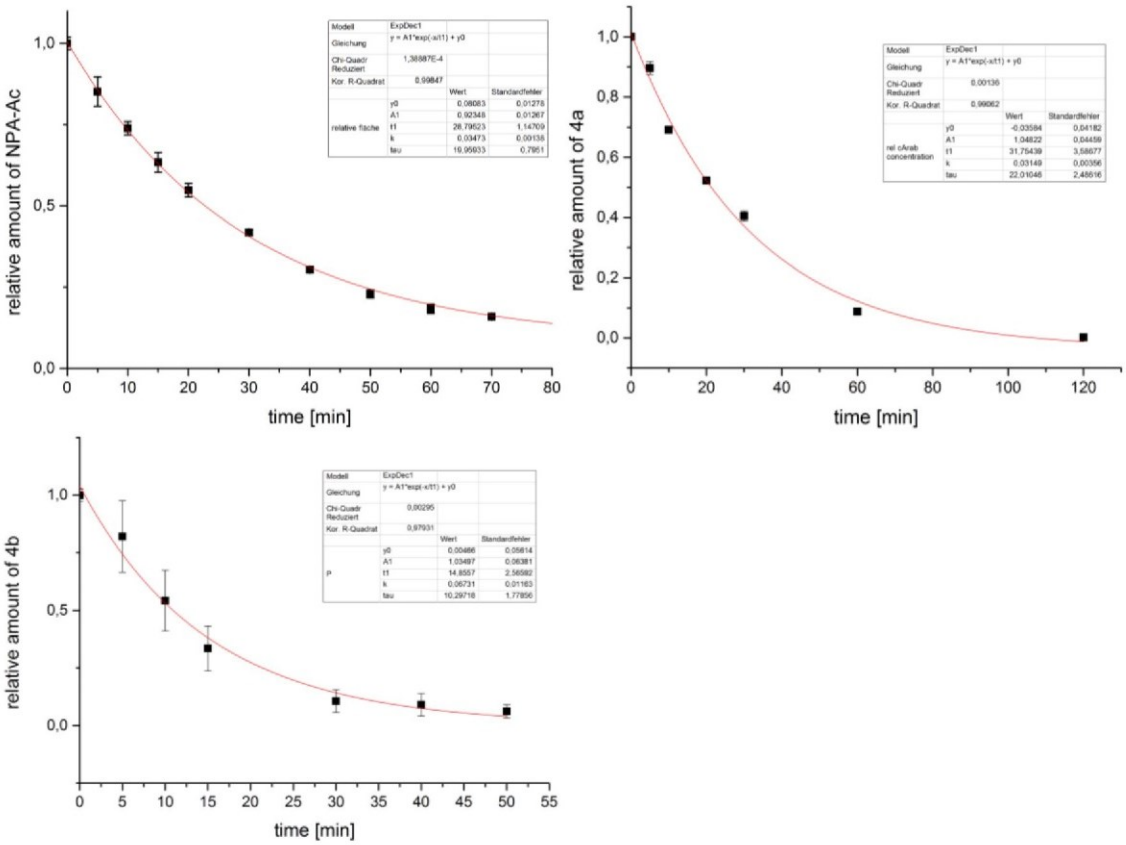

Figure S13. Exponential decay curves of model compound NPA-Ac as well as photocaged arabinose **4a** and **4b**. **NPA-**Ac: 1 mmol in CH_3CN; 375 nm 6.4 mW/cm^2, RT, **4a:** 3 mmol in H_2O; 375 nm 6.4 mW/cm^2, RT, **4b:** 1.5 mmol in H_2O; 375 nm,6.4 mW/cm^2, RT. Measurement (black squares) were fitted with an exponential fit (red line).

The decay of the caged compounds gives us an exponential curve. With the Beer–Lambert law and the rate law we were able to calculate the relative quantum yield in dependency of the intensity of the irradiated light. As the intensity of the irradiated light is the same for all samples, these values are direct proportional to the absolute quantum yields. With the quantum yield of NPA-Ac we determined the following absolute quantum yields. [10,11]

Table S3. Quantification of uncaging quantum yields ϕ_u.

compound	ϕ_u	Reference
NPA-Ac	0.1[10]	[10]
4a	0.11	This study
4b	0.29	This study

3.3 Analysis of stability and toxicity of photocaged arabinose compounds

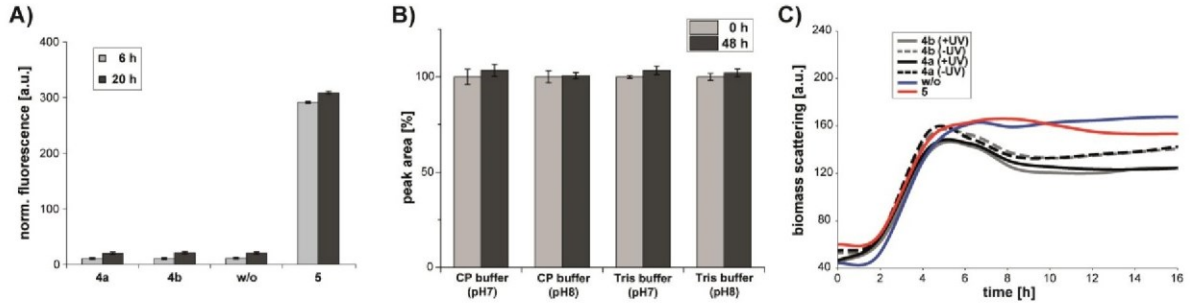

Figure S14. A) GFP expression cultures (supplemented with 100 µM of each compound) in the dark highlighting *in vivo* stability of photocaged arabinose **4a** and **4b**. B) HPLC measurements of photocaged arabinose **4a** stability in different buffers at pH 7 and 8 demonstrating *in vitro* stability at RT (24°C) for 48 h. C) Growth of GFP expression cultures (supplemented with 100 µM of each compound) showing non-toxicity of photocaged arabinose **4a** and **4b** compared to uninduced (w/o) and induced cultures (**5**).

3.4 Analysis of basal expression in uninduced cultures

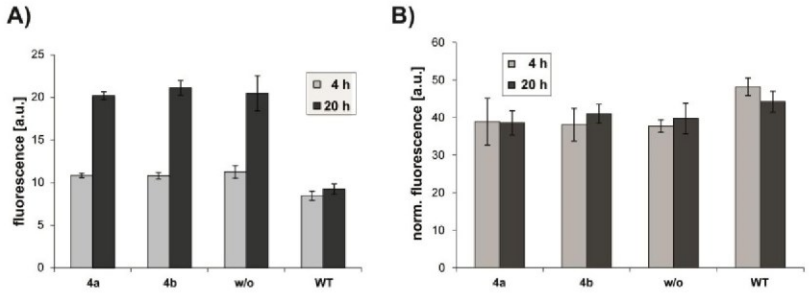

Figure S15. A) Basal fluorescence of unnormalized GFP expression cultures (uninduced; supplemented with 100 µM of each compound) compared to the wildtype (WT: *E. coli* LMG194). For biomass-unnormalized cultures a 1.3-fold (after 4h) and 2.2-fold (after 20 h) basal expression could be detected. B) Basal fluorescence of biomass-normalized expression cultures cultures (uninduced; supplemented with 100 µM of each compound). Fluorescence values refer to an optical density of cultures of 1.0. For biomass-normalized cultures no basal expression could be detected.

3.5 Analysis of unspecific activity and growth at high concentrations

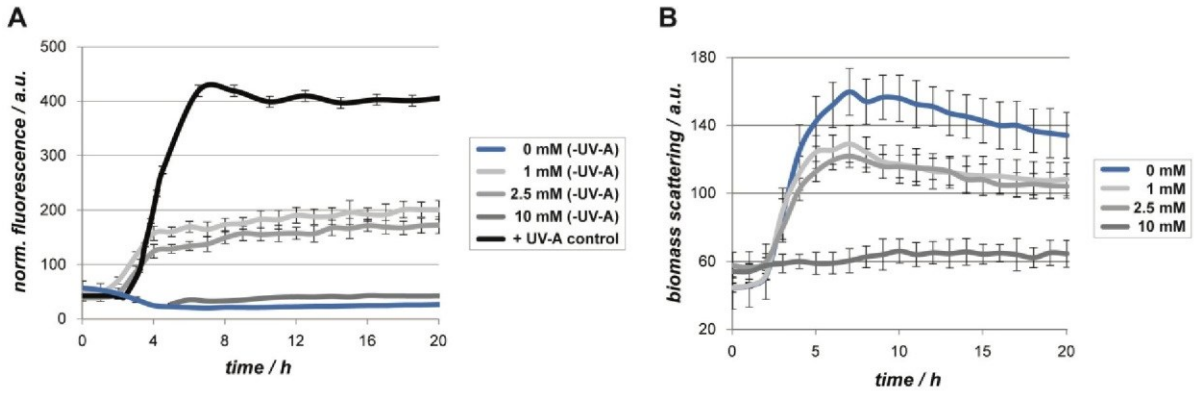

Figure S16. GFP expression cultures at high concentrations of photocaged arabinose **4a**. A) Unspecific activity at 0, 1, 2.5 and 10 mM of photocaged arabinose, compared to activity obtained by light induction using 0.1 mM. B) Growth of unexposed cultures supplemented with different amounts of photocaged arabinose.

3.6 Analysis of conventional arabinose induction with UV-A light

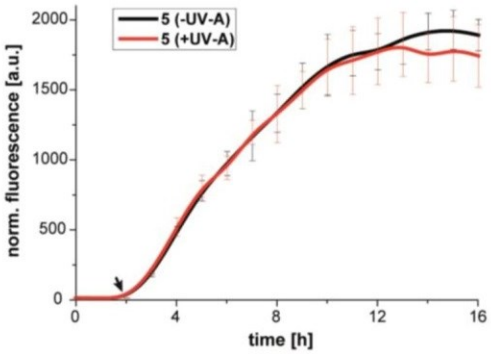

Figure S17. Fluorescence profiles of GFP expression cultures with and without UV-A exposure (365 nm; 10 min; time of induction indicated by arrow). Induction was performed using 25µM of **5**.

3.7 Single cell analysis of conventional and light induction

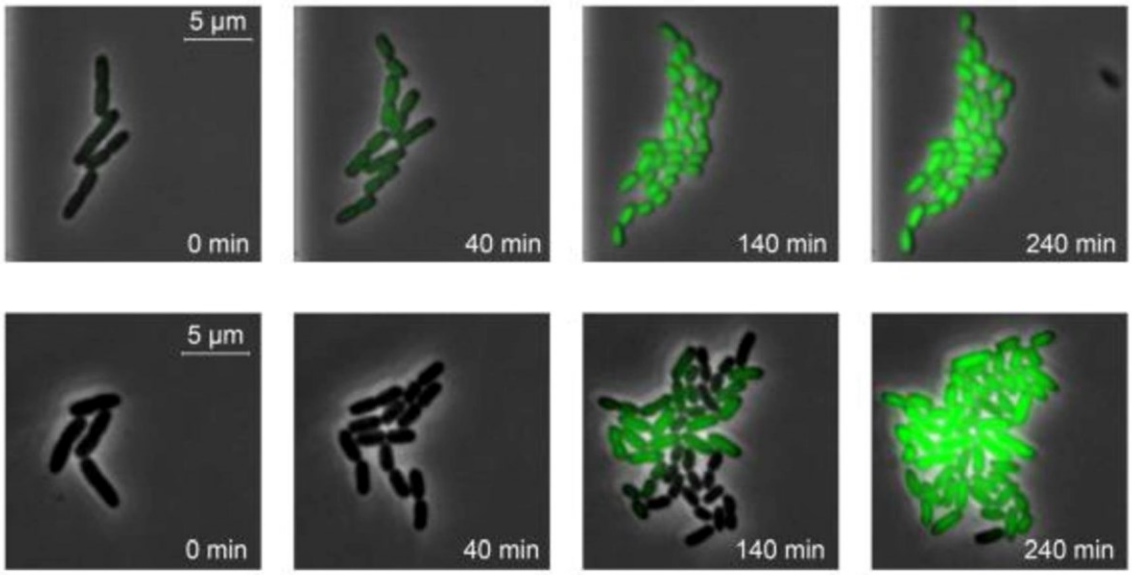

Figure S18. Single cell analysis of *E. coli* LMG194/pAra-GFP expression cultures induced with photocaged arabinose (upper row) and arabinose (lower row). Selected photographs from time lapse microscopy during microfluidic batch cultivation (flow turned off) with 25 µM of **5** (upper row) and 25 µM of **4a** (lower row). Light induction was achieved via 1 min of UV-A light exposure.

3.8 Quantification of UV-A light intensities

Light intensities used for UV-A light induction of gene expression were quantified at a wavelength of 365 nm using a Thermal Power Sensor (S302C, ThorLabs Inc, USA). Expression cultures that were solely covered with a polystyrol cover were exposed with 0.89 mW cm^{-2} (VL-315.BL hand lamp 45 W, Vilber Lourmat, France; distance to flowerplate: 1.5 cm, wavelength quantified: 365 nm). The increasing number of diffusion foil layers (White Diffusion LEE216, LEE Filters, USA) was applied to gradually dim UV-A light intensities (Tab. S4).

Table S4. Quantification of UV-A light intensities that were gradually attenuated using increasing layers of diffusion foils. Measurements were conducted at 365 nm using Thermal Power Sensor (S302C, ThorLabs Inc, USA).

Dimmed [x-fold]	Intensity at 365 nm [mW cm^{-2}]	Percentaged intensity
0	0.89 ± 0.01	100
1	0.55 ± 0.01	62
2	0.42 ± 0.02	48
3	0.35 ± 0.01	40
4	0.30 ± 0.01	34
5	0.22 ± 0.02	25
6	0.09 ± 0.02	10
Dark	0.00 ± 0.01	0

3.9 Comparative analysis of system responsiveness

In order to characterize the light-responsiveness of the established phototrigger using photocaged arabinose **4a** and **4b**, normalized fluorescence profiles of expression cultures with **4a** and **4b** were fitted to a sigmoidal Boltzmann fit using OriginPro 9.0G®. To highlight the rapid responsiveness of the novel phototriggers, the profiles of **4a/b** were further compared to conventional arabinose **5** induction. All normalized expression profiles were fitted and are comparatively illustrated in Figure S19. The half-maximal responsiveness was calculated from fitting parameters (Table S5) using the following standard equation for sigmoidal Boltzmann fitting: $y = \frac{A_1 - A_2}{1 + e^{(x - x_0)idx}} + A_2$

Table S5. Calculation of half-maximal responsiveness $t_{0.5}$ for the AraC/P_{BAD}- and LacI/P_{T7lac}-regulated system using fitting parameters from sigmoidal Boltzmann fits shown in Figure S15. Final half-maximal responsiveness $t_{0.5}$ was calculated as the difference of $t_{0.5}$ calculated and the induction time point t_0.

Inducer	$y_{0.5}$	A_1	A_2	x_0	dx	$T_{0.5}$ [h] calculated	t_0 [h]	$t_{0.5}$ [h] total
4a	0.34852	0.09315	0.97649	4.12943	0.05089	4.10954	2.5	**1.6**
4b	0.34989	0.08992	0.96953	4.15344	0.56368	3.94080	2.5	**1.4**
5	0.34444	0.09103	0.96197	4.92497	0.72228	4.64557	2.5	**2.1**
IPTG	0.48292	0.00279	0.97421	4.39148	0.52338	4.38626	1.5	**2.9**
Caged IPTG	0.39836	0.04587	0.93432	4.96740	0.53670	4.86972	1	**3.9**

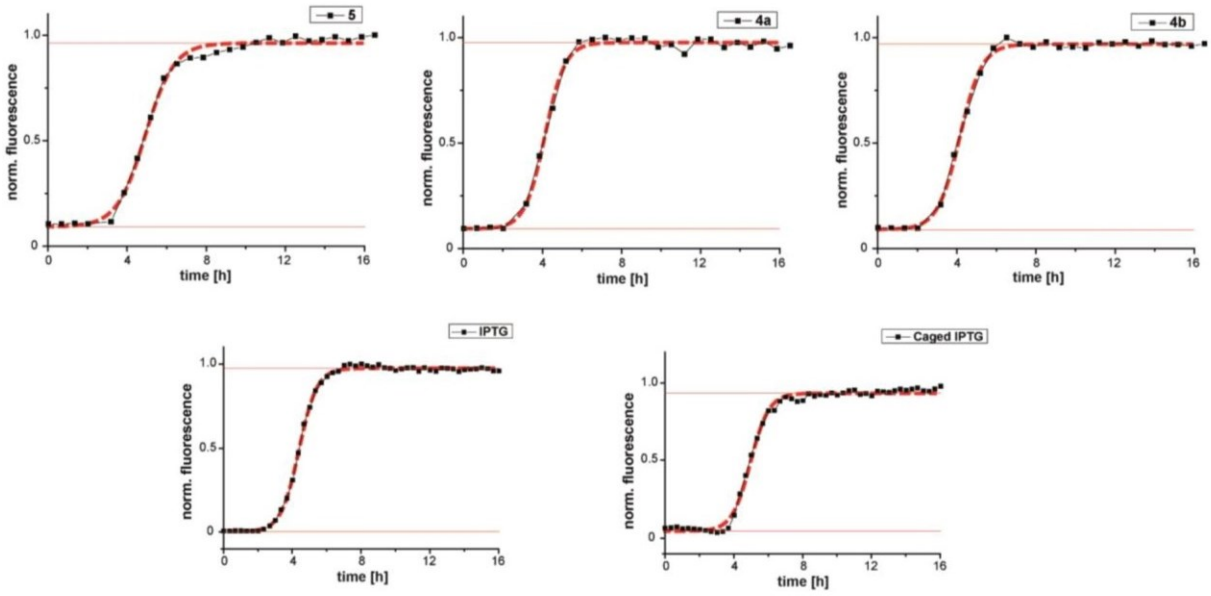

Figure S19. Expression profiles of AraC/P_{BAD}- and LacI/P_{T7lac}-regulated systems using 4a, 4b and 5 as well as IPTG and Caged IPTG. All curves were fitted using a sigmoidal Boltzmann fit.

3.10 Proof of violacein accumulation using HRMS

In order to shown that the expression of the *vioABCDE* gene cluster yielded the product violacein **11** together with its precursor desoxyviolacein **10** HRMS analysis was performed using the ethanol extracts described in section 2.6.

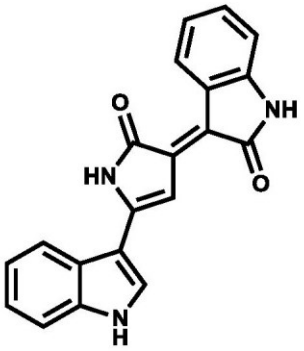

desoxyviolacein

10

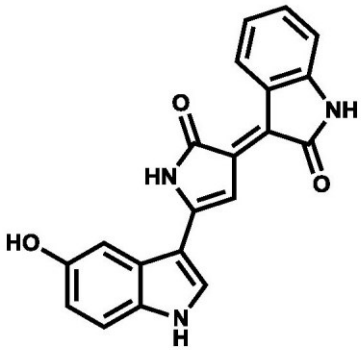

violacein

11

HRMS (ESI, positive mode): $M_{desoxyviolacein} = (C_{20}H_{14}N_3O_2)$, *m/z* =

calculated:	[M+H]	328.1086
found:	[M+H]	328.1079 (100%)

HRMS (ESI, positive mode): $M_{violacein} = (C_{20}H_{14}N_3O_3)$, *m/z* =

calculated:	[M+H]	344.1035
found:	[M+H]	344.1028 (57%)

3.11 Quantification of violacein

In order to determine violacein concentrations within 800 µL expression cultures, violacein was extracted with 500 µL ethanol from the cell pellet as described above and absorption at 575 nm was measured in a ten-fold diluted extract. The concentrations were estimated with an extinction coefficient (ε_{575} = 0.05601 mL μg^{-1} cm^{-1} in ethanol) described by Mendes *et al.* in 2001[11], which was verified in another study to be the best approximation for the determination of violacein concentrations.[12] Absorption was measured in microplates (Nunclon, ThermoScientific) using a Tecan M1000 Pro Microplate reader and correlated with photometer (Genesys10 S UV-Vis spectral photometer, ThermoScientific) absorption (1 mL, 1 cm path length) for the final calculation of the violacein concentrations (Fig. S20).

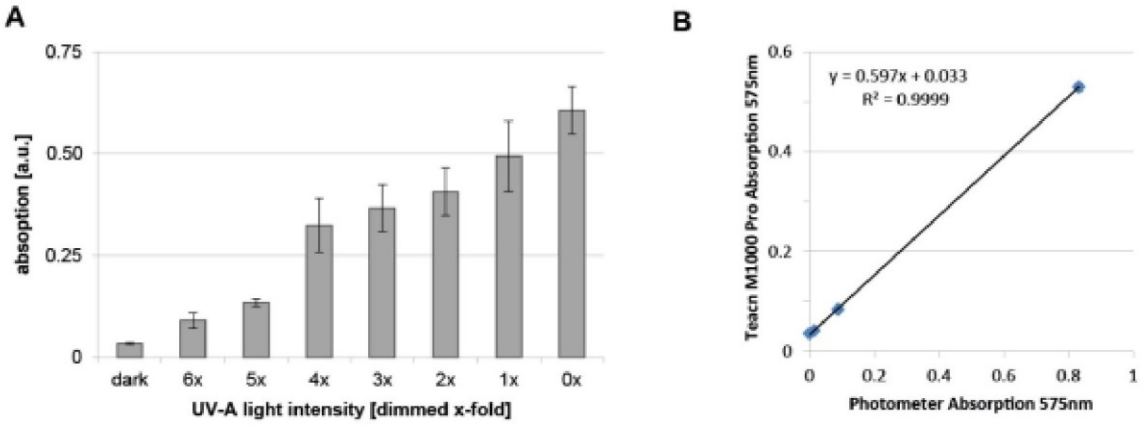

Figure S20. Microplate reader (Tecan M1000Pro) absorption from 10-fold diluted ethanol extracts of differently UV-A light exposed violacein expression cultures (A) and (B) correlation between microplate reader absorption and photometer (Genesys10 S UV-Vis spectral photometer, ThermoScientific) absorption that was used for calculation of violacein yields.

Table S6. Absorption and calculated yields from extracts of differently UV-A light exposed expression cultures.

unit	**dark**	**6x**	**5x**	**4x**	**3x**	**2x**	**1x**	**0x**
Absorption 1*	0.034	0.090	0.134	0.324	0.366	0.407	0.494	0.606
Absorption 2**	0.002	0.095	0.169	0.487	0.558	0.626	0.772	0.960
Estimated yield*** [mg/L]	0.64	27.14	48.27	139.12	159.41	178.83	220.53	274.24

* absorption in Tecan M1000 Pro Microplate reader

** absorption in Genesys10 S UV-Vis spectral photometer, ThermoScientific

*** calculated with ε_{575} = 56.01 L*µg^{-1}*cm^{-1} implying 5/8 volume reduction and 10-fold dilution

4. DNA sequences

DNA sequences of synthetic *ara* regulatory region (including **AraC*^{280}** and the **P_{BAD} promoter**) that was inserted into pSB-M2g via *NdeI*/*BglI* (cleavage sites underlined) restriction:

*GCCACTT*AGGCTGCGCAACTGTTGGGAAGGGCGATCGGTGCGGGCCTCTTCGCTATTACG
CCAGCTGGCGAAAGGGGGATGTGCTGCAAGGCGATTAAGTTGGGTAACGCCAGGGTTTT
CCCAGTCACGACGTTGTAAAACGACGGCCAGTGCCAAGCTTGCATGCCTGCAGGTCGACT
CTAGC**TCAACCGGCACGGAACTCGCTCGGGCTGGCCCCGGTGCATTTTTTAAATACC**
CGCGAGAAATAGAGTTGATCGTCAAAACCAACATTGCGACCGACGGTGGCGATAGG
CATCCGGGTGGTGCTCAAAAGCAGCTTCGCCTGGCTGATACGTTGGTCCTCGCGCC
AGCTTAAGACGCTAATCCCTAACTGCTGGCGGAAAAGATGTGACAGACGCGACGGC
GACAAGCAAACATGCTGTGCGACGCTGGCGATATCAAAATTGCTGTCTGCCAGGTG
ATCGCTGATGTACTGACAAGCCTCGCGTACCCGATTATCCATCGGTGGATGGAGCG
ACTCGTTAATCGCTTCCATGCGCCGCAGTAACAATTGCTCAAGCAGATTTATCGCCA
GCAGCTCCGAATAGCGCCCTTCCCCTTGCCCGGCGTTAATGATTTGCCCAAACAGGT
CGCTGAAATGCGGCTGGTGCGCTTCATCCGGGCGAAAGAACCCCGTATTGGCAAAT
ATTGACGGCCAGTTAAGCCATTCATGCCAGTAGGCGCGCGGACGAAAGTAAACCCA
CTGGTGATACCATTCGCGAGCCTCCGGATGACGACCGTAGTGATGAATCTCTCCTG
GCGGGAACAGCAAAATATCACCCGGTCGGCAAACAAATTCTCGTCCCTGATTTTTCA
CCACCCCCTGACCGCGAATGGTGAGATTGAGAATATAACCTTTCATTCCCAGCGGTC
GGTCGATAAAAAAATCGAGATAACCGTTGGCCTCAATCGGCGTTAAACCCGCCACC
AGATGGGCATTAAACGAGTATCCCGGCAGCAGGGGATCATTTTGCGCTTCAGCCAT
ACTTTTCATACTCCCGCCATTCAGAGAAG**AAACCAATTGTCCATATTGCATCAGACAT**
TGCCGTCACTGCGTCTTTTACTGGCTCTTCTCGCTAACCAAACCGGTAACCCCGCTT
ATTAAAAGCATTCTGTAACAAAGCGGGACCAAAGCCATGACAAAAACGCGTAACAA
AAGTGTCTATAATCACGGCAGAAAAGTCCACATTGATTTATTTGCACGGCGTCACAC
TTTGCTATGCCATAGCATTTTTATCCATAAGATTAGCGGATCCTACCTGACGCTTTTT
ATCGCAACTCTCTACTGTTTCTCCATACCCGTTTTTTGGGCTAACAGGAGGAATTAAC*CA*
TATG

5. Supporting movies

Supporting Movie 1: Single cell analysis of arabinose induced GFP expression.
Single cell cultivation of a representative *E. coli* LMG194/pAra-GFP microcolony was induced with 25 µM arabinose within the LB cultivation medium. Fluorescence and phase contrast images were recorded via time-lapse microcopy every 10 min over a cultivation period of 4 h.

Supporting Movie 2: Single cell analysis of light-induced GFP expression using photocaged arabinose.
Single cell cultivation of a representative *E. coli* LMG194/pAra-GFP microcolony was induced with 1 min of UV-A light exposure and previous supplementation of the LB cultivation medium with 25 µM NP-photocaged arabinose **4a**. Fluorescence and phase contrast images were recorded via time-lapse microcopy every 10 min over a cultivation period of 4 h.

6. Additional references

[1] K. P. R. Kartha, H. J. Jennings, *J. Carbohydr. Chem.* **1990**, *9*, 777–781.

[2] M. Wirkner, J. M. Alonso, V. Maus, M. Salierno, T. T. Lee, A. J. García, A. del Campo, *Adv. Mater.* **2011**, *23*, 3907–10.

[3] L. M. Guzman, D. Belin, M. J. Carson, J. Beckwith, *J. Bacteriol.* **1995**, *177*, 4121–30.

[4] D. Hanahan, *J. Mol. Biol.* **1983**, *166*, 557–80.

[5] S. Balzer, V. Kucharova, J. Megerle, R. Lale, T. Brautaset, S. Valla, *Microb. Cell Fact.* **2013**, *12*, 26.

[6] J. Sambrook, E. F. Fritsch, T. Maniatis, *Molecular Cloning: a Laboratory Manual*, Cold Spring Harbor Laboratory Press, New York City, USA, **1989**.

[7] B. P. Cormack, R. H. Valdivia, S. Falkow, *Gene* **1996**, *173*, 33–8.

[8] S. K. Lee, H. H. Chou, B. F. Pfleger, J. D. Newman, Y. Yoshikuni, J. D. Keasling, *Appl. Environ. Microbiol.* **2007**, *73*, 5711–5.

[9] D. Binder, A. Grünberger, A. Loeschcke, C. Probst, C. Bier, J. Pietruszka, W. Wiechert, D. Kohlheyer, K.-E. Jaeger, T. Drepper, *Integr. Biol. (Camb).* **2014**, *6*, 755–65.

[10] F. Bley, K. Schaper, H. Görner, *Photochem. Photobiol.* **2008**, *84*, 162–71.

[11] B. Bier, PhD thesis, Heinrich-Heine University Düsseldorf (Düsseldorf, Germany), 2011.

[12] A. S. Mendes, J. E. de Carvalho, M. C. T. Duarte, N. Durán, R. E. Bruns, *Biotechnol. Lett.* **2001**, *23*, 1963–1969.

[13] A. L. Rodrigues, N. Trachtmann, J. Becker, A. F. Lohanatha, J. Blotenberg, C. J. Bolten, C. Korneli, A. O. de Souza Lima, L. M. Porto, G. a Sprenger, et al., *Metab. Eng.* **2013**, *20*, 29–41.

V.4 Supporting Information for Chapter II.3.3 – Photocaged Carbohydrates

Photocaged carbohydrates – versatile tools for controlling gene expression by light. (Feature article for *Synthesis, in press*)
Claus Bier, Dennis Binder, Dagmar Drobietz, Anita Loeschcke, Thomas Drepper, Karl-Erich Jaeger, Jörg Pietruszka (2016)

Compound (1a): 2,3,4,6-Tetra-O-acetyl-α-D-galactopyranosyl bromide

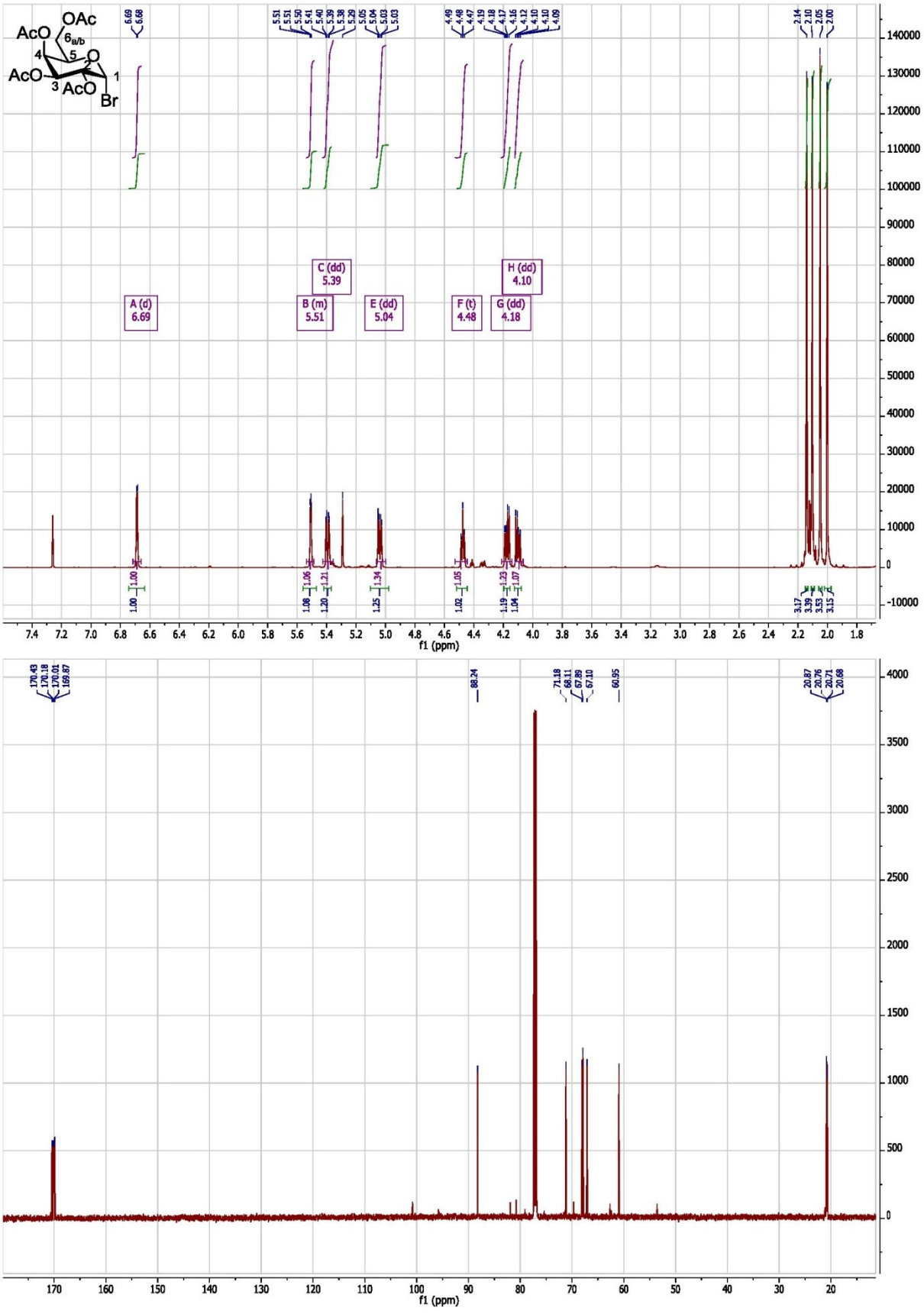

Figure 1: ^{1}H and ^{13}C NMR spectra of compound 1a.

Compound (1b): 2,3,4,6-Tetra-O-acetyl-alpha-D-glucopyranosyl bromide

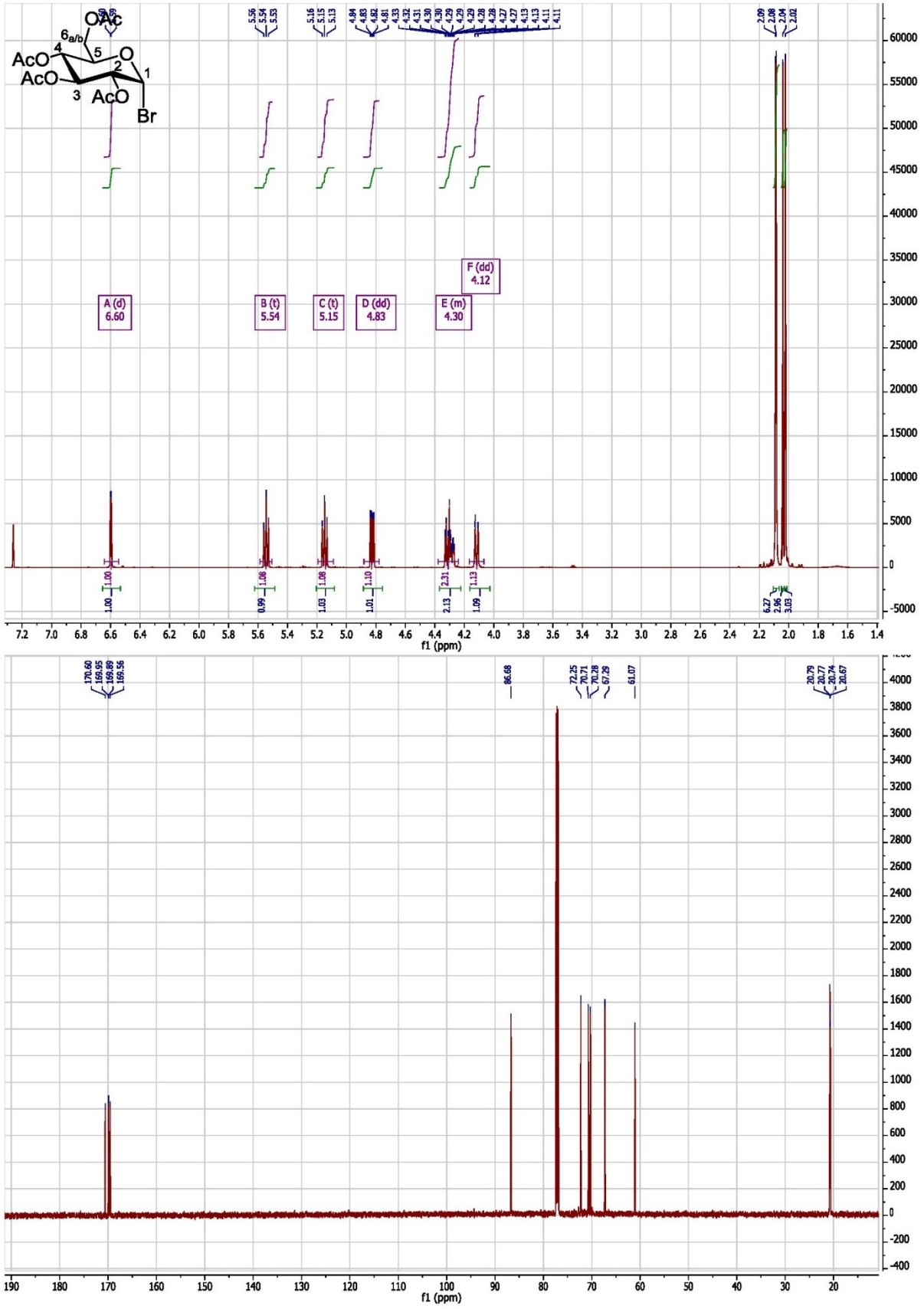

Figure 2: ^{1}H and ^{13}C NMR spectra of compound 1b.

Compound (1c): 2,3,4-Tri-*O*-acetyl-α-rhamnopyranosyl bromide

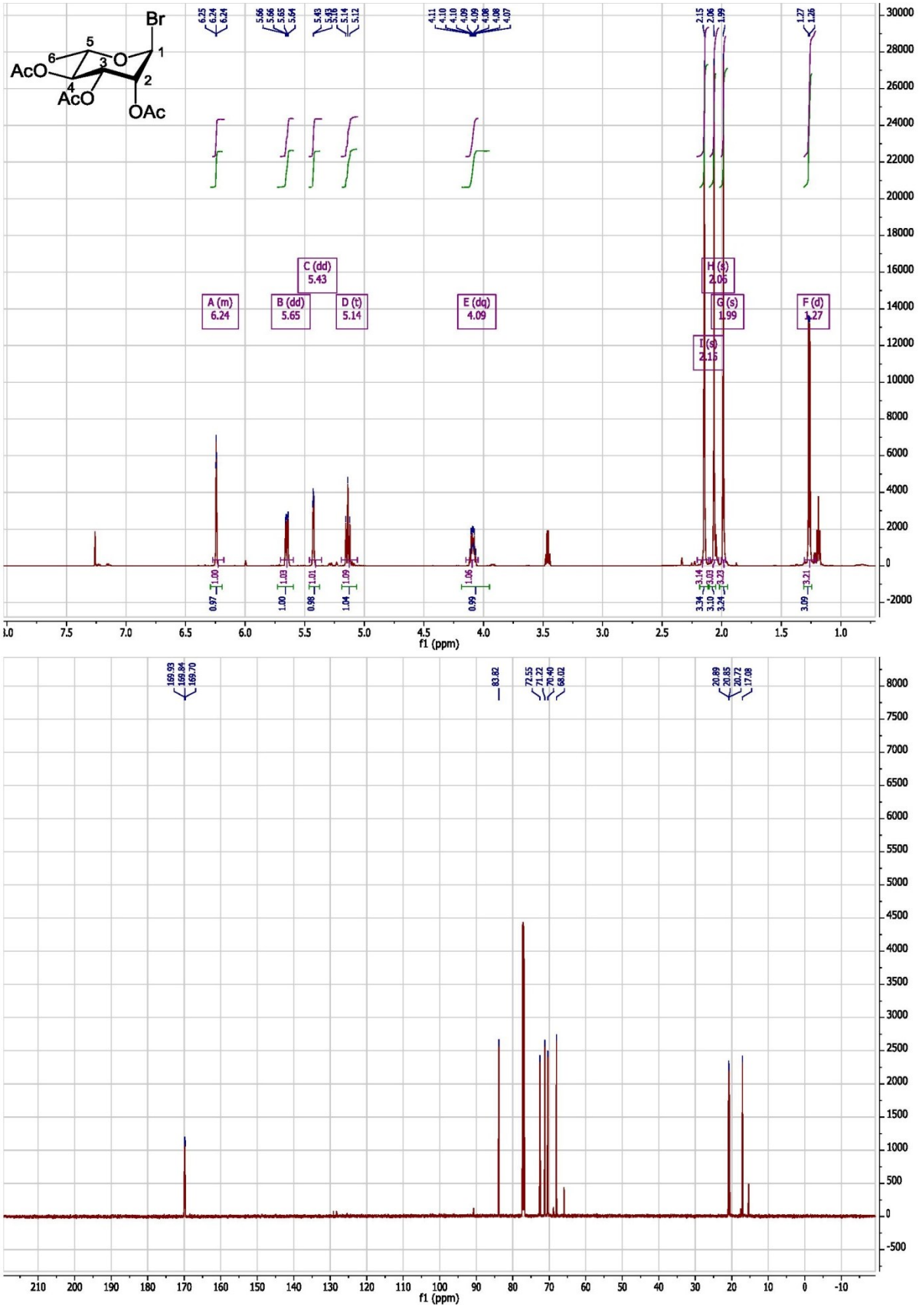

Figure 3: ^{1}H and ^{13}C NMR spectra of compound 1c.

Compound (1e): 2,3,6,2',3',4',6'-Hepta-O-acetyl-α-D-lactosyl bromide

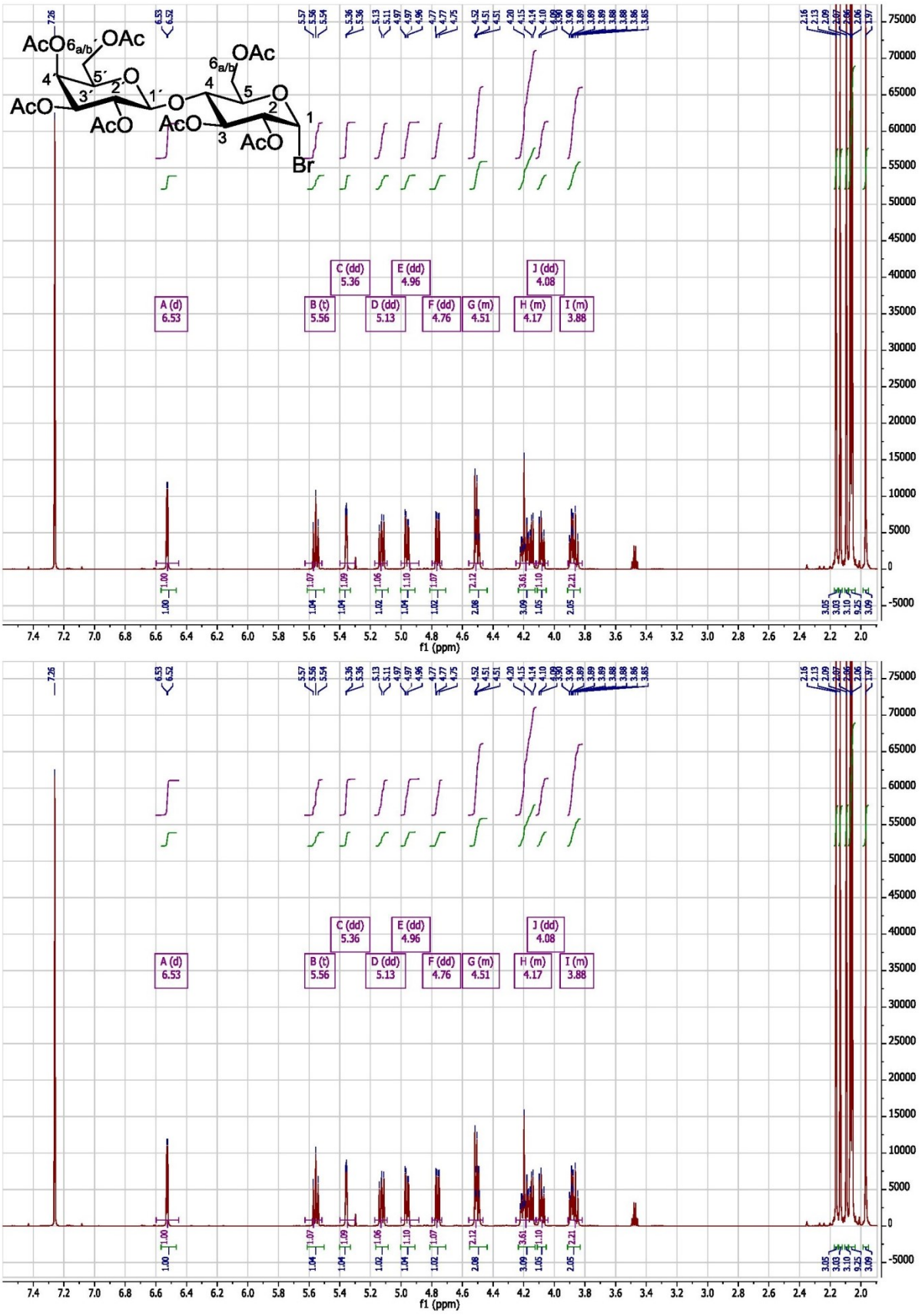

Figure 4: ^{1}H and ^{13}C NMR spectra of compound 1e.

Photocaged Carbohydrates

Compound (6a): cGalactose; 6-nitropiperonyl β-D-galactopyranosid

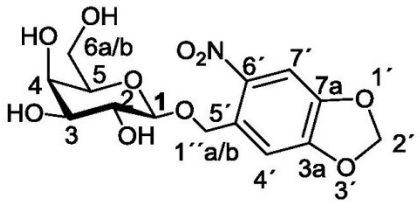

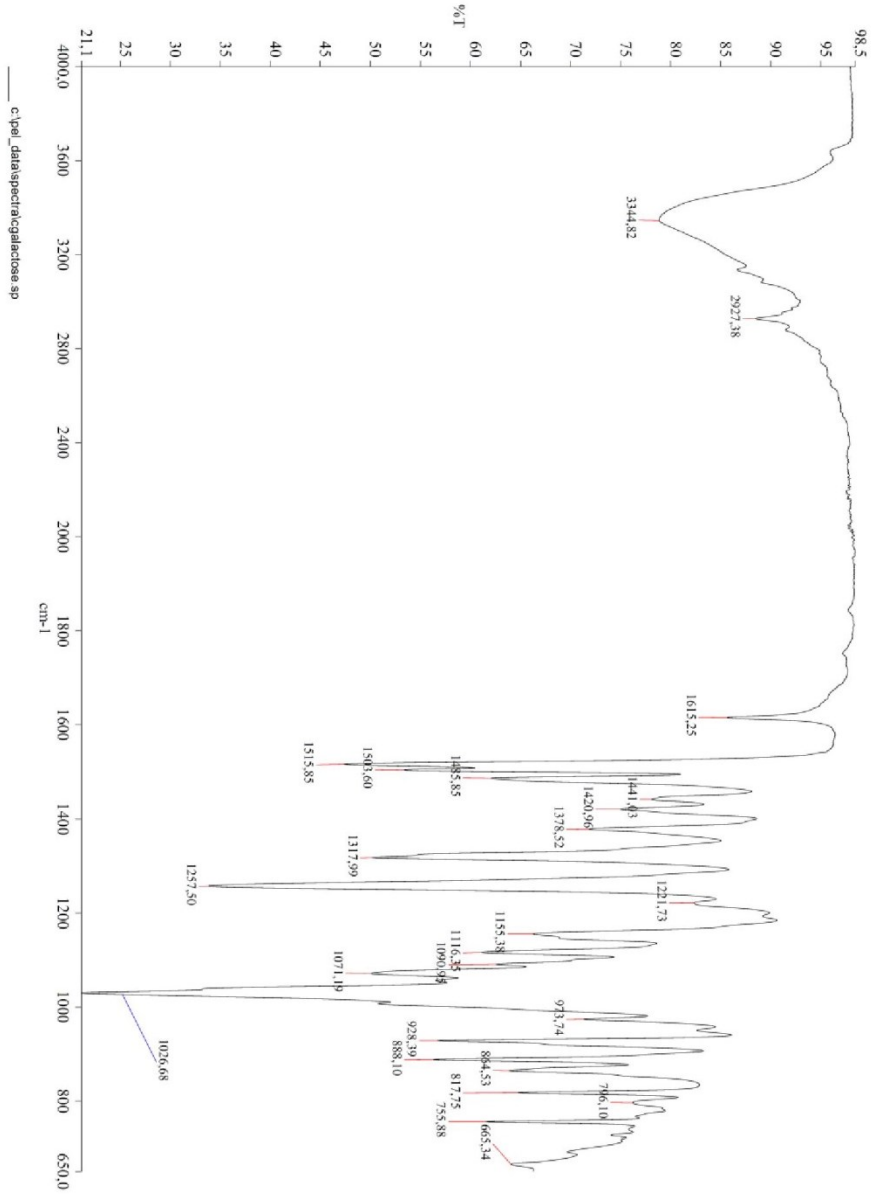

Figure 5: IR Data (ATR) 6a.

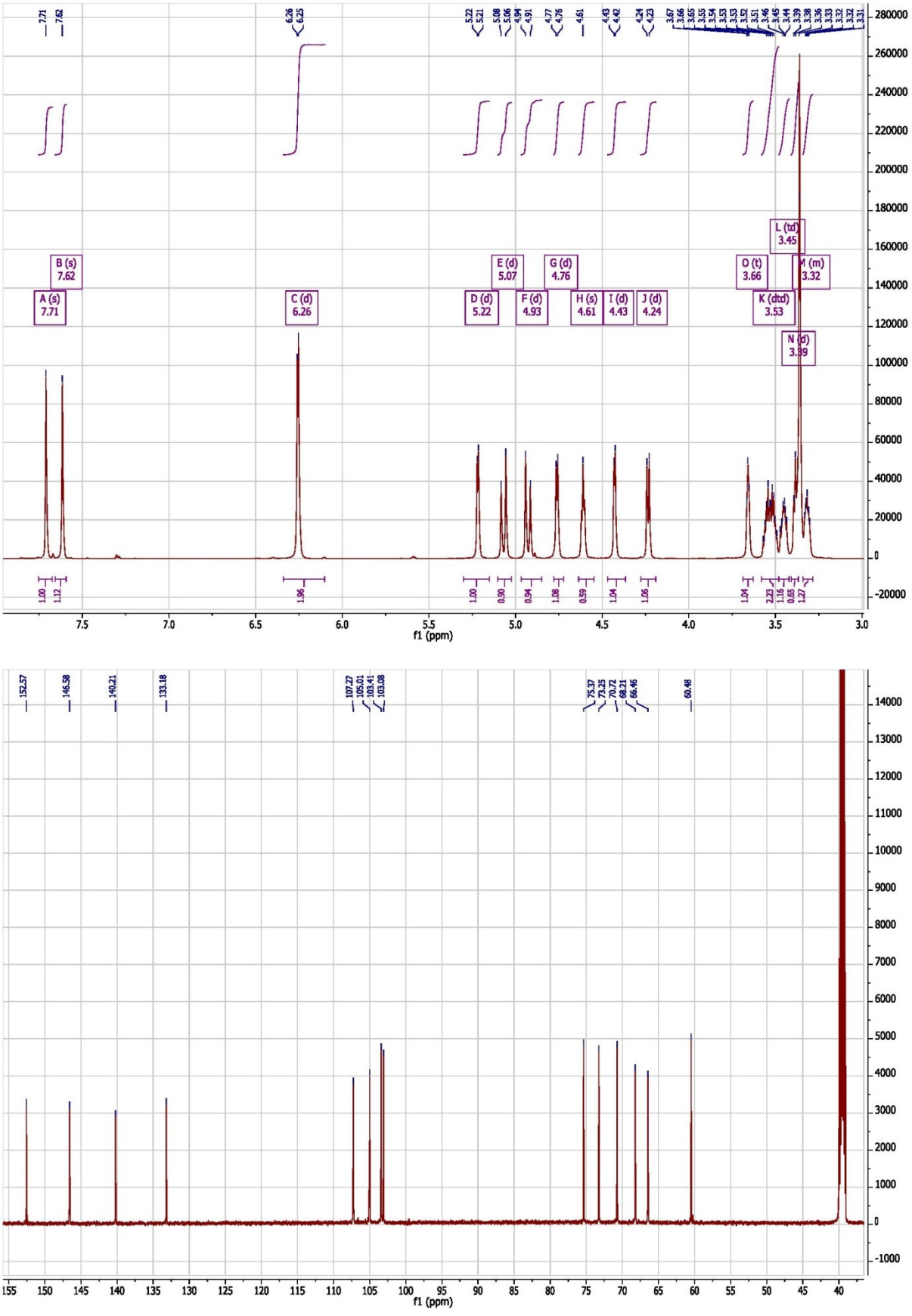

Figure 6: ^{1}H and ^{13}C NMR spectra of compound 6a.

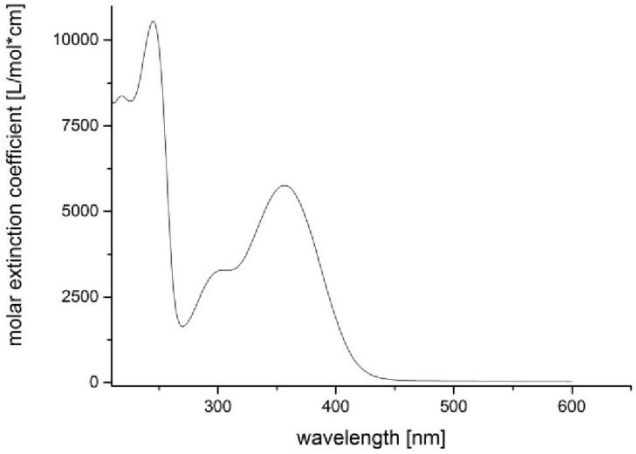

Figure 7 : UV-Vis spectrum of compound 6a.

Compound (6b): cGlucose; 6-nitropiperonyl β-D-glucopyranosid /6-nitropiperonyl α-D-glucopyranosid

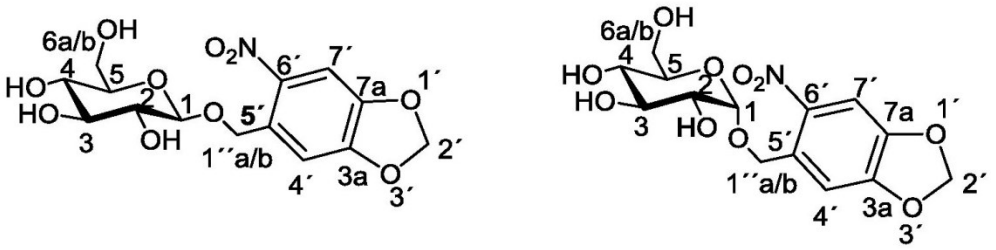

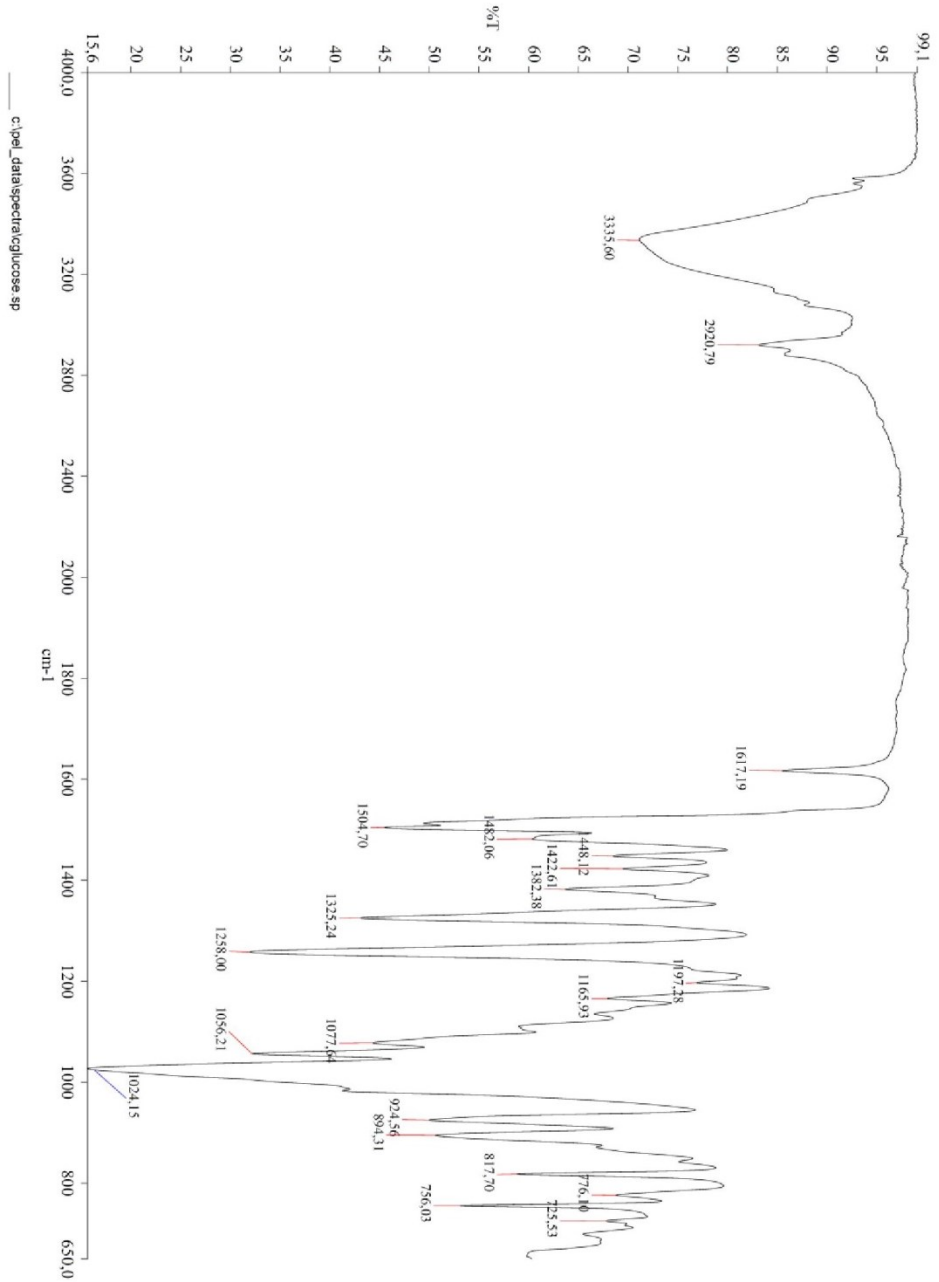

Figure 8: IR (ATR) 6b.

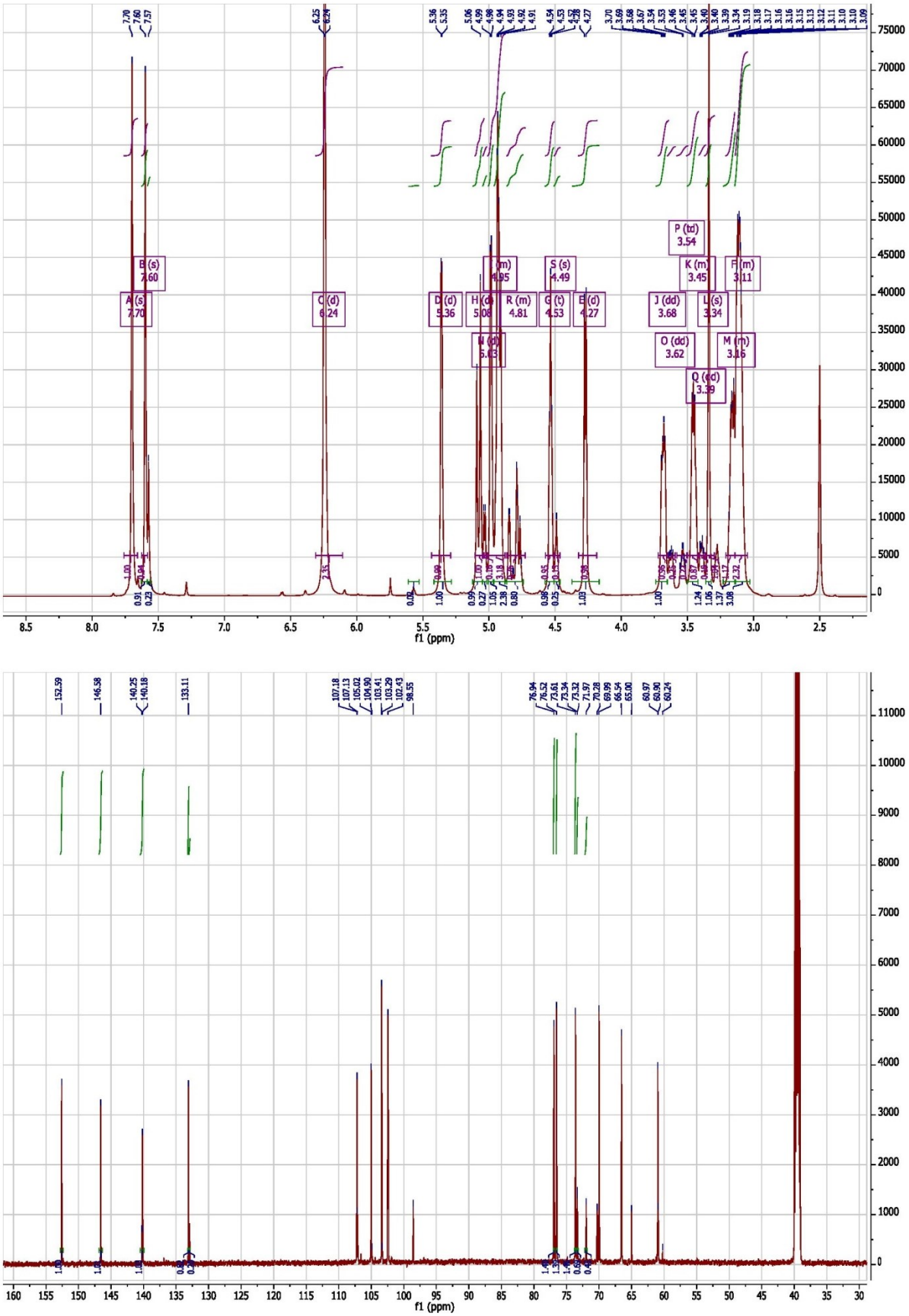

Figure 9: ^{1}H and ^{13}C NMR spectra of compound 6b.

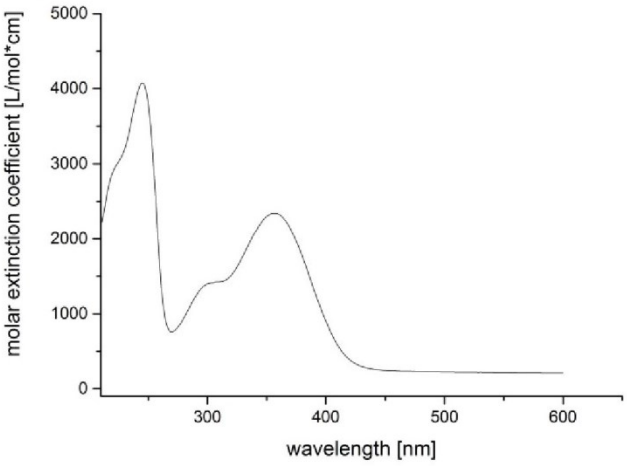

Figure 10: UV-Vis spectrum of compound 6b.

Compound (6c): cRhamnose; 6-nitropiperonyl β-L-rhamnopyranosid

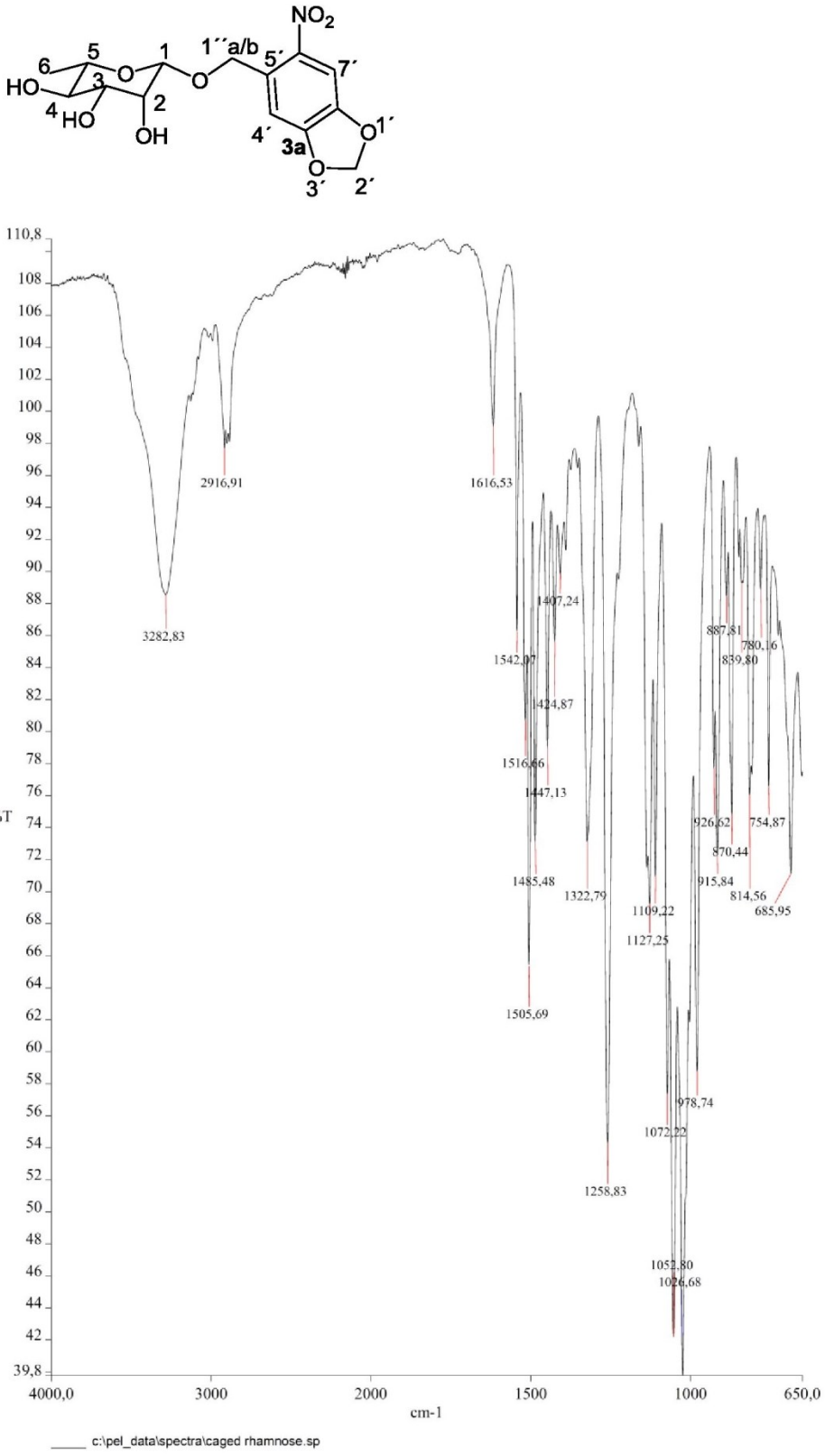

Figure 11: IR (ATR) 6c.

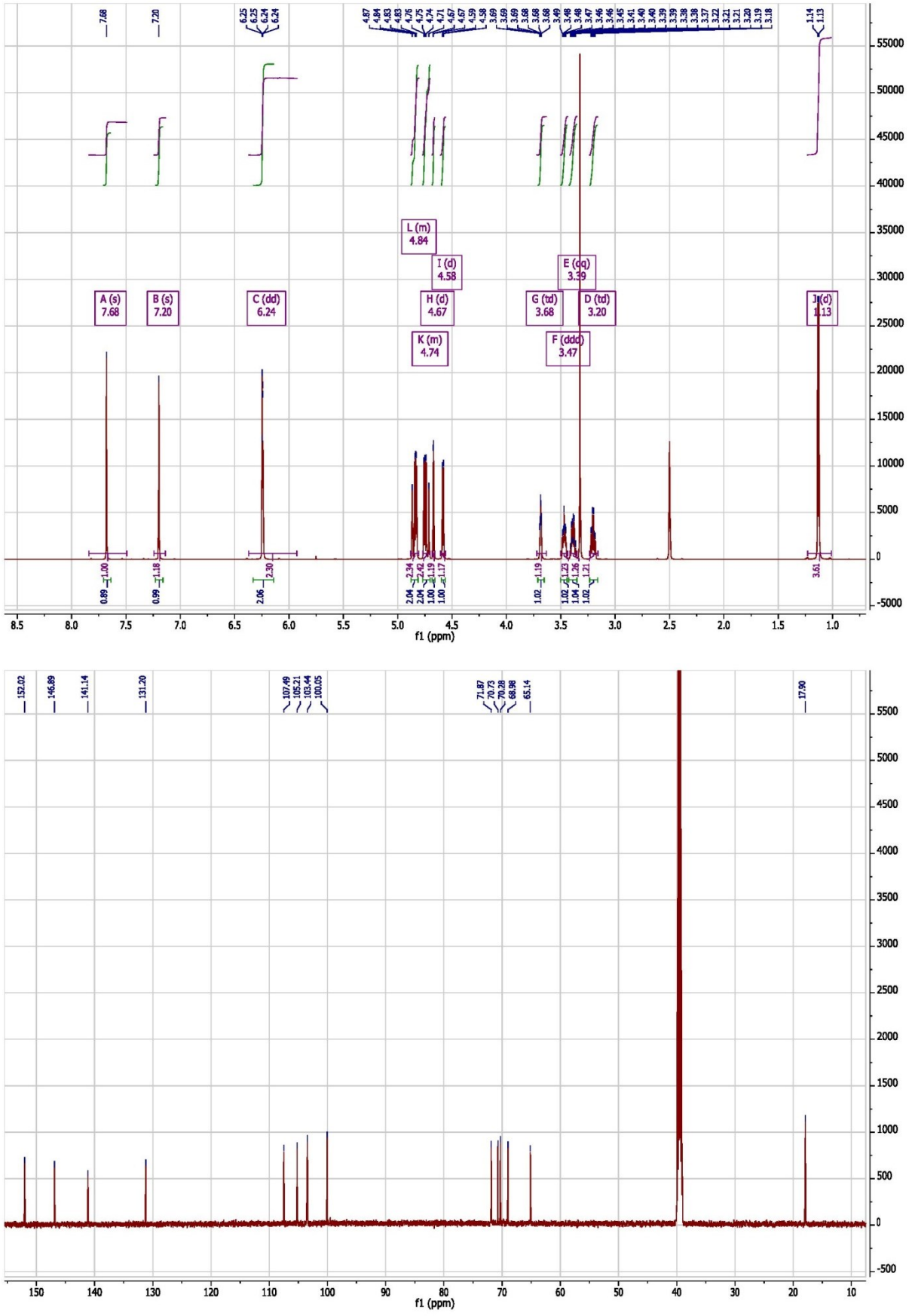

Figure 12: ^{1}H and ^{13}C NMR spectra of compound 6c.

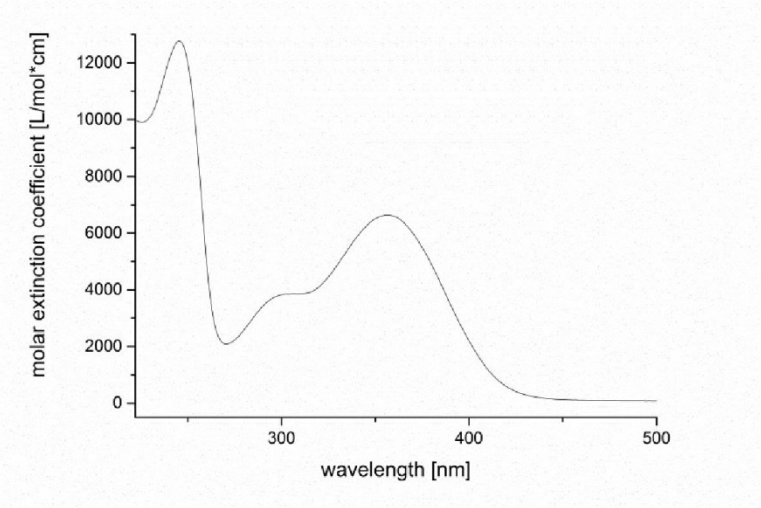

Figure 13: UV-Vis spectrum of compound 6c.

Compound (7c): cMeRhamnose; 1-(6-nitrobenzo[*d*][1,3]dioxol)-5-yl)ethyl β-L-rhamnopyranosid

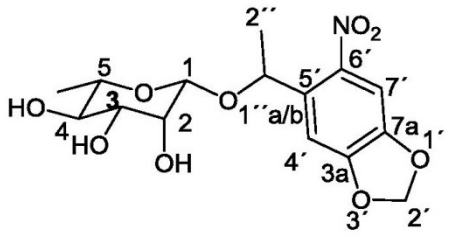

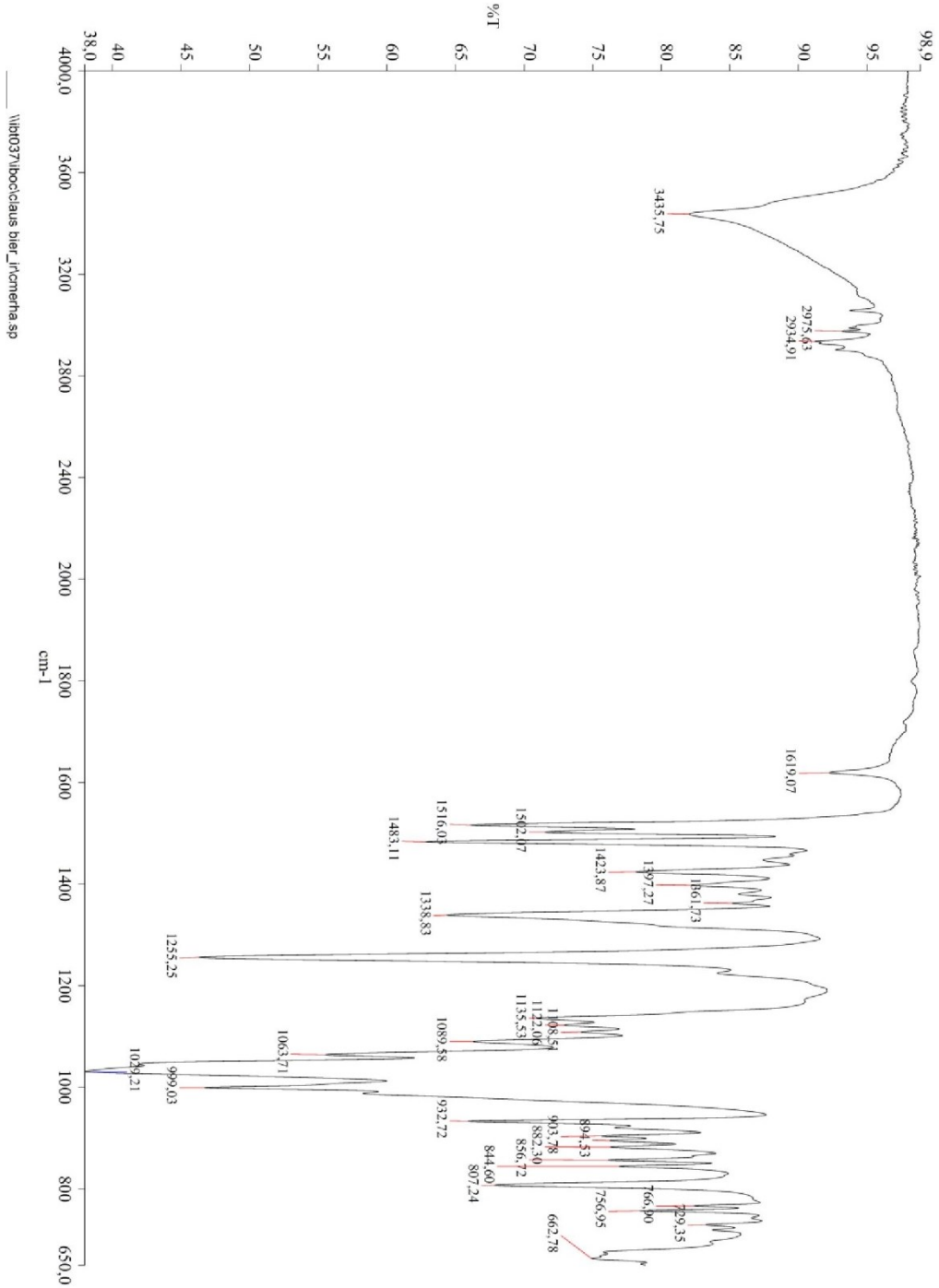

Figure 14: IR (ATR) 7c.

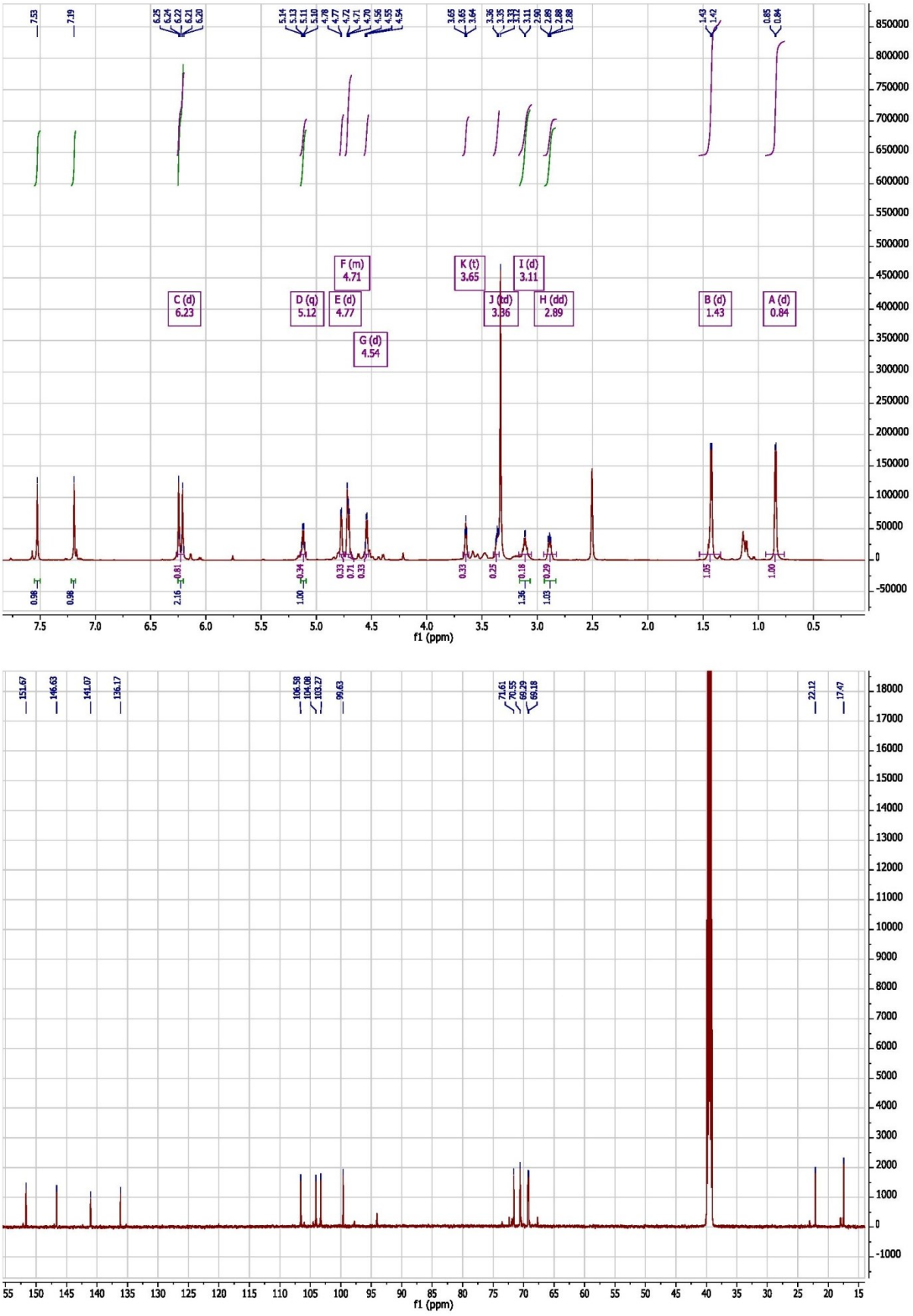

Figure 15: ^{1}H and ^{13}C NMR spectra of compound 7c.

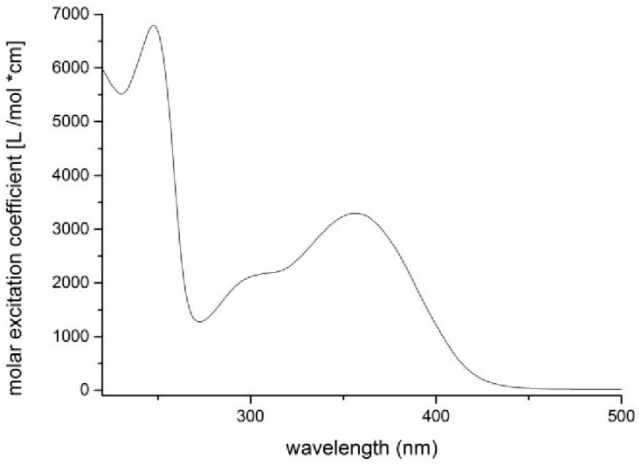

Figure 16: UV-Vis spectrum of compound 7c.

Compound (6e): cLactose; 6-nitropiperonyl-β-D-lactopyranosid /6-nitropiperonyl-α-D-lactopyranosid

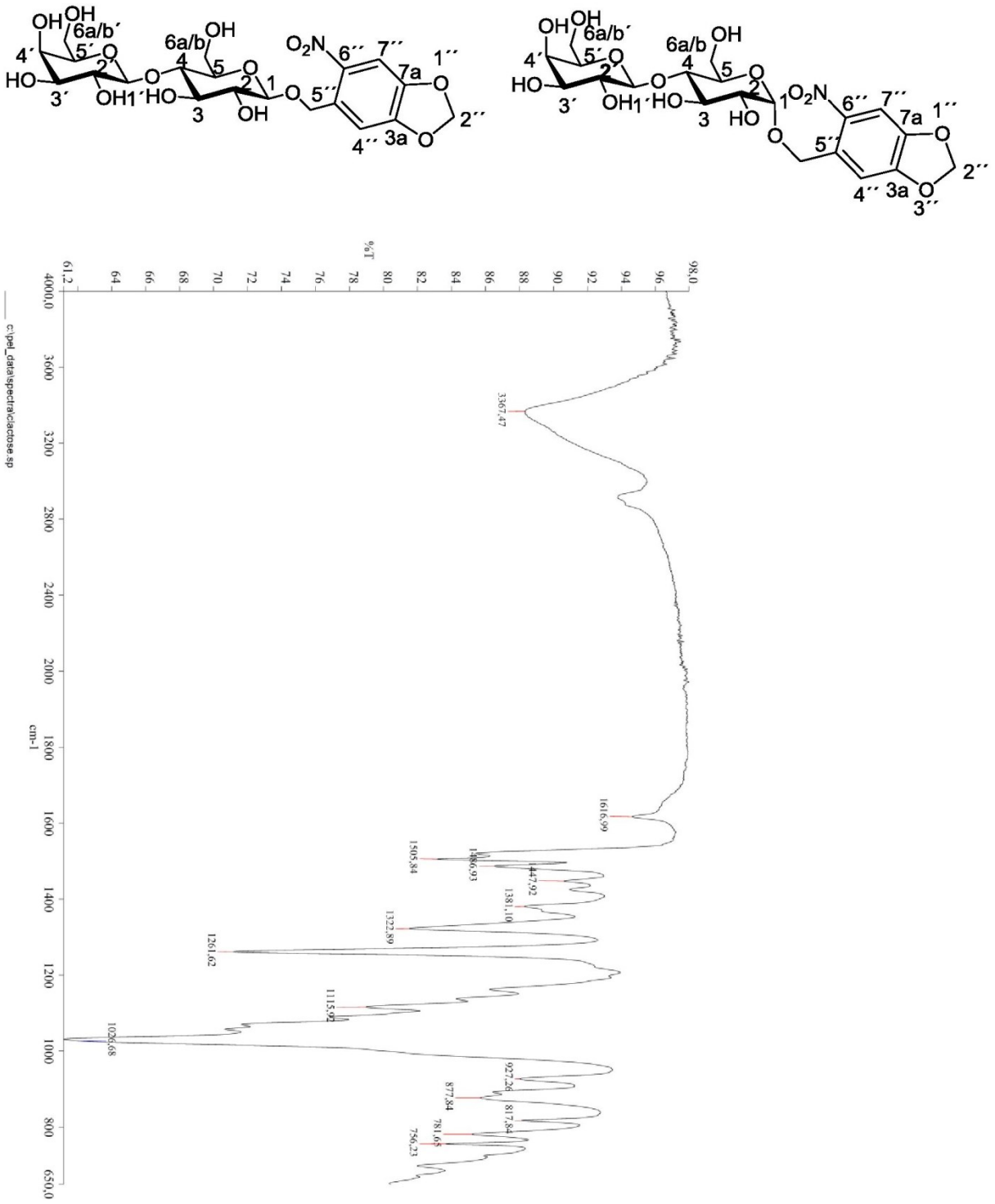

Figure 17: IR (ATR) 6e.

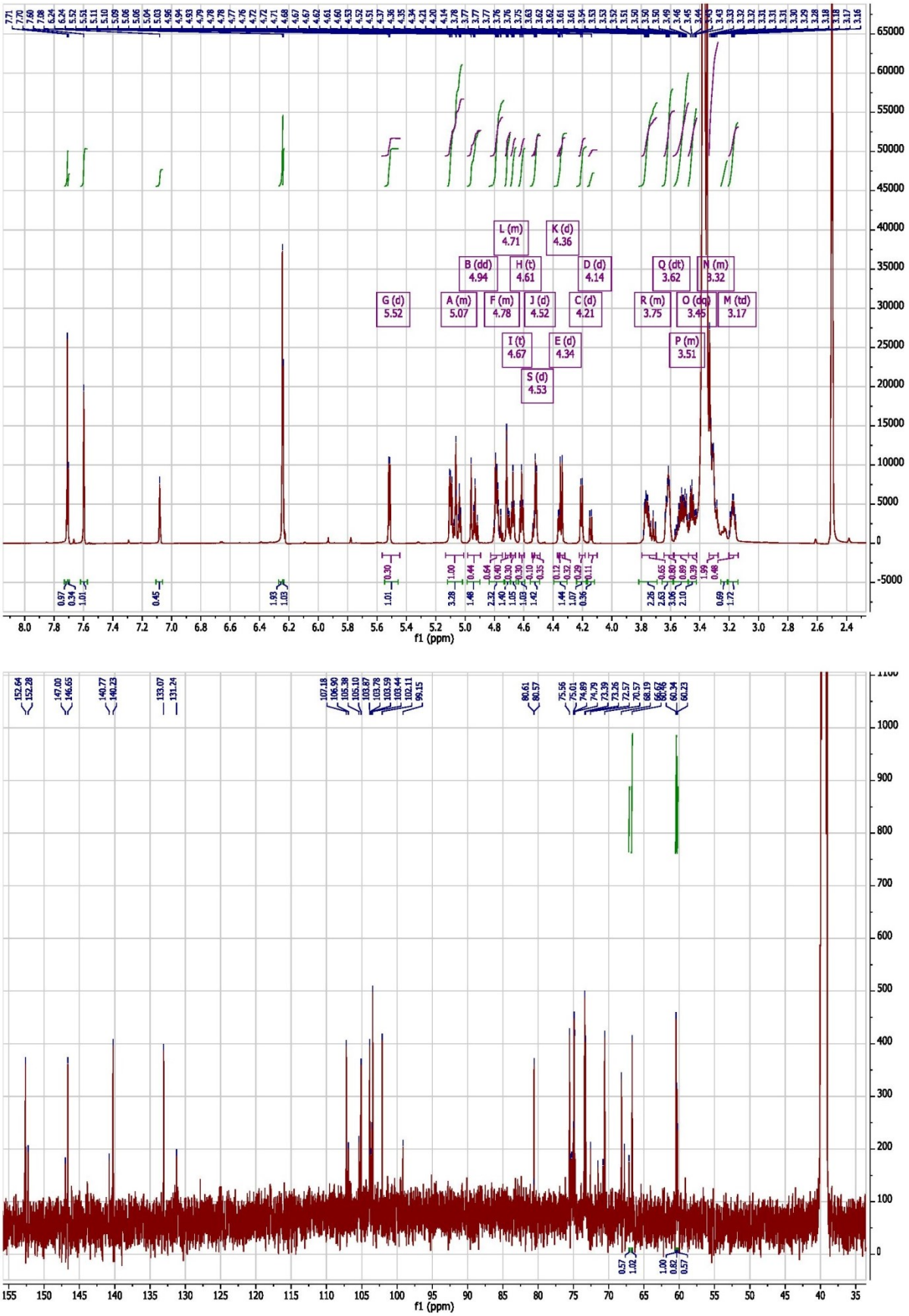

Figure 18: ^{1}H and ^{13}C NMR spectra of compound 6e.

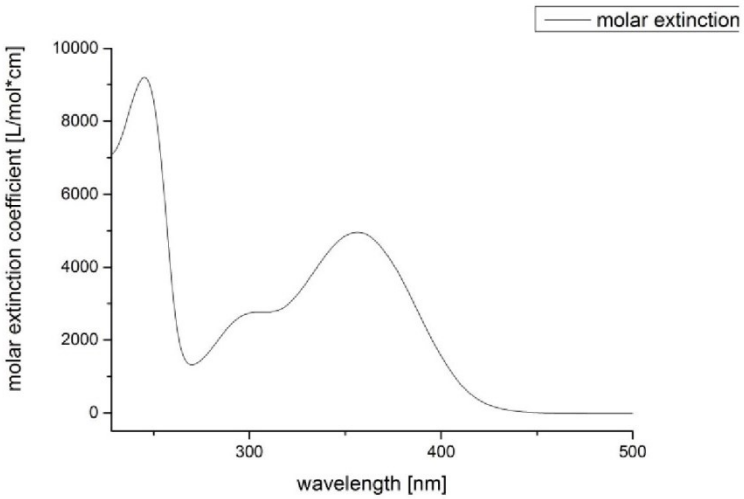

Figure 19: UV-Vis spectrum of compound 6e.

Quantification of uncaging half-life times

For the Quantification of uncaging half-life times a 1 mmol/L solution of each photocaged carbohydrate in demineralized water was prepared. A cuvette was charged with 1 mL of this solution and was irradiated at room temperature in the LUMOS 43 at 375 nm for a defined time period. In the following the sample was analysed on the HPLC (Jaso HPLC system (column: Hyperclone 5 µ ODS (C18) 120 (Phenomenex), MeOH:H_2O, 15:85; 1mL/min, 25 °C, 30 µL). This procedure was repeated for different irradiation durations for each photcaged carbohydrate. The decrease of concentration of the photocaged carbohydrate was measured with an UV detector the amount of freed carbohydrate was determine via a light scattering detector (ELSD ZAM 3000 from AlphaCrom, 80 °C, gasflow 1.5 l_n/min). In order to quantify the exact amount of carbohydrates by the light scattering detector a calibration curve for each carbohydrate had to be made. Curves shown in the figure 20 were fitted using an exponential fit (Epx Dec 1) with OriginPro 9.0G®. The uncaging half-life time was calculated with OriginPro 9.0G®. Fitting parameters are shown in table 1

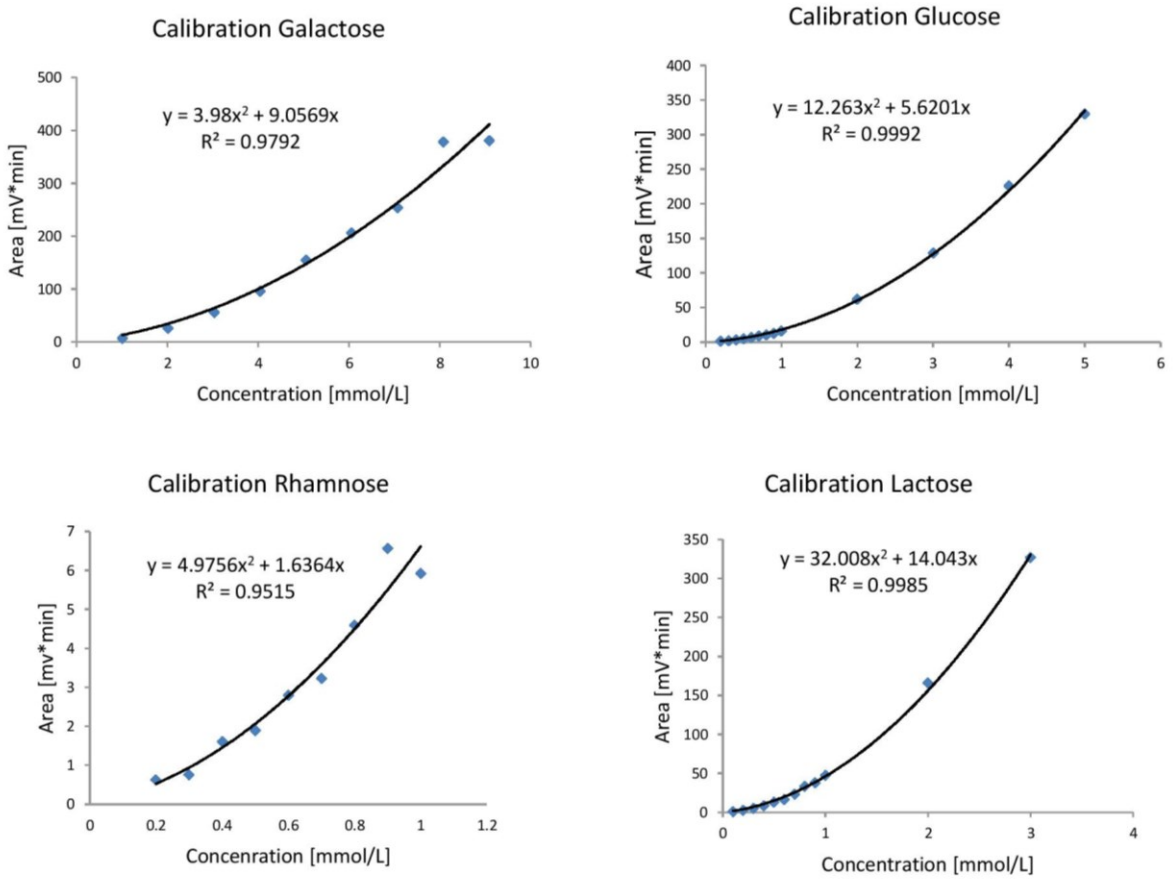

Figure 20: Calibration curves for the light scattering detector (ELSD ZAM 3000 from AlphaCrom, 80 °C, gasflow 1.5 l_n/min); monitored via HPLC analysis(Jaso HPLC system (column: Hyperclone 5 µ ODS (C18) 120 (Phenomenex), MeOH:H_2O, 15:85; 1mL/min, 25 °C, 30 µL). Polynomial fitted Microsoft® Excel® 2010 (14.0.7171.5000).

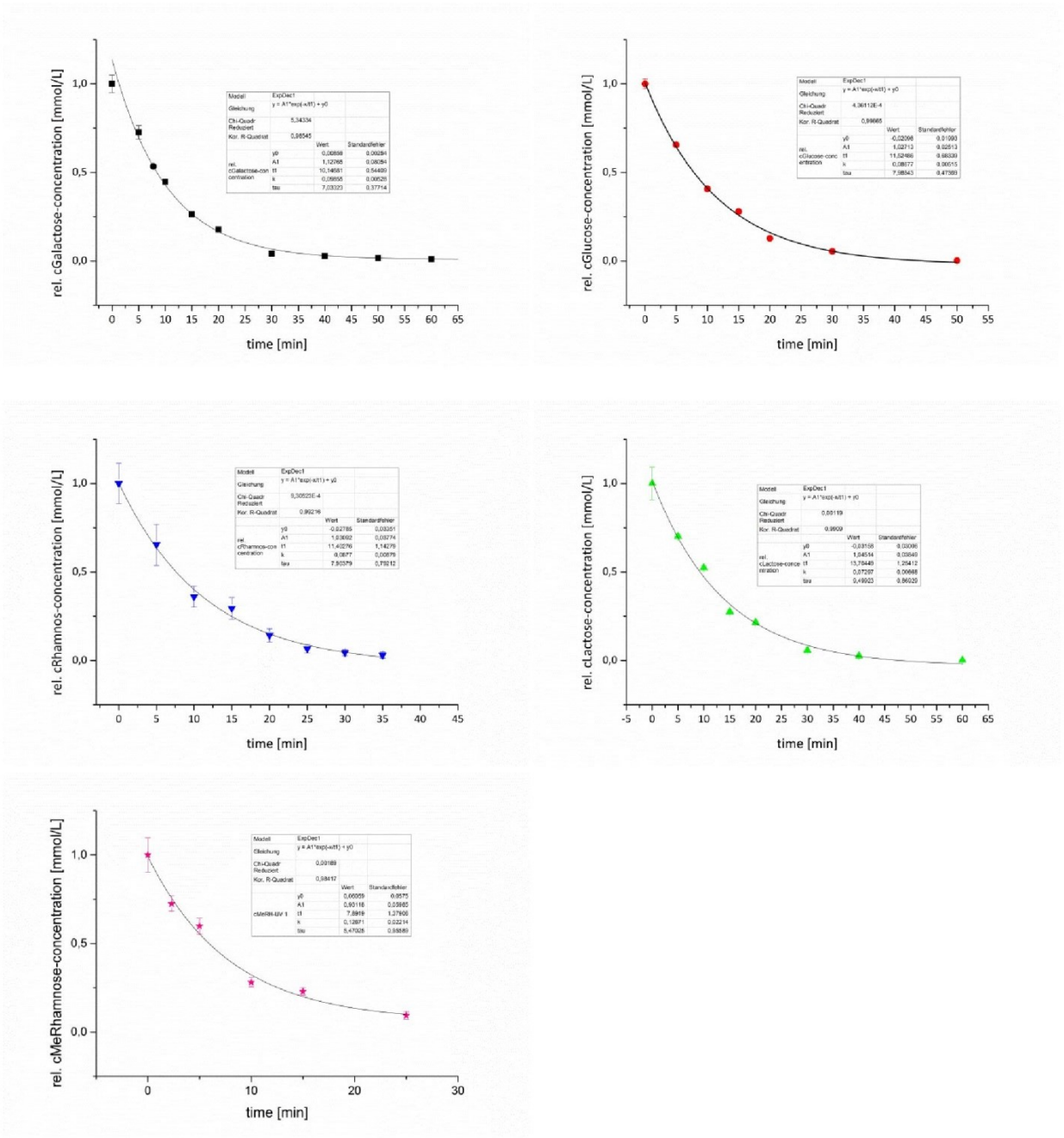

Figure 21 : *In vitro* release of carbohydrates monitored via HPLC analysis, of compound 6a;6b; 6c, 7c, 6e, 1 mmol in H_2O; 375 nm 6.4 mW/cm^2, r.t.

Table 1: Fitting parameters and uncaging half-life times $t_{0.5}$ for photocaged carbohydrates.

Inducer	y_0	A_1	t_1	k	$t_{0.5}$ *[min]*
cGalactose **6a**	-0,00691	1,03447	11,90947	0,08397	8,25501
cGlucose **6b**	-0,02098	1,02713	11,52486	0,08677	7,98843
cRhamnose **6c**	-0,02785	1,03092	11,40276	0,0877	7,90379
cMeRhamnose **7c**	0,06059	0,93118	7,8919	0,12671	5,47025
cLactose **6e**	-0,03158	1,04514	13,70449	0,07297	9,49923

V.5 Supporting Information for Chapter II.4.1 – DMNB Actinometry

Using 1,2-dimethoxy-4-nitrobenzene actinometry to monitor UV-A light exposure in photobiotechnological setups (*In preparation*)

Dennis Binder, Claus Bier, Oliver Klaus, Jörg Pietruszka, Karl-Erich Jaeger, and Thomas Drepper

NMR data of a DMNB solution prior to light exposure:

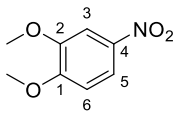

^{1}H NMR (600 MHz, Deuterium Oxide) δ 7.97 (dd, $^3J_{5,6}$ = 9.0 Hz, $^4J_{5,3}$ = 2.5 Hz, 1H, 5-H), 7.84 (d, $^4J_{3,5}$ = 2.5 Hz, 1H, 3-H), 7.13 (d, $^3J_{6,5}$ = 9.0 Hz, 1H, 6-H), 3.95 (s, 3H, CH_3), 3.92 (s, 3H, CH_3).

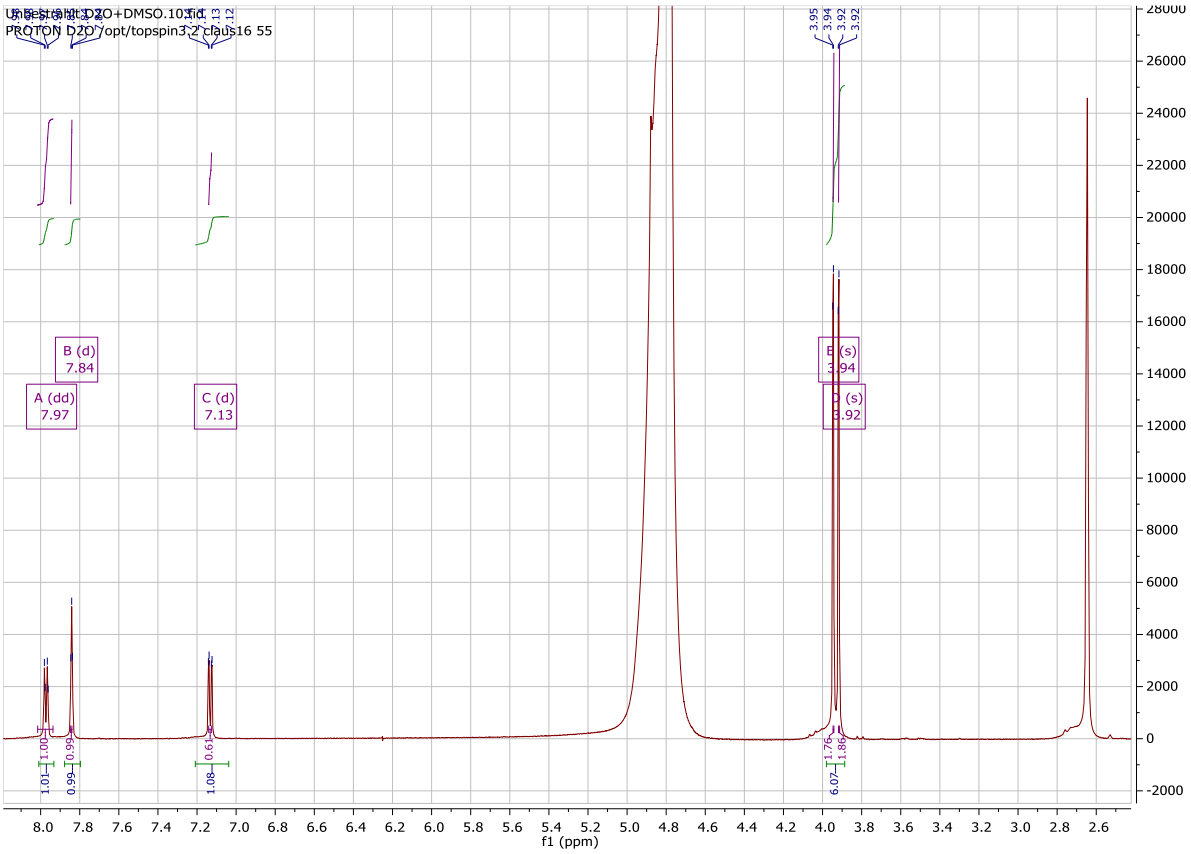

Figure S1. ^{1}H NMR spectrum of an unexposed 1.25 mM 1,2-Dimethoxy-4-nitrobenzene solution (0.5 M KOH, 10% DMSO-d_6) in Deuterium oxide.

NMR data of a DMNB solution upon 60 min of UV-A light exposure:

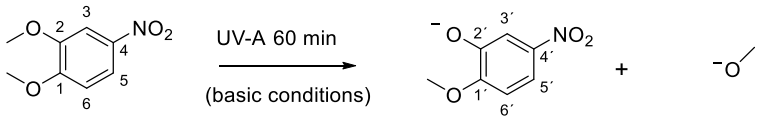

^{1}H NMR (600 MHz, Deuterium Oxide) δ 7.97 (dd, $^{3}J_{5,6}$ = 9.0 Hz, $^{4}J_{5,3}$ = 2.5 Hz, 1H, 5-H) 7.84 (d, $^{4}J_{3,5}$ = 2.5 Hz, 1H, 3-H), 7.47 (dd, $^{3}J_{5',6'}$ = 8.8 Hz, $^{4}J_{5',3'}$ = 2.9 Hz, 1H, 5´-H), 7.28 (d, $^{4}J_{3',5'}$ = 2.9 Hz, 1H, 3´-H), 7.13 (d, $^{3}J_{6,5}$ = 9.0 Hz, 1H, 6-H), 6.87 (d, $^{3}J_{6',5'}$ = 8.8 Hz, 4H), 3.95 (s, 3H, CH_3), 3.92 (s, 3H, CH_3)., 3.83 (s, 3H, CH_3´), 3.30 (s, 3H, $^{-}$OMe).

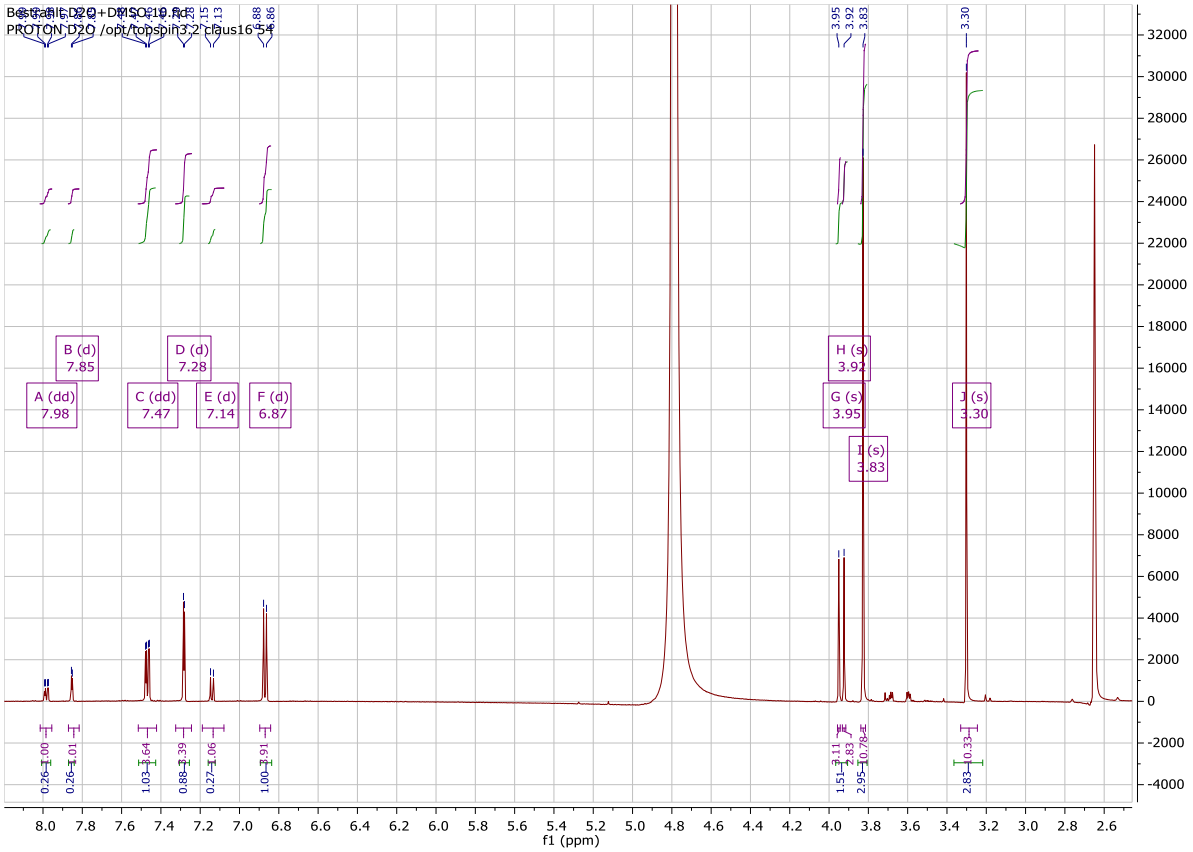

Figure S2. ^{1}H NMR spectrum of a light-exposed (60 min UV-A) 1.25 mM 1,2-Dimethoxy-4-nitrobenzene solution (0.5 M KOH, 10% DMSO-d_6) in Deuterium oxide.

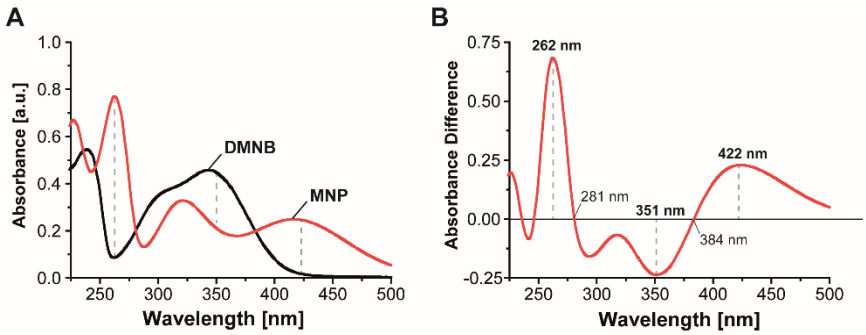

Figure S3. Full UV-Vis (A) and UV-Vis-Difference (B) spectra for fully converted 1.25 mM DMNB solutions measured in a quartz cuvette.

Table S1. Cultivation vessel specifications.

Cultivation vessel	Vessel Specification	Total volume	Working Volume	Liquid surface***	Surface-to-volume-ratio***
MTP	96 well F-Bottom (Greiner Bio-One)	392 µL	100 µL	48.44 mm^2	>0.48 mm^{-1}**
MTP Black	Nunclon F96 Black (Thermo Scientific)	400 µL	100 µL	49.70 mm^2	0.50 mm^{-1}
FP	48 well, flat bottom, black FlowerPlate®, (m2p labs)	3200 µL	800 µL	96.97 mm^2	0.12 mm^{-1}
10 mL Flask*	100 mL Erlenmeyer flask, narrow neck (DURAN®)	n.d.	10 mL	4096 mm^2	>0.41 mm^{-1}**
100 mL Flask*	1000 mL Erlenmeyer flask, narrow neck (DURAN®)	n.d.	100 mL	17161 mm^2	>0.17 mm^{-1}**

* volumina here refer to solution volume not to flask capacity
** due to translucent cultivation vessel: lateral light exposure and thus enlarged exposed surface expected
*** for unshaken cultures

Table S2. Exact UV-A light exposure setups for different cultivation vessels.

Cultivation vessel	Exact distance to vessel	Exposed from	Shaking frequencies
MTP	4.5 cm	Top	1000 rpm
MTP Black	4.5 cm	Top	1000 rpm
FP	1.5 cm*	Top	1000 rpm*
10 ml Flask	1.85 cm	Sideways (9° tilted towards flask)	150 rpm
100 ml Flask	1.85 cm	Sideways (9° tilted towards flask)	150 rpm

*Except for parameter variation experiments shown in Fig. 3.

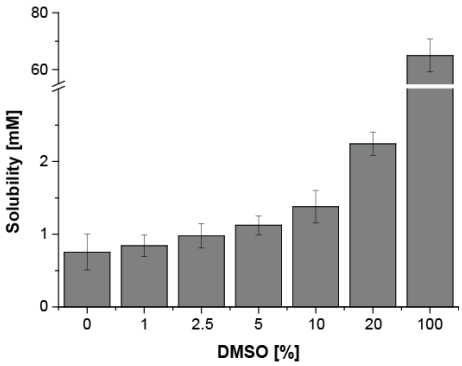

Figure S4. Solubility improvement of DMNB in aqueous potassium hydroxide solutions *via* DMSO.

V.6 Supporting Information for Chapter II.4.2 – Light-induced induction profiling

Light-induced gene expression with photocaged IPTG for induction profiling in a high-throughput screening system

Georg Wandrey, Claus Bier, Dennis Binder, Kyra Hoffmann, Karl-Erich Jaeger, Jörg Pietruska, Thomas Drepper, Jochen Büchs . *Microb Cell Fact 2016,* 15:63.

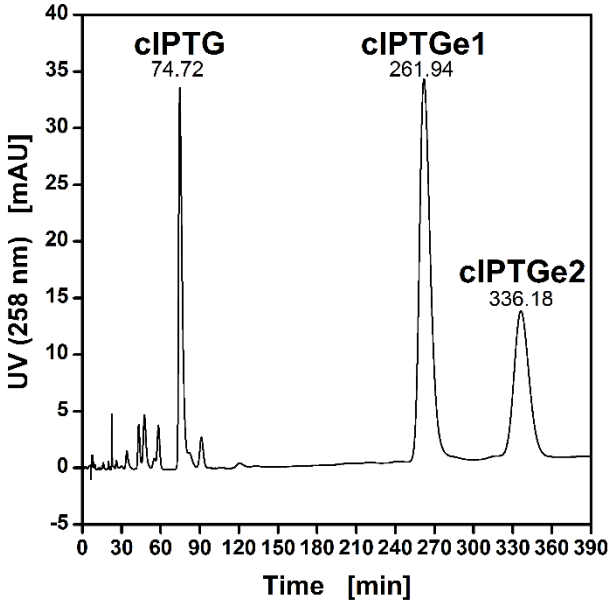

Additional file: 1. cIPTG was dissolved in isopropanol/n-heptan 50/50. (8.3 mg in 2.5 mL) and irradiated for 10 min (375 nm; 6.2 mW/cm²). cIPTG and its ester intermediates (cIPTGe1 and cIPTGe2) were then separated via HPLC (column: Chiralpak IC, 250·10 mm, Daicel, Japan; solvent: n-heptan:2-propanol (30:70); flow rate: 0.5 mL/min; detection: UV 258 nm)

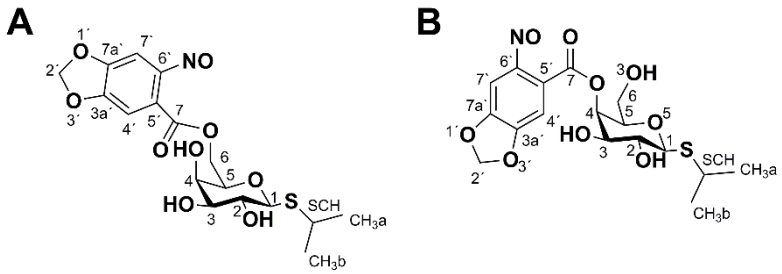

Additional file: 2 . NMR-measurement of ester intermediates. cIPTGe1 (A) and cIPTGe2 (B) were identified via NMR. **cIPTGe1 (A):** 1H-NMR (600 MHz, CDCl3), δ [ppm]: 7.35 (s, 1 H, 4´-CH), 6.01 (s, 1 H, 7´-CH), 6.14 (s, 2 H, 2´-CH2), 4.75 (dd, 2J6a, 6b = 11.5 Hz, 2J6a, 5 = 6.0 Hz, 1 H, 6-CH2), 4.66 (dd, 2J6b, 6a = 11.4 Hz, 2J6b, 5 = 6.6 Hz, 1 H, 6-CH2), 4.39 (m, 1 H, 1-CH), 3.98 (m, 1 H, 4-CH), 3.87 (m, 1 H, 5-CH), 3.63 (m, 2 H, 2-CH, 3-CH), 3.17 (septet, 3JSCH, CH3a/b = 6.70 Hz, 1 H, -SCH), 2.73 (s, 1 H, OH), 2.59 (s, 1 H, OH), 2.45 (s, 1 H, OH), 1.31 (d, 3JCH3a, SCH = 1.70 Hz, 3H, -CH3a), 1.30 (d, 3JCH3b, SCH = 1.80 Hz, 3H,-CH3b). 13C-NMR (151 MHz, CDCl3), δ [ppm]: 166.94 (C-7), 160.67 (C-6´), 153.16 (C-7a´), 150.80 (C-3a´), 133.61 (C-5´), 108.72 (C-4´), 103.36 (C-2´), 89.36 (C-7´), 86.00 (C-1), 75.66 (C-5), 74.34 (C-3), 70.51 (C-2), 68.47 (C-4), 64.69 (C-6), 35.92 (SCH), 24.22 (C- CH3a), 23.99 (C- CH3b). **cIPTGe2 (B):** 1H-NMR (600 MHz, CDCl3), δ [ppm]: 7.42 (s, 1 H, 4´-CH), 6.19 (s, 2 H, 2´-CH2), 6.01 (s, 1 H, 7´-CH), 5.69 (dd, 3J4,3 = 3.6 Hz, 3J4,5 = 1.1 Hz 1 H, 4–CH), 4.47 (d, 3J1,2 = 9.7 Hz, 1 H, 1-CH), 3.86 (m, 1 H, 5-CH), 3,78 (m, 2 H, 6a-CH2, 3-CH), 3.70 (dd, 3J6b, 6a = 11.9 Hz, 3J6b, 5 = 7.1 Hz, 1H, 6-CH2), 3.30 (t, 3J2,1 = 9.4 Hz, 3J2,3 = 9.4 Hz, 1 H, 2-CH2)), 3.18 (m, 1 H, -SCH), 1.31 (d, 3JCH3a/b, SCH = 1.6 Hz, 3H,-CH3a), 1.30 (d, 3JCH3a/b, SCH = 1.5 Hz, 3H,-CH3b)

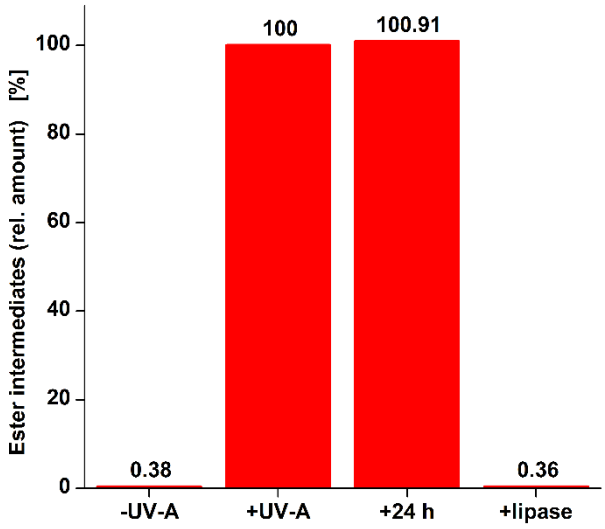

Additional file: 3. Relative amount of cIPTG ester intermediates over time. No ester intermediates are detected without UV-A irradiation (-UV-A). After UV-A irradiation (+UV-A) ester intermediates are detected. They were stable for at least 24 h (+24 h). Addition of lipase PL from *Alcaligenes sp.* fully degrades the ester intermediates (+lipase). HPLC (Jasco HPLC system, column: Hyperclone 5 µ ODS (C18) 120 (Phenomenex), solvent: MeOH:H2O 30:70, flow rate: 1 mL/min, 25 °C, 30 µL, detection: UV 258 nm at 11.46 min). 1000 µM cIPTG in H_2O, irradiation with 6.4 mW/cm² at 375 nm for 10 min and storage at RT for 24 h, addition of 1 mg lipase PL (Alcaligenes sp. lipase 100000 U/g) to 910 µL at 38 °C for 24 h

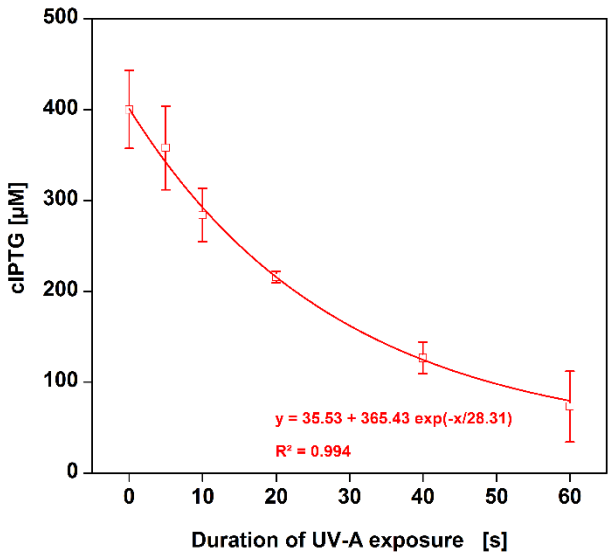

Additional file: 4. Photo-uncaging of cIPTG as a function of UV-A exposure duration. In vitro decomposition of 400 µM cIPTG in H_2O by UV-A irradiation (λ_{max} = 368 nm, I = 52 mW/cm², n = 4) monitored via HPLC–UV. HPLC (Jasco HPLC system, column: Hyperclone 5 µ ODS (C18) 120 (Phenomenex), solvent: MeOH:H2O 30:70, flow rate: 1 mL/min, 25 °C, 30 µL, detection: UV 258 nm at 19.04 min)

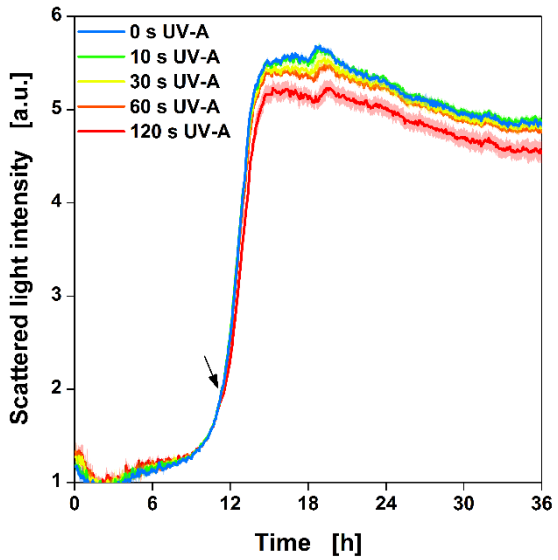

Additional file: 5. Effect of UV-A irradiation on cell growth. Scattered light intensity of non-induced cultures irradiated with UV-A LEDs for 0–120 s (λ_{max} = 368 nm, I = 52 mW/cm²). No cIPTG was added to the medium. The black arrow indicates the time of UV-A exposure in the exponential phase. For up to 60 s of UV-A exposure only minute deviations are detected in the scattered light signal. Exposure for 120 s leads to a slightly lower scattered light signal in the stationary phase. Since exposure durations of up to 40 s were sufficient for optical induction, negative effects of UV-A irradiation are of no concern for the bacteria used in this work. Cultivations were performed in triplicates; standard deviation is shown in the same color as the mean value but at 50 % transparency

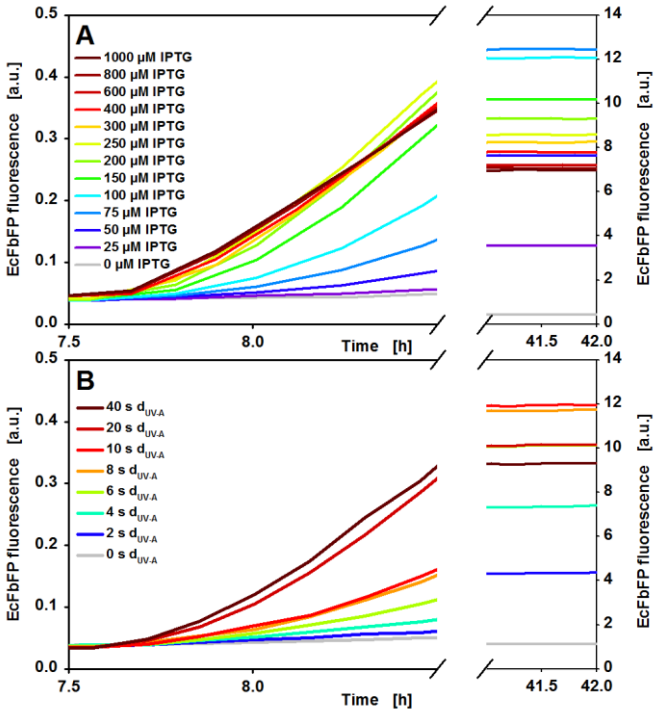

Additional file: 6. Initial product formation after induction. Zoomed view of Fig. 6c and Fig. 6g. FbFP fluorescence of *E. coli* cultures induced after 7.5 h with 0–1000 µM IPTG (A) or 400 µM of cIPTG and 0–40 s of UV-A irradiation (B). The initial product formation gradually increases with increasing IPTG concentrations (0–400 µM) and is saturated for higher concentrations (400–1000 µM) (A). However, the highest product fluorescence at the end of the cultivation after 42 h is reached with 75–100 µM IPTG (A, right side). For optical induction, initial product formation rate is highest for 20–40 s of UV-A irradiation and the highest product concentrations after 42 h are reached with 8–10 s (B). Note the axis scaling and breaks for increased readability. Additionally, note that only 400 µM of cIPTG are available for uncaging in B. Cultivation conditions: 800 µL Wilms-MOPS mineral medium per well in a 48-FlowerPlate, 400 µM cIPTG added to cultures induced with the LED array (λ_{max} = 368 nm, I = 52 mW/cm²), 30 °C, shaking frequency: 1000 rpm, shaking diameter: 3 mm

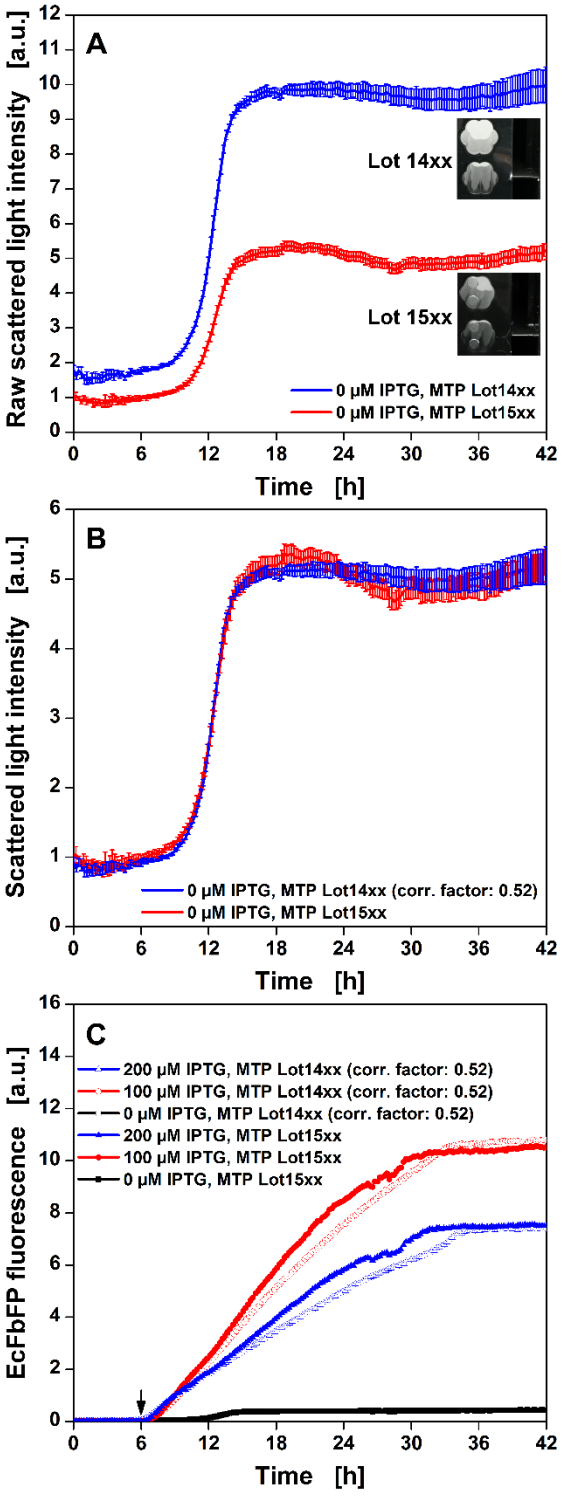

Additional file: 7. Data normalization. Raw scattered light signals are influenced by the microtiter plate lot (A). For normalization the raw signals of cultivations in one lot can be multiplied with a correction factor to match the course of the other cultivation (B). The correction factor is determined by dividing the scattered light intensities at the end of the cultivation after 42 h. This correction factor can also be applied to correct EcFbFP fluorescence signals (C). The normalized signals of cultures induced with 0, 100 or 200 µM IPTG are in good agreement. This demonstrates that reproducible results can be obtained even when different microtiter plate lots are used. Cultivation conditions: 800 µL Wilms-MOPS mineral medium per well in a 48-FlowerPlate, 30 °C, shaking frequency: 1000 rpm, shaking diameter: 3 mm. Error bars in A and B indicate the standard deviation of six reference cultures. Induction in C after 6 h. Data for 0 µM IPTG and lot 14xx is not visible in C because it is almost identical to lot 15xx

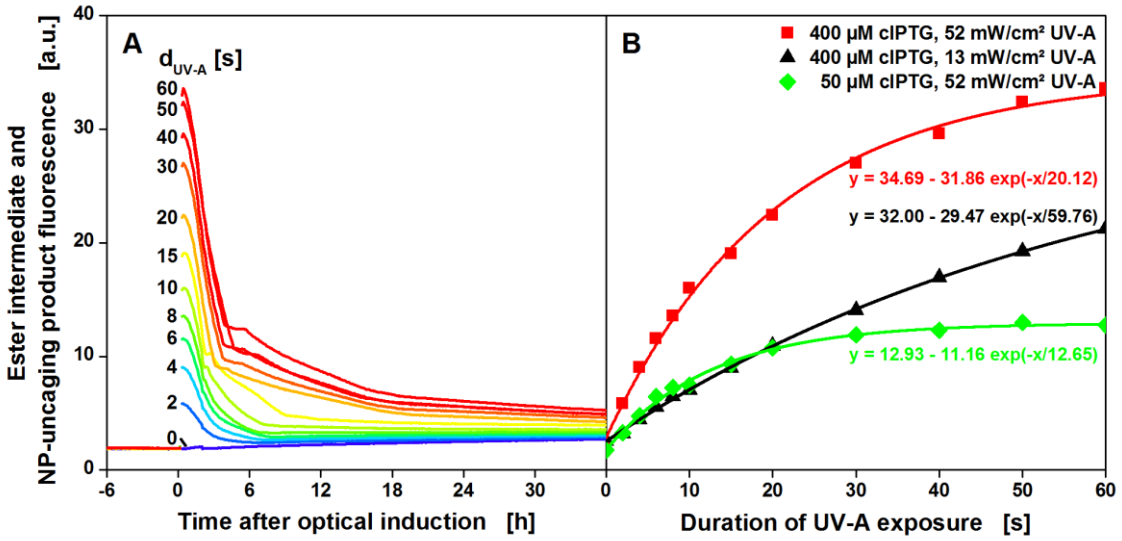

Additional file: 8. Online measurement of cIPTG ester intermediates and NP-uncaging product. This figure shows the full data set of the measurement presented in Fig. 4 where measurements for 8, 15, 40 and 50 s of UV-A irradiation were not shown to increase readability. Fluorescence intensity (λ_{Ex} = 326 nm, λ_{Em} = 407 nm, black cross in Fig. 2) of 12 *E. coli* cultures before and after UV-A irradiation for 0–60 s (A) and fluorescence intensity measured directly after irradiation as a function of duration of UV-A exposure (B). At the beginning of the cultivation, 400 µM cIPTG were added to the medium. After 10 h, optical induction was performed with the LED array (λ_{max} = 368 nm, I = 52 mW/cm²). The amount of ester intermediates increases with increasing duration of UV-A exposure and can be fitted with first-order kinetics (solid lines and equations in B, $R^2 > 0.995$). Reduced irradiance leads to lower rate constants (black triangles, I = 13 mW/cm²) and reduced cIPTG concentration to lower amplitude (green diamonds, 50 µM cIPTG). Cultivation conditions: 800 µL Wilms-MOPS mineral medium (20 g/L glucose, 0.2 M MOPS) per well in a 48-FlowerPlate, 30 °C, shaking frequency: 1000 rpm, shaking diameter: 3 mm

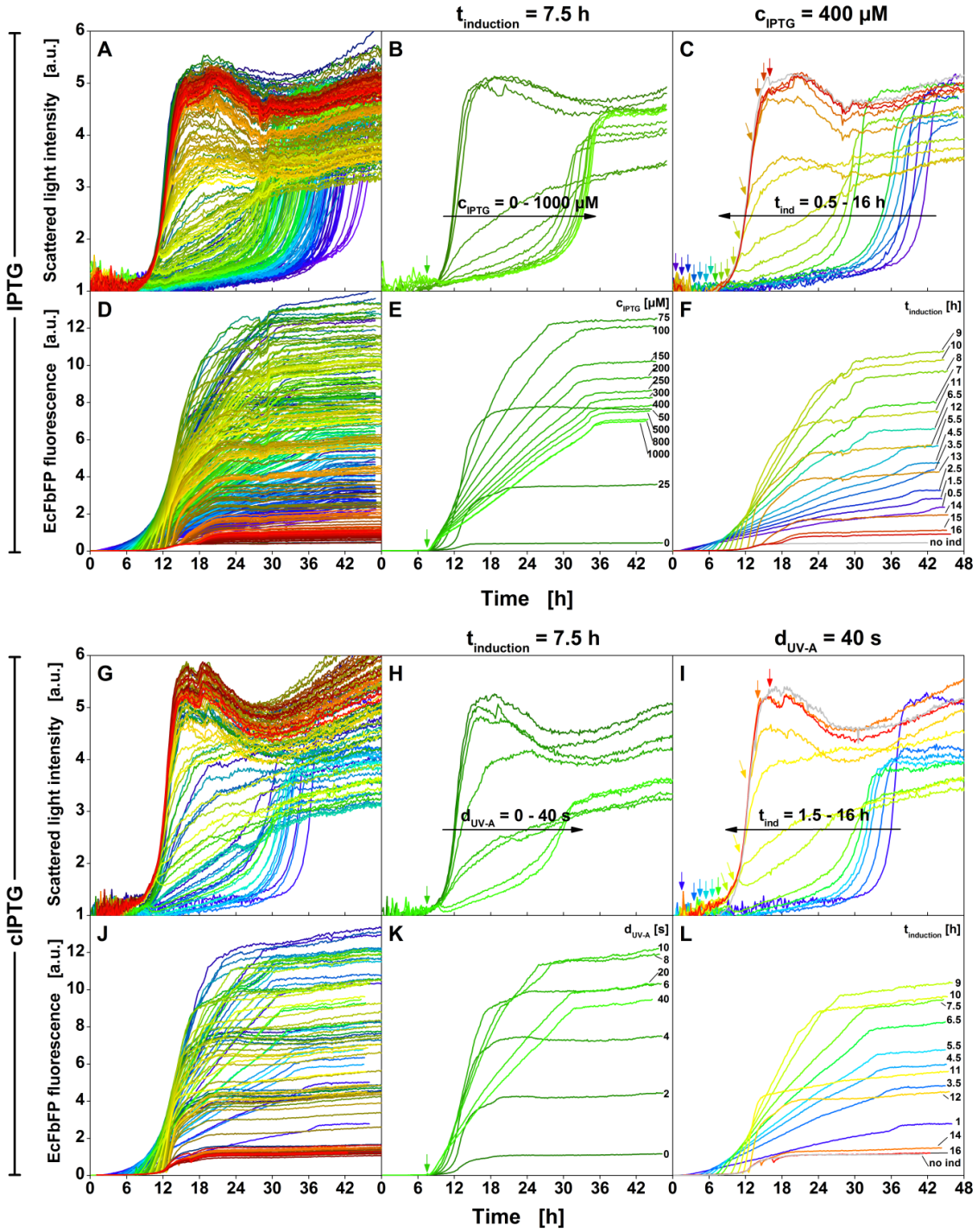

Additional file: 9. Online measurement data for conventional induction profiling with manual addition of IPTG solution and optical induction profiling with cIPTG. This figure shows the full data set of induction profiling experiment presented in Fig. 6. Scattered light and FbFP fluorescence of 304 E. coli cultures induced with IPTG (A-F) and of 96 E. coli cultures induced with cIPTG (G-L). Time of induction and inducer strength (IPTG concentration or duration of UV-A exposure) are varied in full factorial design. Colors from blue to red mark later induction times (0.5–16 h), dull to bright colors mark increasing inducer strength (0–1000 µM IPTG or 0–40 s duration of UV-A exposure). The first column (A,D,G,J) shows the full data set while the second column (B,E,H,K) shows a subset at a fixed induction time of 7.5 h and the third column (C,F,I,L) shows a subset at a fixed inducer strength of 400 µM IPTG or 40 s UV-A exposure. Small colored down-pointing arrows illustrate the time of induction (not all shown). Long horizontal arrows in black illustrate general trends, e.g. impact of increasing inducer concentration on growth (B). Cultivation conditions: 800 µL Wilms-MOPS mineral medium per well in a 48-FlowerPlate, 400 µM cIPTG added to cultures induced with the LED array (λ_{max} = 368 nm, I = 52 mW/cm²), 30 °C, shaking frequency: 1000 rpm, shaking diameter: 3 mm

V.7 Supporting Information for Chapter II.5.1 – Light-controlled Corynebacterium cell factories

Light-controlled cell factories – Employing photocaged IPTG for light-mediated optimization of *lac*-based gene expression and valencene biosynthesis in *Corynebacterium glutamicum*

Dennis Binder,* Jonas Frohwitter,* Regina Mahr, Claus Bier, Alexander Grünberger, Anita Loeschcke, Petra Peters-Wendisch, Dietrich Kohlheyer, Jörg Pietruszka, Julia Frunzke, Karl-Erich Jaeger, Volker Wendisch and Thomas Drepper. *Appl Env Microbiol* 2016. doi: 10.1128/AEM.01457-16

DNA-Sequence of the synthetic codon-usage optimized CnVS gene (oCnVS):

ATGGCGGAAATGTTCAACGGCAACAGCAGCAACGATGGCAGCAGCTGCATGCCGGTGAAAGATGCG
CTGCGCCGCACCGGCAACCATCATCCGAACCTGTGGACCGATGATTTCATCCAGAGCCTGAACAGCC
CGTATAGCGATAGCAGCTATCATAAACATCGCGAAATCCTGATCGATGAAATCCGCGATATGTTCAGC
AACGGCGAAGGCGATGAATTCGGCGTGCTGGAAAACATCTGGTTCGTGGATGTGGTGCAGCGCCTG
GGCATCGATCGCCATTTCCAGGAAGAAATCAAAACCGCGCTGGATTATATCTATAAATTCTGGAACCA
TGATAGCATCTTCGGCGATCTGAACATGGTGGCGCTGGGCTTCCGCATCCTGCGCCTGAACCGCTAT
GTGGCGAGCAGCGATGTGTTCAAAAAATTCAAAGGCGAAGAAGGCCAGTTCAGCGGCTTCGAAAGCA
GCGATCAGGATGCGAAACTGGAAATGATGCTGAACCTGTATAAAGCGAGCGAACTGGATTTCCCGGA
TGAAGATATCCTGAAAGAAGCGCGCGCGTTCGCGAGCATGTATCTGAAACATGTGATCAAAGAATATG
GCGATATCCAGGAAAGCAAAAACCCGCTGCTGATGGAAATCGAATATACCTTCAAATATCCGTGGCGC
TGCCGCCTGCCGCGCCTGGAAGCGTGGAACTTCATCCATATCATGCGCCAGCAGGATTGCAACATCA
GCCTGGCGAACAACCTGTATAAAATCCCGAAAATCTATATGAAAAAAATCCTGGAACTGGCGATCCTG
GATTTCAACATCCTGCAAAGCCAGCATCAGCATGAAATGAAACTGATCAGCACCTGGTGGAAAAACAG
CAGCGCGATCCAGCTGGATTTCTTCCGCCATCGCCATATCGAAAGCTATTTCTGGTGGGCGAGCCCG
CTGTTCGAACCGGAATTCAGCACCTGCCGCATCAACTGCACCAAACTGAGCACCAAAATGTTCCTGCT
GGATGATATCTATGATACCTATGGCACCGTGGAAGAACTGAAACCGTTCACCACCACCCTGACCCGC
TGGGATGTGAGCACCGTGGATAACCATCCGGATTATATGAAAATCGCGTTCAACTTCAGCTATGAAAT
CTATAAAGAAATCGCGAGCGAAGCGGAACGCAAACATGGCCCGTTCGTGTATAAATATCTGCAAAGCT
GCTGGAAAAGCTATATCGAAGCGTATATGCAGGAAGCGGAATGGATCGCGAGCAACCATATTCCGGG
CTTCGATGAATATCTGATGAACGGCGTGAAAAGCAGCGGCATGCGCATCCTGATGATCCATGCGCTG
ATCCTGATGGATACCCCGCTGAGCGATGAAATCCTGGAACAGCTGGATATCCCGAGCAGCAAAAGCC
AGGCGCTGCTGAGCCTGATCACCCGCCTGGTGGATGATGTGAAAGATTTCGAAGATGAACAGGCGCA
TGGCGAAATGGCGAGCAGCATCGAATGCTATATGAAAGATAACCATGGCAGCACCCGCGAAGATGCG
CTGAACTATCTGAAAATCCGCATCGAAAGCTGCGTGCAGGAACTGAACAAAGAACTGCTGGAACCGA
GCAACATGCATGGCAGCTTCCGCAACCTGTATCTGAACGTGGGCATGCGCGTGATCTTCTTCATGCT
GAACGATGGCGATCTGTTCACCCATAGCAACCGCAAAGAAATCCAGGATGCGATCACCAAATTCTTCG
TGGAACCGATCATCCCG<u>TAA</u>

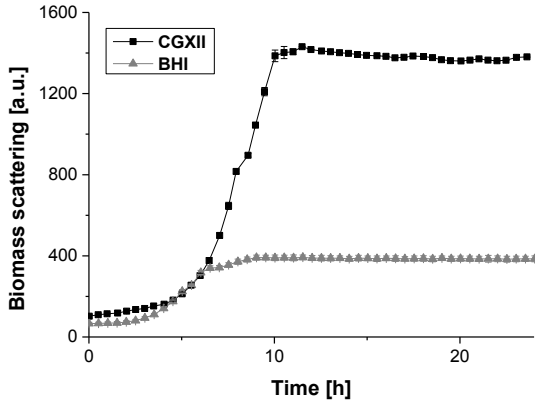

FIG S1 Growth curves of *C. glutamicum* cultures in triplicates in BHI complex (grey triangles) and CGXII minimal medium (black squares).

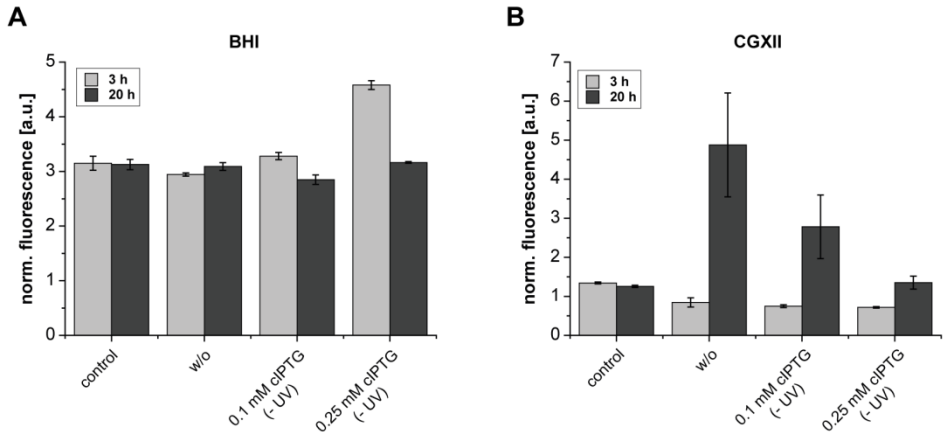

FIG S2 Basal expression background of cIPTG supplemented cultures in BHI (**A**) and CGXII medium (**B**) in the dark. Normalized fluorescence values originate from biomass-normalized triplicates analog to values for induced gene expression depicted in Fig. 2B,D. Control: Wildtype control strain without the pEKEx-2-EYFP plasmid.

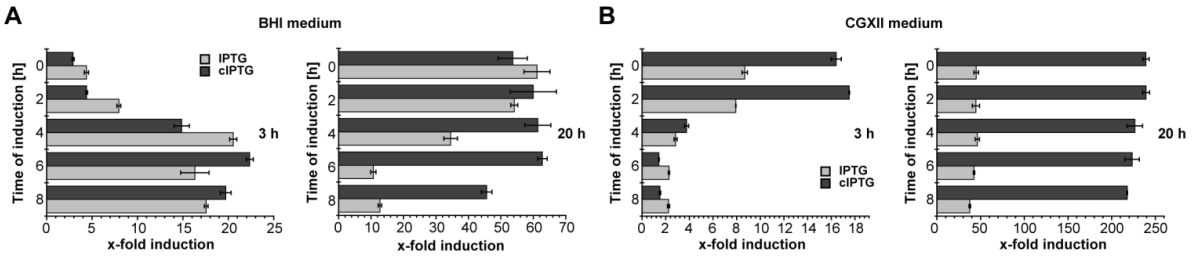

FIG S3 Dynamic range of induction for IPTG (light grey) and cIPTG-based (dark grey) induction after 3 (left) and 20 h (right) of expression in BHI (**A**) and CGXII medium (**B**) using *C. glutamicum* ATCC13032 (pEKEx-2-EYFP). Calculations originate from data depicted in Fig.2 B,C (biomass-normalized fluorescence) and Fig.S2 (basal fluorescence levels).

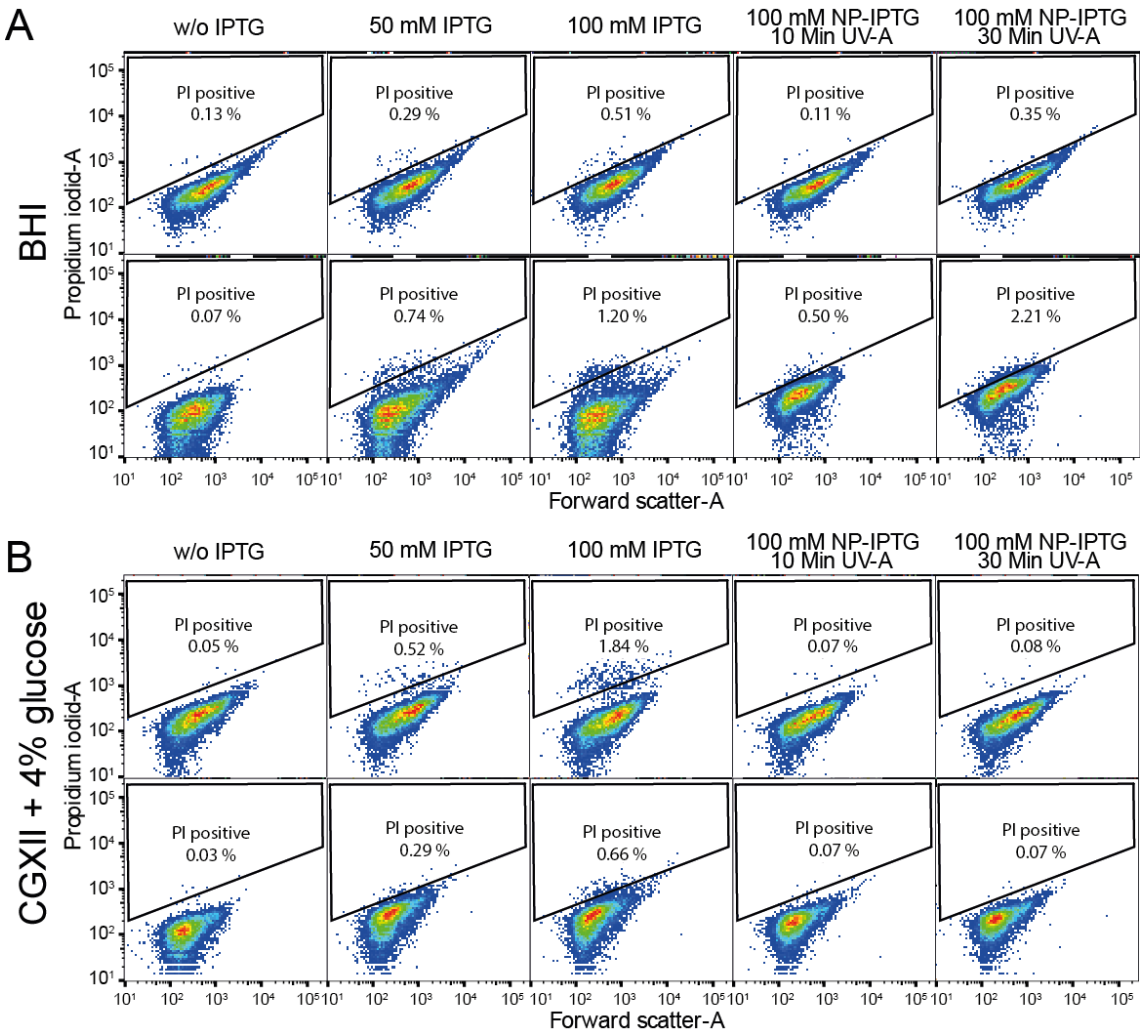

FIG S4 Propidium iodide-based live-dead-staining using flow cytometric single-cell analysis to evaluate cell viability.

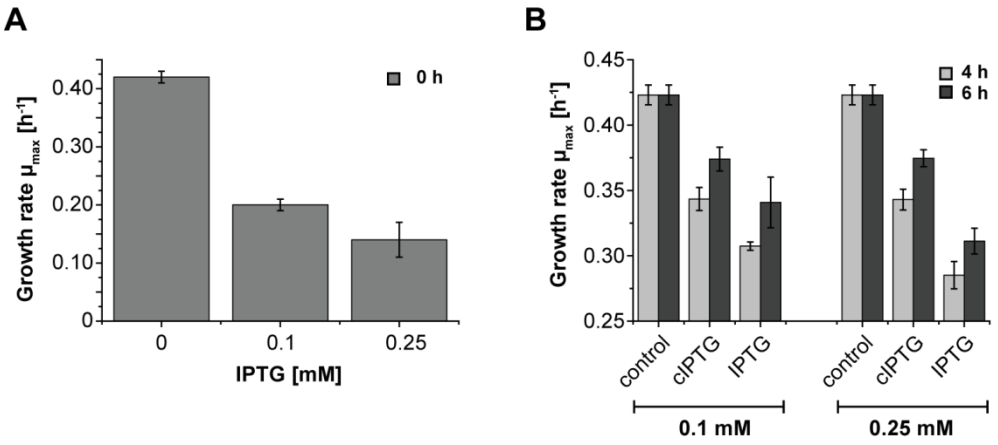

FIG S5 Reduction of growth impairment during (+)-valencene production in VLC6 *via* delayed induction and application of cIPTG-based light induction. **A**) Growth rates of VLC6 cultures for direct induction (0 h) are depicted for different IPTG inducer concentrations. **B**) Growth rates of VLC6 cultures are shown for delayed IPTG and cIPTG-induction after 4 (light grey) and 6 h (dark grey) together with un-induced cultures (control). All means and standard deviation derive from biological triplicates.

TAB S1 Summary titers and productivities for the conducted (+)-valencene productions in different *C. glutamicum* strains using CGXII minimal medium. Values for volumetric productivity were calculated using the overall cultivation times (28 h for induction after 4 h and 30 h for induction after 6 h).

Strain	Condition	Titer [mg l^{-1}]	Final OD_{600}	Volumetric productivity [µg l^{-1} h^{-1}]	Biomass yield [µg g CDW^{-1} h^{-1}]
VLC3	0.1 mM IPTG, 6h, Flask	7.2±0.6	33.5±2.1	240 ± 20	28.7±2.4
VLC4	0.1 mM IPTG, 6h, Flask	10.8±1.1	34.1±1.8	360 ± 37	42.2±4.3
VLC5	0.1 mM IPTG, 6h, Flask	10.5±3.5	33.9±2.3	350 ± 117	41.3±13.8
VLC6	0.1 mM IPTG, 6h, Flask	27.1±0.6	35.2±1.1	903 ± 20	102.7±2.3
VLC6	0.1 mM IPTG, 6h, Flowerplate	29.0±0.1	59.7±3.4	967 ± 3	64.8±0.3
VLC6	0.1 mM IPTG, 4h, Flask	14.8±1.1	30.3±1.2	529 ± 39	69.8±5.2
VLC6	0.1 mM IPTG, 4h, Flowerplate	28.4±1.7	57.8±2.9	1014 ± 61	70.2±4.2
VLC6	0.1 mM cIPTG, full light induction after 4h, Flowerplate	41.0±0.7	60.8±1.9	1464 ± 25	96.3±1.6

Supporting References

1. **Hentschel E, Will C, Mustafi N, Burkovski A, Rehm N, Frunzke J**. 2013. Destabilized eYFP variants for dynamic gene expression studies in *Corynebacterium glutamicum*. Microb Biotechnol **6**:196–201.
2. **Peters-Wendisch PG, Schiel B, Wendisch VF, Katsoulidis E, Möckel B, Sahm H, Eikmanns BJ**. 2001. Pyruvate carboxylase is a major bottleneck for glutamate and lysine production by *Corynebacterium glutamicum*. J Mol Microbiol Biotechnol **3**:295–300.
3. **Frohwitter J, Heider SAE, Peters-Wendisch P, Beekwilder J, Wendisch VF**. 2014. Production of the sesquiterpene (+)-valencene by metabolically engineered *Corynebacterium glutamicum*. J Biotechnol **191**:205–13.
4. **Stansen C, Uy D, Delaunay S, Eggeling L, Goergen J-L, Wendisch VF**. 2005. Characterization of a *Corynebacterium glutamicum* lactate utilization operon induced during temperature-triggered glutamate production. Appl Environ Microbiol **71**:5920–8.

Epilogue & Acknowledgments

The here presented thesis was developed in the framework of a major project that was concerned with new optical sensors and photoregulators for light-mediated control and analysis of molecular systems (OptoSys). In the larger context of developing next generation biotechnological methods (Biotechnology 2020+) the project was funded by the Federal Ministry of Education and Research (BMBF). Consequentially, this thesis benefited from a highly collaborative venture and would not have been feasible in this manner without the assistance of the OptoSys consortium.

Firstly, I thank my doctorate supervisor Prof. Karl-Erich Jaeger for providing me with this appealing project to work on as well as his helpful advice on various concerns and manuscripts.

My sincere thanks go to Dr. Thomas Drepper, who strongly supported and encouraged me during the whole thesis with highly fruitful discussions and friendly guidance. Moreover, I greatly acknowledge him for letting me follow up on own thoughts and concepts.

Furthermore, I would like to thank Dr. Anita Loeschke for valuable comments on so many manuscripts and projects and especially this thesis.

Many thanks belong to Dr. Stephan Thies for sharing his knowledge on e.g. natural products or *P. putida* cultivations as well as valuable notes on this thesis.

Specifically, I would like to express my sincere thanks to Claus Bier and Prof. Dr. Jörg Pietruszka for a great collaboration concerning the photocaged compounds projects as well as so many fruitful discussions at the interface between chemistry and biology. In detail, I thank Claus Bier for the very pleasant collaboration and teaching me a lot about chemistry. Many thanks go to Prof. Dr. Jörg Pietruszka for his kind acceptance as co-referee and the continuous support of this thesis.

The microscale bioengineering group, notably Dr. Alexander Grünberger, Dr. Christopher Probst and Prof. Dr. Dietrich Kohlheyer, I thank for an amazing cooperation in the field of microfluidic single-cell analysis. Special thanks go to Dr. Alexander Grünberger for teaching me a lot about single-cell analysis, pushing so many projects with his unprecedented ambition and for notes on my thesis. Many thanks belong to Dr. Christopher Probst for his huge efforts in image analysis, graphical illustrations and sophisticated technical setups.

I would also like to express my gratitude for a fruitful cooperation with Georg Wandrey and Prof. Dr. Jochen Büchs especially with respect to setting up light-induced induction profiling in a specifically developed photomicrobioreactor.

Moreover, I thank Jonas Frohwitter, Dr. Petra Peters-Wendisch and Prof. Volker Wendisch for a nice collaboration concerning the light-controlled (+)-valence production in *C. glutamicum*.

Further thanks go to Dr. Regina Mahr and Prof. Dr. Julia Frunzke for valuable assistance in setting up *C. glutamicum* cultivations and flow cytometric analyses.

Furthermore, I would like to acknowledge Pia Skoczinski and Dr. Andreas Knapp as well as Sarah Wienecke and Dr. Rebekka Biedendieck for providing strains and helpful advice with regard to setting up expression cultures of *B. subtilis* and *B. megaterium*, respectively.

I sincerely thank Sonja Kubicki and Nora Lisa Bitzenhofer for their high incentive in their bachelor projects.

Many thanks further belong to Fabienne Hilgers for her excellent bachelor and master projects she conducted under my supervision as well as her help in the lab on various issues.

Furthermore, I thank Katrin Troost and Nadine Katzke for advice on GC measurements and terpenoid production.

I would also like to thank Vera Svensson, Dr. Achim Heck and Dr. Armagan Özgür for their excellent advice on so many topics.

For their help on chemical or bioinformatical issues, I would like to express my gratitude to Vera Ophoven and Dr. Thomas Classen as well as Dr. Stefan Helfrich and Dr. Katarina Nöh.

All members of the IMET and especially those of the Drepper lab, I thank for such a friendly and helpful atmosphere. It was a pleasure working with you all!

For a cheerful atmosphere in the office I thank Vera and Maja. Further I have to acknowledge Chris, Armagan, Robin, Woopi, as well as Christopher and Alex for highly humorous spare time activities.

Last but not least, I deeply thank my family, my parents and friends for their continuous and immense support and patience.

Erklärung

Ich versichere an Eides Statt, dass diese Dissertation von mir selbständig und ohne unzulässige fremde Hilfe unter Beachtung der „Grundsätze zur Sicherung guter wissenschaftlicher Praxis an der Heinrich-Heine-Universität Düsseldorf“ erstellt worden ist.

Diese Dissertationsschrift wurde in vorliegender oder ähnlicher Form noch bei keiner anderen Fakultät eingereicht. Ich habe bisher keine erfolglosen Promotionsversuche unternommen.

Düsseldorf, den 06.September 2016